

# **Reactivity of Platinum (II) Complexes with (O,S) Bidentate Ligands towards DNA Model Systems for Cancer Treatment**

## **Dissertation**

**(kumulativ)**

zur Erlangung des akademischen Grades doctor rerum naturalium

(Dr. rer. nat.)

vorgelegt dem Rat der Chemisch-Geowissenschaftlichen Fakultät

der Friedrich-Schiller-Universität Jena

von M.Sc. Micheal Eshak

geboren am 08.06.1988 in Assiut, Ägypten

Gutachter:

1. Prof. Dr. Wolfgang Weigand, IAAC Institut, CGF, FSU-Jena.
2. Prof. Dr. Wolfgang Imhof, Institut für Integrierte Naturwissenschaften, UNI-Koblenz.
- (3. )

Tag der Verteidigung: 03.05.2023

# Contents

Contents .....	III
1. List of Publications .....	1
2. Documentation of Authorship .....	2
2.1 [ME-1] Novel Homoleptic and Heteroleptic Pt(II) $\beta$ -oxodithiocinnamic ester Complexes: Synthesis, Characterization, Interactions with 9-methylguanine and Antiproliferative Activity .....	2
2.2 [ME-2] Platinum(II) and palladium(II) complexes mediated by $\beta$ -hydroxy-dithioesters ferrocenyl derivatives: synthesis, characterization and Antiproliferative Activity .....	2
2.3 [ME-3] Dual Function of $\beta$ -Hydroxy Dithiocinnamic Esters: RAFT Agent and Ligand for Metal Complexation.....	3
2.4 [ME-4] Activating a [FeFe] Hydrogenase Mimic for Hydrogen Evolution under Visible Light	4
2.5 Declaration.....	5
3. Introduction .....	6
3.1 Cancer .....	6
3.1.1 Differences Between Cancer Cells and Normal Cells .....	7
3.1.2 Differences Between Benign and Malignant Tumors .....	8
3.2 Cancer Genes .....	8
3.3 Cancer Develop and Spread .....	9
3.4 Cancer Types .....	11
3.5 Cancer Treatment .....	11
3.5.1 Biomarker Testing for Cancer Treatment .....	11
3.5.2 Hormone Therapy .....	12
3.5.3 Hyperthermia Therapy.....	12
3.5.4 Photodynamic Therapy .....	12
3.5.5 Radiation Therapy .....	12
3.5.6 Immunotherapy .....	13
3.5.7 Targeted Therapy .....	14
3.5.8 Stem Cell Transplant .....	14
3.5.9 Surgery .....	14
3.5.10 Chemotherapy.....	14
3.6 Classification of Chemotherapeutic agents .....	16
3.6.1 Antimetabolites.....	16
3.6.2 Antitumor Antibiotics.....	17
3.6.3 Plant-derived Anticancer Agents.....	19
3.6.4 Hormonal Anticancer Agents .....	21

3.6.5	Alkylating Antineoplastic Agents.....	22
3.6.5.1	Bifunctional Alkylating Agents .....	22
3.6.5.2	Monofunctional Alkylating Agents.....	25
3.6.6	Platinum-based chemotherapeutic drugs.....	26
3.6.6.1	Clinically Approved Platinum(II)-Anticancer Agents. ....	26
3.6.6.2	Platinum Anticancer Drugs currently in clinical trials .....	28
3.7	Cisplatin Mechanism of Action .....	29
3.8	Mechanism of tumor resistance to cisplatin and carboplatin .....	32
3.8.1	Resistance through insufficient DNA binding which happens due to:.....	32
3.8.2	Resistance after DNA binding.....	32
3.9	Platinum(II) complexes with biologically active compounds .....	33
3.10	Monofunctional platinum(II) complexes.....	34
3.11	Platinum(IV) Anticancer Agents .....	35
3.11.1	Platinum(IV) prodrugs with Innocent Axial Ligands .....	37
3.11.2	Platinum(IV) prodrugs with Bioactive or Targeting Axial Ligands.....	38
3.11.3	Photoactivatable Pt(IV) prodrugs.....	47
3.12	Cinnamic Acid and its Derivatives .....	51
3.13	Motivation.....	55
4.	Result and Discussion.....	60
4.1	$\beta$ -Hydroxydithiocinnamic esters .....	60
4.2	Project 1. Novel Homoleptic and Heteroleptic Pt(II) $\beta$ -oxodithiocinnamic ester Complexes: Synthesis, Characterization, Interactions with 9-methylguanine and Antiproliferative Activity .....	61
4.2.1	Synthesis and characterization of $\beta$ -hydroxydithiocinnamic ester Ligands (HL1- HL9) .....	62
4.2.2	Synthesis and characterization of the Homoleptic and Heteroleptic Pt(II) $\beta$ - oxodithiocinnamic ester complexes.....	63
4.2.3	Molecular Structures Determination .....	64
4.2.4	Interactions of the platinum(II) complexes with 9-MeG as a DNA model .....	68
4.2.4.1	Interactions of the [Pt(L6)(DMS)Cl] complex with 9-MeG .....	68
4.2.4.2	Interactions of the [Pt(L6)(DMSO)Cl] complex with 9-MeG .....	68
4.2.4.3	Interactions of the [Pt(L6) <sub>2</sub> ] complex with 9-MeG.....	68
4.2.5	Cytotoxic Activity of the Heteroleptic Platinum Complexes .....	72
4.3	Project 2. Platinum(II) and palladium(II) complexes mediated by $\beta$ -hydroxy- dithioesters ferrocenyl derivatives: synthesis, characterization and antiproliferative activity 73	
4.3.1	Synthesis and characterization of $\beta$ -hydroxy-dithioesters ferrocenyl Ligands (HFr1-HFr3).....	73



4.3.2	Synthesis and characterization of the Heteroleptic Pt(II) and Homoleptic Pd(II) $\beta$ -hydroxy-dithioesters ferrocenyl complexes.....	74
4.3.3	Molecular Structures Determination for [Pt(Fr2)(DMSO)Cl] and [Pd(Fr3) <sub>2</sub> ] complexes .....	75
4.3.4	Interactions of the [Pt(Fr1)(DMSO)Cl] complex with 9-MeG as a DNA model .....	77
4.3.5	Cytotoxic Activity of the free ligands and the Pt/Pd Complexes .....	79
4.4	Project 3. Dual Function of $\beta$ -hydroxydithiocinnamic esters: RAFT Agent and Ligand for Metal Complexation.....	80
4.4.1	Synthesis and characterization of $\beta$ -hydroxydithiocinnamic ester compounds (HA1-HA9) .....	80
4.4.2	Molecular Structures Determination for HA5 and HA6 .....	81
4.4.3	Polymerizations and kinetics.....	82
4.4.4	Synthesis and characterization of the Pt(II) NAM $\beta$ -hydroxydithiocinnamic acid polymer complexes (Dual Function). .....	85
4.4.5	Cytotoxic Activity of the free ligands, NAM-polymers and the Pt(II) NAM- $\beta$ -hydroxydithiocinnamic esters Complexes .....	88
5.	Publications.....	89
5.1	[ME-1].....	89
5.2	[ME-2].....	148
5.3	[ME-3].....	181
5.4	[ME-4].....	220
6.	Summary .....	267
7.	Zusammenfassung .....	272
8.	References.....	277
9.	Acknowledgements.....	291
10.	Curriculum Vitae .....	292
11.	Declaration of Authorship.....	296
12.	Selbstständigkeitserklärung .....	296

## **Abbreviations**

A	Adenine
AR	Androgen Receptor
ATP	Adenosine triphosphate
ATP7A	ATPase copper transporting alpha
ATP7B	ATPase copper transporting beta
AChE	Acetylcholinesterase
AIBN	Azobisisobutyronitrile
BA	n-Butyl acrylate
CS <sub>2</sub>	Carbon disulfide
CTR1	Copper transporter 1
ChB	Chlorambucil
CENUs	Chloroethylnitrosoureas
ChEs	Cholinesterase
COX	Cyclooxygenase
CTA	Chain transfer agent
1R,2R-DACH	1,2-Diaminocyclohexane
DHFR	Dihydrofolate reductase
DCA	Dichloroacetate
DCM	Dichloromethane
DMF	Dimethylformamide
DMSO	Dimethylsulfoxide
DMS	Dimethylsulfide
DNA	Deoxyribonucleic acid
ER	Estrogen Receptor
EA	Ethacrynic acid
EPR	Enhanced permeability and retention
ERCC1	Excision repair cross-complementing-1
5-FU	5-Fluorouracil
FSH	Follicle-stimulating hormone
FDA	Food and Drug Administration
G	Guanine
GLUTs	Glucose transporters
GSH	Glutathione
GSTs	Glutathione S-transferases
GnRH	Gonadotropin-Releasing Hormone

HDAC	Histone deacetylase
HDACi	Histone deacetylase inhibitor
MDM2	Human murine double minute 2 oncoprotein
HSA	Human serum albumin
HPMA	Hydroxypropylmethacrylamide
HMG1	High-mobility group protein 1
HMG2	High-mobility group protein 2
HEA	2-Hydroxyethyl acrylate
IC <sub>50</sub>	Half-maximal inhibitory concentration
ICP-AES	Inductively coupled plasma atomic emission spectroscopy
L	Ligand
LDH	Lactic dehydrogenase
LH	Luteinizing hormone
LED	Light-emitting diode
mRNA	Messenger ribonucleic acid
MMR	Mismatch repair proteins
MTX	Methotrexate
MRP2	Multidrug resistance-associated protein 2
MMA	Methylmethacrylate
9-MeG	9-Methylguanine
MS	Mass spectrometry
N	Nitrogen
Na	Sodium
NMR	Nuclear magnetic resonance
NSCLC	Non-small cell lung cancer
NER	Nucleotide excision repair proteins
NSAIDs	Non-steroidal anti-inflammatory drugs
NAM	N-acryloylmorpholine
OCTs	Organic cation transporters
<sup>t</sup> BuOK	Potassium tert-butoxide
Pt	Platinum
PhB	Phenylbutyrate
PDK	Pyruvate dehydrogenase kinase
PDT	Photodynamic therapy
PARP	Poly (ADP-ribose) polymerase
r. t.	Room temperature
t <sub>R</sub>	Retention time

ROS	Reactive oxygen species
RNA	Ribonucleic acid
RNA pol II	RNA polymerase II
RAFT	Reversible addition-fragmentation chain-transfer
SAR	Structure activity relationship
SCLC	Small cell lung cancer
SERM	Selective estrogen receptor modulator
SGLTs	Sodium-dependent glucose transporters
SMVT	Sodium-dependent multivitamin transporter
SEC	Size exclusion chromatography
TMV	Tobacco mosaic virus
TMV- CP	Tobacco mosaic virus coat protein
TOPO I	Topoisomerase I
TOPO II	Topoisomerase II
UV	Ultraviolet

## 1. List of Publications

**[ME-1]** Novel Homoleptic and Heteroleptic Pt(II)  $\beta$ -oxodithiocinnamic ester Complexes: Synthesis, Characterization, Interactions with 9-methylguanine and Antiproliferative Activity

**Micheal K. Farh**, Norman Häfner, Helmar Görls, Ingo B. Runnebaum, Wolfgang Weigand  
Zeitschrift für anorganische und allgemeine Chemie 2022, submitted.

Manuscript submission number: zaac.202200349

**[ME-2]** Platinum(II) and palladium(II) complexes mediated by  $\beta$ -hydroxy-dithioesters ferrocenyl derivatives: synthesis, characterization and Antiproliferative Activity

**Micheal K. Farh**, Ikrame Louzi, Hassan Abul-Futouh, Helmar Görls, Norman Häfner, Ingo B. Runnebaum, Wolfgang Weigand

Journal of Sulfur Chemistry 2022, accepted.

DOI: 10.1080/17415993.2022.2152285.

**[ME-3]** Dual Function of  $\beta$ -Hydroxy Dithiocinnamic Esters: RAFT Agent and Ligand for Metal Complexation

**Micheal K. Farh**, Franka V. Gruschwitz, Nicole Ziegenbalg, Hassan Abul-Futouh, Helmar Görls, Wolfgang Weigand, Johannes C. Brendel

Macromolecular Rapid Communications 2022, 2200428.

**[ME-4]** Activating a [FeFe] Hydrogenase Mimic for Hydrogen Evolution under Visible Light

Philipp Buday, Chizuru Kasahara, Elisabeth Hofmeister, Daniel Kowalczyk, **Micheal K. Farh**, Saskia Riediger, Martin Schulz, Maria Wächtler, Shunsuke Furukawa, Masaichi Saito, Dirk Ziegenbalg, Stefanie Gräfe, Peter Bäuerle, Stephan Kupfer, Benjamin Dietzek-Ivanšić, Wolfgang Weigand

Angewandte Chemie International Edition 2022, 61, e202202079.

## 2. Documentation of Authorship

### 2.1 [ME-1] Novel Homoleptic and Heteroleptic Pt(II) $\beta$ -oxodithiocinnamic ester Complexes: Synthesis, Characterization, Interactions with 9-methylguanine and Antiproliferative Activity

Micheal K. Farh,<sup>1</sup> Norman Häfner,<sup>2</sup> Helmar Görls,<sup>3</sup> Ingo B. Runnebaum,<sup>4</sup> Wolfgang Weigand<sup>5</sup>

Zeitschrift für anorganische und allgemeine Chemie 2022, submitted

Manuscript submission number: zaac.202200349

Involved in	Authors				
	1	2	3	4	5
Manuscript preparation	x	x	x		
Manuscript Discussion	x	x		x	x
Synthesis of compounds	x				
Analytics	x				
Stability Determinations	x				
DNA-binding behavior	x				
MTT-Assays		x			
X-Ray structure Determination			x		
Strategy of research approach	x				x
Investigation strategy	x	x		x	x
Supervision				x	x
Publication equivalents	1.0				

### 2.2 [ME-2] Platinum(II) and palladium(II) complexes mediated by $\beta$ -hydroxy-dithioesters ferrocenyl derivatives: synthesis, characterization and Antiproliferative Activity

Micheal K. Farh,<sup>1</sup> Ikrame Louzi,<sup>2</sup> Hassan Abul-Futouh,<sup>3</sup> Helmar Görls,<sup>4</sup> Norman Häfner,<sup>5</sup> Ingo B. Runnebaum,<sup>6</sup> Wolfgang Weigand<sup>7</sup>

Journal of Sulfur Chemistry 2022, accepted

Involved in	Authors						
	1	2	3	4	5	6	7
Manuscript preparation	x		x	x	x		
Manuscript Discussion	x		x		x	x	x
Synthesis of compounds	x	x					
Analytics	x						
Cyclic Voltammetry			x				
MTT-Assays					x		
X-Ray structure Determination				x			
Strategy of research approach	x						x
Investigation strategy	x		x		x	x	x
Supervision						x	x
Publication equivalents	1.0						

### 2.3 [ME-3] Dual Function of $\beta$ -Hydroxy Dithiocinnamic Esters: RAFT Agent and Ligand for Metal Complexation

Micheal K. Farh,<sup>1</sup> Franka V. Gruschwitz,<sup>2</sup> Nicole Ziegenbalg,<sup>3</sup> Hassan Abul-Futouh,<sup>4</sup> Helmar Görls,<sup>5</sup> Wolfgang Weigand,<sup>6</sup> Johannes C. Brendel<sup>7</sup>

Macromolecular Rapid Communications 2022, 2200428.

Involved in	Authors						
	1	2	3	4	5	6	7
Manuscript preparation	x	x		x	x		x
Manuscript Discussion	x	x	x	x		x	x
Synthesis of compounds	x	x					
Analytics	x	x	x				
X-Ray structure Determination					x		
Strategy of research approach	x	x				x	x
Investigation strategy	x	x				x	x
Supervision						x	x
Publication equivalents	1.0						

## 2.4 [ME-4] Activating a [FeFe] Hydrogenase Mimic for Hydrogen Evolution under Visible Light

Philipp Buday,<sup>1</sup> Chizuru Kasahara,<sup>2</sup> Elisabeth Hofmeister,<sup>3</sup> Daniel Kowalczyk,<sup>4</sup> **Michael K. Farh**,<sup>5</sup> Saskia Riediger,<sup>6</sup> Martin Schulz,<sup>7</sup> Maria Wächtler,<sup>8</sup> Shunsuke Furukawa,<sup>9</sup> Masaichi Saito,<sup>10</sup> Dirk Ziegenbalg,<sup>11</sup> Stefanie Gräfe,<sup>12</sup> Peter Bäuerle,<sup>13</sup> Stephan Kupfer,<sup>14</sup> Benjamin Dietzek-Ivanšić,<sup>15</sup> Wolfgang Weigand<sup>16</sup>

Angewandte Chemie International Edition 2022, 61, e202202079.

Involved in	Authors															
	1	2	3	4	5	6	7	8	9	10	11	12	13	14	15	16
Manuscript preparation	X		X					X						X		
Manuscript discussion	X	X	X	X		X	X	X		X	X		X	X	X	X
Synthesis of compounds	X	X			X											
Basic characterization	X	X			X											
X-ray structure determination									X							
Ground state spectroscopy	X							X								
Transient spectroscopy			X					X								
Operando spectroscopy	X		X													
Spectroelectro-chemistry			X					X								
Cyclic voltammetry	X															
Theoretical investigations												X		X		
Photocatalysis	X						X									
Design and supply of custom-made photoreactor				X							X					
Conception of research approach														X	X	X
Investigation strategy	X							X						X		
Publication equivalents					0.25											



## 2.5 Declaration

### **Erklärung zu den Eigenanteilen der Promovendin/des Promovenden sowie der weiteren Doktorandinnen/Doktoranden als Co-Autorinnen/-Autoren an den Publikationen und Zweitpublikationsrechten bei einer kumulativen Dissertation**

Für alle in dieser kumulativen Dissertation verwendeten Manuskripte liegen die notwendigen Genehmigungen der Verlage („Reprint permissions“) für die Zweitpublikation vor.

Die Co-Autorinnen/-Autoren der in dieser kumulativen Dissertation verwendeten Manuskripte sind sowohl über die Nutzung, als auch über die oben angegebenen Eigenanteile der weiteren Doktorandinnen/Doktoranden als Co-Autorinnen/-Autoren an den Publikationen und Zweitpublikationsrechten bei einer kumulativen Dissertation informiert und stimmen dem zu.

Die Anteile der Promovendin/des Promovenden sowie der weiteren Doktorandinnen/Doktoranden als Co-Autorinnen/-CoAutoren an den Publikationen und Zweitpublikationsrechten bei einer kumulativen Dissertation sind in der Anlage aufgeführt.

M. Sc. Micheal Eshak                      Jena,

Ich bin mit der Abfassung der Dissertation als publikationsbasierte Dissertation, d.h. kumulativ, einverstanden und bestätige die vorstehenden Angaben.

Prof. Dr. Wolfgang Weigand              Jena,

### 3. Introduction

#### 3.1 Cancer

According to the National cancer institute, “cancer is a genetic disease caused by changes to genes that control the cell's function, especially how they grow and divide. cancer occurred when cells divide uncontrollably and further spread into surrounding tissues”.<sup>1</sup> Cancer can begin nearly anywhere in the body, which consists of trillions of cells. The cells divide to form new cells as the body requires them through a process called cell division. As cells age or become damaged, they die, and new ones replace them. Occasionally, a breakdown in this orderly process can result in abnormal or damaged cells growing and multiplying. These cells may form tumors, which are abnormal lumps of tissue. Tumors can be cancerous (malignant) or not cancerous (benign or nonmalignant).<sup>1-4</sup> Unlike cancerous tumors, benign tumors (Fig. 1) do not spread into nearby tissues and do not usually grow back after removal.<sup>1-4</sup> Sometimes, benign tumors can grow very large and press on nearby organs, tissues, nerves, or blood vessels. Furthermore, some benign tumors can also cause serious symptoms or even be life-threatening, such as benign brain tumors.<sup>1-3</sup> Quite the opposite, cancerous tumors spread into or invade nearby tissues (Fig. 1) and can spread to other parts of the body through the bloodstream or lymph nodes to form new tumors, this process is called metastasis.<sup>1-5</sup> Except for blood cancers, most cancers are solid tumors.<sup>1-3</sup>

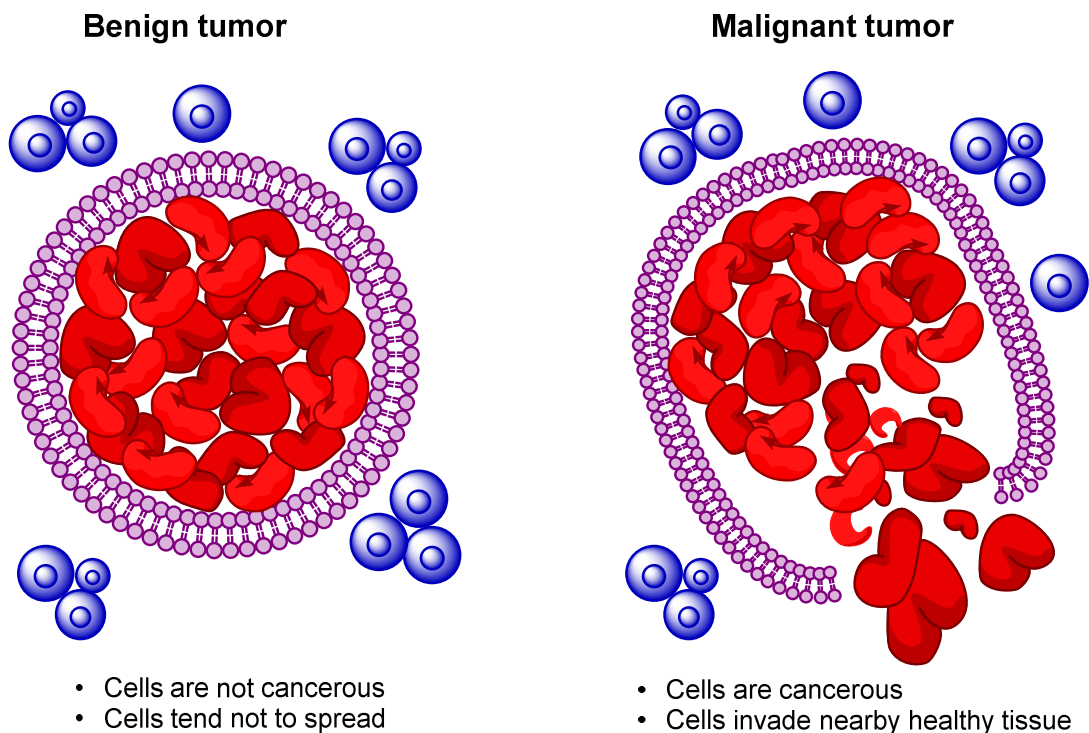


Fig. 1: Benign and Malignant Tumors.

### 3.1.1 Differences Between Cancer Cells and Normal Cells

Cancer cells differ from normal cells in many ways, here are the main ones in Table 1.<sup>1,6,7</sup>

Table 1: Cancer and Normal cells.

Cancer Cells	Normal Cells
<ul style="list-style-type: none"> <li>• Cells grow in the absence of signals.</li> <li>• Ignore signals that normally tell cells to stop dividing or to die (apoptosis).</li> <li>• Invade into nearby areas and spread to other areas of the body.</li> <li>• Hide from the immune system, some cancer cells convince immune cells to protect the tumor instead of attacking it.</li> <li>• Accumulate multiple changes in their chromosomes, such as duplications and deletions of chromosome parts.</li> <li>• Request blood vessels to grow toward tumors, which supply tumors with oxygen, nutrients and remove waste products from tumors.</li> <li>• Rely on different kinds of nutrients. Moreover, some cancer cells make energy from nutrients such as sugars in a different way than most normal cells. This offers cancer cells to grow more quickly.</li> </ul>	<ul style="list-style-type: none"> <li>• Cells only grow when they receive signals.</li> <li>• Show programmed cell death (apoptosis).</li> <li>• Stop growing when they encounter other cells.</li> <li>• The immune system normally eliminates damaged or abnormal cells.</li> </ul>

Thus, researchers must take the advantage of abnormal features of cancer cells that they can't survive without them and develop therapies that target the abnormal behaviors of cancer cells. For instance, angiogenesis inhibitors are unique cancer-fighting agents because they prevent blood vessels from growing toward tumors, which starves the tumor of needed nutrients.<sup>8</sup>

### 3.1.2 Differences Between Benign and Malignant Tumors

In general, both types of tumors have distinct and recognizable differences, compiled a list of the most important ones in Table 2.<sup>1-4</sup>

Table 2: Benign and Malignant Tumors.

Benign Tumors	Malignant Tumors
<ul style="list-style-type: none"> <li>• Cells tend not to spread.</li> <li>• Mostly grow slowly.</li> <li>• Cells do not invade nearby tissue.</li> <li>• Do not metastasize to other parts of the body and tend to have clear boundaries.</li> <li>• Under the microscope, the shape, chromosomes, and DNA of cells appear normal.</li> <li>• Do not secrete chemical signaling molecules except for pheochromocytomas of the adrenal gland.</li> <li>• May not require treatment if not health-threatening.</li> <li>• Unlikely to come back if removed.</li> </ul>	<ul style="list-style-type: none"> <li>• Cells can spread</li> <li>• Usually grow rapidly.</li> <li>• Predominantly invade nearby healthy tissue.</li> <li>• Can spread via the bloodstream, lymphatic system, or by sending "fingers" into nearby tissue.</li> <li>• Cells have abnormal chromosomes, DNA and may have abnormal shape.</li> <li>• Can secrete chemical signaling molecules such as hormones or cytokines that cause fatigue, weakness, and weight loss (paraneoplastic syndrome).</li> <li>• Require urgent treatment, such as surgery, chemotherapy, radiation, and immunotherapy medications.</li> <li>• May recur after removal, sometimes in areas other the original site.</li> </ul>

### 3.2 Cancer Genes

Cancer is caused by changes in DNA. Most cancer-causing DNA changes occurred in sections of DNA called genes (Fig. 2).<sup>1,9</sup> These genes control the way our cell's function, especially how they grow and divide. Genetic changes that cause cancer can happen because of many factors such as errors that occur during the cell divide, DNA damage caused by harmful substances, or they were inherited from our parents.<sup>1,9</sup> Normally immune system eliminates cells with damaged DNA before they turn cancerous,

but as we age the body's ability to do so goes down which explains a higher risk of cancer later in life.<sup>1,9</sup> Genomic changes that contribute to cancer usually two classes of genes: proto-oncogenes and tumor suppressor genes.<sup>9</sup> Such changes are called "drivers of cancer".<sup>1,9</sup>

- a) **Proto-oncogenes** are genes that normally help cells grow and divide. However, when these genes are mutated or are more active than normal, they become cancer-causing genes (oncogenes), which allow cells to grow and divide out of control then lead to cancer.<sup>1,9</sup>
- b) **Tumor suppressor genes** are normal genes that slow down cell division, repair DNA mistakes, and triggering apoptosis. When tumor suppressor genes fail to function, cells can grow out of control, which can also lead to cancer.<sup>1,9</sup>

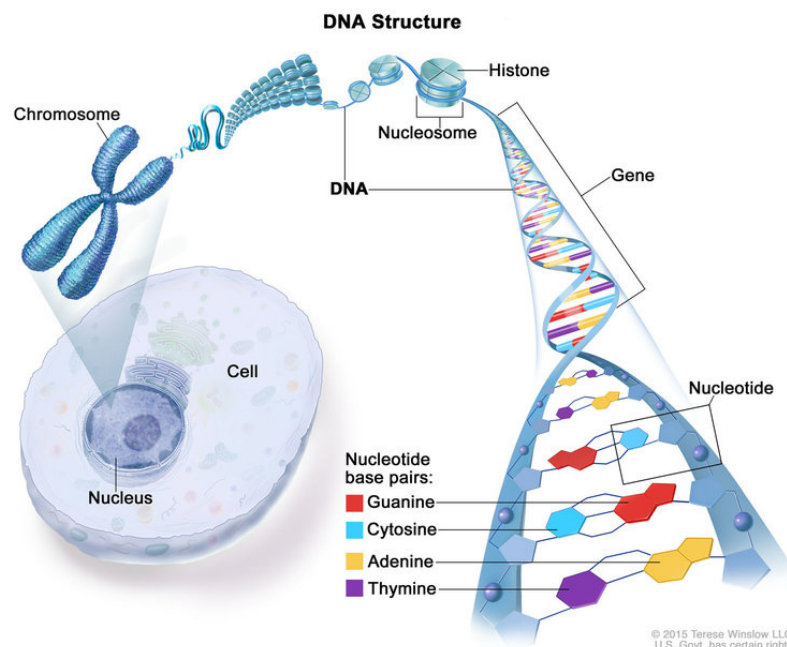
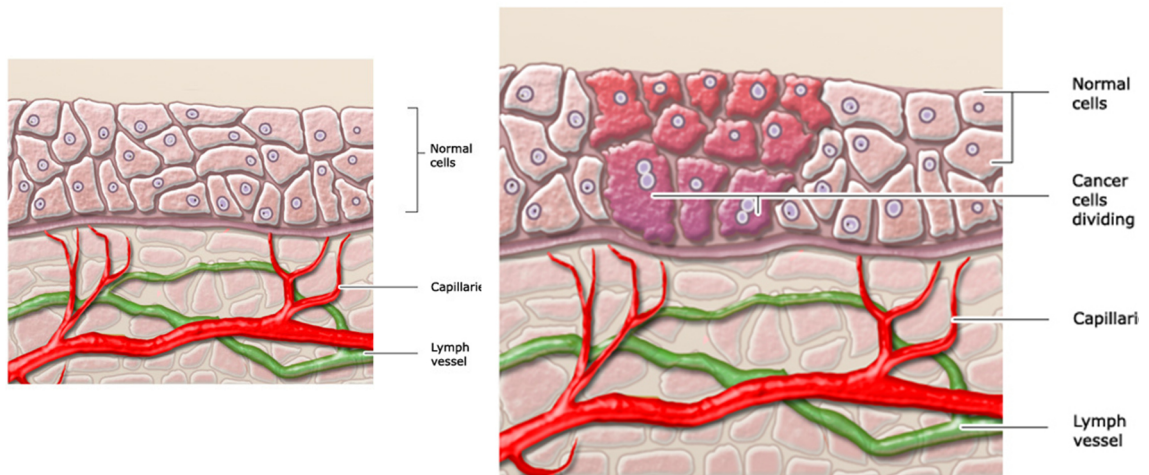


Fig.2: DNA-Structure. Reproduced with permission from National Cancer Institute © (2015) Terese Winslow LLC, U.S. Govt. has certain rights.<sup>1</sup>

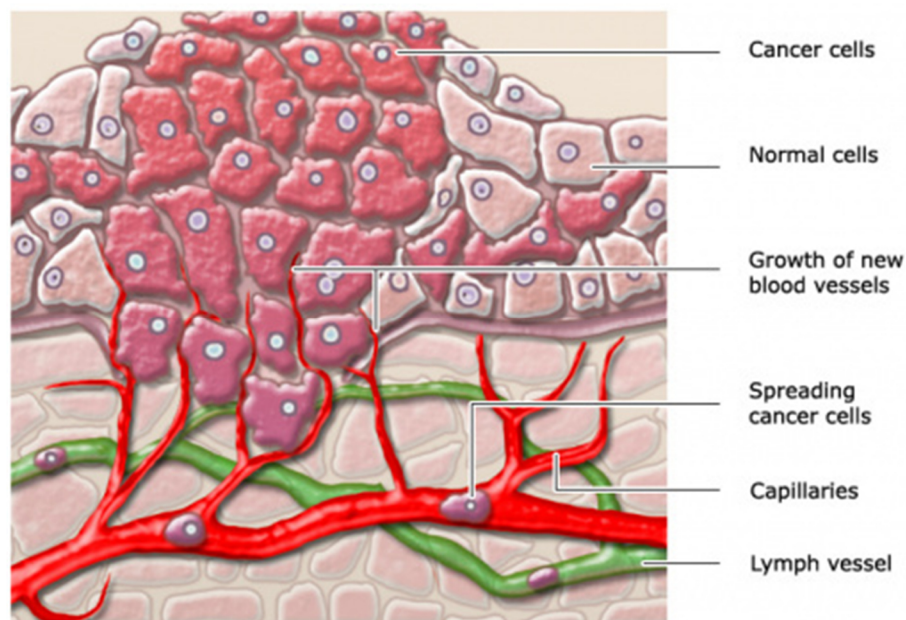
### 3.3 Cancer Develop and Spread

Once cancerous cells begin replicating, they don't behave like normal cells (Fig. 3A).<sup>2,3</sup> If the malignant tumor is found in one area and doesn't spread to adjacent tissue, it is called "carcinoma in situ" (Fig. 3B).<sup>2,10</sup> The moment that the malignant tumors start to create their own blood vessels, that supply them with extra oxygen, glucose, and hormones, this process is called angiogenesis.<sup>10</sup> Therefore, they can continue to grow and divide and during this process, tumors can start to invade surrounding tissues and are classified as "invasive cancer" (Fig. 3C).<sup>2,10</sup>



(A) Normal cells

(B) Carcinoma in situ



(C) Invasive cancer

Fig. 3: Cancer development stages, Reproduced with permission from [gesundheitsinformation.de /IQWiG](http://gesundheitsinformation.de/IQWiG).<sup>3</sup>

Active cancer cells can enter the bloodstream or lymphatic system and travel to other parts of the body (Fig. 4). In other words, they start the tumor-formation process over again elsewhere which is called metastatic or secondary cancer.<sup>1,5</sup> Metastatic cancer has the same name and type of cancer cells as the original or primary cancer. Under a pathologist's microscope, metastatic cancer cells typically appear the same as those of original cancer.<sup>1,5</sup> In addition, metastatic cancer cells and cancer cells from original cancer usually share some molecular features, such as chromosome alterations. For example, colon cancer that forms a metastatic tumor in liver or lung is metastatic colon cancer, not lung or liver cancer (Fig. 4).<sup>1,5</sup>



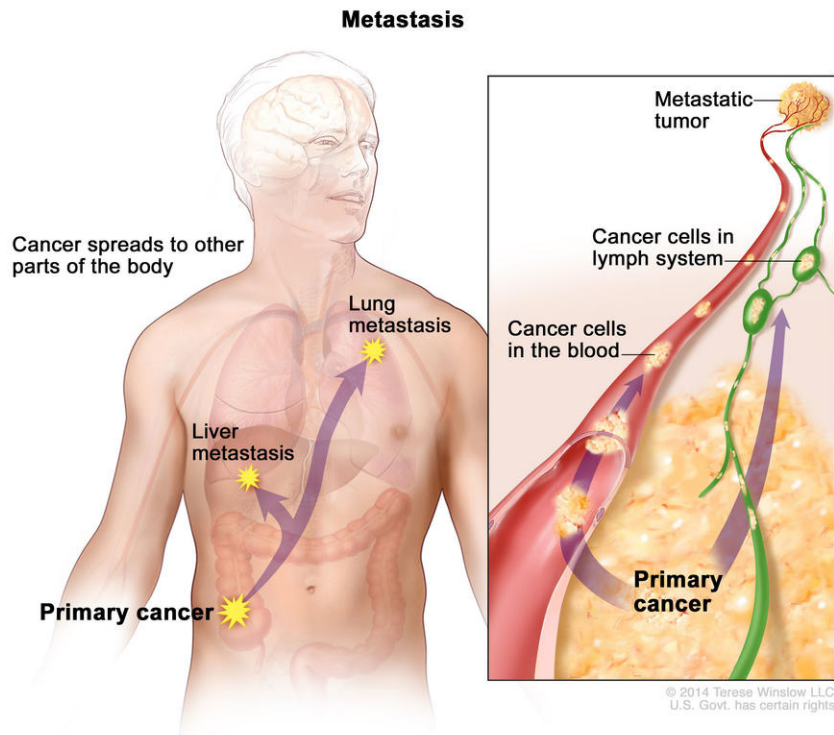


Fig 4: Metastasis. Reproduced with permission from National Cancer Institute © (2014) Terese Winslow LLC, U.S. Govt. has certain rights.<sup>1</sup>

### 3.4 Cancer Types

According to the National cancer institute, there are more than 100 types of cancer.<sup>1</sup> Cancers are usually categorized by which organs or tissues they form. For example, lung cancer starts in the lung, whereas brain cancer starts in the brain. Furthermore, cancers can be also classified according to the type of cell that created them, such as epithelial or squamous cells.<sup>1</sup>

### 3.5 Cancer Treatment

Depending on the cancer type and how advanced is it, there are many types of treatment. Some patients will have only one type of treatment, but most of them need a combination of treatments, such as surgery with chemotherapy and radiation therapy.

#### 3.5.1 Biomarker Testing for Cancer Treatment

Biomarker testing is sometimes referred to as “molecular testing” or “genetic testing”. Cancer biomarkers can be DNA, RNA, protein, or metabolomic profiles that are specific to the tumor.<sup>11,12</sup> Biomarker testing is done by obtaining a small amount of tissue which is called a biopsy from a patient's tumor or blood drawn for blood cancer, that is conduct a series of advanced pathology and molecular profiling tests.<sup>11,12</sup> Biomarker testing can provide information about alterations in the tumor which can be used to decide on the treatment protocol, especially for targeted therapies and immunotherapies.<sup>11,12</sup>

### **3.5.2 Hormone Therapy**

Hormone therapy or endocrine therapy is a treatment that slows or stops the growth of hormone-dependent cancers such as breast, prostate, endometrium, and adrenal cortex cancers.<sup>13-17</sup> Most often, hormone therapy is used in conjunction with other cancer treatments.<sup>16,17</sup> Additionally, hormone therapy is also used to reduce or prevent symptoms in prostate cancer patients who are not candidates for radiation therapy or surgery, making a tumor smaller before surgery or radiation therapy (neoadjuvant therapy)<sup>13,17</sup>, reducing the risk of cancer returning after the main treatment as well as destroy cancer cells that have returned or spread to other parts of your body.<sup>16,17</sup>

### **3.5.3 Hyperthermia Therapy**

Hyperthermia is also called thermal therapy, thermal ablation, or thermotherapy. During the treatment, the body tissue is heated to up to 113°F to help damage and kill cancer cells with as little harm to healthy tissue as possible.<sup>18,19</sup> A hyperthermic treatment can also help other cancer treatments, such as chemotherapy and radiation, work more efficiently.<sup>18,19</sup>

### **3.5.4 Photodynamic Therapy**

Photodynamic therapy (PDT) may be also called photo-radiation therapy, or photochemotherapy, which uses a drug that is activated by light called a photosensitizer.<sup>20,21</sup> Depending on the part of the body being treated, the photosensitizing agent is either injected into a vein or absorbed through the skin.<sup>20,21</sup> When cancer cells that have absorbed photosensitizers are exposed to a specific wavelength of light usually from a laser or LEDs, the photosensitizer is activated and produces a form of oxygen, called reactive oxygen species (ROS), that destroy cancerous and precancerous cells.<sup>20,21</sup>

### **3.5.5 Radiation Therapy**

Radiation therapy also called radiotherapy, is a type of cancer treatment that uses beams of intense energy (ionizing radiation) to kill cancer cells and shrink tumors, most often using X-rays, but protons or other types of energy also can be used.<sup>22-24</sup> Radiotherapy damages cancer cells or slows their growth by destroying the genetic material DNA that controls how cells grow and divide.<sup>22-24</sup> It takes days or weeks for DNA to be damaged sufficiently for cancer cells to die, then, cancer cells keep dying for weeks or months after radiation therapy ends.<sup>22-24</sup> As damaged cells die, they are broken down and excreted by the body.<sup>22-24</sup> For some patients, radiation may be the only needed treatment. But, most often, they will have radiotherapy with other cancer treatments, such



as surgery, chemotherapy, and immunotherapy.<sup>24</sup> Radiotherapy may be given before, during, or after other treatments depending on the type of cancer being treated and whether the goal of radiotherapy is to treat cancer or ease symptoms.<sup>24</sup> When radiotherapy is combined with surgery, it can be given<sup>24, 25</sup>

- a) Before surgery, shrink a cancerous tumor, so it can be removed by surgery and be less likely to return (neoadjuvant therapy).
- b) During surgery, it goes straight to cancer without passing through the skin (intraoperative radiation).
- c) After surgery, to stop the growth of any remaining cancer cells (adjuvant therapy).

### **3.5.6 Immunotherapy**

Immunotherapy is a type of biological therapy that uses substances made from living organisms that help your immune system which is made up of white blood cells, organs, and tissues of the lymph system to fight cancer.<sup>26-28</sup> There are several types of immunotherapies are used to treat cancer including:

- a) **Immune checkpoint inhibitors** are drugs that block immune checkpoints. Checkpoints are normal parts of the immune system that prevent overactive immunity. Immune checkpoint inhibitors drugs block them, allowing immune cells to respond more strongly to cancer.<sup>26,27</sup>
- b) **T-cell transfer therapy** also called adoptive cell therapy, adoptive immunotherapy, or immune cell therapy, is a treatment that boosts the natural ability of the T cells to fight cancer.<sup>26,28</sup> A T cell is a type of lymphocyte and one of the important white blood cells of the immune system that plays a central role in the adaptive immune response [26, 28]. In this treatment, immune cells found in and around tumors which are the most effective ones against this cancer, taken and selected or modified in the lab to better attack the cancer cells, then grown in large batches, and injected back into the body.<sup>26,28</sup>
- c) **Monoclonal antibodies** also called therapeutic antibodies, are immune system proteins designed in the lab to bind specific targets on cancer cells.<sup>26,28</sup> By marking cancer cells with monoclonal antibodies, the immune system will be able to recognize and destroy them more effectively.<sup>26,28</sup>
- d) **Cancer vaccines** that work against cancer by enhancing the immune system's response to cancer cells.<sup>26,27</sup>
- e) **Immune system modulators** are a type of immunotherapy that enhances the body's immune response against cancer.<sup>27</sup> Some of these agents affect specific

parts of the immune system, while others affect the immune system in a more general way.<sup>27</sup>

### **3.5.7 Targeted Therapy**

Targeted therapy is the base of precision medicine, this type of treatment targets proteins that control how cancer cells grow, divide, and spread.<sup>29-31</sup> With a better understanding of the DNA changes and proteins that drive cancer, researchers are better able to design treatments that target these proteins. There are two main types of targeted therapy including either small-molecule drugs or monoclonal antibodies.<sup>29-31</sup>

- a) **Small-molecule drugs** are small enough to penetrate cells easily, so they can be used to treat targets inside cells.<sup>29-31</sup>
- b) **Monoclonal antibodies** are proteins produced in the lab. Proteins such as this are designed to bind to specific targets found on cancer cells.<sup>28</sup> Some monoclonal antibodies are used in Immunotherapy by marking cancer cells so that they will be better seen and destroyed by the immune system. However, other monoclonal antibodies directly inhibit the growth of cancer cells or cause them to self-destruct.<sup>28-31</sup>

### **3.5.8 Stem Cell Transplant**

Stem cell transplants do not usually work against cancer directly instead, are procedures that restore blood-forming stem cells in patients who have had theirs destroyed by the high doses of chemotherapy or radiation therapy.<sup>32</sup> In a stem cell transplant, the patient injects healthy blood-forming stem cells. After entering the bloodstream, stem cells travel to the bone marrow, where they replace the cells that were destroyed by treatment.<sup>32,33</sup>

### **3.5.9 Surgery**

Surgery is a procedure in which a surgeon removes cancer from the patient's body. Different types of cancer are treated with surgery. Surgery is helpful for solid tumors that are contained in one area. In contrast, is not used for leukemia or cancers that have spread.<sup>34,35</sup> Occasionally, surgery will be the only treatment needed. But most often, other cancer treatments such as chemotherapy or radiotherapy are needed.<sup>34,35</sup>

### **3.5.10 Chemotherapy**

Chemotherapy is a type of cancer treatment that uses drugs to kill fast-growing cells and stop them from spreading. Chemotherapy most often attacks dividing cells since

cancer cells grow and multiply much more quickly than normal ones.<sup>36-38</sup> Hair and skin cells are divided often in the body so these cells can also be killed by chemotherapy. Therefore, chemotherapy can cause side effects such as hair loss. However, normal cells can usually recover once treatment ends.<sup>36-38</sup> Chemotherapeutic drugs target cells with several mechanisms of action and at different phases of the cell cycle (Fig. 5)<sup>37,38</sup>, where the cells are formed by the division of their parent cells, a process known as mitosis.<sup>37</sup> The cell cycle can be divided into five phases including (shown in Fig. 5):<sup>37,38</sup>

- I. **G<sub>0</sub> phase**, this is the resting phase while the cell is not dividing. When the cell receives the signal to divide, it comes out of this phase.
- II. **G<sub>1</sub> phase**, where the cell enlarges and makes proteins as well as mRNA to ensure that it is ready for the steps that lead to mitosis.
- III. **S or synthesis phase**, in this phase, DNA replication produces two replicable copies of DNA that can be passed to the daughter cells formed by mitosis.
- IV. **G<sub>2</sub> phase**, during this phase, the cell continues to grow between the synthesis stage and the mitosis stage. In turn, a checkpoint control mechanism ensures the cell is ready to progress into mitosis.
- V. **M phase or mitosis**, the cell ceases to grow and begins to divide into two daughter cells. Another checkpoint mechanism ensures the cell is ready to split.

In general, cancer cells that are actively undergoing cell cycle phases are highly chemosensitive, while cells in a resting state G<sub>0</sub> are relatively insensitive.<sup>37-39</sup>

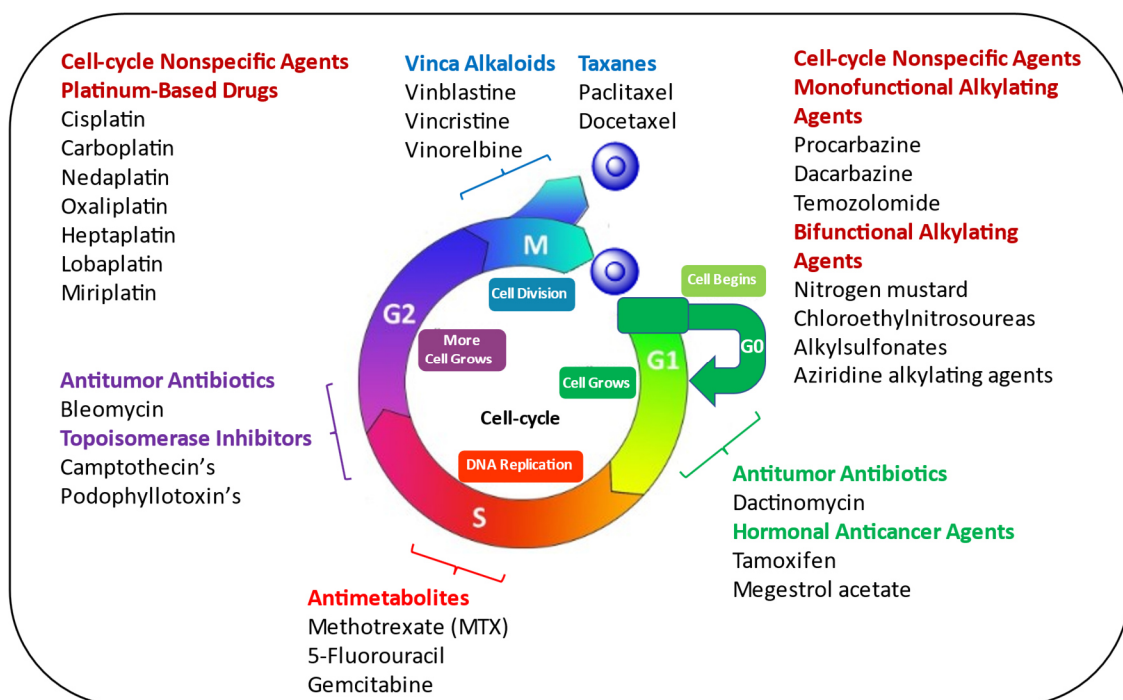


Fig. 5: Cell cycle and Chemotherapeutic drugs during different phases of the cell cycle.

### 3.6 Classification of Chemotherapeutic agents

Chemotherapeutic agents can be classified according to the mechanism of action to:

#### 3.6.1 Antimetabolites

Antimetabolites are structural and chemical analogs of naturally occurring components of the metabolic pathways that lead to the synthesis of purines, pyrimidines, and nucleic acids.<sup>37,40-43</sup> These agents mostly affect the S phase of the cell cycle and replace the normal DNA or RNA with other analogs, thus interfering with cell replication and proliferation. When this happens, the DNA can't make copies of itself, and the cell can't reproduce.<sup>37,40-43</sup> They are typically used to treat leukemias, as well as breast, ovary, and intestinal tract cancers.<sup>37,40-43</sup>

Examples of antimetabolites and mechanism of action:

##### a) Methotrexate (MTX)

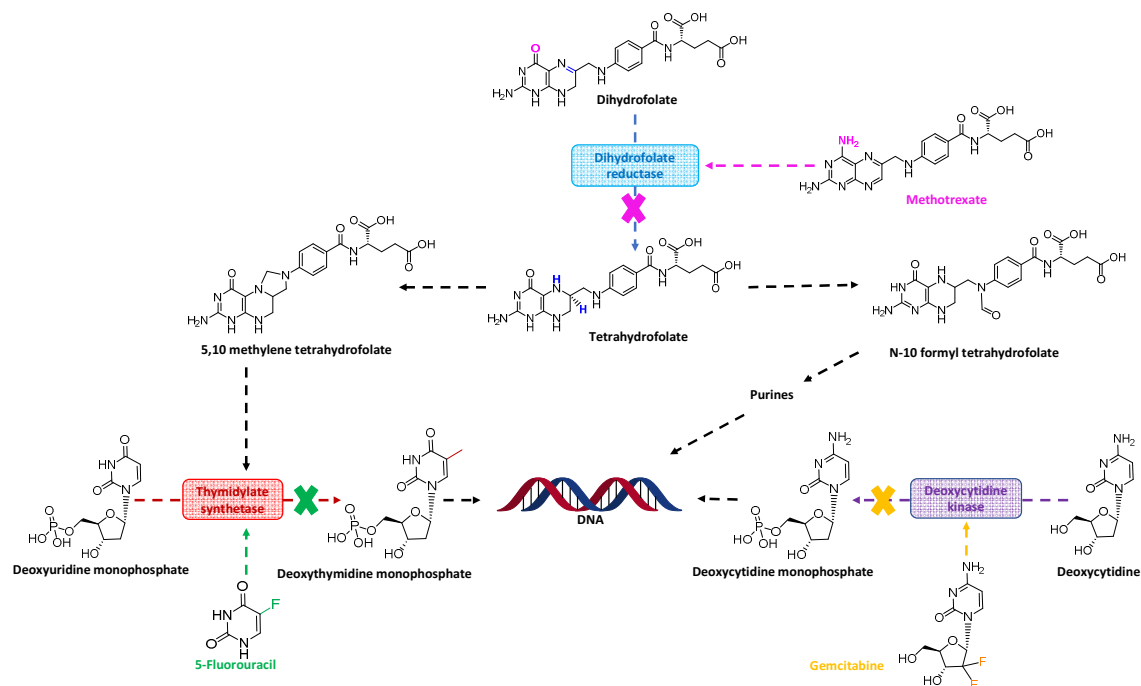
Methotrexate (MTX) historically known as amethopterin, is a dihydrofolate analog and an FDA-approved drug used for the treatment of many solid tumors and hematologic malignancies.<sup>41</sup> Methotrexate binds tightly to dihydrofolate reductase and blocks the reduction of dihydrofolate to tetrahydrofolate, thus reversibly inhibits the enzyme dihydrofolate reductase (DHFR) as shown in Scheme 1. As a result, thymidylate synthetase and various steps in purine synthesis are halted and leads to the arrest of DNA, RNA, and protein synthesis.<sup>37,40-42</sup>

##### b) 5-Fluorouracil

5-Fluorouracil (5-FU) is thymine analog and acts as a thymidine synthetase inhibitor to block DNA replication as shown in Scheme 1.<sup>37,43</sup> Occasionally it is paired with cisplatin during chemoradiation of cervical cancer or used in topical form for the treatment of vaginal intraepithelial neoplasia.<sup>37,43</sup>

##### c) Gemcitabine

Gemcitabine is a synthetic deoxycytidine analog, that undergoes multiple phosphorylations to form the triphosphate active metabolite.<sup>44</sup> The resulting triphosphate is incorporated into DNA as a counterfeit base pair. Afterward, one additional deoxynucleotide is added to the end of the DNA chain before replication is terminated, and thereby, DNA synthesis is halted as shown in Scheme 1.<sup>37,38,44</sup> Gemcitabine is FDA approved to be used with other agents for the treatment of metastatic breast, bladder, pancreas, and ovarian cancers as well as non-small cell lung cancer and soft-tissue sarcoma.<sup>37,38,44</sup>



Scheme 1: Methotrexate, 5-Fluorouracil, and Gemcitabine Mechanism of Action.<sup>37,38</sup>

### 3.6.2 Antitumor Antibiotics

The antitumor antibiotics are generally produced from *Streptomyces* bacteria.<sup>37,38</sup> The commonly used types of antitumor antibiotics are bleomycin, dactinomycin, and anthracyclines.<sup>37,38</sup> These compounds have a wide spectrum of activity against leukemias, lymphomas, breast, stomach, uterine, ovarian, bladder, and lung cancers.<sup>37,38</sup> In general, antitumor antibiotics exert their cytotoxic effects by DNA intercalation throughout multiple phases of the cell cycle. As a group, they are considered cell-cycle specific.<sup>37,38</sup> The mechanisms of actions of these drugs include free radical damage to DNA, topoisomerase II inhibition, binding of DNA *via* intercalation causing obstruction in DNA and RNA, and alteration of cell membrane fluidity as well as transport of ions.<sup>37,38</sup>

#### a) Bleomycin

Bleomycin (Fig. 6) is FDA approved antitumor antibiotic that was discovered by umezama and colleagues in 1962.<sup>45</sup> It is produced by the bacterium *streptomyces verticillus*.<sup>45,46</sup> Bleomycin is usually used with other cancer medications for the treatment of Hodgkin's lymphoma, non-Hodgkin's lymphoma, testicular cancer, ovarian cancer, and cervical cancer.<sup>47,48</sup> The mechanism of action includes DNA cleavage in presence of oxygen and metal ions, bleomycin chelates metal ions (primarily iron), producing a pseudo-enzyme that reacts with oxygen to produce oxygen-free radicals, which cause DNA-strand breaks and cell death.<sup>49,50</sup> It is maximally effective during the G<sub>2</sub> phase.<sup>37,49</sup>

## b) Dactinomycin

Dactinomycin (Fig. 6) is also known as actinomycin D.<sup>51</sup> It is FDA approved as a single agent or as part of combination chemotherapy to treat Wilms tumor, rhabdomyosarcoma, ewing's sarcoma, trophoblastic neoplasm, testicular cancer, and certain types of ovarian cancers.<sup>37,51</sup> Mechanism of Action, dactinomycin is shown to have the ability to inhibit DNA to RNA transcription, by binding into the purine-pyrimidine DNA base pairs at the transcription initiation complex and preventing elongation of RNA chain by RNA polymerase.<sup>37,51</sup> It also produces toxic oxygen-free radicals that cause DNA breaks. Messenger RNA (mRNA) is created when segments of DNA are transcribed into RNA molecules that can encode proteins.<sup>51</sup> As result, dactinomycin is most effective in the G<sub>1</sub> phase.<sup>37,51</sup>

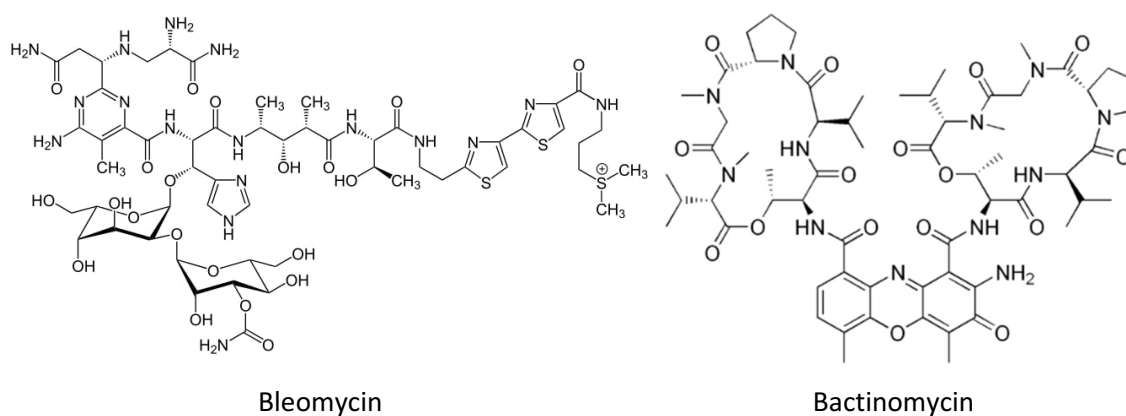
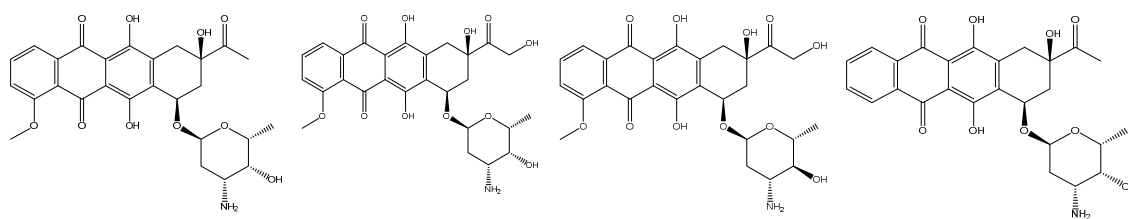


Fig. 6: Structure of Bleomycin,<sup>45</sup> and Bactinomycin.<sup>51</sup>

## c) Anthracyclines

Anthracyclines is a class of chemotherapy drugs that extracted from *Streptomyces bacterium*.<sup>38, 52,53</sup> Structurally, anthracyclines are tetracyclic molecules with an anthraquinone backbone attached by a glycosidic linkage to a sugar moiety. Daunorubicin was the first discovered anthracycline and the most important clinically anthracyclines are doxorubicin, daunorubicin, epirubicin, and idarubicin (Fig.7).<sup>52,54</sup> Doxorubicin is used in the treatment of Hodgkin's and non-Hodgkin's lymphoma, myelomas, sarcomas, and breast, lung, ovarian, and thyroid cancers. while the main use of daunorubicin is in the treatment of acute leukemias.<sup>52</sup> Epirubicin is used in breast and gastroesophageal cancers.<sup>52</sup> Idarubicin is the newest anthracycline, which is approved in in the treatment of acute myelogenous leukemia.<sup>52</sup> These drugs act mainly by intercalates into DNA, form a stable anthracycline-DNA-topoisomerase II ternary complex thus "poisoning" the enzyme and impeding the religation of double-stranded DNA breaks which finally lead to the programmed cell death.<sup>52,55,56</sup>



Daunorubicin

Doxorubicin

Epirubicin

Idarubicin

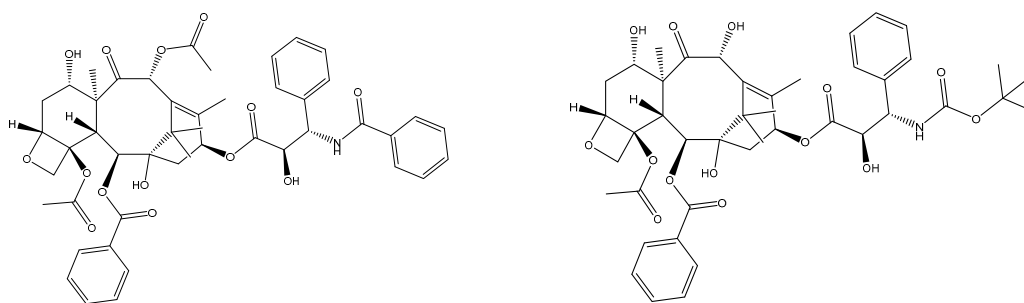
Fig. 7: Structures of Daunorubicin, Doxorubicin, Epirubicin, and Idarubicin.<sup>52,54</sup>

### 3.6.3 Plant-derived Anticancer Agents

For centuries, plants have been exploited as sources of numerous cancer chemotherapeutic agents. Good examples of anticancer compounds of clinical significance today include taxanes, vinca alkaloids, and topoisomerase inhibitors including both camptothecins and podophyllotoxins.<sup>37,38,52</sup> Taxanes are originally derived from the bark of the Pacific Yew tree (*taxus*) while the vinca alkaloids are from the periwinkle plant (*catharanthus rosea*).<sup>52</sup> Taxanes and vinca alkaloids are also known as antimicrotubule agents.<sup>37,38,52</sup> In addition, camptothecin was isolated from the bark and stem of the camptothecin tree while epipodophyllotoxins are substances naturally occurring in the root of the American mayapple plant (*Podophyllum peltatum*).<sup>37,38,52</sup>

#### a) Taxanes

Paclitaxel and docetaxel are the commonly used taxanes (Fig. 8).<sup>57,58</sup> They have activity in several solid tumors, including breast, ovarian, lung, gastroesophageal, prostate, bladder, neck, and head cancers.<sup>37,52,57,58</sup> In addition, they are cell cycle-specific agents that have maximal activity during the M phase, thus, taxanes are mitotic inhibitors.<sup>37,52</sup> They act by interfering “poison” the mitotic spindle, stabilizing the microtubule polymer, and preventing it from disassembly into tubulin monomers. As a result, chromosomes are unable to achieve a metaphase spindle configuration.<sup>37,52,57,58</sup> The activated mitotic checkpoint blocks mitosis from progressing and triggers apoptosis or reversion to the G<sub>0</sub>-phase of the cell cycle without cell division.<sup>37,52,57,58</sup>



Paclitaxel

Docetaxel

Fig. 8: Structures of Paclitaxel, and Docetaxel.<sup>57,58</sup>

## b) Vinca alkaloids

Vinca alkaloids are a set of anti-mitotic and anti-microtubule alkaloid agents.<sup>37,52</sup> Vincristine, vinblastine, and vinorelbine are examples of vinca alkaloids (Fig. 9). They act in the M phase of the cancer cell cycle.<sup>37,52</sup> Moreover, vincristine is used in acute leukemias, lymphomas, Wilms' tumor, and neuroblastoma. Vinblastine is used for lymphomas, neuroblastoma, Kaposi's sarcoma, and testicular carcinoma. And vinorelbine is used in breast cancer and non-small cell lung cancer.<sup>52</sup> Such compounds act in contrast to the taxanes, by preventing the assembly of tubulin dimers to form microtubules and block the formation of the mitotic spindle.<sup>37,52</sup>

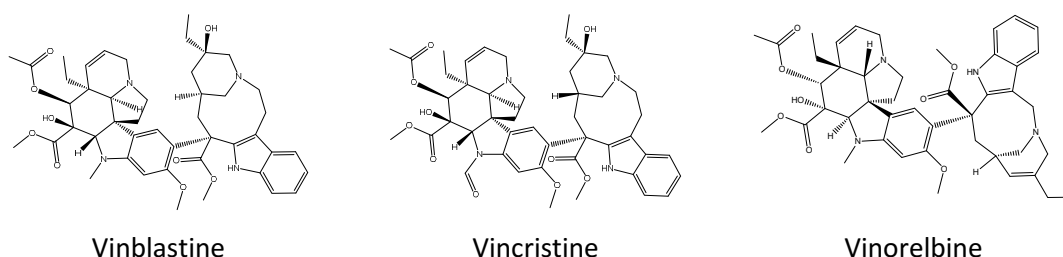


Fig. 9: Structures of Vinblastine, Vincristine, and Vinorelbine.<sup>52</sup>

## c) Topoisomerase inhibitors

This group of agents divided into two categories based on the specific topoisomerase enzyme they inhibit. The camptothecin (Fig. 10) inhibits topoisomerase I (TOPO I). Topotecan and irinotecan (Fig. 10) are camptothecin analogs that have been approved and are used in chemotherapy.<sup>37,52</sup> While the podophyllotoxins (Fig. 10) inhibit topoisomerase II (TOPO II). Etoposide and teniposide (Fig. 10) are semisynthetic derivatives of podophyllotoxin.<sup>37,52</sup> Topotecan is used as second-line therapy for advanced ovarian cancer and for small cell lung cancer. Irinotecan is used to treat metastatic colorectal cancer and small cell lung cancer. Etoposide and teniposide are used in combination drug regimens for therapy of lymphoma, lung, germ cell, and gastric cancers.<sup>37,52</sup> Topoisomerase-I is a nuclear enzyme that relieves torsional strain in DNA by opening single-strand breaks.<sup>59</sup> Once topoisomerase-I creates a single-strand break, the DNA can rotate in front of the advancing replication fork.<sup>59</sup> Topoisomerase-II is an enzyme that creates temporary double-stranded DNA breaks (dsDNA) in one DNA double-strand, allowing another to pass through and re-ligate the broken strands.<sup>59</sup> Topotecan and irinotecan act by binding to and stabilize a transient TOPO I-DNA complex, this prevents DNA re-ligation, therefore causes DNA damage, and promotes apoptosis of the cancer cell.<sup>52,59</sup> On the other side, etoposide and teniposide display binding activity to the enzyme topoisomerase II during the late S and early G<sub>2</sub> phases of the cell cycle.<sup>60</sup> This drug “poisons” the TOPO II enzyme by stabilizing the transient TOPO



II-DNA complex, disrupts the reparation of the breakthrough through which the double-stranded DNA passes, and consequently stops DNA unwinding and replication.<sup>60</sup>

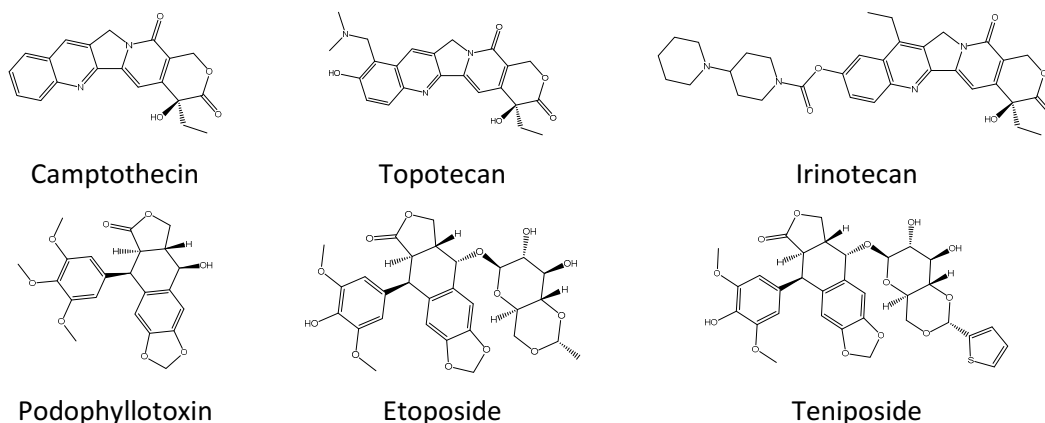


Fig. 10: Structures of Camptothecin's and Podophyllotoxin's.<sup>37,52</sup>

### 3.6.4 Hormonal Anticancer Agents

A hormone is a biochemical messenger substance that helps to control how certain types of cells work.<sup>13,17</sup> Hormonal agents alter the internal and extracellular environment.<sup>52</sup> Breast, prostate, endometrium, and adrenal cortex cancers are examples of tumors that are sensitive to hormonal manipulation.<sup>37,52</sup> The action of hormones or hormone antagonists depends on the presence of hormone receptors in the tumors themselves (i.e., estrogen receptors in breast cancers).<sup>37,52</sup> For instance, tamoxifen (Fig. 11) is a selective estrogen receptor modulator (SERM), used to treat breast cancer. It metabolizes into a high-affinity antagonist of the estrogen receptor in breast tissue. Moreover, it competes with estrogen for receptor binding but does not activate the receptor, thus inhibiting breast cancer cell growth. Tamoxifen is most effective during G<sub>0</sub> or G<sub>1</sub> phase.<sup>37,52</sup> Megestrol acetate (Fig. 11) is a synthetic derivative of progesterone that has activity on tumors through its antiestrogenic effects. It is also used to treat breast cancer and endometrial cancer.<sup>37</sup> Leuprolide, goserelin, and nafarelin are gonadotropin-releasing hormone (GnRH) agonists, effective in prostatic carcinoma. They inhibit the release of pituitary luteinizing hormone (LH) and follicle-stimulating hormone (FSH).<sup>52</sup> Furthermore, anastrozole and letrozole inhibit aromatase, the enzyme that catalyzes the conversion of androstenedione to estrone and they are used in advanced breast cancer.<sup>52</sup>



Fig. 11: Structures of Tamoxifen, and Megestrol acetate.<sup>37,52</sup>

### 3.6.5 Alkylating Antineoplastic Agents

The alkylating agents are cell-cycle nonspecific agents that work at any phase of active replication.<sup>37,52</sup> They are classified as bifunctional- and monofunctional-alkylating agents. Mostly, they act by alkylating the nucleophilic groups on DNA bases, particularly the N-7 position of guanine, which causes cross-linking of bases, abnormal base-pairing, or DNA strand breakage, and leads to death by apoptosis or necrosis.<sup>37,52</sup> However, tumor cell resistance to these drugs occurs through increased DNA repair, and the production of trapping agents such as thiols.<sup>37,52</sup>

#### Classification of alkylating agents:

##### 3.6.5.1 Bifunctional Alkylating Agents

Bifunctional alkylating agents are a broad spectrum of compounds such as nitrogen mustard, chloroethylnitrosoureas, alkylsulfonates, and aziridines.<sup>52</sup> In general, they act by covalently binding two complementary strands of DNA, preventing effective cell division, and causing cell death.<sup>52</sup>

##### a) Nitrogen mustard

Such as chlorambucil, bendamustine, melphalan, uramustine, cyclophosphamide, and ifosfamide (Fig. 12). Chlorambucil and bendamustine are used to treat chronic lymphocytic leukemia, Hodgkin lymphoma, and non-Hodgkin lymphoma. Melphalan is used to treat multiple myeloma, ovarian cancer, and melanoma.<sup>61</sup> Uramustine is used to treat non-Hodgkin's lymphoma.<sup>61</sup> Cyclophosphamide and ifosfamide are used to treat different cancers including leukemia, non-Hodgkin's lymphoma, breast cancer, ovarian cancer, testicular cancer, bladder cancer, cervical cancer, neuroblastoma, small cell lung cancer, and sarcoma.<sup>52,61</sup> Nitrogen mustards have bis(2-chloroethyl) amine functional group.<sup>61,62</sup> The mechanism of action includes the formation of active aziridinium rings through intramolecular displacement of the chloride by the amine nitrogen. The aziridinium ion alkylates DNA strands at guanine N-7 position then a second alkylation occurring after the displacement of the second chloride, that results in the formation of N7G-N7G interstrand cross-links as shown in scheme 2. This process is irreversible and force the cell to undergo apoptosis.<sup>61,62</sup>

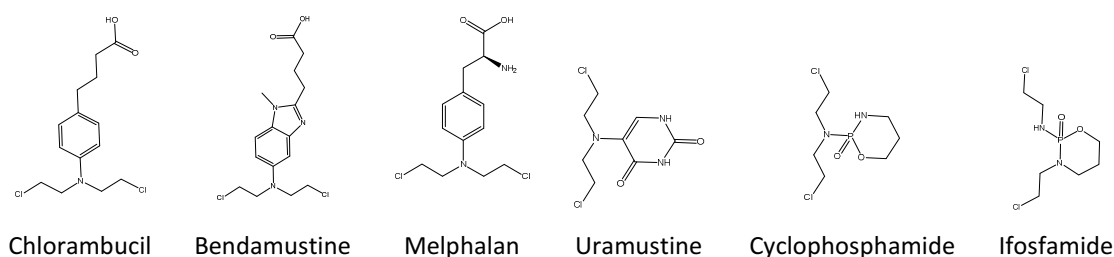
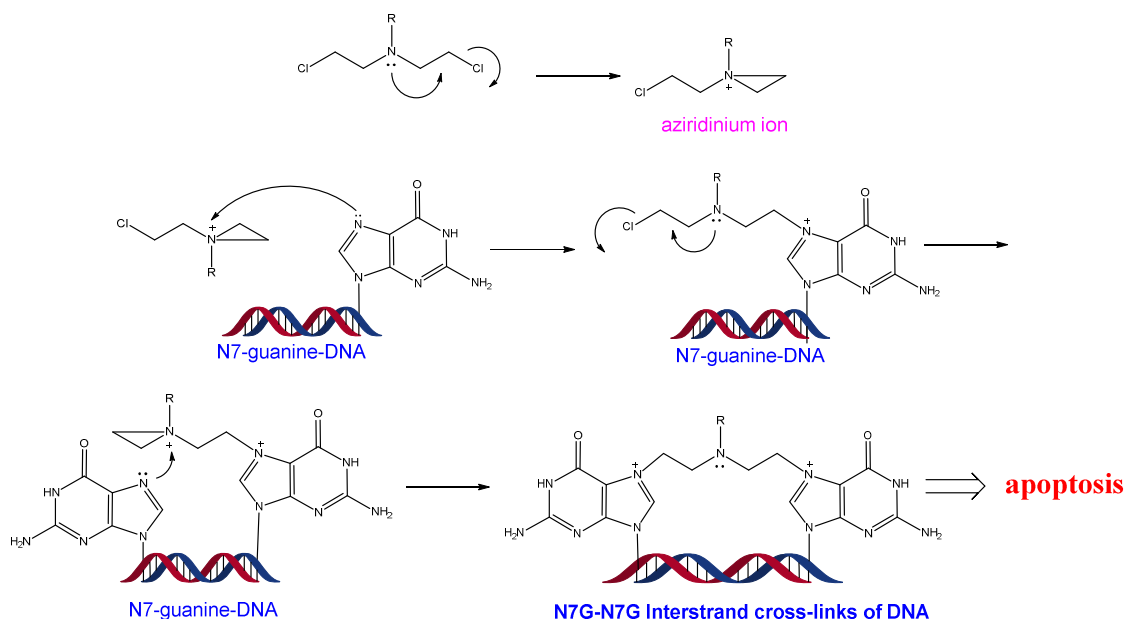


Fig. 12: Structures of some Nitrogen mustards derivatives.<sup>61,62</sup>



Scheme 2: Alkylating mechanism of nitrogen mustard agent toward DNA-guanine bases leading to apoptosis.<sup>61,62</sup>

#### b) Chloroethylnitrosoureas (CENUs)

Typical CENU chemotherapies include carmustine and lomustine (Fig. 13). Chloroethylnitrosoureas have been demonstrated to be efficient for treating brain tumors, including glioblastoma, astrocytoma, oligodendroglioma, and medulloblastoma, due to their highly lipid-solubility, thus penetrating the blood-brain barrier.<sup>63,64</sup>

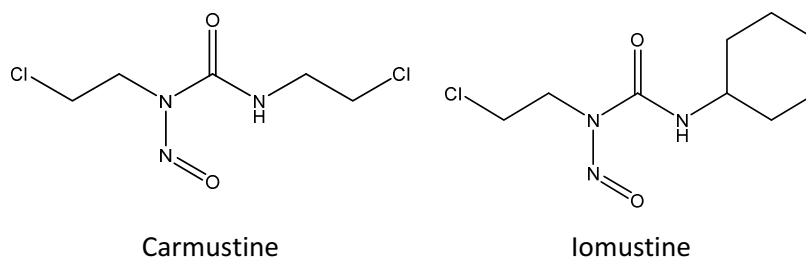
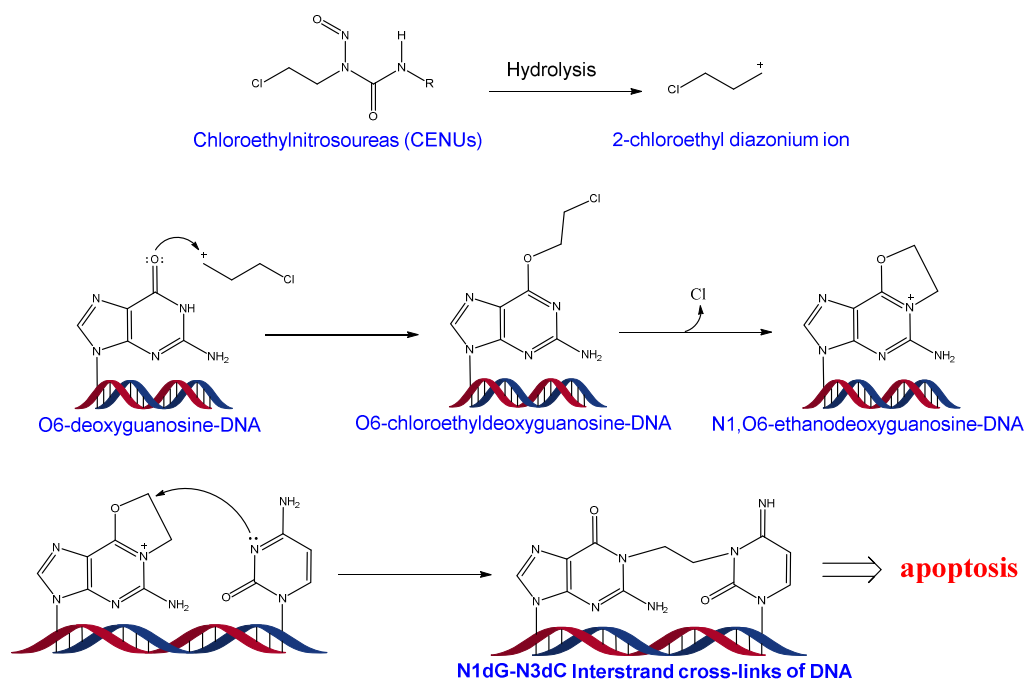


Fig. 13: Structures of Carmustine and Lomustine.<sup>63, 64</sup>

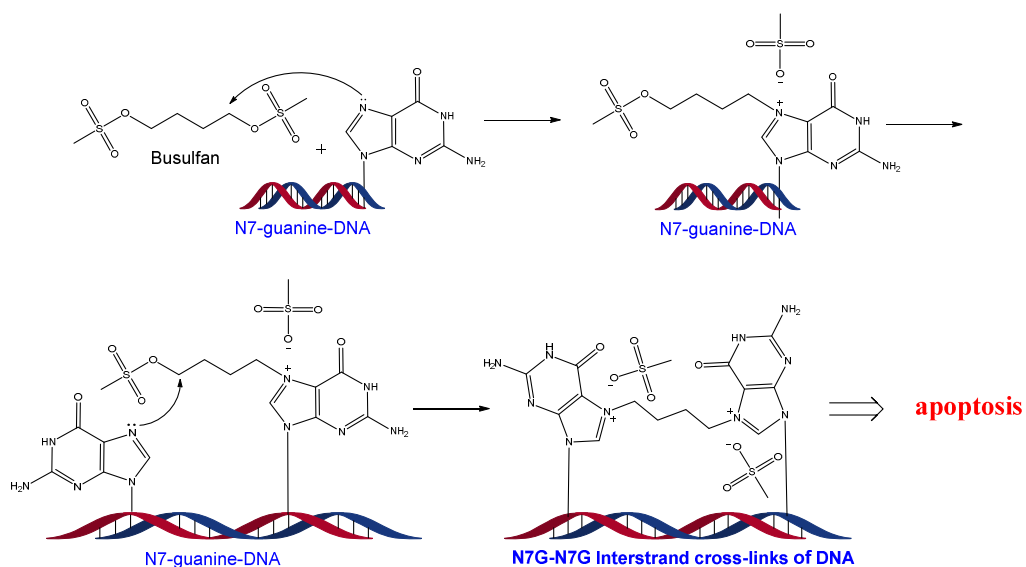
CENUs are apt to undergo spontaneous hydrolysis under physiological conditions and yield 2-chloroethyl diazonium ion, which alkylate O6-deoxyguanosine. The resulting O6-chloroethyldeoxyguanosine undergoes intramolecular cyclization to form N1,O6-ethanodeoxyguanosine, that attacks the complementary deoxycytidine to produce interstrand crosslink between the N1 of deoxyguanosine and the N3 of deoxycytidine (dG-dC crosslink) as shown in scheme 3.<sup>64,65</sup>



Scheme 3: Alkylating mechanism of Chloroethylnitrosoureas (CENUs) leading to apoptosis.<sup>64,65</sup>

### c) Alkylsulfonates

Alkyl sulfonates are esters of alkane sulfonic acids with the general formula R-SO<sub>2</sub>-O-R'. Busulfan is the alkyl sulfonate which is currently used for the treatment of chronic myeloid leukemia.<sup>52,66</sup> As nitrogen mustards, this compound causes DNA crosslinks as shown in Scheme 4 but has different biological and clinical effects.<sup>52,66</sup> In addition, busulfan has the interesting property of having much less effect on lymphoid cells than the immunosuppressive nitrogen mustards.<sup>52,66</sup>



Scheme 4: Alkylating mechanism of Busulfan.<sup>52,66</sup>

#### d) Aziridine alkylating agents

Aziridine is an organic compound consisting of the three-membered heterocycle  $(\text{CH}_2)_2\text{NH}$ .<sup>66, 67</sup> The aziridine alkylating agents, which are used significantly in cancer therapy, are thiotepa and mitomycin C (Fig. 14).<sup>52, 66, 67</sup> Mitomycin C, an antibiotic extracted from a microorganism which acts against hypoxic tumor cells and is used in combination regimens for adenocarcinomas of the cervix, stomach, pancreas, and lung.<sup>52</sup> The best results of thiotepa are found in the treatment of adenocarcinoma of breast and ovary, as well as papillary thyroid and bladder cancers.<sup>67</sup> Aziridine alkylating agents structurally resemble nitrogen mustards but react with DNA with uncharged aziridine rings.<sup>66, 67</sup> These rings are less reactive than the aziridinium intermediates through which the nitrogen mustards alkylate DNA.<sup>66, 67</sup> The interstrand crosslink formed by thiotepa appears similar to the nitrogen mustards, with two aziridine carbons reacting with the N7 of guanylates in complementary strands.<sup>66, 67</sup> Mitomycin C is a bioreductive activated antitumor drug that not only specifically yields interstrand crosslink between the C<sub>2</sub>-NH<sub>2</sub> groups of two guanines sites in the complementary strands but also forms intrastrand crosslink and monoadducts.<sup>64, 68</sup>

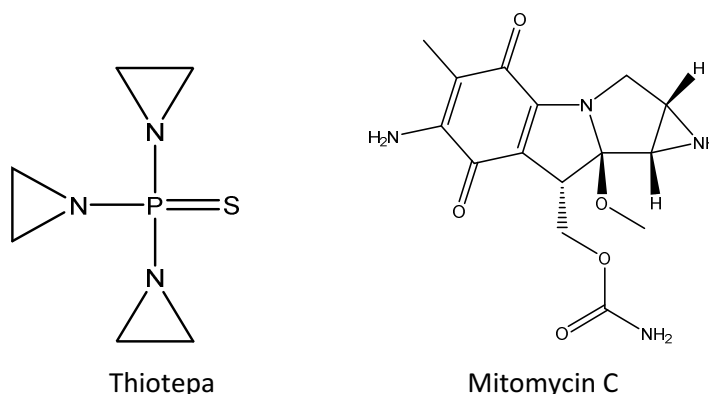


Fig. 14: Structures of Thiotepa,<sup>67</sup> and Mitomycin C.<sup>68</sup>

#### 3.6.5.2 Monofunctional Alkylating Agents

The most frequently used monofunctional alkylating agents are procarbazine, dacarbazine, and temozolomide (Fig. 15).<sup>66</sup> Procarbazine and temozolomide are used in the treatment of brain tumors, while dacarbazine is used in the treatment of malignant melanoma.<sup>66</sup> These compounds are metabolized to produce a very reactive methyl diazonium, which methylates the O6 position of guanylate in DNA. As result, the DNA mismatch repair and other enzymes recognize the presence of the abnormal DNA base and attempt to repair or remove the methylated guanylate which appears to be the major mechanism of cellular damage produced by these compounds.<sup>66</sup>

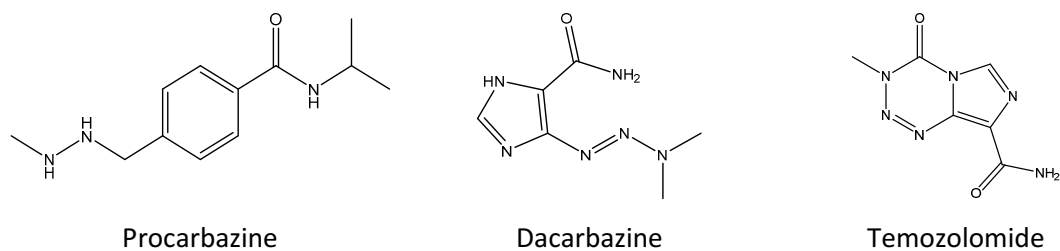


Fig. 15: Structures of Procarbazine, Dacarbazine and Temozolomide.<sup>66</sup>

### 3.6.6 *Platinum-based chemotherapeutic drugs*

Platinum anticancer agents represent a significant success story in the field of medicinal inorganic chemistry and show how a combination of serendipity and rational design can lead to a successful drug development process.<sup>69</sup> They are sometimes described as "alkylating-like" because of similar effects as alkylating antineoplastic agents, despite the absence of an alkyl group.<sup>37,52,69</sup> Moreover, they are in general cell-cycle nonspecific agents that work at any phase of active replication, in particular during the S phase.<sup>37,52,69</sup>

#### 3.6.6.1 *Clinically Approved Platinum(II)-Anticancer Agents.*

Since Barnett Rosenberg discovered the therapeutic potential of *cis*-diamminedichloridoplatinum(II) or cisplatin (Fig. 16) in 1964,<sup>70</sup> it became an essential component in chemotherapy regimens.<sup>71-73</sup> Cisplatin was approved by FDA in 1978 for the treatment of testicular and ovarian cancers.<sup>71</sup> Currently, it is used to treat ovarian, testicular, bladder, non-small cell lung, and small cell lung cancers, as well as lymphomas, myelomas, and melanoma.<sup>71-73</sup> Six other platinum drugs (Fig. 16) have been approved for clinical use in the USA and other countries. Carboplatin and Nedaplatin (Fig. 16) are considered second-generation platinum-based drugs.<sup>71</sup> Carboplatin was approved by FDA in 1989 and is primarily used to treat ovarian cancer.<sup>71</sup> Nedaplatin was approved in Japan in 1995 and was primarily used for small cell lung and non-small cell lung cancers.<sup>71</sup> Carboplatin and Nedaplatin contain the same non-leaving group as cisplatin, but different leaving groups, 1,1-cyclobutanedicarboxylate and glycolate in carboplatin and nedaplatin respectively.<sup>71</sup> In carboplatin, the 1,1-cyclobutanedicarboxylate binds to Pt(II) strictly, due to the chelation effect, which results in a much slower aquation, and activation rate compared with cisplatin.<sup>74</sup> The slower activation rate of carboplatin makes it much gentler to off-target biological nucleophiles and thus has a lower toxicity profile. Therefore, carboplatin can be administered at a higher dosage than cisplatin.<sup>74,75</sup> Also, it exhibits the same cross-resistance, and the same platinum DNA adducts as cisplatin since they share the same non-leaving group.<sup>76</sup> Nedaplatin contains a glycolate group as a leaving group which contributes to nedaplatin's higher water solubility than cisplatin and lower

nephrotoxicity than both cisplatin and carboplatin.<sup>77</sup> Oxaliplatin is third-generation platinum-based anticancer drugs and was approved by the FDA in 2002 mainly for colorectal cancer treatment.<sup>71</sup> Oxaliplatin (Fig. 16) is the first clinically approved platinum drug that can overcome cisplatin resistance.<sup>76</sup> It shows oxalate as a chelating leaving group, which is less susceptible to aquation and has a different non-leaving group 1R,2R-diaminocyclohexane (1R,2R-DACH), thus shows different sensitivity to cancer cell lines compared to cisplatin and carboplatin.<sup>76</sup> Oxaliplatin accumulation appears to be less dependent on copper transporters and more dependent on organic cation transporters (OCTs), which are often overexpressed in colon cancer.<sup>78,79</sup> Lobaplatin (Fig. 16) is also a third-generation platinum anticancer drug, approved by China in 2003 and is currently used for the treatment of chronic myelogenous leukemia, inoperable metastatic breast cancer, and small cell lung cancer.<sup>71,80</sup> It has R, R and S, S cyclobutane-1,2-bis(methylamine) racemic mixture as the non-leaving group ligand and the S-lactate as the leaving group. Thus, lobaplatin is a mixture of diastereomers.<sup>71</sup> Heptaplatin (Fig. 16), approved by South Korea in 1999, is used for gastric cancer treatment.<sup>71</sup> It has malonate as a chelating leaving group and 2-(1-methylethyl)-1,3-dioxolane-4,5-dimethanamine as the non-leaving group.<sup>71</sup> The *in vitro* and *in vivo* cytotoxicity of heptaplatin was equal, or superior, to cisplatin in various cell lines.<sup>81</sup> Furthermore, it displayed high stability in solution and potent anticancer activity toward cisplatin-resistant cells without remarkable toxicity.<sup>81</sup> Miriplatin (Fig. 16) was approved by pharmaceuticals and medical devices agency of Japan (PMDA) and is used to treat hepatocellular carcinoma. It is a lipophilic platinum complex containing myristates as leaving groups and the same non-leaving group as oxaliplatin.<sup>82</sup>

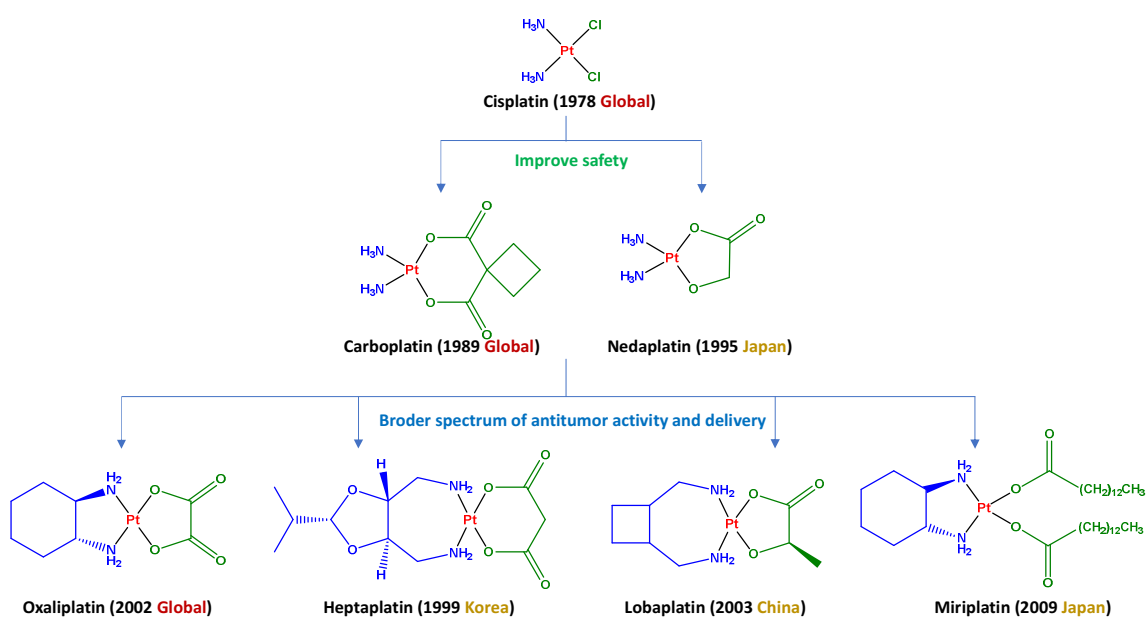


Fig. 16: Clinically Approved Platinum(II)-Anticancer Agents.<sup>71</sup>

### 3.6.6.2 *Platinum Anticancer Drugs currently in clinical trials*

There are currently four drugs in various stages of clinical trials Picoplatin, ProLindac™, Lipoplatin, and Satraplatin.<sup>71</sup> Picoplatin (Fig. 17) or *cis*-amminedichlorido(2-methylpyridine) platinum(II) was entered clinical trials in November 1997.<sup>83</sup> Structurally, the pyridine ring is almost perpendicular to the plane of the platinum atom, thus placing the ligand's methyl group directly over the metal center and providing steric hindrance for nucleophiles, particularly thiols, to attack the drug.<sup>83</sup> Furthermore, the *in vitro* studies have shown picoplatin's anticancer properties in resistant cell lines to cisplatin, carboplatin, and oxaliplatin.<sup>84,85</sup> A promising alternative strategy to the discovery and development of brand-new platinum complexes for cancer treatment is the creation of improved delivery technologies for the known cytotoxic agent. The goal is to enhance their delivery to tumors, especially to the DNA of tumor cells and reduce the cytotoxic agent's toxicity. ProLindac™ (Fig. 17) and Lipoplatin will become the first polymer and liposomal-based platinum drugs if approved. ProLindac™ (AP5346) is a nanopolymer consisting of [Pt(1R,2R-DACH)], the active moiety of oxaliplatin, bound to a hydrophilic biocompatible polymer hydroxypropylmethacrylamide (HPMA) to better target solid cancers through the enhanced permeability and retention effect.<sup>71,86,87</sup> The structure is denoted as poly(HPMA)-GGG-Ama-Pt-(1R,2R-DACH), where HPMA is the polymer backbone, GGG is the tripeptide glycyl-glycyl-glycine, Ama is the N,O-amidomalonate chelate and 1R,2R-DACH is the diaminocyclohexane chelate.<sup>86,87</sup> The amidomalonate–platinum chelate is stable at physiological pH but the low pH which is found in the extracellular space of hypoxic tumors and/or the intracellular lysosomal compartment enables the sustained release of the active platinum complex via breakage of these bonds.<sup>71,87</sup> Both preclinical and clinical study data indicate that ProLindac™ exhibits efficacy at least equal to, and likely superior to oxaliplatin, while demonstrating excellent tolerability and activity against several cisplatin-resistant cell lines.<sup>71,87</sup> Lipoplatin is a liposomal cisplatin encapsulated into liposome nanoparticles with an average diameter of 110 nm. It is composed of 8.9% cisplatin and 91.1% lipids (w/w). Lipoplatin's liposomes are reverse-miscelles, composed of soy phosphatidyl choline (SPC-3), cholesterol, dipalmitoyl phosphatidyl glycerol (DPPG), and methoxy-polyethylene glycol-distearoyl phosphatidylethanolamine (mPEG2000-DSPE).<sup>71,88,89</sup> Lipoplatin crosses cell membranes more easily than cisplatin due to the fusogenic nature of the DPPG lipids, which unlocks the cell membrane barrier by promoting a direct fusion with the cell membrane. Also, the presence of a PEG coating prevents detection by immunogenic entities.<sup>71,89</sup> Lipoplatin was developed to reduce cisplatin's systemic toxicity profile so that it can be administered in higher doses whilst improving the targeting of primary tumors and metastases.<sup>71,89</sup> Lipoplatin showed superior cytotoxicity in all tumor cell models and less toxicity in normal cells than cisplatin,



suggesting a greater therapeutic index for Lipoplatin as a new substitute for cisplatin.<sup>71,89</sup> Satraplatin or [bis-(acetato)-amminedichloro-(cyclohexylamine)platinum(IV), JM216] (Fig. 17), has emerged as a novel oral active platinum (IV) drug that has a better toxicity profile than cisplatin and more hydrophobic than cisplatin or oxaliplatin.<sup>90</sup> It has a single amine and cyclohexylamine group as non-leaving groups, dichloro leaving groups, and a pair of acetate ligands in axial positions of the octahedral structure.<sup>71,90</sup> Satraplatin is readily absorbed by the gastrointestinal mucosa, and once in the bloodstream, it is reduced into six different platinum(II) compounds, of which cis-amminedichlorido(cyclohexylamine)platinum(II) is the most active and abundant one.<sup>71,90</sup> It has anticancer activity against several platinum-sensitive and resistant cell lines including human lung, ovary, cervix, and prostate.<sup>71,90</sup>

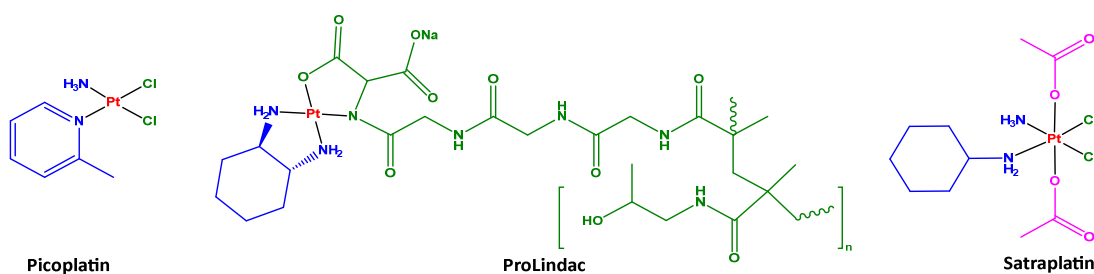


Fig. 17: Platinum Anticancer Agents in Clinical trials. Not shown: Lipoplatin.<sup>71</sup>

### 3.7 Cisplatin Mechanism of Action

Cisplatin and related FDA-approved platinum-based anticancer drugs act in four steps as described below:<sup>92</sup>

#### a) Cellular uptake

The platinum anticancer agent's efficacy depends on its ability to enter the cell and penetrate the nucleus, where DNA is located.<sup>93</sup> Cisplatin is mostly taken up by cells via passive diffusion through the plasma membrane and active transport mediated by membrane proteins.<sup>92-95</sup> A transmembrane protein involved in copper homeostasis, copper transporter 1 (CTR1), was also reported to play an important role in the uptake of cisplatin (Fig. 19).<sup>96</sup>

#### b) Aquation and activation

Once inside the cells, where the chloride concentration is much lower (4–10 mM) than in the bloodstream (100 mM) (Fig. 19)<sup>92-94</sup>, cisplatin undergoes a ligand substitution event prior to DNA binding in which a chloride ligand is replaced by a water molecule.<sup>92</sup> This reaction affords the potent electrophilic cations, the mono-aqua  $cis\text{-[Pt(NH}_3\text{)}_2\text{Cl(OH}_2\text{)]}^+$  and the diaqua  $cis\text{-[Pt(NH}_3\text{)}_2\text{(OH}_2\text{)}_2\text{]}^{2+}$ , which readily bind DNA (Fig. 18).<sup>92-94</sup> In comparison to

aqua species, mono-aqua species may play a more dominant intracellular role than the diaqua species.<sup>92</sup>

### c) DNA binding

The aquated cisplatin species can enter the nucleus, then the water molecule substituted by nucleophilic centers on DNA-purine bases, particularly the N7 positions of guanine and adenosine residues.<sup>92-94</sup> The two reactive sites on the platinum center permit the formation of a cross-link between two adjacent guanines on the same strand or on different strands, giving rise to intrastrand and interstrand DNA cross-links, respectively.<sup>92,94</sup> The most prevalent lesion is 1,2-d(GpG) (intrastrand cross-linking two adjacent guanines)(60–65%), but 1,2-(ApG)(intrastrand cross-linking adjacent adenine and guanine)(20–25%) and 1,3-d(GpTpG)(intrastrand cross-linking two guanines separated by another intervening base) (10%) also form along with small amounts of GG (interstrand crosslinks two adjacent guanines)(2–6%), monofunctional adduct on guanines (approximately 2%) and DNA–platinum–protein cross-link (Fig. 18).<sup>92,94,97,98</sup>

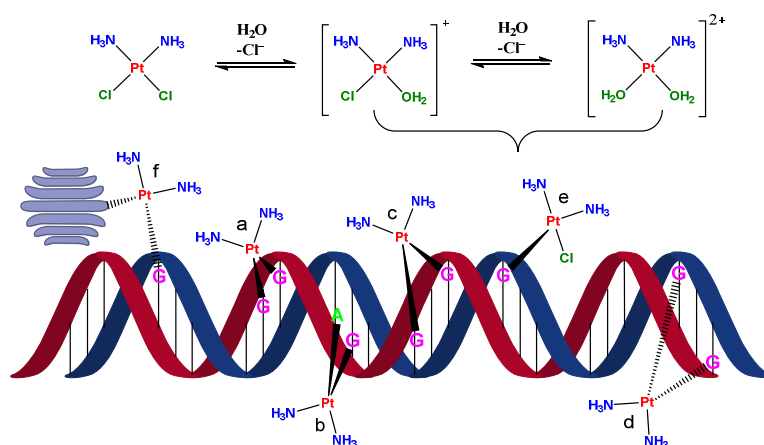


Fig. 18: Cisplatin aquation and the most prevalent DNA-lesion.

a) 1,2-d(GpG) intrastrand crosslinking two adjacent guanines; b) 1,2-(ApG) intrastrand crosslinking adjacent guanine and adenine; c) 1,3-d(GpTpG) intrastrand crosslinking two guanines separated by another intervening base; d) GG interstrand cross-link; e) monofunctional adduct; f) DNA–platinum–protein cross-link.<sup>92,94,97,98</sup>

### d) Cellular processing of DNA lesions leading to apoptosis

Cisplatin–DNA intrastrand cross-links that are formed cause significant structural distortion in the DNA double-helix, thus inhibiting transcription and replication and triggering cell death pathways.<sup>92-94,99</sup> These Pt-DNA adducts are recognized by several cellular proteins including non-histone chromosomal high-mobility group proteins 1 and 2 (HMG1 and HMG2), nucleotide excision repair (NER) proteins, and mismatch repair

(MMR) proteins leading to the repair, replication bypass, or initiation of apoptosis.<sup>92-94</sup> Among these proteins is the nucleotide excision repair (NER) pathway, comprising the cellular DNA repair machinery for the removal of platinum-DNA adducts and DNA damage repair.<sup>93,100,101</sup> A cellular defect in this pathway resulted in hypersensitivity to cisplatin.<sup>100-102</sup> On the contrary, enhanced NER activity is associated with cisplatin resistance.<sup>93,100,101</sup> Alternatively, other proteins can potentiate the activity of cisplatin.<sup>103</sup> High mobility group (HMG)-domain proteins are mainly involved in gene regulation and chromatin structure,<sup>94</sup> selectively bind to 1,2-d(GpG) intrastrand cross-links adduct,<sup>104,105</sup> and subsequently induce apoptosis.<sup>104-106</sup> HMG proteins also increase the efficacy of these cytotoxic platinum lesions by blocking the access of proteins required for the NER repair pathway.<sup>94,107,108</sup> This phenomenon is called "repair shielding". In addition, HMG1 and HMG2 proteins promote the binding of p53 to DNA, resulting in the transactivation of several genes involved in cell cycle progression (p21), DNA repair, and apoptosis.<sup>94</sup> Hence, high expression levels of HMG-domain proteins may increase cellular cisplatin sensitivity.<sup>93,109</sup> Finally, the mismatch repair (MMR) protein complex does not actually repair cisplatin-DNA adducts but rather attempts to repair DNA damage, after failing to repair DNA damage, it also triggers apoptosis.<sup>94</sup>

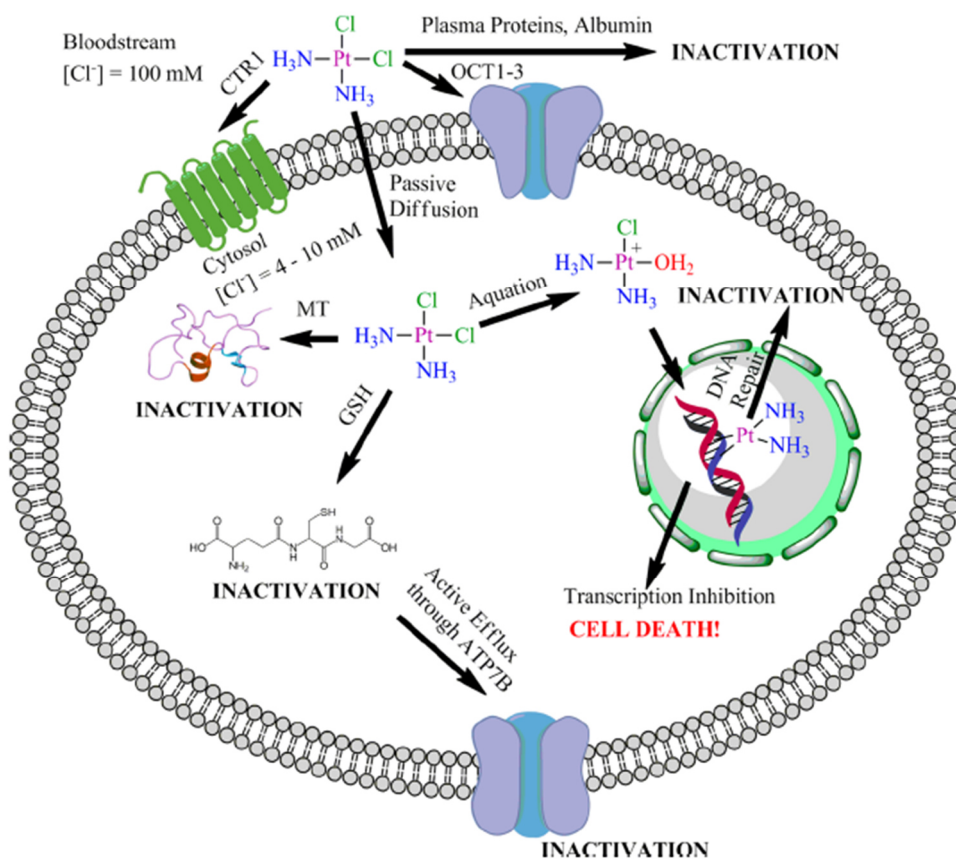


Fig. 19: Mechanism of action of cisplatin and resistance to the drug. Reproduced with permission from ref. 93, Copyright © 2013, American Chemical Society.

### **3.8 Mechanism of tumor resistance to cisplatin and carboplatin**

Cisplatin and carboplatin drug resistance has been studied in cell lines, and two broad mechanisms of resistance have been suggested.<sup>110</sup> The first one is due to an inadequate amount of platinum reaching the target DNA, thus creating resistance through insufficient DNA binding, and the second one is because of a failure to achieve cell death after DNA binding.<sup>110</sup>

#### **3.8.1 Resistance through insufficient DNA binding which happens due to:**

- a) Reduce uptake and increase efflux

Current platinum drugs are all administered intravenously, where they can interact with blood components, including human serum albumin (HSA), the most abundant protein in the human bloodstream, that inhibits the action of platinum drugs (Fig. 19).<sup>92</sup> Also, downregulation of copper transporter 1 (CTR1), which plays an important role in the uptake of cisplatin results in less platinum entering cells and, consequently, drug resistance.<sup>94,110-112</sup> On the other hand, copper-extruding P-type ATPases, ATP7A and ATP7B was found to participate in platinum drug resistance.<sup>94,110,112</sup> Cisplatin is sequestered in vesicular structures by ATP7A, preventing further drug distribution, while ATP7B is responsible for cisplatin efflux from the cell (Fig. 19),<sup>94,110,112-114</sup> thus, patients with high levels of ATP7A and ATP7B had significantly poorer overall survival.<sup>115,116</sup>

- b) Increase inactivation

In the cytoplasm, the activated aqua species bind to cytoplasmic sulfur-containing nucleophiles such as glutathione (GSH), metallothionein, methionine, and other cysteine-rich proteins before the DNA binding (Fig. 19).<sup>94,110</sup> Consequently, the cytoplasmic antioxidant reserve is depleted, and the cells experience oxidative stress leading to apoptotic pathways.<sup>94</sup> On the other hand, these nucleophilic species act as scavengers, decreasing the availability of reactive cisplatin and contributing to cisplatin resistance.<sup>94,110</sup> The conjugation of cisplatin with glutathione is catalyzed by glutathione S-transferases (GSTs), which makes the compound more anionic and readily excreted out of the cells by multidrug resistance protein MRP2, a member of the ABC family ATPases.<sup>117,118</sup> In addition, it was observed high levels of glutathione or glutathione-S-transferase in cisplatin-resistant cells.<sup>119,120</sup>

#### **3.8.2 Resistance after DNA binding**

After Pt–DNA adducts have been formed, cellular survival and therefore tumor drug resistance occur either by DNA repair and increase removal of lesions or by tolerance mechanisms.<sup>110</sup>

#### a) DNA repair

Nucleotide-excision repair (NER) is known as the major pathway to remove cisplatin lesions from DNA,<sup>100,101,110</sup> increasing NER, especially through the activation of the endonuclease protein ERCC1 (excision repair cross-complementing-1) can increase the removal of DNA adducts before triggering apoptotic signalling pathways, thus lead to platinum drug resistance.<sup>100,101,121</sup>

#### b) Tolerance

Tolerance to the platinum-induced DNA damage can occur through loss or downregulation of the mismatch repair (MMR) protein with respect to cisplatin–DNA adducts, resulting in reduced apoptosis and, consequently, drug resistance.<sup>110,122,123</sup> In addition, another tolerance mechanism involves enhanced replicative bypass of the cisplatin–DNA adducts through  $\beta$  and  $\eta$  DNA polymerases (Translesion synthesis pathway of DNA repair).<sup>124</sup> Loss of pol  $\eta$  results in a remarkable sensitivity to cisplatin and other platinum agents, whereas overexpression of pol  $\eta$  provides resistance to cisplatin.<sup>125,126</sup> Finally, tolerance can also occur through decreased expression of apoptotic signalling pathways, mediated by various proteins such as tumor suppressor (p53), Bcl-2 family, and c-Jun N-terminal kinases (JNKs).<sup>110,127,128</sup>

### 3.9 Platinum(II) complexes with biologically active compounds

Many medicinal-chemistry efforts produced compounds of the general formula  $cis\text{-PtA}_2\text{X}_2$ , where A is ammine or a substituted amine non-leaving group and X or  $\text{X}_2$  is an anionic leaving group.<sup>92,94</sup> A biologically active compounds attached either to the leaving or non-leaving group to uncover novel mechanisms of cell killing, modify the spectrum of activity, and raise cancers susceptible to platinum therapy.<sup>92,94</sup> It was shown, for instance, VP-128 (Fig. 20), is estradiol tethered platinum complex with excellent receptor binding affinity.<sup>129</sup> This estradiol-linked platinum(II) complex showed markedly improved in *vitro* and in *vivo* activity towards ER $\alpha$  (+) breast cancer (MCF-7), which has weak sensitivity toward cisplatin and without an increase in systemic toxicity.<sup>130</sup> The glucose-conjugated oxaliplatin-based complex Glu-Pt (Fig. 20) was developed for targeted drug delivery *via* glucose uptake by cancer cells,<sup>131</sup> and it is reported that cancer cells require much higher levels of glucose to supply the energy of cell division.<sup>132</sup> Glu-Pt exhibits the same mechanistic principles of oxaliplatin with improved potency in cytotoxicity and 150 times much higher aqueous solubility.<sup>131</sup> Another approach, the combination of platinum with intercalator ligands might enable DNA binding *via* two different sites, through covalent bonds of the platinum moiety and by intercalation of the ligand between the DNA base

pairs.<sup>94,133</sup> The acridine-platinum compounds  $cis-[Pt\{AO(CH_2)_6en\}Cl_2]^+$  (Fig. 20), is one of the first complexes prepared by Lippard and co-workers that contained acridine orange as an intercalator.<sup>133</sup> It showed the same sequence selectivity in DNA cross-linking as with cisplatin, and the acridine ligand intercalated into the DNA at one or two base pairs from the Pt-DNA adduct.<sup>133</sup>

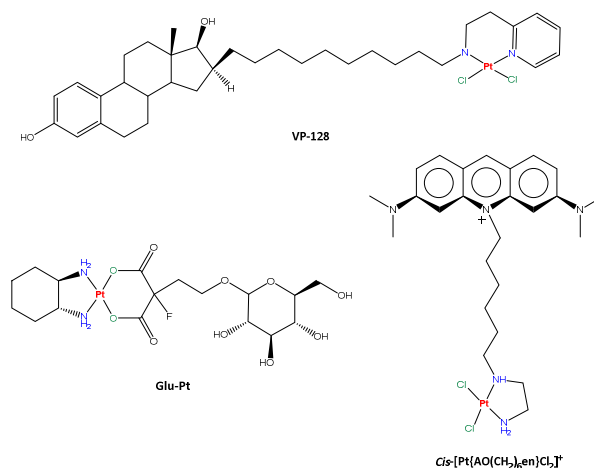


Fig. 20: Structure of VP-128,<sup>129,130</sup> Glu-Pt,<sup>131</sup> and  $cis-[Pt\{AO(CH_2)_6en\}Cl_2]^+$ .<sup>133</sup>

### 3.10 Monofunctional platinum(II) complexes

Monofunctional platinum(II) complexes represent another class of non-traditional anticancer agents that feature only one labile ligand and are expected to form only one covalent bond to DNA.<sup>92-94</sup> The earliest studies have demonstrated that the monofunctional platinum(II) complexes such as  $[Pt(NH_3)_3Cl]^+$  and  $[Pt(dien)Cl]^+$  (dien = diethylenetriamine) are inactive both in *vitro* and in *vivo*.<sup>134-136</sup> According to the prevailing view, only neutral and square-planar platinum(II) complexes with a pair of inert ligands in a *cis*-configuration could have anticancer activity.<sup>92,137,138</sup> However, this belief was overturned when the cationic monofunctional  $cis-[Pt(NH_3)_2(Am)Cl]^+$  (Am is an N-heterocyclic amine) could inhibited tumor cells growth in *vitro* and in P388 as well as L1210 leukemia mouse models.<sup>92</sup> Another group of monofunctional compounds has been developed in Lippard's laboratory with a general formula  $cis-[Pt(NH_3)_2(Am)Cl]^+$ , where Am was a planar aromatic base such as pyridine, purine, pyrimidine, or phenanthridine.<sup>139</sup> *Cis*-diamminepyridinechloroplatinum(II), also referred to as Pyriplatin (Fig. 21), had a remarkable affinity for organic cation transporters OCTs, even far better than those of oxaliplatin.<sup>92,140,141</sup> thus cells with high OCTs expression were more sensitive to pyriplatin treatment than those with low OCTs levels.<sup>92,94,140,141</sup> Pyriplatin is expected to form only one covalent bond with the N7 site of a deoxyguanosine residue, which induces only a little distortion on the DNA double helix,<sup>140,142</sup> precluding the bending induced by bifunctional platinum complexes such as cisplatin.<sup>140</sup> In addition, such a significant type

of DNA adducts formed by pyriplatin, might have a novel spectrum of activity. This adduct was able to stall RNA polymerase II (RNA pol II), and transcription inhibition was proposed to be the origin of its cytotoxicity.<sup>140,143</sup> Monofunctional lesions formed by pyriplatin are mainly repaired by NER, but not with the same efficiency as bifunctional lesions of the clinically used platinum drugs.<sup>93,144</sup> Pyriplatin cytotoxicity was lower than that of cisplatin in all tested cell lines,<sup>145</sup> which motivated a search for more active analogs. Since the structural analysis of RNA polymerase II stalled at a site-specific pyriplatin lesion suggested that, by increasing the steric hindrance of the N-heterocyclic ligand for enzyme inhibition, it might be possible to increase transcription inhibition and consequential cytotoxicity.<sup>140,143</sup> Therefore, the pyridine in pyriplatin was substituted by phenanthridine. This process quickly led to the discovery of *cis*-[Pt(NH<sub>3</sub>)<sub>2</sub>(phenanthridine)Cl]<sup>+</sup> (phenanthriplatin) (Fig. 21) as the most potent complex of this series.<sup>139,140,142</sup> Studies of translesion DNA synthesis past phenanthriplatin adducts demonstrated that this complex can inhibit both RNA polymerases and DNA polymerases (pol η).<sup>140,146</sup> Moreover, phenanthriplatin cellular uptake is higher than that of cisplatin and pyriplatin, and the steric hindrance provides protection from thiol deactivation like picoplatin.<sup>93</sup> Phenanthriplatin has significantly greater potency than cisplatin, in contrast to pyriplatin.<sup>140</sup>

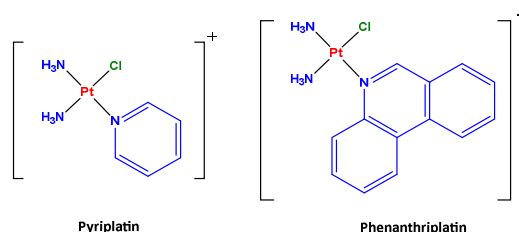


Fig. 21: Structure of Pyriplatin,<sup>92,94,140-143</sup> and Phenanthriplatin.<sup>139,140,142,146</sup>

### 3.11 Platinum(IV) Anticancer Agents

Platinum(II) drugs still have some serious drawbacks including inherent or acquired resistance, dose limiting, as well as severe side effects that patients have to deal with during chemotherapy.<sup>110,147,148</sup> Square planar platinum (II) complexes, with a d<sup>8</sup> electronic configuration, are semi-labile and hence they easily undergo non-selective ligand substitution with various biological nucleophiles prior to reaching the tumor,<sup>94,110,149</sup> this results in low bioavailability and increased side effects.<sup>110,148,149</sup> Various strategies have been suggested to improve the efficiency and overcome the shortcomings of platinum (II) drugs, one of the most promising approaches is to use platinum (IV) complexes as prodrugs.<sup>92,94</sup> Platinum(IV) complexes are prepared by oxidative addition of the square planar Pt(II) complexes, usually with hydrogen peroxide, to give the octahedral

complex which retains the original coordination sphere of platinum(II) at the equatorial positions and adds two hydroxides at the axial positions.<sup>150,151</sup> The physicochemical properties of platinum(IV) agents are significantly different from those of their platinum(II) counterparts.<sup>92,150,152</sup> Platinum(IV) complexes exhibit kinetic inertness and a low-spin  $d^6$  coordinatively saturated octahedral geometry, rendering them more resistant to ligand substitution reactions than the platinum(II) centers, thus minimizing unwanted side reactions with biological nucleophiles prior to DNA binding and reducing associated side effects.<sup>92,150,152, 153</sup> Furthermore, the axial ligands determine the chemical and biological properties of each complex and can be specifically designed to fulfill certain tasks such as increasing lipophilicity, solubility, cellular uptake, improving tumor targeting, interfering with cellular processes, changing the reduction potential, and enhancing cytotoxicity by incorporating additional bioactive agents to obtain dual- and multi-action drugs. (Fig. 22).<sup>92-94,150,152-154</sup> The intracellular activation of the platinum(IV) complexes takes place primarily by cellular reducing agents such as ascorbic acid or glutathione (GSH) through a two-electron reductive elimination reaction, resulting in the release of the original platinum(II) drug along with the two axial ligands.<sup>150,152</sup> The reduction process depends upon the composition of the platinum(IV) agent as well as the nature of the biological reducing agent involved.<sup>92,155-157</sup> Platinum(IV) complexes are considered ideal candidates for prodrugs as they are reasonably non-reactive toward extracellular nucleophiles but are activated by a plethora of reducing agents inside the cancer cells.<sup>150,152,155</sup>

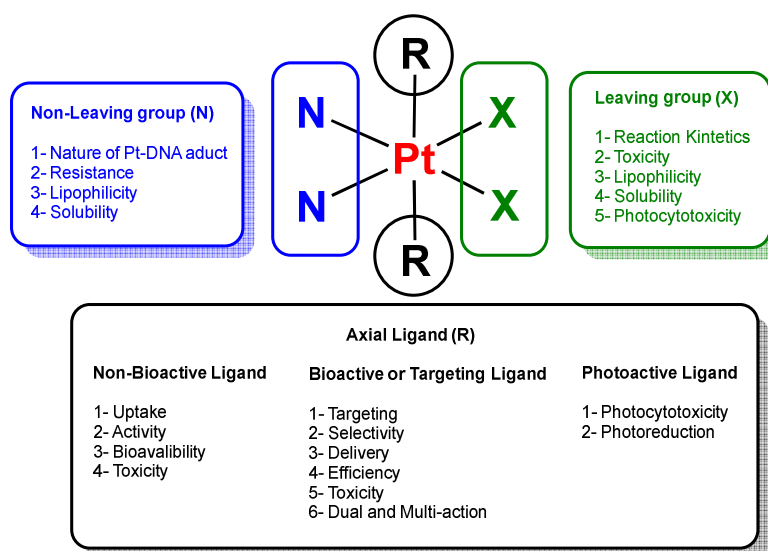


Fig. 22: General structure for platinum(IV) prodrugs and the role of Non-leaving, Leaving and Axial ligands.<sup>92-94,150,152-155</sup>

Platinum(IV) prodrugs can be classified into three main categories according to the type of the axial ligand: complexes with innocent axial ligands (hydroxides, chlorides, acetates, etc.) that do not have a specific biological activity, complexes with bioactive



axial ligands (anti-proliferative agents, enzyme inhibitors, FDA approved drugs, etc.) that affect cellular processes and contribute to the death of the cancer cells or targeting axial ligands (glycosyl, biotin, estrogen, tamoxifen, cyanonilutamide, etc.) are designed to confer selectivity towards cancer cells, and finally the photoactivatable platinum(IV) prodrugs.<sup>94,152</sup>

### 3.11.1 Platinum(IV) prodrugs with Innocent Axial Ligands

Ormaplatin, iproplatin, satraplatin, and LA-12 (Fig. 23) are platinum(IV) complexes without bioactive axial ligands that entered clinical trials.<sup>94</sup> Ormaplatin, also known as tetraplatin was one of the first platinum(IV) agents to undergo clinical trials. Ormaplatin is rapidly reduced to dichloro(trans-1,2- diaminocyclohexane)platinum(II) in tissue culture medium ( $t_{1/2} = 5-15$  min) and undiluted rat plasma ( $t_{1/2} = 3$  s).<sup>158</sup> Ormaplatin, despite undergoing six phase I clinical trials,<sup>159</sup> has not proceeded to any phase II clinical trial due to severe cumulative neurotoxicity, most probably attributable to the rapid reduction to its platinum(II) counterpart by biological reducing agents.<sup>71,94</sup> Iproplatin, in contrast, is less prone to reduction and deactivation by biological reducing agents than ormaplatin, despite being involved in 38 clinical trials from phase I to phase III,<sup>92</sup> it did not exhibit overall effectiveness that surpassed that of cisplatin or carboplatin, and no further trials were undertaken.<sup>71,92,94</sup> Satraplatin was the first lipophilic platinum(IV) drug developed for oral administration.<sup>90,91</sup> Phase III trials found that the complex increased progression-free survival and reduced the risk of disease progression by 40% in hormone-refractory prostate cancer. However, because of the lack of convincing benefit in terms of overall survival, approval by FDA did not follow.<sup>94</sup> Satraplatin is currently being evaluated in Phase I, II, and III clinical trials with a variety of drugs to treat prostate and non-small cell lung cancers as well as advanced solid tumors. Since these studies are in their infancy and will require further funding, it is unlikely that the company will continue to develop satraplatin. LA-12 is an analog of satraplatin in which the cyclohexylamine is replaced with adamantylamine.<sup>160,161</sup> Furthermore, LA-12 showed promising *in vivo* activity in mice bearing ADJ/PC6 plasmacytoma and A2780 ovarian cancer.<sup>161</sup>

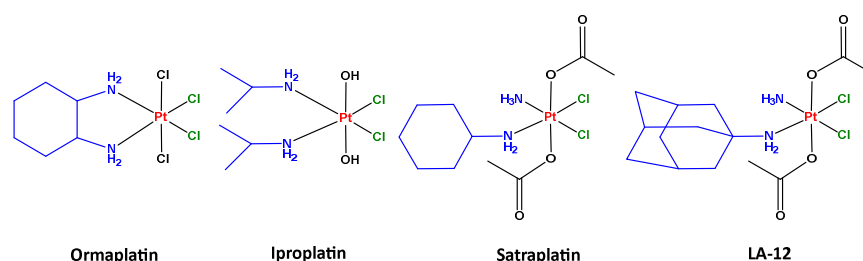


Fig. 23: Structure of Pt(IV) complexes with innocent axial ligands, Ormaplatin,<sup>71,94,158,59</sup> Iproplatin,<sup>71,92,94</sup> Satraplatin,<sup>90,91,94</sup> and LA-12.<sup>160,161</sup>

In spite of numerous clinical studies and many promising results, platinum(IV) prodrug has yet to reach the clinic, thus researchers have turned their attention to developing targeted drug design and action by refining what were once "innocent" axial ligands into designer ligands with additional functions.

### 3.11.2 Platinum(IV) prodrugs with Bioactive or Targeting Axial Ligands

Here we will discuss the most prominent examples:

a) Platinum(IV) prodrugs including histone deacetylase inhibitors (HDACi)

Histone deacetylases (HDAC) are enzymes that remove acetyl groups from the lysine residues of histones, allowing the histones to wrap the DNA more tightly, which is generally associated to a decrease in chromatin accessibility.<sup>162,163</sup> HDAC inhibitors (HDACi) promote the open form of chromatin thereby making the nuclear DNA more accessible for DNA platination, which can improve cytotoxicity.<sup>162,163</sup> Nonetheless, they are epigenetic antiproliferative agents, inhibiting proliferation epigenetically through changing the expression of oncogenes and tumor suppressor genes.<sup>163</sup> Vorinostat and belinostat are FDA approved hydroxamate based HDAC inhibitors, very potent with IC<sub>50</sub> values in the low nM range. On the other hand, organic acids such as valproic acid (Val), butyric acid or 4-phenylbutyric acid (PhB) are very weak extracellular HDAC inhibitors with IC<sub>50</sub> values in the mM range.<sup>164</sup> Pt(IV) derivative of cisplatin with two valproate axial ligands *cis*-[Pt(NH<sub>3</sub>)<sub>2</sub>(Val)<sub>2</sub>Cl<sub>2</sub>](Fig. 24A), is the first Pt(IV)-HDACi complex reported, has μM IC<sub>50</sub> values in several cancer cell lines and more potent than cisplatin.<sup>165,166</sup> Shen and co-workers contend that the high cytotoxicity was due of the synergism between platinum and valproic acid.<sup>165</sup> While Osella and coworkers concluded that the enhanced efficacy of the compound compared to cisplatin was only due to increased accumulation.<sup>166</sup> Pt(IV) derivative based on 4-phenylbutyrate, *cis*-[Pt(NH<sub>3</sub>)<sub>2</sub>(PhB)<sub>2</sub>Cl<sub>2</sub>] (Fig. 24B), was even more potent than *cis*-[Pt(NH<sub>3</sub>)<sub>2</sub>(VPA)<sub>2</sub>Cl<sub>2</sub>] in promoting cytotoxicity.<sup>167</sup> Almotairy and co-workers reported Pt(IV) complexes based on carboplatin and 4-phenylbutyrate (Fig. 24C), but the antitumor activity was lower than that induced by cisplatin analogs.<sup>168</sup>

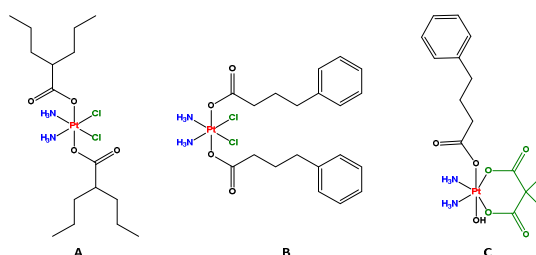


Fig. 24: Structure of Pt(IV) prodrugs based on valproic acid and 4-phenylbutyric acid (HDACi) (A,<sup>165,166</sup> B,<sup>167</sup> and C<sup>168</sup>).

b) Platinum(IV) prodrugs including glutathione-S-transferase (GST) inhibitor axial ligands

Glutathione-S-transferase (GST) enzymes have been demonstrated to be the most important factors in drug resistance.<sup>117,118</sup> Ethacraplatin (Fig. 25A) is a Pt(IV)-ethacrynic acid (EA) prodrug, that in the cell releases cisplatin as well as two ethacrynic acid (EA) molecules which is inhibitor of GST.<sup>169</sup> In addition, ethacraplatin inhibits the cellular activity of GST much more effectively than ethacrynic acid, and its cellular uptake was 10-fold higher than cisplatin.<sup>169</sup> Many years later, Ang co-workers discovered that mono Pt(IV)-EA (Fig. 25B) is more cytotoxic than ethacraplatin.<sup>170</sup>

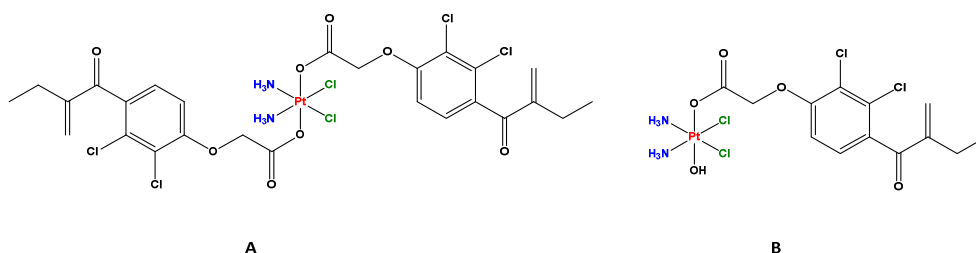


Fig. 25: Structure of Pt(IV) prodrugs based on ethacrynic acid (EA) (A,<sup>169</sup> and B<sup>170</sup>).

c) Platinum(IV) prodrug including a p53 activator (chalcone)

In fact, p53 serves as a "guardian angel" for genome integrity and it plays a crucial role in triggering apoptosis or cell-cycle arrest in response to platinum-DNA damage.<sup>150,171</sup> Nevertheless, p53 function can be inhibited by direct interactions with the human murine double minute 2 protein (MDM2) oncoprotein.<sup>172</sup> A well-known p53-MDM2 inhibitor, chalcone, inhibits the interaction between p53 and MDM2 at a concentration in the micromolar range.<sup>173</sup> Chalcoptatin (Fig. 26) is Pt(IV) anticancer prodrug based on cisplatin and chalcone.<sup>174</sup> The results showed that chalcoptatin significantly activated the p53 pathway, as well as increased cellular accumulation, compared to cisplatin, it exhibited a markedly higher cytotoxicity (10-fold) for wild-type p53 cells.<sup>174</sup> Additionally, chalcoptatin caused cell cycle arrest at both S and G2/M phases of the cell cycle, while cisplatin and chalcone caused cell cycle arrest mainly during the S or G2/M phases, respectively.<sup>174</sup>

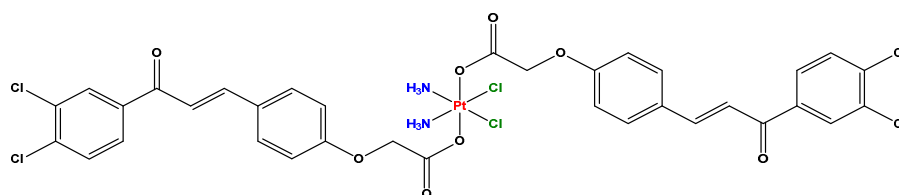


Fig. 26: Structure of Chalcoptatin.<sup>174</sup>

d) Platinum(IV) prodrugs including cyclooxygenase (COX) inhibitors axial ligands

According to the clinical data, cancer progression is often accompanied by chronic inflammation, related to increased cyclooxygenase (COX) expression, including COX-1 and COX-2.<sup>175,176</sup> The non-steroidal anti-inflammatory drugs (NSAIDs) such as aspirin, ibuprofen, indomethacin, and naproxen are known cyclooxygenase (COX) inhibitors.<sup>177,178</sup> A number of recent publications have focused on designing Pt(IV)-NSAIDs prodrugs, which have high lipophilicity and can penetrate tumor cells and release the cytotoxic metabolite and NSAID intracellularly, thereby reducing side effects and increasing the impact of platinum chemotherapy.<sup>178-187</sup> Pt(IV)-aspirin prodrug also called Platin-A (Fig. 27A) showed no significant advantage over cisplatin as a cytotoxic agent in the LNCap, DU145, and PC3 cell lines but was more potent than cisplatin in the MCF-7, A549, HepG2, and A549R cell lines, with IC<sub>50</sub> values in the low μM.<sup>179,180</sup> Using indomethacin and ibuprofen as COX inhibitors, Hey-Hawkins and coworkers conjugated Pt(IV) derivatives of both cisplatin and oxaliplatin.<sup>181,182</sup> In spite of indomethacin being a much better inhibitor of COX-1 and COX-2 than ibuprofen, the bis-ibuprofen Pt(IV) derivatives (Fig. 27B) were more potent than its indomethacin analogs (Fig. 27C) against HCT-116 and MDA-MB-231 cancer cell lines.<sup>181,182</sup> Which can be explained through the ability of ibuprofen to induce cell death by other modes such as apoptosis and cell cycle block in colon carcinoma cells,<sup>188</sup> or these complexes exert their cytotoxicity *via* COX-independent mechanisms. Moreover, the cisplatin derivative with ibuprofen was nearly 5-fold more potent than its oxaliplatin analog.<sup>181,182</sup> Recently, another series of naproxen-containing Pt(IV) prodrugs was obtained.<sup>183-185</sup> Two highly potent cisplatin-based naproxen prodrugs, mono-naproxen Pt(IV) derivative reported by Tolan (Fig. 27D),<sup>183</sup> and bis-naproxen Pt(IV) derivative which reported by Jin (Fig. 27E).<sup>185</sup> Both demonstrated outstanding antiproliferative activity toward the breast cancer cell lines MCF-7, MDA-MB-231, and MDA-MB-435.<sup>183,185</sup> Where the bis-naproxen Pt(IV) derivative, IC<sub>50</sub> values from 0.34 to 0.17 μM, which is 187-fold more higher cytotoxic than that of cisplatin, while mono-naproxen Pt(IV) derivative showed IC<sub>50</sub> values from 0.4 to 1.11 μM is 26-fold higher cytotoxic than cisplatin.<sup>183,185</sup>

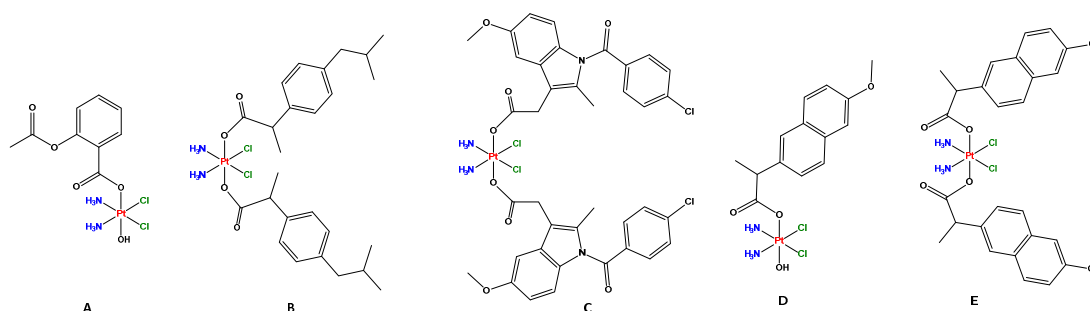


Fig. 27: Structure of Pt(IV) prodrugs based on NSAID (A,<sup>179,180</sup> B,<sup>181,182</sup> C,<sup>181,182</sup> D,<sup>183</sup> and E<sup>185</sup>).

e) Platinum(IV) prodrug including pyruvate dehydrogenase kinase (PDK) inhibitor axial ligands

Normal cells get most of their required energy from the mitochondria through the action of the citric acid cycle and oxidative phosphorylation,<sup>189</sup> while cancer cells obtain a larger proportion of their energy by aerobic glycolysis (Warburg effect), due to the hypoxic conditions present in many tumor tissues.<sup>189,190</sup> Dichloroacetate (DCA) is an inhibitor of pyruvate dehydrogenase kinase (PDK) that plays a key role in glycolysis.<sup>191</sup> With the purpose of inhibiting glycolysis, Lippard and coworkers prepared mitaplatin, a “dual action” Pt(IV) derivative based on cisplatin and two DCA axial ligands. (Fig. 28).<sup>191</sup> Mitaplatin exhibited a dual killing activity against cancer cells, including DNA damage by cisplatin, and decreasing the mitochondrial membrane potential gradient, leading to apoptosis by promoting the release and translocation of cytochrome c as well as apoptosis-inducing factor (AIF).<sup>191</sup> Compared to cisplatin, mitaplatin displayed comparable cytotoxicity and selectively killed cancer cells in co-culture with normal fibroblasts.<sup>191</sup> In later studies, mitaplatin was found to be more potent than cisplatin in both sensitive and resistant epidermoid adenocarcinoma and hepatoma cells.<sup>192</sup>

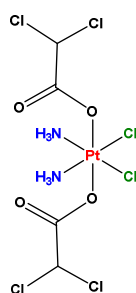


Fig. 28: Structure of Mitaplatin.<sup>191,192</sup>

f) Platinum(IV) prodrugs including glycosyl axial ligands targeting glucose transporters (GLUTs)

According to the Warburg effect, human malignancies are characterized by increased glycolysis and overexpression of glucose transporters (GLUTs) especially GLUT1 and sodium-dependent glucose transporters (SGLTs).<sup>189,190,193</sup> Carbohydrate uptake occurs mainly *via* both glucose transporters (GLUTs) and sodium-dependent glucose transporters (SGLTs).<sup>189,190</sup> Thus, sugar combined with antitumor agents has become an attractive cancer treatment strategy. Wang and co-workers synthesized a series of glycosylated Pt(IV) complexes with protected, and de-protected glucose, mannose, galactose, and rhamnose, the potent compounds are shown in (Fig. 29).<sup>193-196</sup> The glycosylated Pt(IV) complexes protected by acetyl groups (Fig. 29A-F), were found to be comparable or even superior to cisplatin or oxaliplatin in different cell lines such as HeLa,

MCF-7, LNCaP, PC3, HepG-2, A549, and A549R.<sup>193-195</sup> In general, Pt(IV) complexes with the cisplatin core were more effective than their oxaliplatin counterparts.<sup>193-195</sup> The cellular uptake and DNA-platination of the Pt(IV) compounds are enhanced in comparison with Pt(II) drugs.<sup>193-195</sup> Different glycosyl groups exert remarkable influences on their activity, where mannose, galactose, and rhamnose more active than glucose.<sup>193-195</sup> Based on the reduction studies, a lower pH in the cancer microenvironment may facilitate the reduction of mono- glycosylated platinum(IV) complexes to release active platinum(II) complexes.<sup>193-195</sup> Furthermore, mono- glycosylated platinum(IV) complexes exhibited low toxicity to normal cells.<sup>193-195</sup> In further studies, Wang and co-workers investigated whether the transformation of acetyl glycosylated Pt(IV) complexes was associated with GLUTs. Phlorizin was used as a GLUT inhibitor to study how it affected the antitumor activities.<sup>193,196</sup> Based on their findings, GLUT inhibition had no effect on the IC<sub>50</sub> values of the tested complexes, which indicates that glucose transporters (GLUT) were not involved in the transfer of the tested acetyl glycosylated platinum(IV) complexes.<sup>193,196</sup> In contrast, the pyranoside-conjugated platinum(IV) complex with galactose, glucose, and mannose (Fig. 29G-I) demonstrated the ability to exploit GLUT1 and OCT2, as well as specific tumor-targeting properties *in vitro*.<sup>196</sup> They showed high cytotoxicity (IC<sub>50</sub> 0.24–3.97 μM) and 166-fold higher antitumor activity than the positive controls cisplatin, oxaliplatin, and satraplatin.<sup>196</sup> Moreover, having a hexadecanoic chain allowed binding to human serum albumin (HSA) for drug delivery, which not only enhanced the stability of Pt(IV) prodrugs but also decreased their reduction by reductants found in the blood.<sup>196</sup>

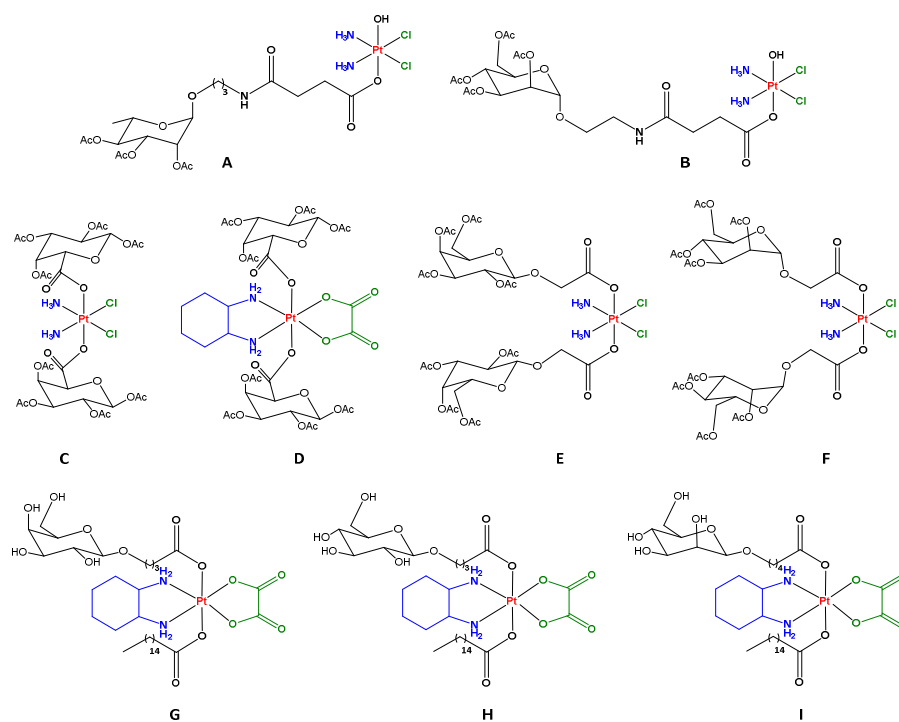


Fig. 29: Glycosylated Platinum(IV) prodrugs (29A-F,<sup>193-195</sup> and 29G-I<sup>196</sup>).

g) Platinum(IV) prodrugs including biotin axial ligands targeting sodium-dependent multivitamin transporter (SMVT)

Biotin also known as vitamin B7 or coenzyme R, is transported into cells by the sodium-dependent multivitamin transporter (SMVT).<sup>197</sup> Biotin receptors are overexpressed in several cancer cell lines, such as MCF-7, MDA-MB-231, A549, RENCA, HeLa, and HepG2.<sup>197</sup> Guo and Wang described Pt(IV) derivatives of cisplatin (Fig. 30A) with axial biotin and chloride ligands, cisplatin with one or two axial biotin ligands (Fig. 30B and C), as well as cisplatin with one axial biotin and the other axial was indomethacin ligands (Fig. 30D) to investigate the impact of biotin targeting on cytotoxicity and selectivity of Pt(IV) prodrugs.<sup>198-200</sup> Biotin-Pt(IV)-Cl (Fig. 30A) exhibited effective cytotoxicity against cancer cell lines (HepG2, MCF7, SGC-7901, and SGC-7901/Cis), which was 2.0–9.6-fold more potent than cisplatin.<sup>198</sup> It has cancer cell uptake better than that of cisplatin, especially in cisplatin-resistant SGC-7901/Cis cancer cells.<sup>198</sup> Moreover, it is reduced rapidly to cisplatin by glutathione or ascorbic acid under biologically relevant conditions.<sup>198</sup> In further study, Wang and co-workers investigated the cytotoxicity of the mono- and di-biotinylated Pt(IV) complexes (Fig. 30B and C) against the human breast cancer MCF-7 and MDA-MB-231 as well as human mammary epithelial MCF-10A/vector cell lines.<sup>199</sup> Both them exhibited time-dependent cytotoxicity, where at 72 h being stronger than that at 48 h. Mono-biotinylated Pt(IV) complex has comparable cytotoxicity to cisplatin against MCF-7 cells at 72 h, much higher cytotoxicity against cisplatin-insensitive MDA-MB-231 cells at 48 and 72 h, and around 4.2-4.5 fold less cytotoxic than cisplatin toward MCF-10A/vector cells at 48 and 72 h.<sup>199</sup> In general, the cytotoxicity of the di-biotinylated Pt (IV) complex was notably lower than that of the mono-biotinylated Pt(IV) complex and cisplatin against MCF-7 cells at 48 and 72 h but against MDA-MB-231 cells was higher than cisplatin at 48 and 72h, also still lower than the mono-biotinylated Pt(IV) complex.<sup>199</sup> Importantly, the cellular association levels (in terms of Pt distribution) of mono- and di-biotinylated Pt(IV) complexes in cancerous MCF-7 and MDA-MB-231 cell lines were much higher than cisplatin. In particular, the di-biotinylated Pt(IV) complexes > mono-biotinylated Pt(IV) complexes > cisplatin. While the platinum content in the non-cancerous MCF-10A/vector cell lines about five-fold lower than in the cancerous MCF-7 and MDA-MB-231 cells and around two-fold lower than cisplatin.<sup>199</sup> However, the platinum content and the cytotoxicity do not match up; for instance, the di-biotinylated Pt(IV) complex has the highest total platinum content but has the least cytotoxicity.<sup>199</sup> In short, adding one or two biotin groups to cisplatin increases the selectivity of the Pt(IV) prodrug toward cancerous cells that overexpress biotin receptors and reducing its content in non-cancerous tissues.<sup>199</sup> A Pt(IV) prodrug composed of biotin and COX inhibitor indomethacin (Fig. 30D) was developed by Gou and co-workers.<sup>200</sup> They investigated the cytotoxicity of this complex

against malignant cell lines HCT-116 (colorectal cancer), HepG-2 (hepatocellular carcinoma), PC-3 (prostate carcinoma), SGC7901 (gastric cancer), and SGC7901/CDDP (cisplatin-resistant gastric cancer) as well as against normal cell lines LO-2 (normal liver), and EA.hy926 (umbilical vein endothelial cell).<sup>200</sup> The biotin-Pt(IV)-indomethacin complex showed lesser activity than cisplatin on nearly all malignant cells. However, it showed maximum cytotoxicity towards the cisplatin-resistant cell line SGC7901/CDDP around 9-fold higher than cisplatin.<sup>200</sup> Moreover, it was 17- and 5-fold less toxic than cisplatin to normal cells LO-2 and EA.hy926, indicating a significant selectivity of biotin-Pt(IV)-indomethacin complex for cancer cells.<sup>200</sup>

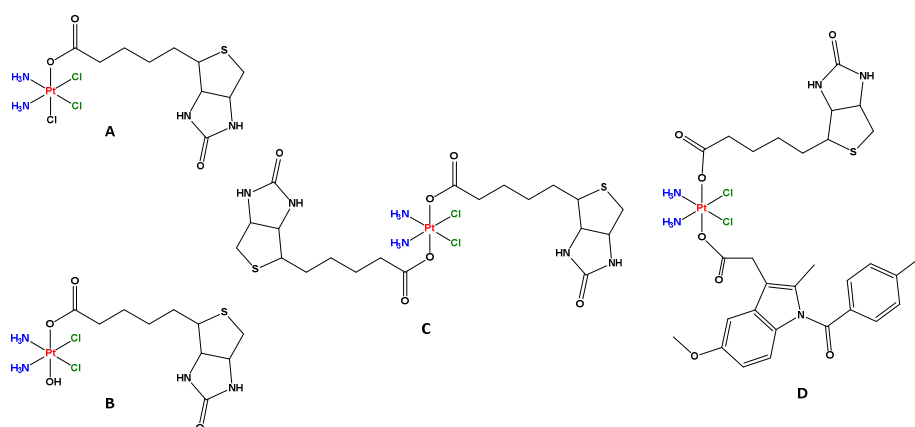


Fig. 30: Structure of Pt(IV) prodrugs based on biotin (A,<sup>198</sup> B,<sup>199</sup> C,<sup>199</sup> and D<sup>200</sup>).

#### h) Platinum(IV) prodrugs including axial ligands that targeting Estrogen Receptor (ER) and Androgen Receptor (AR)

The addition of estrogen to ER+ breast cancer cells increase the expression of HMGB1, which binds to the major cisplatin-DNA adducts 1,2-intrastrand d (GpG) and d(ApG) cross-links, inhibiting DNA repair by the NER and increasing the sensitivity of cancer cells to cisplatin.<sup>109</sup> Therefore, Lippard and co-workers designed a series of Pt(IV) derivatives with estrogen axial ligands, having general structure bis-estrogen-cis-diamminedichloroplatinum (IV). According to their finding, all the synthesized complexes induced overexpression of HMGB1 in ER+ MCF-7 cells compared with ER- HCC-1937 cells.<sup>201</sup> The Pt(IV)-estrogen complex (Fig. 31A) was 1.8-fold more cytotoxic to ER+ MCF-7 cells than it was to ER- HCC-1937 cells as predicted on the basis of the construct design.<sup>201</sup> Tamoxifen as a selective estrogen receptor modulator (SERM) has been widely used across all stages of breast cancer with positive estrogen receptors (ER+).<sup>37,52</sup> Gou's group reported four Pt(IV)-tamoxifen complexes, shown in (Figure 31B).<sup>202</sup> The Pt(IV)-tamoxifen complexes are selectively effective against MCF-7 (ER $\alpha$  positive breast cancer cells), while less effective against MDA-MB-231 (ER $\alpha$ -negative breast cancer cells).<sup>202</sup> Moreover, they could also reverse the tamoxifen resistance of the TamR-MCF-7 cell



line.<sup>202</sup> On the other hand, targeting androgen receptor (AR) which is overexpressed in castration-resistant prostate cancer (CRPC).<sup>203</sup> Pt(IV) prodrug targeting AR was reported also by Gou's group (Figure 31C), based on cisplatin with androgen antagonists (cyanonilutamide) and coumarin axial ligands.<sup>203</sup> This compound exhibited satisfactory AR binding affinity and antagonist activity. As a result of its AR affinity, it selectively accumulates in more abundant quantities in LNCaP (AR+) cells than in PC-3 (AR-) with more potency than cisplatin.<sup>203</sup>

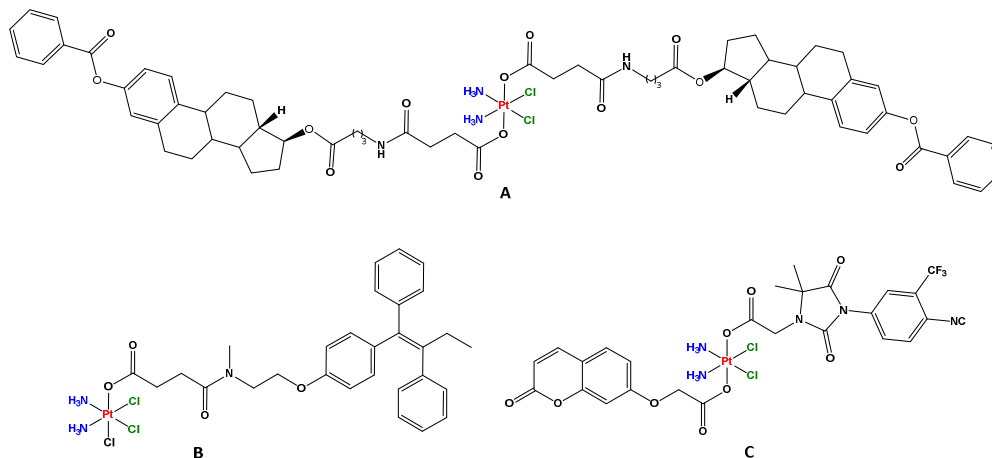


Fig. 31: Pt(IV) prodrugs targeting Estrogen Receptor (ER) (A,<sup>201</sup> and B<sup>202</sup>), and Androgen Receptor (AR) (C<sup>203</sup>).

i) Platinum(IV) prodrugs including FDA-approved bioactive axial ligands

Nitrogen mustards such as cyclophosphamide, and chlorambucil (ChB), have been approved by the FDA to treat chronic lymphocytic leukemia and other cancers as discussed before.<sup>61,62</sup> As with Pt(II) complexes, its clinical application was hindered by serious drug resistance and toxicities.<sup>61,62</sup> A series of Pt(IV)-chlorambucil derivatives with cisplatin, oxaliplatin, and carboplatin (Fig. 32A-D) were reported by Xu's and Gou's groups.<sup>204-206</sup> Xu's group showed the mono ChB-Pt(IV)-OH and bi ChB-Pt(IV)-ChB complexes based on cisplatin,<sup>204</sup> They exhibited significant antitumor activities against all the tested cancer cell lines, such as A549, HeLa, MCF-7, and MDA-MB-231 and were more potent than cisplatin or the combination of cisplatin and chlorambucil.<sup>204</sup> The ChB-Pt(IV)-ChB prodrug (Fig. 32A) penetrated cells at a much higher quantities than cisplatin, resulting in a greater damage to DNA which also provide the synergism between chlorambucil and cisplatin in targeting DNA.<sup>204</sup> Gou and co-workers showed ChB-Pt(IV)-Cl prodrugs based on cisplatin and carboplatin (Fig. 32C and D) respectively.<sup>205,206</sup> ChB-Pt(IV)-Cl based on cisplatin (Fig. 32C) displayed potent antitumor activity against both cisplatin-sensitive (HCT-116, HepG-2, SGC7901) and cisplatin-resistant (SGC7901/CDDP) cells lines.<sup>205</sup> This potent behavior was due to the improved cellular

uptake and the inhibition of PARP-1 protein which is involved in DNA repair.<sup>205</sup> In comparison with cisplatin, carboplatin, or chlorambucil, the ChB-Pt(IV)-Cl based on carboplatin (Fig. 32D) exhibited also superior antitumor activity against cisplatin-resistant cell lines SGC-7901/CDDP and A549/CDDP.<sup>206</sup> According to mechanistic studies, this compound exhibited such potent antitumor activity due to suppressing DNA damage repair and reversing drug resistance.<sup>206</sup>

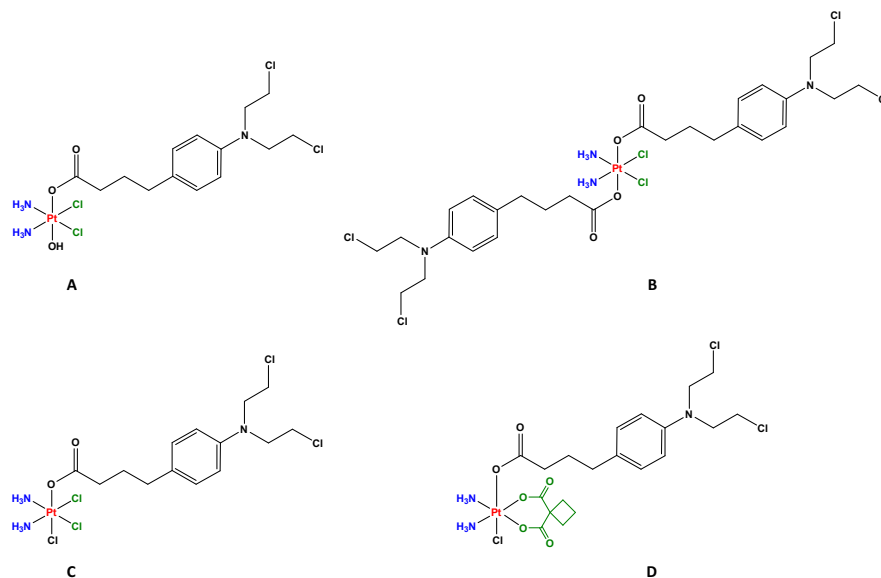


Fig. 32: Pt(IV) prodrugs based on chlorambucil (A,<sup>204</sup> B,<sup>204</sup> C,<sup>205</sup> and D<sup>206</sup>).

Gibson and co-workers reported a series of so-called dual-, triple-, and quadruple-action platinum(IV) prodrugs with one or two different FDA-approved bioactive axial ligands (Fig. 33A-D).<sup>207-209</sup> The  $[\text{Pt}(\text{NH}_3)_2(\text{Paclitaxel})(\text{OH})\text{Cl}_2]$  (Fig. 33A) is dual-action Pt(IV) prodrug based on cisplatin and mitotic inhibitor (paclitaxel), while  $[\text{Pt}(\text{NH}_3)_2(\text{Gemcitabine})(\text{PhB})\text{Cl}_2]$  (Fig. 33B) is triple-action prodrug base on cisplatin, antimetabolite (gemcitabine) and HDAC inhibitor (phenyl butyrate).<sup>207</sup> These compounds formed *via* carbonate bridge between the OH of the Pt(IV) and the OH of paclitaxel or gemcitabine.<sup>207</sup> Upon reduction of the Pt(IV), the carbonated ligand loses  $\text{CO}_2$  and generate the original bioactive molecules.<sup>207</sup> Both of them exhibited low nM  $\text{IC}_{50}$  values for a panel of cancer cells and  $[\text{Pt}(\text{NH}_3)_2(\text{Gemcitabine})(\text{PhB})\text{Cl}_2]$  prodrug was less toxic and more potent than gemcitabine, cisplatin, and co-administration of cisplatin and gemcitabine.<sup>207</sup> Gibson's group also reported a series of eight triple-action Pt(IV) prodrugs based on cisplatin with HDAC, COX, and PDK inhibitors:  $[\text{Pt}(\text{NH}_3)_2(\text{COXi})(\text{PDKi})\text{Cl}_2]$ ,  $[\text{Pt}(\text{NH}_3)_2(\text{COXi})(\text{HDACi})\text{Cl}_2]$  and  $[\text{Pt}(\text{NH}_3)_2(\text{HDACi})(\text{PDKi})\text{Cl}_2]$ , where COXi (aspirin or ibuprofen), HDACi (valproate or phenylbutyrate), and PDKi (dichloroacetate).<sup>208</sup> Most of these compounds were significantly more potent than cisplatin with average  $\text{IC}_{50}$  values against a panel of six cancer cell lines being 0.37–1.46  $\mu\text{M}$  compared to 12.5  $\mu\text{M}$  for

cisplatin. The most promising candidate among the eight studied compounds was  $[\text{Pt}(\text{NH}_3)_2(\text{DCA})(\text{PhB})\text{Cl}_2]$  (Fig. 33C), which is active against cisplatin- and oxaliplatin-resistant cell lines.<sup>208</sup> A quadruple-action Pt(IV) prodrug (Fig. 33D) that released four different bioactive moieties, cisplatin, Pt56MeSS, DCA, and PhB in KRAS-mutated cancer cells (Fig. 33D) was also reported by Gibson's group.<sup>209</sup> Compared with cisplatin, this Pt(IV) prodrug is 200-450-fold more effective against KRAS-mutated pancreatic and colon cancers, and 40-fold more selective towards KRAS mutated cells than normal cells.<sup>209</sup>

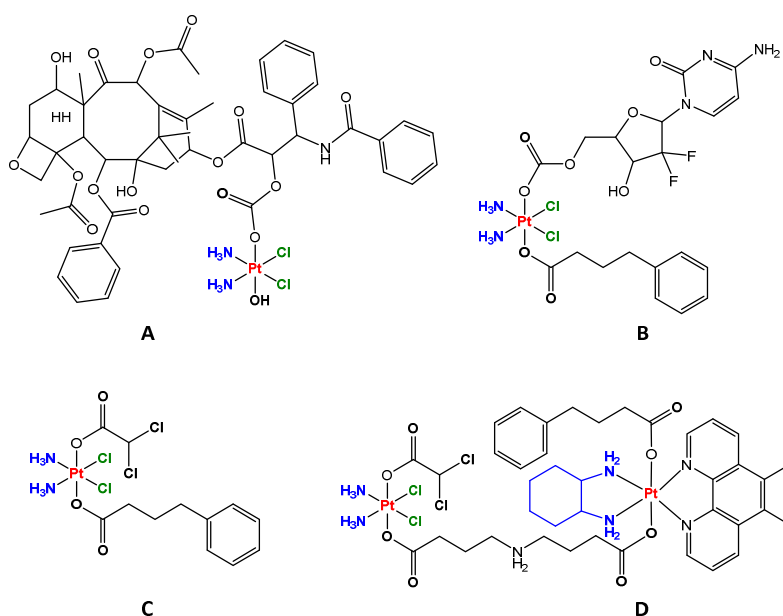


Fig. 33: Dual-, Triple-, and Quadruple-action platinum(IV) prodrugs (A,<sup>207</sup> B,<sup>207</sup> C,<sup>208</sup> and D<sup>209</sup> respectively).

### 3.11.3 Photoactivatable Pt(IV) prodrugs

Using photoactivatable groups to facilitate the release of desired active species upon irradiation is a promising cancer treatment strategy.<sup>20,21,157,210-212</sup> Recently, photoactivatable platinum(IV) prodrugs development has been significant to controllable spatiotemporal activation.<sup>157</sup> In the dark, these prodrugs are non-toxic and stable even in the presence of cellular reducing agents, but upon irradiation at specific wavelengths, they are efficiently reduced to toxic platinum(II) species. As a result, photoactivatable platinum(IV) prodrugs have a significantly lower level of off-target effects in normal tissues, as well as reduce side effects.<sup>210-212</sup> According to the structural scaffold of the prodrugs, photoactivatable platinum(IV) prodrugs can be divided into two classes. The first class is the diiodo- and diazido-Pt(IV) photoactive prodrugs and their derivatives. The second class is photoactivatable platinum(IV) prodrugs based on clinically approved platinum(II) drugs such as cisplatin, carboplatin and oxaliplatin.<sup>157</sup>

### a) Diiodo- and diazido-Pt(IV) photoactive prodrugs

The diiodo-Pt(IV) photoactive complexes bind irreversibly to DNA under visible light, and its photolysis products are cytotoxic to human cancer cells.<sup>210,212,213</sup> Even so, these complexes showed poor stability in the presence of biological reductants in the darkness, and there is no significant difference between dark and light toxicity (low phototoxic index).<sup>210-213</sup> Considering these drawbacks, further development of these types of complexes as photoactivatable anticancer agents was shelved.<sup>210-213</sup> According to Vogler's group in the 1980s, the diazido-Pt(IV) complexes undergo reductive elimination of azide ligands under irradiation.<sup>214</sup> In addition, they are highly stable against biological reductants and exhibit very low cytotoxicity in the dark, both desirable characteristics for photoactivatable drugs.<sup>215,216</sup> Intriguingly, the all-*trans* photoactive Pt(IV) prodrug, *trans,trans,trans*-[Pt(N<sub>3</sub>)<sub>2</sub>(OH)<sub>2</sub>(NH<sub>3</sub>)<sub>2</sub>] (Fig. 34B), exhibited higher aqueous solubility, more intense and red-shifted ligand-to-metal charge-transfer (LMCT) band compared with *cis,trans,cis*-[Pt(N<sub>3</sub>)<sub>2</sub>(OH)<sub>2</sub>-(NH<sub>3</sub>)<sub>2</sub>] isomer (Fig. 34A).<sup>216</sup> In the dark, both were not toxic to human skin cells (keratinocytes), but when irradiated with UVA light for 50 minutes, they were as cytotoxic as cisplatin.<sup>216</sup> In light of the outstanding properties of *trans*-diazido-Pt(IV) complexes, researchers formulated a series of *trans*-diazido-Pt(IV) complexes with various N-donor ligands, including aromatic N-donors and aliphatic amines, to explore the structure-activity relationship of Pt(IV) prodrugs and to find more potent photoactivatable ones. Among them, *trans,trans,trans*-[Pt(N<sub>3</sub>)<sub>2</sub>(OH)<sub>2</sub>(NH<sub>3</sub>)(Py)] complex (Fig. 34C), that exhibited superior photocytotoxicity and darkness stability even in the presence of glutathione.<sup>217</sup> Upon irradiation with UVA, it showed 80- and 15-fold higher photocytotoxicity in both cisplatin-sensitive A2780 cells and cisplatin-resistant A2780cisR cells respectively, compared with cisplatin.<sup>217</sup> As the above-mentioned complexes are activated by UV light, which limited their clinical application due to poor tissue penetration depth.<sup>157,210</sup> To extend the wavelength spectrum of photoactivation, *trans,trans,trans*-[Pt(N<sub>3</sub>)<sub>2</sub>(OH)<sub>2</sub>(py)<sub>2</sub>] complex (Fig. 34D) was developed, that can be photoactivated over a range of wavelengths.<sup>218</sup> When irradiated with visible light (420 nm), it demonstrated remarkable photocytotoxicity against some human cancer cell lines. In HaCaT cells, the IC<sub>50</sub> value was 9.5 μM under irradiation with a low dose of blue light, which was more powerful than cisplatin.<sup>218</sup> Taking advantage of the success of diazido-Pt(IV) photoactivatable prodrugs, in particular the *trans,trans,trans*-[Pt(N<sub>3</sub>)<sub>2</sub>(OH)<sub>2</sub>(py)<sub>2</sub>] complex, it is now possible to enhance their cytotoxicity by adding bioactive or targeting axial ligands. Recently, Sadler's group reported two biotinylated diazido-Pt(IV) complexes *trans,trans,trans*-[Pt(N<sub>3</sub>)<sub>2</sub>(biotin)(OH)(py)<sub>2</sub>] (Fig. 34E) and *trans,trans,trans*-[Pt(N<sub>3</sub>)<sub>2</sub>(biotin)(DCA)(py)<sub>2</sub>] (Fig. 34E) by conjugating either biotin or biotin and dichloroacetate (PDK inhibitor) to the axial position of the diazido-Pt(IV) complex.<sup>219</sup> They

exhibited high dark stability and promising photocytotoxicity against A2780 ovarian, A549 lung, and PC3 prostate cancer cells upon irradiation with low-dose blue light (465 nm, 4.8 mW cm<sup>-2</sup>, 1h), with high photocytotoxicity indices.<sup>219</sup> Furthermore, the photoreactions of the two biotinylated diazido-Pt(IV) complexes with guanosine monophosphate (5'-GMP) at 310 K in the dark for 1 h, then irradiated by blue light (420 nm) for 1 h resulted in the formation of the monofunctional [Pt<sup>II</sup>(CH<sub>3</sub>CN)(py)<sub>2</sub>(GMP-H)]<sup>+</sup> as the major Pt-GMP product.<sup>219</sup>

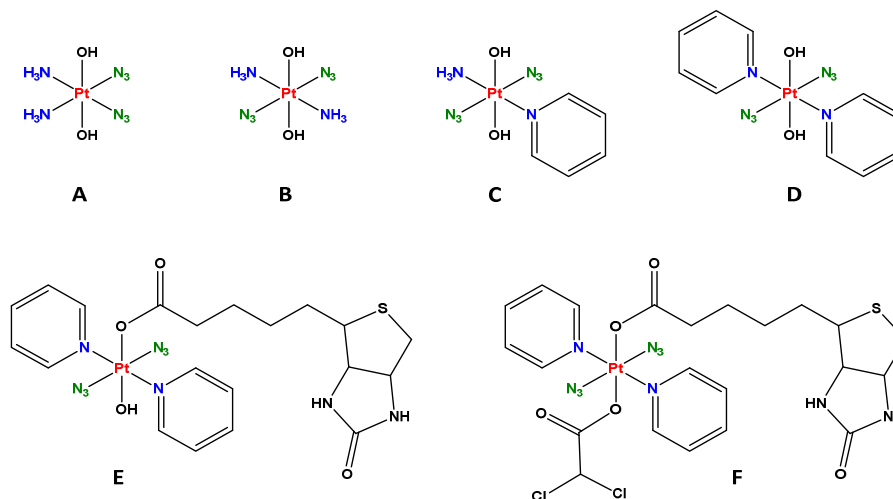


Fig. 34: Diazido-Pt(IV) photoactive prodrugs (A,<sup>216</sup> B,<sup>216</sup> C,<sup>217</sup> D,<sup>218</sup> E,<sup>219</sup> and F<sup>219</sup>).

b) Photoactivatable platinum(IV) prodrugs based on clinically approved platinum(II) drugs

Recently, many publications have focused on the functionalization of platinum(IV) prodrugs with photosensitizer axial ligands to control both the photoactivation and photoreduction of platinum(IV) prodrugs.<sup>220-222</sup> Based on this hypothesis, Zhu's group reported two potent photoactivatable Pt(IV) prodrugs, phorbiplatin and BODI-Pt.<sup>220,221</sup> Phorbiplatin (Fig. 35A) is a red light photoactivatable Pt(IV) prodrug based on oxaliplatin and pyropheophorbide A (PPA) at axial position.<sup>220</sup> Pyropheophorbide and its derivatives are used as photosensitizers for photodynamic therapy (PDT) *in vivo* and as photocatalysts to catalyze redox reactions *via* electron transfer under irradiation.<sup>223</sup> As expected, phorbiplatin was stable in the dark in both buffers and cell lysates, whereas under low-intensity red light irradiation (650 nm, 7 mW/cm<sup>2</sup>), it rapidly reduced to oxaliplatin by reducing agents such as ascorbic acid or GSH.<sup>220</sup> Furthermore, phorbiplatin was non-toxic toward A2780, A2780cisR and MCF-7 cancer cells (IC<sub>50</sub> > 10 μM) in the darkness.<sup>220</sup> While the IC<sub>50</sub> values of treated cells A2780, A2780cisR, and MCF-7 after irradiation with red light were 0.13 μM, 0.19 μM, and 0.044 μM respectively, which were 523-, 974-, and 1786-fold lower than those of oxaliplatin, respectively.<sup>220</sup> The BODI-Pt(IV)

prodrug (Fig. 35B) is a green light activatable carboplatin-based Pt(IV) prodrug, with boron dipyrromethene photosensitizer axial position.<sup>221</sup> It was quite stable in a PBS buffer even in the presence of reducing agents such as ascorbate but was easily reduced to carboplatin upon irradiated with green light (13 mW/cm<sup>2</sup>).<sup>221</sup> In the darkness, the BODI–Pt(IV) was not toxic to normal cells, but it was more toxic to cancer cells than carboplatin.<sup>221</sup> For instance, in MCF-7 cells, BODI-Pt showed 11 times higher cytotoxicity than carboplatin under dark conditions and 39 times higher cytotoxicity under irradiation conditions.<sup>221</sup> Gibson and Gasser reported recently a multi-action photoactivatable cisplatin-based Pt(IV) prodrug, with Ru(II) polypyridine complex as a photosensitizer and phenylbutyrate as HDAC inhibitor at axial positions (Fig. 35C).<sup>222</sup> The [Ru(4,7-diphenyl-1,10-phenanthroline)<sub>2</sub>(4,4'-dimethyl-2,2'-bipyridine)]<sup>2+</sup> complex used as photosensitizer, also it exhibited a photo-toxic effect from 480 nm up to clinically relevant 595 nm.<sup>224</sup> The Pt(IV) prodrug showed higher cytotoxicity in the cancerous cell line (HeLa) compared to the noncancerous cell line (RPE-1) in the dark as well as upon irradiation at 480 or 595 nm.<sup>222</sup> Furthermore, it exhibited remarkable photocytotoxicity in the μM range against human ovarian carcinoma (A2780) cells, and its cisplatin-resistant line (A2780 cis) as well as its doxorubicin-resistant line (A2780 ADR) upon irradiation at 480 or 595 nm and was more potent than cisplatin.<sup>222</sup> This novel approach of combining Pt(IV) prodrug and photosensitizer has a great potential for further development of photodynamic therapy (PDT).

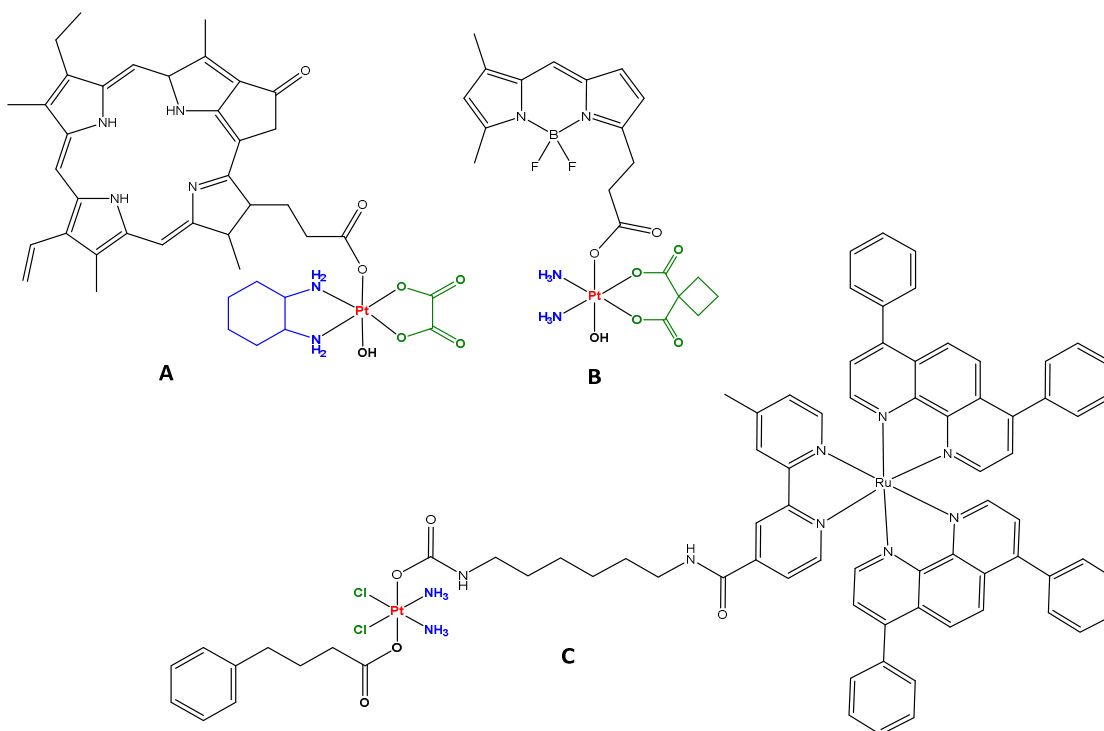


Fig. 35: Pt(IV) prodrug including photosensitizer at axial position (A,<sup>220</sup> B,<sup>221</sup> and C<sup>222</sup>).

### 3.12 Cinnamic Acid and its Derivatives

Bioactive phytochemical compounds that play an essential role in the development, reproduction, and defense system of various plant species, have significant potential for use as therapeutic agents.<sup>225-227</sup> Among the numerous classes, cinnamic acid and its derivatives such as *p*-coumaric, caffeic, chlorogenic, ferulic, and sinapic acids (Fig. 36).<sup>225-227</sup> Where they showed several potential therapeutic activities including anti-inflammatory, antiviral, antibacterial, antifungal, antioxidant, and anticancer activities.<sup>225-227</sup> Cinnamic acid is found in vegetal species, especially *Cinnamomum cassia* (Chinese cinnamon).<sup>227</sup> It is one of the auxins plant hormones that regulate cell growth and differentiation, and often displays a low toxicity level to several living organisms.<sup>227</sup> Natural hydroxyl cinnamates are essential constituents of the biochemical pathway that forms lignin, the second most abundant biopolymer after cellulose.<sup>227</sup> Furthermore, they are highly effective antitumor agents.<sup>225-227</sup> Cinnamic acid and its derivatives possess three main reactive sites: aromatic ring available for substituent, carboxylic acid for functionality, and  $\alpha,\beta$ -unsaturated carbonyl moiety (Michael-acceptor) which is an active moiety often employed in the design of anticancer drugs.<sup>227,228</sup>

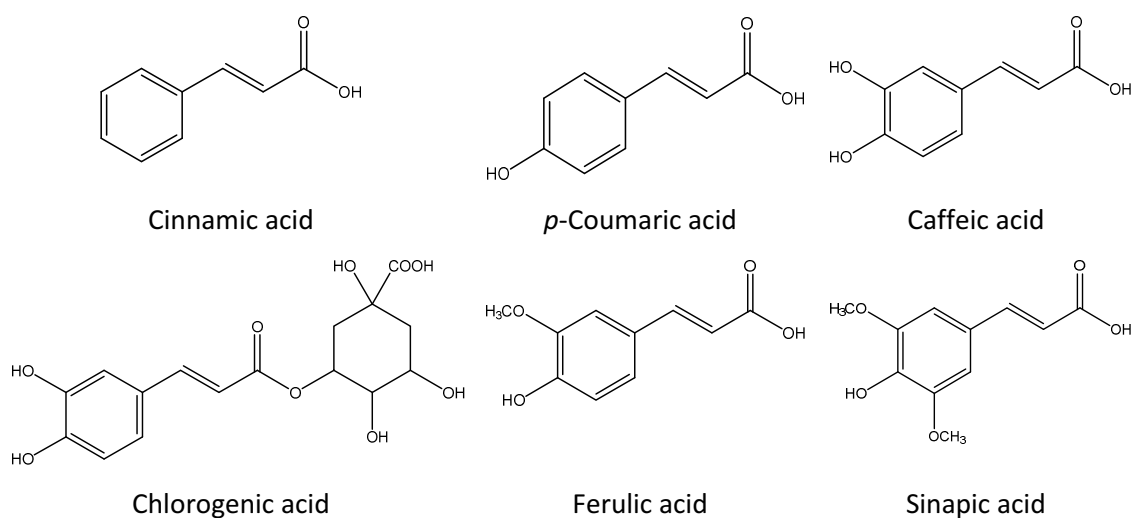
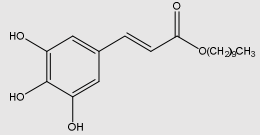
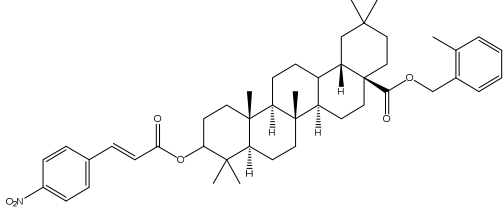
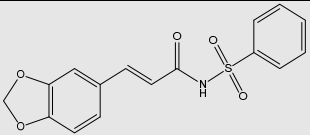
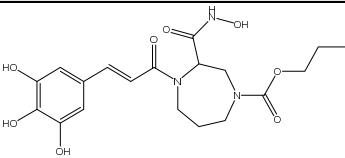
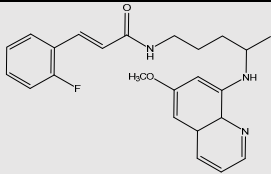
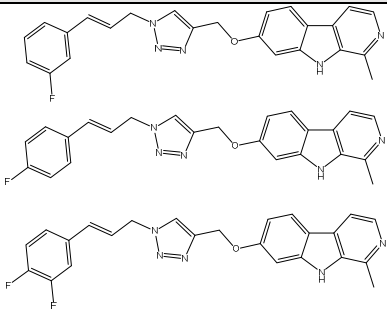
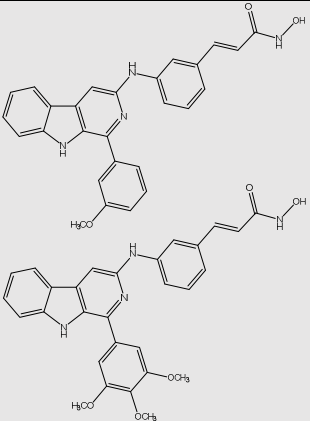


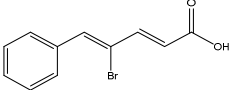
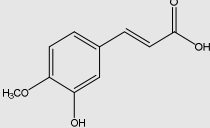
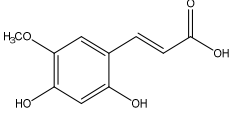
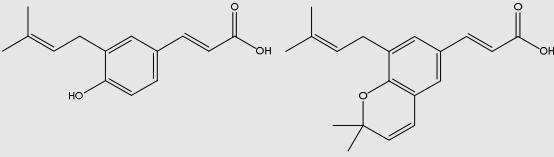
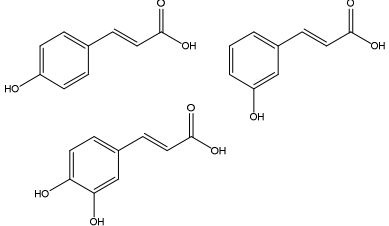
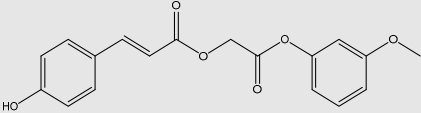
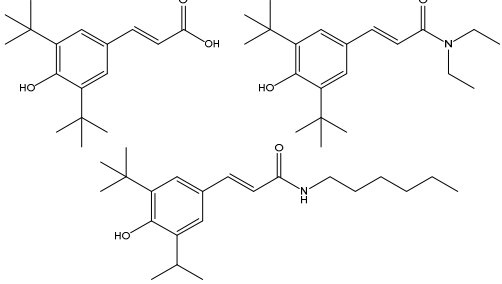
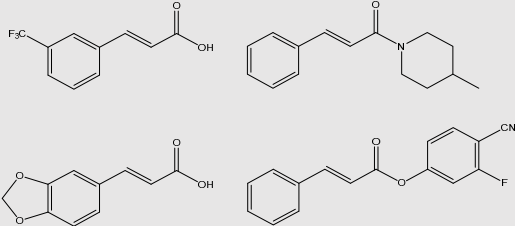
Fig. 36: Cinnamic acid and some of its natural derivatives.<sup>225-227</sup>

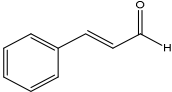
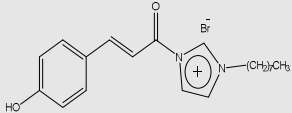
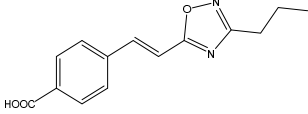
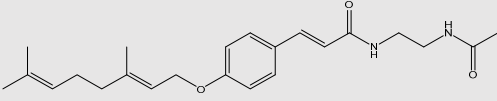
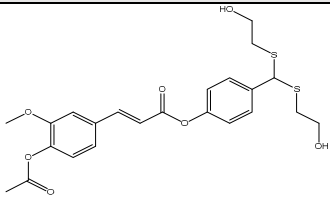
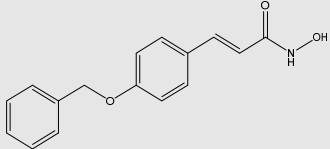
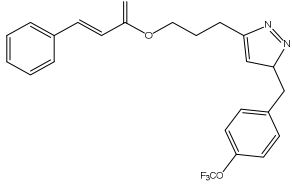
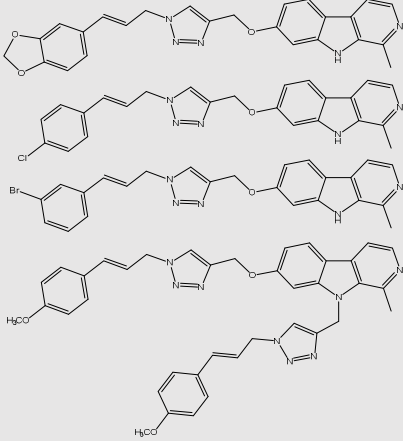
Several synthetic routes have been successfully used to synthesize cinnamic acid and its derivatives in large quantities. Additionally, they have several therapeutic applications against diabetes, infectious diseases, and degenerative diseases as well as antioxidant and anticancer activities, which made them candidates for therapeutic agents.<sup>225,226,229-231</sup> Some examples of the recent reported potent bioactive cinnamic acid derivatives are shown in Table 3.

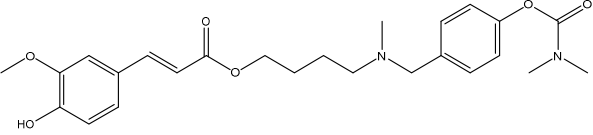
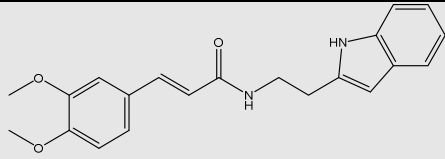
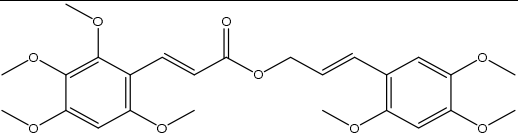
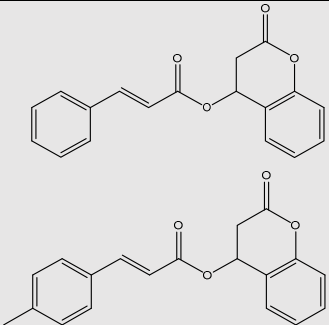
Table 3: Bioactive cinnamic acid derivatives.

Structure	Bioactivity	Mechanism of action	Ref
	Anticancer (Breast and prostatic)	Cell growth inhibition via apoptosis	232
	Anticancer (Cervical)	Apoptosis and autophagy	229
	Anticancer (Breast)	Tubulin inhibitor	233
	Anticancer (Lung)	Matrix metalloproteinase inhibitor	234
	Anticancer (Breast)	Cell growth inhibition via apoptosis	235
	Anticancer (Liver)	-	236
	Anticancer (Hepatocellular carcinoma)	HDAC-inhibitors	237



	Antioxidant	Lipid peroxidation inhibition	238
	Antioxidant	Lipid peroxidation inhibition	239
	Antioxidant	Lipid peroxidation inhibition	240
	Antioxidant	Lipid peroxidation inhibition	241
	Melanogenic regulator	Tyrosinase Inhibition	242
	Melanogenic regulator	Tyrosinase Inhibition	243
	anti-inflammatory	COX-2 inhibitors	244
	Antifungal ( <i>Cochliobolus lunatus</i> , <i>Aspergillus niger</i> , and <i>Pleurotus ostreatus</i> )	CYP53A15 Inhibition	245

	<p>Antimicrobial (<i>Escherichia coli</i>, <i>Staphylococcus aureus</i>, and <i>Enterococcus hirae</i>)</p>	<p>- 246</p>
	<p>Antimicrobial (<i>Staphylococcus aureus</i>, and <i>Staphylococcus epidermidis</i>)</p>	<p>- 247</p>
	<p>Antitubercular (<i>Mycobacterium tuberculosis</i>)</p>	<p>- 248</p>
	<p>Antitubercular (<i>Mycobacterium tuberculosis</i>)</p>	<p>- 249</p>
	<p>Anti-Tobacco mosaic virus (TMV)</p>	<p>TMV-CP binding 250</p>
	<p>Anti-hepatitis C virus (HCV)</p>	<p>HDACs-inhibitor 251</p>
	<p>Anti-leishmanial</p>	<p>Leishmania braziliensis 252</p>
	<p>Antimalarial</p>	<p>Plasmodium falciparum 236</p>

	Alzheimer's disease	ChEs-inhibitor	253
	Alzheimer's disease	AChE-inhibitor	254
	Anticonvulsant	LDH-inhibitor	255
	Antidiabetic Activity	$\alpha$ -Glucosidase Inhibitor	256

### 3.13 Motivation

The FDA-approved platinum(II) drugs cisplatin, carboplatin, and oxaliplatin, are the mainstays of present chemotherapy regimens. Nevertheless, there are a variety of severe side effects, including nephrotoxicity, neurotoxicity, ototoxicity, and nausea as well as the problems of drug resistance and dosage limitations.<sup>92-94,110,147,148</sup> In addition, the current platinum(II) drugs are all administered intravenously, where they can interact with blood components, including human serum albumin (HSA), the most abundant protein in the human bloodstream, that inhibits the action of platinum(II) drugs.<sup>92-94</sup> In the cytoplasm, the activated drug species bind to cytoplasmic sulfur-containing nucleophiles such as glutathione (GSH), metallothionein, methionine, and other cysteine-rich proteins before the DNA binding.<sup>94,110</sup> Consequently, these nucleophilic species act as scavengers, decreasing the availability of reactive species and contributing to drug resistance.<sup>94,110</sup> Further, most of the side effects can be attributed to unselective biomolecules binding especially the sulfur-containing nucleophiles, and the accumulation in both normal and cancerous tissues. Cisplatin, carboplatin, and oxaliplatin have a general formula  $cis-PtA_2X_2$ , where the soft Pt(II) center coordinated to non-leaving group (A) ammonia for cisplatin and carboplatin and 1R,2R-DACH for oxaliplatin, as well as chloride, 1,1-cyclobutanedicarboxylate and oxalate as an anionic leaving group (X) for cisplatin,

carboplatin, and oxaliplatin, respectively. Both the non-leaving and the leaving groups possess nitrogen, chloride or oxygen donor atoms and are classified as hard lewis bases, thus leads to substitution of the leaving groups by the soft biomolecular sulfur-containing nucleophiles according to the hard and soft acids and bases (HSAB) principle. Therefore, using non-leaving groups that contains soft donor atoms might reduce the affinity of the platinum(II) complexes towards biomolecular sulfur donors. In this work, we present a design of platinum(II) complexes based on antisymbiosis (trans effect), and HSAB principles, with the aim of reducing the affinity of the synthesized platinum(II) complexes towards sulfur-containing nucleophiles, thus reducing the side effects as well as overcoming the drug inhibition and resistance drawbacks. Nowadays, cinnamic acid and its derivatives showed several potential therapeutic activities as discussed before.<sup>225-227,229-256</sup> Furthermore, the  $\beta$ -hydroxydithiocinnamic acid derivatives act as non-leaving bidentate chelating ligands for the synthesis of platinum (II) complexes and have been well established within the Weigand group,<sup>257-266</sup> and are now attracting interest from others.<sup>267-270</sup> Inspired by the promising results obtained from the different  $\beta$ -hydroxydithiocinnamic acid metal complexes and as an extension of our group work, we are interested in the synthesis of different designs from  $\beta$ -hydroxydithiocinnamic ester ligands, which can be utilized in the following three projects:

**Project 1.** Synthesis, Characterization, 9-MeG binding, and Antiproliferative Activity of Homoleptic and Heteroleptic Pt(II)  $\beta$ -oxodithiocinnamic ester Complexes (Fig. 37).

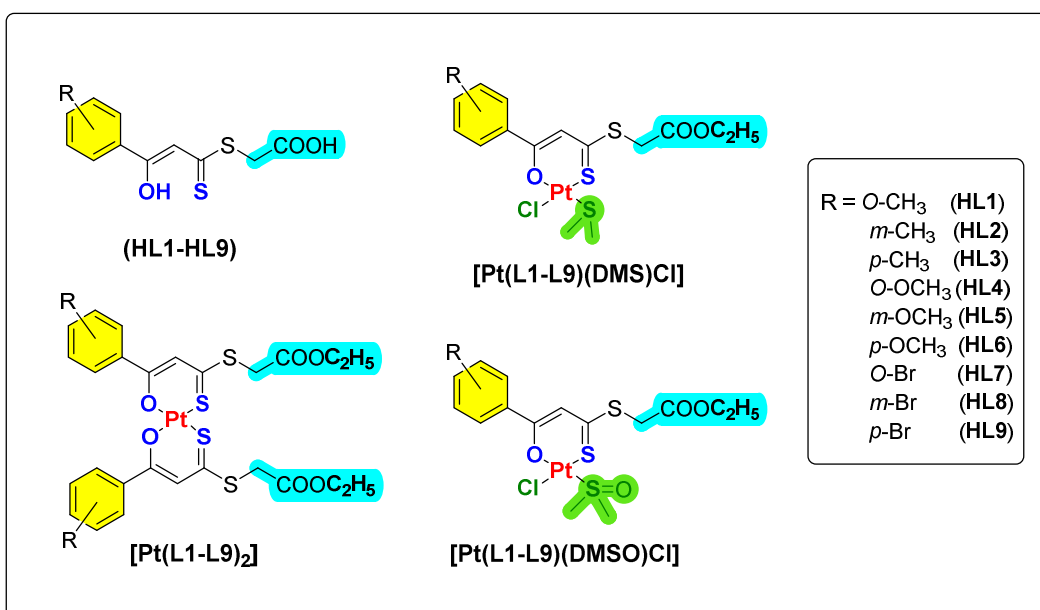


Fig. 37: Structure of  $\beta$ -hydroxydithiocinnamic ester ligands HL1-HL9 and their corresponding complexes  $[\text{Pt}(\text{L1-L9})_2]$ ,  $[\text{Pt}(\text{L1-L9})(\text{DMS})\text{Cl}]$ , and  $[\text{Pt}(\text{L1-L9})(\text{DMSO})\text{Cl}]$ .

- 1- Synthesis and characterization of  $\beta$ -hydroxydithiocinnamate- $\beta'$ -acetic acid ligands (HL1-HL9), as a first set of ligands.
- 2- Synthesis and characterization of the homoleptic bis-chelate complexes  $[\text{Pt}(\text{HL1-HL9})_2]$ , as well as the heteroleptic mono-chelate complexes with dimethyl sulfide  $[\text{Pt}(\text{L1-L9})(\text{DMS})\text{Cl}]$  or dimethyl sulfoxide  $[\text{Pt}(\text{L1-L9})(\text{DMSO})\text{Cl}]$  and one chloride ligands as leaving groups.
- 3- Molecular structures determination of the free ligands, the homoleptic and heteroleptic complexes.
- 4- Investigation of the reaction between the synthesized Pt(II) complexes and 9-methylguanine (9-MeG) as a DNA model.
- 5- Cytotoxic screening of the synthesized Pt(II) complexes.

**Project 2.** Synthesis, Characterization, 9-MeG binding, and Antiproliferative Activity of Heteroleptic Pt(II) and Homoleptic Pd(II)  $\beta$ -hydroxydithioesters ferrocenyl Complexes (Fig. 38).

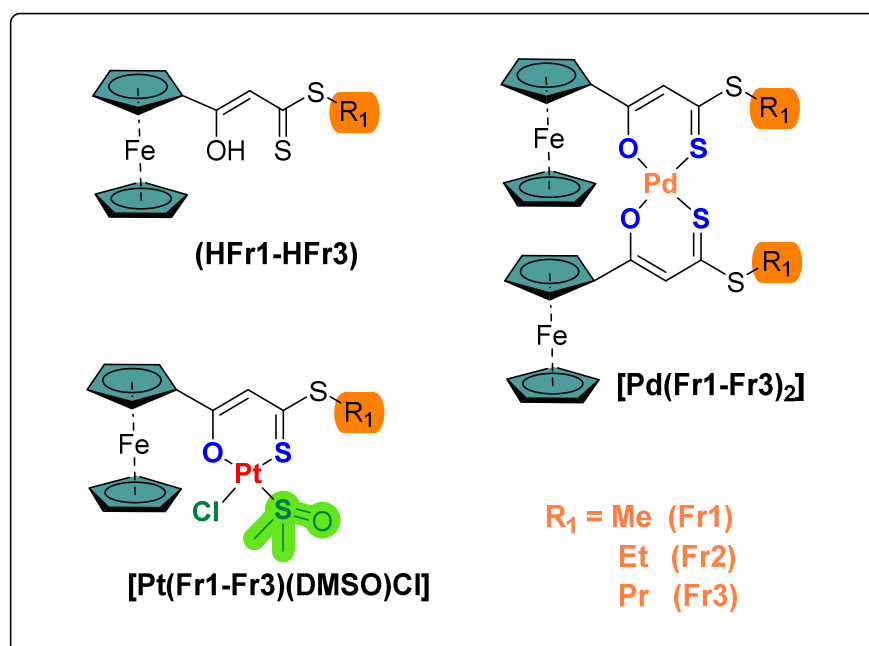


Fig. 38: Structure of  $\beta$ -hydroxydithioesters ferrocenyl ligands HFr1-HFr3 and their corresponding complexes  $[\text{Pt}(\text{Fr1-Fr3})(\text{DMS})\text{Cl}]$ , and  $[\text{Pd}(\text{Fr1-Fr3})_2]$ .

- 1- Synthesis and characterization of  $\beta$ -hydroxydithioesters ferrocenyl ligands (HFr1-HFr3), as ferrocene mimics of the  $\beta$ -hydroxydithiocinnamic acid derivatives.
- 2- Synthesis and characterization of the heteroleptic mono-chelate complexes  $[\text{Pt}(\text{Fr1-Fr3})(\text{DMSO})\text{Cl}]$  with dimethyl sulfoxide and a chloride ligands as leaving groups, as well as the homoleptic bis-chelate complexes  $[\text{Pd}(\text{Fr1-Fr3})_2]$ .

- 3- Molecular structures determination of the homoleptic Pd(II) and the heteroleptic Pt(II) complexes.
- 4- Investigation of the reaction between the synthesized Pt(II) complexes and 9-methylguanine (9-MeG) as a DNA model.
- 5- Cytotoxic screening of the synthesized compounds.

**Project 3.** Dual Function of  $\beta$ -hydroxydithiocinnamic esters: RAFT Agent and Ligand for Metal Complexation (Fig. 39).

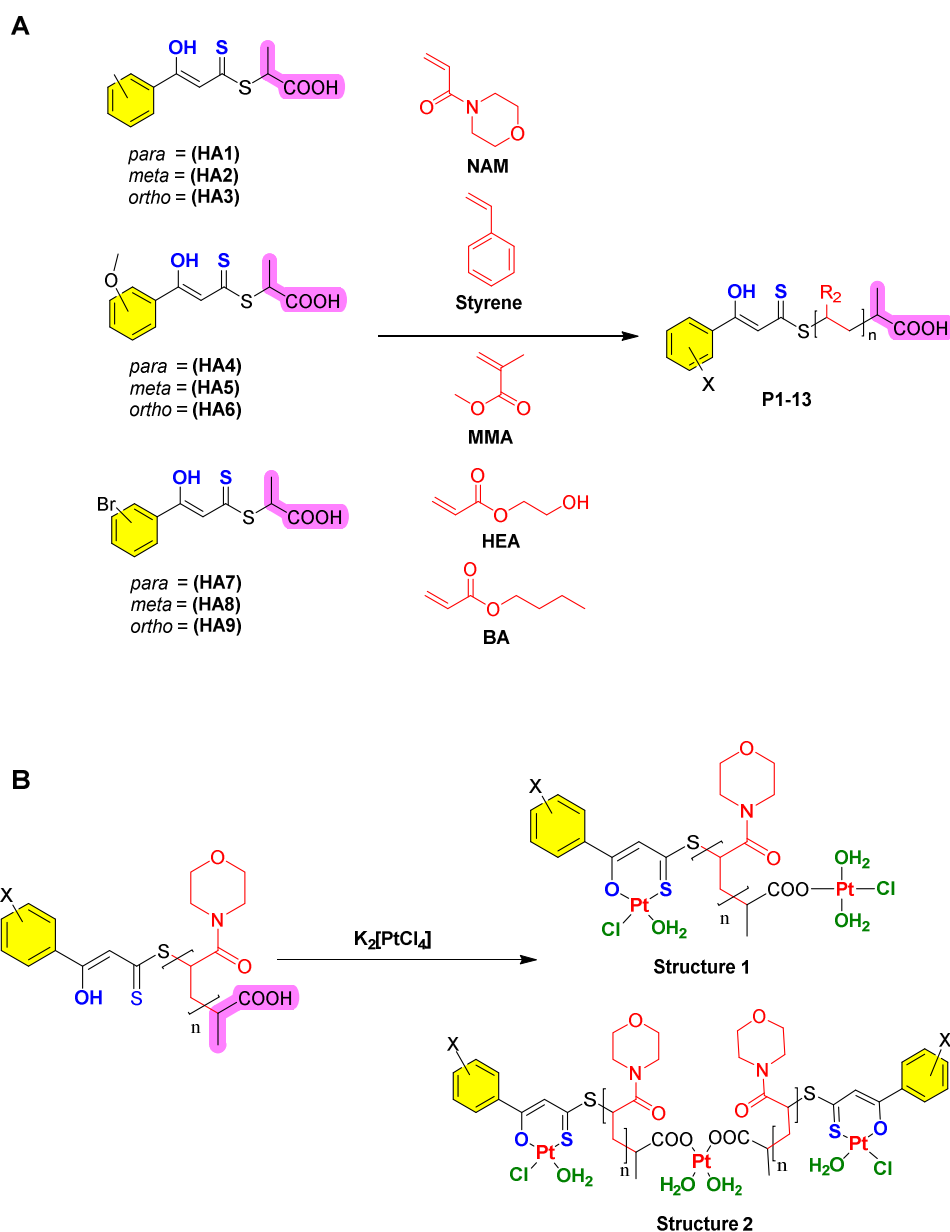
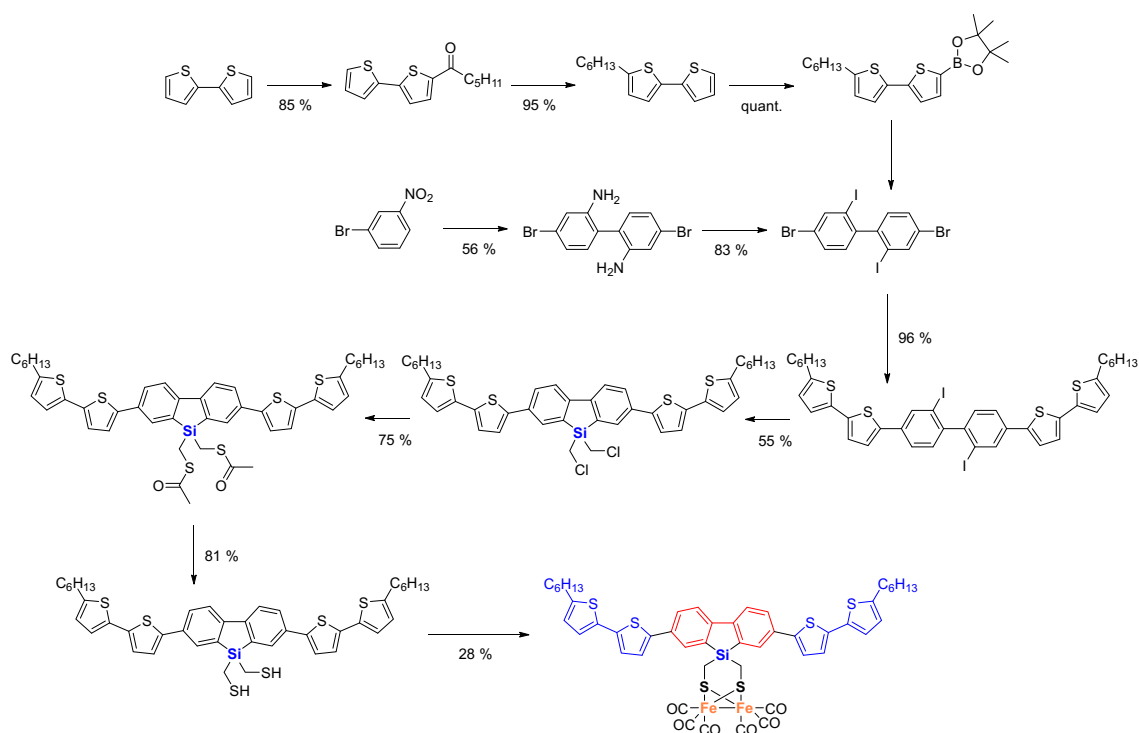


Fig. 39: A) Chemical structures of the ligands, monomers, and the resulting polymers (P1-P13); B) The two potentially formed structures during the complexation of Pt(II) by the RAFT-polymers based on NAM.

- 1- Synthesis and characterization of  $\beta$ -hydroxydithiocinnamate- $\beta'$ -2- propionic acid ligands (HA1-HA9), which utilized as CTA agents for RAFT polymerization of acrylates, acrylamides, and styrene.
- 2- Polymerizations (the tested monomers include the acrylates n-butyl acrylate (BA) and 2-hydroxyethyl acrylate (HEA), the acrylamide N-acryloyl morpholine (NAM), and styrene).
- 3- Synthesis and characterization of the Pt(II) complexes from the water-soluble N-acryloylmorpholine- $\beta$ -hydroxydithiocinnamate- $\beta'$ -2-propionic acid polymers (Dual Function).
- 4- Cytotoxic screening of the synthesized compounds.

**Project 4.** During my work, project 4 is a side project that focuses on synthesis, characterization, and photoactivity of a photoactive [FeFe] Hydrogenase mimic for hydrogen evolution under visible light irradiation.



Scheme 5: Synthetic pathway of the photoactive [FeFe] Hydrogenase mimic.

## 4. Result and Discussion

### 4.1 $\beta$ -Hydroxydithiocinnamic esters

$\beta$ -Hydroxydithiocinnamic esters are derivatives from the  $\beta$ -oxodithioesters.<sup>271</sup> In addition,  $\beta$ -oxodithioesters are highly efficient intermediates in organic synthesis and considered parallel synthons for  $\beta$ -ketoester chemistry.<sup>271-275</sup> Where,  $\beta$ -Hydroxydithiocinnamic esters contain polyfunctional groups with three nucleophilic and two electrophilic centers, as shown in Figure 40 A, and B. Synthons containing both electrophilic and nucleophilic centers have significant potential to use as a valuable building block in the synthesis of various heterocyclic systems.<sup>272-275</sup>  $\beta$ -Hydroxydithiocinnamic esters exhibit keto-enol tautomerism (Fig.40 A and B), that is shifted towards the enol form due to the high electronegativity of the  $\beta$ -keto group that makes the  $\alpha$ -protons more acidic.<sup>271</sup> The enol form is stabilized by intramolecular hydrogen bonding and the conjugated system (Fig. 40 C).

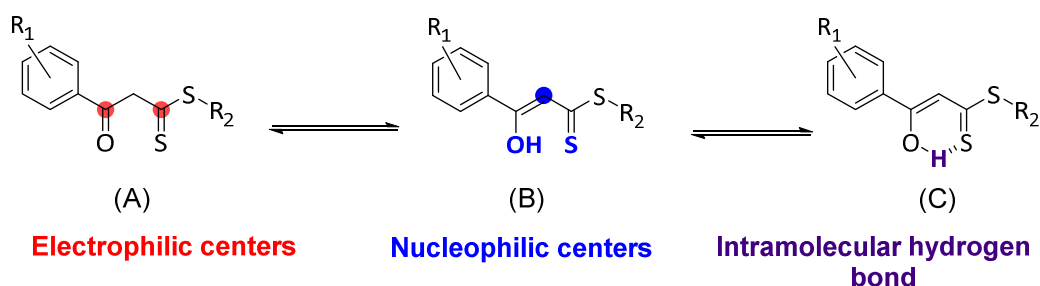
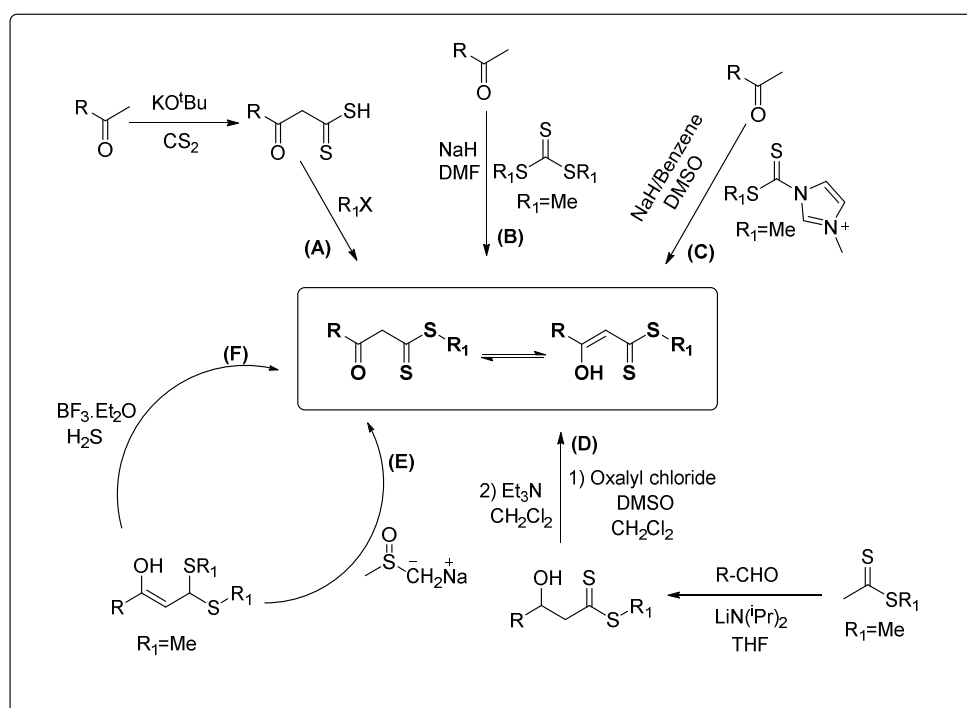


Fig. 40: Structure of  $\beta$ -hydroxydithiocinnamic ester derivatives (Electrophilic, Nucleophilic centers, and the intramolecular hydrogen bond).

Several synthetic methods have been described for the synthesis of  $\beta$ -oxodithioesters, the most prominent ones are shown in Scheme 6.<sup>276-281</sup> Thuillier et al. utilize enolizable ketones as acetophenone derivatives that, when treated with a strong base, generate active methylene compounds, which further react with  $CS_2$  to provide the sodium salt of dithiocarboxylic acid that can be alkylated to the respective  $\beta$ -oxodithioesters (Scheme 6A).<sup>276</sup> Another convenient method was described by Junjappa and co-workers, in which the active methylene ketones were treated with (S,S)-dimethyltrithiocarbonate in a DMF-hexane mixture affording the desired  $\beta$ -oxodithioesters (Scheme 6B).<sup>277</sup> Also, Junjappa et al., by using 3-methylimidazolium-1-carbodithioic acid methyl ester instead of (S,S)-dimethyltrithiocarbonate with active methylene compounds,  $\beta$ -oxodithioesters can be also obtained (Scheme 6C).<sup>278</sup> Another method described by Beslin and Houtteville, through regiocontrolled condensation of dithioester with aldehyde, followed by oxidation to the corresponding  $\beta$ -oxodithioesters (Scheme 6D).<sup>279</sup> Alternatively,  $\beta$ -oxodithioesters can also be obtained from the selective demethylation of  $\alpha$ -



oxoketene-S,S-dithioacetals using sodium methylsulfinylmethylide (dimsyl sodium), reported by Nair and co-workers (Scheme 6E).<sup>280</sup> In addition, they conducted a convenient method, which involves sulfo-hydrolysis of the  $\alpha$ -oxoketene-S,S-dithioacetals using hydrogen sulfide catalyzed by  $\text{BF}_3 \cdot \text{Et}_2\text{O}$  to the respective  $\beta$ -oxodithioesters (Scheme 6F).<sup>281</sup> It is worth mentioning that the  $\beta$ -hydroxydithiocinnamic esters derivatives used in projects 1 and 3 were prepared according to the Thuillier method with some modifications, while those used in project 2 were prepared according to the method described by Junjappa and co-workers also with modifications.



Scheme 6: Synthetic pathways of  $\beta$ -oxodithioesters derivatives.

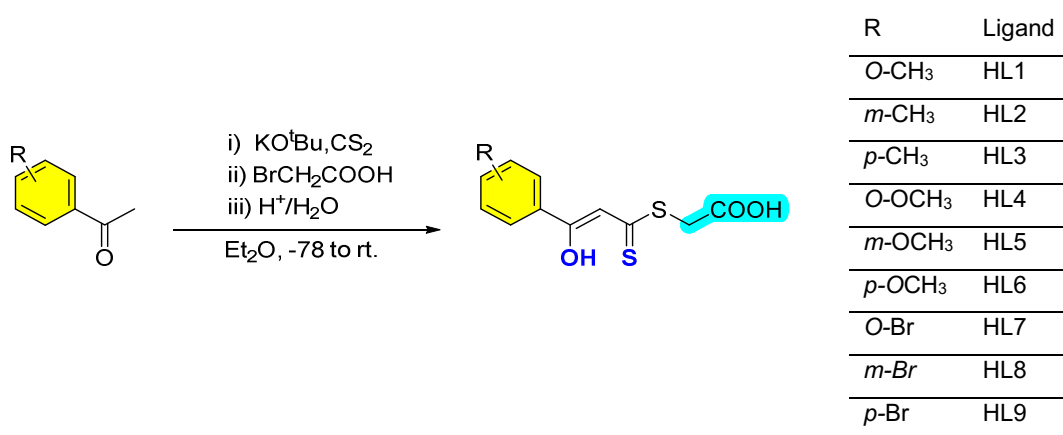
#### 4.2 Project 1. Novel Homoleptic and Heteroleptic Pt(II) $\beta$ -oxodithiocinnamic ester Complexes: Synthesis, Characterization, Interactions with 9-methylguanine and Antiproliferative Activity

Utilizing the  $\beta$ -hydroxydithiocinnamic acid derivatives as O,S-binding bidentate chelating ligands for the synthesis of several nickel(II), palladium(II), platinum(II), ruthenium(II), and osmium(II) complexes which possess anticancer activities, have been well established in the Weigand group.<sup>257-266</sup> Inspired by the promising results obtained,

we are interested in the synthesis of new designs from  $\beta$ -hydroxydithiocinnamic ester ligands and their potentially cytotoxic platinum(II) complexes.

#### 4.2.1 Synthesis and characterization of $\beta$ -hydroxydithiocinnamic ester Ligands (HL1-HL9)

Acetophenone derivatives were first treated with potassium tert-butoxide and then  $\text{CS}_2$  to obtain the sodium salt of dithiocarboxylic acid that can be reacted in situ with 2-bromoacetic acid instead of the normal alkyl halide as established in the Thuillier synthetic methods, affording finally the new class of  $\beta$ -hydroxydithiocinnamic ligands (HL1-HL9), bearing *O*-/*m*-/*p*-( $\text{CH}_3$ ,  $\text{OCH}_3$ , or Br) as substituent R in the phenyl ring (Scheme 7).



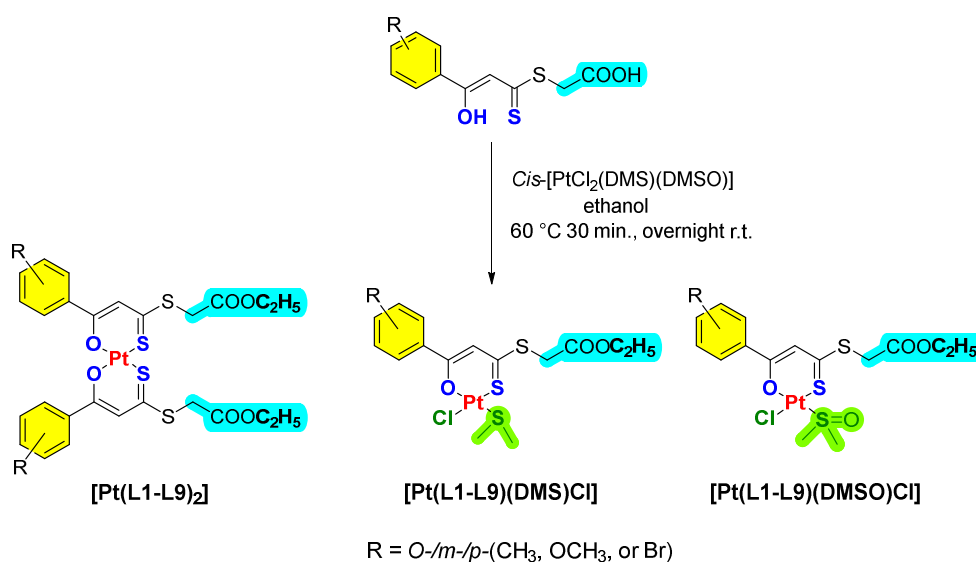
Scheme 7: Synthesis of  $\beta$ -hydroxydithiocinnamic ligands (HL1-HL9).

All ligands were obtained in moderate yield, which is higher in case of *ortho* and *para*-substituted ligands than the *meta*-substituted ones. Moreover, they are characterized by different NMR spectroscopy, mass spectrometry, and elemental analysis. Recrystallization of HL3 produced suitable single crystals for X-ray diffraction studies. The most characteristic signals in the NMR spectra of the free ligands HL1–HL9 are as follows. First, in the  $^1\text{H}$  NMR spectra, HL1-HL9 display a single resonance in the range  $\delta$  14.49-15.17 ppm belonging to the hydroxyl group ( $-\text{OH}$ ) proton. whereas the methine proton ( $=\text{CH}-$ ) was found at  $\delta$  6.66-7.44 ppm. A single resonance at  $\delta$  11.40-13.07 ppm corresponds to the ( $-\text{COOH}$ ) proton. In the  $^{13}\text{C}\{^1\text{H}\}$  NMR spectra, resonances for the ( $\text{C}-\text{OH}$ ) carbon were found in the range  $\delta$  168.91–174.11 ppm. The methine ( $=\text{CH}-$ ) carbon of the free ligands was found in the range  $\delta$  106.64–111.22 ppm. And the quaternary thiocarbonyl carbon ( $\text{C}=\text{S}$ ) was found at  $\delta$  213.50–216.37 ppm. Furthermore, these ligands show some interesting features: (i) O,S-bidentate chelating ligand, (ii) keto-enol tautomerism, (iii) having both hard oxygen and soft sulfur donor atoms, and (iv) the different functional groups on the benzene ring and terminal carboxylic group which may influence the electronic and steric properties. In view of these features, we now present

the synthesis of the homoleptic and heteroleptic platinum(II)  $\beta$ -hydroxydithiocinnamic ester complexes.

#### 4.2.2 Synthesis and characterization of the Homoleptic and Heteroleptic Pt(II) $\beta$ -oxodithiocinnamic ester complexes

*Cis*-[PtCl<sub>2</sub>(DMS)(DMSO)] precursor complex that was synthesized following the reported procedure in the literature<sup>282</sup>, reacted with the  $\beta$ -hydroxydithiocinnamic ester ligands (HL1-HL9) in ethanolic solution to generate three different classes of compounds: homoleptic bis-chelate complexes [Pt(L1-L9)<sub>2</sub>] and two heteroleptic mono-chelate complexes with dimethyl sulfide [Pt(L1-L9)(DMS)Cl] or dimethyl sulfoxide [Pt(L1-L9)(DMSO)Cl] and one chloride ligands as shown in Scheme 8. It is also noteworthy that, the terminal carboxylic group was esterified during the coordination, as indicated by X-ray analysis, NMR spectroscopy, and mass spectrometry.



Scheme 8: Synthesis of the Pt(II)-complexes [Pt(L1-L9)<sub>2</sub>], [Pt(L1-L9)(DMS)Cl], and [Pt(L1-L9)(DMSO)Cl].

All compounds were characterized by different NMR spectroscopy, mass spectrometry, and elemental analysis. Recrystallization of [Pt(L2)<sub>2</sub>], [Pt(L2)(DMSO)Cl] and [Pt(L6)(DMS)Cl] complexes produced suitable single crystals for X-ray diffraction studies. In the <sup>1</sup>H NMR spectra of the synthesized Pt(II) complexes, it was noted the disappearance of the resonances corresponding to the hydroxyl group (–OH) and the (–COOH) protons of the free ligand. Furthermore, the appearance of additional signals at  $\delta$  1.30 ppm (triplet) and  $\delta$  4.24 ppm (quartet) in the <sup>1</sup>H NMR spectra of the complexes and a downfield shift of around 0.23 and 0.5 ppm, respectively, compared to ethanol signals, which confirm the esterification of the carboxylic group during the coordination of the

ligands.<sup>283</sup> In the  $^{13}\text{C}\{^1\text{H}\}$  NMR spectra of the synthesized complexes, resonances for the (C–OH) carbon were found in the range 171.52–177.35 ppm. The methine (=CH-) carbon of the free ligands was found in the range  $\delta$  106.64–111.22 ppm is slightly downfield shifted by  $\approx 5$  ppm in the complexes to  $\delta$  111.53–116.71 ppm, due to the slight deshielding effect through the delocalization of the electrons in the chelating ring, which is consistent with those of similar analogues reported in the literature.<sup>261–266</sup> In contrast, a considerable upfield shift is observed for the quaternary thiocarbonyl carbon (C=S) at  $\delta$  174.27–180.47 ppm in the complexes, compared to the free ligands ( $\delta$  213.50–216.37 ppm). As a result of coordinating  $\beta$ -hydroxydithiocinnamic esters to the platinum(II) center, the  $\beta$ -oxo carbon is deshielded, while the thiocarbonyl sulfur atom accepts the  $\pi$ -backbonding electrons from the platinum(II) center, which enriches the electron density and thus shields the thiocarbonyl carbon.<sup>261–264</sup> The heteroleptic  $[\text{Pt}(\text{L1-L9})(\text{DMS})\text{Cl}]$  complexes exhibit a characteristic signal for the coordinated dimethyl sulfide (DMS) in both  $^1\text{H}$  and  $^{13}\text{C}\{^1\text{H}\}$  NMR spectra. In the  $^1\text{H}$  NMR spectra, the methyl groups were found as a singlet with platinum satellites  $^3J_{\text{Pt-H}} \approx 50$  Hz, whereas in the  $^{13}\text{C}\{^1\text{H}\}$  NMR spectra, they were found at  $\delta$  24 ppm with platinum–carbon coupling  $^2J_{\text{Pt-C}} \approx 18$  Hz. In addition, there is a downfield shift by 0.5 and 6 ppm compared to free DMS in both  $^1\text{H}$  and  $^{13}\text{C}\{^1\text{H}\}$  NMR, respectively.<sup>284</sup> On the other side, the methyl groups of the coordinated dimethyl sulfoxide (DMSO) in the heteroleptic  $[\text{Pt}(\text{L1-L9})(\text{DMSO})\text{Cl}]$  complexes observed at  $\delta$  3.60 ppm as a singlet accompanied by platinum satellites  $^3J_{\text{Pt-H}} \approx 22$  Hz in the  $^1\text{H}$  NMR spectra and  $\delta$  46 ppm with platinum–carbon coupling  $^2J_{\text{Pt-C}} \approx 50$  Hz in the  $^{13}\text{C}\{^1\text{H}\}$  NMR spectra, respectively. Compared to the free DMSO, there is a downfield shift by 1.1 and 6 ppm in both  $^1\text{H}$  and  $^{13}\text{C}\{^1\text{H}\}$  spectra, respectively which also confirm the coordination of the DMSO towards the Pt(II) center and is consistent with those of similar analogues reported in Weigand group.<sup>261–266</sup>  $^{195}\text{Pt}$  NMR spectra for the bis-chelate complexes  $[\text{Pt}(\text{L1-L9})_2]$  as well as the heteroleptic  $[\text{Pt}(\text{L1-L9})(\text{DMS})\text{Cl}]$  and  $[\text{Pt}(\text{L1-L9})(\text{DMSO})\text{Cl}]$  complexes were obtained. The signals appeared in the range of (–2267 to –2350 ppm) and (–2879 to –3079 ppm), for the bis-chelate and the mono-chelate heteroleptic complexes, respectively.

#### 4.2.3 Molecular Structures Determination

Recrystallization from  $\text{CH}_2\text{Cl}_2$  and cyclohexane mixture (1:1) of  $[\text{Pt}(\text{L2})_2]$ ,  $[\text{Pt}(\text{L2})(\text{DMSO})\text{Cl}]$ , and  $[\text{Pt}(\text{L6})(\text{DMS})\text{Cl}]$  complexes and HL3 ligand provided suitable single crystals for X-ray diffraction studies. Molecular structures are provided in Figure 41 with ellipsoids drawn at the 50% probability level. Crystal data and refinement details for the X-ray structure determinations are summarized in Table 4. Selected bond lengths and angles for HL3,  $[\text{Pt}(\text{L2})_2]$ ,  $[\text{Pt}(\text{L6})(\text{DMS})\text{Cl}]$  and  $[\text{Pt}(\text{L2})(\text{DMSO})\text{Cl}]$  are shown in Table 5.

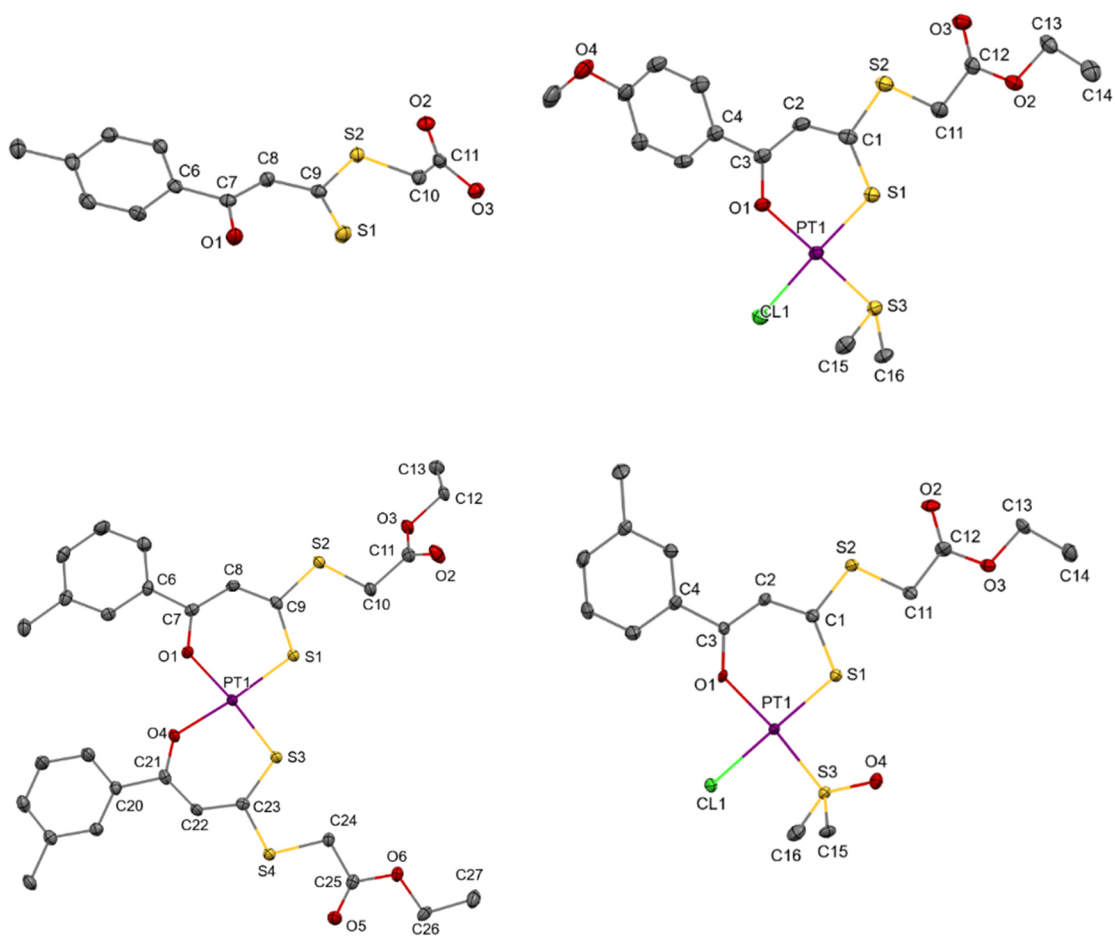


Fig. 41: Depiction of solid-state molecular structures of HL3 (top-left), [Pt(L2)<sub>2</sub>] (down-left), [Pt(L6)(DMS)Cl] (top-right) and [Pt(L2)(DMSO)Cl] (down-right). Thermal ellipsoids are given at the 50% probability level and hydrogen atoms are omitted for clarity.

Table 4: Crystal data and refinement details for the X-ray structure determinations.

Compound	HL3	[Pt(L2) <sub>2</sub> ]	[Pt(L6)(DMS)Cl]	[Pt(L2)(DMSO)Cl]
formula	C <sub>12</sub> H <sub>12</sub> O <sub>3</sub> S <sub>2</sub>	C <sub>28</sub> H <sub>30</sub> O <sub>6</sub> PtS <sub>4</sub>	C <sub>17</sub> H <sub>23</sub> Cl <sub>3</sub> O <sub>4</sub> PtS <sub>3</sub>	C <sub>17</sub> H <sub>23</sub> Cl <sub>3</sub> O <sub>4</sub> PtS <sub>3</sub>
fw (g·mol <sup>-1</sup> )	268.34	785.85	688.97	688.97
T/°C	-140(2)	-140(2)	-140(2)	-140(2)
crystal system	orthorhombic	monoclinic	orthorhombic	orthorhombic
space group	P 2 <sub>1</sub> 2 <sub>1</sub> 2 <sub>1</sub>	P 2 <sub>1</sub> /c	P 2 <sub>1</sub> 2 <sub>1</sub> 2 <sub>1</sub>	P n a 2 <sub>1</sub>
a/ Å	6.0945(2)	16.5228(3)	7.1099(1)	12.5038(2)
b/ Å	7.1789(2)	23.6316(4)	13.8320(2)	25.9893(5)
c/ Å	27.4196(8)	7.34570(10)	23.5265(4)	7.1057(1)
α/°	90	90	90	90
β/°	90	93.172(1)	90	90
γ/°	90	90	90	90
V/Å <sup>3</sup>	1199.66(6)	2863.81(8)	2313.69(6)	2309.10(7)
Z	4	4	4	4
ρ (g·cm <sup>-3</sup> )	1.486	1.823	1.978	1.982
μ (cm <sup>-1</sup> )	4.36	52.33	67.03	67.16
measured data	8666	38773	19126	30377
data with I > 2σ(I)	2617	6116	5021	5146
unique data (R <sub>int</sub> )	2705/0.0340	6570/0.0366	5292/0.0354	5275/0.0284
wR <sub>2</sub> (all data, on F <sup>2</sup> ) <sup>a)</sup>	0.0614	0.0493	0.0383	0.0348
R <sub>1</sub> (I > 2σ(I)) <sup>a)</sup>	0.0270	0.0238	0.0197	0.0166
S <sup>b)</sup>	1.078	1.147	1.066	1.080
Res. dens./e·Å <sup>-3</sup>	0.216/-0.186	0.562/-0.712	0.454/-0.441	0.412/-0.527
Flack-parameter	0.04(4)	-	0.375(9)	0.494(8)
absorpt method	multi-scan	multi-scan	multi-scan	multi-scan
absorpt corr	0.6933/0.7456	0.5637/0.7456	0.6141/0.7456	0.5334/0.7456
T <sub>min</sub> /max				
CCDC No.	2211752	2211753	2211754	2211755

<sup>a)</sup> Definition of the R indices:  $R_1 = (\sum ||F_o| - |F_c||) / \sum |F_o|$ ;

$wR_2 = \{\sum [w(F_o^2 - F_c^2)^2] / \sum [w(F_o^2)^2]\}^{1/2}$  with  $w^{-1} = \sigma^2(F_o^2) + (aP)^2 + bP$ ;  $P = [2F_c^2 + \text{Max}(F_o^2)]/3$ ;

<sup>b)</sup>  $S = \{\sum [w(F_o^2 - F_c^2)^2] / (N_o - N_p)\}^{1/2}$ .

Table 5. Selected bond lengths and angles for HL3, [Pt(L2)<sub>2</sub>], [Pt(L6)(DMS)Cl], and [Pt(L2)(DMSO)Cl].

HL3				[Pt(L2) <sub>2</sub> ]			
Bond lengths [Å]		Bond angles [°]		Bond lengths [Å]		Bond angles [°]	
C6-C7	1.472(2)			Pt-O1	2.0117(19)	O1-Pt-S1	95.68(6)
C3-C12	1.508(3)			Pt-O4	2.0022(19)	S1-Pt-S3	89.50(3)
C9-S2	1.7533(18)			Pt-S1	2.2286(7)	O4-Pt-S3	95.94(6)
C8-H8	0.95(2)			Pt-S3	2.2347(7)	O1-Pt-O4	78.90(8)
S1-C9	1.6795(18)					O1-Pt-S3	174.75(6)
C7-C8	1.378(2)			S1-C9	1.696(3)	O4-Pt-S1	174.21(6)
C8-C9	1.418(2)			C7-C8	1.402(4)		
O1-C7	1.325(2)	O1-C7-C8	122.85(16)	C8-C9	1.398(4)	Pt-O1-C7	132.62(19)
		C7-C8-C9	125.69(16)	O1-C7	1.277(3)	O1-C7-C8	125.4(3)
		C8-C9-S1	126.60(14)	S3-C23	1.702(3)	C7-C8-C9	127.4(3)
				C21-C22	1.405(4)	C8-C9-S1	130.3(2)
				C22-C23	1.390(4)	C9-S1-Pt	108.45(10)
				O4-C21	1.275(3)	Pt-O4-C21	132.76(19)
						O4-C21-C22	125.3(3)
						C21-C22-C23	127.7(3)
						C22-C23-S3	130.3(2)
						C23-S3-Pt	108.01(10)
[Pt(L6)(DMS)Cl]				[Pt(L2)(DMSO)Cl]			
Bond lengths [Å]		Bond angles [°]		Bond lengths [Å]		Bond angles [°]	
Pt-O1	2.017(3)	O1-Pt-S1	96.74(9)	Pt-O1	2.011(2)	O1-Pt-S1	96.17(7)
Pt-S1	2.2338(10)	S1-Pt-S3	84.12(4)	Pt-S1	2.2526(8)	S1-Pt-S3	89.81(3)
Pt-S3	2.2575(11)	S3-Pt-Cl	93.49(4)	Pt-S3	2.1987(8)	S3-Pt-Cl	89.60(3)
Pt-Cl	2.3496(9)	O1-Pt-Cl	85.65(9)	Pt-Cl	2.3335(8)	O1-Pt-Cl	84.42(7)
		S1-Pt-Cl	177.61(4)			S1-Pt-Cl	179.38(5)
S1-C1	1.701(4)	O1-Pt-S3	178.32(16)	S1-C1	1.710(3)	O1-Pt-S3	174.02(7)
C1-C2	1.385(6)			C1-C2	1.387(5)		
C2-C3	1.397(6)	Pt-O1-C3	129.5(3)	C2-C3	1.400(5)	Pt-O1-C3	131.9(2)
O1-C3	1.291(5)	O1-C3-C2	127.4(4)	O1-C3	1.276(4)	O1-C3-C2	125.9(3)
		C3-C2-C1	128.7(4)			C3-C2-C1	128.1(3)
		C2-C1-S1	128.7(3)	S3-O4	1.465(3)	C2-C1-S1	130.1(3)
S3-C15	1.798(7)	C1-S1-Pt	108.90(14)	S3-C15	1.770(8)	C1-S1-Pt	107.55(12)
S3-C16	1.798(7)			S3-C16	1.783(9)		
						O4-S3-C15	107.9(5)
						O4-S3-C16	109.4(5)
		C15-S3-C16	99.8(2)			C15-S3-C16	102.76(19)
						O4-S3-Pt	117.30(12)
		C15-S3-Pt	106.4(3)			C15-S3-Pt	109.4(3)
		C16-S3-Pt	108.9(3)			C16-S3-Pt	109.1(3)

#### 4.2.4 Interactions of the platinum(II) complexes with 9-MeG as a DNA model

In Cisplatin's mechanism of action, the chloride ligands undergo aquation and form the two potent electrophilic cations  $cis\text{-}[\text{Pt}(\text{NH}_3)_2\text{Cl}(\text{H}_2\text{O})]^+$  and  $cis\text{-}[\text{Pt}(\text{NH}_3)_2(\text{H}_2\text{O})_2]^{2+}$ .<sup>92-94</sup> These active species can enter the nucleus, and the water molecule is substituted by nucleophilic centers on DNA-purine bases, particularly the N7 positions of guanosine and adenosine residues.<sup>92-94</sup> As a DNA model, 9-methylguanine (9-MeG) was selected in this study to react with three representative complexes  $[\text{Pt}(\text{L6})_2]$ ,  $[\text{Pt}(\text{L6})(\text{DMS})\text{Cl}]$ , and  $[\text{Pt}(\text{L6})(\text{DMSO})\text{Cl}]$ . Where 1 eq. of each complex was incubated with 8 eq. from 9-MeG in  $\text{CH}_3\text{CN-PBS}$  (pH 7.4; 1:1) at 37 °C for 72 hours, and the reaction was analyzed by LC-ESI-MS to identify the formed Pt/9-MeG adducts.

##### 4.2.4.1 Interactions of the $[\text{Pt}(\text{L6})(\text{DMS})\text{Cl}]$ complex with 9-MeG

Upon the reaction of the  $[\text{Pt}(\text{L6})(\text{DMS})\text{Cl}]$  complex with 9-MeG, two major peaks at  $m/z = 835.6$  ( $t_R = 8.98$  min), and  $732.7$  ( $t_R = 9.33$  min) were found, assignable to the bifunctional adduct  $[\text{Pt}(\text{L6})(9\text{-MeG})_2]^+$  and the monofunctional adduct  $[\text{Pt}(\text{L6})(\text{DMS})(9\text{-MeG})]^+$ , respectively (Fig. 42). Furthermore, a minor peak at  $m/z = 670.9$  ( $t_R = 8.98$  min) was observed and can be assigned to the N7,O6-bidentate 9-MeG adduct  $[\text{Pt}(\text{L6})(\text{N7},\text{O6}\text{-}9\text{-MeG})]^+$  (Fig. 42). Interestingly, the absence of any peaks attributed to  $[\text{Pt}(\text{L6})(\text{DMS})\text{Cl}]$  complex after 24 h, indicates that the initial quantity has been consumed. Also, there are no significant changes in spectral composition over time (24, 48 and 72 h) (Fig. 42).

##### 4.2.4.2 Interactions of the $[\text{Pt}(\text{L6})(\text{DMSO})\text{Cl}]$ complex with 9-MeG

In the reaction between  $[\text{Pt}(\text{L6})(\text{DMSO})\text{Cl}]$  complex with 9-MeG, the main peak was found at  $m/z = 835.6$  ( $t_R = 8.98$  min), which can be assigned to the bifunctional adduct  $[\text{Pt}(\text{L6})(9\text{-MeG})_2]^+$ . Nevertheless, the minor peak at  $m/z = 670.8$  ( $t_R = 8.98$  min) assignable to  $[\text{Pt}(\text{L6})(\text{N7},\text{O6}\text{-}9\text{-MeG})]^+$  adduct was also detected (Fig. 43). Intrinsically, there are no peaks attributed to  $[\text{Pt}(\text{L6})(\text{DMSO})\text{Cl}]$  complex after 24 h, indicating the consumption of the whole compound. There are no significant changes in spectral composition over time (24, 48, and 72 h) (Fig. 43).

##### 4.2.4.3 Interactions of the $[\text{Pt}(\text{L6})_2]$ complex with 9-MeG

Conversely, the ESI spectrum of  $[\text{Pt}(\text{L6})_2]$  complex with 9-MeG, shows a major peak at  $m/z = 817.6$  ( $t_R = 15.99$  min), attributed to the non-reacted complex as well as a minor peak at  $m/z = 835.6$  ( $t_R = 8.98$  min) assigned to the bifunctional adduct  $[\text{Pt}(\text{L6})(9\text{-MeG})_2]^+$  (Fig. 44). Also, there are no significant changes in spectral composition over time (24, 48, and 72 h) (Fig. 44). Unsurprisingly, such kind of bis-chelate complexes exhibited the lowest 9-MeG binding.



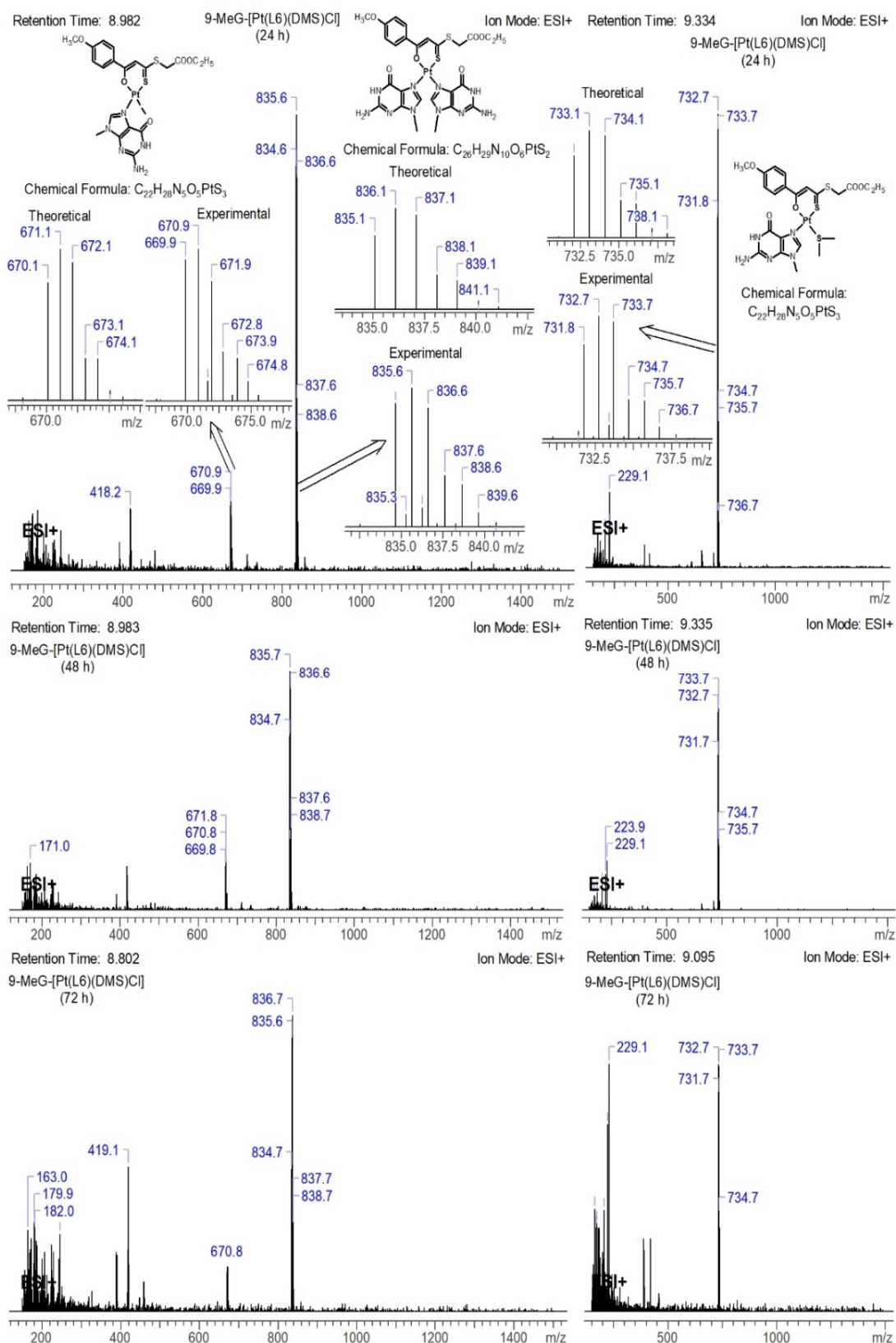


Figure 42: ESI-MS spectra of the adducts formed between 9-MeG and [Pt(L6)(DMS)Cl] complex in  $CH_3CN$ -PBS (pH 7.4; 1:1) at 37 °C after; A) 24 h (top), B) 48 h (middle), and C) 72 h (bottom). The insets show the theoretical as well as the experimental isotope patterns of  $m/z = 835.6$  ( $t_R = 8.98$  min),  $732.7$  ( $t_R = 9.33$  min), and  $670.9$  ( $t_R = 8.98$  min).

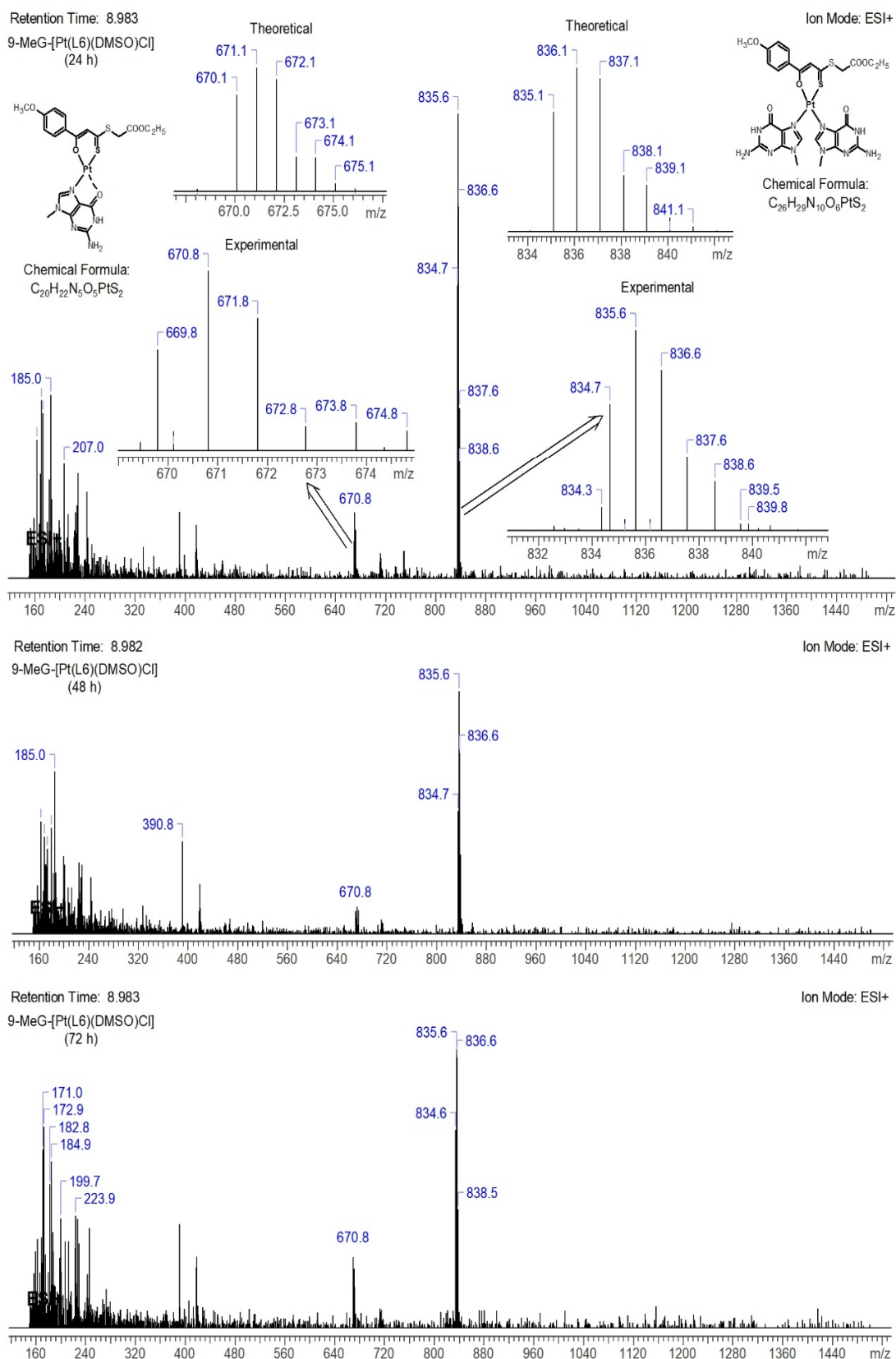


Figure 43: ESI-MS spectra of the adducts formed between 9-MeG and [Pt(L6)(DMSO)Cl] complex in  $CH_3CN$ -PBS (pH 7.4; 1:1) at 37 °C after; A) 24 h (top), B) 48 h (middle), and C) 72 h (bottom). The insets show the theoretical as well as the experimental isotope patterns of  $m/z = 835.6$  ( $t_R = 8.98$  min), and  $670.8$  ( $t_R = 8.98$  min).

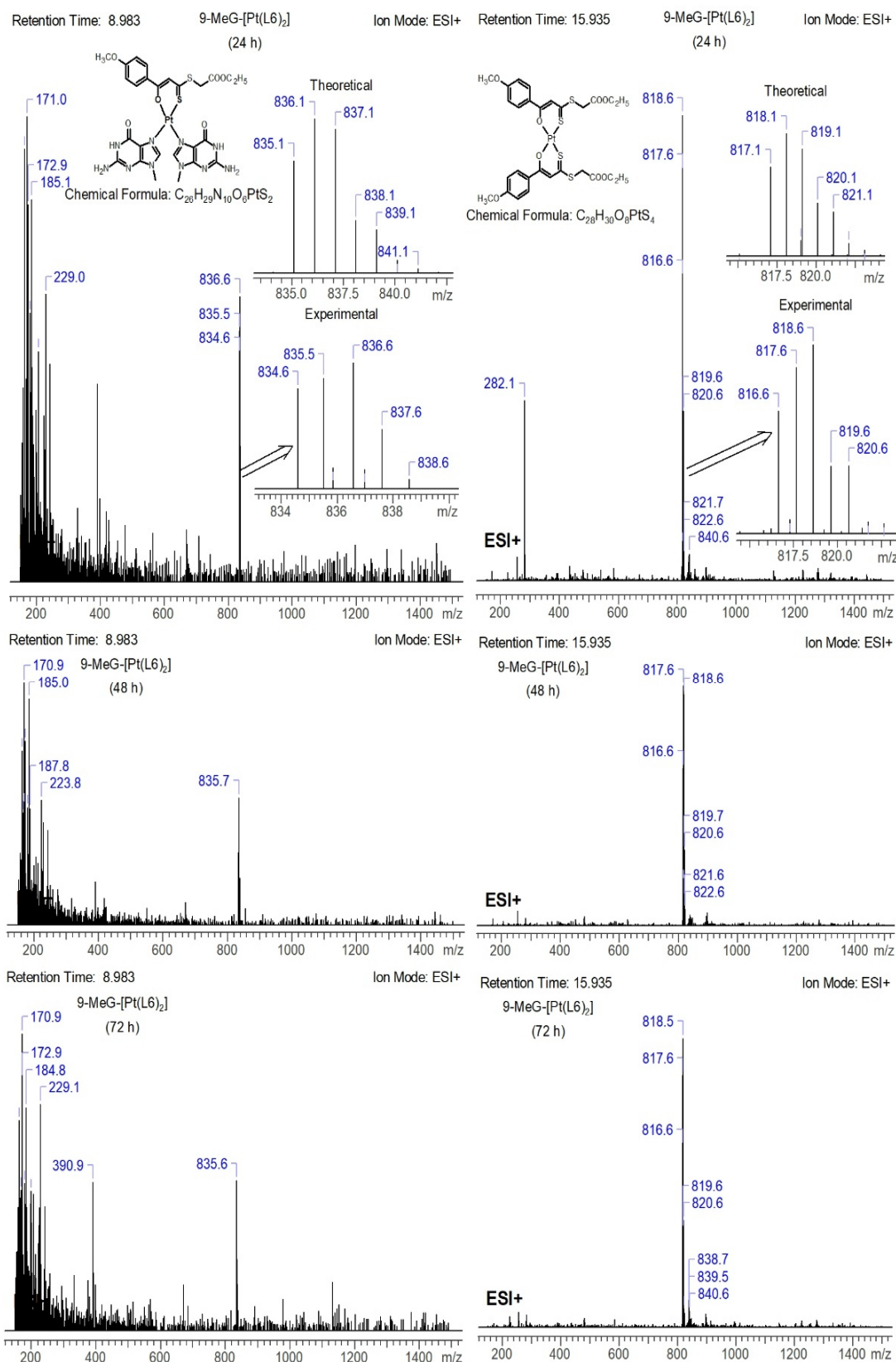


Figure 44: ESI-MS spectra of the adducts formed between 9-MeG and [Pt(L6)<sub>2</sub>] complex in CH<sub>3</sub>CN-PBS (pH 7.4; 1:1) at 37 °C after; A) 24 h (top), B) 48 h (middle), and C) 72 h (bottom). The insets show the theoretical as well as the experimental isotope patterns of  $m/z = 835.6$  ( $t_R = 8.98$  min), and the non-reacted complex at  $817.6$  ( $t_R = 15.93$  min).

#### 4.2.5 Cytotoxic Activity of the Heteroleptic Platinum Complexes

The anti-proliferative activity of the heteroleptic [Pt(L1-L9)(DMS)Cl] and [Pt(L1, L2, L4, L5, and L7-L9)(DMSO)Cl] complexes against the epithelial ovarian cancer cell lines A2780 and Skov3 and their cisplatin-resistant subcultures was determined after 48 h incubation with varying concentrations of the compounds by the MTT assay. The mean IC<sub>50</sub> values of the tested compounds and the calculated resistance factors (RF) for A2780 and Skov3 are shown in Table 6. Most compounds affected both sensitive and cisplatin-resistant cells similarly or showed higher activity against resistant cells resulting in resistance factors (RF = IC<sub>50, resistant</sub> / IC<sub>50, sensitive</sub>) RF ≤ 1 as shown in Table 6.

Table 6: Mean IC<sub>50</sub> values of the tested compounds and calculated resistance factors (RF).

		A2780	A2780 Cis	RF A2780	Skov3	Skov3 Cis	RF Skov3	mean IC50
Pt(L)(DMS) Cl	L1	33.3 (±6.8)	16.0 (±5.1)	0.5	76.1 (±16.8)	46.2 (±10.2)	0.6	34.4
	L2	2056.6 (±489.2)	355.0 (±115.5)	0.2	685.8 (±245.3)	183.1 (±52.1)	0.3	656.1
	L3	56.1 (±11.5)	60.5 (±19.2)	1.1	57.5 (±17.0)	41.4 (±11.8)	0.7	43.3
	L4	55.0 (±10.8)	72.2 (±26.4)	1.3	60.6 (±17.1)	53.2 (±12.6)	0.9	48.5
	L5	93.0 (±9.7)	59.1 (±14.7)	0.6	119.9 (±20.1)	69.6 (±13.6)	0.6	68.4
	L6	59.5 (±12.4)	46.4 (±13.1)	0.8	86.6 (±10.4)	69.7 (±11.4)	0.8	52.6
	L7	28.1 (±4.1)	44.7 (±11.7)	1.6	63.9 (±16.2)	53.7 (±13.2)	0.8	38.4
	L8	42.6 (±15.3)	50.7 (±14.3)	1.2	66.3 (±16.9)	63.7 (±18.5)	1.0	44.9
	L9	32.9 (±14.5)	39.4 (±19.8)	1.2	60.6 (±15.4)	52.6 (±12.8)	0.9	37.3
Pt(L)(DMSO) Cl	L1	25.6 (±10.1)	55.3 (±10.7)	2.2	336.8 (±62.4)	99.4 (±16.2)	0.3	103.8
	L2	164.4 (±45.2)	50.4 (±12.5)	0.3	380.9 (±96.1)	103.6 (±20.5)	0.3	139.9
	L3				n.a.			
	L4	16.5 (±4.5)	73.3 (±25.0)	4.5	146.1 (±28.1)	92.8 (±17.4)	0.6	66.6
	L5	224.6 (±64.2)	58.5 (±13.6)	0.3	777.3 (±270.5)	95.5 (±21.0)	0.1	231.2
	L6				n.a.			
	L7	102.8 (±56.4)	56.3 (±13.3)	0.5	646.9 (±196.8)	182.8 (±70.5)	0.3	197.9
	L8	64.6 (±32.2)	48.2 (±12.4)	0.7	87.6 (±15.0)	54.9 (±11.2)	0.6	51.2
	L9	153.8 (±35.7)	76.8 (±25.1)	0.5	403.9 (±127.3)	163.6 (±60.3)	0.4	159.7
CIS	6.8 (±2.4)	15.4 (±4.8)	2.3	12.5 (±2.8)	28.6 (±4.2)	2.3	13.1	

Both [Pt(L)(DMS)Cl], and [Pt(L)(DMSO)Cl] complexes have a similar mean activity (mean IC<sub>50</sub> 132 μM and 135 μM, respectively) but exhibit cell line-specific differences. Whereas [Pt(L)(DMS)Cl] complexes are less cytotoxic for A2780 than for Skov3 (mean IC<sub>50</sub> 212 μM and 118 μM), the opposite is detected for [Pt(L)(DMSO)Cl] complexes (mean IC<sub>50</sub> 84 μM and 255 μM, respectively). Thus, cell line-specific detoxification, DNA damage repair, or cell death signaling processes influencing the cytotoxic activity may affect the two compound groups differently. The first in-vitro studies using ovarian cancer cell lines revealed no superior activity of these complexes compared to cisplatin but point to a



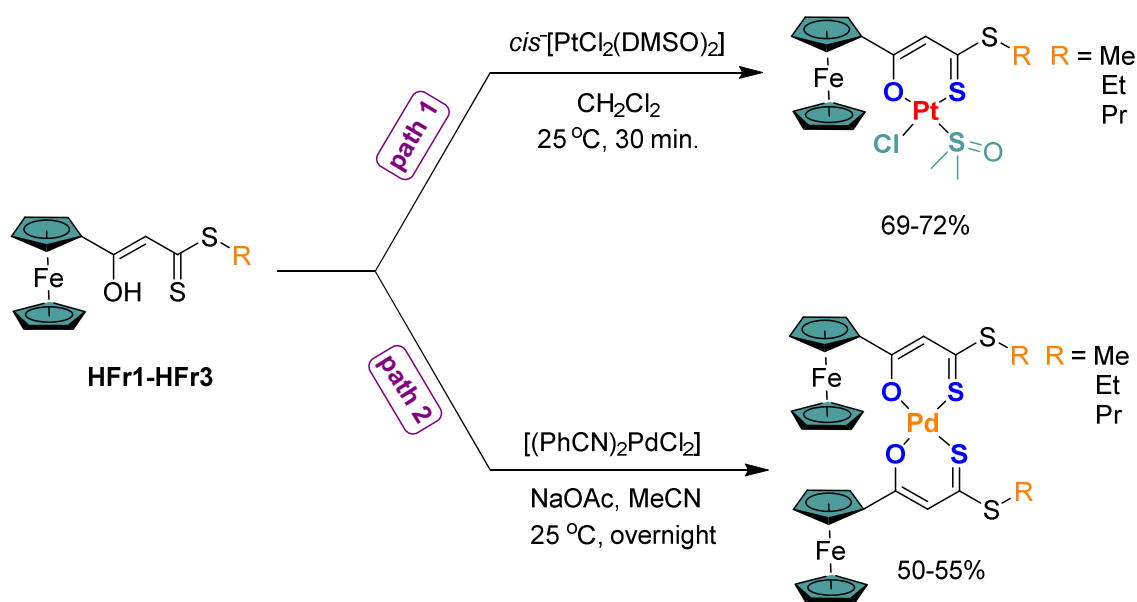
All compounds were characterized by spectroscopic methods ( $^1\text{H}$  NMR,  $^{13}\text{C}\{^1\text{H}\}$  NMR, and IR), mass spectrometry, and elemental analysis. The  $^1\text{H}$  NMR spectra of HFr1-HFr3 exhibit a resonance signal in the range at  $\delta$  6.61-6.56 ppm for the methine proton ( $=\text{CH}-$ ), whereas a single resonance appeared at a strong downfield shift at  $\delta$  15.10 ppm assigned to hydroxyl group ( $-\text{OH}$ ) proton. Additionally, the ferrocene nine protons appear in the area between  $\delta$  4.82 and 4.22 ppm, while the protons of the alkyl substituents R of HFr1-HFr3 free ligands were detected in the range  $\delta$  3.25-1.06 ppm. The  $^{13}\text{C}\{^1\text{H}\}$  NMR spectrum of HFr1-HFr3 shows a resonance signal located at a low field  $\delta$  211.8-212.5 ppm, which is assigned to the thiocarbonyl carbon atom. The  $\beta$ -oxo carbon atoms appear at  $\delta$  176.4-176.8 ppm, while those of the methine groups are found around  $\delta$  107.6 ppm.

#### **4.3.2 Synthesis and characterization of the Heteroleptic Pt(II) and Homoleptic Pd(II) $\beta$ -hydroxy-dithioesters ferrocenyl complexes**

The free ligands HFr1-HFr3 were reacted with the precursor complex *cis*- $[\text{PtCl}_2(\text{DMSO})_2]$ , which was synthesized following the reported procedure in the literature [34], affording after column chromatography, the heteroleptic complexes  $[\text{Pt}(\text{Fr1-Fr3})(\text{DMSO})\text{Cl}]$  in 69-72% yield as shown in Scheme 10 (path 1). All complexes were characterized by elemental analyses, multinuclear NMR and FTIR spectroscopy, mass spectrometry as well as X-ray analysis for complex  $[\text{Pt}(\text{Fr2})(\text{DMSO})\text{Cl}]$ . In the  $^1\text{H}$  NMR spectra of the synthesized  $[\text{Pt}(\text{Fr1-Fr3})(\text{DMSO})\text{Cl}]$  complexes, it was noted the disappearance of the resonances corresponding to the hydroxyl group ( $-\text{OH}$ ) of the free ligand (HFr1-HFr3). Furthermore, the methyl groups of the coordinated dimethyl sulfoxide (DMSO) in the heteroleptic  $[\text{Pt}(\text{Fr1-Fr3})(\text{DMSO})\text{Cl}]$  complexes observed at  $\delta$  3.63 ppm as a singlet accompanied by platinum satellites  $^3J_{\text{Pt-H}} \approx 22$  Hz in the  $^1\text{H}$  NMR spectra and  $\delta$  46.8 ppm with platinum-carbon coupling  $^2J_{\text{Pt-C}} \approx 58$  Hz in the  $^{13}\text{C}\{^1\text{H}\}$  NMR spectra, respectively. Compared to the free DMSO, there is a downfield shift by 1 and 6 ppm in both  $^1\text{H}$  and  $^{13}\text{C}\{^1\text{H}\}$  spectra, respectively which also confirm the coordination of the DMSO towards the Pt(II) center and is consistent with those of similar analogues reported in Weigand group.<sup>261-266</sup> In the  $^{13}\text{C}\{^1\text{H}\}$  NMR spectra of the Pt(II) complexes, resonances for the  $\beta$ -oxo carbon were found in the range 172.6-173.5 ppm, the methine carbon are slightly downfield shifted by  $\approx 5$  ppm (deshielded), while the thiocarbonyl carbon atom is shifted upfield (shielded) around  $\delta$  181 ppm compared to their parent ligands HFr1-HFr3 ( $\delta$  111.5 ppm). Both the downfield and upfield shift of the methine and thiocarbonyl carbons, respectively, was due to the coordinated oxygen atoms possessing  $\sigma$ -donating properties towards the metal center, while the coordinated sulfur atom can act as an electron acceptor for  $\pi$ -backbonding from the metal center. The  $^{195}\text{Pt}$  NMR spectra exhibit

signals at  $\delta$  -3123.5, -3124.2, -3121.4 ppm, respectively, which is attributed to Pt-Cl bond and is in accordance with the literature.<sup>294</sup>

The synthesis of the homoleptic  $[\text{Pd}(\text{Fr1-Fr3})_2]$  complexes was carried out in two steps. First, HFr1-HFr3 were deprotonated using sodium acetate. The latter was then treated with half equivalent of bis(benzonitrile)palladium(II) chloride and stirred overnight at room temperature. After workup through extraction with diethyl ether, the desired homoleptic complexes could be obtained as red-volatile crystalline solids in 50-55% yields as shown in Scheme 10 (path 2). The  $^1\text{H}$  and  $^{13}\text{C}\{^1\text{H}\}$  NMR spectra of the homoleptic bis-chelates complexes  $[\text{Pd}(\text{Fr1-Fr3})_2]$  is similar to those of the corresponding mono-chelated complexes  $[\text{Pt}(\text{Fr1-Fr3})(\text{DMSO})\text{Cl}]$ , with the only difference being the non-existent of the DMSO ligands. The  $^1\text{H}$  NMR spectra  $[\text{Pd}(\text{Fr1-Fr3})_2]$  complexes display signal around  $\delta$  6.71 ppm for the methine proton, beside the disappearance of the proton belonging to the hydroxyl group located at 15.10 ppm in the parent ligands HFr1-HFr3. The  $^{13}\text{C}\{^1\text{H}\}$  NMR spectra of  $[\text{Pd}(\text{Fr1-Fr3})_2]$  complexes display a signal around  $\delta$  184.5 ppm for the thiocarbonyl carbon atom and a signal around  $\delta$  174.9 ppm for the  $\beta$ -oxo carbon atom. The signal of the carbon atom of the methine moiety was also detected around  $\delta$  111.5 ppm.



Scheme 10: Synthetic pathways of the Heteroleptic Pt(II) and Homoleptic Pd(II) complexes.

#### 4.3.3 Molecular Structures Determination for $[\text{Pt}(\text{Fr2})(\text{DMSO})\text{Cl}]$ and $[\text{Pd}(\text{Fr3})_2]$ complexes

Recrystallization from  $\text{CH}_2\text{Cl}_2$  and cyclohexane mixture (1:1) of complexes  $[\text{Pt}(\text{Fr2})(\text{DMSO})\text{Cl}]$ , and  $[\text{Pd}(\text{Fr3})_2]$  provided suitable single crystals for X-ray diffraction



studies. Molecular structures are provided in Figure 45 with ellipsoids drawn at the 50% probability level.

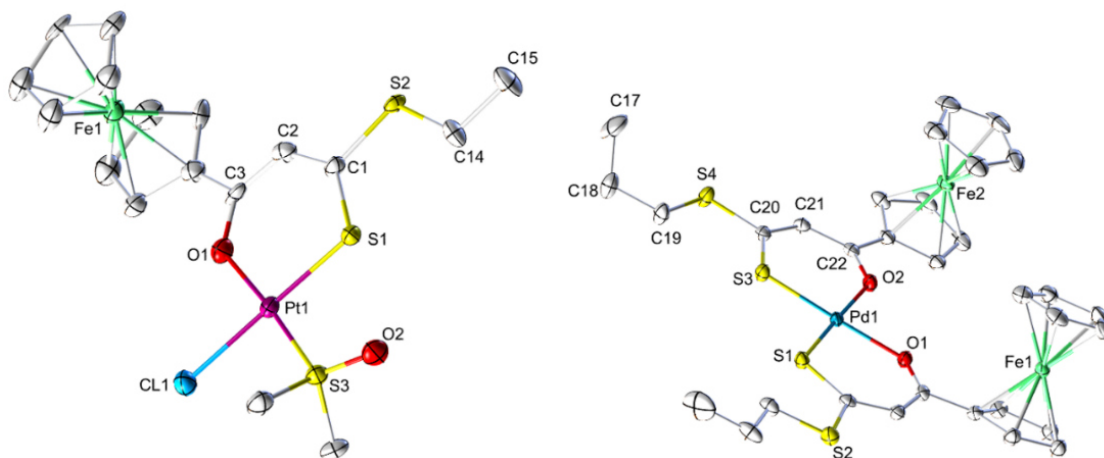


Fig. 45: Molecular structures of complexes [Pt(Fr2)(DMSO)Cl] (left), and [Pd(Fr3)<sub>2</sub>] (right). Hydrogen atoms have been omitted for clarity.

#### Crystal Data for [Pt(Fr2)(DMSO)Cl]

C<sub>17</sub>H<sub>21</sub>ClFeO<sub>2</sub>PtS<sub>3</sub>, Mr = 639.91 g mol<sup>-1</sup>, red-brown prism, size 0.082 x 0.044 x 0.042 mm<sup>3</sup>, triclinic, space group P  $\bar{1}$ , a = 7.1055(7), b = 11.8777(9), c = 12.8066(9) Å,  $\alpha$  = 112.261(5),  $\beta$  = 97.436(4),  $\gamma$  = 92.556(6)°, V = 986.69(14) Å<sup>3</sup>, T = -140 °C, Z = 2,  $\rho_{\text{calcd.}}$  = 2.154 g cm<sup>-3</sup>,  $\mu$  (Mo-K $\alpha$ ) = 82.78 cm<sup>-1</sup>, multi-scan, transmin: 0.5428, transmax: 0.7456, F(000) = 616, 4448 reflections in h(-9/9), k(-15/15), l(-16/16), measured in the range 2.906° ≤  $\Theta$  ≤ 27.482°, completeness  $\Theta_{\text{max}}$  = 98.5%, 4448 independent reflections, R<sub>int</sub> = 0.0495, 3943 reflections with F<sub>o</sub> > 4 $\sigma$ (F<sub>o</sub>), 230 parameters, 30 restraints, R1<sub>obs</sub> = 0.0728, wR<sub>obs</sub><sup>2</sup> = 0.1964, R1<sub>all</sub> = 0.0829, wR<sub>all</sub><sup>2</sup> = 0.2051, GOOF = 1.128, largest difference peak and hole: 6.203 / -5.815 e Å<sup>-3</sup>.

#### Crystal Data for [Pd(Fr3)<sub>2</sub>]

C<sub>32</sub>H<sub>34</sub>Fe<sub>2</sub>O<sub>2</sub>PdS<sub>4</sub>, Mr = 796.93 g mol<sup>-1</sup>, red-brown prism, size 0.108 x 0.102 x 0.098 mm<sup>3</sup>, orthorhombic, space group P c c n, a = 17.9485(3), b = 27.1924(4), c = 12.7899(2) Å, V = 6242.27(17) Å<sup>3</sup>, T = -140 °C, Z = 8,  $\rho_{\text{calcd.}}$  = 1.696 g cm<sup>-3</sup>,  $\mu$  (Mo-K $\alpha$ ) = 17.84 cm<sup>-1</sup>, multi-scan, transmin: 0.6462, transmax: 0.7456, F(000) = 3232, 46577 reflections in h(-23/23), k(-35/35), l(-16/16), measured in the range 2.094° ≤  $\Theta$  ≤ 27.478°, completeness  $\Theta_{\text{max}}$  = 99.8%, 7151 independent reflections, R<sub>int</sub> = 0.0542, 6411 reflections with F<sub>o</sub> > 4 $\sigma$ (F<sub>o</sub>), 372 parameters, 0 restraints, R1<sub>obs</sub> = 0.0296, wR<sub>obs</sub><sup>2</sup> = 0.0542, R1<sub>all</sub> = 0.0363, wR<sub>all</sub><sup>2</sup> = 0.0566, GOOF = 1.090, largest difference peak and hole: 0.522 / -0.655 e Å<sup>-3</sup>.



#### **4.3.4 Interactions of the [Pt(Fr1)(DMSO)Cl] complex with 9-MeG as a DNA model**

As a DNA model, 9-methylguanine (9-MeG) was selected to react with [Pt(Fr1)(DMSO)Cl] complex. Where 1 eq. (1 mg) of the complex was incubated with 8 eq. (2.1 mg) from 9-MeG in CH<sub>3</sub>CN-PBS (pH 7.4; 2:1) at 37 °C for 72 hours, and the reaction was analyzed by LC-ESI-MS to identify the formed Pt/9-MeG adducts. After 12 h, two major peaks at  $m/z = 837.6$  ( $t_R = 8.76$  min), and  $735.7$  ( $t_R = 9.33$  min) were found, assignable to the monofunctional adducts [Pt(Fr1)(DMSO)(9-MeG)]<sup>+</sup>.2CH<sub>3</sub>CN, and [Pt(Fr1)(CH<sub>3</sub>CN)(9-MeG)]<sup>+</sup>.H<sub>2</sub>O, respectively (Fig. 46). The latter was observed again without the water molecule as  $m/z = 716.8$  ( $t_R = 9.06$  min) (Fig. 46). The ESI spectra clearly show an additional peak at  $m/z = 611.6$  assigned to [(Pt(Fr1)(CH<sub>3</sub>CN)<sub>2</sub>]<sup>+</sup> ( $t_R = 9.47$  min, Fig. 46), implying the efficient replacement of the chloride and DMSO ligands, thus affording the bi-solvolytic species. The formation of such adduct indicates the solvolysis of both DMSO and Cl ligands, even though no bifunctional adduct was observed after 12 h. As the incubation time was extended to 24 h, the compounds decomposed into brown precipitates, and no adducts were detected, which might explain the lower cytotoxic activity of such ferrocenyl-based complexes.

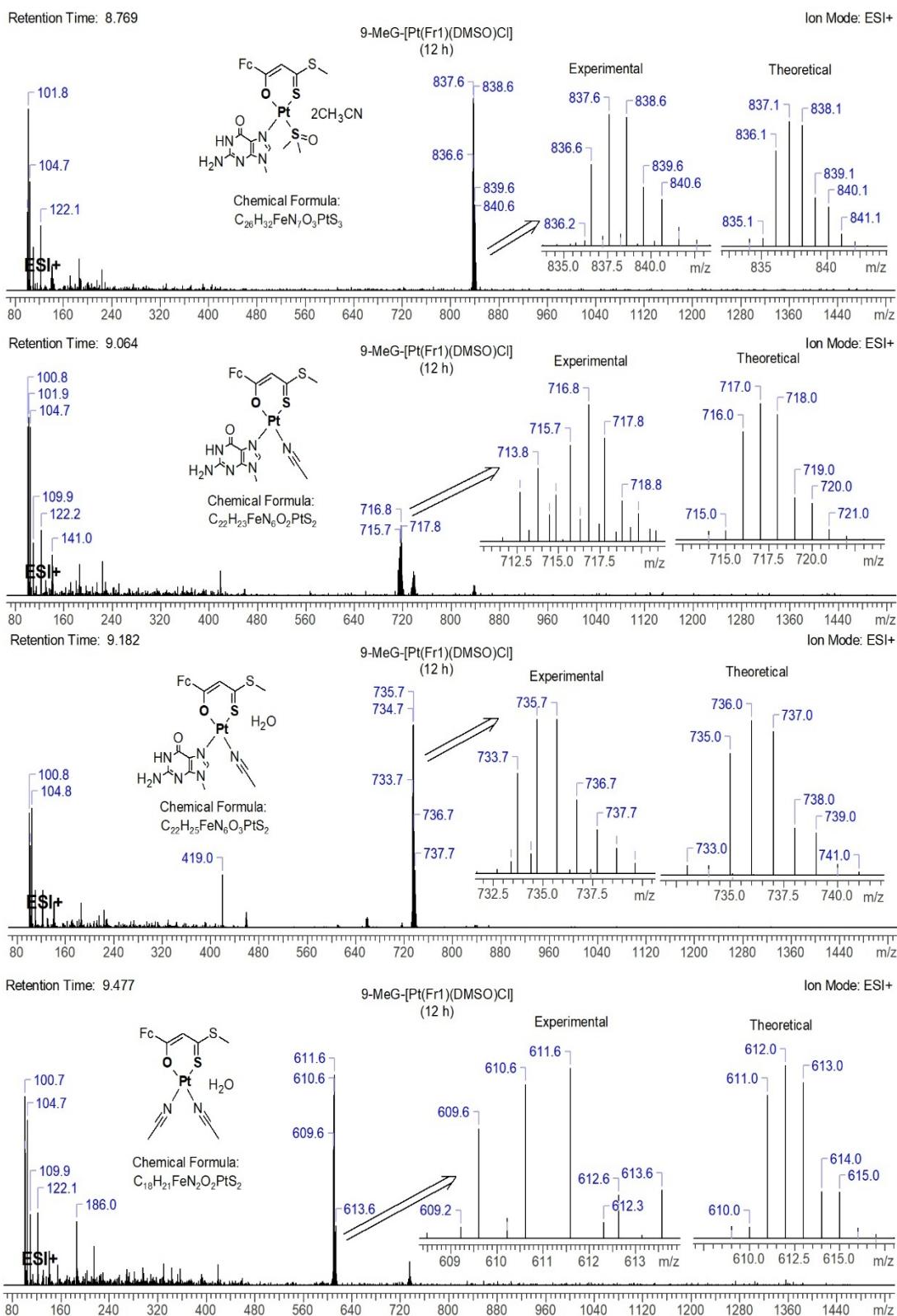


Figure 46: ESI-MS spectra of the adducts formed between 9-MeG and [Pt(Fr1)(DMSO)Cl] complex in  $CH_3CN$ -PBS (pH 7.4; 2:1) at 37 °C after 12 h; at  $t_R = 8.76$  min. (first spectrum)  $m/z = 837.6$ ,  $t_R = 9.06$  min. (second spectrum)  $m/z = 716.8$ ,  $t_R = 9.18$  min. (third spectrum)  $m/z = 735.7$ , and  $t_R = 9.47$  min. (forth spectrum)  $m/z = 611.6$ . The insets show the theoretical and the experimental isotope patterns, Fc = Ferrocene.

#### 4.3.5 Cytotoxic Activity of the free ligands and the Pt/Pd Complexes

The anti-proliferative activity of the free ligand HFr1-HFr3 as well as their Pt/Pd complexes against the epithelial ovarian cancer cell lines A2780 and Skov3 and their cisplatin-resistant subcultures was determined. The IC<sub>50</sub> values of the tested compounds and the calculated resistance factors (RF) for A2780 and Skov3 are shown in Table 7. Cytotoxicity assays of the synthesized compounds showed low toxicity towards ovarian cancer cells, but the compounds are not affected by cisplatin resistance mechanisms. The Pt(II) complexes [Pt(Fr1-Fr3)(DMSO)Cl] exhibited higher activity in comparison to both the free ligands (HFr1-HFr3) and the Pd(II) complexes [Pd(Fr1-Fr3)<sub>2</sub>]. The alkyl substituent strongly influenced the activity of these complexes, where the cytotoxic activity increases with the length of the alkyl chain, thus the [Pt(Fr3)(DMSO)Cl] complex exhibiting a mean IC<sub>50</sub> of 56 μM, which confirms the structure-activity relationships. Both the Pt(II) and Pd(II) ferrocenyl-based complexes included in this study exhibited a lower cytotoxic activity than the normal β-hydroxy-dithiocinnamic acid complexes reported before in our group,<sup>263,266</sup> this might be caused by the low stability of the ferrocenyl-adducts or the steric effects inhibiting the binding to the target biomolecules as shown before in the 9-MeG binding experiment.

Table 7: IC<sub>50</sub> values ± SD of analyzed compounds [μM] of the tested compounds and the calculated resistance factors (RF) for A2780 and Skov3.

		A2780	A2780 Cis	RF A2780	Skov3	Skov3 Cis	RF Skov3	mean IC50
	<b>HFr1</b>	226.9±81.2	780.1±115.7	3.4	1831.2±258.1	301.7±65.5	0.2	785.0
<b>Ligand</b>	<b>HFr2</b>	183.5±31.6	61.1±14.6	0.3	289.4±94.5	435.3±105.4	1.5	242.3
	<b>HFr3</b>	124.1±47.1	118.5±39.2	1.0	195.2±24.2	70.4±16.2	0.4	127.0
	<b>Fr1</b>	540.4±100.5	118.1±29.2	0.2	2509.7±752.4	408.5±103.2	0.2	894.2
<b>Pt complex</b>	<b>Fr2</b>	37.8±11.7	62.9±21.4	1.7	149.0±25.3	42.6±19.2	0.3	73.1
	<b>Fr3</b>	17.9±4.8	58.6±19.1	3.3	103.6±31.6	46.8±22.0	0.5	56.7
	<b>Fr1</b>	970.5±273.2	231.3±35.9	0.2	1018.6±328.9	424.0±315.1	0.4	661.1
<b>Pd complex</b>	<b>Fr2</b>	n.c.	n.c.		881.7±215.6	473.2±120.1	0.5	677.5
	<b>Fr3</b>	n.c.	n.c.		1543.3±485.0	273.4±76.1	0.2	908.4

(RF – resistance factor, n.c. – could not be calculated by regression analysis)

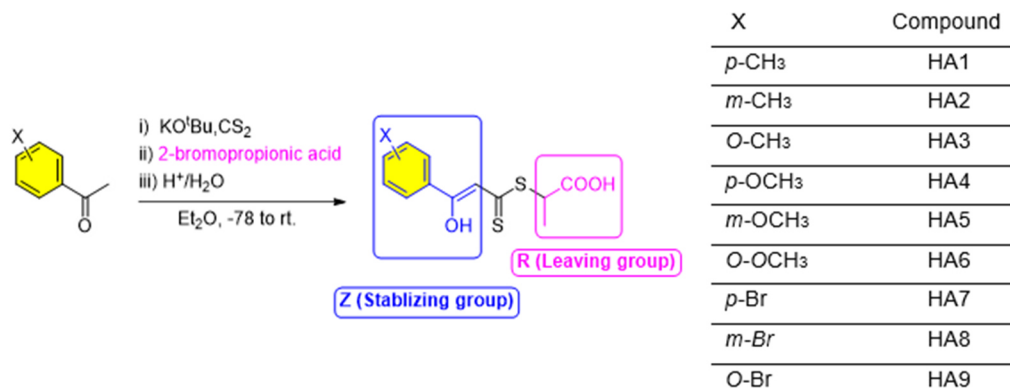
#### **4.4 Project 3. Dual Function of $\beta$ -hydroxydithiocinnamic esters: RAFT Agent and Ligand for Metal Complexation.**

Polymer and liposomal-based platinum drugs such as ProLindac™ and Lipoplatin represent a promising alternative strategy to the discovery and development of brand-new platinum complexes for cancer treatment, which enhance the drug delivery, especially to the DNA of tumor cells, and reduce the toxicity of known cytotoxic agents.<sup>71,86-89</sup> In recent years, several approaches have been proposed to improve the delivery of cytotoxic agents using supramolecules, miktoarm star polymers, and micelles.<sup>295-297</sup> For instance, Lim and co-workers loaded the known anticancer drug doxorubicin in amphiphilic poly(D,L-Lactide-Co-Glycolide)-b-poly(N-acryloylmorpholine) as AB<sub>2</sub> miktoarm star block copolymers to enhance the drug delivery.<sup>295</sup> They also reported the supramolecular poly(N-acryloylmorpholine)-b-poly(D,L-lactide) pseudo block copolymer which is used to enhance the drug delivery and synthesized *via* host-guest interaction.<sup>296</sup> Recently, Hasegawa and co-workers investigated the thioether-based polymeric micelles with fine-tuned oxidation sensitivities for chemotherapeutic drug delivery.<sup>297</sup> In this project, we are interested in the synthesis of new designs from  $\beta$ -hydroxydithiocinnamic ester ligands which are utilized as CTA agents for RAFT polymerization of acrylates, acrylamides, and styrene. In addition, the synthesis of the platinum (II) complexes from the water-soluble N-acryloylmorpholine - $\beta$ -hydroxydithiocinnamate- $\beta'$ -2- propionic acid polymers.

##### **4.4.1 Synthesis and characterization of $\beta$ -hydroxydithiocinnamic ester compounds (HA1-HA9)**

The synthesis of HA1-HA9 compounds was according to Thuillier synthetic methods and with the same modified procedures used for the synthesis of HL1-HL9 in project 1, with the only difference being using 2-bromopropionic acid instead of 2-bromoacetic acid, affording the new class of  $\beta$ -hydroxydithiocinnamic compounds (HA1-HA9), which can be utilized as chain transfer agent (CTA), bearing *O-/m-/p-*(CH<sub>3</sub>, OCH<sub>3</sub>, or Br) as substituent X in the stabilizing group, and CH(CH<sub>3</sub>)COOH as leaving group for RAFT polymerization (Scheme 11). All compounds were obtained in moderate to high yield, which is higher in case of *para*- and *ortho*-substituted ligands than the *meta*-substituted ones. Moreover, they are characterized by different NMR spectroscopy, mass spectrometry, and elemental analysis. Recrystallization of HA5 and HA6 produced suitable single crystals for X-ray diffraction studies. Both <sup>1</sup>H NMR and <sup>13</sup>C{<sup>1</sup>H} NMR spectra for HA1-HA9 are generally similar to the previously synthesized free ligands in project 1 (HL1-1L9), with the only difference in the terminal S-group. In the <sup>1</sup>H NMR spectra, HA1-HA9 displays resonances at  $\delta$  1.77 ppm (d, 3H, CH-CH<sub>3</sub>) and  $\delta$  4.77 ppm

(q, 1H, S-CH-), which is not observed in HL1-HL9 (average values given). In the  $^{13}\text{C}\{^1\text{H}\}$  NMR spectra of HA1-HA9, resonances for the ( $\text{CH}_3$ ) and (S-CH-) carbons were found at  $\delta$  17 and  $\delta$  46 ppm, respectively, which is not observed also in HL1-HL9 (average values given).



Scheme 11: Synthesis of  $\beta$ -hydroxydithiocinnamic compounds (HA1-HA9).

#### 4.4.2 Molecular Structures Determination for HA5 and HA6

Recrystallization from  $\text{CH}_2\text{Cl}_2$  and cyclohexane mixture (1:1) of HA5 and HA6 provided suitable single crystals for X-ray diffraction studies. Molecular structures are provided in Figure 47 with ellipsoids drawn at the 50% probability level.

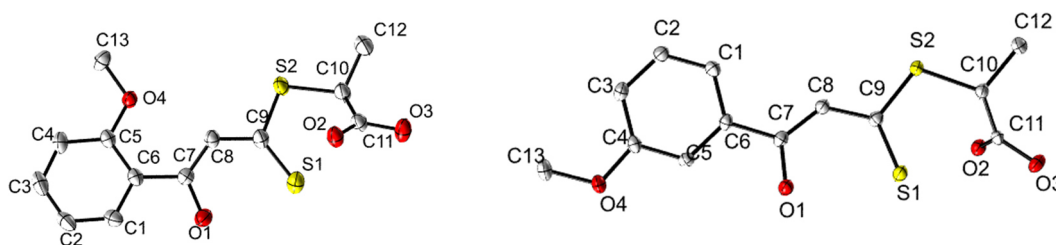


Fig. 47: Molecular structures of HA5 (left), and HA6 (right) (probability 50%). Hydrogen atoms have been omitted for clarity.

**Crystal Data for HA6:**  $\text{C}_{13}\text{H}_{14}\text{O}_4\text{S}_2$ ,  $M_r = 298.36 \text{ gmol}^{-1}$ , yellow prism, size  $0.102 \times 0.092 \times 0.088 \text{ mm}^3$ , monoclinic, space group  $P 2_1/c$ ,  $a = 12.5849(3)$ ,  $b = 10.3771(2)$ ,  $c = 10.9319(2) \text{ \AA}$ ,  $\beta = 104.836(1)^\circ$ ,  $V = 1380.05(5) \text{ \AA}^3$ ,  $T = -140 \text{ }^\circ\text{C}$ ,  $Z = 4$ ,  $\rho_{\text{calcd.}} = 1.436 \text{ gcm}^{-3}$ ,  $\mu (\text{Mo-K}\alpha) = 3.92 \text{ cm}^{-1}$ , multi-scan,  $\text{transmin} = 0.7190$ ,  $\text{transmax} = 0.7456$ ,  $F(000) = 624$ , 10180 reflections in  $h(-16/16)$ ,  $k(-13/13)$ ,  $l(-14/14)$ , measured in the range  $1.674^\circ \leq \Theta \leq 27.445^\circ$ , completeness  $\Theta_{\text{max}} = 99.3\%$ , 3143 independent reflections,  $R_{\text{int}} = 0.0213$ , 3033 reflections with  $F_o > 4\sigma(F_o)$ , 217 parameters, 0 restraints,  $R1_{\text{obs}} = 0.0670$ ,  $wR2_{\text{obs}} = 0.1631$ ,  $R1_{\text{all}} = 0.0686$ ,  $wR2_{\text{all}} = 0.1642$ , GOOF = 1.100, largest difference peak and hole:  $1.476 / -0.948 \text{ e \AA}^{-3}$ .

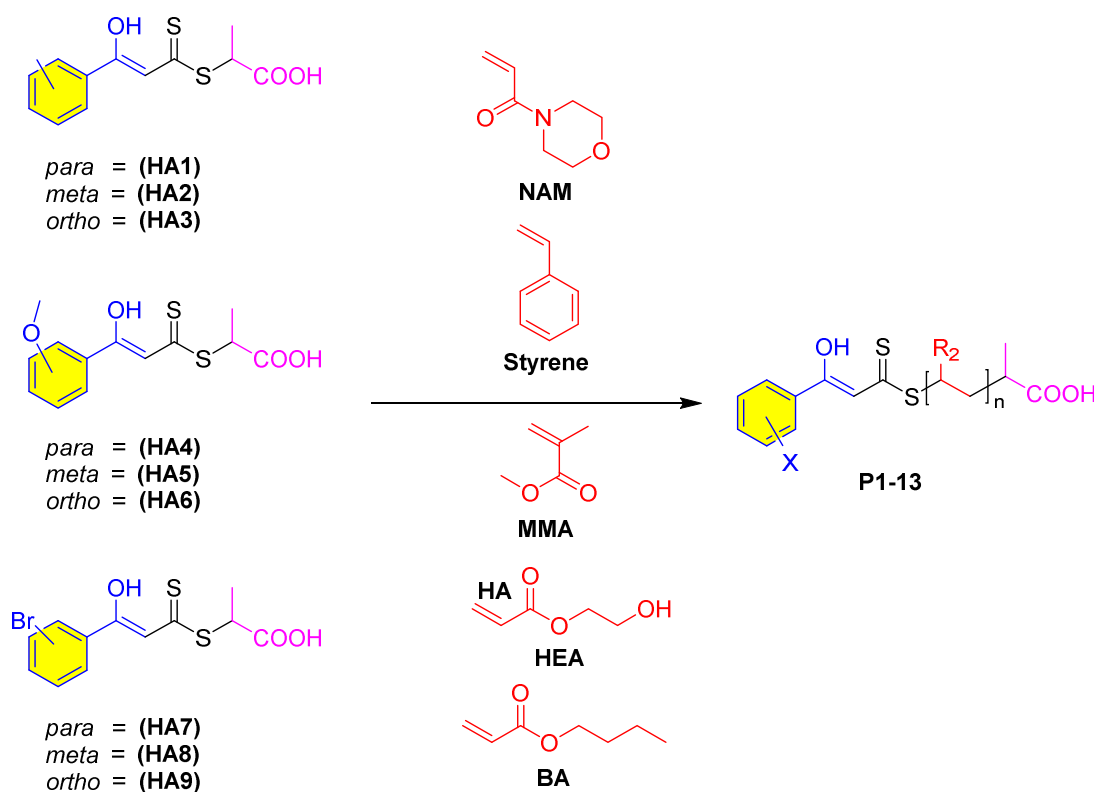
**Crystal Data for HA5:** C<sub>13</sub>H<sub>14</sub>O<sub>4</sub>S<sub>2</sub>, Mr = 298.36 g mol<sup>-1</sup>, yellow prism, size 0.100 x 0.082 x 0.080 mm<sup>3</sup>, monoclinic, space group P 2<sub>1</sub>/c, a = 5.40870(10), b = 11.3630(2), c = 21.5531(4) Å, β = 92.936(1)°, V = 1322.89(4) Å<sup>3</sup>, T = -140 °C, Z = 4, ρ<sub>calcd.</sub> = 1.498 g cm<sup>-3</sup>, μ (Mo-K<sub>α</sub>) = 4.09 cm<sup>-1</sup>, multi-scan, transmin: 0.7146, transmax: 0.7456, F(000) = 624, 8072 reflections in h(-6/7), k(-14/14), l(-21/27), measured in the range 2.027° ≤ Θ ≤ 27.484°, completeness Θ<sub>max</sub> = 99.7%, 3018 independent reflections, R<sub>int</sub> = 0.0147, 2848 reflections with F<sub>o</sub> > 4σ(F<sub>o</sub>), 228 parameters, 0 restraints, R<sub>1obs</sub> = 0.0256, wR<sub>2obs</sub><sup>2</sup> = 0.0652, R<sub>1all</sub> = 0.0273, wR<sub>2all</sub><sup>2</sup> = 0.0665, GOOF = 1.035, largest difference peak and hole: 0.369 / -0.208 e Å<sup>-3</sup>.

#### 4.4.3 Polymerizations and kinetics

The reversible addition-fragmentation chain-transfer (RAFT) process has become a versatile tool for polymeric architectures and is suitable for the preparation of defined polymers tolerating a large variety of functional groups with a wide variety of monomers.<sup>298-305</sup> Generally, trithiocarbonates and aromatic dithioesters as effective chain transfer agents (CTAs), which are used to polymerize more activated monomers, such as styrenes, (meth)acrylates or (meth)acrylamides, but only a few examples have been reported, where the resulting end groups are directly considered for a secondary use besides controlling the polymerization.<sup>306,307</sup> Herein, it is demonstrated that β-hydroxy dithiocinnamic esters represent a hitherto overlooked class of materials, which are originally designed for the complexation of transition metals but may as well act as reversible CTAs. Modified with a suitable leaving group (R-group), these vinyl conjugated dithioesters might provide reasonable control over the polymerization of acrylates, acrylamides, or styrene *via* the RAFT process. In fact, the literature is rich with numerous examples of chain transfer agents (CTA) that contain reactive moieties either attached to the functional leaving group R or the stabilizing unit Z.<sup>308-321</sup> Nevertheless, the bivalent uses of the inherent RAFT motif as a reactive moiety remain scarce in the literature, which is partly related to the limited option in the structural design of the CTA without sacrificing its ability to control the polymerization.<sup>306,322</sup> Interesting, but so far overlooked compounds are β-hydroxydithiocinnamic esters, which are well known for their ability to form complexes with a variety of metals including Ni, Pd, Pt, Ru, and Os.<sup>257-270</sup> The structure differs from common CTAs based on trithiocarbonates or dithiobenzoates, but the conjugation of the vinyl benzenemoiety (Z-group) might still be sufficient to stabilize the intermediate radical in the RAFT process. The group of Destarac and co-workers have previously examined dithiocinnamic acid derivatives as CTAs in RAFT, but the vinylogous character of their RAFT agents caused severe retardation during polymerization.<sup>323</sup> The β-hydroxy modified ligands presented in this work might circumvent the observed

degeneration by a Diels-Alder reaction, as the additional hydroxy group increases the steric hindrance and electron density at the vinyl group.

In the polymerization of  $\beta$ -hydroxydithiocinnamic esters compounds, azobisisobutyronitrile (AIBN) was used as the initiator (CTA/initiator ratio: 20/1). Given a temperature of 70 °C and a polymerization time of 24 h, around 95% of the initiator should be decomposed resulting in a theoretical livingness of all polymers of >95%, if an initiator efficiency of 0.5 is assumed. Herin HA1 was chosen to first evaluate the general potential of these compounds for controlling the polymerization of the different monomer types. The tested monomers include the acrylates n-butyl acrylate (BA) and 2-hydroxyethyl acrylate (HEA), the acrylamide N-acryloyl morpholine (NAM), and styrene which are all known to be polymerizable with common trithiocarbonate and aromatic dithioester based RAFT-agents.<sup>306,307</sup> While the methylmethacrylate (MMA) was further included as a representative for methacrylates, but the R-group of our  $\beta$ -hydroxydithiocinnamic acid derivatives might not be suitable for efficient chain transfer. The impact of different substituents on the benzene ring was investigated using the monomer N-acryloyl morpholine (NAM). Scheme 12 depicts an overview of the examined  $\beta$ -hydroxydithiocinnamic acid derivatives and the set of monomers tested during the RAFT polymerization. The resulted polymers (P1-P13) were characterization by NMR and size exclusion chromatography (SEC).



Scheme 12: Chemical structures of the ligands, monomers, and the resulting polymers.

An overview of all combinations and the resulting polymers (after 24 h of polymerization) is given in Table 8. Narrowly distributed polymers were obtained for the acrylates and styrene ( $\mathcal{D} < 1.2$ ), while the dispersity is slightly increased for NAM. However, MMA could not be controlled by these compounds, which corresponds to observations for established CTAs with similar poor leaving groups R.

Table 8: Summary of all prepared polymers.

Polymer	Monomer	CTA (X)	Conversion, <sup>a</sup> 24 h [%]	$M_{n,theo}$ <sup>b</sup> [kg mol <sup>-1</sup> ]	$M_{n,NMR}$ <sup>c</sup> [kg mol <sup>-1</sup> ]	$M_{n,SEC}$ <sup>d</sup> [kg mol <sup>-1</sup> ]	$\mathcal{D}$ <sup>d</sup>
P1	NAM	HA1 (Me)	79	5.9	7.8	7.1	1.24
P2	BA	HA1 (Me)	92	6.2	8.2	8.4	1.18
P3	Styrene	HA1 (Me)	18	1.2	2.4	2.9	1.11
P4	HEA	HA1 (Me)	96	5.9	6.3	10.4	1.18
P5	MMA	HA1 (Me)	60	-	-	213.0	1.88
P6	NAM	HA2 (Me)	68	5.1	6.6	5.8	1.23
P7	NAM	HA3 (Me)	67	5.0	5.6	5.3	1.23
P8	NAM	HA6 (OMe)	83	6.2	8.3	6.4	1.29
P9	NAM	HA5 (OMe)	78	5.8	6.4	5.5	1.31
P10	NAM	HA4 (OMe)	82	6.1	6.8	5.8	1.31
P11	NAM	HA9 (Br)	71	5.4	6.6	5.9	1.26
P12	NAM	HA8 (Br)	40	3.2	4.0	2.6	1.40
P13	NAM	HA7 (Br)	55	4.2	5.0	4.4	1.32

<sup>a</sup> Determined from <sup>1</sup>H-NMR; <sup>b</sup> Calculated from conversion and the targeted DP of 50; <sup>c</sup> Precipitated polymers, determined from ratio of aromatic signals to signals of repeating units in <sup>1</sup>H NMR (precipitated polymers); <sup>d</sup> Precipitated polymers, determined by SEC (Eluent: DMAc + 0.21 wt% LiCl, PMMA-calibration).

Detailed kinetic studies revealed a linear evolution of molar masses with conversion. It has however to be considered that the increased reactivity of the vinyl moiety in the Z-group might still cause side reaction, if extended reaction times are applied. Nevertheless, the resulting polymer chains can successfully be chain extended, if shorter polymerization times are applied, verifying a high-end group fidelity and the living character of the polymerization. The substitution pattern on the adjacent benzene has overall only a minor impact on the polymerization behavior. Only in the case of the rather reactive bromine substituents reduced conversions and a broadening of the molar mass distribution was observed, which became particularly prominent for the meta and para-substituted compounds.



#### **4.4.4 Synthesis and characterization of the Pt(II) NAM $\beta$ -hydroxydithiocinnamic acid polymer complexes (Dual Function).**

In order to investigate whether the  $\beta$ -hydroxydithiocinnamic ester end group is still capable of fulfilling its second function, the complexation of metals. Therefore, we have exemplarily chosen the water-soluble NAM-polymers P1 and P6–P11 that react with  $K_2PtCl_4$  to form the corresponding complexes PtP1 and PtP6-11. The Pt(II) complexes were characterized using NMR spectroscopy and inductively coupled plasma atomic emission spectroscopy (ICP-AES). The  $^1H$  NMR spectra of the resulting complexes PtP1 and PtP6-11 are very similar compared to the spectra of the corresponding precursor's polymer P1 and P6-11. However, the disappearance of the signal around 15 ppm indicates that the coordination occurred through the  $\beta$ -oxo atom. Furthermore, the  $^{13}C\{^1H\}$  NMR spectra of PtP1 and PtP6-11 display a downfield shift ( $\approx 3$ – $7$  ppm) for the methine carbon atom and a high field shift ( $\approx 27$ – $37$  ppm) for the quaternary thiocarbonyl carbon atom (C=S), compared to the corresponding precursor's polymer P1 and P6-11. The disappearance of the signal around 15 ppm in the  $^1H$  NMR spectra and both the downfield and upfield shift of the methine and thiocarbonyl carbons, respectively, were due to the coordination of  $\beta$ -hydroxydithiocinnamic ester end group towards the Pt(II) as O,S-chelate unit. ICP-AES was used to quantify the amount of coordinated Pt in the polymers P1 and P6-11.<sup>324-327</sup> Interestingly, in most polymers the Pt content was found, which is considerably higher than expected for a complexation of one equivalent of Pt, despite excessive washing steps and thorough purification. These calculations were based on average molar masses or number of repeating units, respectively, estimated from the  $^1H$  NMR signals (aromatic protons vs protons of repeating units) of the precipitated polymers (Table 9). Although the  $M_n$  values might deviate from absolute molar masses (e.g., by the loss of the end group), this determination should still reflect the real content of active complexation sites in the sample independent of the molar masses. Therefore, these deviations cannot be related to false molar mass values. Instead, we assume that the additional binding of Pt is caused by the carboxylic acid groups present at the  $\alpha$  end of the polymer chains (Figure 48a), which were initially chosen to simplify the purification of the  $\beta$ -hydroxydithiocinnamic esters. The SEC analysis of the exemplarily chosen complex PtP6 further corroborated our assumption, as a bimodal distribution is observed (Figure 48b), which reflects the expected composition comprising a polymer distribution close to the initial polymer P6 and second distribution representing a coupled species at double molar mass. Given the proposed two structures A and B, we estimated that PtP6 must consist of 42% A and 58% B considering a measured Pt content of 47.16 mg(Pt)/g(sample) (ICP-AES), and an  $M_n$  (NMR) of 6.6 kg mol $^{-1}$  for the polymer P6. Independent of the discrepancies in the expected and observed Pt content, the high

amount of Pt bound in the polymers can only be explained if the  $\beta$ -hydroxydithiocinnamic ester moiety is still able to bind the metal. Therefore, this data confirms that the functionality of the end group is maintained during the polymerization and the desired Pt complexes can be formed.

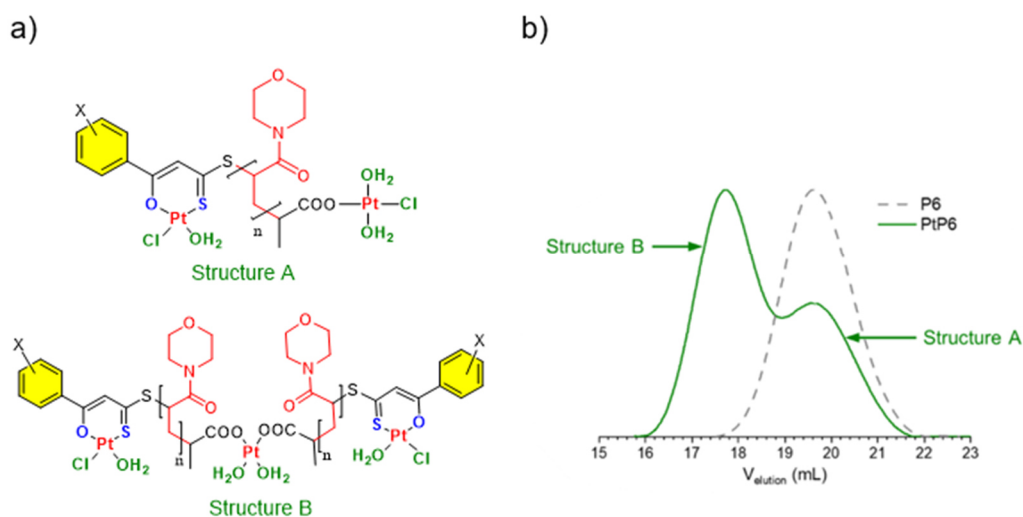


Fig. 48: a) The two potentially formed structures during the complexation of Pt by the RAFT-polymers based on NAM; b) corresponding SEC of the complex PtP6 (green solid line) in comparison with the initial polymer P6 (grey dashed line) (DMAc/LiCl, RI-detection, PMMA-calibration).

### Calculations of compositions

More than one equivalent of Pt was found per chain in all samples, which is explained by the formation of the following two potential structures A and B (Figure 48a). The experimentally determined mass of Pt for 1 g of sample is related to the ratio of the two proposed structures according to the equation

$$m(\text{Pt}) = \left[ x(A) \frac{2}{M(A)} + x(B) \frac{3}{M(B)} \right] A(\text{Pt})$$

where  $x(A)$  and  $x(B)$  are the molar ratios of structures A and B in the sample,  $M(A)$  and  $M(B)$  are the average molar masses of the corresponding structures (average degrees of polymerization ( $n$ ) were estimated from the  $^1\text{H}$  NMR spectra of the precipitated polymers), and  $A(\text{Pt})$  is the atomic weight of Pt. The numbers 2 and 3 in the numerators correspond to the number of Pt atoms in the corresponding structures A and B, respectively.

With  $x(B) = 1 - x(A)$  we can resolve the equation to estimate  $x(A)$  according to

$$x(A) = \left[ \frac{m(\text{Pt})}{M(\text{Pt})} - \frac{3}{M(B)} \right] / \left[ \frac{2}{M(A)} - \frac{3}{M(B)} \right]$$

So, Table 9 summarizes the composition of the synthesized PtP1 and PtP6-11 complexes.

Table 9: Concentrations on the Pt emission signal at 214.423 nm using ICP-AES.

Pt(II) complexes	Pt content (Theor.)[mg/g]	Pt content (Exp.)[mg/g]	Calculated composition x(A) + x(B)(in %)
<b>PtP1 (structure A)</b> Pt <sub>2</sub> C <sub>384</sub> H <sub>601</sub> N <sub>53</sub> O <sub>112</sub> S <sub>2</sub> Cl <sub>2</sub> M.W.= 8277.48 g/mol	47.14		
<b>PtP1 (structure B)</b> Pt <sub>3</sub> C <sub>768</sub> H <sub>1198</sub> N <sub>106</sub> O <sub>222</sub> S <sub>4</sub> Cl <sub>2</sub> M.W.= 16252.94 g/mol	36.01	39.60	32% (A) + 68% (B)
<b>PtP6 (structure A)</b> Pt <sub>2</sub> C <sub>328</sub> H <sub>513</sub> N <sub>45</sub> O <sub>96</sub> S <sub>2</sub> Cl <sub>2</sub> M.W.= 7148.12 g/mol	54.58		
<b>PtP6 (structure B)</b> Pt <sub>3</sub> C <sub>656</sub> H <sub>1022</sub> N <sub>90</sub> O <sub>190</sub> S <sub>4</sub> Cl <sub>2</sub> M.W.= 13994.22 g/mol	41.82	47.16	42% (A) + 58% (B)
<b>PtP7 (structure A)</b> Pt <sub>2</sub> C <sub>279</sub> H <sub>436</sub> N <sub>38</sub> O <sub>82</sub> S <sub>2</sub> Cl <sub>2</sub> M.W.= 6159.93 g/mol	63.34		
<b>PtP7 (structure B)</b> Pt <sub>3</sub> C <sub>558</sub> H <sub>868</sub> N <sub>76</sub> O <sub>162</sub> S <sub>4</sub> Cl <sub>2</sub> M.W.= 12017.84 g/mol	48.70	52.80	28% (A) + 72% (B)
<b>PtP8 (structure A)</b> Pt <sub>2</sub> C <sub>412</sub> H <sub>645</sub> N <sub>57</sub> O <sub>121</sub> S <sub>2</sub> Cl <sub>2</sub> M.W.= 8858.16 g/mol	44.05		
<b>PtP8 (structure B)</b> Pt <sub>3</sub> C <sub>824</sub> H <sub>1286</sub> N <sub>114</sub> O <sub>240</sub> S <sub>4</sub> Cl <sub>2</sub> M.W.= 17414.30 g/mol	33.61	37.8	40% (A) + 60% (B)
<b>PtP9 (structure A)</b> Pt <sub>2</sub> C <sub>314</sub> H <sub>491</sub> N <sub>43</sub> O <sub>93</sub> S <sub>2</sub> Cl <sub>2</sub> M.W.= 6881.78 g/mol	56.70		
<b>PtP9 (structure B)</b> Pt <sub>3</sub> C <sub>628</sub> H <sub>978</sub> N <sub>86</sub> O <sub>184</sub> S <sub>4</sub> Cl <sub>2</sub> M.W.= 13461.54 g/mol	43.48	48.90	41% (A) + 59% (B)
<b>PtP10 (structure A)</b> Pt <sub>2</sub> C <sub>335</sub> H <sub>524</sub> N <sub>46</sub> O <sub>99</sub> S <sub>2</sub> Cl <sub>2</sub> M.W.= 7305.29 g/mol	53.41		
<b>PtP10 (structure B)</b> Pt <sub>3</sub> C <sub>670</sub> H <sub>1044</sub> N <sub>92</sub> O <sub>196</sub> S <sub>4</sub> Cl <sub>2</sub> M.W.= 14308.56 g/mol	40.90	45.00	33% (A) + 67% (B)
<b>PtP11 (structure A)</b> Pt <sub>2</sub> C <sub>320</sub> H <sub>499</sub> N <sub>44</sub> O <sub>94</sub> S <sub>2</sub> BrCl <sub>2</sub> M.W.= = 7071.82 g/mol	55.17		
<b>PtP11 (structure B)</b> Pt <sub>3</sub> C <sub>640</sub> H <sub>994</sub> N <sub>88</sub> O <sub>186</sub> S <sub>4</sub> Br <sub>2</sub> Cl <sub>2</sub> M.W.= 13841.62 g/mol	42.28	47.50	40% (A) + 60% (B)

Considering the unexpected formation of the Pt-carboxylate complexes, we would like to emphasize that although these simple complexes appear quite robust, significantly higher binding constants can be expected for the Pt complexes with  $\beta$ -hydroxydithiocinnamic esters considering the bidentate character of this O,S-ligands. The carboxylic acid moiety at the R-leaving group further represents a versatile group for additional modifications of the polymers regarding potential applications. These findings open a versatile new route to tailor-made polymer-bound metal complexes. Further studies in this direction are under consideration in our groups, which should further underline the importance of the dual use of the presented CTAs.

#### 4.4.5 Cytotoxic Activity of the free ligands, NAM-polymers and the Pt(II) NAM- $\beta$ -hydroxydithiocinnamic esters Complexes

The anti-proliferative activity of selected samples from the free ligands (HA2, HA4, and HA9), NAM- $\beta$ -hydroxydithiocinnamic esters polymers (P6, P10, and P11) and their Pt complexes (PtP6, PtP10, and PtP11) against the epithelial ovarian cancer cell lines A2780 and Skov3 and their cisplatin-resistant subcultures was determined in Table 10.

Table 10: Mean IC<sub>50</sub> values of the tested compounds for ovarian cancer cell lines [ $\mu$ M].

		A2780	A2780CIS	SKOV3	SKOV3CIS
CIS	IC50	1.718	11.87	24.92	49.66
	95% CI IC50	1.29 - 2.28	7.71 - 18.25	11.87 - 52.32	38.41 - 64.20
HA9	IC50	458.09	149.82	501.99	not calculated
	95% CI IC50	38.28 - 548.12	78.43 - 286.20	383.19 - 657.61	
HA2	IC50	1891.86	527.14	not calculated	1157.35
	95% CI IC50	1095.9 - 3266.6	232.34 - 1195.96		507.96 - 2636.94
HA4	IC50	307.17	184.39	265.39	1917.87
	95% CI IC50	112.21 - 840.87	129.38 - 262.78	205.01 - 343.55	1898.0 - 1938.6
P11	IC50	216.01	214.74	388.67	857.13
	95% CI IC50	80.35 - 580.71	117.68 - 391.88	272.26 - 554.86	714.22 - 1028.65
P6	IC50	1059.44	1847.24	1283.77	not calculated
	95% CI IC50	141.09 - 7955.45	222.55 - 15330.06	767.25 to 2148.01	
P10	IC50	not calculated	not calculated	702.79	not calculated
	95% CI IC50			531.84 - 928.68	
PtP11	IC50	108.41	120.5	78.24	273.54
	95% CI IC50	84.12 - 139.72	94.59 - 153.51	51.70 - 118.41	193.45 - 386.79
PtP6	IC50	139.99	305.04	496.75	636.2
	95% CI IC50	111.78 - 175.33	128.12 - 726.25	89.59 - 2754.37	323.70 - 1250.41
PtP10	IC50	338.62	375.17	139.4	392.59
	95% CI IC50	145.41 - 788.57	208.51 - 675.02	105.14 - 184.81	249.79 - 617.02

(Where CI - confidence interval)

Missing data are caused by the absence of a measurable effect on cell viability.

They were evaluated as ineffective. Nevertheless, structure modifications, for instance, the polymerization of other monomers that can bind to a known anticancer drug might improve the cytotoxicity of such kind of promising compounds

Furthermore, these dual-function compounds are attractive candidates to directly prepare functional polymers for several applications, for instance, wastewater treatment since they could chelate many transition and heavy metals. Additionally, replacing the Pt element with Ti, Gd, or Lu might make them useful for bioimaging.

## 5. Publications

### 5.1 [ME-1]

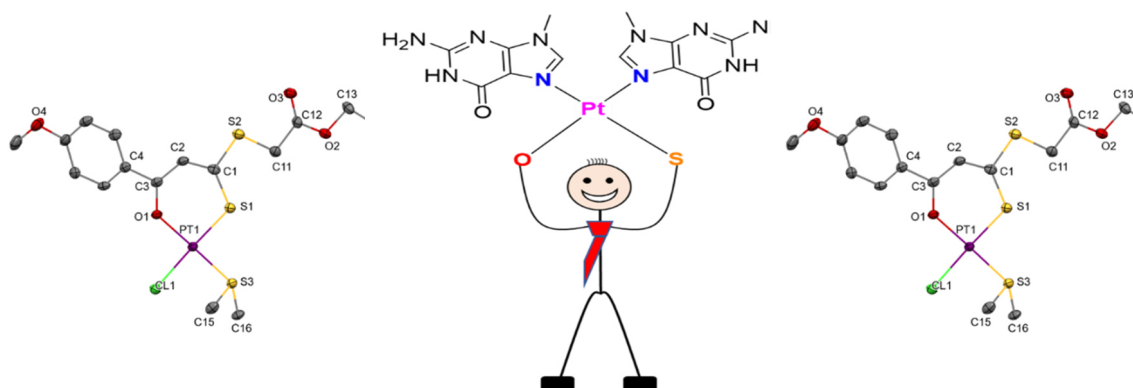
#### **Novel Homoleptic and Heteroleptic Pt(II) $\beta$ -oxodithiocinnamic ester Complexes: Synthesis, Characterization, Interactions with 9-methylguanine and Antiproliferative Activity**

Micheal K. Farh, Norman Häfner, Helmar Görls, Ingo B. Runnebaum, Wolfgang Weigand

Zeitschrift für anorganische und allgemeine Chemie **2022**, submitted.

Manuscript submission number: zaac.202200349

Reproduced by permission of Micheal K. Farh, Norman Häfner, Helmar Görls, Ingo B. Runnebaum, Wolfgang Weigand



**Submission Confirmation for Novel Homoleptic and Heteroleptic Pt(II)  $\beta$ -oxodithiocinnamic ester Complexes: Synthesis, Characterization, Interactions with 9-methylguanine and Antiproliferative Activity**

You are being carbon copied ("cc:'d") on an e-mail "To" "Wolfgang Weigand" wolfgang.weigand@uni-jena.de CC: "Micheal K. Farh" micheal.eshak@uni-jena.de, "Norman Häfner" norman.haefner@med.uni-jena.de, "Helmar Görls" helmar.goerls@uni-jena.de, "Ingo B. Runnebaum" direktion-gyn@med.uni-jena.de

Dear Prof. Dr. Weigand,

Your submission entitled "Novel Homoleptic and Heteroleptic Pt(II)  $\beta$ -oxodithiocinnamic ester Complexes: Synthesis, Characterization, Interactions with 9-methylguanine and Antiproliferative Activity" has been received by Zeitschrift für anorganische und allgemeine Chemie

The submission number for your Research Article is zaac.202200349.

To check on the progress of your paper, please go to <https://www.editorialmanager.com/zaac/> and log in as an Author using your username (Your username is: \*\*\*\*\*) and password. If you have forgotten your password, please use the "Send Access Credentials" option given on the login screen.

If the manuscript is accepted for publication, this author's affiliation will be used to determine eligibility for some open access funding (click [here](https://authorservices.wiley.com/author-resources/Journal-Authors/open-access/affiliation-policies-payments/institutional-funder-payments.html) for details).

This journal offers a number of license options; information about this is available here: <https://authorservices.wiley.com/author-resources/Journal-Authors/licensing/index.html>  
The submitting author has confirmed that all co-authors have the necessary rights to grant in the submission, including in light of each co-author's funder policies. If any author's funder has a policy that restricts which kinds of license they can sign, for example if the funder is a member of Coalition S, please make sure the submitting author is aware.

We will contact you again with the decision on this paper as soon as possible.

Kind regards,  
Editorial Office Staff  
*Zeitschrift für anorganische und allgemeine Chemie*

---

WILEY-VCH 69469 Weinheim  
Boschstrasse 12 Germany  
phone: +49-6201-606-574 fax: +49-6201-606-203  
e-mail: [zaac-office@wiley-vch.de](mailto:zaac-office@wiley-vch.de)  
<http://www.zaac.wiley-vch.de>

---

# Novel Homoleptic and Heteroleptic Pt(II) $\beta$ -oxodithiocinnamic ester Complexes: Synthesis, Characterization, Interactions with 9-methylguanine and Antiproliferative Activity

Micheal K. Farh,<sup>[a,b]</sup> Norman Häfner,<sup>[c]</sup> Helmar Görls,<sup>[a]</sup> Ingo B. Runnebaum,<sup>\*,[c]</sup> and Wolfgang Weigand,<sup>\*,[a,d]</sup>

Dedication ((optional))

**Abstract:** Three new series of homoleptic and heteroleptic platinum(II)  $\beta$ -oxodithiocinnamic ester complexes, [Pt(L1-L9)<sub>2</sub>], [Pt(L1-L9)(DMS)Cl] and [Pt(L1-L9)(DMSO)Cl], were synthesized and characterized using elemental analysis, mass spectrometry, and different NMR spectroscopy (<sup>1</sup>H, <sup>13</sup>C{<sup>1</sup>H} and <sup>195</sup>Pt). The  $\beta$ -oxodithiocinnamic esters coordinate towards the platinum(II) centre as O,S-bidentate chelating ligands. The structures of HL3, [Pt(L2)<sub>2</sub>], [Pt(L6)(DMS)Cl] as well as [Pt(L2)(DMSO)Cl] have been confirmed through the X-ray crystallography, where the platinum(II) complexes exhibit a slightly distorted square planar geometry. In this article, we also investigated the solvolysis of three representative Pt(II) complexes, as well as the interaction with 9-methylguanine as a DNA model system, by utilizing the LC-ESI-MS technique. A selection of the complexes was assessed for their use as anticancer agents, and cytotoxicity assays with these complexes showed modest toxicity on both Cisplatin sensitive and resistant ovarian cancer cell lines. However, the compounds cytotoxicity was not affected by the Cisplatin resistance mechanisms and a specific selection of the ligands may modify the cell line specificity.

## Introduction

$\beta$ -oxodithioesters are highly efficient intermediates in organic synthesis, and despite their differing reactivities, considered parallel synthons for  $\beta$ -ketoester chemistry.<sup>[1-7]</sup> Also, they

exhibit keto-enol tautomerism (Fig. 1), which is shifted towards the enol form due to the high electronegativity of the  $\beta$ -keto group that makes the  $\alpha$ -protons more acidic.<sup>[1]</sup> The enol form is also stabilized by the intramolecular hydrogen bonding and the conjugated system (Fig. 1A).<sup>[1]</sup> Furthermore,  $\beta$ -oxodithioesters contain polyfunctional groups with multi-reactive centers including three nucleophilic and two electrophilic centers, as shown in (Fig. 1B and 1C). Synthons containing both electrophilic and nucleophilic centers have significant potential for developing more effective reaction pathways during the construction of various heterocyclic systems.<sup>[1-4]</sup> As a result of those active centers and the specific advantages of easy preparation and versatile reactivity,  $\beta$ -oxodithioesters have been widely applied as a valuable building block in the synthesis of several organosulfur moieties, in which sulfur acts either as an internal or external substituent.<sup>[1-7]</sup> In addition,  $\beta$ -oxodithioesters have been employed as O,S-chelating ligands in the synthesis of several homo and heteroleptic transition metal complexes.<sup>[8-16]</sup> Several zinc(II), cadmium (II), nickel(II), and copper (II)  $\beta$ -oxodithioester complexes have been reported by Singh and co-workers to catalyze the transformation of many organic reactions.<sup>[8-10]</sup> Moreover, some nickel(II), palladium(II), and platinum(II)  $\beta$ -oxodithioester complexes exhibited antileishmanial activities.<sup>[11]</sup> A series of nickel(II), palladium(II), platinum(II), ruthenium(II), and osmium(II)  $\beta$ -oxodithioester complexes have been also reported by Weigand and co-workers to possess anticancer activities.<sup>[12-17]</sup> It is worth mentioning that the co-operative effects of electronic and geometric properties in metal-organic ligand structures ultimately promote highly diverse interactions with biological targets, providing opportunities for drug activity and development.<sup>[12-18]</sup> Although Cisplatin is one of the most effective cancer drugs<sup>[19-25]</sup>, there is a significant adverse effect on normal cells and tissues, cross-resistance, and severe side effects that make it critical

[a] M. K. Farh, Dr. H. Görls, Prof. Dr. W. Weigand  
Institut für Anorganische und Analytische Chemie, Friedrich-Schiller-Universität  
Humboldtstraße 8, 07743 Jena, Germany  
E-mail: wolfgang.weigand@uni-jena.de

[b] M. K. Farh  
Department of Chemistry, Faculty of Science, Assiut University  
Assiut 71515, Egypt

[c] Dr. N. Häfner, Prof. Dr. I. B. Runnebaum  
Department of Gynecology, Jena University Hospital—Friedrich-Schiller University Jena  
Am Klinikum 1, 07747 Jena, Germany  
Direktion-Gyn@med.uni-jena.de

[d] Prof. Dr. W. Weigand  
Jena Center for Soft Matter (JCSM), Friedrich Schiller University  
Philosophenweg 7, 07743 Jena, Germany

Supporting information for this article is given via a link at the end of the document

to find new platinum-based drugs with a manageable set of side effects applicable for clinical use.<sup>[26-28]</sup>

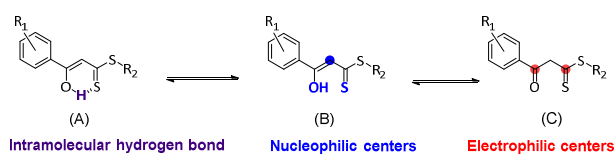
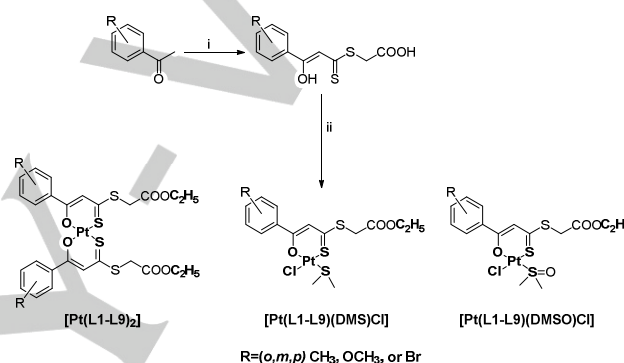


**Figure 1:** Structure of  $\beta$ -hydroxydithiocinnamic ester derivatives (intramolecular hydrogen bond, and active sites).

## Results and Discussion

Several advanced methods have been developed for the synthesis of  $\beta$ -oxodithioesters. Thuillier *et al.* utilize enolizable ketones as acetophenone derivatives that, when treated with a strong base, generate active methylene compounds, which further react with  $\text{CS}_2$  to provide the sodium salt of dithiocarboxylic acid that can be alkylated to the respective  $\beta$ -oxodithioesters.<sup>[29]</sup> Another convenient method was described by Junjappa and co-workers, in which the active methylene ketones were treated with (S,S)-dimethyl trithiocarbonate in a DMF–hexane mixture affording the desired  $\beta$ -oxodithioesters.<sup>[30]</sup> Alternatively, Junjappa *et al.* by using 3-methylimidazolium-1-carbodithioic acid methyl ester instead of (S,S)-dimethyl trithiocarbonate with active methylene compounds,  $\beta$ -oxodithioesters can be also obtained.<sup>[31]</sup>  $\beta$ -hydroxydithiocinnamic esters used in this study were prepared according to the Thuillier method with some modifications. The acetophenone derivatives were first treated with potassium tert-butoxide and then carbon disulfide to obtain the sodium salt of dithiocarboxylic acid that can be reacted in situ with 2-bromoacetic acid instead of the normal alkyl halide as established in the previous synthetic methods, affording finally the new class of  $\beta$ -hydroxydithiocinnamic ligands (Scheme 1). These ligands show some interesting features: (i) O,S-bidentate chelating ligand, (ii) keto-enol tautomerism (iii) having both hard oxygen and soft sulfur donor atoms, (iv) different functional groups on the benzene ring and terminal carboxylic group which may influence the electronic and steric properties. In view of these features, we now present the synthesis of the platinum(II)  $\beta$ -hydroxydithiocinnamic ester complexes using the platinum(II) precursor complex *cis*-[PtCl<sub>2</sub>(DMS)(DMSO)]. *Cis*-[PtCl<sub>2</sub>(DMS)(DMSO)] was prepared according to previous literature procedure<sup>[32]</sup> and reacts with the  $\beta$ -hydroxydithiocinnamic ester ligands in ethanolic solution to generate the desired platinum(II) complexes (Scheme 1). Three different classes of compounds were obtained through

this method: homoleptic bis-chelate complexes [Pt(L1-L9)<sub>2</sub>] and two heteroleptic mono-chelate complexes with dimethyl sulfide [Pt(L1-L9)(DMS)Cl] or dimethyl sulfoxide [Pt(L1-L9)(DMSO)Cl] and one chloride ligand (Scheme 1). It is also noteworthy that the terminal carboxylic group was esterified during the coordination, as indicated by X-ray structure analysis, NMR spectroscopy and mass spectrometry. The bonding of the soft platinum(II) ions towards soft (S) and hard (O and Cl<sup>-</sup>) donors are based on antisymbiosis and HSAB principles, where each two sulfur donors are coordinated *cis* to each other, while *trans* to hard donors (O or Cl<sup>-</sup>).<sup>[33,34]</sup> This coordination may make significant differences in the stability of Pt–Cl, Pt–O, and Pt–S bond polarity and hence the reactivity of the complexes.



**Scheme 1:** Synthesis of  $\beta$ -hydroxydithiocinnamic ester ligands HL1–HL9 and their corresponding complexes [Pt(L1-L9)<sub>2</sub>], [Pt(L1-L9)(DMS)Cl], and [Pt(L1-L9)(DMSO)Cl]: i, KO<sup>t</sup>Bu (2 eq.), diethyl ether (40 mL), -78 °C, 2-bromoacetic acid (1 eq.), r.t.; ii, [PtCl<sub>2</sub>(DMS)(DMSO)] (1 eq.), ethanol (40 mL), 60 °C 30 min., overnight r.t.

## Spectroscopic characterization

All compounds were characterized by NMR spectroscopy, mass spectrometry and elemental analysis. The chemical shifts in <sup>1</sup>H NMR and <sup>13</sup>C{<sup>1</sup>H} NMR spectra for ligands HL1–HL9 are generally in good agreement with previously reported values.<sup>[8-17, 35-39]</sup> In the <sup>1</sup>H NMR spectra, HL1–HL9 display a single resonance signal in the range of  $\delta$  14.49–15.17 ppm belonging to the hydroxyl group (–OH) proton, which is not observed in the complexes [Pt(L1-L9)<sub>2</sub>], [Pt(L1-L9)(DMS)Cl], and [Pt(L1-L9)(DMSO)Cl]. The methine proton (=CH–) found at  $\delta$  6.66–7.44 ppm and  $\delta$  6.76–7.32 ppm for the ligands and complexes, respectively, is virtually unchanged. A single resonance signal at  $\delta$  11.40–13.07 ppm corresponding to the (–COOH) proton of the free ligands HL1–HL9 is disappeared in the <sup>1</sup>H NMR spectra of the complexes [Pt(L1-L9)<sub>2</sub>], [Pt(L1-L9)(DMS)Cl], and [Pt(L1-L9)(DMSO)Cl]. Furthermore, the appearance of additional signals at  $\delta$  1.30 ppm (triplet) and  $\delta$  4.24 ppm (quartet) in the <sup>1</sup>H NMR spectra of the complexes



and a downfield shift of around 0.23 and 0.5 ppm, respectively, compared to ethanol signals, confirm the esterification of the carboxylic group during the coordination of the ligands.<sup>[40]</sup> In the  $^{13}\text{C}\{^1\text{H}\}$  NMR spectra, resonances for the (C–OH) carbon were found in the range of  $\delta$  168.91–174.11 and  $\delta$  171.52–177.35 ppm, for the ligands and complexes, respectively. The methine (=CH–) carbon of the free ligands found in the range of  $\delta$  106.64–111.22 ppm is slightly downfield shifted by  $\approx 5$  ppm in the complexes to  $\delta$  111.53–116.71 ppm, because of the slightly deshielding effect through the delocalization of the electrons in the chelating ring.<sup>[13–16]</sup> In contrast, a considerable upfield shift is observed for the quaternary thiocarbonyl carbon (C=S) at  $\delta$  174.27–180.47 ppm in the complexes, compared to the free ligands ( $\delta$  213.50–216.37 ppm). As a result of coordinating  $\beta$ -hydroxydithiocinnamic esters to the platinum(II) center, the  $\beta$ -oxo carbon atom is deshielded, while the thiocarbonyl group accepts the  $\pi$ -backbonding electron density from the platinum(II) center and thus shields the thiocarbonyl carbon atom.<sup>[8–17]</sup>  $[\text{Pt}(\text{L1-L9})(\text{DMS})\text{Cl}]$  complexes exhibit a characteristic signal for the coordinated dimethyl sulfide (DMS) in both  $^1\text{H}$  and  $^{13}\text{C}\{^1\text{H}\}$  NMR spectra. The methyl groups were found at  $\delta$  2.60 ppm as a singlet with platinum satellites  $^3J_{\text{Pt-H}} \approx 50$  Hz in the  $^1\text{H}$  NMR spectra and  $\delta$  24 ppm with platinum–carbon coupling  $^2J_{\text{Pt-C}} \approx 18$  Hz in the  $^{13}\text{C}\{^1\text{H}\}$  NMR spectra. Also, there is a downfield shift by 0.5 and 6 ppm compared to free DMS in both  $^1\text{H}$  and  $^{13}\text{C}\{^1\text{H}\}$  NMR spectra, respectively.<sup>[41]</sup> The methyl groups of the coordinated dimethyl sulfoxide (DMSO) in  $[\text{Pt}(\text{L1-L9})(\text{DMSO})\text{Cl}]$  complexes were observed at  $\delta$  3.60 ppm as a singlet accompanied by platinum satellites  $^3J_{\text{Pt-H}} \approx 22$  Hz in the  $^1\text{H}$  NMR spectra and  $\delta$  46 ppm with platinum–carbon coupling  $^2J_{\text{Pt-C}} \approx 50$  Hz in the  $^{13}\text{C}\{^1\text{H}\}$  NMR spectra, respectively. Compared to the free DMSO, there is observed a downfield shift by 1.1 and 6 ppm in both  $^1\text{H}$  and  $^{13}\text{C}\{^1\text{H}\}$  NMR spectra, respectively, which also confirm the formation of a mono-chelate complex with S-coordinated DMSO ligand which is in accordance with previously described Pt–DMSO complexes.<sup>[13–16,35–39,42–46]</sup>  $^{195}\text{Pt}$  NMR spectra for the bis-chelate complexes  $[\text{Pt}(\text{L1-L9})_2]$  as well as the mono-chelate complexes  $[\text{Pt}(\text{L1-L9})(\text{DMS})\text{Cl}]$  and  $[\text{Pt}(\text{L1-L9})(\text{DMSO})\text{Cl}]$  were obtained. The signals appeared in the range of (–2267 to –2350 ppm) and (–2879 to –3079 ppm), for the bis-chelate and mono-chelate complexes, respectively, which is in good agreement with the previously reported values.<sup>[42–46]</sup>

## Molecular structures

Recrystallization from a mixture of  $\text{CH}_2\text{Cl}_2$  and cyclohexane (1:1) of  $[\text{Pt}(\text{L2})_2]$ ,  $[\text{Pt}(\text{L2})(\text{DMSO})\text{Cl}]$  and  $[\text{Pt}(\text{L6})(\text{DMS})\text{Cl}]$  complexes as well as HL3 ligand at 20 °C produced suitable single crystals for X-ray diffraction studies. Molecular structures are provided in Figure 2 with ellipsoids drawn at the 50% probability level. Crystallographic data as well as structure solution and refinement details are summarized in Table S1. Selected bond lengths and angles are given in Table S2. The platinum(II) metal centers in each of the platinum(II) complexes is found in a slightly distorted square-planar coordination mode. In the case of complexes  $[\text{Pt}(\text{L2})(\text{DMSO})\text{Cl}]$  and  $[\text{Pt}(\text{L6})(\text{DMS})\text{Cl}]$ , the sulfur atoms (S3) of the DMSO or DMS moiety are coordinated *cis* to the sulfur atom (S1) of the O,S bidentate ligand, while *trans* to each of the soft sulfur atom is located a hard donor atom (O1 or Cl). The bond lengths of platinum and their donor atoms are decreasing as following:  $\text{Pt-Cl} > \text{Pt-S1} \approx \text{Pt-S3} > \text{Pt-O1}$ . Moreover,  $[\text{Pt}(\text{L2})(\text{DMSO})\text{Cl}]$  coordination sphere angles comes close to 90° for  $\text{S1-Pt-S3}$  (89.81(3)°) and  $\text{S3-Pt-Cl}$  (89.60(3)°), is smaller for  $\text{O1-Pt-Cl}$  (84.42(7)°) and larger in the case of  $\text{O1-Pt-S1}$  (96.17(7)°). Meanwhile, the angles in the coordination sphere of  $[\text{Pt}(\text{L6})(\text{DMS})\text{Cl}]$  are higher than 90° for  $\text{O1-Pt-S1}$  (96.74(9)°) and  $\text{S3-Pt-Cl}$  (93.49(4)°), and smaller for  $\text{O1-Pt-Cl}$  (85.65(9)°) and  $\text{S1-Pt-S3}$  (84.12(4)°). Upon coordination, the chelating ligand also undergoes structural changes, the C3-O1 bond is significantly shorter, while the C1-S1 bond is elongated, reflecting an increasing double-bond character for the C-O bond and an increasing single-bond character for the C-S bond. Additionally, all carbon-carbon bonds and carbon skeleton angles in the 6-membered chelating ring are almost equal, which confirms a good delocalization of electron density there. This behavior agrees with the  $^{13}\text{C}\{^1\text{H}\}$  NMR data obtained for both complexes. The chelating unit's angles are widened to achieve square-planar coordination towards the platinum center. The angle  $\text{Pt-O1-C3}$  is the widest (131.9(2)° in  $[\text{Pt}(\text{L2})(\text{DMSO})\text{Cl}]$  and 129.5(5)° in  $[\text{Pt}(\text{L6})(\text{DMS})\text{Cl}]$ ) whereas, the  $\text{Pt-S1-C1}$  angle is the smallest (107.55(12)° in  $[\text{Pt}(\text{L2})(\text{DMSO})\text{Cl}]$  and 108.90(14)° in  $[\text{Pt}(\text{L6})(\text{DMS})\text{Cl}]$ ). The bis-chelate complex  $[\text{Pt}(\text{L2})_2]$  is almost identical to those of the corresponding mono-chelated species, with the only difference being non-existent of DMS or DMSO ligands. The two ligands are *cis* coordinated, as reported earlier for analogous structures.<sup>[13–16]</sup> The angles of the coordination sphere are larger than 90° for  $\text{O1-Pt-S1}$  (95.68(6)°), and  $\text{O4-Pt-S3}$  (95.94(6)°), close to 90° for  $\text{S1-Pt-S3}$  (89.50(3)°) and

therefore smaller than  $90^\circ$  for O1-Pt-O4 ( $76.90(8)^\circ$ ). The chelating units are planar with slightly widened angles, as it was observed for [Pt(L2)(DMSO)Cl] and [Pt(L6)(DMS)Cl] complexes.

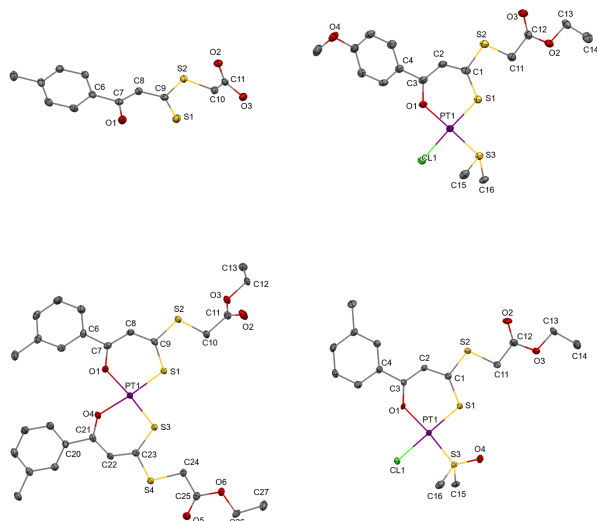


**Figure 2:** Depiction of solid-state molecular structures of HL3 (top-left), [Pt(L2)<sub>2</sub>] (down-left), [Pt(L6)(DMS)Cl] (top-right) and [Pt(L6)(DMSO)Cl] (down-right). Thermal ellipsoids are given at the 50% probability level and hydrogen atoms are omitted for clarity.

### Stability and solvolysis of the Pt(II) complexes

The solvolysis of three representative Pt(II) complexes [Pt(L6)<sub>2</sub>], [Pt(L6)(DMS)Cl], and [Pt(L6)(DMSO)Cl] in CH<sub>3</sub>CN-PBS (pH 7.4; 1:1) at 37 °C for 72 hours was monitored by LC-ESI-MS spectroscopy (positive ion mode) (Figs. S1-S3). The ESI spectra of the [Pt(L6)(DMS)Cl], and [Pt(L6)(DMSO)Cl] complexes clearly show a peak at  $m/z = 587.6$  assigned to [(Pt(L6)(CH<sub>3</sub>CN)<sub>2</sub>]<sup>+</sup> ( $t_R = 9.48$  min, Figs. S2, and S3), implying the efficient replacement of the chloride, DMS, or DMSO ligands. In the ESI spectrum of the [Pt(L6)(DMS)Cl] complex, an additional peak at  $m/z = 608.6$  was observed and assigned to the [(Pt(L6)(DMS)(CH<sub>3</sub>CN))]<sup>+</sup> ( $t_R = 9.6$  min, Fig. S2), demonstrating that only the Pt-Cl bond undergoes solvolysis, thus affording the mono-solvolysis species. Whereas the ESI spectrum of [Pt(L6)<sub>2</sub>] complex shows a peak at  $m/z = 817.6$  ( $t_R = 15.99$  min, Fig. S1), corresponding to the non-solvolysed complex and a less abundant peak at  $m/z = 587.7$  ( $t_R = 9.48$  min, Fig. S1) was also observed. As shown in Figs. S1-S3, there is no significant change in the spectral composition over time (24, 48 and 72 h). Based on these findings, the O,S-Pt(II) chelate units are stable under the study conditions, while the chloride, DMS, and DMSO ligands undergo solvolysis.

### Interactions of the Pt(II) complexes with 9-methylguanine

As part of Cisplatin's mechanism of action, one or both chloride ligands are replaced by water molecules, thereby producing the potent electrophilic cations *cis*-[Pt(NH<sub>3</sub>)<sub>2</sub>Cl(H<sub>2</sub>O)]<sup>+</sup> and *cis*-[Pt(NH<sub>3</sub>)<sub>2</sub>(H<sub>2</sub>O)<sub>2</sub>]<sup>2+</sup>.<sup>[47-49]</sup> Afterwards, the aquated species can enter the nucleus, and the water molecule substituted by nucleophilic centers on DNA-purine bases, particularly the N7 positions of guanosine and adenosine residues.<sup>[47-49]</sup> In order to investigate the reaction of the synthesized Pt(II) complexes with 9-methylguanine (9-MeG) as a DNA model the representative Pt(II) complexes [Pt(L6)<sub>2</sub>], [Pt(L6)(DMS)Cl], and [Pt(L6)(DMSO)Cl] (1 eq.) were incubated with 9-MeG (8 eq.) in CH<sub>3</sub>CN-PBS (pH 7.4; 1:1) at 37 °C for 72 hours. The reaction was monitored by LC-ESI-MS (positive ion mode) to identify the formed Pt/9-MeG adducts (Figs. 3, S4-S6). Upon reaction of the [Pt(L6)(DMS)Cl] complex with 9-MeG, two major peaks at  $m/z = 835.6$  ( $t_R = 8.98$  min), and  $732.7$  ( $t_R = 9.33$  min) were found, assignable to the bifunctional adduct [Pt(L6)(9-MeG)<sub>2</sub>]<sup>+</sup> and the monofunctional adduct [Pt(L6)(DMS)(9-MeG)]<sup>+</sup>, respectively (Figs. 3, and S5). In addition, a minor peak at  $m/z = 670.9$  ( $t_R = 8.98$  min) was observed and can be assigned to the N7,O6-bidentate 9-MeG adduct [Pt(L6)(N7,O6-9-MeG)]<sup>+</sup>, (Figs. 3, and S5). In the ESI spectrum of the reaction between [Pt(L6)(DMSO)Cl] complex and 9-MeG, the main peak was found at  $m/z = 835.6$  ( $t_R = 8.98$  min), which can be assigned to the bifunctional adduct [Pt(L6)(9-MeG)<sub>2</sub>]<sup>+</sup>. However, the minor peak at  $m/z = 670.8$  ( $t_R = 8.98$  min) assignable to [Pt(L6)(N7,O6-9-MeG)]<sup>+</sup> adduct was also detected (Fig. S6). Interestingly, the absence of any peaks attributed to [Pt(L6)(DMS)Cl], and [Pt(L6)(DMSO)Cl] complexes after 24 h indicates that the substitution reaction was completed. Also, there are no significant changes in spectral composition over time (24, 48 and 72 h) (Figs. S5, and S6). In contrast, the ESI spectrum of [Pt(L6)<sub>2</sub>] complex with 9-MeG, shows a major peak at  $m/z = 817.6$  ( $t_R = 15.99$  min), corresponding to the non-reacted complex as well as a minor peak at  $m/z = 835.6$  ( $t_R = 8.98$  min, Fig. S4) assigned to the bifunctional adduct [Pt(L6)(9-MeG)<sub>2</sub>]<sup>+</sup>. In agreement with its non-solvolytic behavior, this bis-chelate complex also exhibited the lowest 9-MeG binding. According to this study, such complexes, especially the heteroleptic mono-chelate complexes [Pt(L1-L9)(DMS)Cl] and [Pt(L1-L9)(DMSO)Cl] are capable of binding DNA-purine bases as well as forming stable mono- and bifunctional adducts.

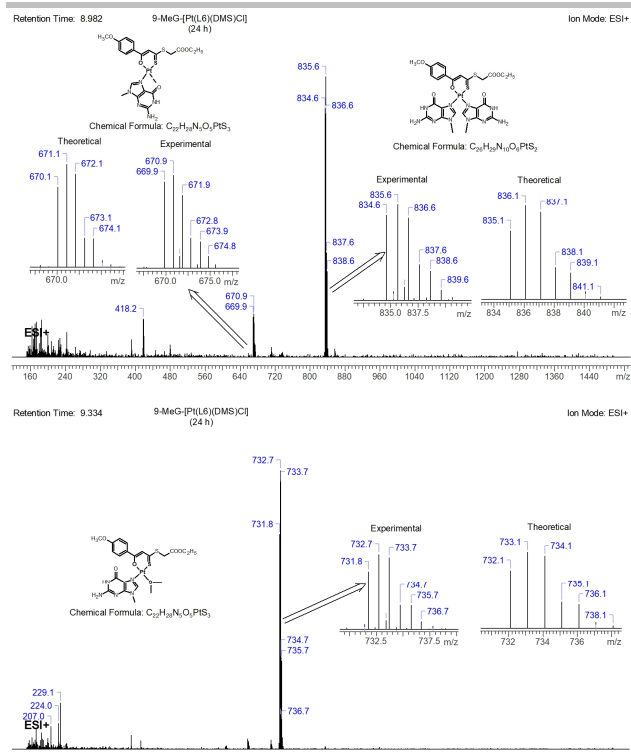


**Figure 3:** ESI-MS spectra of the adducts formed between 9-MeG and [Pt(L6)(DMS)Cl] complex after incubation 24 h at 37 °C. The insets show the theoretical as well as the experimental isotope patterns of  $m/z = 835.6$  ( $t_R = 8.98$  min), 732.7 ( $t_R = 9.33$  min), and 670.9 ( $t_R = 8.98$  min).

### Cytotoxic activity

The activity against the epithelial ovarian cancer cell lines A2780 and Skov3 and their Cisplatin-resistant subcultures was determined after 48 h incubation with varying concentrations of the compounds by the MTT assay as described before [15], (see the experimental section). The tested complexes [Pt(L1-L9)(DMS)Cl] and [Pt(L1, L2, L4, L5, and L7-L9)(DMSO)Cl], did not exhibit a high cytotoxic activity and showed  $IC_{50}$  values higher than 16.0  $\mu M$  (Tab. 1, for mean  $IC_{50}$  values with standard deviation see supplementary data Tab. S3). Moreover, for several compounds the calculated  $IC_{50}$  values are outside the range of analyzed concentrations (>100  $\mu M$ ). Therefore, these compounds should be evaluated as ineffective. This is mainly the case for the Cisplatin sensitive but not resistant cell lines. The analysis of higher concentrations was not compatible with the requirement of low solvent concentrations (< 0.5% DMSO) for cell culture experiments.[15] Most compounds affected both sensitive and Cisplatin-resistant cells similarly or showed a higher activity against resistant cells resulting in resistance factors ( $RF = IC_{50, resistant} / IC_{50, sensitive}$ )  $RF \leq 1$ . These results are in agreement to earlier data of platinum(II) complexes with  $\beta$ -hydroxydithiocinnamic acid derivatives as O,S-

chelating ligands.[15] Moreover, structure-activity relationships (SAR) can be revealed by the data and this may improve the design of future, more active organo-metal-based compounds. DMS and DMSO containing compounds have a similar mean activity (mean  $IC_{50}$  132  $\mu M$  and 135  $\mu M$ , respectively) but exhibit cell line specific differences. Whereas DMS compounds are less cytotoxic for A2780 than for Skov3 (mean  $IC_{50}$  212  $\mu M$  and 118  $\mu M$ ) the opposite is detected for DMSO compounds (mean  $IC_{50}$  84  $\mu M$  and 255  $\mu M$ , respectively). Thus, cell line specific detoxification, DNA damage repair or cell death signaling processes influencing the cytotoxic activity may affect the two compound groups differently.

**Table 1:** Mean  $IC_{50}$  values of the tested compounds and calculated resistance factors (RF) for A2780 and Skov3.

		A2780	A2780 Cis	RF A2780	Skov3	Skov3 Cis	RF Skov3	mean $IC_{50}$
DMS	L1	33.3	16.0	0.5	76.1	46.2	0.6	34.4
	L2	2056.6	355.0	0.2	685.8	183.1	0.3	656.1
	L3	56.1	60.5	1.1	57.5	41.4	0.7	43.3
	L4	55.0	72.2	1.3	60.6	53.2	0.9	48.5
	L5	93.0	59.1	0.6	119.9	69.6	0.6	68.4
	L6	59.5	46.4	0.8	86.6	69.7	0.8	52.6
	L7	28.1	44.7	1.6	63.9	53.7	0.8	38.4
	L8	42.6	50.7	1.2	66.3	63.7	1.0	44.9
	L9	32.9	39.4	1.2	60.6	52.6	0.9	37.3
DMSO	L1	25.6	55.3	2.2	336.8	99.4	0.3	103.8
	L2	164.4	50.4	0.3	380.9	103.6	0.3	139.9
	L3				n.a.			
	L4	16.5	73.3	4.5	146.1	92.8	0.6	66.6
	L5	224.6	58.5	0.3	777.3	95.5	0.1	231.2
	L6				n.a.			
	L7	102.8	56.3	0.5	646.9	182.8	0.3	197.9
	L8	64.6	48.2	0.7	87.6	54.9	0.6	51.2
	L9	153.8	76.8	0.5	403.9	163.6	0.4	159.7
CIS		6.8	15.4	2.3	12.5	28.6	2.3	13.1

The comparison of compounds differing (i) in the position of the substituent (R) at the benzyl ring (meta; para; ortho position) or (ii) in the substituent itself (-CH<sub>3</sub>; -OCH<sub>3</sub>; -Br) did not reveal any general relationship to the cytotoxic activity. Again, DMS and DMSO-containing compounds differed regarding the substance group with the lowest activity (meta and para orientation for DMS and DMSO compounds, respectively; Fig. 4). In agreement with earlier observations, the activity of such kind of platinum(II)  $\beta$ -hydroxydithiocinnamic acid complexes increases with increasing the lipophilicity of the terminal S-alkyl chain.[15] Therefore, the herein-presented compounds with the terminal

hydroneutral ester group ( $\text{S-CH}_2\text{COOC}_2\text{H}_5$ ) are less active than the previously reported platinum(II) complexes containing higher lipophilic  $\beta$ -hydroxydithiocinnamic acid derivatives.<sup>[15]</sup>

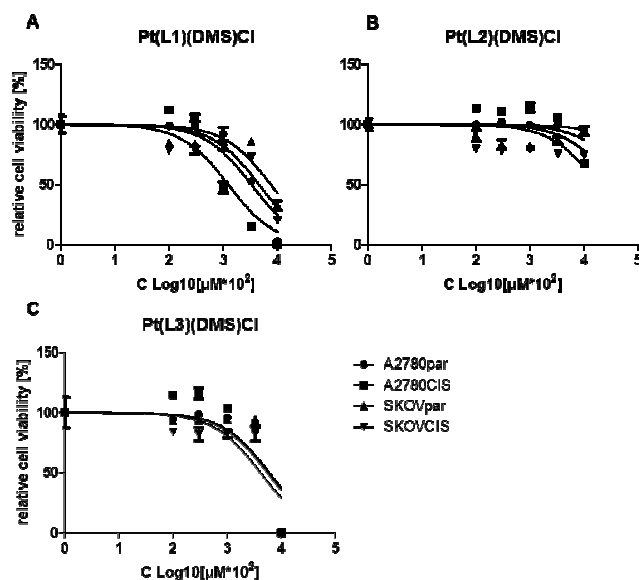


**Figure 4:** Exemplary data for the  $\text{IC}_{50}$  determination of the  $[\text{Pt}(\text{L}1\text{-L}3)(\text{DMS})\text{Cl}]$  compounds with ortho- (A), meta- (B), or para- (C) substituent methyl group, respectively.

## Conclusions

Here we reported on the synthesis of nine novel  $\beta$ -hydroxydithiocinnamic ester ligands HL1–HL9, that coordinated to the platinum(II) center of the precursor complex  $\text{cis-}[\text{PtCl}_2(\text{DMS})(\text{DMSO})]$  affording overall 27 platinum(II) complexes. Among them nine homoleptic bis-chelate complexes  $[\text{Pt}(\text{L}1\text{-L}9)_2]$ , where two  $\beta$ -hydroxydithiocinnamic ester ligands coordinated *cis* to each other and 18 heteroleptic mono-chelate complexes with dimethyl sulfide  $[\text{Pt}(\text{L}1\text{-L}9)(\text{DMS})\text{Cl}]$ , or dimethyl sulfoxide  $[\text{Pt}(\text{L}1\text{-L}9)(\text{DMSO})\text{Cl}]$  and chloride co-ligands. Structure determination was conceivable for the HL3 ligand as well as the platinum(II) complexes  $[\text{Pt}(\text{L}2)_2]$ ,  $[\text{Pt}(\text{L}2)(\text{DMSO})\text{Cl}]$  and  $[\text{Pt}(\text{L}6)(\text{DMS})\text{Cl}]$ . A slightly distorted square-planar coordination mode was found in all the platinum(II) complexes. In the solvolysis experiment of the  $[\text{Pt}(\text{L}6)(\text{DMSO})\text{Cl}]$  complex, both chlorido and DMSO ligands were rapidly replaced by two  $\text{CH}_3\text{CN}$  molecules, affording only the bi-solvolysis species

$[\text{Pt}(\text{L}6)(\text{CH}_3\text{CN})_2]^+$ . The interaction of this complex with 9-MeG resulted in the formation of the bi-functional adduct  $[\text{Pt}(\text{L}6)(9\text{-MeG})_2]^+$ , and also the N7,O6-bi-dentate 9-MeG adduct  $[\text{Pt}(\text{L}6)(\text{N}7,\text{O}6\text{-}9\text{-MeG})]^+$  was observed. Alternatively, the solvolysis of  $[\text{Pt}(\text{L}6)(\text{DMS})\text{Cl}]$  complex gives both the mono-solvolysis  $[\text{Pt}(\text{L}6)(\text{DMS})(\text{CH}_3\text{CN})]^+$  and the bi-solvolysis  $[\text{Pt}(\text{L}6)(\text{CH}_3\text{CN})_2]^+$  species, which also reflected on the interaction with the 9-MeG where subsequently the monofunctional adduct  $[\text{Pt}(\text{L}6)(\text{DMS})(9\text{-MeG})]^+$  as well as the bifunctional  $[\text{Pt}(\text{L}6)(9\text{-MeG})_2]^+$  and the N7,O6-bidentate 9-MeG  $[\text{Pt}(\text{L}6)(\text{N}7,\text{O}6\text{-}9\text{-MeG})]^+$  adducts were obtained. In summary, these findings indicate that such heteroleptic mono-chelate complexes can bind guanines similarly to Cisplatin and its analogues. First *in-vitro* studies using ovarian cancer cell lines revealed no superior activity compared to Cisplatin but point to a different mode-of-action because Cisplatin resistant cells respond similar or even better (lower  $\text{IC}_{50}$ ) than Cisplatin sensitive cells to these compounds.

## Experimental Section

### Materials and techniques

All syntheses were carried out under nitrogen atmosphere. The  $^1\text{H}$ ,  $^{13}\text{C}\{^1\text{H}\}$ ,  $^{195}\text{Pt}$  NMR spectra were recorded with a Bruker Avance 400, 500 and 600 MHz spectrometer and the chemical shifts are given in ppm with  $\text{SiMe}_4$  as internal references. Mass spectra were recorded with a Finnigan MAT SSQ 710 instrument. Elemental analysis was performed with a Leco CHNS-932 apparatus. TLC was performed by using Merck TLC aluminum sheets (Silica gel 60 F254). Solvents from Fisher Scientific and other chemicals from TCI, abcr and Sigma-Aldrich were used without further purification.

### Synthesis of free ligands (HL1–HL9).

2'-Methylacetophenone (2.68 g, 2.62 ml, 20 mmol) for (HL1), 3'-methylacetophenone (2.68 g, 2.72 ml, 20 mmol) for (HL2), 4'-methylacetophenone (2.68 g, 2.67 ml, 20 mmol) for (HL3), 2'-methoxyacetophenone (3.00 g, 2.75 ml, 20 mmol) for (HL4), 3'-methoxyacetophenone (3.00 g, 2.75 ml, 20 mmol) for (HL5), 4'-methoxyacetophenone (3.00 g, 20 mmol) for (HL6), 2'-bromoacetophenone (3.98 g, 2.70 ml, 20 mmol) for (HL7), 3'-Bromoacetophenone (3.98 g, 2.65 ml, 20 mmol) for (HL8) and 4'-bromoacetophenone (3.98 g, 20 mmol) for (HL9), in dry diethyl ether (20 mL) were added slowly and separately to a precooled suspension of potassium tert-butoxide (4.49 g, 40 mmol) in dry diethyl ether (40 mL) at  $-78^\circ\text{C}$ . Carbon disulfide (1.7 ml, 28 mmol) was added dropwise to the solution under vigorous stirring, the mixture maintained at  $-78^\circ\text{C}$  for 3 hours



and allowed to warm up to room temperature then a solution of 2-bromoacetic acid (2.28 g, 20 mmol) in dry diethyl ether (10 mL) was added dropwise with stirring to the formed dithiolate anion, the mixture is stirred protected from light at room temperature for a further 18 hours. For workup, the solvent was removed, and dichloromethane (100 ml) was added to the yellow crude product. Sulfuric acid (aqueous solution, 2M, 100 ml) was added to the suspension and stirred for 30 minutes at room temperature. The two-phased system was separated, and the aqueous phase extracted with dichloromethane (3x35 ml). The combined organic phases were washed with water (3x20 ml), dried with sodium sulfate. After filtration, the solvent was removed, and the yellow crude product washed three times with n-pentane then recrystallized from (dichloromethane/acetone) affording the pure ligands HL1–HL9 with yields ranging from 7.21 % to 49.51 %. All compounds were characterized by NMR spectroscopy, mass spectrometry and elemental analyses (Ligand characterization data are described in detail in the supporting information).

#### General procedure for the Synthesis of platinum(II) complexes.

A hot ethanolic solution of HL1–HL9 (1 equiv.) (20 mL) was added separately to a stirred suspension of *cis*-[PtCl<sub>2</sub>(DMS)(DMSO)], (1 equiv.) in ethanol (20 mL). The resulting solution was stirred for 30 min. in hot water bath over 60 °C and then overnight at room temperature. The yellow solution turned red, and the solvent was removed under reduced pressure. The residue was purified by column chromatography using (cyclohexane/CH<sub>2</sub>Cl<sub>2</sub>/acetone,5:2:1) as eluent affording three different classes of complexes, the first fraction is the bis-chelates [Pt(L1–L9)<sub>2</sub>] while the second and third fractions are the mono-chelates [Pt(L1–L9)(DMS)Cl] and [Pt(L1–L9)(DMSO)Cl], respectively. The products were obtained as a red or orange solids. (<sup>1</sup>H, <sup>13</sup>C{<sup>1</sup>H} and <sup>195</sup>Pt NMR spectra are shown in the supporting information Fig. S7–S63)

**1- HL1 (265 mg, 0.99 mmol), *cis*-[PtCl<sub>2</sub>(DMS)(DMSO)] (400 mg, 0.99 mmol).**

**[Pt(L1)<sub>2</sub>] (PtC<sub>28</sub>H<sub>30</sub>O<sub>6</sub>S<sub>4</sub>) (Mol. Wt.: 785.87 g/mol)**

Red solid; yield: 70.30 mg (9.08 %); Rf= 0.8 (cyclohexane/CH<sub>2</sub>Cl<sub>2</sub>/acetone,5:2:1).

<sup>1</sup>H NMR (400 MHz, CD<sub>2</sub>Cl<sub>2</sub>) δ 7.48 – 7.39 (m, 2H), 7.39 – 7.30 (m, 2H), 7.19 (t, *J* = 7.0 Hz, 4H), 6.78 (s, 2H, =CH-), 4.24 (q, *J* = 7.1 Hz, 4H), 3.97 (s, 4H), 2.38 (s, 6H), 1.31 (t, *J* = 7.1 Hz, 6H), <sup>13</sup>C{<sup>1</sup>H} NMR (101 MHz, CD<sub>2</sub>Cl<sub>2</sub>) δ 180.28 (-C=S), 173.97, 167.35, 139.95, 136.54, 131.26, 130.02, 126.98, 125.64, 116.71 (=CH-), 62.16, 36.44, 20.28, 13.93, <sup>195</sup>Pt NMR

(85.7 MHz, CD<sub>2</sub>Cl<sub>2</sub>) δ -2296 ppm. ESI-MS: (positive mode *m/z*) 808.8 [M+Na]<sup>+</sup>, elemental analysis for PtC<sub>28</sub>H<sub>30</sub>O<sub>6</sub>S<sub>4</sub>: C 42.79, H 3.85, S 16.32; found: C 42.57, H: 3.93 S: 16.29.

**[Pt(L1)(DMS)Cl] (PtC<sub>16</sub>H<sub>21</sub>O<sub>3</sub>S<sub>3</sub>Cl) (Mol. Wt.: 588.06 g/mol)**

Orange solid; yield: 162.2 mg (28 %); Rf = 0.6 (cyclohexane/CH<sub>2</sub>Cl<sub>2</sub>/acetone,5:2:1).

<sup>1</sup>H NMR (400 MHz, CD<sub>2</sub>Cl<sub>2</sub>) δ 7.42 (d, *J* = 7.7 Hz, 1H), 7.37 (td, *J* = 7.6, 1.2 Hz, 1H), 7.31 – 7.14 (m, 2H), 6.84 (s, 1H, =CH-), 4.23 (q, *J* = 7.1 Hz, 2H), 3.94 (s, 2H), 2.57 (s w/Pt satellites, <sup>3</sup>J<sub>Pt-H</sub> = 51.04 Hz, 6H), 2.41 (s, 3H), 1.28 (t, *J* = 7.1 Hz, 3H), <sup>13</sup>C{<sup>1</sup>H} NMR (101 MHz, CD<sub>2</sub>Cl<sub>2</sub>) δ 179.48 (-C=S), 173.85, 167.31, 139.46, 137.19, 131.48, 130.32, 127.21, 125.66, 115.75 (=CH-), 62.20, 36.47, 23.88 (s w/Pt satellites, <sup>2</sup>J<sub>Pt-C</sub> = 18.78 Hz, CH<sub>3</sub>(DMS)), 20.74, 13.93, <sup>195</sup>Pt NMR (85.7 MHz, CD<sub>2</sub>Cl<sub>2</sub>) δ -2892 ppm, ESI-MS: (positive mode *m/z*) 611.1 [M+Na]<sup>+</sup>, elemental analysis for PtC<sub>16</sub>H<sub>21</sub>O<sub>3</sub>S<sub>3</sub>Cl: C 32.68, H 3.60, S 16.36, Cl 6.03; found: C 32.65, H: 3.68 S: 16.47 Cl 5.96.

**[Pt(L1)(DMSO)Cl] (PtC<sub>16</sub>H<sub>21</sub>O<sub>4</sub>S<sub>3</sub>Cl) (Mol. Wt.: 604.05 g/mol)**

Orange solid; yield: 148 mg (24.87 %); Rf = 0.5 (cyclohexane/CH<sub>2</sub>Cl<sub>2</sub>/acetone,5:2:1).

<sup>1</sup>H NMR (400 MHz, CD<sub>2</sub>Cl<sub>2</sub>) δ 7.42 (d, *J* = 7.7 Hz, 1H), 7.37 (t, *J* = 7.5 Hz, 1H), 7.21 (m, 2H), 6.81 (s, 1H, =CH-), 4.22 (q, *J* = 7.1 Hz, 2H), 3.98 (s, 2H), 3.59 (s w/Pt satellites, <sup>3</sup>J<sub>Pt-H</sub> = 20.88 Hz, 6H), 2.41 (s, 3H), 1.27 (t, *J* = 7.1 Hz, 3H), <sup>13</sup>C{<sup>1</sup>H} NMR (101 MHz, CD<sub>2</sub>Cl<sub>2</sub>) δ 180.47 (-C=S), 177.35, 167.21, 138.54, 137.51, 131.52, 130.62, 127.71, 125.71, 115.64 (=CH-), 62.31, 46.68 (s w/Pt satellites, <sup>2</sup>J<sub>Pt-C</sub> = 50 Hz, CH<sub>3</sub>(DMSO)), 36.54, 20.81, 13.88, <sup>195</sup>Pt NMR (85.7 MHz, CD<sub>2</sub>Cl<sub>2</sub>) δ -3035 ppm, ESI-MS: (positive mode *m/z*) 626.9 [M+Na]<sup>+</sup>, elemental analysis for PtC<sub>16</sub>H<sub>21</sub>O<sub>4</sub>S<sub>3</sub>Cl: C 31.81, H 3.50, S 15.92, Cl 5.87; found: C 32.05, H: 3.66 S: 15.83 Cl 5.89.

**2- HL2 (265 mg, 0.99 mmol), *cis*-[PtCl<sub>2</sub>(DMS)(DMSO)] (400 mg, 0.99 mmol).**

**[Pt(L2)<sub>2</sub>] (PtC<sub>28</sub>H<sub>30</sub>O<sub>6</sub>S<sub>4</sub>) (Mol. Wt.: 785.87 g/mol)**

Red solid; yield: 50.7 mg (6.55 %); Rf = 0.7 (cyclohexane/CH<sub>2</sub>Cl<sub>2</sub>/acetone,5:2:1).

<sup>1</sup>H NMR (400 MHz, CD<sub>2</sub>Cl<sub>2</sub>) δ 7.83 (s, 2H), 7.75 (d, *J* = 7.8 Hz, 2H), 7.35 (d, *J* = 7.6 Hz, 2H), 7.27 (t, *J* = 7.7 Hz, 2H), 7.23 (s, 2H, =CH-), 4.16 (q, *J* = 7.1 Hz, 4H), 3.89 (s, 4H), 2.38 (s, 6H), 1.22 (t, *J* = 7.1 Hz, 6H), <sup>13</sup>C{<sup>1</sup>H} NMR (101 MHz, CD<sub>2</sub>Cl<sub>2</sub>) δ 175.19 (-C=S), 173.63, 167.48, 138.84, 138.21, 132.59, 128.71, 128.15, 124.39, 112.93 (=CH-), 62.14, 36.52, 21.23, 13.94, <sup>195</sup>Pt NMR (85.7 MHz, CD<sub>2</sub>Cl<sub>2</sub>) δ -2322 ppm, ESI-MS: (positive mode *m/z*) 808.8 [M+Na]<sup>+</sup>, elemental

analysis for PtC<sub>28</sub>H<sub>30</sub>O<sub>6</sub>S<sub>4</sub>: C 42.79, H 3.85, S 16.32; found: C 43.35, H: 3.87 S: 16.26.

**[Pt(L2)(DMS)Cl] (PtC<sub>16</sub>H<sub>21</sub>O<sub>3</sub>S<sub>3</sub>Cl) (Mol. Wt.: 588.06 g/mol)**

Orange solid; yield: 82 mg (14.15 %); R<sub>f</sub> = 0.5 (cyclohexane/CH<sub>2</sub>Cl<sub>2</sub>/acetone,5:2:1).

<sup>1</sup>H NMR (500 MHz, CD<sub>2</sub>Cl<sub>2</sub>) δ 7.74 (d, *J* = 7.3 Hz, 2H), 7.40 (d, *J* = 7.4 Hz, 1H), 7.32 (t, *J* = 8.0 Hz, 1H), 7.23 (s, 1H, =CH-), 4.23 (q, *J* = 7.1 Hz, 2H), 3.96 (s, 2H), 2.56 (s w/Pt satellites, <sup>3</sup>J<sub>Pt-H</sub> = 50.40 Hz, 6H), 2.42 (s, 3H), 1.28 (t, *J* = 7.1 Hz, 3H), <sup>13</sup>C{<sup>1</sup>H} NMR (126 MHz, CD<sub>2</sub>Cl<sub>2</sub>) δ 175.49 (-C=S), 173.77, 167.78, 139.20, 138.29, 133.10, 129.11, 128.42, 125.16, 112.63 (=CH-), 62.55, 36.86, 24.24 (s w/Pt satellites, <sup>2</sup>J<sub>Pt-C</sub> = 18 Hz, CH<sub>3</sub>(DMS)), 21.49, 14.29, <sup>195</sup>Pt NMR (107 MHz, CD<sub>2</sub>Cl<sub>2</sub>) δ -2917 ppm, ESI-MS: (positive mode *m/z*) 611.1 [M+Na]<sup>+</sup>, elemental analysis for PtC<sub>16</sub>H<sub>21</sub>O<sub>3</sub>S<sub>3</sub>Cl: C 32.68, H 3.60, S 16.36, Cl 6.03; found: C 32.87, H: 3.88 S: 16.21 Cl 5.81.

**[Pt(L2)(DMSO)Cl] (PtC<sub>16</sub>H<sub>21</sub>O<sub>4</sub>S<sub>3</sub>Cl) (Mol. Wt.: 604.05 g/mol)**

Orange solid; yield: 97.3 mg (13.13 %); R<sub>f</sub> = 0.4 (cyclohexane/CH<sub>2</sub>Cl<sub>2</sub>/acetone,5:2:1).

<sup>1</sup>H NMR (400 MHz, CD<sub>2</sub>Cl<sub>2</sub>) δ 7.75 (d, *J* = 5.9 Hz, 2H), 7.41 (d, *J* = 7.5 Hz, 1H), 7.33 (t, *J* = 8.0 Hz, 1H), 7.20 (s, 1H, =CH-), 4.24 (q, *J* = 7.1 Hz, 2H), 4.01 (s, 2H), 3.62 (s w/Pt satellites, <sup>3</sup>J<sub>Pt-H</sub> = 21.60 Hz, 6H), 2.42 (s, 3H), 1.29 (t, *J* = 7.1 Hz, 3H), <sup>13</sup>C{<sup>1</sup>H} NMR (101 MHz, CD<sub>2</sub>Cl<sub>2</sub>) δ 176.81(-C=S), 176.15, 167.32, 138.87, 137.04, 133.15, 128.76, 128.39, 125.15, 112.12 (=CH-), 62.29, 46.76(s w/Pt satellites, <sup>2</sup>J<sub>Pt-C</sub> = 57.4 Hz, CH<sub>3</sub>(DMSO)), 36.58, 21.12, 13.87, <sup>195</sup>Pt NMR (85.7 MHz, CD<sub>2</sub>Cl<sub>2</sub>) δ -3058 ppm, ESI-MS: (positive mode *m/z*) 626.9 [M+Na]<sup>+</sup>, elemental analysis for PtC<sub>16</sub>H<sub>21</sub>O<sub>4</sub>S<sub>3</sub>Cl: C 31.81, H 3.50, S 15.92, Cl 5.87; found: C 32.01, H: 3.73 S: 15.87 Cl 5.72.

**3- HL3 (265 mg, 0.99 mmol), cis-[PtCl<sub>2</sub>(DMS)(DMSO)] (400 mg, 0.99 mmol).**

**[Pt(L3)<sub>2</sub>] (PtC<sub>28</sub>H<sub>30</sub>O<sub>6</sub>S<sub>4</sub>) (Mol. Wt.: 785.87 g/mol)**

Red solid; yield: 50 mg (6.46 %); R<sub>f</sub> = 0.7 (cyclohexane/CH<sub>2</sub>Cl<sub>2</sub>/acetone,5:2:1).

<sup>1</sup>H NMR (400 MHz, CD<sub>2</sub>Cl<sub>2</sub>) δ 7.95 (d, *J* = 8.3 Hz, 4H), 7.29 (d, *J* = 8.1 Hz, 4H), 7.20 (s, 2H, =CH-), 4.24 (q, *J* = 7.1 Hz, 4H), 3.97 (s, 4H), 2.38 (s, 6H), 1.31 (t, *J* = 7.1 Hz, 6H), <sup>13</sup>C{<sup>1</sup>H} NMR (101 MHz, CD<sub>2</sub>Cl<sub>2</sub>) δ 175.26 (-C=S), 172.98, 167.55, 142.79, 135.63, 129.65, 129.32, 127.69, 127.39, 112.82 (=CH-), 62.13, 36.49, 21.44, 13.93, <sup>195</sup>Pt NMR (85.7 MHz, CD<sub>2</sub>Cl<sub>2</sub>) δ -2330 ppm, ESI-MS: (positive mode *m/z*) 808.8 [M+Na]<sup>+</sup>, elemental analysis for PtC<sub>28</sub>H<sub>30</sub>O<sub>6</sub>S<sub>4</sub>: C 42.79, H 3.85, S 16.32; found: C 42.63, H: 3.91 S: 16.22.

**[Pt(L3)(DMS)Cl] (PtC<sub>16</sub>H<sub>21</sub>O<sub>3</sub>S<sub>3</sub>Cl) (Mol. Wt.: 588.06 g/mol)**

Orange solid; yield: 102 mg (17.60 %); R<sub>f</sub> = 0.5 (cyclohexane/CH<sub>2</sub>Cl<sub>2</sub>/acetone,5:2:1).

<sup>1</sup>H NMR (400 MHz, CD<sub>2</sub>Cl<sub>2</sub>) δ 7.85 (d, *J* = 8.2 Hz, 2H), 7.23 (s, 1H, =CH-), 7.23 (d, *J* = 8.0 Hz, 2H), 4.22 (q, *J* = 7.1 Hz, 2H), 3.94 (s, 2H), 2.55 (s w/Pt satellites, <sup>3</sup>J<sub>Pt-H</sub> = 49.60 Hz, 6H), 2.34 (s, 3H), 1.27 (t, *J* = 7.1 Hz, 3H), <sup>13</sup>C{<sup>1</sup>H} NMR (101 MHz, CD<sub>2</sub>Cl<sub>2</sub>) δ 174.90 (-C=S), 172.85, 167.48, 143.09, 135.09, 129.65, 127.69, 111.93 (=CH-), 62.18, 36.50, 23.89 (s w/Pt satellites, <sup>2</sup>J<sub>Pt-C</sub> = 19.79 Hz, CH<sub>3</sub>(DMS)), 21.43, 13.93, <sup>195</sup>Pt NMR (85.7 MHz, CD<sub>2</sub>Cl<sub>2</sub>) δ -2923 ppm, ESI-MS: (positive mode *m/z*) 611.1 [M+Na]<sup>+</sup>, elemental analysis for PtC<sub>16</sub>H<sub>21</sub>O<sub>3</sub>S<sub>3</sub>Cl: C 32.68, H 3.60, S 16.36, Cl 6.03; found: C 32.75, H: 3.83 S: 16.44 Cl 6.11.

**[Pt(L3)(DMSO)Cl] (PtC<sub>16</sub>H<sub>21</sub>O<sub>4</sub>S<sub>3</sub>Cl) (Mol. Wt.: 604.05 g/mol)**

Orange solid; yield: 45 mg (7.56 %); R<sub>f</sub> = 0.3 (cyclohexane/CH<sub>2</sub>Cl<sub>2</sub>/acetone,5:2:1).

<sup>1</sup>H NMR (600 MHz, CD<sub>2</sub>Cl<sub>2</sub>) δ 7.87 (d, *J* = 8.3 Hz, 2H), 7.26 (d, *J* = 8.0 Hz, 2H), 7.22 (s, 1H, =CH-), 4.23 (q, *J* = 7.1 Hz, 2H), 4.00 (s, 2H), 3.61 (s w/Pt satellites, <sup>3</sup>J<sub>Pt-H</sub> = 17.60 Hz, 6H), 2.37 (s, 3H), 1.29 (t, *J* = 7.1 Hz, 3H), <sup>13</sup>C{<sup>1</sup>H} NMR (151 MHz, CD<sub>2</sub>Cl<sub>2</sub>) δ 176.31 (-C=S), 175.96, 167.56, 143.80, 134.33, 129.82, 128.18, 111.90 (=CH-), 62.45, 46.90 (s w/Pt satellites, <sup>2</sup>J<sub>Pt-C</sub> = 49.5 Hz, CH<sub>3</sub>(DMSO)), 36.71, 21.59, 14.03. <sup>195</sup>Pt NMR (85.7 MHz, CD<sub>2</sub>Cl<sub>2</sub>) δ -3067 ppm, ESI-MS: (positive mode *m/z*) 626.9 [M+Na]<sup>+</sup>, elemental analysis for PtC<sub>16</sub>H<sub>21</sub>O<sub>4</sub>S<sub>3</sub>Cl: C 31.81, H 3.50, S 15.92, Cl 5.87; found: C 32.13, H: 3.69 S: 16.04 Cl 5.76.

**4- HL4 (280 mg, 0.99 mmol), cis-[PtCl<sub>2</sub>(DMS)(DMSO)] (400 mg, 0.99 mmol).**

**[Pt(L4)<sub>2</sub>] (PtC<sub>28</sub>H<sub>30</sub>O<sub>6</sub>S<sub>4</sub>) (Mol. Wt.: 817.86 g/mol)**

Red solid; yield: 37.5 mg (4.65 %); R<sub>f</sub> = 0.8 (cyclohexane/CH<sub>2</sub>Cl<sub>2</sub>/acetone,5:2:1).

<sup>1</sup>H NMR (400 MHz, CD<sub>2</sub>Cl<sub>2</sub>) δ 7.74 (dd, *J* = 7.7, 1.6 Hz, 2H), 7.56 – 7.42 (m, 2H), 7.23 (s, 2H, =CH-), 7.08 – 6.89 (m, 4H), 4.24 (q, *J* = 7.1 Hz, 4H), 3.96 (s, 4H), 3.89 (s, 6H), 1.30 (t, *J* = 7.1 Hz, 6H), <sup>13</sup>C{<sup>1</sup>H} NMR (101 MHz, CD<sub>2</sub>Cl<sub>2</sub>) δ 175.69 (-C=S), 171.90, 167.52, 156.99, 132.33, 130.31, 128.75, 120.82, 117.68, 112.11 (=CH-), 62.09, 55.85, 36.47, 13.92, <sup>195</sup>Pt NMR (85.7 MHz, CD<sub>2</sub>Cl<sub>2</sub>) δ -2300 ppm, ESI-MS: (positive mode *m/z*) 840 [M+Na]<sup>+</sup>, elemental analysis for PtC<sub>28</sub>H<sub>30</sub>O<sub>6</sub>S<sub>4</sub>: C 41.12, H 3.70, S 15.68; found: C 40.99, H: 3.68 S: 15.71.

**[Pt(L4)(DMS)Cl] (PtC<sub>16</sub>H<sub>21</sub>O<sub>4</sub>S<sub>3</sub>Cl) (Mol. Wt.: 604.05 g/mol)**

Orange solid; yield: 60 mg (10.10 %); R<sub>f</sub> = 0.7 (cyclohexane/CH<sub>2</sub>Cl<sub>2</sub>/acetone,5:2:1).

$^1\text{H}$  NMR (400 MHz,  $\text{CD}_2\text{Cl}_2$ )  $\delta$  7.71 (dd,  $J = 7.8, 1.6$  Hz, 1H), 7.58 – 7.42 (m, 1H), 7.32 (s, 1H, =CH-), 7.10 – 6.89 (m, 2H), 4.22 (q,  $J = 7.1$  Hz, 2H), 3.94 (s, 2H), 3.89 (s, 3H), 2.56 (s w/Pt satellites,  $^3J_{\text{Pt-H}} = 49.20$  Hz, 6H), 1.27 (t,  $J = 7.0$  Hz, 3H),  $^{13}\text{C}\{^1\text{H}\}$  NMR (101 MHz,  $\text{CD}_2\text{Cl}_2$ )  $\delta$  174.91 (-C=S), 171.80, 167.43, 156.96, 132.59, 130.88, 128.18, 120.99, 116.84, 112.07 (=CH-), 62.13, 55.87, 36.51, 23.86 (s w/Pt satellites,  $^2J_{\text{Pt-C}} = 19.79$  Hz,  $\text{CH}_3(\text{DMSO})$ ), 13.92,  $^{195}\text{Pt}$  NMR (85.7 MHz,  $\text{CD}_2\text{Cl}_2$ )  $\delta$  -2905 ppm,

ESI-MS: (positive mode  $m/z$ ) 626.9  $[\text{M}+\text{Na}]^+$ , elemental analysis for  $\text{PtC}_{16}\text{H}_{21}\text{O}_4\text{S}_3\text{Cl}$ : C 31.81, H 3.50, S 15.92, Cl 5.87; found: C 31.75, H: 3.64 S: 16.07 Cl 5.59.

**[Pt(L4)(DMSO)Cl] (PtC<sub>16</sub>H<sub>21</sub>O<sub>5</sub>S<sub>3</sub>Cl) (Mol. Wt.: 620.05 g/mol)**

Orange solid; yield: 45 mg (7.37 %);  $R_f = 0.4$  (cyclohexane/ $\text{CH}_2\text{Cl}_2$ /acetone,5:2:1).

$^1\text{H}$  NMR (400 MHz,  $\text{CD}_2\text{Cl}_2$ )  $\delta$  7.75 (dd,  $J = 7.8, 1.7$  Hz, 1H), 7.56 – 7.42 (m, 1H), 7.35 (s, 1H, =CH-), 7.11 – 6.92 (m, 2H), 4.22 (q,  $J = 7.1$  Hz, 2H), 3.99 (s, 2H), 3.90 (s, 3H), 3.61 (s w/Pt satellites,  $^3J_{\text{Pt-H}} = 20.80$  Hz, 6H), 1.28 (t,  $J = 7.1$  Hz, 3H),  $^{13}\text{C}\{^1\text{H}\}$  NMR (101 MHz,  $\text{CD}_2\text{Cl}_2$ )  $\delta$  175.60 (-C=S), 175.33, 167.32, 157.40, 133.04, 131.24, 127.14, 120.99, 116.65, 112.05 (=CH-), 62.23, 55.88, 46.71 (s w/Pt satellites,  $^2J_{\text{Pt-C}} = 59.67$  Hz,  $\text{CH}_3(\text{DMSO})$ ), 36.57, 13.86,  $^{195}\text{Pt}$  NMR (85.7 MHz,  $\text{CD}_2\text{Cl}_2$ )  $\delta$  -3048 ppm, ESI-MS: (positive mode  $m/z$ ) 642.9  $[\text{M}+\text{Na}]^+$ , elemental analysis for  $\text{PtC}_{16}\text{H}_{21}\text{O}_5\text{S}_3\text{Cl}$ : C 30.99, H 3.41, S 15.51, Cl 5.72; found: C 30.87, H: 3.56 S: 15.48 Cl 5.66.

**5- HL5 (182 mg, 0.64 mmol), cis-[PtCl<sub>2</sub>(DMS)(DMSO)] (260 mg, 0.64 mmol).**

**[Pt(L5)<sub>2</sub>] (PtC<sub>28</sub>H<sub>30</sub>O<sub>8</sub>S<sub>4</sub>) (Mol. Wt.: 817.86 g/mol)**

Red solid; yield: 31.70 mg (6.05 %);  $R_f = 0.8$  (cyclohexane/ $\text{CH}_2\text{Cl}_2$ /acetone,5:2:1).

$^1\text{H}$  NMR (600 MHz,  $\text{CD}_2\text{Cl}_2$ )  $\delta$  7.63 (s, 2H), 7.59 (d,  $J = 7.9$  Hz, 2H), 7.34 (t,  $J = 8.0$  Hz, 2H), 7.21 (s, 2H, =CH-), 7.14 (ddd,  $J = 8.2, 2.6, 0.7$  Hz, 2H), 4.25 (q,  $J = 7.1$  Hz, 4H), 3.97 (s, 4H), 3.88 (s, 6H), 1.31 (t,  $J = 7.1$  Hz, 6H),  $^{13}\text{C}\{^1\text{H}\}$  NMR (151 MHz,  $\text{CD}_2\text{Cl}_2$ )  $\delta$  174.87 (-C=S), 174.18, 167.63, 160.35, 139.93, 129.90, 119.56, 117.96, 113.13, 112.60 (=CH-), 62.34, 55.55, 36.71, 14.08,  $^{195}\text{Pt}$  NMR (85.7 MHz,  $\text{CD}_2\text{Cl}_2$ )  $\delta$  -2316 ppm, ESI-MS: (positive mode  $m/z$ ) 840  $[\text{M}+\text{Na}]^+$ , elemental analysis for  $\text{PtC}_{28}\text{H}_{30}\text{O}_8\text{S}_4$ : C 41.12, H 3.70, S 15.68; found: C 41.27, H: 3.90 S: 15.59.

**[Pt(L5)(DMS)Cl] (PtC<sub>16</sub>H<sub>21</sub>O<sub>4</sub>S<sub>3</sub>Cl) (Mol. Wt.: 604.05 g/mol)**

Orange solid; yield: 54.40 mg (14.09 %);  $R_f = 0.7$  (cyclohexane/ $\text{CH}_2\text{Cl}_2$ /acetone,5:2:1).

$^1\text{H}$  NMR (400 MHz,  $\text{CD}_2\text{Cl}_2$ )  $\delta$  7.52 (d,  $J = 7.8$  Hz, 1H), 7.48 (s, 1H), 7.34 (t,  $J = 8.0$  Hz, 1H), 7.22 (s, 1H, =CH-), 7.12 (dd,  $J = 8.0, 2.2$  Hz, 1H), 4.23 (q,  $J = 7.1$  Hz, 2H), 3.95 (s, 2H), 3.85 (s, 3H), 2.56 ((s w/Pt satellites,  $^3J_{\text{Pt-H}} = 50$  Hz, 6H), 1.28 (t,  $J = 7.1$  Hz, 3H),  $^{13}\text{C}\{^1\text{H}\}$  NMR (101 MHz,  $\text{CD}_2\text{Cl}_2$ )  $\delta$  174.52 (-C=S), 173.91, 167.42, 160.09, 139.37, 129.86, 119.84, 117.79, 112.74, 112.22 (=CH-), 62.22, 55.42, 36.57, 23.92 (s w/Pt satellites,  $^2J_{\text{Pt-C}} = 23.83$  Hz,  $\text{CH}_3(\text{DMSO})$ ), 13.93,  $^{195}\text{Pt}$  NMR (85.7 MHz,  $\text{CD}_2\text{Cl}_2$ )  $\delta$  -2912 ppm, ESI-MS: (positive mode  $m/z$ ) 626.9  $[\text{M}+\text{Na}]^+$ , elemental analysis for  $\text{PtC}_{16}\text{H}_{21}\text{O}_4\text{S}_3\text{Cl}$ : C 31.81, H 3.50, S 15.92, Cl 5.87; found: C 31.65, H: 3.58 S: 16.03 Cl 5.76.

**[Pt(L5)(DMSO)Cl] (PtC<sub>16</sub>H<sub>21</sub>O<sub>5</sub>S<sub>3</sub>Cl) (Mol. Wt.: 620.05 g/mol)**

Orange solid; yield: 67.10 mg (16.90 %);  $R_f = 0.5$  (cyclohexane/ $\text{CH}_2\text{Cl}_2$ /acetone,5:2:1).

$^1\text{H}$  NMR (400 MHz,  $\text{CD}_2\text{Cl}_2$ )  $\delta$  7.52 (d,  $J = 7.9$  Hz, 1H), 7.48 (s, 1H), 7.35 (t,  $J = 8.0$  Hz, 1H), 7.18 (s, 1H, =CH-), 7.12 (dd,  $J = 8.2, 2.4$  Hz, 1H), 4.23 (q,  $J = 7.1$  Hz, 2H), 4.01 (s, 2H), 3.85 (s, 3H), 3.62 (s w/Pt satellites,  $^3J_{\text{Pt-H}} = 18.50$  Hz, 6H), 1.29 (t,  $J = 7.2$  Hz, 3H),  $^{13}\text{C}\{^1\text{H}\}$  NMR (101 MHz,  $\text{CD}_2\text{Cl}_2$ )  $\delta$  177.31 (-C=S), 175.42, 167.32, 160.05, 138.42, 129.85, 120.17, 118.18, 113.04, 112.02 (=CH-), 62.31, 55.42, 46.76 (s w/Pt satellites,  $^2J_{\text{Pt-C}} = 58.7$  Hz,  $\text{CH}_3(\text{DMSO})$ ), 36.65, 13.87,  $^{195}\text{Pt}$  NMR (85.7 MHz,  $\text{CD}_2\text{Cl}_2$ )  $\delta$  -3053 ppm, ESI-MS: (positive mode  $m/z$ ) 642.9  $[\text{M}+\text{Na}]^+$ , elemental analysis for  $\text{PtC}_{16}\text{H}_{21}\text{O}_5\text{S}_3\text{Cl}$ : C 30.99, H 3.41, S 15.51, Cl 5.72; found: C 31.02, H: 3.45 S: 15.43 Cl 5.80.

**6- HL6 (140 mg, 0.49 mmol), cis-[PtCl<sub>2</sub>(DMS)(DMSO)] (200 mg, 0.49 mmol).**

**[Pt(L6)<sub>2</sub>] (PtC<sub>28</sub>H<sub>30</sub>O<sub>8</sub>S<sub>4</sub>) (Mol. Wt.: 817.86 g/mol)**

Red solid; yield: 32 mg (7.94 %);  $R_f = 0.8$  (cyclohexane/ $\text{CH}_2\text{Cl}_2$ /acetone,5:2:1).

$^1\text{H}$  NMR (400 MHz,  $\text{CD}_2\text{Cl}_2$ )  $\delta$  8.04 (d,  $J = 8.9$  Hz, 4H), 7.19 (s, 2H, =CH-), 6.98 (d,  $J = 8.9$  Hz, 4H), 4.24 (q,  $J = 7.1$  Hz, 4H), 3.96 (s, 4H), 3.88 (s, 6H), 1.31 (t,  $J = 7.1$  Hz, 6H),  $^{13}\text{C}\{^1\text{H}\}$  NMR (101 MHz,  $\text{CD}_2\text{Cl}_2$ )  $\delta$  174.66 (-C=S), 171.88, 167.67, 162.79, 130.72, 129.50, 114.22, 112.53 (=CH-), 62.11, 55.54, 36.46, 13.94,  $^{195}\text{Pt}$  NMR (85.7 MHz,  $\text{CD}_2\text{Cl}_2$ )  $\delta$  -2350 ppm, ESI-MS: (positive mode  $m/z$ ) 840  $[\text{M}+\text{Na}]^+$ , elemental analysis for  $\text{PtC}_{28}\text{H}_{30}\text{O}_8\text{S}_4$ : C 41.12, H 3.70, S 15.68; found: C 40.69, H: 3.65 S: 15.78.

**[Pt(L6)(DMS)Cl] (PtC<sub>16</sub>H<sub>21</sub>O<sub>4</sub>S<sub>3</sub>Cl) (Mol. Wt.: 604.05 g/mol)**

Orange solid; yield: 33 mg (11.07%);  $R_f = 0.7$  (cyclohexane/ $\text{CH}_2\text{Cl}_2$ /acetone,5:2:1).

$^1\text{H}$  NMR (500 MHz,  $\text{CD}_2\text{Cl}_2$ )  $\delta$  7.95 (d,  $J = 9.0$  Hz, 2H), 7.22 (s, 1H, =CH-), 6.93 (d,  $J = 9.0$  Hz, 2H), 4.22 (q,  $J = 7.1$  Hz,

2H), 3.94 (s, 2H), 3.85 (s, 3H), 2.55 ((s w/Pt satellites,  $^3J_{\text{Pt-H}} = 46.50$  Hz, 6H), 1.28 (t,  $J = 7.1$  Hz, 3H),  $^{13}\text{C}\{^1\text{H}\}$  NMR (126 MHz,  $\text{CD}_2\text{Cl}_2$ )  $\delta$  174.31 (-C=S), 171.72, 167.62, 163.01, 130.11, 129.91, 114.22, 111.57 (=CH-), 62.18, 55.55, 36.48, 23.87(s w/Pt satellites,  $^2J_{\text{Pt-C}} = 19.50$  Hz,  $\text{CH}_3(\text{DMS})$ ), 13.96,  $^{195}\text{Pt}$  NMR (107 MHz,  $\text{CD}_2\text{Cl}_2$ )  $\delta$  -2937 ppm, ESI-MS: (positive mode  $m/z$ ) 626.9  $[\text{M}+\text{Na}]^+$ , elemental analysis for  $\text{PtC}_{16}\text{H}_{21}\text{O}_4\text{S}_3\text{Cl}$ : C 31.81, H 3.50, S 15.92, Cl 5.87; found: C 32.05, H: 3.53 S: 16.13 Cl 5.93.

**[Pt(L6)(DMSO)Cl] (PtC<sub>16</sub>H<sub>21</sub>O<sub>5</sub>S<sub>3</sub>Cl) (Mol. Wt.: 620.05 g/mol)**

Orange solid; yield: 7 mg (2.29%);  $R_f = 0.4$  (cyclohexane/ $\text{CH}_2\text{Cl}_2$ /acetone,5:2:1).

$^1\text{H}$  NMR (500 MHz,  $\text{CD}_2\text{Cl}_2$ )  $\delta$  7.97 (d,  $J = 9.0$  Hz, 2H), 7.21 (s, 1H, =CH-), 6.94 (d,  $J = 9.0$  Hz, 2H), 4.23 (q,  $J = 7.1$  Hz, 2H), 3.99 (s, 2H), 3.86 (s, 3H), 3.61 (s w/Pt satellites,  $^3J_{\text{Pt-H}} = 18.68$  Hz, 6H), 1.29 (t,  $J = 7.1$  Hz, 3H),  $^{13}\text{C}\{^1\text{H}\}$  NMR (126 MHz,  $\text{CD}_2\text{Cl}_2$ )  $\delta$  175.30 (-C=S), 174.88, 167.52, 163.39, 130.29, 129.20, 114.24, 111.43 (=CH-), 62.27, 55.58, 46.75(s w/Pt satellites,  $^2J_{\text{Pt-C}} = 59.87$  Hz,  $\text{CH}_3(\text{DMSO})$ ), 36.52, 13.89,  $^{195}\text{Pt}$  NMR 107 MHz,  $\text{CD}_2\text{Cl}_2$ )  $\delta$  -3079 ppm, ESI-MS: (positive mode  $m/z$ ) 642.9  $[\text{M}+\text{Na}]^+$ , elemental analysis for  $\text{PtC}_{16}\text{H}_{21}\text{O}_5\text{S}_3\text{Cl}$ : C 30.99, H 3.41, S 15.51, Cl 5.72; found: C 31.04, H: 3.52 S: 15.63 Cl 5.59.

**7- HL7 (300 mg, 0.91 mmol), cis-[PtCl<sub>2</sub>(DMS)(DMSO)] (370 mg, 0.91 mmol).**

**[Pt(L7)<sub>2</sub>] (PtC<sub>26</sub>H<sub>24</sub>O<sub>6</sub>S<sub>4</sub>Br<sub>2</sub>) (Mol. Wt.: 915.60 g/mol)**

Red solid; yield: 50 mg (5.99 %);  $R_f = 0.8$  (cyclohexane/ $\text{CH}_2\text{Cl}_2$ /acetone,5:2:1).

$^1\text{H}$  NMR (400 MHz,  $\text{CDCl}_3$ )  $\delta$  7.55 (dd,  $J = 7.8, 1.2$  Hz, 2H), 7.51 (dd,  $J = 7.5, 1.9$  Hz, 2H), 7.32 – 7.22 (m, 4H), 6.76 (s, 2H, =CH-), 4.27 (q,  $J = 7.1$  Hz, 4H), 3.98 (s, 4H), 1.33 (t,  $J = 7.1$  Hz, 6H),  $^{13}\text{C}\{^1\text{H}\}$  NMR (101 MHz,  $\text{CDCl}_3$ )  $\delta$  177.01(-C=S), 175.06, 167.29, 141.25, 133.76, 131.06, 129.46, 127.23, 119.87, 116.89 (=CH-), 62.27, 36.52, 14.15,  $^{195}\text{Pt}$  NMR (85.7 MHz,  $\text{CDCl}_3$ )  $\delta$  -2267 ppm, ESI-MS: (positive mode  $m/z$ ) 938.8  $[\text{M}+\text{Na}]^+$ , elemental analysis for  $\text{PtC}_{26}\text{H}_{24}\text{O}_6\text{S}_4\text{Br}_2$ : C 34.11, H 2.64, S 14.01, Br 17.45; found: C 34.23, H: 2.88 S: 14.07, Br 17.36.

**[Pt(L7)(DMS)Cl] (PtC<sub>15</sub>H<sub>18</sub>O<sub>3</sub>S<sub>3</sub>BrCl) (Mol. Wt.: 652.92 g/mol)**

Orange solid; yield: 139.40 mg (23.43 %);  $R_f = 0.6$  (cyclohexane/ $\text{CH}_2\text{Cl}_2$ /acetone,5:2:1).

$^1\text{H}$  NMR (400 MHz,  $\text{CDCl}_3$ )  $\delta$  7.56 (dd,  $J = 7.6, 1.4$  Hz, 1H), 7.51 (dd,  $J = 7.4, 2.0$  Hz, 1H), 7.36 – 7.20 (m, 2H), 6.85 (s, 1H, =CH-), 4.26 (q,  $J = 7.1$  Hz, 2H), 3.95 (s, 2H), 2.61 (s w/Pt satellites,  $^3J_{\text{Pt-H}} = 48.80$ Hz, 6H), 1.30 (t,  $J = 7.1$  Hz, 3H),

$^{13}\text{C}\{^1\text{H}\}$  NMR (101 MHz,  $\text{CDCl}_3$ )  $\delta$  176.51 (-C=S), 174.42, 167.24, 140.99, 133.72, 131.21, 129.88, 127.39, 119.59, 116.48 (=CH-), 62.30, 36.50, 24.14(s w/Pt satellites,  $^2J_{\text{Pt-C}} = 15.65$  Hz,  $\text{CH}_3(\text{DMS})$ ), 14.13,  $^{195}\text{Pt}$  NMR (85.7 MHz,  $\text{CDCl}_3$ )  $\delta$  -2879 ppm, ESI-MS: (positive mode  $m/z$ ) 675.8  $[\text{M}+\text{Na}]^+$ , elemental analysis for  $\text{PtC}_{15}\text{H}_{18}\text{O}_3\text{S}_3\text{BrCl}$ : C 27.59, H 2.78, S 14.73, Br 12.24, Cl 5.43; found: C 27.75, H: 2.94 S: 14.57, Br 12.18, Cl 5.52.

**[Pt(L7)(DMSO)Cl] (PtC<sub>15</sub>H<sub>18</sub>O<sub>4</sub>S<sub>3</sub>BrCl) (Mol. Wt.: 668.92 g/mol)**

Orange solid; yield: 96.6 mg (15.85 %);  $R_f = 0.5$  (cyclohexane/ $\text{CH}_2\text{Cl}_2$ /acetone,5:2:1).

$^1\text{H}$  NMR (400 MHz,  $\text{CDCl}_3$ )  $\delta$  7.58 (dd,  $J = 7.7, 1.2$  Hz, 1H), 7.50 (dd,  $J = 7.5, 1.9$  Hz, 1H), 7.38 – 7.25 (m, 2H), 6.82 (s, 1H, =CH-), 4.26 (q,  $J = 7.1$  Hz, 2H), 4.04 (s, 2H), 3.65 (s w/Pt satellites,  $^3J_{\text{Pt-H}} = 18.80$  Hz, 6H), 1.31 (t,  $J = 7.1$  Hz, 3H),  $^{13}\text{C}\{^1\text{H}\}$  NMR (101 MHz,  $\text{CDCl}_3$ )  $\delta$  178.37 (-C=S), 177.20, 167.10, 140.10, 133.82, 131.45, 130.05, 127.42, 119.99, 116.18 (=CH-), 62.42, 46.80 (s w/Pt satellites,  $^2J_{\text{Pt-C}} = 58.07$  Hz,  $\text{CH}_3(\text{DMSO})$ ), 36.67, 14.09,  $^{195}\text{Pt}$  NMR (85.7 MHz,  $\text{CDCl}_3$ )  $\delta$  -3033 ppm, ESI-MS: (positive mode  $m/z$ ) 691.8  $[\text{M}+\text{Na}]^+$ , elemental analysis for  $\text{PtC}_{15}\text{H}_{18}\text{O}_4\text{S}_3\text{BrCl}$ : C 26.93, H 2.71, S 14.38, Br 11.95, Cl 5.30; found: C 26.87, H: 2.56 S: 14.47, Br 12.03, Cl 5.32.

**8- HL8 (300 mg, 0.91 mmol), cis-[PtCl<sub>2</sub>(DMS)(DMSO)] (370 mg, 0.91 mmol).**

**[Pt(L8)<sub>2</sub>] (PtC<sub>26</sub>H<sub>24</sub>O<sub>6</sub>S<sub>4</sub>Br<sub>2</sub>) (Mol. Wt.: 915.60 g/mol)**

Red solid; yield: 64.8 mg (7.77 %);  $R_f = 0.8$  (cyclohexane/ $\text{CH}_2\text{Cl}_2$ /acetone,5:2:1).

$^1\text{H}$  NMR (400 MHz,  $\text{CDCl}_3$ )  $\delta$  8.15 (s, 2H), 7.91 (d,  $J = 7.9$  Hz, 2H), 7.67 (d,  $J = 7.9$  Hz, 2H), 7.30 (t,  $J = 7.9$  Hz, 2H), 7.07 (s, 2H, =CH-), 4.27 (q,  $J = 7.1$  Hz, 4H), 3.96 (s, 4H), 1.33 (t,  $J = 7.1$  Hz, 6H),  $^{13}\text{C}\{^1\text{H}\}$  NMR (101 MHz,  $\text{CDCl}_3$ )  $\delta$  175.32 (-C=S), 172.47, 167.37, 140.14, 134.38, 130.53, 130.37, 125.67, 123.25, 112.54 (=CH-), 62.27, 36.63, 14.17,  $^{195}\text{Pt}$  NMR (85.7 MHz,  $\text{CDCl}_3$ )  $\delta$  -2270 ppm, ESI-MS: (positive mode  $m/z$ ) 938.8  $[\text{M}+\text{Na}]^+$ , elemental analysis for  $\text{PtC}_{26}\text{H}_{24}\text{O}_6\text{S}_4\text{Br}_2$ : C 34.11, H 2.64, S 14.01, Br 17.45; found: C 34.28, H: 2.86 S: 13.87, Br 17.33.

**[Pt(L8)(DMS)Cl] (PtC<sub>15</sub>H<sub>18</sub>O<sub>3</sub>S<sub>3</sub>BrCl) (Mol. Wt.: 652.92 g/mol)**

Orange solid; yield: 100 mg (16.81 %);  $R_f = 0.6$  (cyclohexane/ $\text{CH}_2\text{Cl}_2$ /acetone,5:2:1).

$^1\text{H}$  NMR (400 MHz,  $\text{CDCl}_3$ )  $\delta$  8.06 (s, 1H), 7.92 (d,  $J = 8.0$  Hz, 1H), 7.68 (d,  $J = 8.0$  Hz, 1H), 7.33 – 7.26 (m, 1H), 7.15 (s, 1H, =CH-), 4.27 (q,  $J = 7.1$  Hz, 2H), 3.96 (s, 2H), 2.62 (s w/Pt satellites,  $^3J_{\text{Pt-H}} = 47.20$  Hz, 6H), 1.31 (t,  $J = 7.1$  Hz, 3H),



$^{13}\text{C}\{^1\text{H}\}$  NMR (101 MHz,  $\text{CDCl}_3$ )  $\delta$  174.92(-C=S), 173.08, 167.32, 139.92, 134.64, 130.44, 130.37, 126.50, 122.97, 112.19 (=CH-), 62.33, 36.53, 24.17(s w/Pt satellites,  $^2J_{\text{Pt-C}}$  = 18.50 Hz,  $\text{CH}_3(\text{DMSO})$ ), 14.16,  $^{195}\text{Pt}$  NMR (85.7 MHz,  $\text{CDCl}_3$ )  $\delta$  -2902 ppm, ESI-MS: (positive mode  $m/z$ ) 675.8 [M+Na] $^+$ , elemental analysis for  $\text{PtC}_{15}\text{H}_{18}\text{O}_3\text{S}_3\text{BrCl}$ : C 27.59, H 2.78, S 14.73, Br 12.24, Cl 5.43; found: C 27.88, H: 2.96 S: 14.54, Br 12.11, Cl 5.64.

**[Pt(L8)(DMSO)Cl] (PtC<sub>15</sub>H<sub>18</sub>O<sub>4</sub>S<sub>3</sub>BrCl) (Mol. Wt.: 668.92 g/mol)**

Orange solid; yield: 65 mg (10.66 %); Rf = 0.5 (cyclohexane/ $\text{CH}_2\text{Cl}_2$ /acetone,5:2:1).

$^1\text{H}$  NMR (400 MHz,  $\text{CDCl}_3$ )  $\delta$  8.05 (s, 1H), 7.89 (d,  $J$  = 7.9 Hz, 1H), 7.66 (d,  $J$  = 8.0 Hz, 1H), 7.29 (t,  $J$  = 7.9 Hz, 1H), 7.09 (s, 1H, =CH-), 4.26 (q,  $J$  = 7.1 Hz, 2H), 4.04 (s, 2H), 3.65 (s w/Pt satellites,  $^3J_{\text{Pt-H}}$  = 18.40 Hz, 6H), 1.31 (t,  $J$  = 7.1 Hz, 3H),  $^{13}\text{C}\{^1\text{H}\}$  NMR (101 MHz,  $\text{CDCl}_3$ )  $\delta$  178.58 (-C=S), 173.75, 167.19, 138.99, 135.02, 130.71, 130.41, 126.66, 123.00, 111.92 (=CH-), 62.44, 46.87(s w/Pt satellites,  $^2J_{\text{Pt-C}}$  = 56.86 Hz,  $\text{CH}_3(\text{DMSO})$ ), 36.70, 14.10,  $^{195}\text{Pt}$  NMR (85.7 MHz,  $\text{CDCl}_3$ )  $\delta$  -3054 ppm, ESI-MS: (positive mode  $m/z$ ) 691.8 [M+Na] $^+$ , elemental analysis for  $\text{PtC}_{15}\text{H}_{18}\text{O}_4\text{S}_3\text{BrCl}$ : C 26.93, H 2.71, S 14.38, Br 11.95, Cl 5.30; found: C 27.12, H: 2.99 S: 14.27, Br 11.83, Cl 5.44.

**9- HL9 (330 mg, 0.99 mmol), cis-[PtCl<sub>2</sub>(DMS)(DMSO)] (400 mg, 0.99 mmol).**

**[Pt(L9)<sub>2</sub>] (PtC<sub>26</sub>H<sub>24</sub>O<sub>6</sub>S<sub>4</sub>Br<sub>2</sub>) (Mol. Wt.: 915.60 g/mol)**

Red solid; yield: 51 mg (5.65 %); Rf = 0.8 (cyclohexane/ $\text{CH}_2\text{Cl}_2$ /acetone,5:2:1).

$^1\text{H}$  NMR (400 MHz,  $\text{CDCl}_3$ )  $\delta$  7.86 (d,  $J$  = 8.6 Hz, 4H), 7.59 (d,  $J$  = 8.5 Hz, 4H), 7.11 (s, 2H, =CH-), 4.27 (q,  $J$  = 7.1 Hz, 4H), 3.98 (s, 4H), 1.33 (t,  $J$  = 7.1 Hz, 6H),  $^{13}\text{C}\{^1\text{H}\}$  NMR (101 MHz,  $\text{CDCl}_3$ )  $\delta$  174.02 (-C=S), 171.28, 167.29, 137.57, 132.15, 128.71, 126.47, 112.86 (=CH-), 62.14, 36.55, 14.06,  $^{195}\text{Pt}$  NMR (85.7 MHz,  $\text{CDCl}_3$ )  $\delta$  -2303 ppm, ESI-MS: (positive mode  $m/z$ ) 938.8 [M+Na] $^+$ , elemental analysis for  $\text{PtC}_{26}\text{H}_{24}\text{O}_6\text{S}_4\text{Br}_2$ : C 34.11, H 2.64, S 14.01, Br 17.45; found: C 34.33, H: 2.82 S: 13.87, Br 17.61.

**[Pt(L9)(DMS)Cl] (PtC<sub>15</sub>H<sub>18</sub>O<sub>3</sub>S<sub>3</sub>BrCl) (Mol. Wt.: 652.92 g/mol)**

Orange solid; yield: 113 mg (17.57%); Rf = 0.6 (cyclohexane/ $\text{CH}_2\text{Cl}_2$ /acetone,5:2:1).

$^1\text{H}$  NMR (500 MHz,  $\text{CDCl}_3$ )  $\delta$  7.84 (d,  $J$  = 8.7 Hz, 2H), 7.52 (d,  $J$  = 8.7 Hz, 2H), 7.16 (s, 1H, =CH-), 4.24 (q,  $J$  = 7.1 Hz, 2H), 3.93 (s, 2H), 2.60 (s w/Pt satellites,  $^3J_{\text{Pt-H}}$  = 44.60 Hz, 6H), 1.29 (t,  $J$  = 7.1 Hz, 3H),  $^{13}\text{C}\{^1\text{H}\}$  NMR (126 MHz,  $\text{CDCl}_3$ )  $\delta$  174.27 (-C=S), 173.46, 167.41, 136.67, 132.14, 129.29,

126.89, 111.92 (=CH-), 62.33, 36.51, 24.26 (s w/Pt satellites,  $^2J_{\text{Pt-C}}$  = 18.25 Hz,  $\text{CH}_3(\text{DMSO})$ ), 14.17,  $^{195}\text{Pt}$  NMR (107 MHz,  $\text{CDCl}_3$ )  $\delta$  -2907 ppm, ESI-MS: (positive mode  $m/z$ ) 675.8 [M+Na] $^+$ , elemental analysis for  $\text{PtC}_{15}\text{H}_{18}\text{O}_3\text{S}_3\text{BrCl}$ . 0.25 cyclohexane: C 29.40, H 3.14, S 14.27, Br 11.85, Cl 5.26; found: C 29.12, H: 2.93 S: 14.24, Br 11.70, Cl 5.48.

**[Pt(L9)(DMSO)Cl] (PtC<sub>15</sub>H<sub>18</sub>O<sub>4</sub>S<sub>3</sub>BrCl) (Mol. Wt.: 668.92 g/mol)**

Orange solid; yield: 87 mg (13.20%); Rf = 0.5 (cyclohexane/ $\text{CH}_2\text{Cl}_2$ /acetone,5:2:1).

$^1\text{H}$  NMR (500 MHz,  $\text{CDCl}_3$ )  $\delta$  7.82 (d,  $J$  = 8.7 Hz, 2H), 7.54 (d,  $J$  = 8.7 Hz, 2H), 7.11 (s, 1H, =CH-), 4.26 (q,  $J$  = 7.2 Hz, 2H), 4.03 (s, 2H), 3.65 (s w/Pt satellites,  $^3J_{\text{Pt-H}}$  = 17.95 Hz, 6H), 1.30 (t,  $J$  = 7.1 Hz, 3H),  $^{13}\text{C}\{^1\text{H}\}$  NMR (126 MHz,  $\text{CDCl}_3$ )  $\delta$  177.87 (-C=S), 174.17, 167.29, 135.75, 132.17, 129.52, 127.34, 111.67 (=CH-), 62.43, 46.86 (s w/Pt satellites,  $^2J_{\text{Pt-C}}$  = 55.87 Hz,  $\text{CH}_3(\text{DMSO})$ ), 36.68, 14.12,  $^{195}\text{Pt}$  NMR (107 MHz,  $\text{CDCl}_3$ )  $\delta$  -3060 ppm, ESI-MS: (positive mode  $m/z$ ) 691.8 [M+Na] $^+$ , elemental analysis for  $\text{PtC}_{15}\text{H}_{18}\text{O}_4\text{S}_3\text{BrCl}$ : C 26.93, H 2.71, S 14.38, Br 11.95, Cl 5.30; found: C 27.00, H: 2.83 S: 14.41, Br 12.05, Cl 5.28.

**Stability and solvolysis of the Pt(II) complexes**

As a typical experiment, 0.21–0.29 mg of [Pt(L6)<sub>2</sub>], [Pt(L6)(DMS)Cl], and [Pt(L6)(DMSO)Cl] complexes were dissolved in 1 mL of  $\text{CH}_3\text{CN}$ : PBS buffer (pH 7.4;1:1), to obtain a 0.35 mM solution, which was incubated at 37 °C for 72 hours. The ESI-MS spectra were recorded after 24, 48 and 72 hours

**Interactions of the Pt(II) complexes with 9-methylguanine**

As a typical experiment, 0.21–0.29 mg of [Pt(L6)<sub>2</sub>], [Pt(L6)(DMS)Cl], and [Pt(L6)(DMSO)Cl] complexes were dissolved in 1 mL of  $\text{CH}_3\text{CN}$ : PBS buffer (pH 7.4;1:1), to obtain a 0.35 mM solution, then (8 eq. 0.47 mg) of 9-MG was added and the mixtures were incubated at 37 °C for 72 hours. The ESI-MS spectra were recorded after 24, 48 and 72 hours.

**IC<sub>50</sub> determination**

Cancer cell lines were cultured under standard conditions (5 %  $\text{CO}_2$ , 37 °C, 90 % humidity) in RPMI medium supplemented with 10 % FCS, 100 U/ml penicillin and 100  $\mu\text{g}/\text{ml}$  streptomycin (Life Technologies, Germany). The tested Pt(II) complexes was dissolved in DMSO. Determinations of IC<sub>50</sub> values were carried out using the CellTiter96 non-radioactive proliferation assay (MTT assay, Promega). After seeding 5000 cells per well in a 96 well plate cells were

allowed to attach for 24 h and were incubated for 48 h with different concentrations of the substances ranging from 0 to 100  $\mu\text{M}$  for Metal complexes (0, 1, 3, 10, 33, 100  $\mu\text{M}$ ). Each measurement was done in triplicate and repeated 3-times. The proportion of live cells was quantified by the MTT assay and after background subtraction relative values compared to the mean of medium controls were calculated. Non-linear regression analyses applying the Hill-slope were run in GraphPad 5.0 software.

## Acknowledgements

M.K.F. is grateful to the Katholischer Akademischer Ausländer-Dienst (KAAD) for a Ph.D. scholarship. The authors would further like to thank Umicore AG & Co. KG Hanau-Wolfgang, Germany for the donation of  $\text{K}_2\text{PtCl}_4$ .

**Keywords:** Platinum(II) complexes •  $\beta$ -hydroxydithiocinnamic esters ligands • O,S-bidentate chelating ligands • Stability and solvolysis • 9-methylguanine binding

1. M. S. Singh, G. C. Nandi, T. Chanda, *RSC Adv.* **2013**, *3*, 14183-14198.
2. J. Li, W. Ma, W. Ming, C. Xu, N. Wei, M. Wang, *J. Org. Chem.* **2015**, *80*, 11138-11142.
3. S. Soni, S. Koley, M. S. Singh, *Tetrahedron Lett.* **2017**, *58*, 2512-2516.
4. R. K. Chellu, S. Kurva, A. K. Soda, S. K. Chilaka, J. B. Nanubolu, S. Madabhushi, *Asian J. Org. Chem.* **2021**, *10*, 1432-1435.
5. I. H. Chanu, L. M. Devi, T. P. Singh, S. J. Singh, R. R. Singh, O. Mukherjee Singh, *ChemistrySelect* **2020**, *5*, 7447-7451.
6. D. Yadav, A. Srivastava, M. A. Ansari, M. S. Singh, *J. Org. Chem.* **2021**, *86*, 5908-5921.
7. S. T. Bhaskaran, P. Mathew, *J. Mol. Struct.* **2022**, *1251*, 132071.
8. K. Kumari, S. Kumar, K. N. Singh, M. G. B. Drew, N. Singh, *New J. Chem.* **2020**, *44*, 12143-12153.
9. C. L. Yadav, Anamika, G. Rajput, K. Kumar, M. G. B. Drew, N. Singh, *Inorg. Chem.* **2020**, *59*, 11417-11431.
10. K. Kumari, A. S. Singh, K. K. Manar, C. L. Yadav, V. K. Tiwari, M. G. B. Drew, N. Singh, *New J. Chem.* **2019**, *43*, 1166-1176.
11. M. K. Yadav, G. Rajput, K. Srivastava, R. K. Singh, R. Mishra, M. G. B. Drew, N. Singh, *New J. Chem.* **2015**, *39*, 6358-6366.
12. J. Hildebrandt, N. Häfner, D. Kritsch, H. Görls, M. Dürst, I. B. Runnebaum, W. Weigand, *Int. J. Mol. Sci.* **2022**, *23*, 4976
13. C. Mügge, R. Liu, H. Görls, C. Gabbiani, E. Michelucci, N. Rüdiger, J. H. Clement, L. Messori, W. Weigand, *Dalton Trans.* **2014**, *43*, 3072-3086.
14. C. Mügge, T. Marzo, L. Massai, J. Hildebrandt, G. Ferraro, P. Rivera-Fuentes, N. Metzler-Nolte, A. Merlino, L. Messori, W. Weigand, *Inorg. Chem.* **2015**, *54*, 8560-8570.
15. J. Hildebrandt, N. Häfner, H. Görls, D. Kritsch, G. Ferraro, M. Dürst, I. B. Runnebaum, A. Merlino, W. Weigand, *Dalton Trans.* **2016**, *45*, 18876-18891.
16. J. Hildebrandt, H. Görls, N. Häfner, G. Ferraro, M. Dürst, I. B. Runnebaum, W. Weigand, A. Merlino, *Dalton Trans.* **2016**, *45*, 12283-12287.
17. J. Hildebrandt, N. Häfner, H. Görls, M.-C. Barth, M. Dürst, I. B. Runnebaum, W. Weigand, *Int. J. Mol. Sci.* **2022**, *23*, 6669.
18. L. Tabrizi, B. Zouchoune, A. Zaiter, *RSC Adv.* **2019**, *9*, 287-300.
19. B. Lippert, *Cisplatin: chemistry and biochemistry of a leading anticancer drug*, Verlag Helv. Chim. Acta, Zürich, **1999**, <https://doi.org/10.1002/9783906390420>.
20. J. Reedijk, *Eur. J. Inorg. Chem.* **2009**, *2009*, 1303-1312.
21. M. D. Hall, M. Okabe, D. W. Shen, X. J. Liang, M. M. Gottesman, *Annu. Rev. Pharmacol. Toxicol.* **2008**, *48*, 495-535.
22. Y. Wang, J. Lv, X. Ma, D. Wang, H. Ma, Y. Chang, G. Nie, L. Jia, X. Duan, X.-J. Liang, *Curr. Drug Metab.* **2010**, *11*, 507-515.
23. D.-w. Shen, I. Pastan, M. M. Gottesman, *Cancer Res.* **1998**, *58*, 268-275.
24. Z. Guo, P. J. Sadler, *Angew. Chem. Int. Ed.* **1999**, *38*, 1512-1531.
25. G. M. Mavligit, A. A. Zukwiski, L. M. Ellis, V. P. Chuang, S. Wallace, *Cancer* **1995**, *75*, 2083-2088.
26. I. Kostova, *Recent Patents on Anti-Cancer Drug Discovery* **2006**, *1*, 1-22.
27. H. P. Varbanov, S. M. Valiahi, C. R. Kowol, M. A. Jakupec, M. Galanski, B. K. Keppler, *Dalton Trans.* **2012**, *41*, 14404-14415.
28. J. Zhao, S. Gou, Y. Sun, L. Fang, Z. Wang, *Inorg. Chem.* **2012**, *51*, 10317-10324.
29. A. Thuillier, J. Vialle, *Bull. Soc. Chim. Fr.* **1962**, 2182-2186.
30. G. Singh, S. S. Bhattacharjee, H. Ila, H. Junjappa, *Synthesis* **1982**, 1982, 693-694.
31. H. Junjappa and H. Ila, *PCT Int. Appl.* **2004**, 2004101530.
32. P. Kapoor, K. Löqvist, Å. Oskarsson, *J. Mol. Struct.* **1998**, *470*, 39-47.
33. C. K. Jorgensen, *Inorg. Chem.* **1964**, *3*, 1201-1202.
34. R. G. Pearson, *Inorg. Chem.* **1973**, *12*, 712-713.
35. M. K. Farh, F. V. Gruschwitz, N. Ziegenbalg, H. Abul-Futouh, H. Görls, W. Weigand, J. C. Brendel, *Macromol. Rapid Commun.* **2022**, *n/a*, 2200428.
36. R. Saumweber, C. Robl, W. Weigand, *Inorganica Chim. Acta* **1998**, *269*, 83-90.
37. K. Schubert, R. Saumweber, H. Görls, W. Weigand, *Z. Anorg. Allg. Chem.* **2003**, *629*, 2091-2096.
38. K. Schubert, T. Alpermann, T. Niksch, H. Görls, W. Weigand, *Z. Anorg. Allg. Chem.* **2006**, *632*, 1033-1042.
39. K. Schubert, H. Görls, W. Weigand, *Z. Naturforsch. B* **2007**, *62*, 475-482.
40. G. R. Fulmer, A. J. M. Miller, N. H. Sherden, H. E. Gottlieb, A. Nudelman, B. M. Stoltz, J. E. Bercaw, K. I. Goldberg, *Organometallics* **2010**, *29*, 2176-2179.
41. M. Kazemnejadi, A. Shakeri, M. Nikoogar, R. Shademani, M. Mohammadi, *R. Soc. Open Sci.* **2018**, *5*, 171541.
42. D. Nieto, A. M. González-Vadillo, S. Bruña, C. J. Pastor, C. Ríos-Luci, L. G. León, J. M. Padrón, C. Navarro-Ranninger, I. Cuadrado, *Dalton Trans.* **2012**, *41*, 432-441.
43. C. López, A. Caubet, S. Pérez, X. Solans, M. Font-Bardía, E. Molins, *Eur. J. Inorg. Chem.* **2006**, *2006*, 3974-3984.

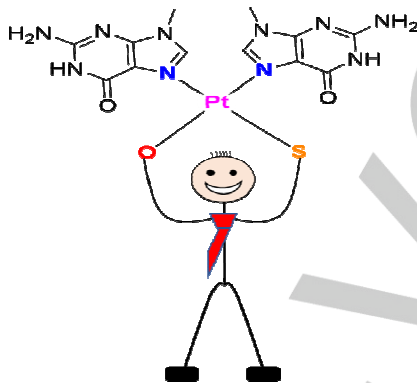
- 
44. C. López, S. Pérez, X. Solans, M. Font-Bardía, T. Calvet, *New J. Chem.* **2010**, *34*, 676-685.
45. D. Talancón, C. López, M. Font-Bardía, T. Calvet, J. Quirante, C. Calvis, R. Messeguer, R. Cortés, M. Cascante, L. Baldomà, J. Badia, *J. Inorg. Biochem.* **2013**, *118*, 1-12.
46. R. Cortés, M. Tarrado-Castellarnau, D. Talancón, C. López, W. Link, D. Ruiz, J. J. Centelles, J. Quirante, M. Cascante, *Metallomics* **2014**, *6*, 622-633.
47. A. M. J. Fichtinger-Schepman, J. L. Van der Veer, J. H. J. Den Hartog, P. H. M. Lohman, J. Reedijk, *Biochemistry* **1985**, *24*, 707-713.
48. V. Brabec, O. Hrabina, J. Kasparkova, *Coord. Chem. Rev.* **2017**, *351*, 2-31.
49. T. C. Johnstone, J. J. Wilson, S. J. Lippard, *Inorg. Chem.* **2013**, *52*, 12234-12249
-

**Entry for the Table of Contents** (Please choose one layout)

Layout 1:

**FULL PAPER**

The reactions of the O,S-bidentate  $\beta$ -hydroxydithiocinnamic ester ligands with *cis*-[PtCl<sub>2</sub>(DMS)(DMSO)] afford a series of homoleptic and heteroleptic platinum(II) complexes. Particularly, the heteroleptic ones are capable of binding 9-methylguanine as a DNA model system, forming stable mono- and bifunctional adducts similar to that formed by Cisplatin and its analogues.



Micheal K. Farh, Norman Häfner,  
Helmar Görls, Ingo B. Runnebaum\*,  
Wolfgang Weigand\*

**Page No. – Page No.**

**Title**

Layout 2:

**FULL PAPER**

((Insert TOC Graphic here; max. width: 11.5 cm; max. height: 2.5 cm))

*Author(s), Corresponding Author(s)\**

**Page No. – Page No.**

**Title**

Text for Table of Contents

Additional Author information for the electronic version of the article.

Micheal K. Farh: ORCID identifier 0000-0003-3669-9127  
Norman Häfner: ORCID identifier 0000-0002-7012-483X  
Wolfgang Weigand: ORCID identifier 0000-0001-5177-1006

# **Novel Homoleptic and Heteroleptic Pt(II) $\beta$ -oxodithiocinnamic ester Complexes: Synthesis, Characterization, Interactions with 9-methylguanine and Antiproliferative Activity**

Micheal K. Farh,<sup>[a,b]</sup> Norman Häfner,<sup>[c]</sup> Helmar Görls,<sup>[a]</sup> Ingo B. Runnebaum,<sup>\*[c]</sup> Wolfgang Weigand,<sup>[a,d]\*</sup>

<sup>a</sup> *Institut für Anorganische und Analytische Chemie, Friedrich-Schiller-Universität, Humboldtstraße 8, 07743 Jena, Germany*

<sup>b</sup> *Department of Chemistry, Faculty of Science, Assiut University, Assiut 71515, Egypt*

<sup>c</sup> *Department of Gynecology, Jena University Hospital—Friedrich-Schiller University Jena, Am Klinikum 1, 07747 Jena, Germany*

<sup>d</sup> *Jena Center for Soft Matter (JCSM), Friedrich Schiller University Jena, Philosophenweg 7, 07743 Jena, Germany*

\* Corresponding authors: [wolfgang.weigand@uni-jena.de](mailto:wolfgang.weigand@uni-jena.de)

[Direktion-Gyn@med.uni-jena.de](mailto:Direktion-Gyn@med.uni-jena.de)

## Stability and solvolysis of the [Pt(L6)<sub>2</sub>], [Pt(L6)(DMS)Cl], and [Pt(L6)(DMSO)Cl] complexes

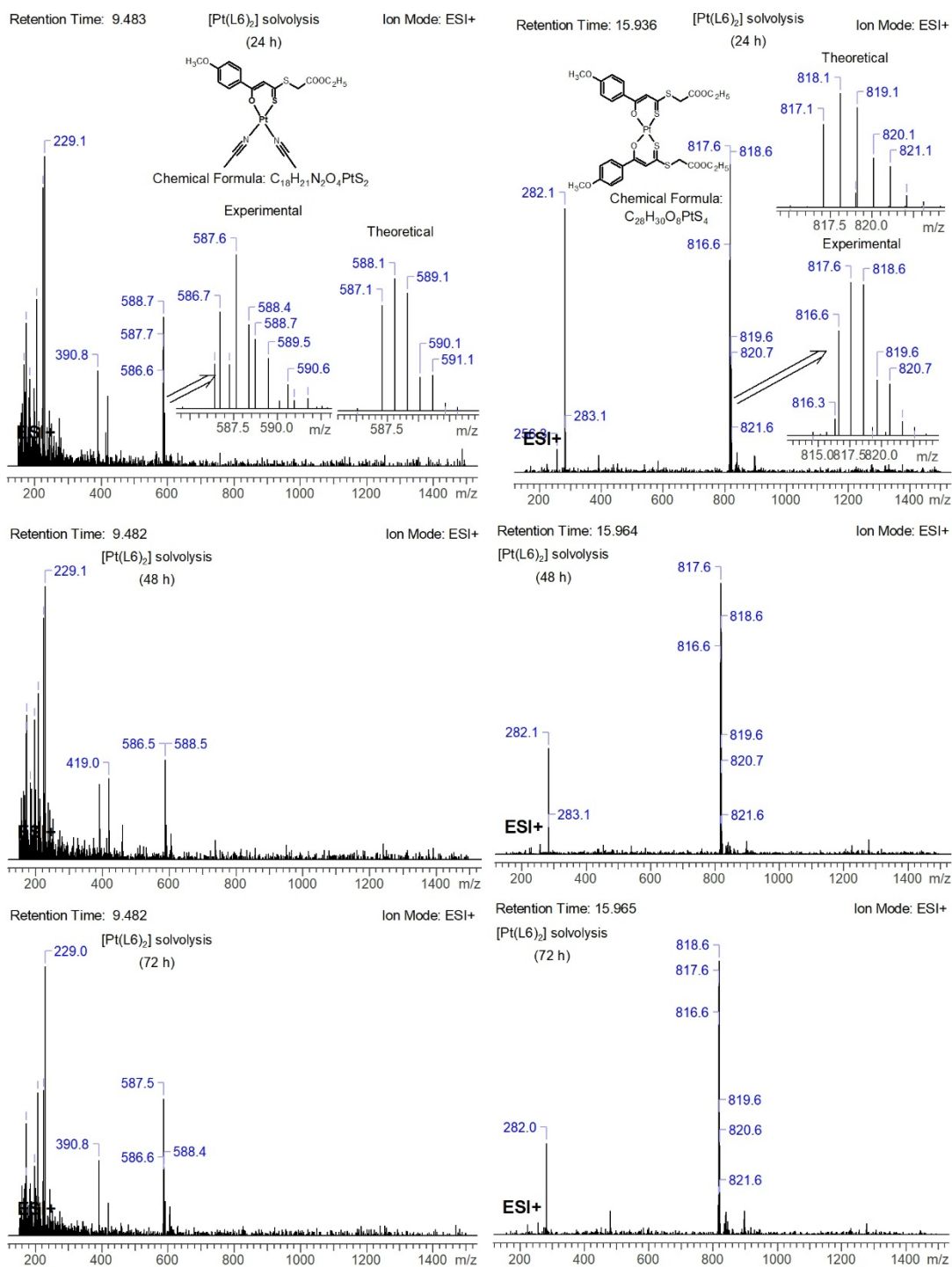


Figure S1: ESI-MS spectra for the solvolysis of [Pt(L6)<sub>2</sub>] in CH<sub>3</sub>CN-PBS (pH 7.4; 1:1) at 37 °C after; A) 24 h (top), B) 48 h (middle), and C) 72 h (bottom). The insets show the isotope patterns of  $m/z = 587.7$ , and  $817.6$  as well as the theoretically produced cations.



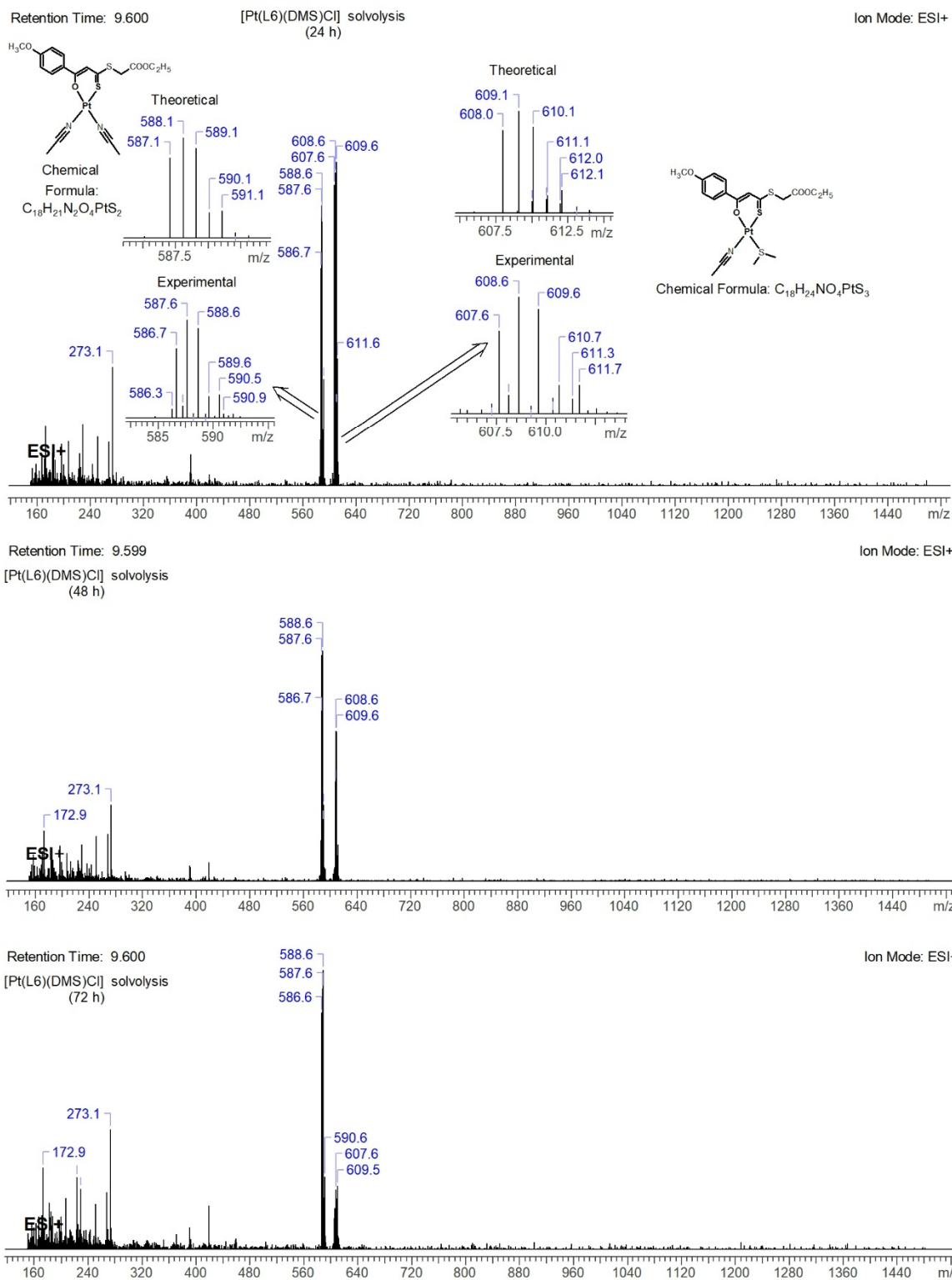


Figure S2: ESI-MS spectra for the solvolysis of [Pt(L6)(DMS)Cl] in  $CH_3CN$ -PBS (pH 7.4; 1:1) at 37 °C after; A) 24 h (top), B) 48 h (middle), and C) 72 h (bottom). The insets show the isotope patterns of  $m/z = 587.6$ , and 608.6 as well as the theoretically produced cations.

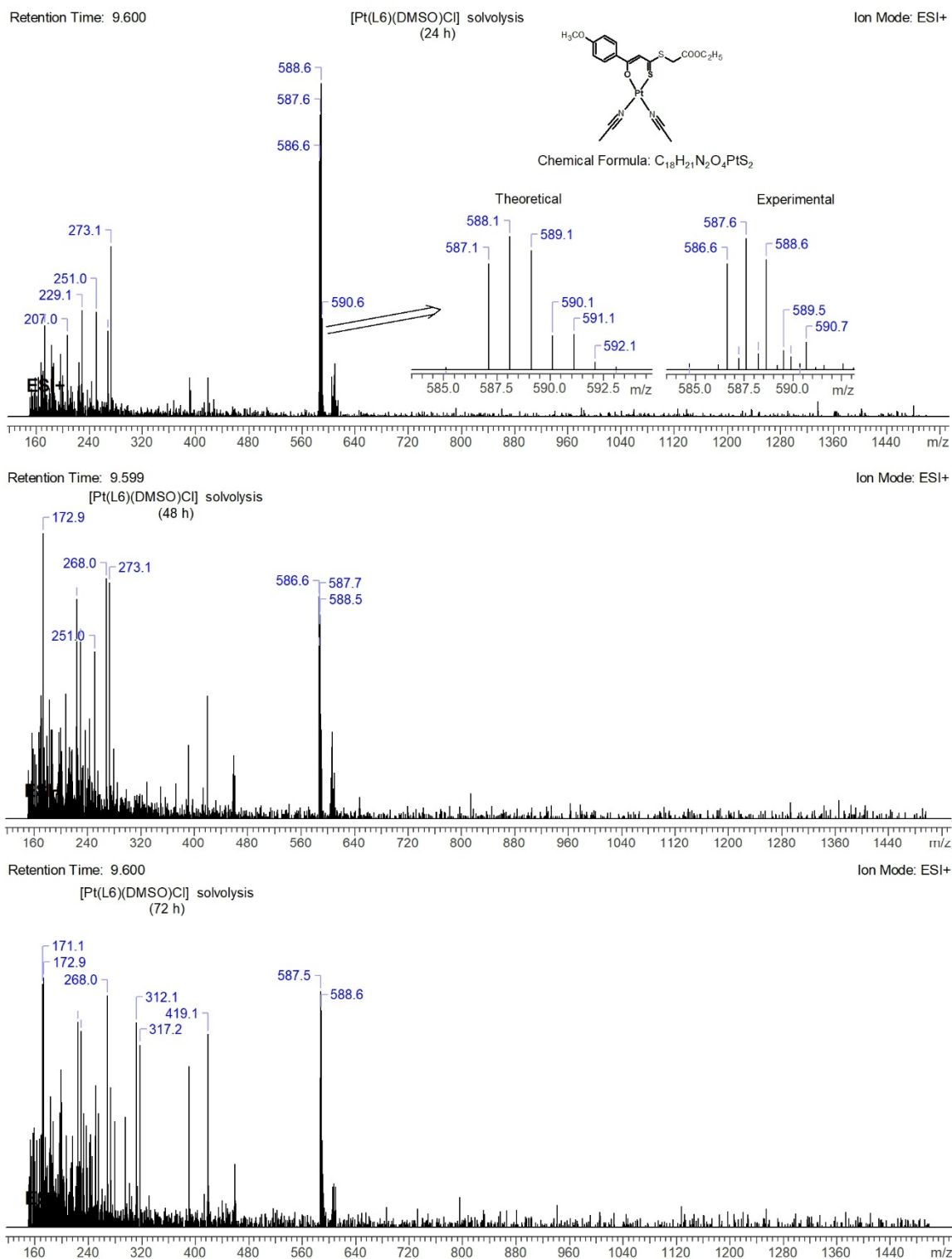


Figure S3: ESI-MS spectra for the solvolysis of [Pt(L6)(DMSO)Cl] in  $CH_3CN$ -PBS (pH 7.4; 1:1) at 37 °C after; A) 24 h (top), B) 48 h (middle), and C) 72 h (bottom). The insets show the isotope pattern of  $m/z = 587.6$  as well as the theoretically produced cations.



## Interactions of the [Pt(L6)<sub>2</sub>], [Pt(L6)(DMS)Cl], and [Pt(L6)(DMSO)Cl] complexes with 9-MeG.

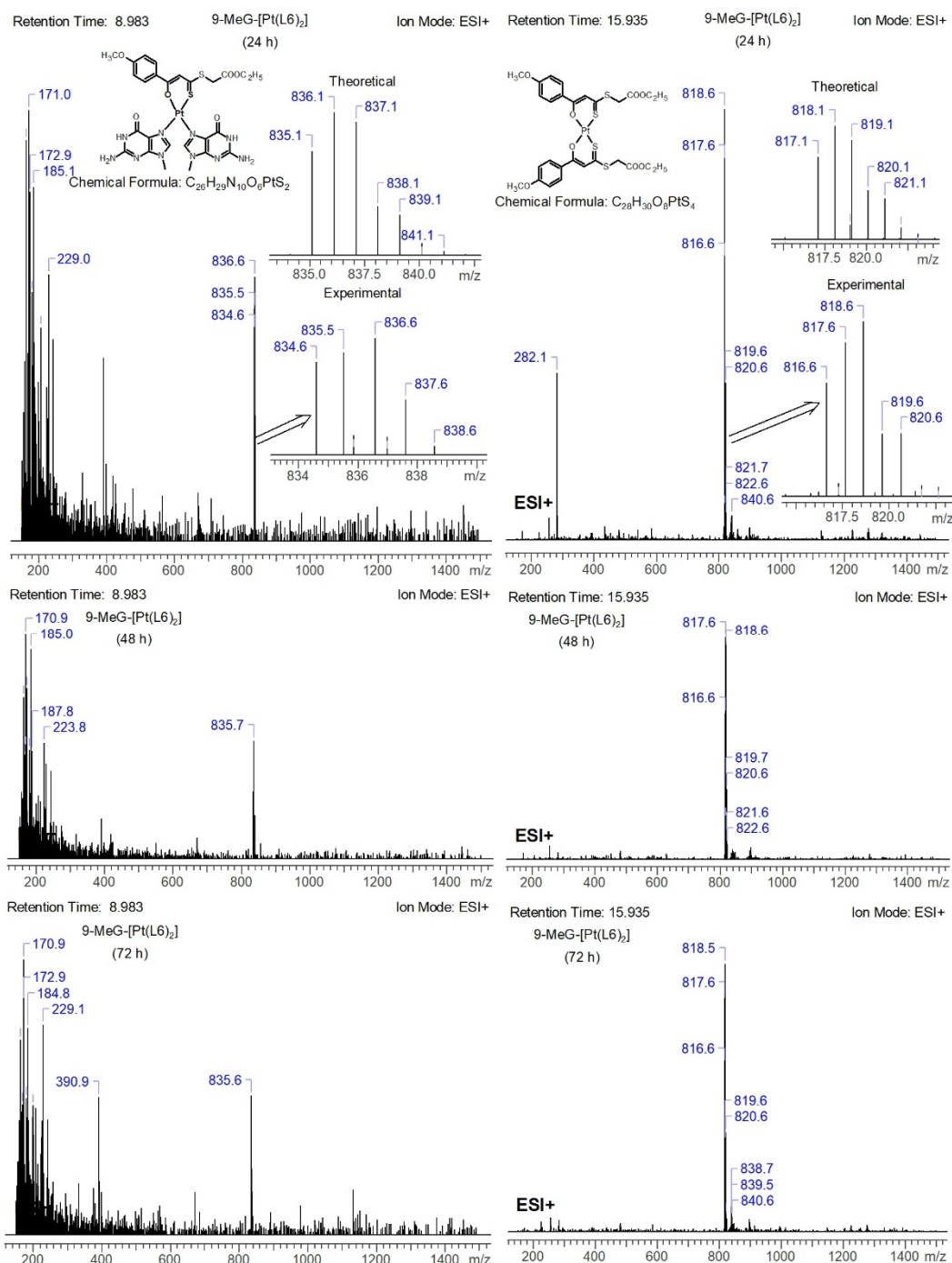


Figure S4: ESI-MS spectra of the adducts formed between 9-MeG and [Pt(L6)<sub>2</sub>] complex in CH<sub>3</sub>CN-PBS (pH 7.4; 1:1) at 37 °C after; A) 24 h (top), B) 48 h (middle), and C) 72 h (bottom). The insets show the theoretical as well as the experimental isotope patterns of  $m/z = 835.6$  ( $t_R = 8.98$  min), and the non-reacted complex at 817.6 ( $t_R = 15.93$  min).

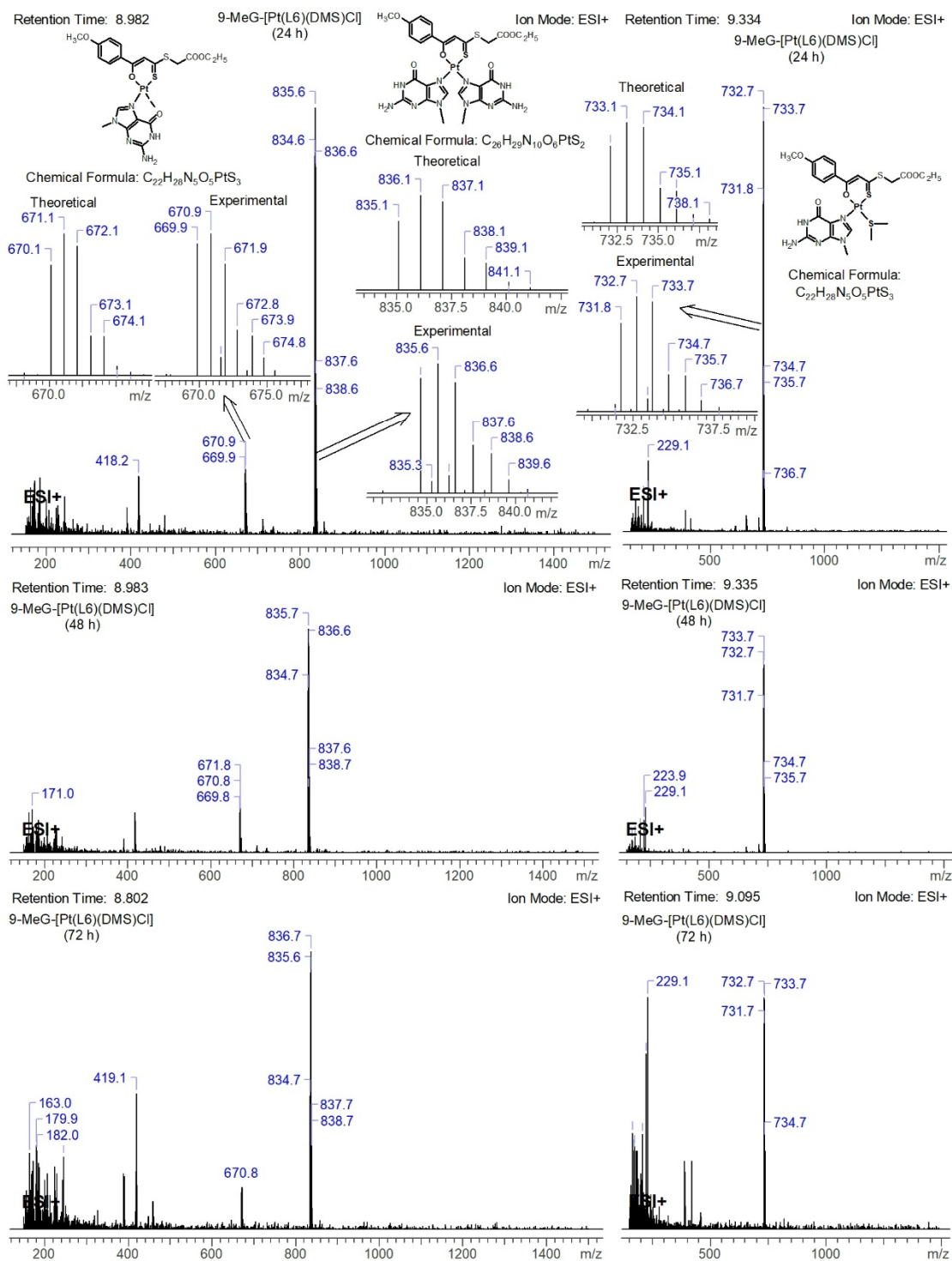


Figure S5: ESI-MS spectra of the adducts formed between 9-MeG and [Pt(L6)(DMS)Cl] complex in  $CH_3CN$ -PBS (pH 7.4; 1:1) at 37 °C after; A) 24 h (top), B) 48 h (middle), and C) 72 h (bottom). The insets show the theoretical as well as the experimental isotope patterns of  $m/z = 835.6$  ( $t_R = 8.98$  min), 732.7 ( $t_R = 9.33$  min), and 670.9 ( $t_R = 8.98$  min).

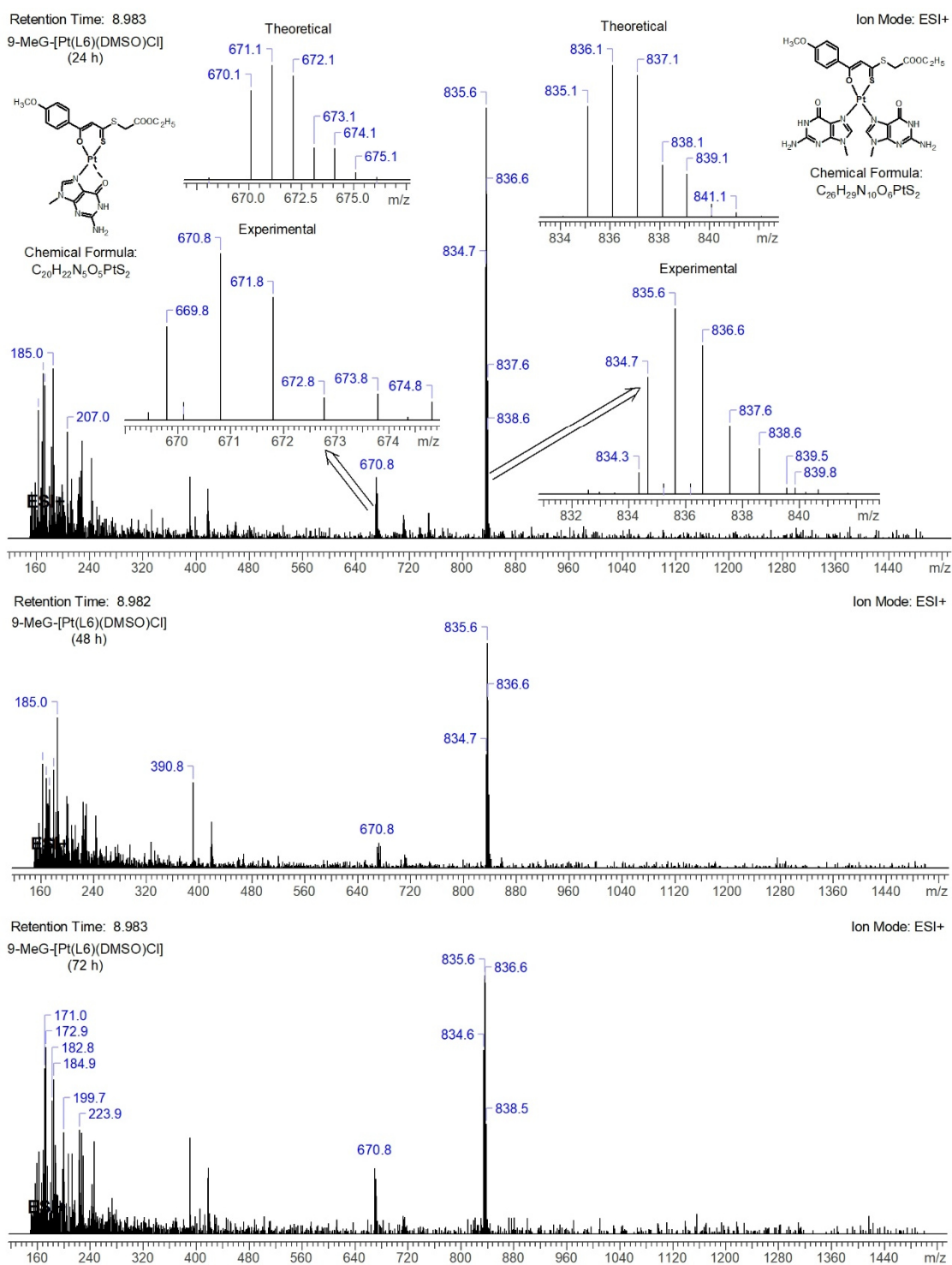
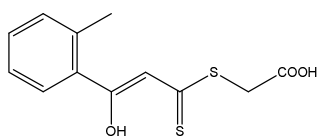


Figure S6: ESI-MS spectra of the adducts formed between 9-MeG and [Pt(L6)(DMSO)Cl] complex in  $CH_3CN$ -PBS (pH 7.4; 1:1) at 37 °C after; A) 24 h (top), B) 48 h (middle), and C) 72 h (bottom). The insets show the theoretical as well as the experimental isotope patterns of  $m/z = 835.6$  ( $t_R = 8.98$  min), and 670.8 ( $t_R = 8.98$  min).

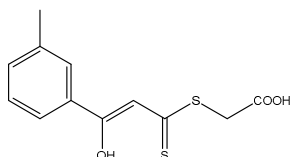
## Characterization data of the synthesized ligands HL1- HL9

### 2-((3-hydroxy-3-(o-tolyl)prop-2-enethioyl)thio)acetic acid (HL1)



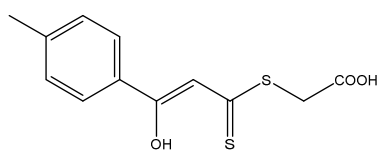
Yield: 1.49 g (27.76 %) as yellow crystals.  $^1\text{H}$  NMR (400 MHz, acetone- $d_6$ ):  $\delta$  15.01 (s, 1H, -C-OH), 11.20 (s, 1H, -COOH), 7.55 (d,  $J = 7.6$  Hz, 1H), 7.43 (t,  $J = 7.4$  Hz, 1H), 7.32 (m, 2H), 6.74 (s, 1H, =CH-), 4.23 (s, 2H), 2.48 (s, 3H),  $^{13}\text{C}\{^1\text{H}\}$  NMR (101 MHz, acetone):  $\delta$  216.02 (-C=S), 174.11 (-C-OH), 167.83 (COOH), 136.87, 134.75, 131.35, 130.91, 128.53, 126.16, 111.22 (=CH-), 35.34, 19.87, MS (ESI)  $m/z$ : 267.1 [M-H] $^-$ , elemental analysis: calculated for  $\text{C}_{12}\text{H}_{12}\text{O}_3\text{S}_2$ : C 53.71, H 4.51, S 23.90; found: C 54.01, H 4.45, S 24.18.

### 2-((3-hydroxy-3-(m-tolyl)prop-2-enethioyl)thio)acetic acid (HL2)



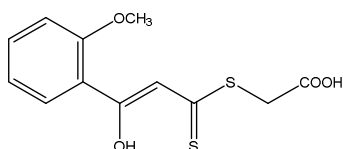
Yield: 1.01 g (18.82 %) as yellow crystals.  $^1\text{H}$  NMR (400 MHz,  $\text{dms}\text{-}d_6$ ):  $\delta$  15.00 (s, 1H, -C-OH), 13.04 (s, 1H, -COOH), 7.74-7.95 (m, 2H), 7.38-7.55 (m, 2H), 7.33 (s, 1H, =CH-), 4.17 (s, 2H), 2.39 (s, 3H),  $^{13}\text{C}\{^1\text{H}\}$  NMR (101 MHz,  $\text{dms}\text{-}d_6$ ):  $\delta$  216.28 (-C=S), 171.14 (-C-OH), 170.02 (COOH), 139.88, 134.80, 134.35, 130.32, 128.63, 125.50, 108.95 (=CH-), 37.30, 22.25, MS (ESI)  $m/z$ : 267.1 [M-H] $^-$ , elemental analysis: calculated for  $\text{C}_{12}\text{H}_{12}\text{O}_3\text{S}_2$ : C 53.71, H 4.51, S 23.90; found: C 53.47, H 4.49, S 24.13.

### 2-((3-hydroxy-3-(p-tolyl)prop-2-enethioyl)thio)acetic acid (HL3)



Yield: 2.28 g (42.48 %) as yellow crystals.  $^1\text{H}$  NMR (400 MHz,  $\text{dms}\text{-}d_6$ ):  $\delta$  14.80 (s, 1H, -C-OH), 13.07 (s, 1H, -COOH), 7.85 (d,  $^3J_{\text{H-H}} = 7.6$  Hz, 2H), 7.29 (d,  $^3J_{\text{H-H}} = 7.84$  Hz, 2H), 7.26 (s, 1H, =CH-), 4.10 (s, 2H), 2.35 (s, 3H),  $^{13}\text{C}\{^1\text{H}\}$  NMR (101 MHz,  $\text{dms}\text{-}d_6$ ): 216.37 (-C=S), 171.54 (-C-OH), 170.40 (COOH), 142.61, 133.52, 129.80, 127.38, 107.35 (=CH-), 36.34, 21.60, MS (ESI)  $m/z$ : 267.1 [M-H] $^-$ , elemental analysis: calculated for  $\text{C}_{12}\text{H}_{12}\text{O}_3\text{S}_2$ : C 53.71, H 4.51, S 23.90; found: C 53.33, H 4.72, S 23.94.

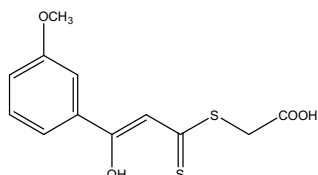
### 2-((3-hydroxy-3-(2-methoxyphenyl)prop-2-enethioyl)thio)acetic acid (HL4)



Yield: 1.29 g (22.68 %) as yellow crystals.  $^1\text{H}$  NMR (400 MHz, acetone- $d_6$ ):  $\delta$  15.09 (s, 1H, -C-OH), 11.40 (s, 1H, -COOH), 7.89 (dd,  $^3J_{\text{H-H}} = 8.00$  Hz,  $^4J_{\text{H-H}} = 1.76$  Hz, 1H), 7.55 (t,  $^3J_{\text{H-H}} = 8.04$  Hz,

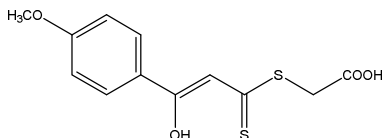
1H), 7.44 (s, 1H, =CH-), 7.19 (d,  $^3J_{H-H}$  = 8.4 Hz, 1H), 7.01 (t,  $^3J_{H-H}$  = 7.80 Hz, 1H), 4.21 (s, 2H), 3.98 (s, 3H),  $^{13}\text{C}\{^1\text{H}\}$  NMR (101 MHz, acetone- $d_6$ ):  $\delta$  215.00 (-C=S), 168.81 (-C-OH), 167.92 (COOH), 158.36, 133.47, 129.90, 122.23, 120.79, 112.40, 112.28 (=CH-), 55.48, 35.38, MS (ESI)  $m/z$ : 283.1 [M-H] $^-$ , elemental analysis: calculated for  $\text{C}_{12}\text{H}_{12}\text{O}_4\text{S}_2$ : C 50.69, H 4.25, S 22.55; found: C 51.05, H 4.20, S 22.43.

### 2-((3-hydroxy-3-(3-methoxyphenyl)prop-2-enethioyl)thio)acetic acid (HL5)



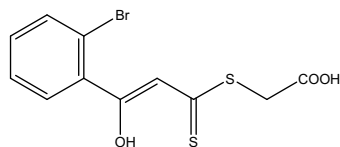
Yield: 0.41 g (7.21 %) as yellow crystals.  $^1\text{H}$  NMR (400 MHz,  $\text{dms}\text{-}d_6$ ):  $\delta$  14.95 (s, 1H, -C-OH), 12.66 (s, 1H, -COOH), 7.30-7.56 (m, 3H), 7.23 (s, 1H, =CH-), 7.07 (s, 1H), 4.07 (s, 2H), 3.80 (s, 3H),  $^{13}\text{C}\{^1\text{H}\}$  NMR (101 MHz,  $\text{dms}\text{-}d_6$ ):  $\delta$  213.56 (-C=S), 171.71 (-C-OH), 170.75 (COOH), 160.13, 135.20, 129.93, 119.12, 118.25, 111.92, 107.90 (=CH-), 55.15, 35.21, MS (ESI)  $m/z$ : 283.1 [M-H] $^-$ , elemental analysis: calculated for  $\text{C}_{12}\text{H}_{12}\text{O}_4\text{S}_2$ : C 50.69, H 4.25, S 22.55; found: C 50.44, H 4.28, S 22.54.

### 2-((3-hydroxy-3-(4-methoxyphenyl)prop-2-enethioyl)thio)acetic acid (HL6)



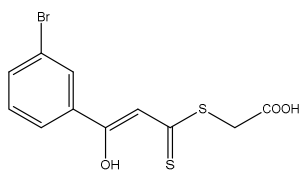
Yield: 1.78 g (31.30 %) as yellow crystals.  $^1\text{H}$  NMR (400 MHz, acetone- $d_6$ ):  $\delta$  15.17 (s, 1H, -C-OH), 11.40 (s, 1H, -COOH), 8.02 (d,  $^3J_{H-H}$  = 8.90 Hz, 2H), 7.21 (s, 1H, =CH-), 7.08 (d,  $^3J_{H-H}$  = 8.90 Hz, 2H), 4.21 (s, 2H), 3.90 (s, 3H),  $^{13}\text{C}\{^1\text{H}\}$  NMR (101 MHz, acetone- $d_6$ ):  $\delta$  213.50 (-C=S), 170.84 (-C-OH), 168.05 (COOH), 163.60, 129.04, 125.40, 114.41, 106.64 (=CH-), 55.15, 35.21, MS (ESI)  $m/z$  = 283.1 [M-H] $^-$ , elemental analysis: calculated for  $\text{C}_{12}\text{H}_{12}\text{O}_4\text{S}_2$ : C 50.69, H 4.25, S 22.55; found: C 51.05, H 4.20, S 22.43%.

### 2-((3-(2-bromophenyl)-3-hydroxyprop-2-enethioyl)thio)acetic acid (HL7)



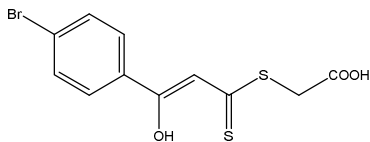
Yield: 1.54 g (23.11 %) as yellow crystals.  $^1\text{H}$  NMR (400 MHz,  $\text{dms}\text{-}d_6$ ):  $\delta$  14.49 (s, 1H, -C-OH), 13.04 (s, 1H, -COOH), 7.75 (d,  $^3J_{H-H}$  = 7.84 Hz, H), 7.39-7.62 (m, 3H), 6.66 (s, 1H, =CH-), 4.14 (s, 2H),  $^{13}\text{C}\{^1\text{H}\}$  NMR (101 MHz,  $\text{dms}\text{-}d_6$ ):  $\delta$  216.32 (-C=S), 170.89 (-C-OH), 169.21 (COOH), 133.93, 132.57, 130.83, 128.46, 120.68, 113.33, 109.59 (=CH-), 36.87, MS (ESI)  $m/z$  = 331 [M-H] $^-$ , elemental analysis: calculated for  $\text{C}_{12}\text{H}_9\text{O}_3\text{S}_2\text{Br}$ : C 39.65, H 2.72, S 19.24, Br 23.98; found: C 39.22, H 2.53, S 19.19, Br 24.15.

## 2-((3-(3-bromophenyl)-3-hydroxyprop-2-enethioyl)thio)acetic acid (HL8)



Yield: 2.30 g (34.51 %) as yellow crystals.  $^1\text{H}$  NMR (400 MHz,  $\text{dms}\text{-d}_6$ ):  $\delta$  14.92 (s, 1H, -C-OH), 13.04 (s, 1H, -COOH), 8.20 (s, 1H), 8.02 (d,  $^3J_{\text{H-H}}=8.04$  Hz, H), 7.80 (dd,  $^3J_{\text{H-H}}=7.84$  Hz,  $^4J_{\text{H-H}}=1.2$  Hz, H), 7.49 (t,  $^3J_{\text{H-H}}=8$  Hz, H), 7.40 (s, 1H, =CH-), 4.18 (s, 2H),  $^{13}\text{C}\{^1\text{H}\}$  NMR (101 MHz,  $\text{dms}\text{-d}_6$ ):  $\delta$  216.58 (-C=S), 169.02 (-C-OH), 167.70 (COOH), 136.04, 135.59, 131.61, 129.70, 126.34, 122.87, 108.49 (=CH-), 36.59, MS (ESI)  $m/z$ : 331 [M-H] $^-$ , elemental analysis: calculated for  $\text{C}_{12}\text{H}_9\text{O}_3\text{S}_2\text{Br}$ : C 39.65, H 2.72, S 19.24, Br 23.98; found: C 40.06, H 2.56, S: 19.47, Br 24.07.

## 2-((3-(4-bromophenyl)-3-hydroxyprop-2-enethioyl)thio)acetic acid (HL9)



Yield: 3.30 g (49.51 %) as yellow crystals.  $^1\text{H}$  NMR (400 MHz,  $\text{dms}\text{-d}_6$ ): 14.95 (s, 1H, -C-OH), 13.06 (s, 1H, -COOH), 7.96 (d,  $^3J_{\text{H-H}}=8.76$  Hz, H), 7.73 (d,  $^3J_{\text{H-H}}=8.60$  Hz, H), 7.35 (s, 1H, =CH-), 4.17 (s, 2H),  $^{13}\text{C}\{^1\text{H}\}$  NMR (101 MHz,  $\text{dms}\text{-d}_6$ ):  $\delta$  216.05 (-C=S), 169.04 (-C-OH), 168.54 (COOH), 132.80, 132.55, 129.28, 126.90, 108.11 (=CH-), 36.50, MS (ESI)  $m/z$ : 331 [M-H] $^-$ , elemental analysis: calculated for  $\text{C}_{12}\text{H}_9\text{O}_3\text{S}_2\text{Br}$ : C 39.65, H 2.72, S 19.24, Br 23.98; found: C 39.37, H 2.57, S 19.58, Br 23.83.

$^1\text{H}$ ,  $^{13}\text{C}\{^1\text{H}\}$  and  $^{195}\text{Pt}$  NMR spectra of  $[\text{Pt}(\text{L1-L9})_2]$ ,  $[\text{Pt}(\text{L1-L9})(\text{DMS})\text{Cl}]$  and  $[\text{Pt}(\text{L1-L9})(\text{DMSO})\text{Cl}]$  complexes.

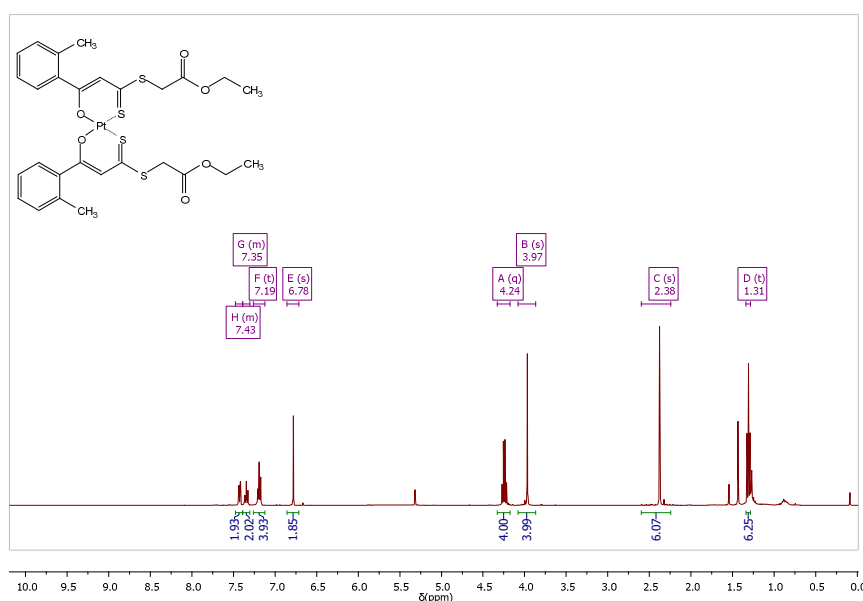


Figure S7.  $^1\text{H}$ -NMR (400 MHz,  $\text{CD}_2\text{Cl}_2$ ):  $[\text{Pt}(\text{L1})_2]$

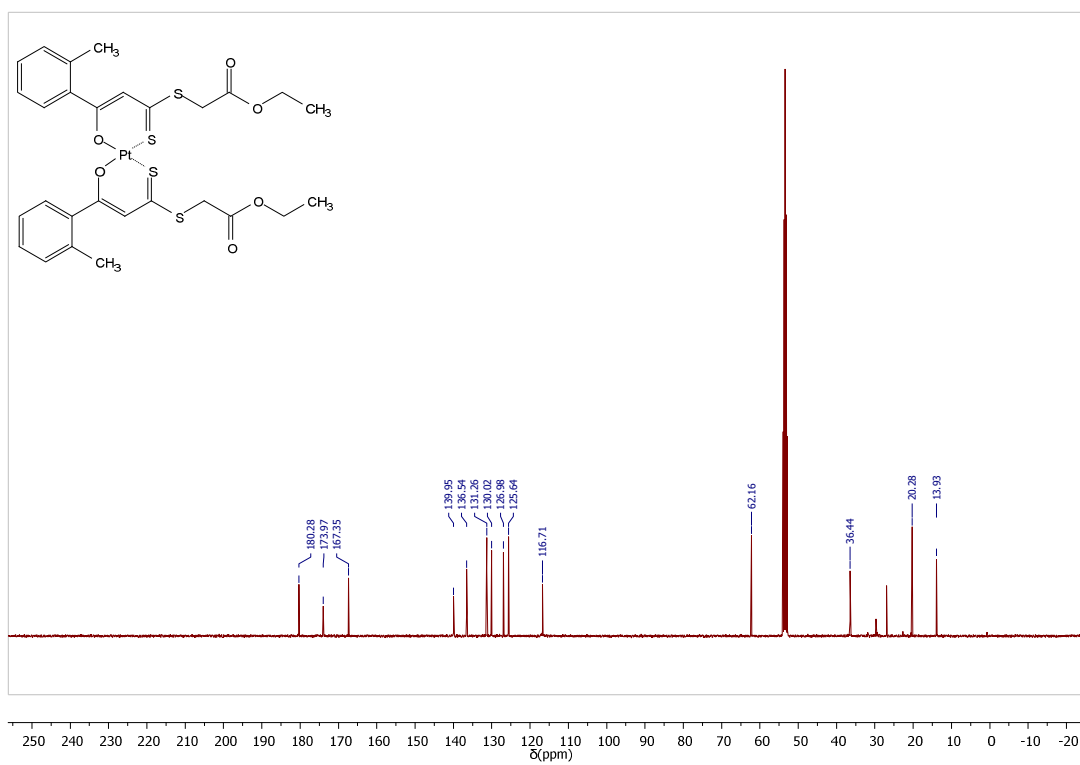


Figure S8. <sup>13</sup>C{<sup>1</sup>H} NMR (101 MHz, CD<sub>2</sub>Cl<sub>2</sub>): [Pt(L1)<sub>2</sub>]

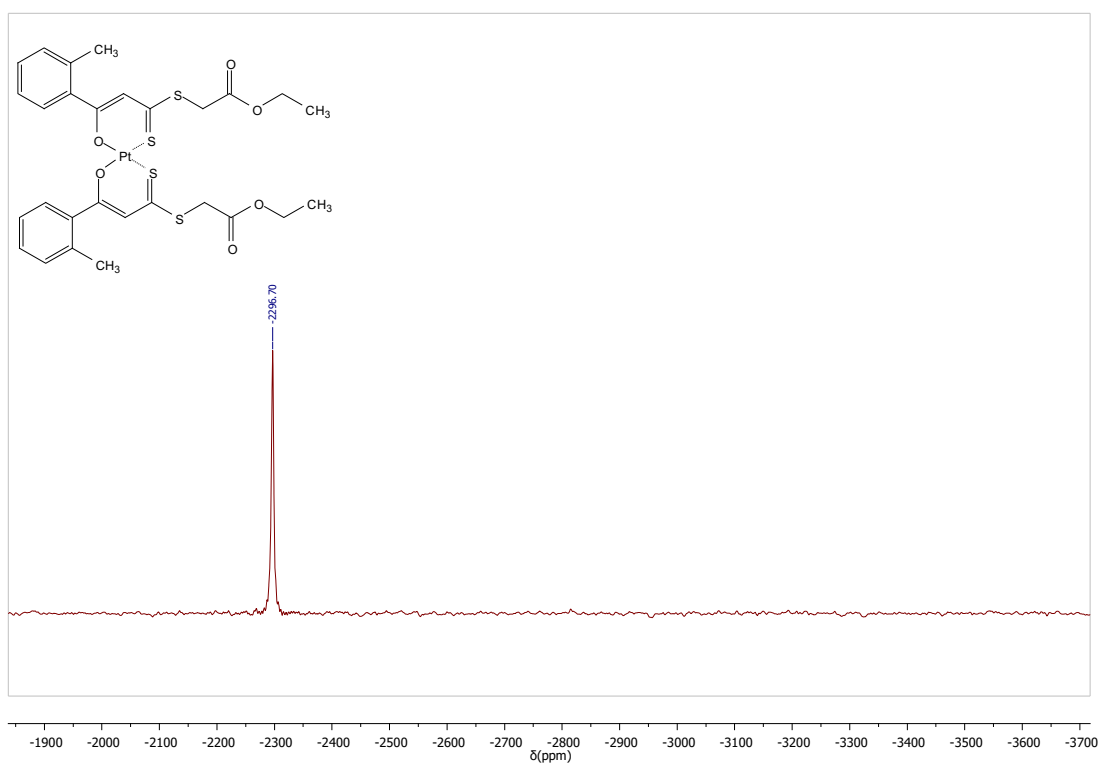


Figure S9. <sup>195</sup>Pt NMR (85.7 MHz, CD<sub>2</sub>Cl<sub>2</sub>): [Pt(L1)<sub>2</sub>]

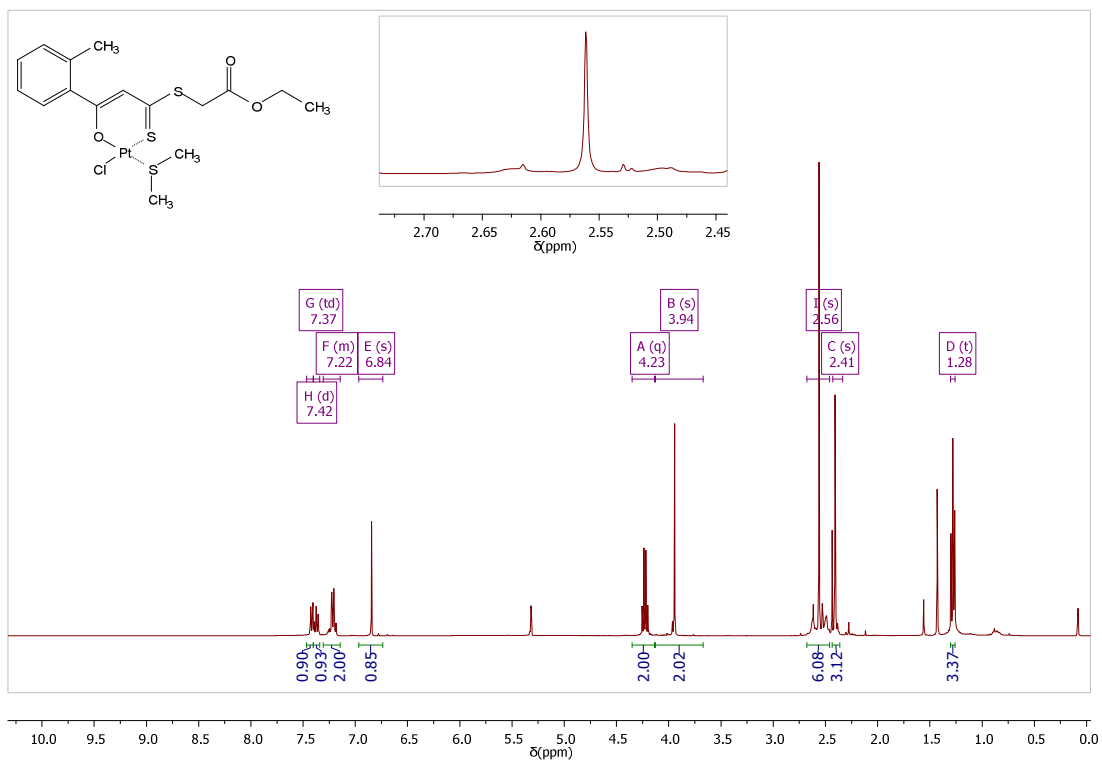


Figure S10. <sup>1</sup>H-NMR (400 MHz, CD<sub>2</sub>Cl<sub>2</sub>): [Pt(L1)(DMS)Cl]

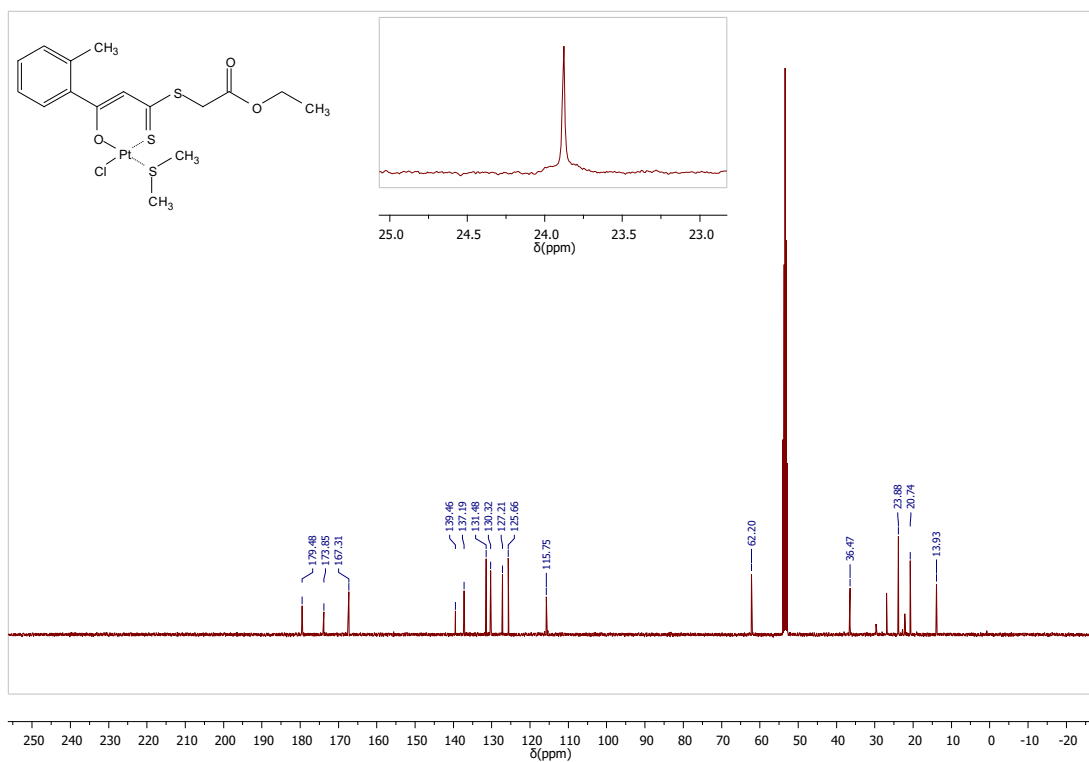


Figure S11. <sup>13</sup>C{<sup>1</sup>H} NMR (101 MHz, CD<sub>2</sub>Cl<sub>2</sub>): [Pt(L1)(DMS)Cl]



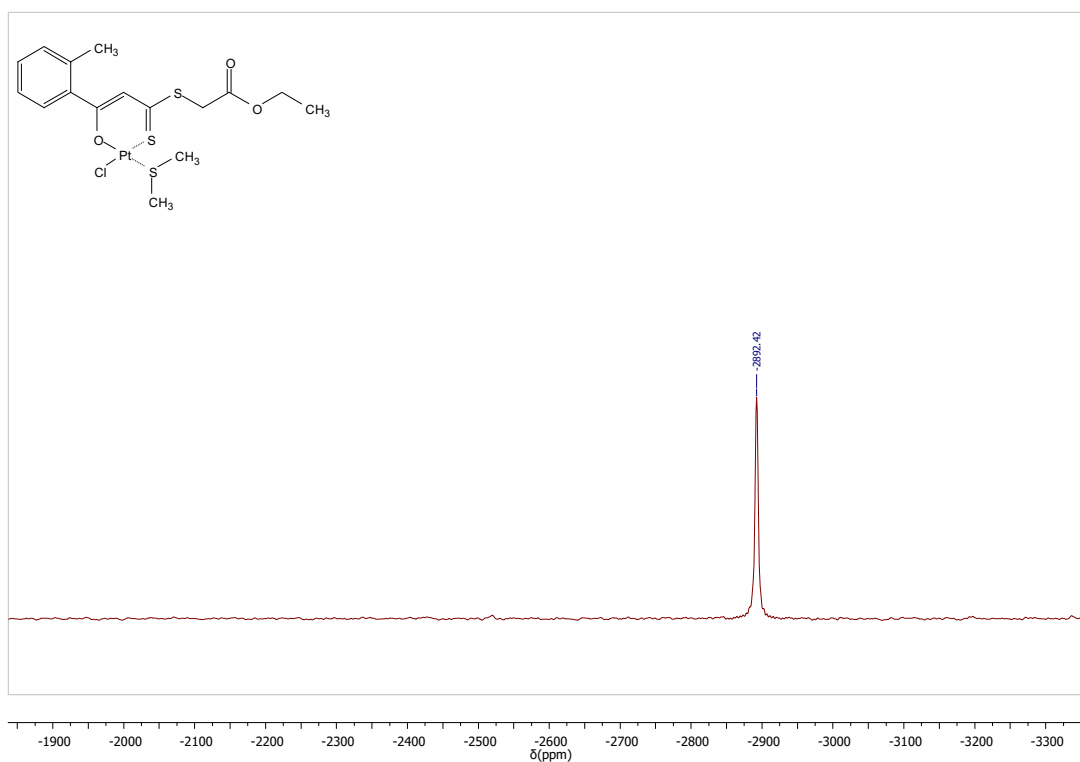


Figure S12.  $^{195}\text{Pt}$  NMR (85.7 MHz,  $\text{CD}_2\text{Cl}_2$ ):  $[\text{Pt}(\text{L1})(\text{DMS})\text{Cl}]$

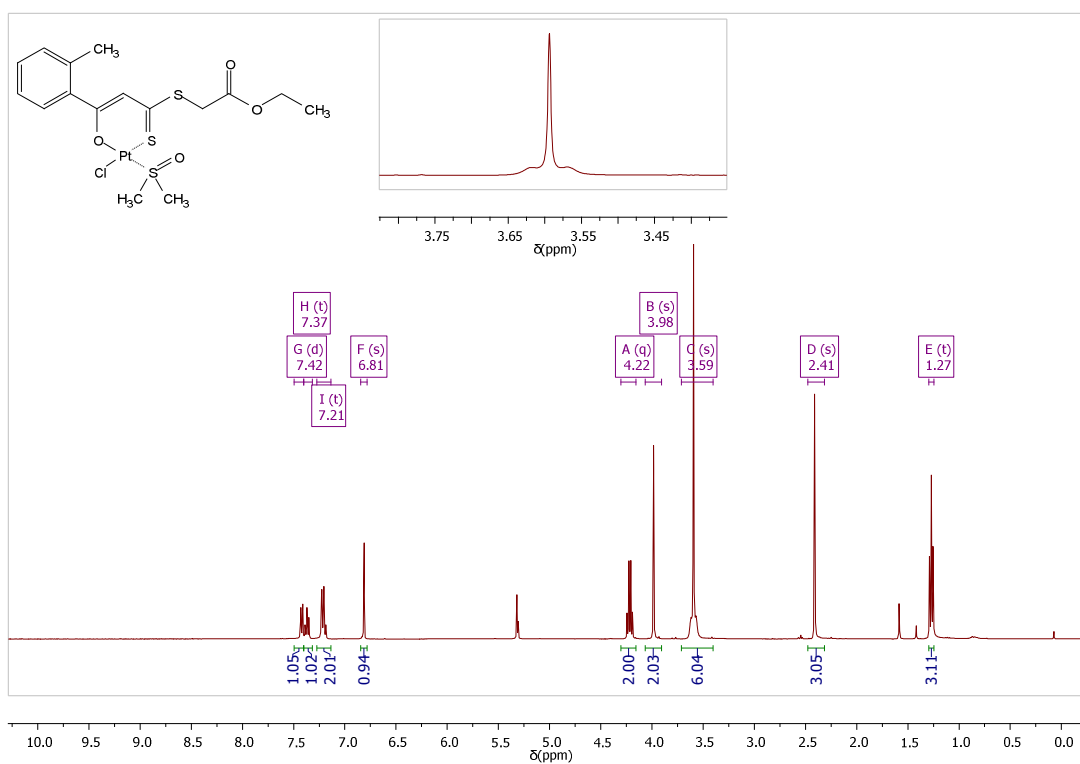


Figure S13.  $^1\text{H}$ -NMR (400 MHz,  $\text{CD}_2\text{Cl}_2$ ):  $[\text{Pt}(\text{L1})(\text{DMSO})\text{Cl}]$

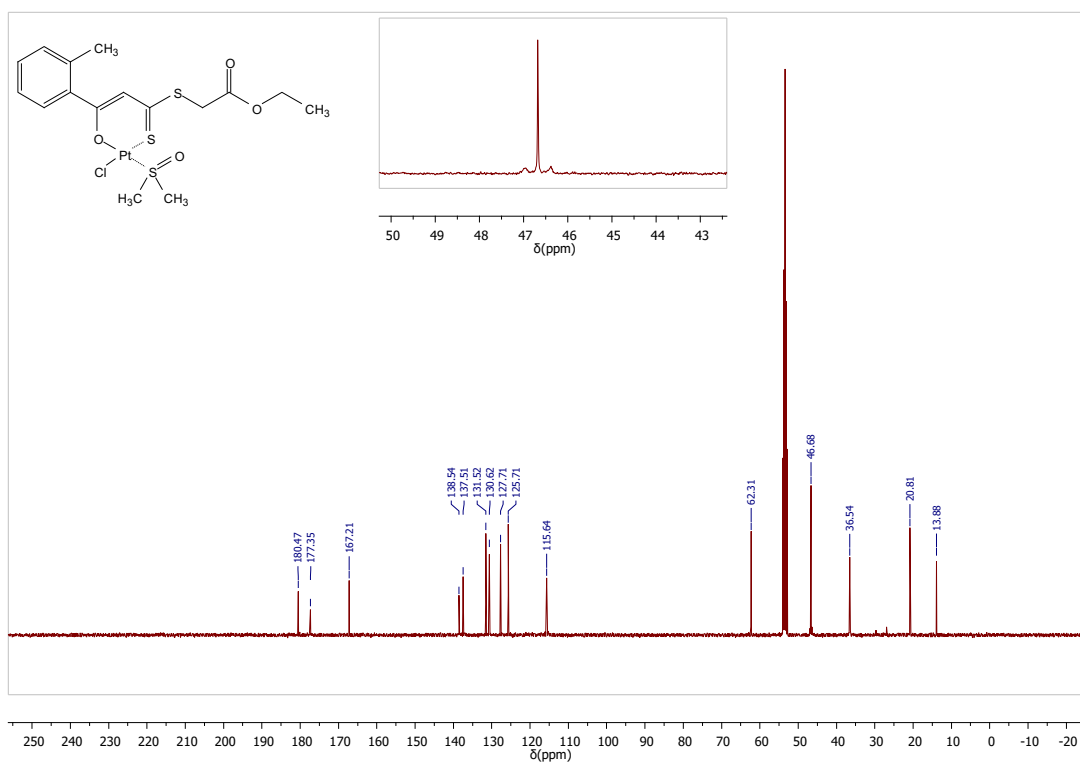


Figure S14.  $^{13}\text{C}\{^1\text{H}\}$  NMR (101 MHz,  $\text{CD}_2\text{Cl}_2$ ): [Pt(L1)(DMSO)Cl]

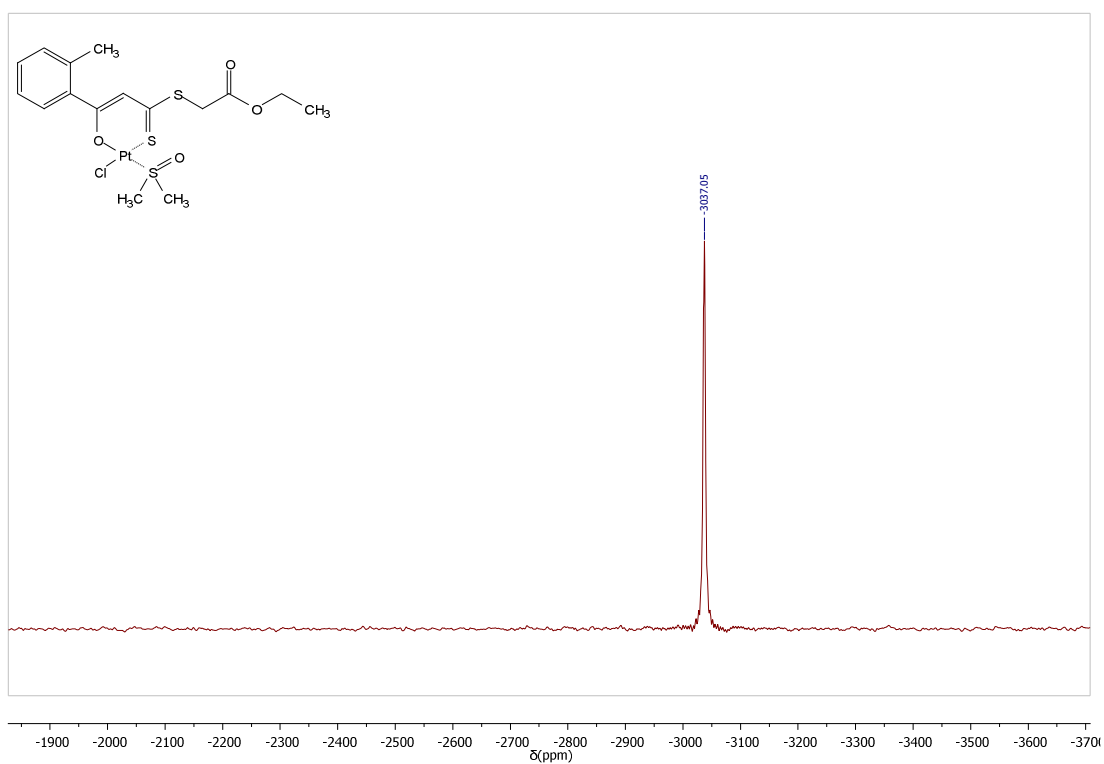


Figure S15.  $^{195}\text{Pt}$  NMR (85.7 MHz,  $\text{CD}_2\text{Cl}_2$ ): [Pt(L1)(DMSO)Cl]

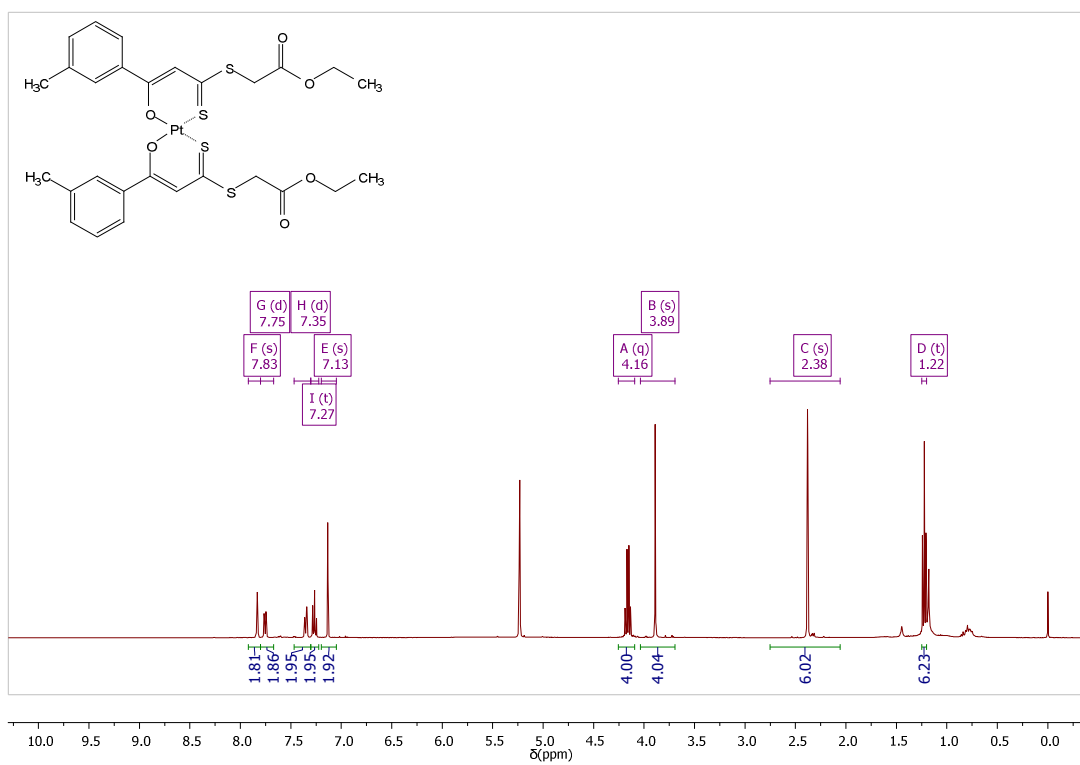


Figure S16.  $^1\text{H-NMR}$  (400 MHz,  $\text{CD}_2\text{Cl}_2$ ):  $[\text{Pt}(\text{L}2)_2]$

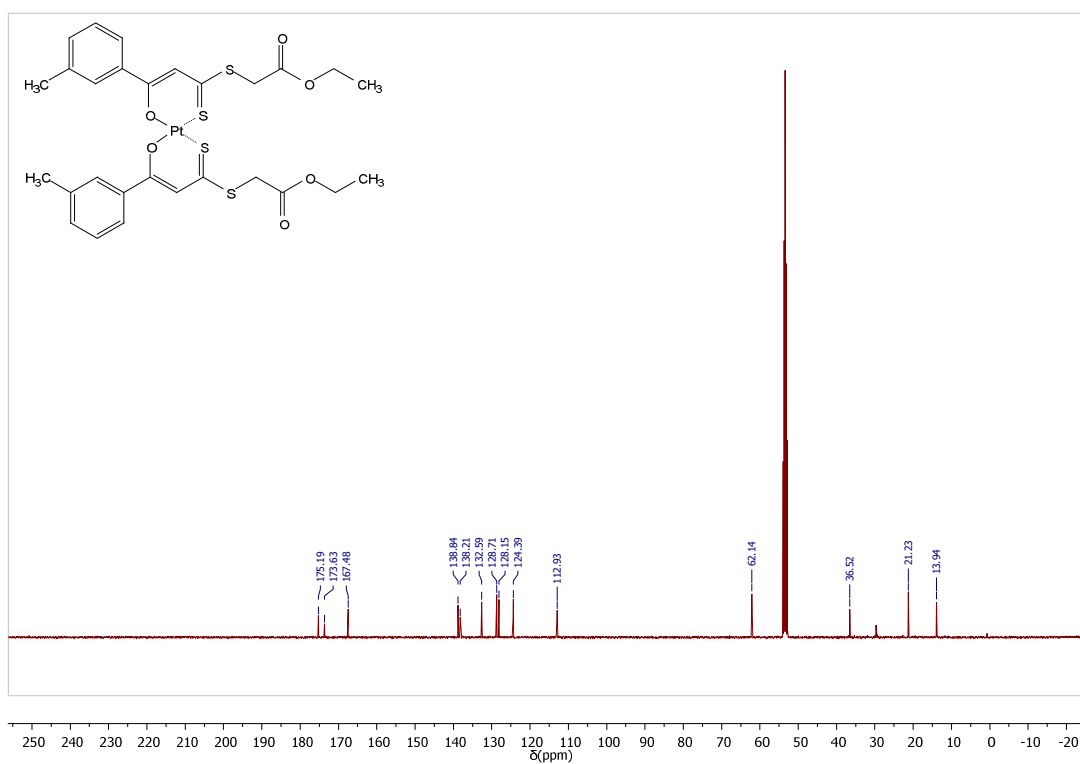


Figure S17.  $^{13}\text{C}\{^1\text{H}\}$  NMR (101 MHz,  $\text{CD}_2\text{Cl}_2$ ):  $[\text{Pt}(\text{L}2)_2]$

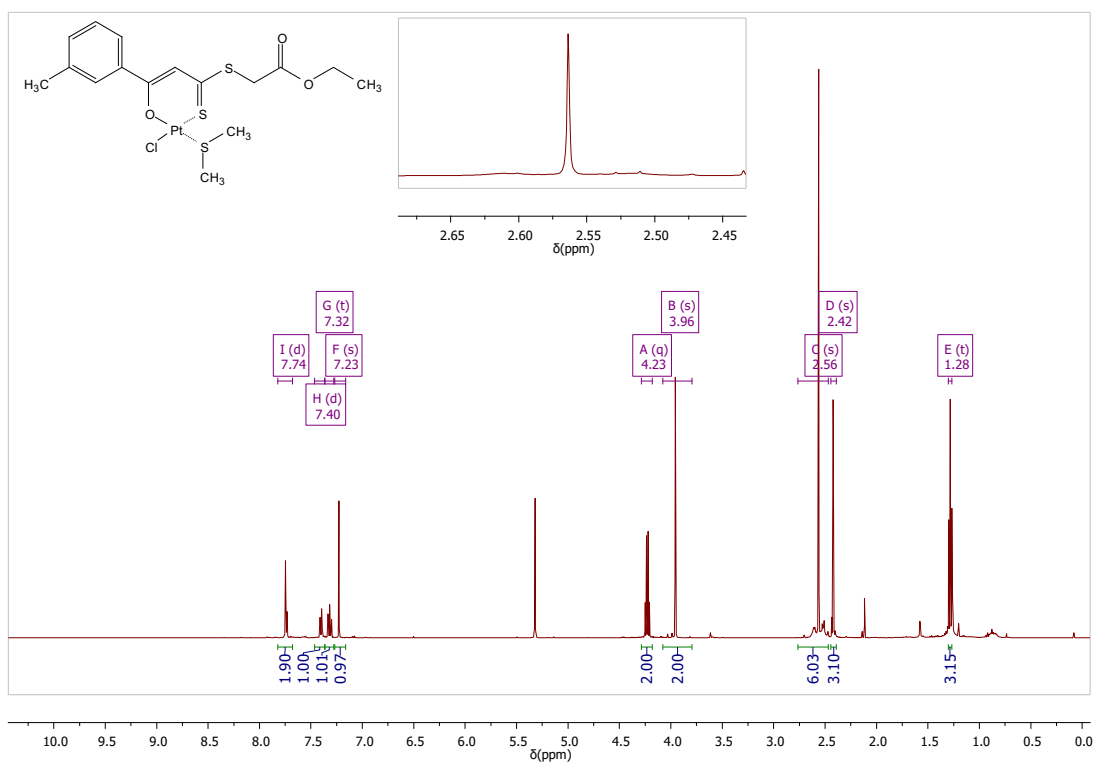


Figure S18.  $^1\text{H-NMR}$  (500 MHz,  $\text{CD}_2\text{Cl}_2$ ): [Pt(L2)(DMS)Cl]

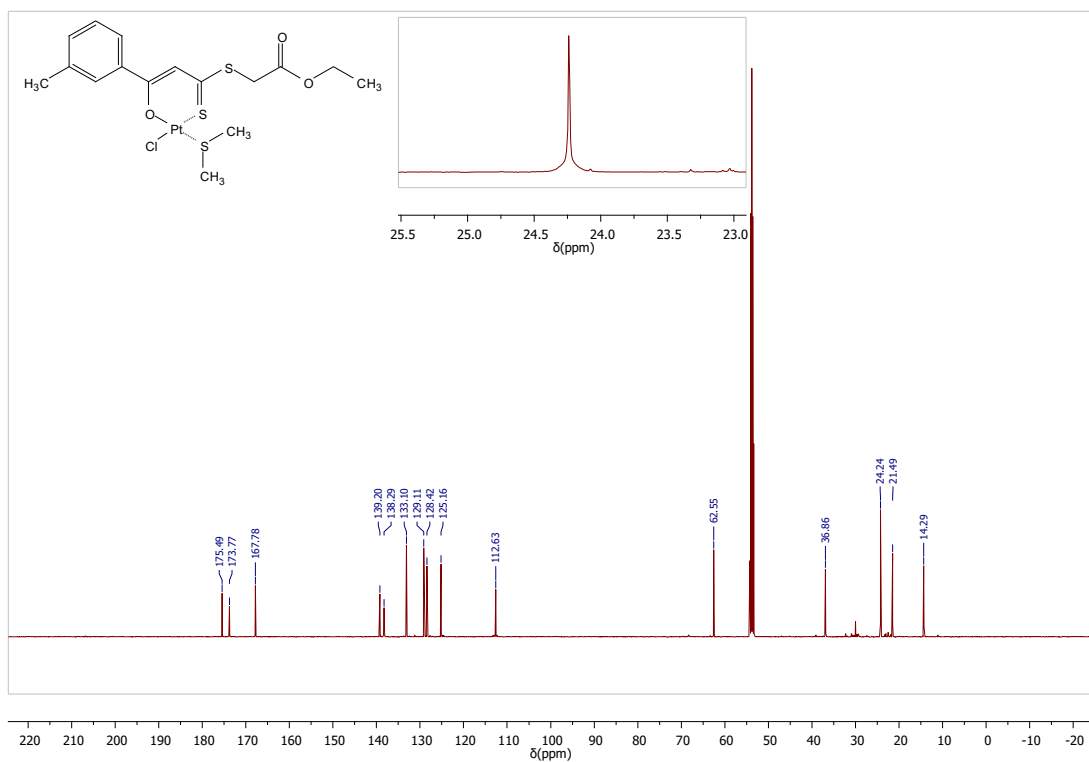


Figure S19.  $^{13}\text{C}\{^1\text{H}\}$  NMR (126 MHz,  $\text{CD}_2\text{Cl}_2$ ): [Pt(L2)(DMS)Cl]

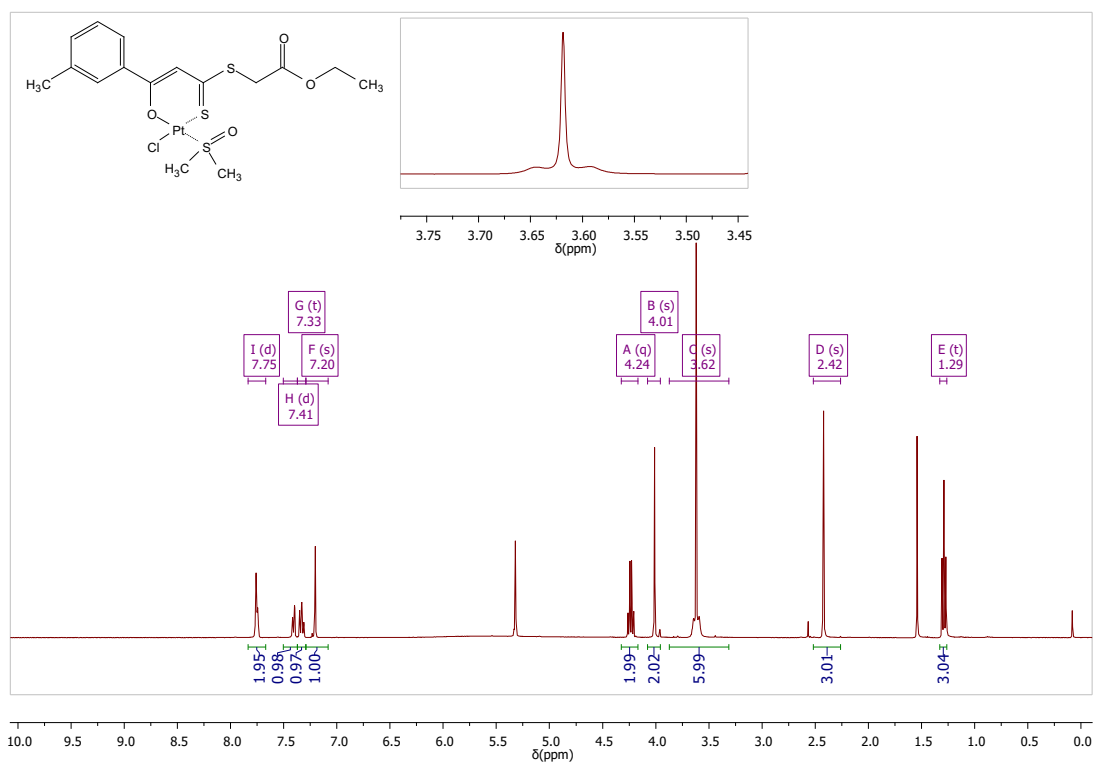


Figure S20. <sup>1</sup>H-NMR (500 MHz, CD<sub>2</sub>Cl<sub>2</sub>): [Pt(L2)(DMSO)Cl]

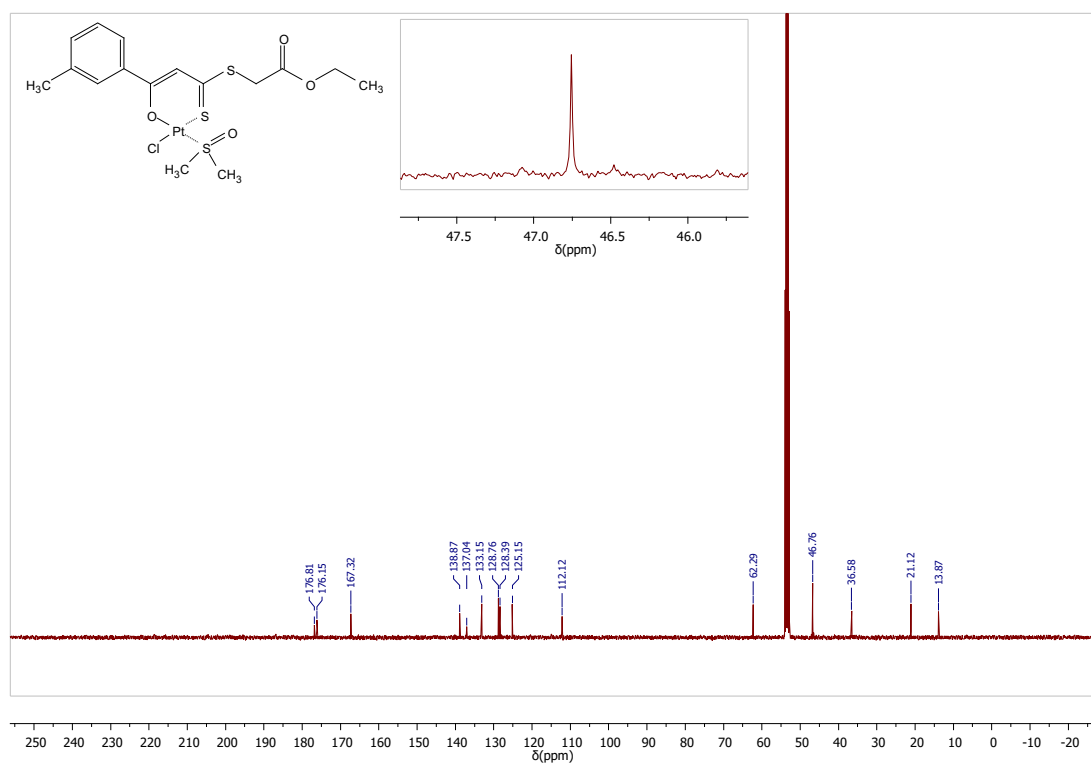


Figure S21. <sup>13</sup>C{<sup>1</sup>H} NMR (126 MHz, CD<sub>2</sub>Cl<sub>2</sub>): [Pt(L2)(DMSO)Cl]

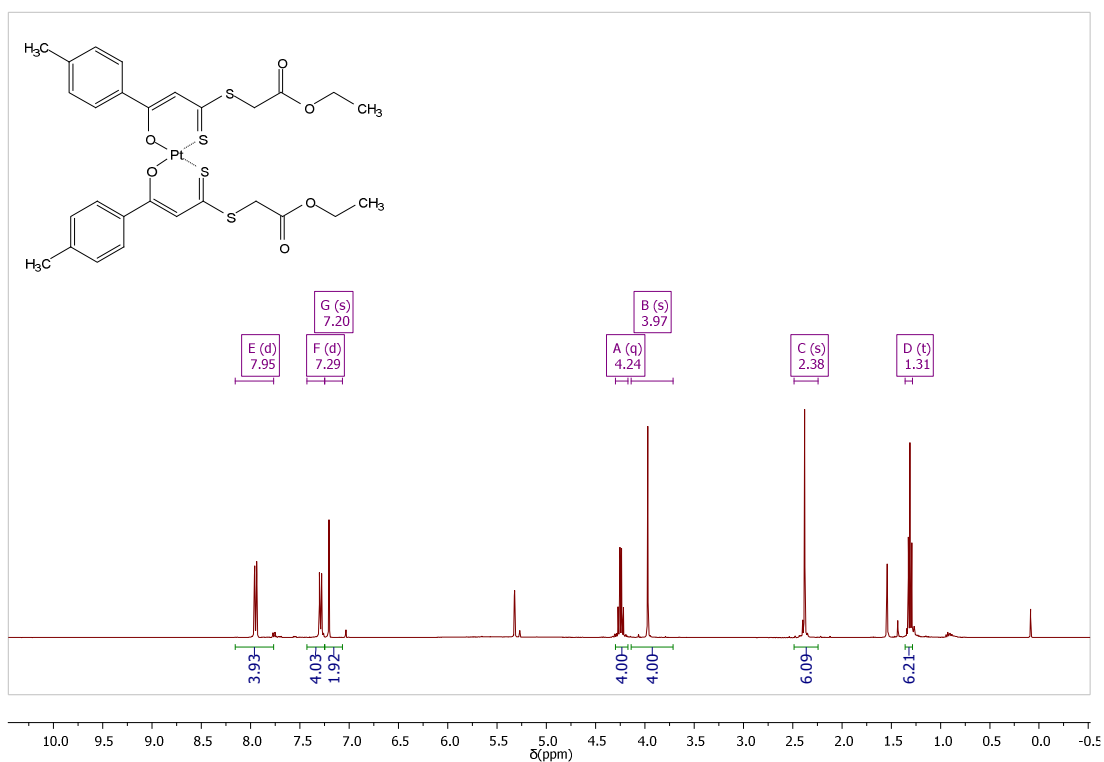


Figure S22.  $^1\text{H-NMR}$  (400 MHz,  $\text{CD}_2\text{Cl}_2$ ):  $[\text{Pt}(\text{L3})_2]$

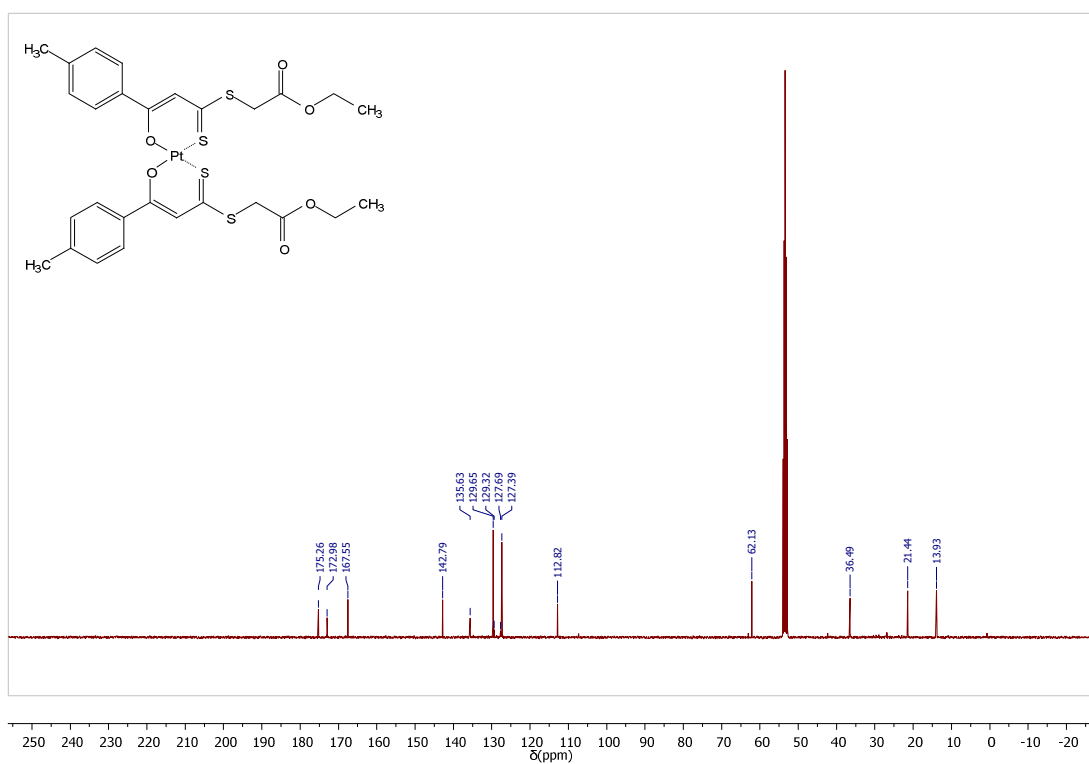


Figure S23.  $^{13}\text{C}\{^1\text{H}\}$  NMR (101 MHz,  $\text{CD}_2\text{Cl}_2$ ):  $[\text{Pt}(\text{L3})_2]$

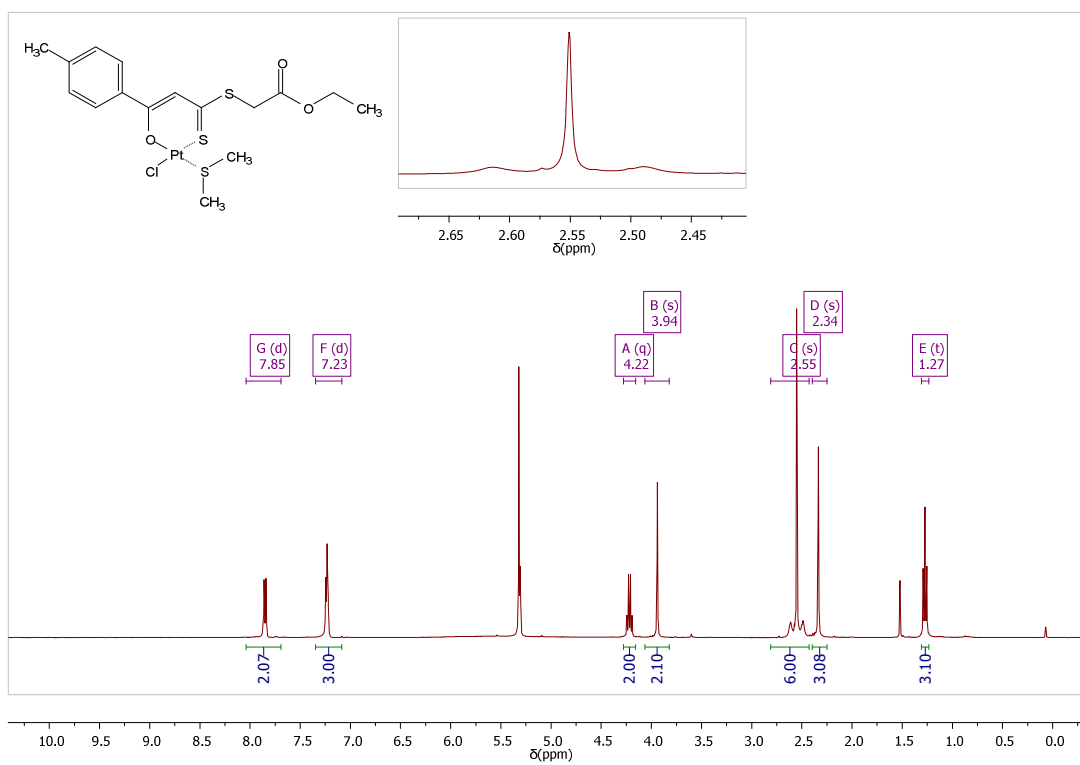


Figure S24. <sup>1</sup>H-NMR (400 MHz, CD<sub>2</sub>Cl<sub>2</sub>): [Pt(L3)(DMS)Cl]

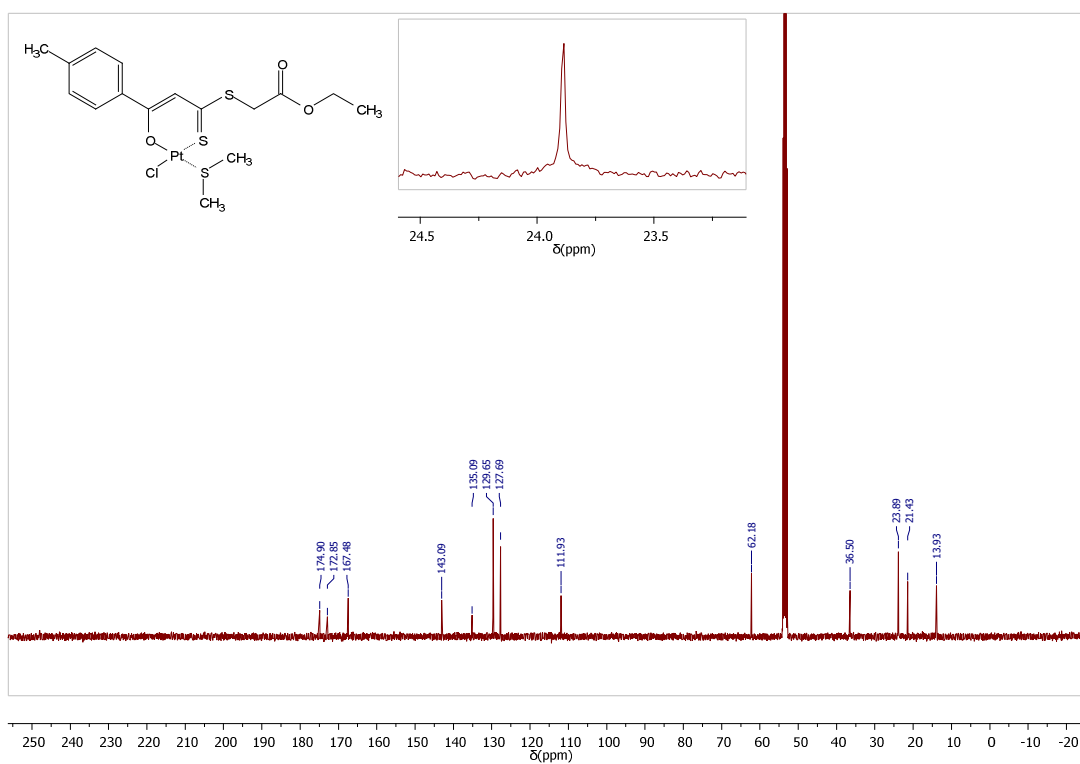


Figure S25. <sup>13</sup>C{<sup>1</sup>H} NMR (101 MHz, CD<sub>2</sub>Cl<sub>2</sub>): [Pt(L3)(DMS)Cl]

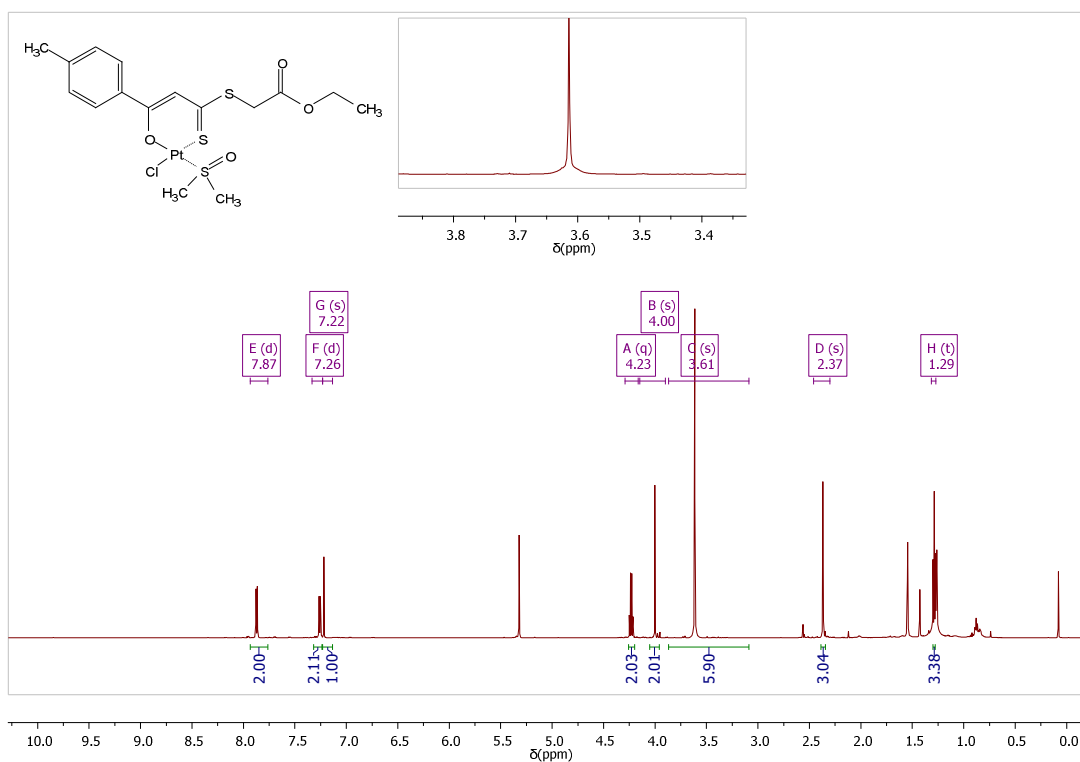


Figure S26.  $^1H$ -NMR (600 MHz,  $CD_2Cl_2$ ):  $[Pt(L3)(DMSO)Cl]$

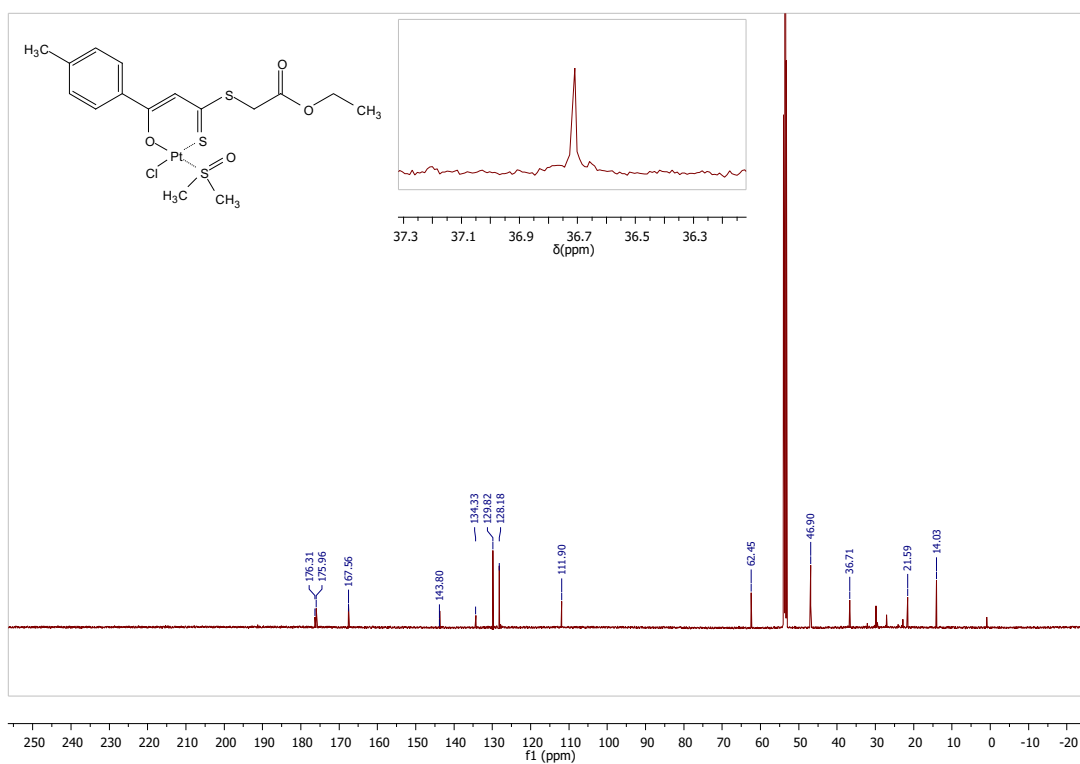


Figure S27.  $^{13}C$   $\{^1H\}$  NMR (151 MHz,  $CD_2Cl_2$ ):  $[Pt(L3)(DMSO)Cl]$



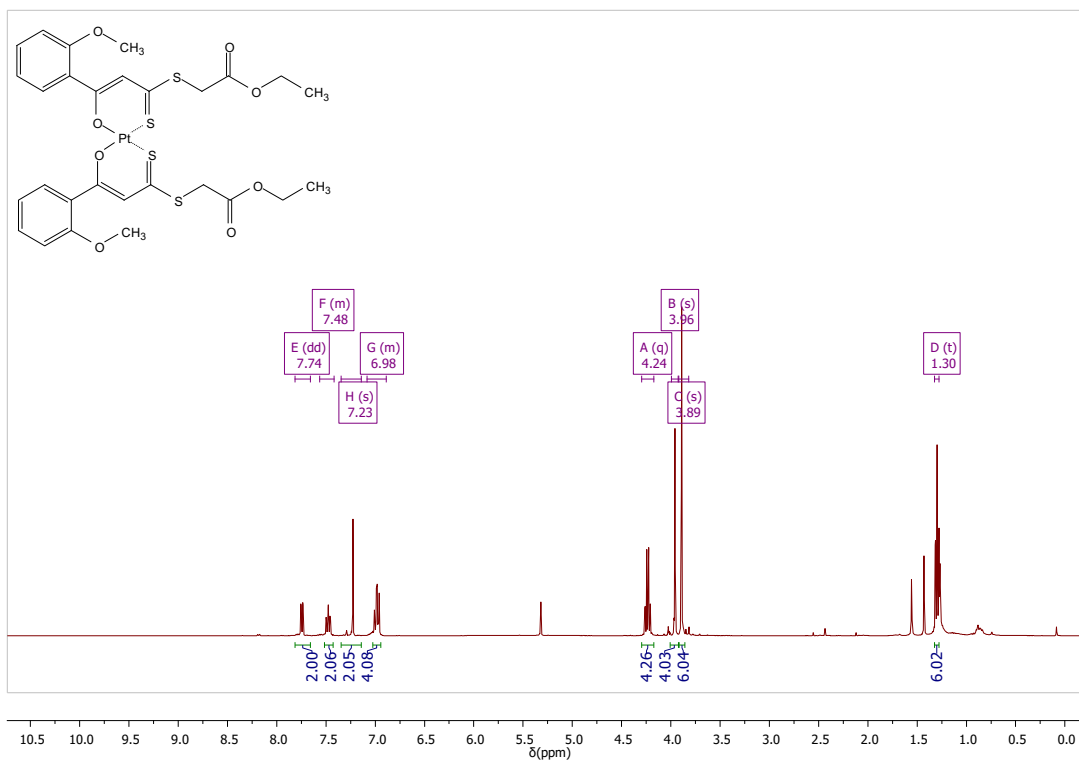


Figure S28.  $^1\text{H-NMR}$  (400 MHz,  $\text{CD}_2\text{Cl}_2$ ):  $[\text{Pt}(\text{L4})_2]$

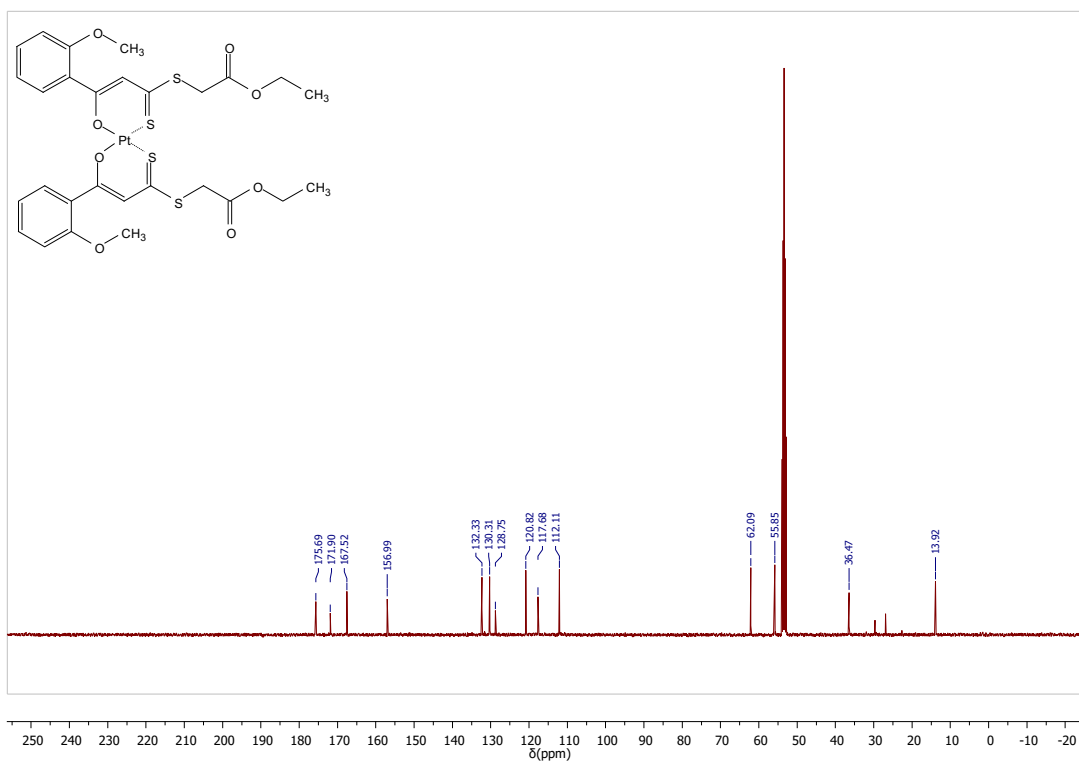


Figure S29.  $^{13}\text{C}\{^1\text{H}\}$  NMR (101 MHz,  $\text{CD}_2\text{Cl}_2$ ):  $[\text{Pt}(\text{L4})_2]$

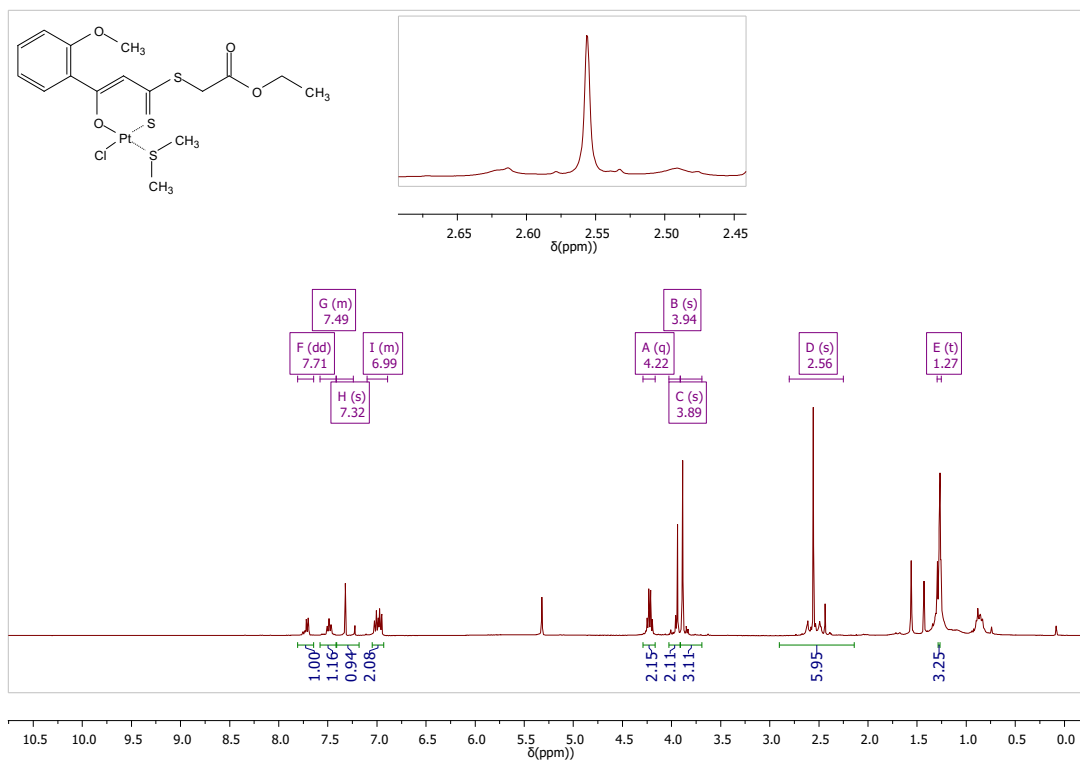


Figure S30.  $^1\text{H-NMR}$  (400 MHz,  $\text{CD}_2\text{Cl}_2$ ):  $[\text{Pt}(\text{L4})(\text{DMS})\text{Cl}]$

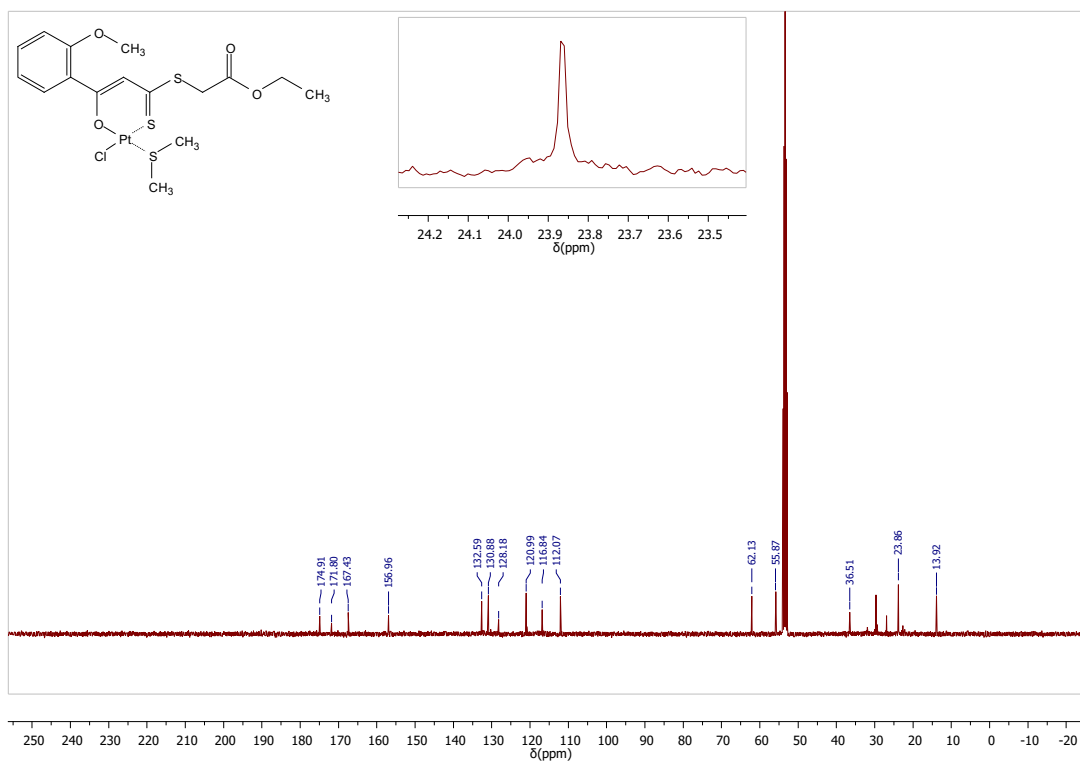


Figure S31.  $^{13}\text{C}\{^1\text{H}\}$  NMR (101 MHz,  $\text{CD}_2\text{Cl}_2$ ):  $[\text{Pt}(\text{L4})(\text{DMS})\text{Cl}]$

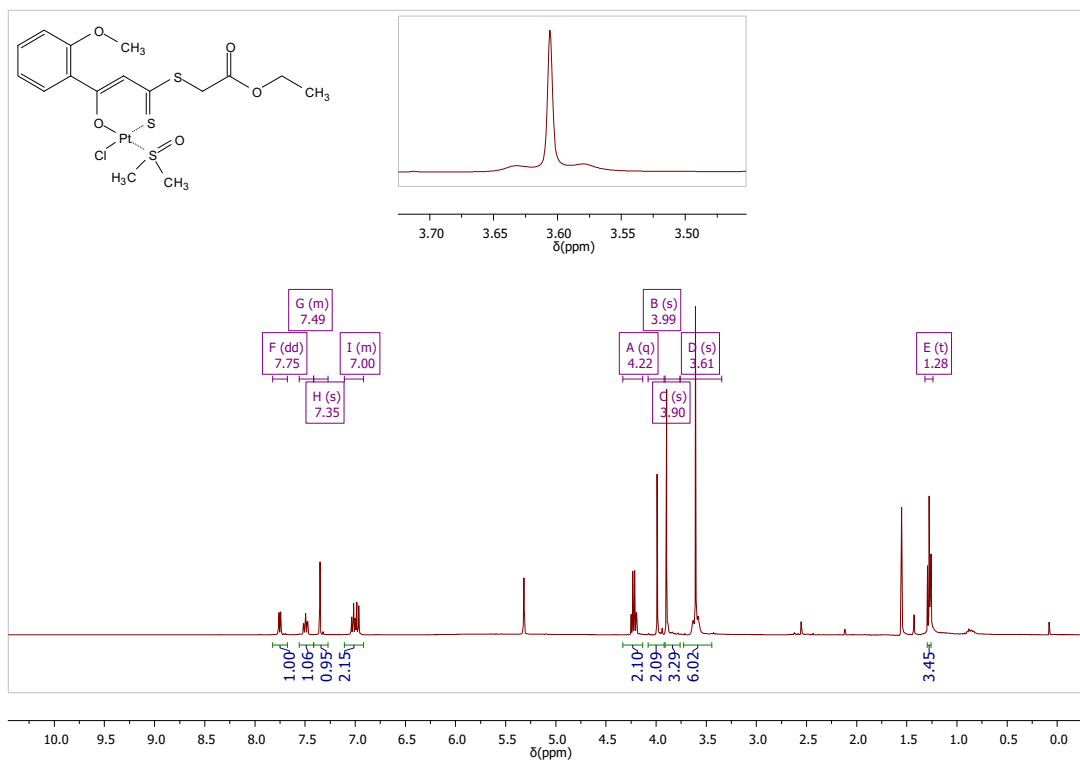


Figure S32.  $^1\text{H-NMR}$  (400 MHz,  $\text{CD}_2\text{Cl}_2$ ):  $[\text{Pt}(\text{L4})(\text{DMSO})\text{Cl}]$

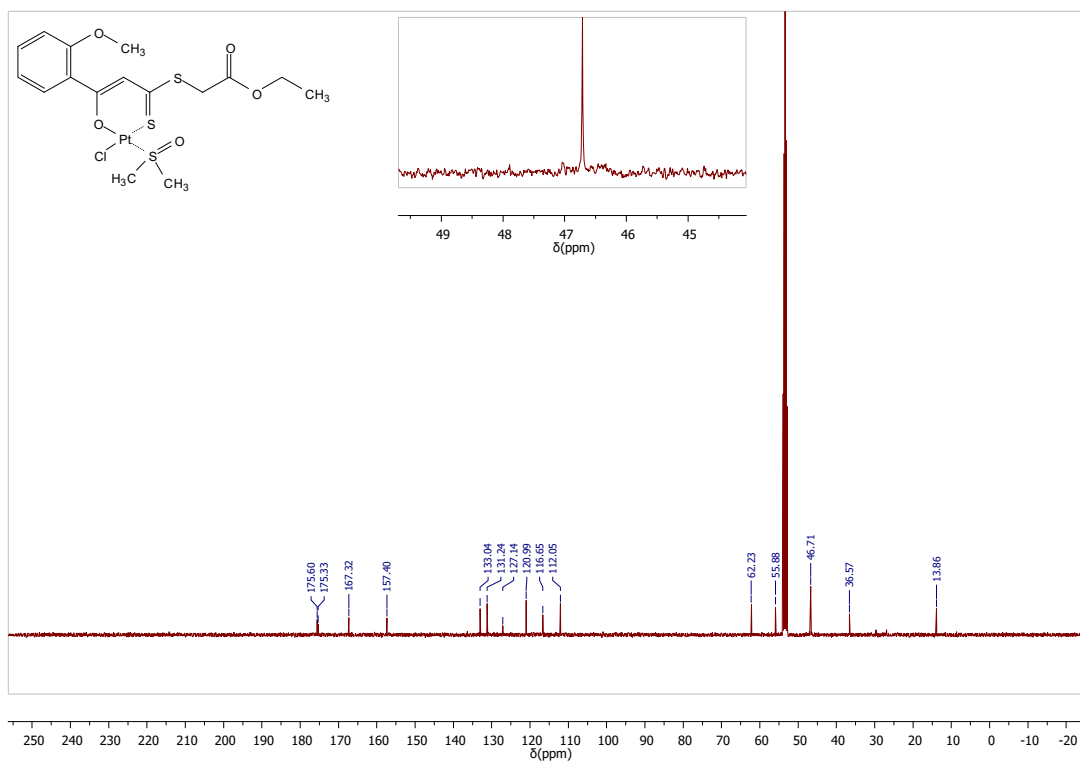


Figure S33.  $^{13}\text{C}\{^1\text{H}\}$  NMR (101 MHz,  $\text{CD}_2\text{Cl}_2$ ):  $[\text{Pt}(\text{L4})(\text{DMSO})\text{Cl}]$

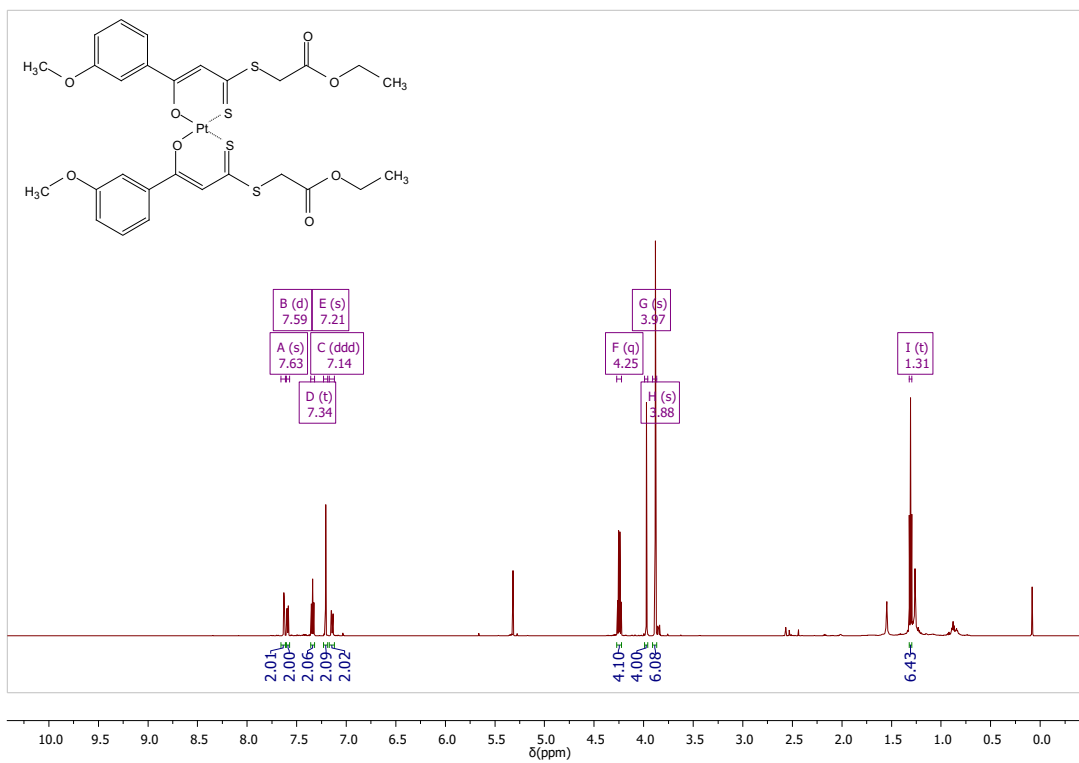


Figure S34. <sup>1</sup>H-NMR (600 MHz, CD<sub>2</sub>Cl<sub>2</sub>): [Pt(L5)<sub>2</sub>]

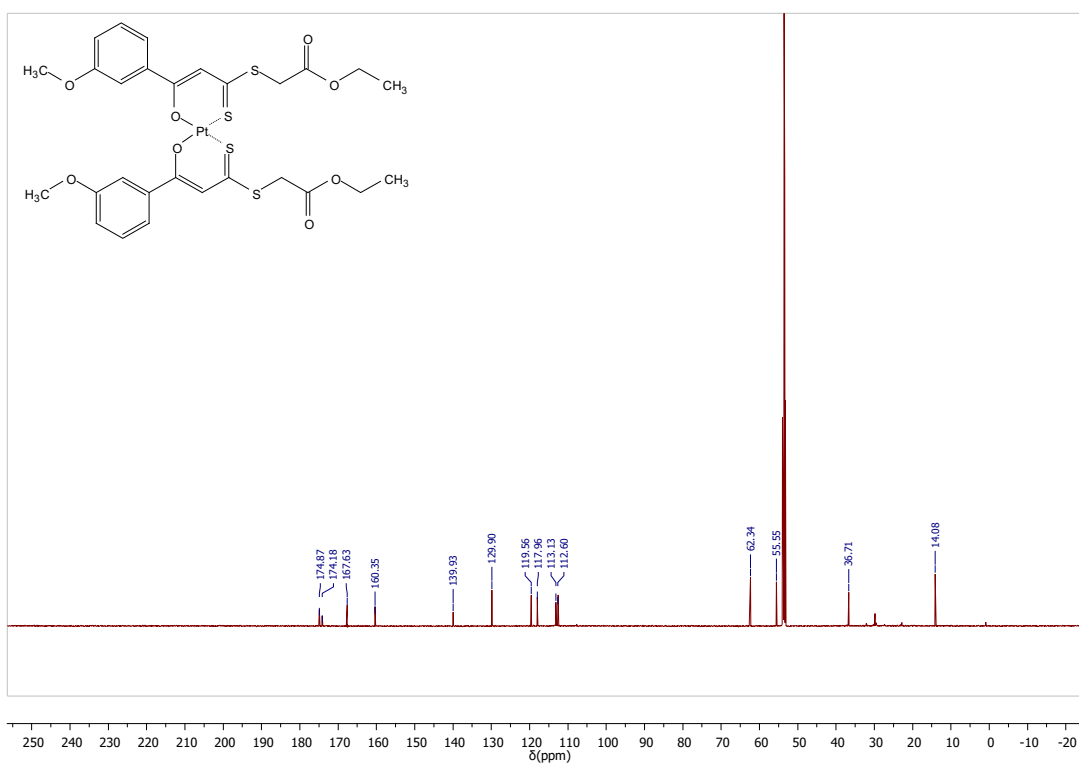


Figure S35. <sup>13</sup>C{<sup>1</sup>H} NMR (151 MHz, CD<sub>2</sub>Cl<sub>2</sub>): [Pt(L5)<sub>2</sub>]

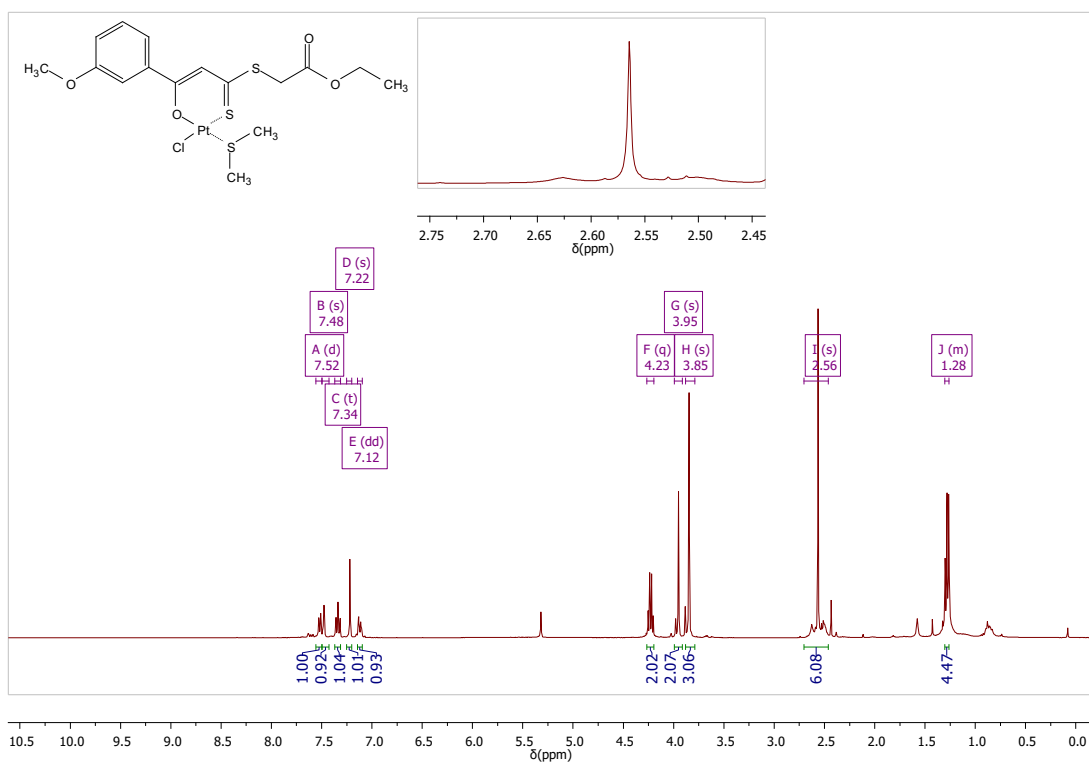


Figure S36.  $^1\text{H-NMR}$  (400 MHz,  $\text{CD}_2\text{Cl}_2$ ):  $[\text{Pt}(\text{L5})(\text{DMS})\text{Cl}]$

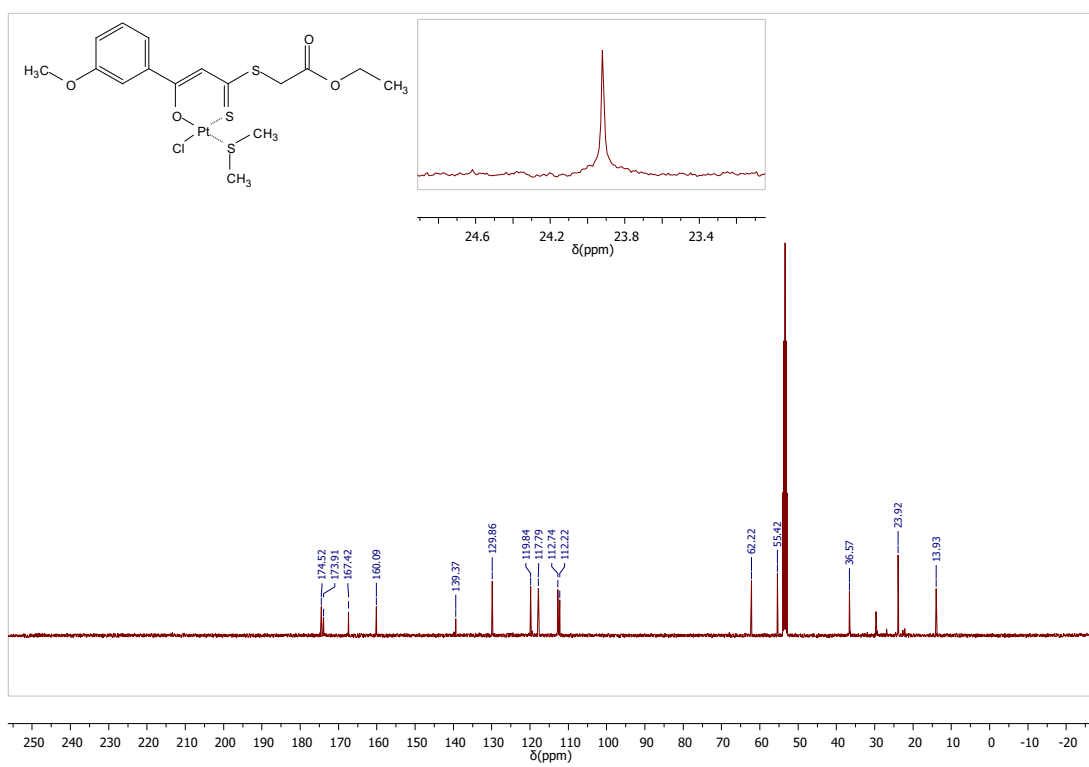


Figure S37.  $^{13}\text{C}\{^1\text{H}\}$  NMR (101 MHz,  $\text{CD}_2\text{Cl}_2$ ):  $[\text{Pt}(\text{L5})(\text{DMS})\text{Cl}]$

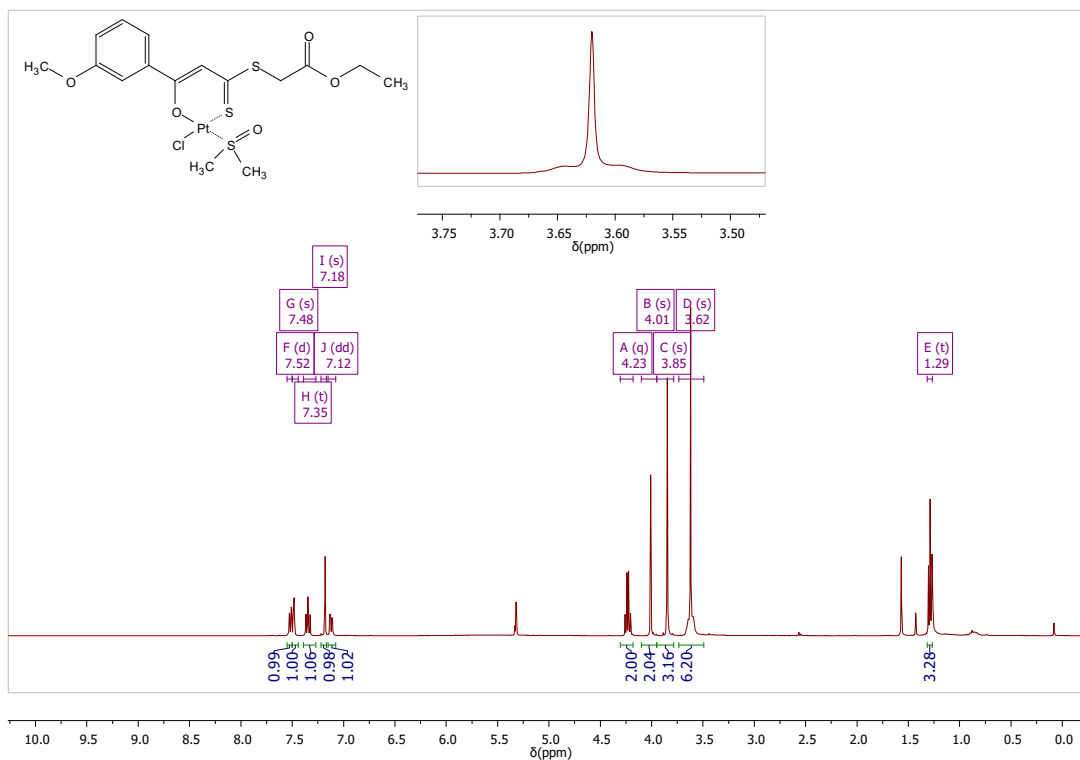


Figure S38.  $^1\text{H-NMR}$  (400 MHz,  $\text{CD}_2\text{Cl}_2$ ):  $[\text{Pt}(\text{L5})(\text{DMSO})\text{Cl}]$

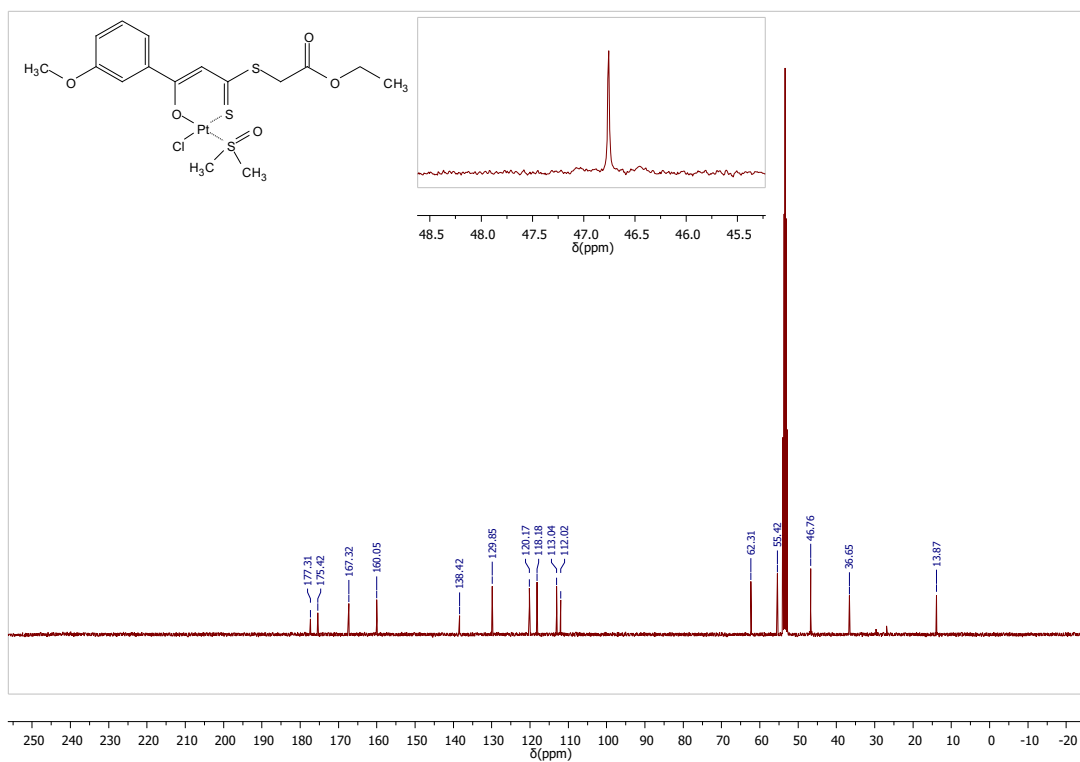


Figure S39.  $^{13}\text{C}\{^1\text{H}\}$  NMR (101 MHz,  $\text{CD}_2\text{Cl}_2$ ):  $[\text{Pt}(\text{L5})(\text{DMSO})\text{Cl}]$

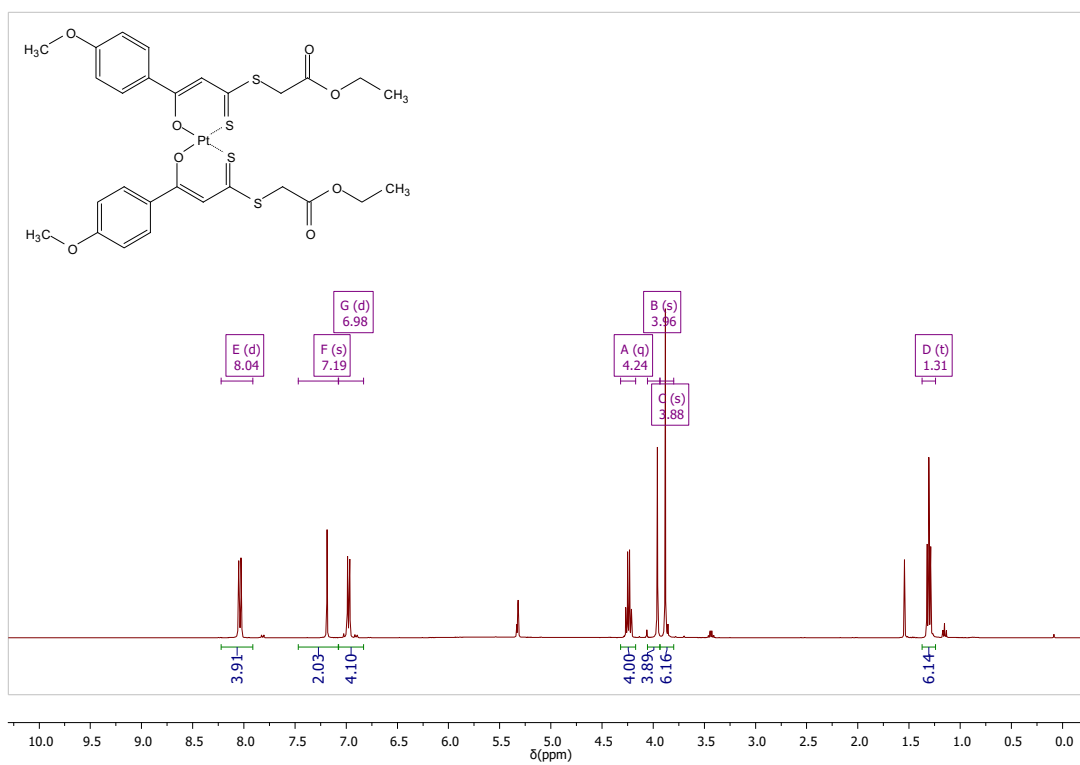


Figure S40. <sup>1</sup>H-NMR (400 MHz, CD<sub>2</sub>Cl<sub>2</sub>): [Pt(L6)<sub>2</sub>]

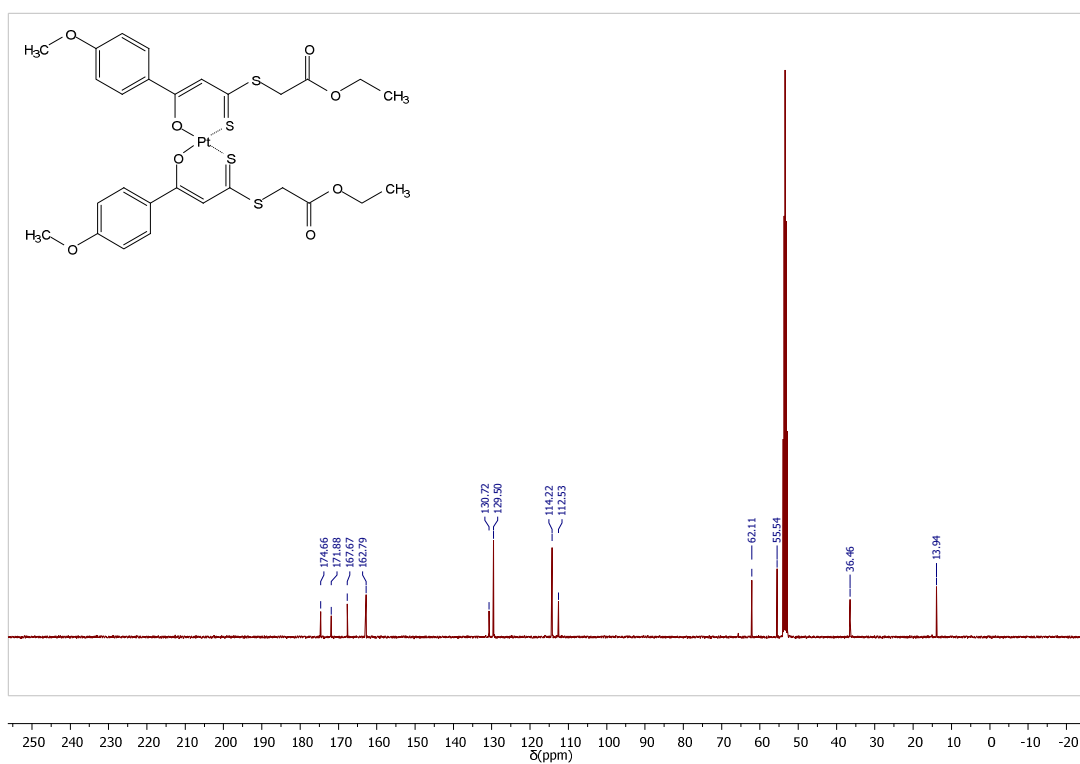


Figure S41. <sup>13</sup>C{<sup>1</sup>H} NMR (101 MHz, CD<sub>2</sub>Cl<sub>2</sub>): [Pt(L6)<sub>2</sub>]

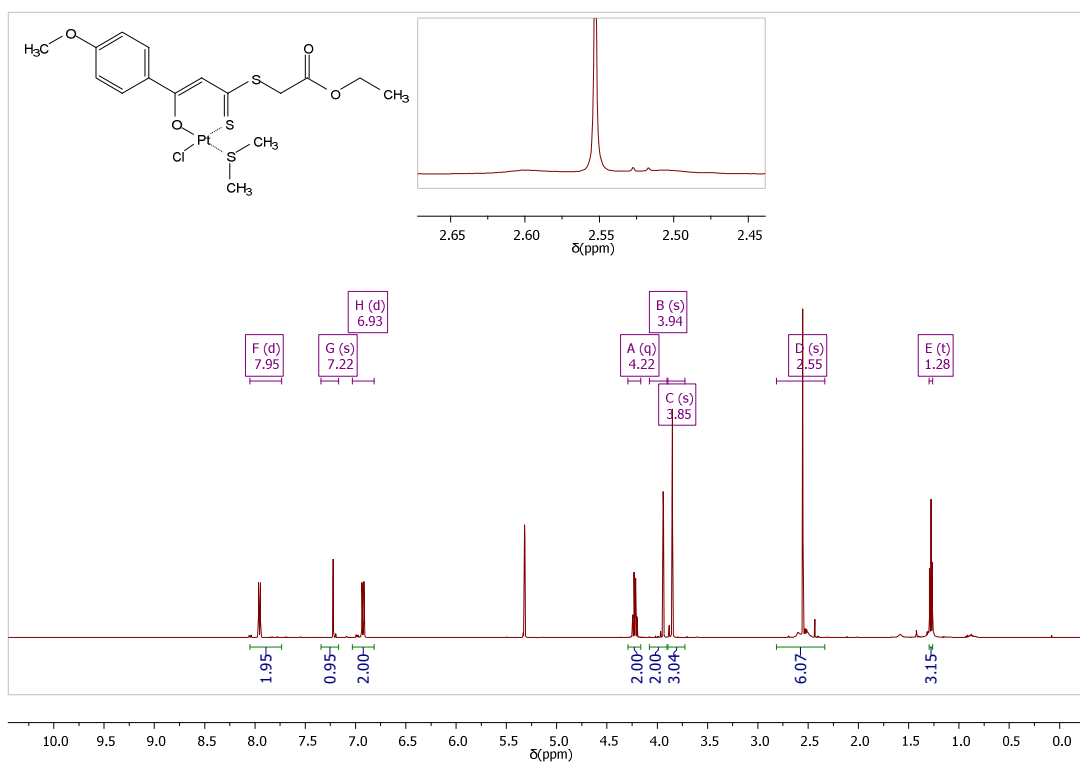


Figure S42.  $^1\text{H-NMR}$  (500 MHz,  $\text{CD}_2\text{Cl}_2$ ):  $[\text{Pt}(\text{L6})(\text{DMS})\text{Cl}]$

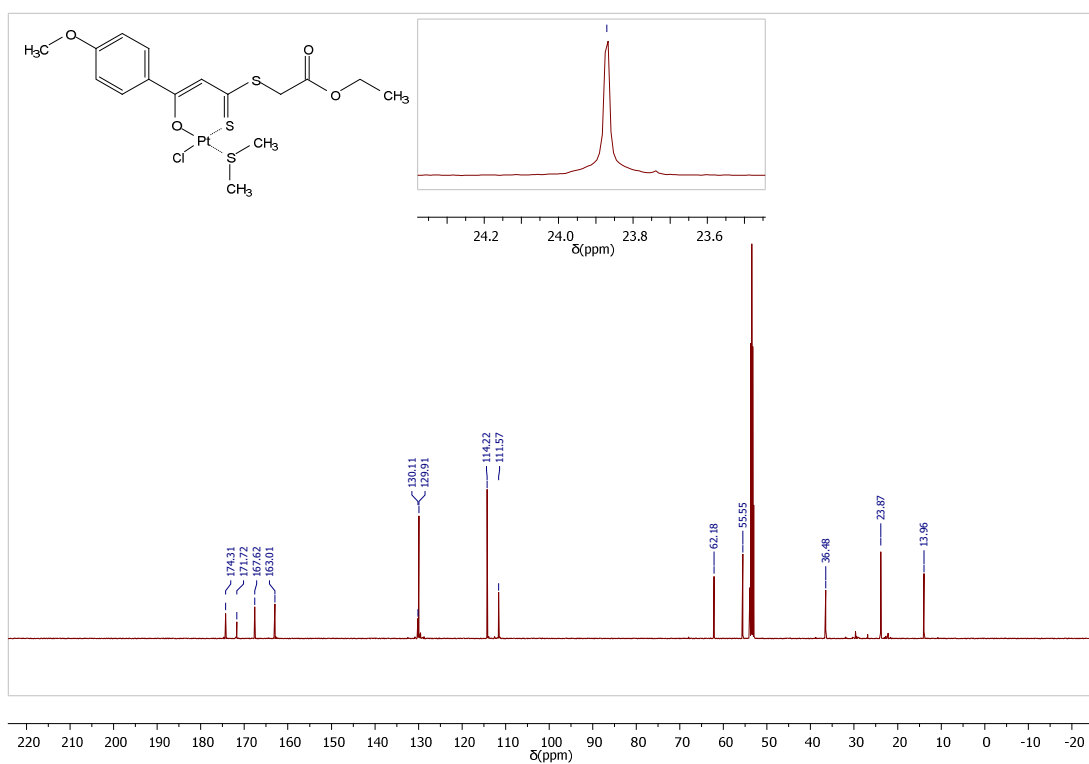


Figure S43.  $^{13}\text{C}\{^1\text{H}\}$  NMR (126 MHz,  $\text{CD}_2\text{Cl}_2$ ):  $[\text{Pt}(\text{L6})(\text{DMS})\text{Cl}]$



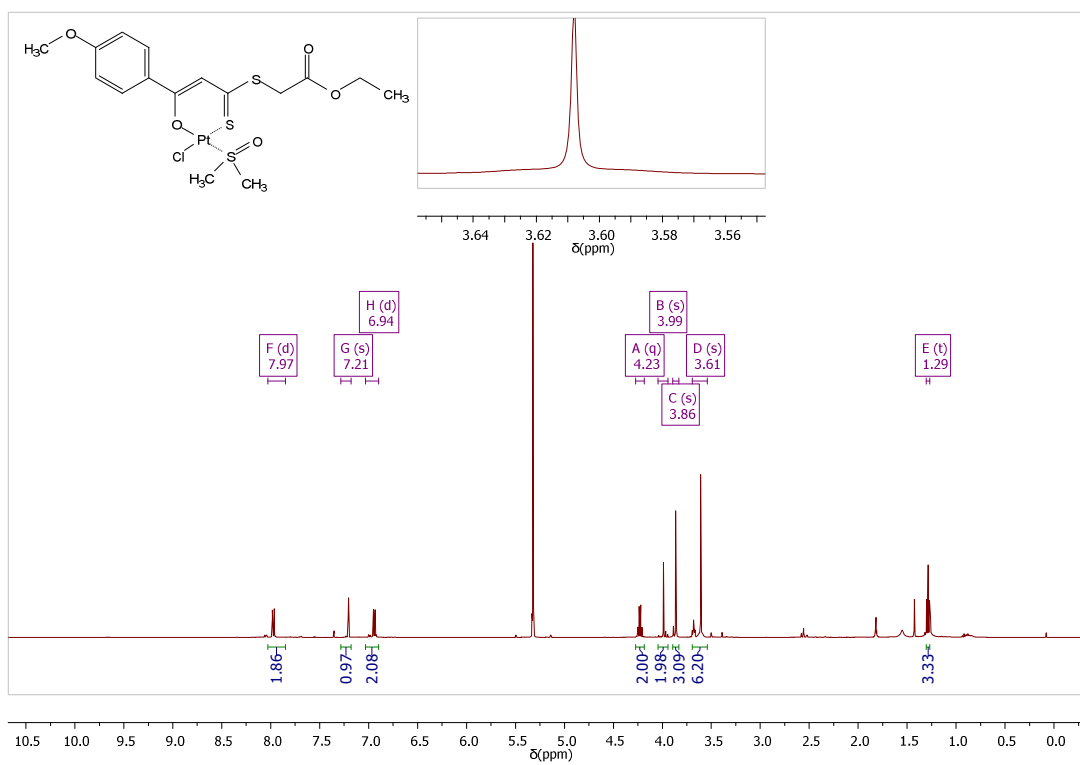


Figure S44. <sup>1</sup>H-NMR (500 MHz, CD<sub>2</sub>Cl<sub>2</sub>): [Pt(L6)(DMSO)Cl]

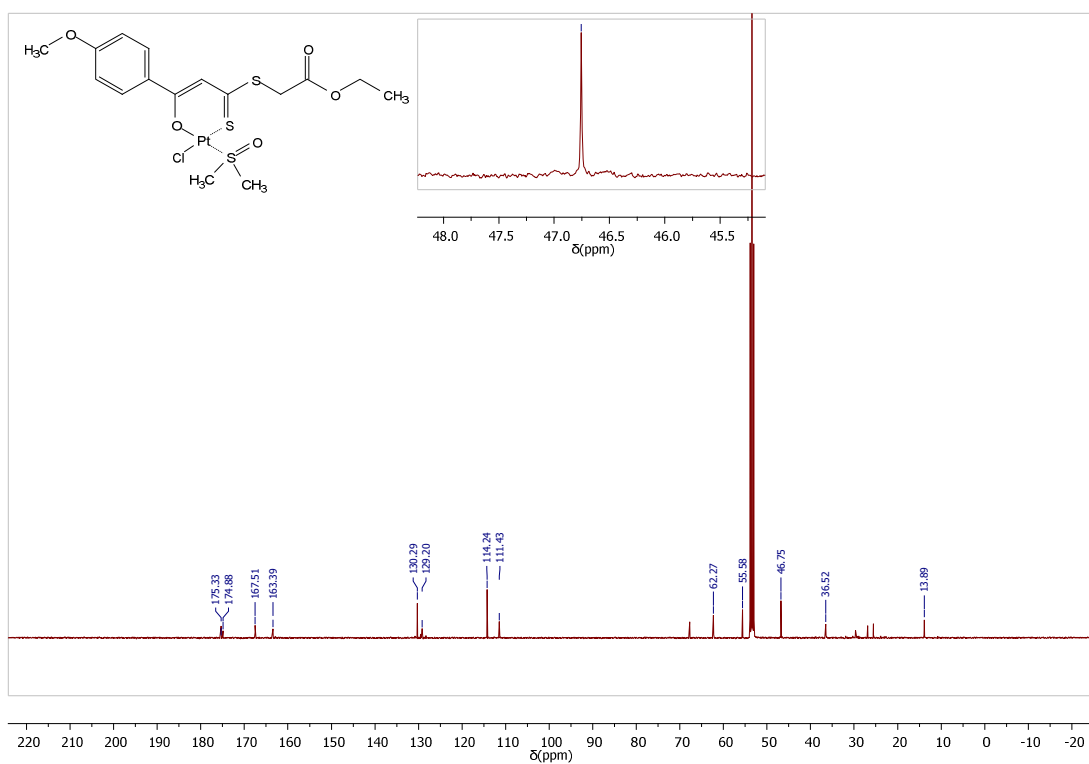


Figure S45. <sup>13</sup>C{<sup>1</sup>H} NMR (126 MHz, CD<sub>2</sub>Cl<sub>2</sub>): [Pt(L6)(DMSO)Cl]

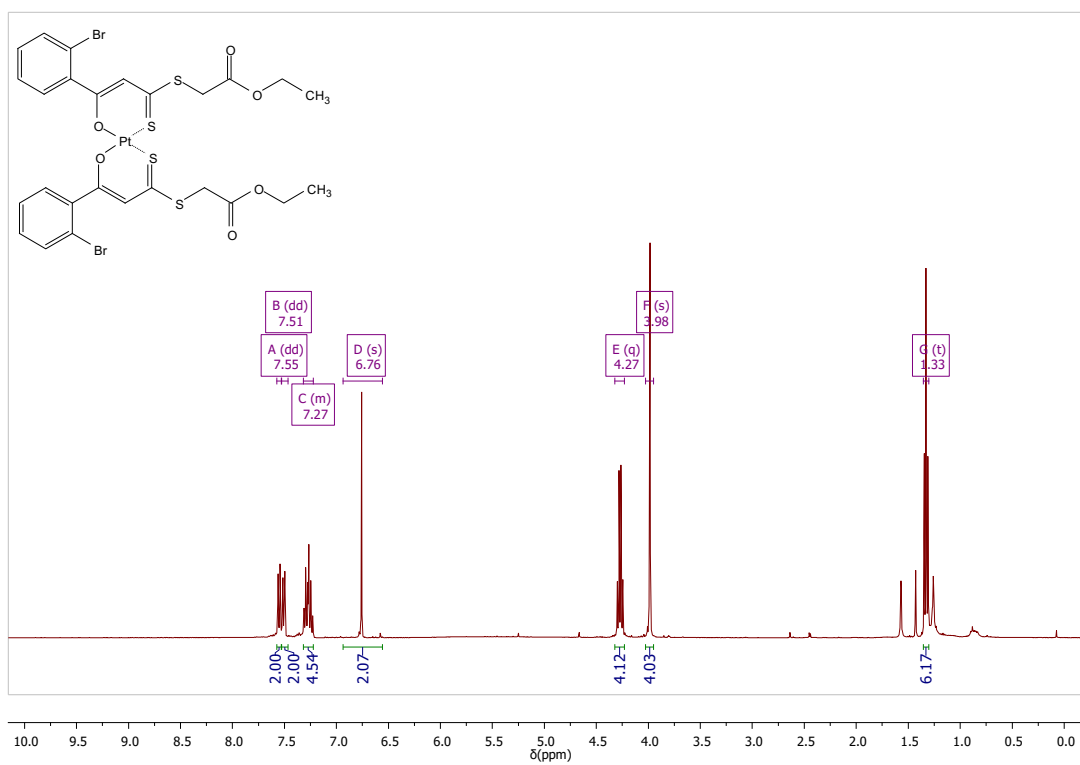


Figure S46. <sup>1</sup>H-NMR (400 MHz, CDCl<sub>3</sub>): [Pt(L7)<sub>2</sub>]

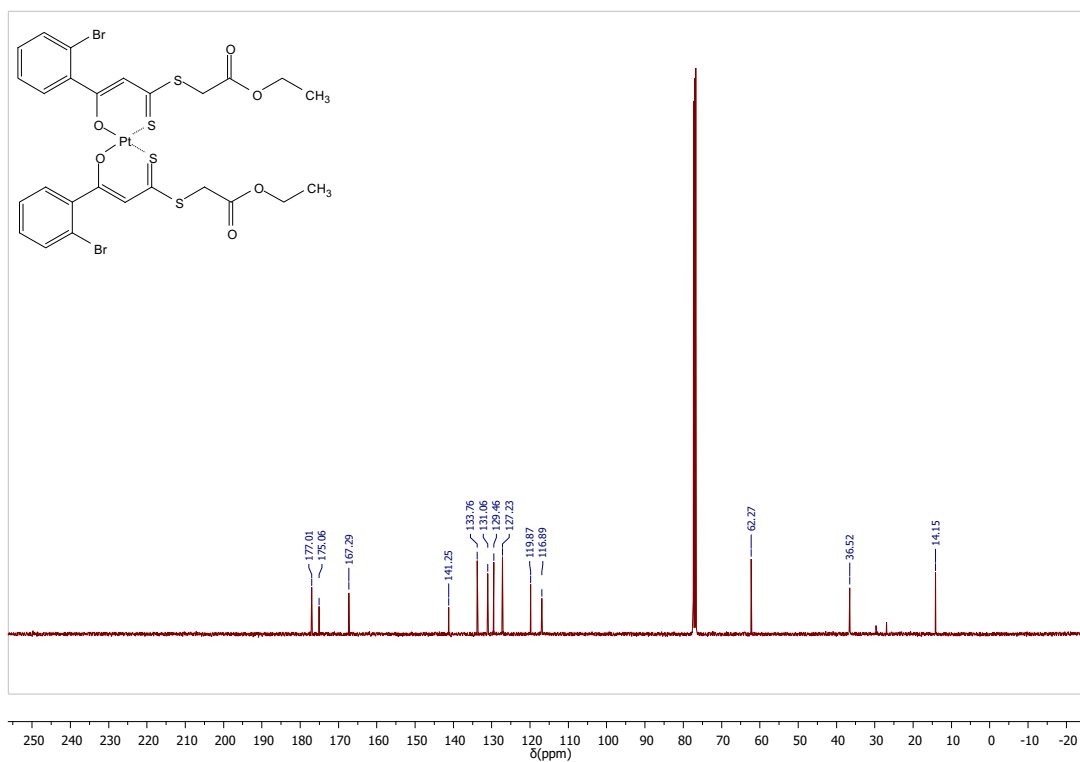


Figure S47. <sup>13</sup>C{<sup>1</sup>H}-NMR (101 MHz, CDCl<sub>3</sub>): [Pt(L7)<sub>2</sub>]

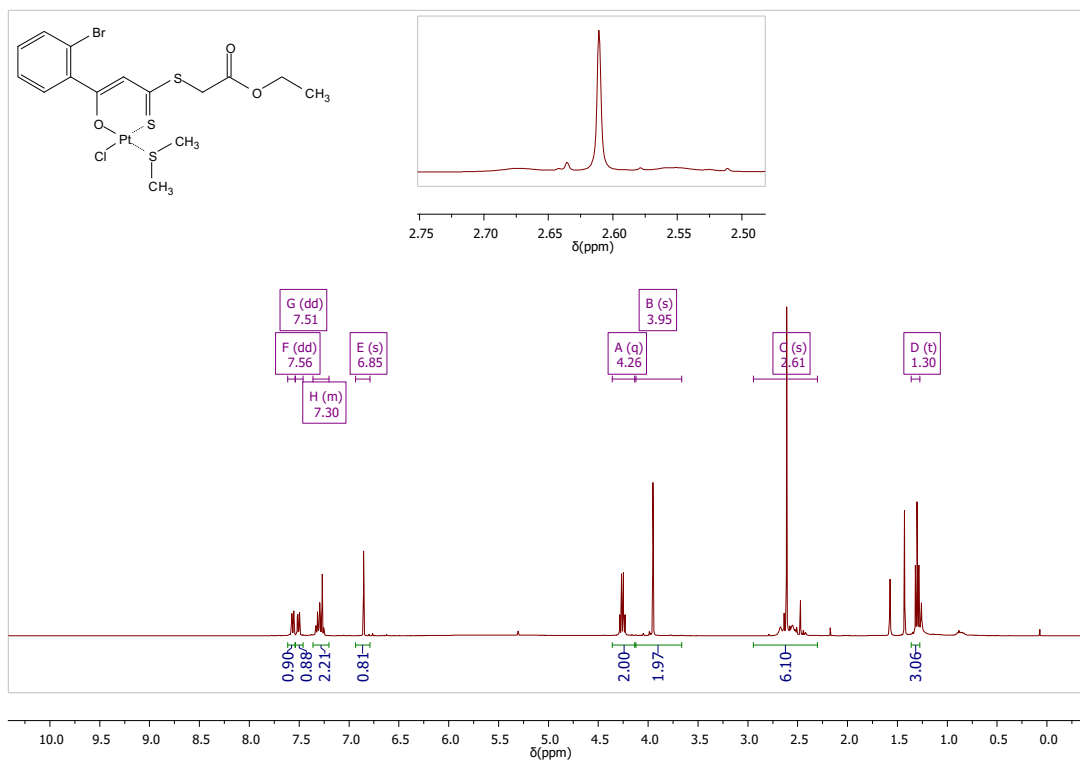


Figure S48. <sup>1</sup>H-NMR (400 MHz, CDCl<sub>3</sub>): [Pt(L7)(DMS)Cl]

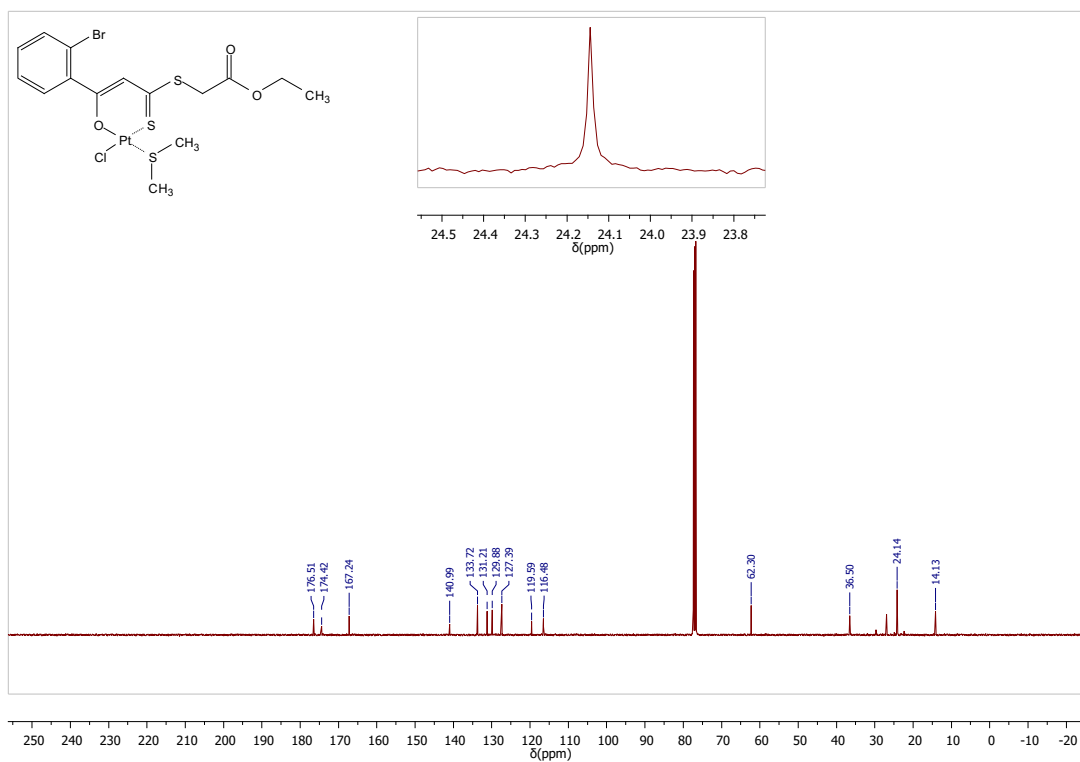


Figure S49. <sup>13</sup>C{<sup>1</sup>H} NMR (101 MHz, CDCl<sub>3</sub>): [Pt(L7)(DMS)Cl]

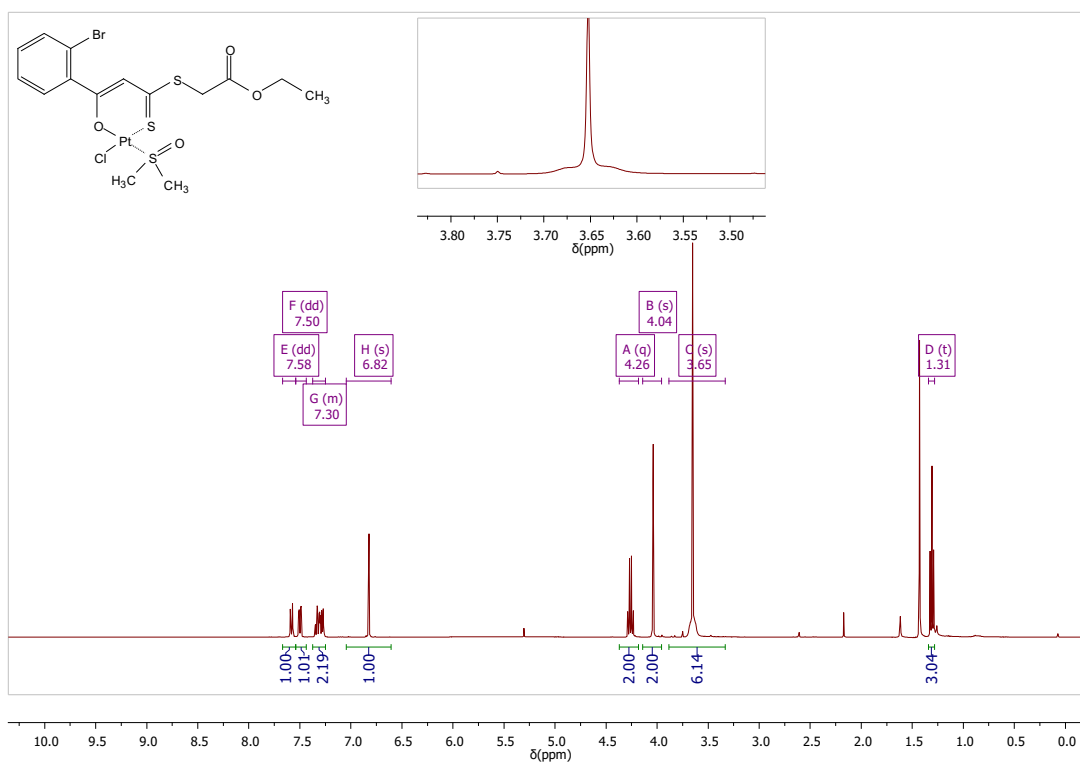


Figure S50.  $^1H$ -NMR (400 MHz,  $CDCl_3$ ):  $[Pt(L7)(DMSO)Cl]$

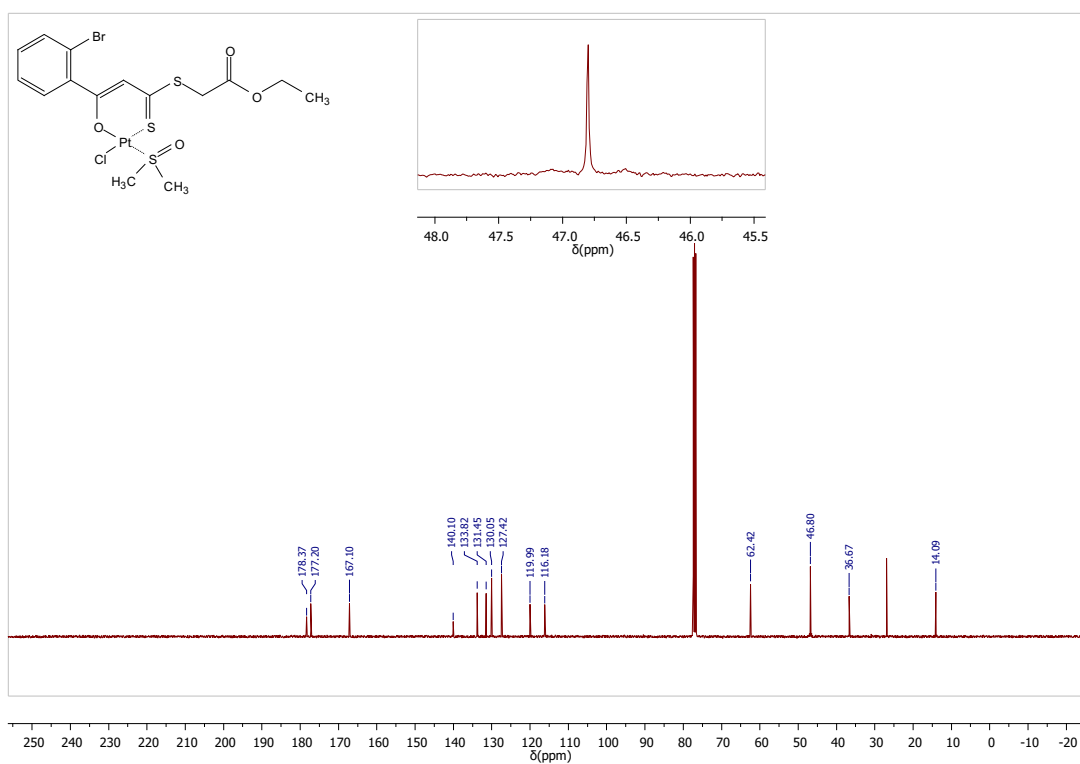


Figure S51.  $^{13}C\{^1H\}$  NMR (101 MHz,  $CDCl_3$ ):  $[Pt(L7)(DMSO)Cl]$

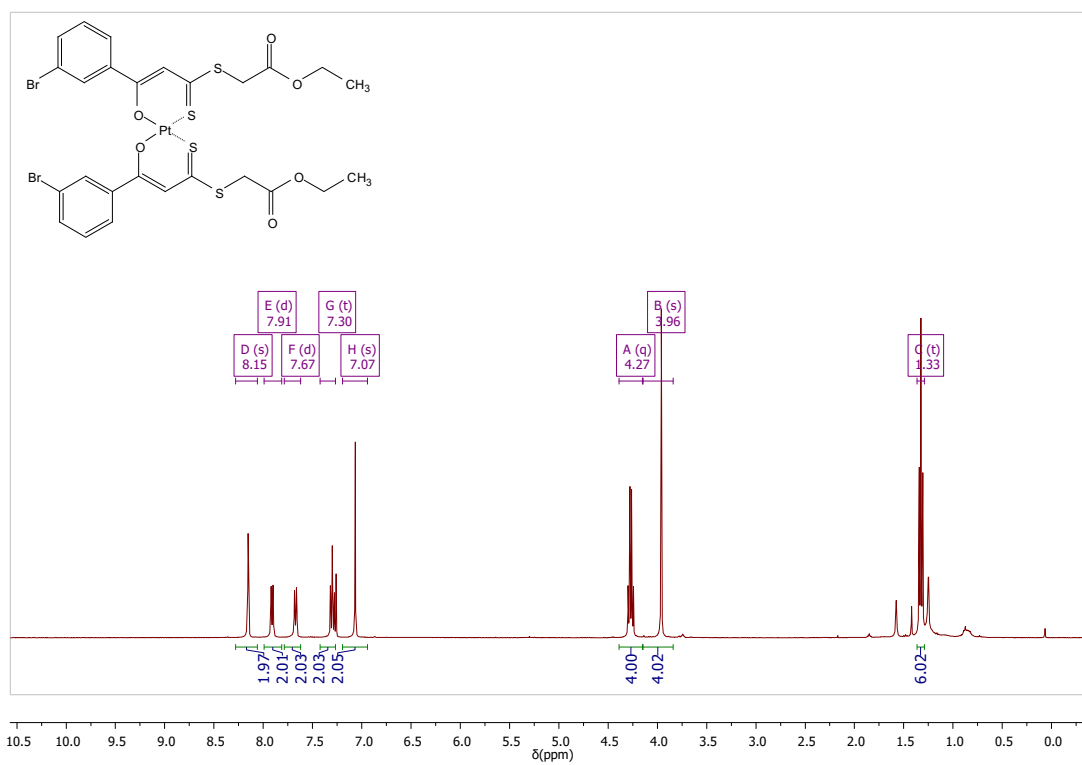


Figure S52. <sup>1</sup>H-NMR (400 MHz, CDCl<sub>3</sub>): [Pt(L8)<sub>2</sub>]

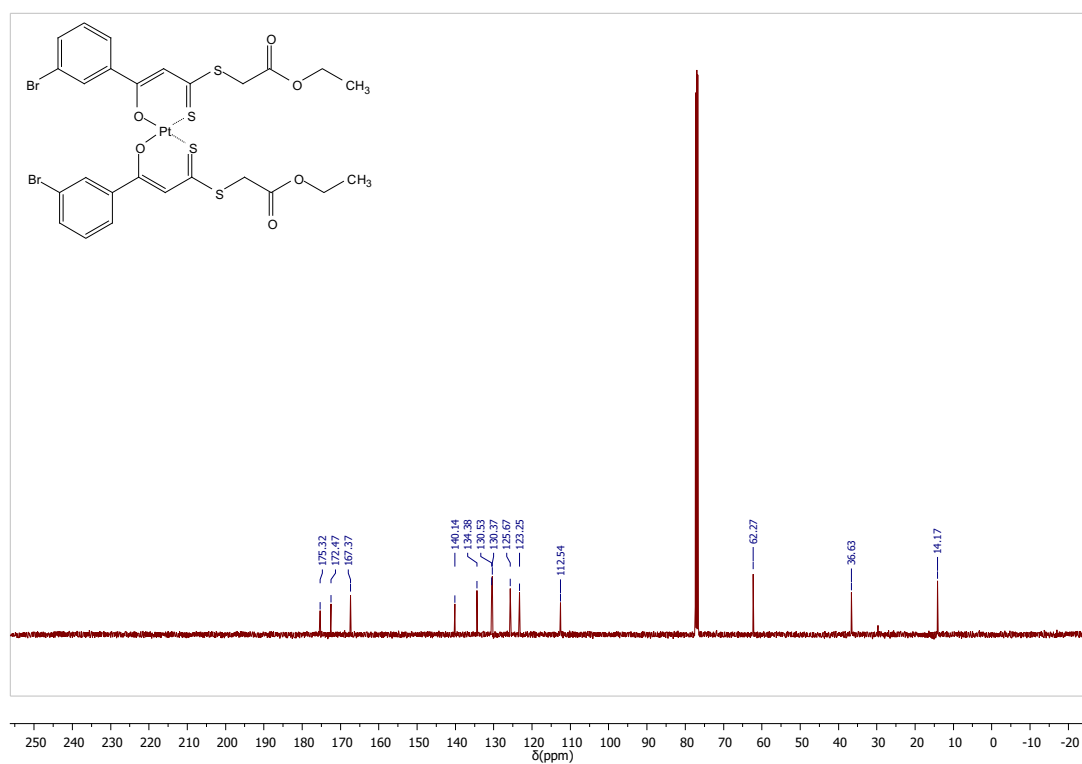


Figure S53. <sup>13</sup>C{<sup>1</sup>H} NMR (101 MHz, CDCl<sub>3</sub>): [Pt(L8)<sub>2</sub>]

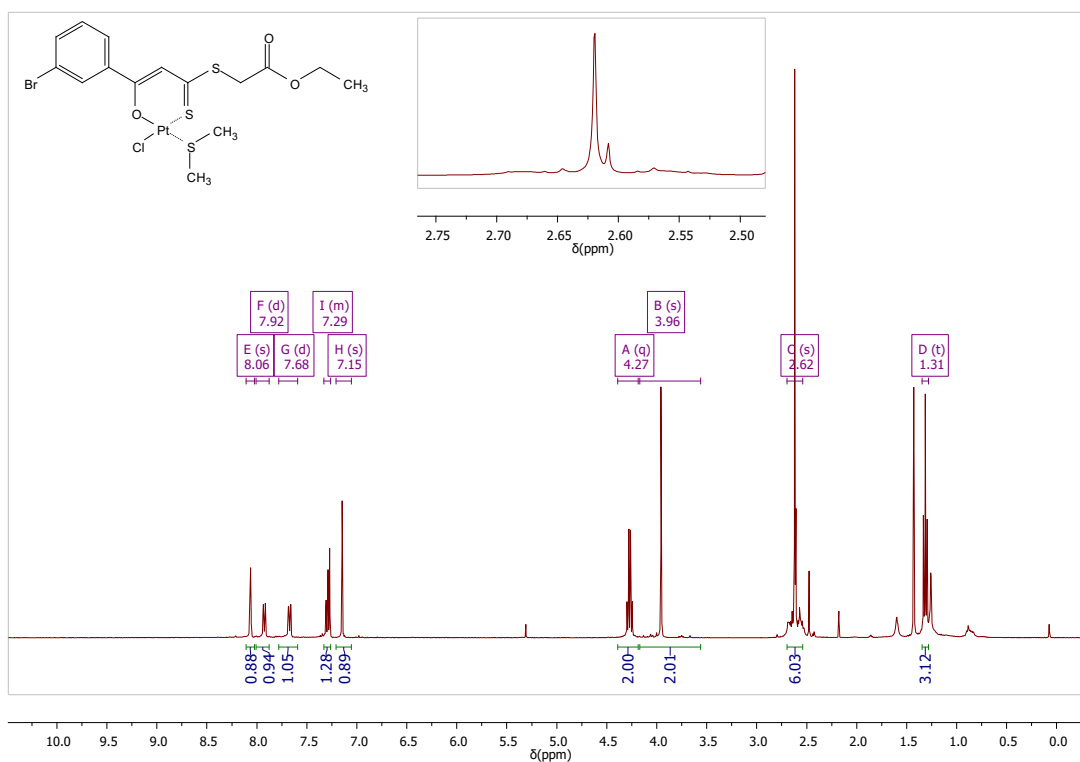


Figure S54. <sup>1</sup>H-NMR (400 MHz, CDCl<sub>3</sub>): [Pt(L8)(DMS)Cl]

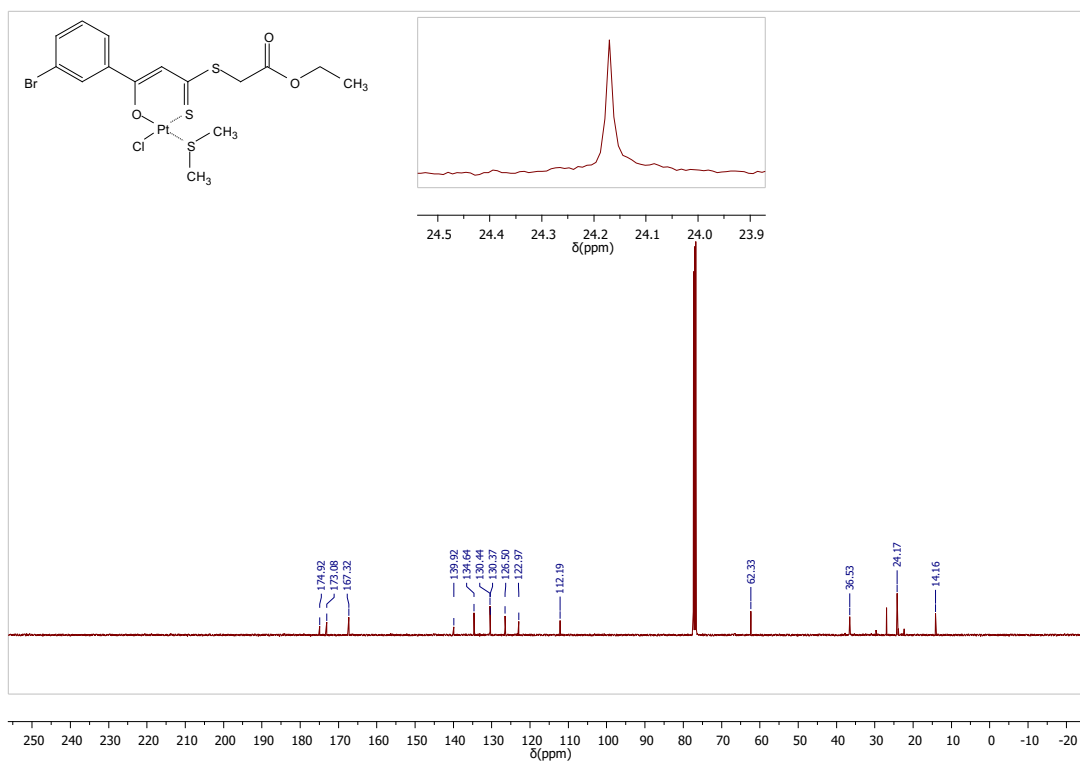


Figure S55. <sup>13</sup>C{<sup>1</sup>H} NMR (101 MHz, CDCl<sub>3</sub>): [Pt(L8)(DMS)Cl]

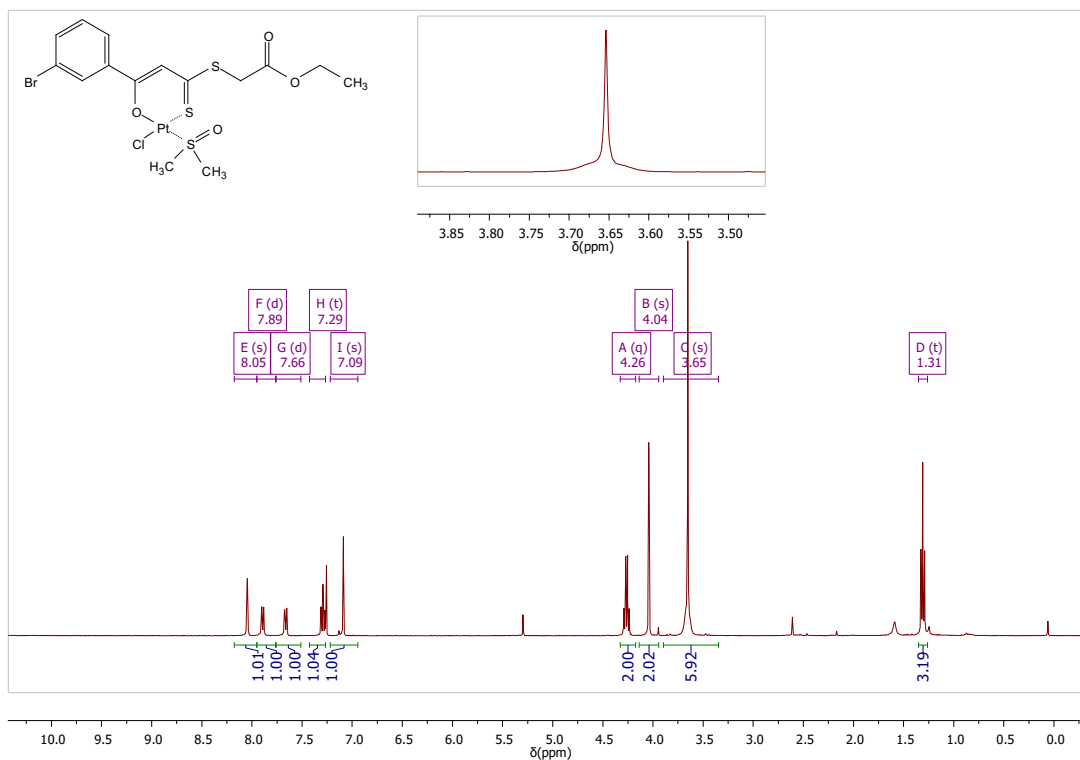


Figure S56.  $^1\text{H-NMR}$  (400 MHz,  $\text{CDCl}_3$ ):  $[\text{Pt}(\text{L8})(\text{DMSO})\text{Cl}]$

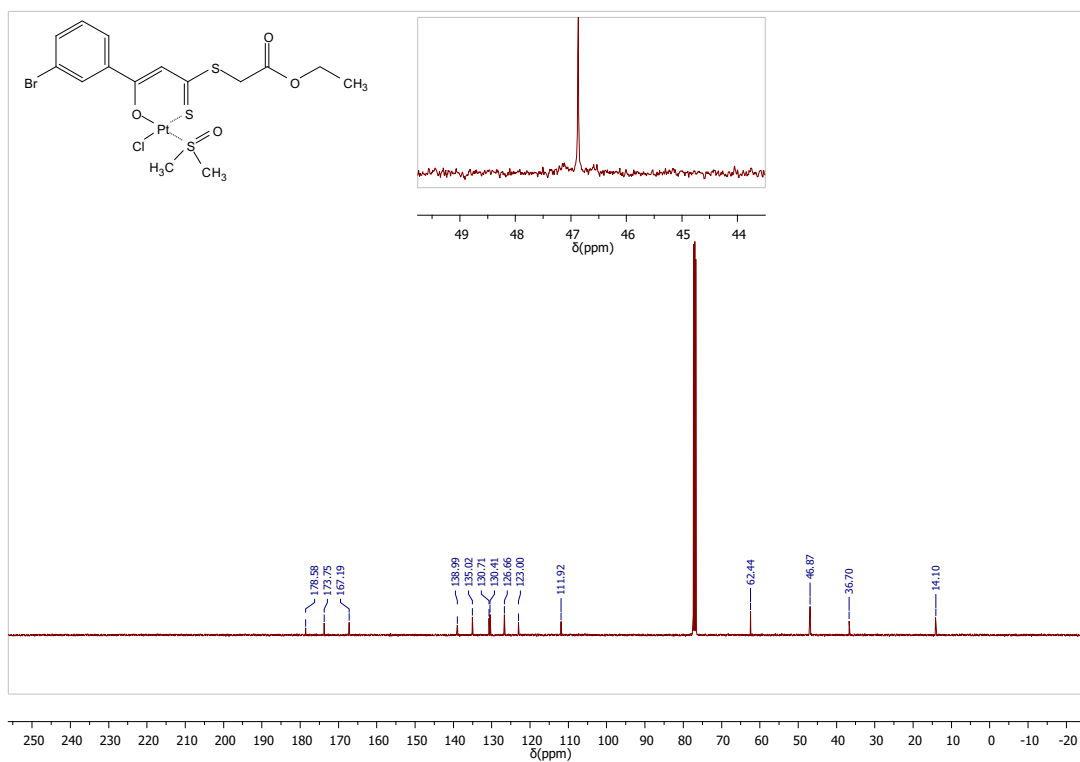


Figure S57.  $^{13}\text{C}\{^1\text{H}\}$  NMR (101 MHz,  $\text{CDCl}_3$ ):  $[\text{Pt}(\text{L8})(\text{DMSO})\text{Cl}]$

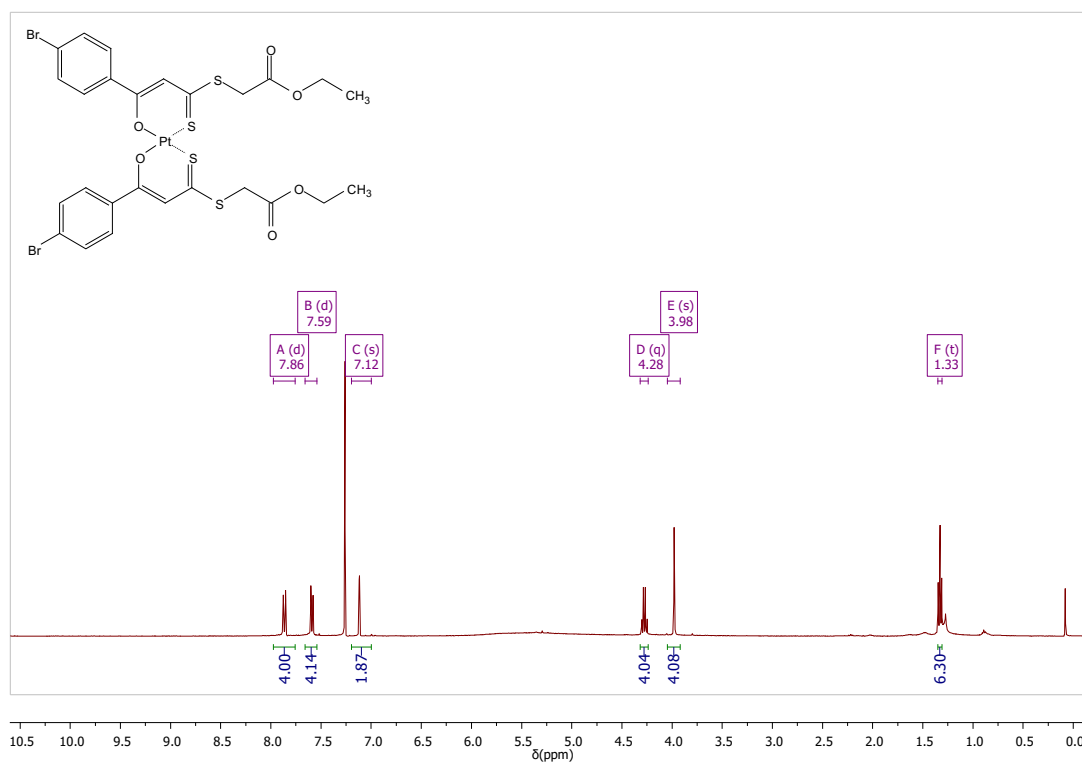


Figure S58. <sup>1</sup>H-NMR (400 MHz, CDCl<sub>3</sub>): [Pt(L9)<sub>2</sub>]

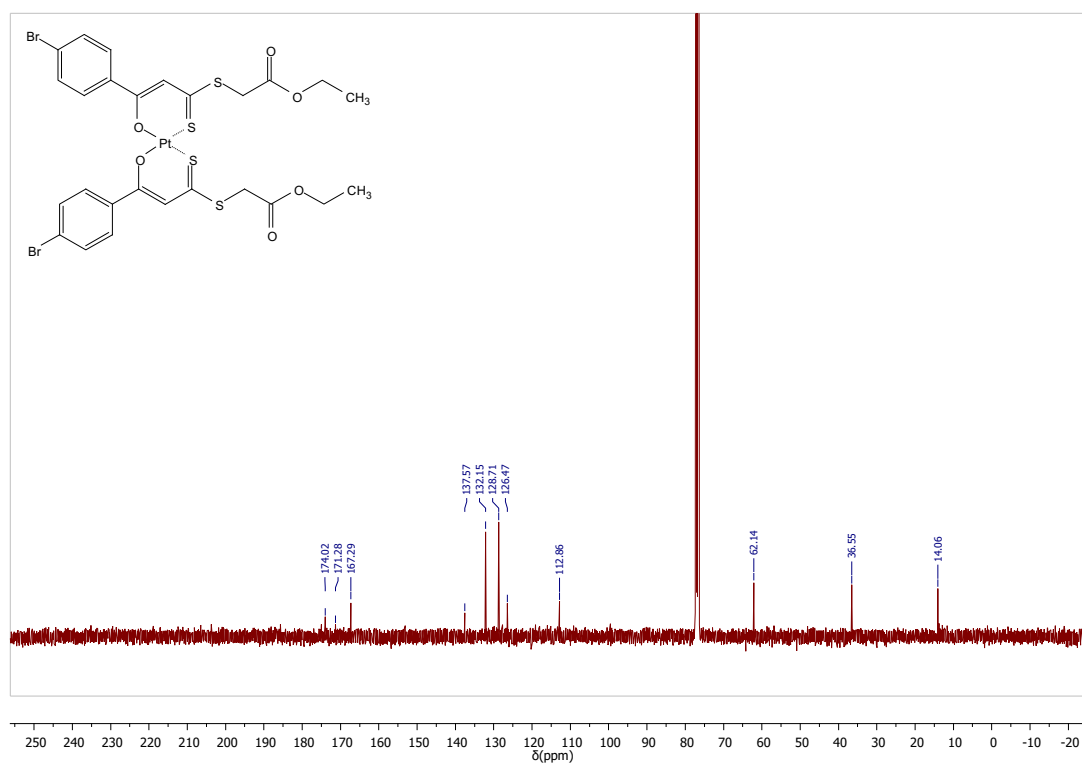


Figure S59. <sup>13</sup>C{<sup>1</sup>H} NMR (101 MHz, CDCl<sub>3</sub>): [Pt(L9)<sub>2</sub>]



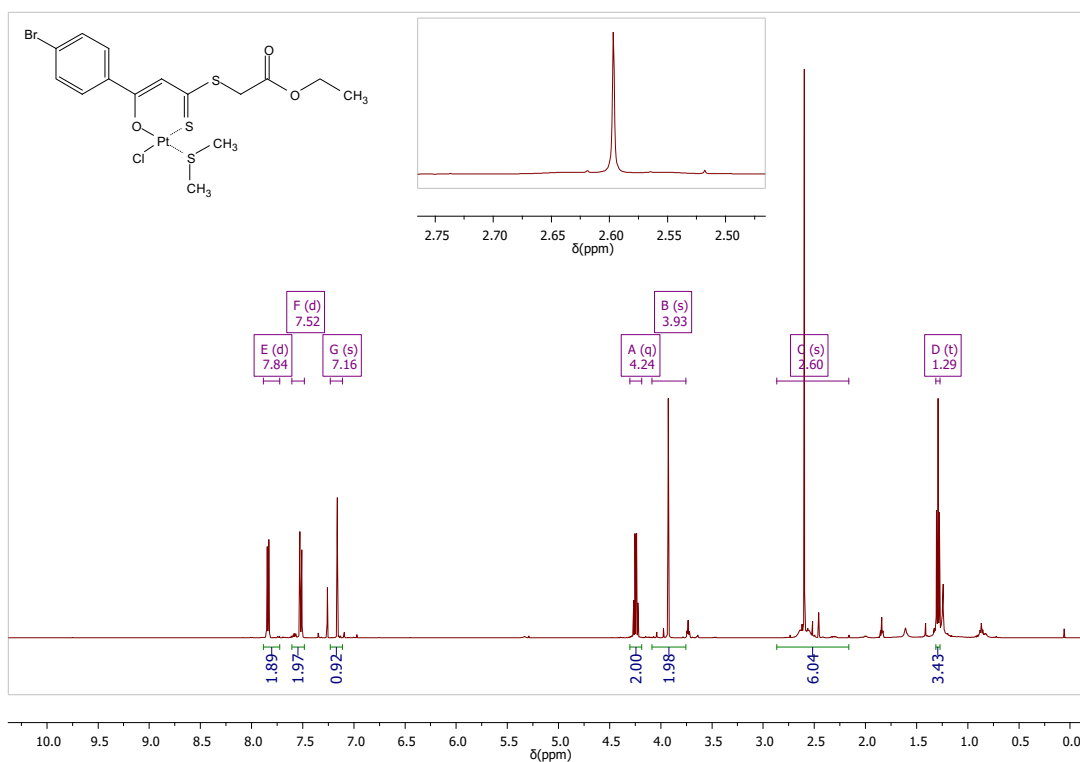


Figure S60.  $^1\text{H-NMR}$  (500 MHz,  $\text{CDCl}_3$ ): [Pt(L9)(DMS)Cl]

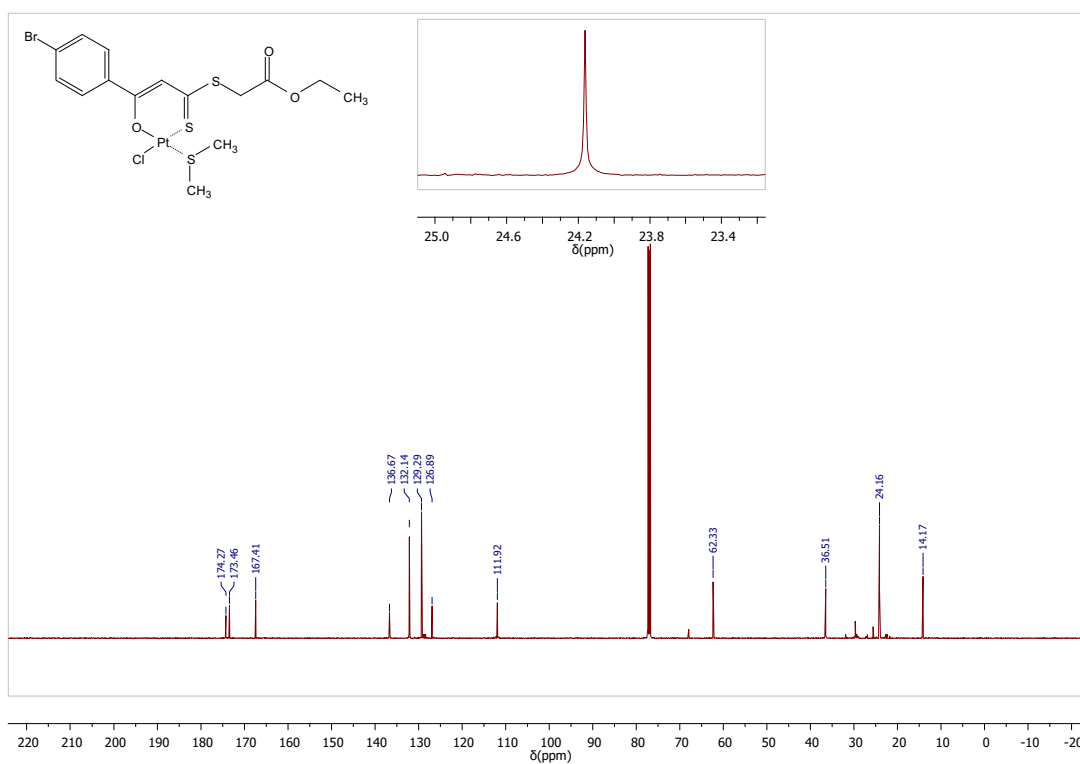


Figure S61.  $^{13}\text{C}\{^1\text{H}\}$  NMR (126 MHz,  $\text{CDCl}_3$ ): [Pt(L9)(DMS)Cl]

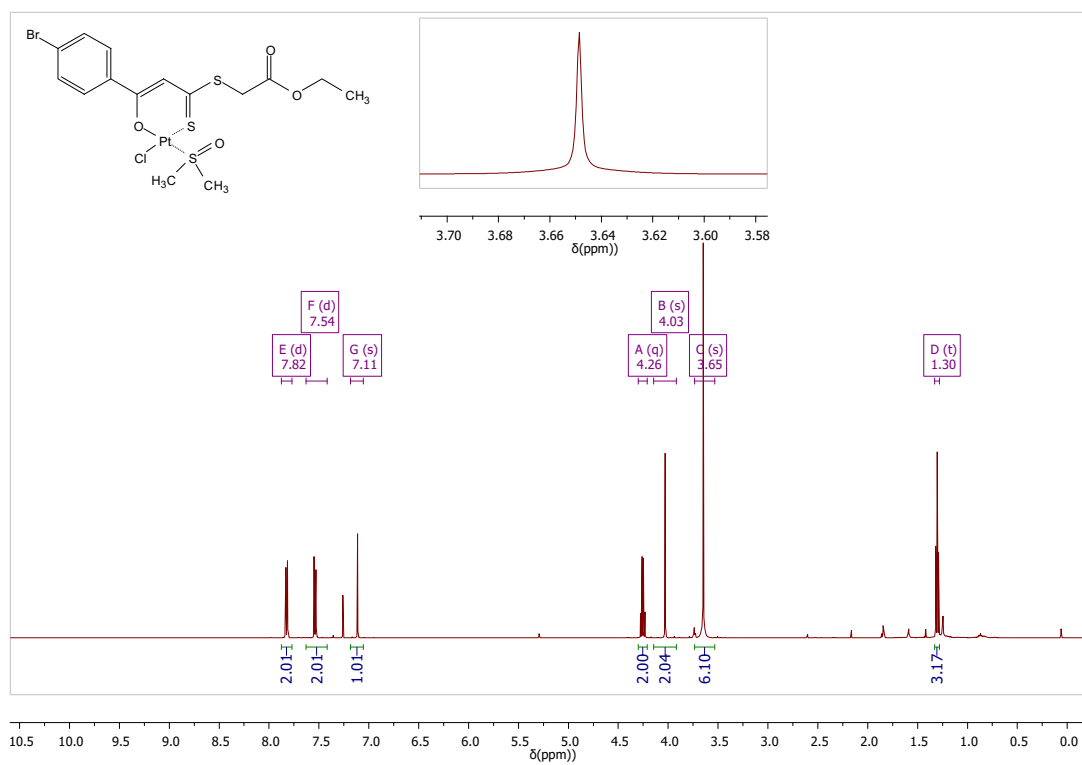


Figure S62.  $^1\text{H-NMR}$  (500 MHz,  $\text{CDCl}_3$ ):  $[\text{Pt}(\text{L9})(\text{DMSO})\text{Cl}]$

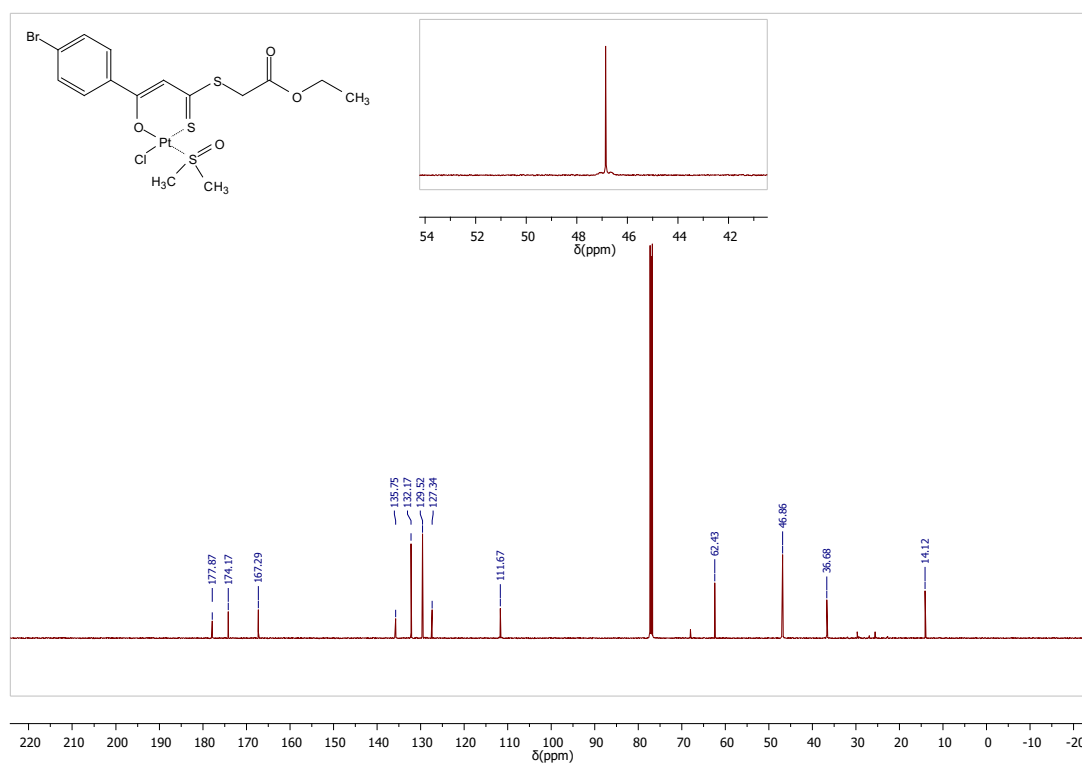


Figure S63.  $^{13}\text{C}\{^1\text{H}\}$  NMR (126 MHz,  $\text{CDCl}_3$ ):  $[\text{Pt}(\text{L9})(\text{DMSO})\text{Cl}]$

### Structure Determinations.

The intensity data for the compounds were collected on a Nonius KappaCCD diffractometer using graphite-monochromated Mo-K $\alpha$  radiation. Data were corrected for Lorentz and polarization effects; absorption was taken into account on a semi-empirical basis using multiple scans.<sup>[1-4]</sup> The structures were solved by intrinsic methods (SHELXT<sup>[5]</sup>) and refined by full-matrix least squares techniques against Fo<sup>2</sup> SHELXL-2018<sup>[6]</sup>. The hydrogen atoms of the organic compound **HL3** were located by difference Fourier synthesis and refined isotropically. All hydrogen atoms of the heavy metal complexes were included at calculated positions with fixed thermal parameters. All non-hydrogen atoms were refined anisotropically.<sup>[6]</sup> Crystallographic data as well as structure solution and refinement details are summarized in Table S1. MERCURY<sup>[7]</sup> was used for structure representations.

**Supporting Information available:** Crystallographic data (excluding structure factors) has been deposited with the Cambridge Crystallographic Data Centre as supplementary publication CCDC-2211752 for **HL3**, CCDC-2211753 for **[Pt(L2)<sub>2</sub>]**, CCDC-2211754 for **[Pt(L6)(DMS)Cl]**, and CCDC-2211755 for **[Pt(L2)(DMSO)Cl]**. Copies of the data can be obtained free of charge on application to CCDC, 12 Union Road, Cambridge CB2 1EZ, UK [E- mail: deposit@ccdc.cam.ac.uk].

**Table S1.** Crystal data and refinement details for the X-ray structure determinations.

Compound	HL3	[Pt(L2) <sub>2</sub> ]	[Pt(L6)(DMS)Cl]	[Pt(L2)(DMSO)Cl]
formula	C <sub>12</sub> H <sub>12</sub> O <sub>3</sub> S <sub>2</sub>	C <sub>28</sub> H <sub>30</sub> O <sub>6</sub> PtS <sub>4</sub>	C <sub>17</sub> H <sub>23</sub> Cl <sub>3</sub> O <sub>4</sub> PtS <sub>3</sub>	C <sub>17</sub> H <sub>23</sub> Cl <sub>3</sub> O <sub>4</sub> PtS <sub>3</sub>
fw (g·mol <sup>-1</sup> )	268.34	785.85	688.97	688.97
T/°C	-140(2)	-140(2)	-140(2)	-140(2)
crystal system	orthorhombic	monoclinic	orthorhombic	orthorhombic
space group	P 2 <sub>1</sub> 2 <sub>1</sub> 2 <sub>1</sub>	P 2 <sub>1</sub> /c	P 2 <sub>1</sub> 2 <sub>1</sub> 2 <sub>1</sub>	P n a 2 <sub>1</sub>
<i>a</i> / Å	6.0945(2)	16.5228(3)	7.1099(1)	12.5038(2)
<i>b</i> / Å	7.1789(2)	23.6316(4)	13.8320(2)	25.9893(5)
<i>c</i> / Å	27.4196(8)	7.34570(10)	23.5265(4)	7.1057(1)
<i>α</i> /°	90	90	90	90
<i>β</i> /°	90	93.172(1)	90	90
<i>γ</i> /°	90	90	90	90
<i>V</i> /Å <sup>3</sup>	1199.66(6)	2863.81(8)	2313.69(6)	2309.10(7)
<i>Z</i>	4	4	4	4
<i>ρ</i> (g·cm <sup>-3</sup> )	1.486	1.823	1.978	1.982
<i>μ</i> (cm <sup>-1</sup> )	4.36	52.33	67.03	67.16
measured data	8666	38773	19126	30377
data with <i>I</i> > 2σ( <i>I</i> )	2617	6116	5021	5146
unique data ( <i>R</i> <sub>int</sub> )	2705/0.0340	6570/0.0366	5292/0.0354	5275/0.0284
<i>wR</i> <sub>2</sub> (all data, on <i>F</i> <sup>2</sup> ) <sup>a)</sup>	0.0614	0.0493	0.0383	0.0348
<i>R</i> <sub>1</sub> ( <i>I</i> > 2σ( <i>I</i> )) <sup>a)</sup>	0.0270	0.0238	0.0197	0.0166
<i>S</i> <sup>b)</sup>	1.078	1.147	1.066	1.080
Res. dens./e·Å <sup>-3</sup>	0.216/-0.186	0.562/-0.712	0.454/-0.441	0.412/-0.527
Flack-parameter	0.04(4)	-	0.375(9)	0.494(8)
absorpt method	multi-scan	multi-scan	multi-scan	multi-scan
absorpt corr T <sub>min</sub> /max	0.6933/0.7456	0.5637/0.7456	0.6141/0.7456	0.5334/0.7456
CCDC No.	2211752	2211753	2211754	2211755

<sup>a)</sup> Definition of the *R* indices:  $R_1 = (\sum ||F_o| - |F_c||) / \sum |F_o|$ ;

$wR_2 = \{\sum [w(F_o^2 - F_c^2)^2] / \sum [w(F_o^2)^2]\}^{1/2}$  with  $w^{-1} = \sigma^2(F_o^2) + (aP)^2 + bP$ ;  $P = [2F_c^2 + \text{Max}(F_o^2)]/3$ ;

<sup>b)</sup>  $s = \{\sum [w(F_o^2 - F_c^2)^2] / (N_o - N_p)\}^{1/2}$ .

**Table S2.** Selected bond lengths and angles for HL3, [Pt(L2)<sub>2</sub>], [Pt(L6)(DMS)Cl] and [Pt(L2)(DMSO)Cl].

HL3				[Pt(L2) <sub>2</sub> ]			
Bond lengths [Å]		Bond angles [°]		Bond lengths [Å]		Bond angles [°]	
C6-C7	1.472(2)			Pt-O1	2.0117(19)	O1-Pt-S1	95.68(6)
C3-C12	1.508(3)			Pt-O4	2.0022(19)	S1-Pt-S3	89.50(3)
C9-S2	1.7533(18)			Pt-S1	2.2286(7)	O4-Pt-S3	95.94(6)
C8-H8	0.95(2)			Pt-S3	2.2347(7)	O1-Pt-O4	78.90(8)
						O1-Pt-S3	174.75(6)
S1-C9	1.6795(18)			S1-C9	1.696(3)	O4-Pt-S1	174.21(6)
C7-C8	1.378(2)			C7-C8	1.402(4)		
C8-C9	1.418(2)			C8-C9	1.398(4)	Pt-O1-C7	132.62(19)
O1-C7	1.325(2)	O1-C7-C8	122.85(16)	O1-C7	1.277(3)	O1-C7-C8	125.4(3)
		C7-C8-C9	125.69(16)			C7-C8-C9	127.4(3)
		C8-C9-S1	126.60(14)	S3-C23	1.702(3)	C8-C9-S1	130.3(2)
				C21-C22	1.405(4)	C9-S1-Pt	108.45(10)
				C22-C23	1.390(4)		
				O4-C21	1.275(3)	Pt-O4-C21	132.76(19)
						O4-C21-C22	125.3(3)
						C21-C22-C23	127.7(3)
						C22-C23-S3	130.3(2)
						C23-S3-Pt	108.01(10)
[Pt(L6)(DMS)Cl]				[Pt(L2)(DMSO)Cl]			
Bond lengths [Å]		Bond angles [°]		Bond lengths [Å]		Bond angles [°]	
Pt-O1	2.017(3)	O1-Pt-S1	96.74(9)	Pt-O1	2.011(2)	O1-Pt-S1	96.17(7)
Pt-S1	2.2338(10)	S1-Pt-S3	84.12(4)	Pt-S1	2.2526(8)	S1-Pt-S3	89.81(3)
Pt-S3	2.2575(11)	S3-Pt-Cl	93.49(4)	Pt-S3	2.1987(8)	S3-Pt-Cl	89.60(3)
Pt-Cl	2.3496(9)	O1-Pt-Cl	85.65(9)	Pt-Cl	2.3335(8)	O1-Pt-Cl	84.42(7)
		S1-Pt-Cl	177.61(4)			S1-Pt-Cl	179.38(5)
S1-C1	1.701(4)	O1-Pt-S3	178.32(16)	S1-C1	1.710(3)	O1-Pt-S3	174.02(7)
C1-C2	1.385(6)			C1-C2	1.387(5)		
C2-C3	1.397(6)	Pt-O1-C3	129.5(3)	C2-C3	1.400(5)	Pt-O1-C3	131.9(2)
O1-C3	1.291(5)	O1-C3-C2	127.4(4)	O1-C3	1.276(4)	O1-C3-C2	125.9(3)
		C3-C2-C1	128.7(4)			C3-C2-C1	128.1(3)
		C2-C1-S1	128.7(3)	S3-O4	1.465(3)	C2-C1-S1	130.1(3)
S3-C15	1.798(7)	C1-S1-Pt	108.90(14)	S3-C15	1.770(8)	C1-S1-Pt	107.55(12)
S3-C16	1.798(7)			S3-C16	1.783(9)		
						O4-S3-C15	107.9(5)
						O4-S3-C16	109.4(5)
		C15-S3-C16	99.8(2)			C15-S3-C16	102.76(19)
						O4-S3-Pt	117.30(12)
		C15-S3-Pt	106.4(3)			C15-S3-Pt	109.4(3)
		C16-S3-Pt	108.9(3)			C16-S3-Pt	109.1(3)

**Table S3.** IC<sub>50</sub> values of analyzed compounds for ovarian cancer cell lines mean (±SD)

		<b>A2780</b>	<b>A2780 Cis</b>	<b>RF A2780</b>	<b>Skov3</b>	<b>Skov3 Cis</b>	<b>RF Skov3</b>	<b>mean IC50</b>
Pt(L)(DMS)Cl	L1	33.3 (±6.8)	16.0 (±5.1)	0.5	76.1 (±16.8)	46.2 (±10.2)	0.6	34.4
	L2	2056.6 (±489.2)	355.0 (±115.5)	0.2	685.8 (±245.3)	183.1 (±52.1)	0.3	656.1
	L3	56.1 (±11.5)	60.5 (±19.2)	1.1	57.5 (±17.0)	41.4 (±11.8)	0.7	43.3
	L4	55.0 (±10.8)	72.2 (±26.4)	1.3	60.6 (±17.1)	53.2 (±12.6)	0.9	48.5
	L5	93.0 (±9.7)	59.1 (±14.7)	0.6	119.9 (±20.1)	69.6 (±13.6)	0.6	68.4
	L6	59.5 (±12.4)	46.4 (±13.1)	0.8	86.6 (±10.4)	69.7 (±11.4)	0.8	52.6
	L7	28.1 (±4.1)	44.7 (±11.7)	1.6	63.9 (±16.2)	53.7 (±13.2)	0.8	38.4
	L8	42.6 (±15.3)	50.7 (±14.3)	1.2	66.3 (±16.9)	63.7 (±18.5)	1.0	44.9
	L9	32.9 (±14.5)	39.4 (±19.8)	1.2	60.6 (±15.4)	52.6 (±12.8)	0.9	37.3
Pt(L)(DMSO)Cl	L1	25.6 (±10.1)	55.3 (±10.7)	2.2	336.8 (±62.4)	99.4 (±16.2)	0.3	103.8
	L2	164.4 (±45.2)	50.4 (±12.5)	0.3	380.9 (±96.1)	103.6 (±20.5)	0.3	139.9
	L3				n.a.			
	L4	16.5 (±4.5)	73.3 (±25.0)	4.5	146.1 (±28.1)	92.8 (±17.4)	0.6	66.6
	L5	224.6 (±64.2)	58.5 (±13.6)	0.3	777.3 (±270.5)	95.5 (±21.0)	0.1	231.2
	L6				n.a.			
	L7	102.8 (±56.4)	56.3 (±13.3)	0.5	646.9 (±196.8)	182.8 (±70.5)	0.3	197.9
	L8	64.6 (±32.2)	48.2 (±12.4)	0.7	87.6 (±15.0)	54.9 (±11.2)	0.6	51.2
	L9	153.8 (±35.7)	76.8 (±25.1)	0.5	403.9 (±127.3)	163.6 (±60.3)	0.4	159.7
CIS		6.8 (±2.4)	15.4 (±4.8)	2.3	12.5 (±2.8)	28.6 (±4.2)	2.3	13.1

## References

- [1] COLLECT, Data Collection Software; Nonius B.V., Netherlands, **1998**.
- [2] „Processing of X-Ray Diffraction Data Collected in Oscillation Mode“: Otwinowski, Z.; Minor, W. in Carter, C. W.; Sweet, R. M. (eds.): *Methods in Enzymology, Vol. 276, Macromolecular Crystallography, Part A*, pp. 307-326, Academic Press **1997**.
- [3] SADABS 2.10, Bruker-AXS inc., 2002, Madison, WI, U.S.A.
- [4] Bruker (2020) APEX3 Bruker AXS LLC, Madison, WI, USA.
- [5] Sheldrick, G. M. *Acta Cryst.* (2015). **A71**, 3-8.
- [6] Sheldrick, G. M. *Acta Cryst.* (2015). **C71**, 3-8.
- [7] MERCURY, Macrae CF, Edgington PR, McCabe P, Pidcock E, Shields GP, Taylor R, Towler M, van de Streek J (2006) *J Appl Cryst* 39:453

## 5.2 [ME-2]

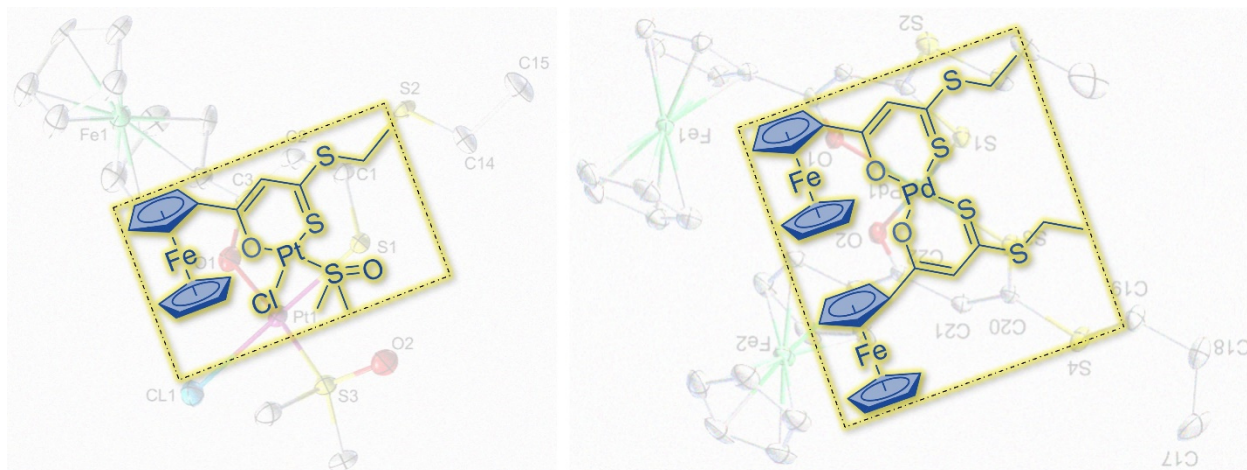
### Platinum(II) and palladium(II) complexes mediated by $\beta$ -hydroxy-dithioesters ferrocenyl derivatives: synthesis, characterization and Antiproliferative Activity

Micheal K. Farh, Ikrame Louzi, Hassan Abul-Futouh, Helmar Görls, Norman Häfner, Ingo B. Runnebaum, Wolfgang Weigand

Journal of Sulfur Chemistry **2022**, accepted

DOI: 10.1080/17415993.2022.2152285.

Reproduced by permission from the Journal of Sulfur Chemistry



This article published by Taylor & Francis in Journal of Sulfur Chemistry, acceptance date 22.11.2022, available at: <https://doi.org/10.1080/17415993.2022.2152285>.

It is deposited under the terms of the Creative Commons Attribution-NonCommercial License (<http://creativecommons.org/licenses/by-nc/4.0/>), which permits non-commercial re-use, distribution, and reproduction in any medium, provided the original work is properly cited.”



**Journal of Sulfur Chemistry - Decision on Manuscript ID GSRP-2022-0164.R1**

22-Nov-2022

Dear Professor Wolfgang Weigand:

Ref: Platinum(II) and palladium(II) complexes mediated by  $\beta$ -hydroxy-dithioesters ferrocenyl derivatives: synthesis, characterization and antiproliferative activity

I have now considered your paper and have recommended publication in Journal of Sulfur Chemistry. We are pleased to accept your paper in its current form subject to an originality check using the Crossref Similarity Check™ software. Once the originality check is complete, the paper will be forwarded to the Production Editor for copy editing and typesetting.

You will receive proofs for checking, and instructions for transfer of copyright in due course.

The publisher also requests that proofs are checked and returned within 48 hours of receipt.

Thank you for your contribution to Journal of Sulfur Chemistry and we look forward to receiving further submissions from you.

Sincerely,  
Dr Clennan  
Editor, Journal of Sulfur Chemistry  
[sulfchem@uwyo.edu](mailto:sulfchem@uwyo.edu)

**Platinum(II) and palladium(II) complexes mediated by  $\beta$ -hydroxy-dithioesters ferrocenyl derivatives: synthesis, characterization and antiproliferative activity**

Micheal K. Farh,<sup>a,b</sup> Ikrame Louzi,<sup>a</sup> Hassan Abul-Futouh,<sup>c\*</sup> Helmar Görls,<sup>a</sup> Norman Häfner,<sup>d</sup> Ingo B. Runnebaum,<sup>d\*</sup> Wolfgang Weigand<sup>a,e\*</sup>

*<sup>a</sup>Department of Inorganic and Analytical Chemistry (IAAC), Friedrich Schiller University Jena, Humboldtstraße 8, 07743 Jena, Germany; <sup>b</sup>Department of Chemistry, Faculty of Science, Assiut University, Assiut 71515, Egypt; <sup>c</sup>Department of Chemistry, Faculty of Science, The Hashemite University, P.O. Box 330127, Zarqa 13133, Jordan; <sup>d</sup>Department of Gynecology, Jena University Hospital- Friedrich Schiller University Jena, Am Klinikum 1, 07747 Jena, Germany; <sup>e</sup>Jena Center for Soft Matter (JCSM), Friedrich Schiller University Jena, Philosophenweg 7, 07743 Jena, Germany.*

Wolfgang Weigand, Department of Inorganic and Analytical Chemistry (IAAC), Friedrich Schiller University Jena, Humboldtstraße 8, 07743 Jena, Germany.  
[wolfgang.weigand@uni-jena.de](mailto:wolfgang.weigand@uni-jena.de).

# Platinum(II) and palladium(II) complexes mediated by $\beta$ -hydroxy-dithioesters ferrocenyl derivatives: synthesis, characterization and antiproliferative activity

Ferrocene and its derivatives compounds have shown a significant role in medicinal organometallic chemistry as an antiparasitic or antibacterial. Therefore, we herein report on the utilization of dithioesters ferrocenyl derivatives as proligands for the synthesis of heteroleptic platinum(II) and homoleptic palladium(II) complexes bearing a conserved *O,S* binding moiety. The resulting complexes [Pt(L1)(DMSO)Cl] (**1**), [Pt(L2)(DMSO)Cl] (**2**), [Pt(L3)(DMSO)Cl] (**3**), [Pd(L1)<sub>2</sub>] (**4**), [Pd(L2)<sub>2</sub>] (**5**), and [Pd(L3)<sub>2</sub>] (**6**), in which HL1 = methyl 3-hydroxy-3-ferroceneprop-2-enedithioate, HL2= ethyl 3-hydroxy-3-ferroceneprop-2-enedithioate and HL3 = propyl 3-hydroxy-3-ferroceneprop-2-enedithioate, were fully characterized employing a variety of analytical techniques (NMR spectroscopy, elemental analysis, and mass spectrometry and X-ray structure determination of complexes **2** and **6**). Cytotoxicity assays of the synthesized ligands as well as the Pt/Pd metal complexes showed low toxicity towards ovarian cancer cells, but the compounds are not affected by cisplatin resistance mechanisms. Pt(II) complexes exhibited the highest activity, and the alkyl substituent strongly influenced the activity of these complexes and the free ligands. The cytotoxic activity increases with the length of the alkyl chain with **3** exhibiting a mean IC<sub>50</sub> of 56  $\mu$ M.

Keywords: Ferrocene; platinum; palladium; sulfur; cytotoxicity

## Introduction

Nowadays, great efforts have been deployed towards the development of novel platinum drugs, such as cisplatin, carboplatin and oxaliplatin, which are considered a cornerstone in many chemotherapeutic treatments [1-7]. However, most of these drugs are still causing severe side effects including emesis, nausea, vomiting, nephrotoxicity, neurotoxicity, myelosuppression, or ototoxicity and their activity is affected by resistance mechanisms both limiting their clinical use [8,9]. Therefore, the improvement of such metal-based drugs to minimize its toxicity as well as overcoming the natural resistance without affecting its biological activity has been

considered as an interesting target for research [10,11].

In fact, ferrocenyl-containing compounds have shown an important role in medicinal organometallic chemistry as an antiparasitic or antibacterial agent [12-14]. Furthermore, the neutral ferrocene derivatives ferrocifens that elaborate iron-based mimics of the organic drugs tamoxifen and hydroxy tamoxifen as well as some cationic ferrocenium salts display cytotoxic behavior and reduce the expansion of tumors in vivo [15-21]. Moreover, an interesting synthetic approach of ferrocifens utilizing alkyl ferrocenyl thioketones based on the Barton-Kellogg reaction was described by Mlostoń and co-workers [22]. Compared to commonly traditional methods, such as McMurry coupling, the sulfur approach offers a more straightforward procedure with comparable yields [22]. In addition, the ferrocene unit has also been connected to platinum or palladium metal to investigate their cooperative biological effects between the two active metals [23-29]. For example, the heterometallic platinum (II) compound with  $\beta$ -aminoethylferrocene moiety reported by Cuadrado and co-workers has shown a greater activity profile in a colon cancer cell line compared to that of standard cisplatin drug [29].

In recent publications, we have shown different types of  $\beta$ -hydroxy-dithiocinnamic acid derivatives that were utilized as ligands for the synthesis of Ni(II), Pd(II), Pt(II), Ru(II) and Os(II) complexes bearing a conserved *O,S* binding moiety (Figure 1) as experimental anticancer agents [30-38].

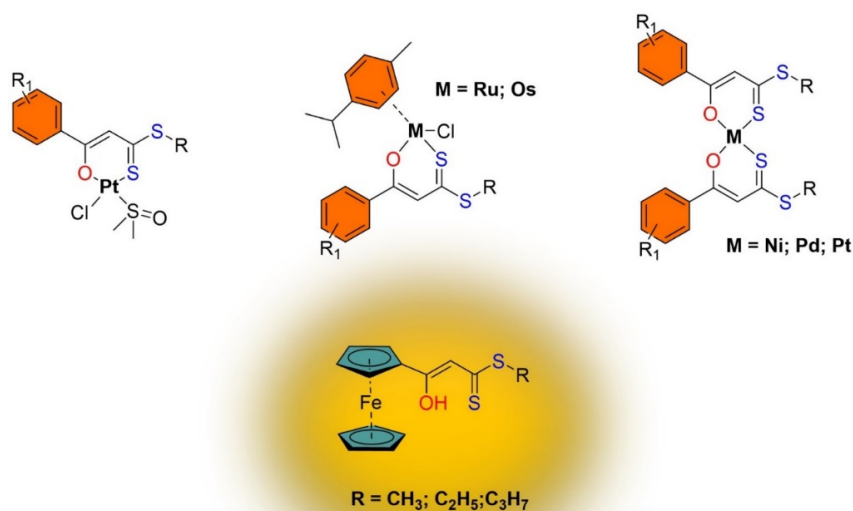


**Figure 1.** Ni(II), Pd(II), Pt(II), Ru(II) and Os(II) complexes mediated by  $\beta$ -hydroxy-dithiocinnamic acid as a ligand (top) and  $\beta$ -hydroxy-dithioesters ferrocenyl derivatives compounds used in this study (bottom).

Moreover, we have also indicated that the characteristics of such type of complexes could be tuned by changing the substituent at the aromatic moiety as well as the chain length of the alkyl substituent. Investigations on this class of complexes revealed an acceptable solubility profile in mixed DMSO–buffer solutions and a considerable stability at physiological pH as determined from analysis of their time-course UV-visible absorption spectra [36-38].

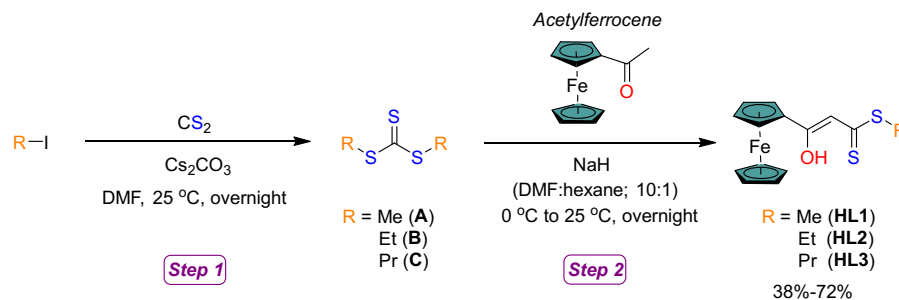
Motivated by our results obtained with platinum (II) complexes with  $\beta$ -hydroxy-dithiocinnamic acid derivatives, we recently become interested in using  $\beta$ -hydroxy-dithioesters ferrocenyl derivatives (Figure 1) as proligands for the synthesis of new potentially cytotoxic heterometallic platinum (II) and palladium (II) complexes. It is worth mentioning that the stability of the ferrocenyl group in aqueous solution under aerobic environment, the possibility of numerous derivatives, and its convenient electrochemical features have made ferrocene-based complexes of particular interest in medicinal chemistry [39]. Therefore, the aim of this study is to investigate the reactivity of the chelating system of  $\beta$ -hydroxy-dithioesters ferrocenyl derivatives towards *cis*-[PtCl<sub>2</sub>(DMSO)<sub>2</sub>] and (PhCN)<sub>2</sub>PdCl<sub>2</sub> complexes to generate new electroactive heterometallic Pt/Pd-based complexes. The expected metal complexes with *O,S*-chelating ligand have been characterized using a variety of spectroscopic techniques (NMR, IR, MS), elemental analysis, and by X-ray analysis. Moreover, the electrochemical properties of the obtained complexes were studied by cyclic voltammetry and their cytotoxic activities were tested against epithelial ovarian cancer cell lines.

## Results and Discussion

### *Synthesis and Characterization of the free ligands HL1-3*

The synthetic pathway and characterization of precursors **A-C** (Scheme 1, step 1) needed for the synthesis of  $\beta$ -hydroxy-dithioesters ferrocenyl ligands, **HL1-3**, are described in detail in the ESI according to the reported literature method [40]. The known compound **HL1** was prepared in a modified procedure described by Singh *et al.* [41,42] through the reaction of acetylferrocene with dimethyl trithiocarbonate (**A**) in the presence of sodium hydride (NaH) in dimethylformamide (DMF)-hexane mixture. Similarly, the reaction of precursor **B** (or **C**) with acetylferrocene in DMF-

hexane in the presence of NaH at room temperature afforded the *O,S*-chelating ligands **HL2** and **HL3**, respectively, as shown in Scheme 1, step 2.



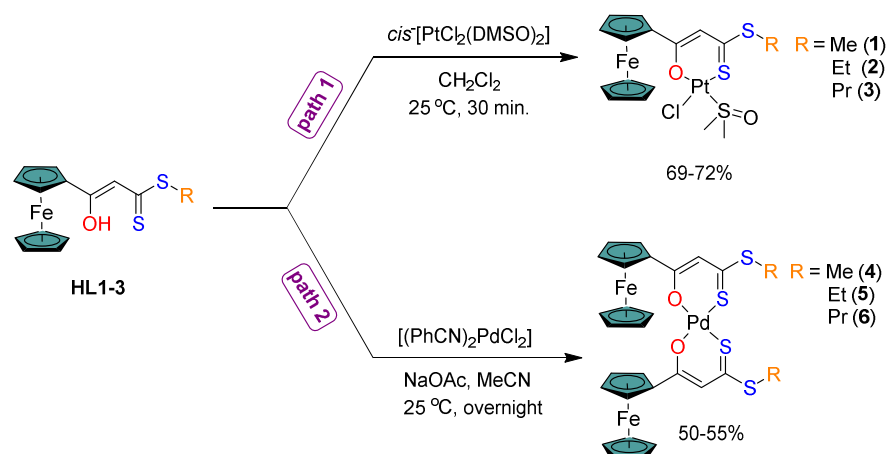
**Scheme 1.** Synthetic pathways of precursors A-C (step 1) and the free ligands **HL1-3** (step 2).

The resulting compounds **HL1-3** have been characterized by spectroscopic methods (<sup>1</sup>H NMR, <sup>13</sup>C{<sup>1</sup>H} NMR, and IR), mass spectrometry, and elemental analysis. The <sup>1</sup>H NMR spectra of these compounds exhibit a resonance signal at 6.61 (**HL1**), 6.56 (**HL2**) and 6.58 (**HL3**) ppm for the methine proton, whereas the signal appeared at strong downfield shift (15.10 ppm) could be assigned to the proton belonging to the hydroxyl group (average values given), which is consistent with those of similar analogues reported in the literature [36-38,41,42]. This reflects the formation of the expected *cis*-enolic structure of the target compounds as well as the existence of an intramolecular hydrogen bond with the sulfur atom of the thiocarbonyl moiety. Additionally, the nine protons of the ferrocene moiety appear in the area between 4.82 and 4.22 ppm, while the protons of the alkyl substituents of compounds **HL1-3** were detected in the range of 3.25-1.06 ppm. The <sup>13</sup>C{<sup>1</sup>H} NMR spectrum of each compound shows a resonance signal located at low field (~ 212 ppm), which is assigned to the thiocarbonyl carbon atom. The β-oxo carbon atoms appear at 176 ppm, while those of the methine groups are found at 107 ppm (average values given). In the FTIR spectra, characteristic broad bands are detected around 3090 cm<sup>-1</sup> for the enolic OH group in compounds **HL1-3**, which reflects the existence of hydrogen bonds. Very strong absorption bands around 1600, 1484, and 1256 cm<sup>-1</sup> are assigned to stretching vibrations of C=C, C-O, and C=S respectively. Desorption Electron Impact (DEI) mass spectrometric analysis allows the assignment of [M]<sup>+</sup> peak for compounds **HL1-3**.

### ***Synthesis and Characterization of *O,S*-chelating Pt/Pd(II) complexes***

In order to obtain the target *O,S*-chelating platinum(II) complexes, the free ligands **HL1-3** were reacted with *cis*-[PtCl<sub>2</sub>(DMSO)<sub>2</sub>], that was synthesized following the

reported procedure in the literature [43]. The slow addition of one equivalent of **HL1-3**, respectively, to a solution of *cis*-[PtCl<sub>2</sub>(DMSO)<sub>2</sub>] dissolved in CH<sub>2</sub>Cl<sub>2</sub> followed by subsequent column chromatography afforded the heteroleptic complexes [Pt(**L1-L3**)(DMSO)Cl] in 69-72% yield as shown in Scheme 2 (path 1).



**Scheme 2.** Synthetic pathways of obtaining *O,S*-chelating Pt/Pd(II) complexes **1-6**.

All complexes were characterized by elemental analyses, multinuclear NMR and FTIR spectroscopy, mass spectrometry as well as X-ray analysis for complex [Pt(**L2**)(DMSO)Cl] (**2**). It is worth pointing out that the coordination of the ligands **HL1-3** towards the Pt(II) center results in changing the chemical shift values of their <sup>1</sup>H and <sup>13</sup>C{<sup>1</sup>H} NMR spectra. This is because the oxygen atoms in **1-3** complexes possess σ-donating properties towards the metal center, while the sulfur atom can act as an electron acceptor for π-backbonding from the metal center. Overall, the β-oxo carbon atom in complexes **1-3** and the thiocarbonyl carbon atom is shifted upfield (shielded) compared to their parent ligands **HL1-3**. Moreover, the chemical shift values of the proton and carbon atoms of the methine moiety in complexes **1-3** are slightly shifted to higher frequency (deshielded) due to the delocalization of electron density in the six-membered chelating ring. Additionally, the <sup>1</sup>H and <sup>13</sup>C{<sup>1</sup>H} NMR spectra of complexes **1-3** show the appearance of signals at 3.63 and 46.8 ppm, respectively, accompanied by <sup>195</sup>Pt satellites, which can be assigned to the methyl groups of the coordinated DMSO ligand. These frequencies are shifted downfield relative to those of free DMSO [44]. These results are consistent with those of *O,S*-chelating platinum(II) analogues [36-38]. The <sup>195</sup>Pt NMR spectra of **1-3** exhibit signals at -3123.5, -3124.2, -3121.4 ppm, respectively, which is attributed to Pt-Cl bond and is in accordance with the literature [45].

On the other hand, the synthesis of *bis*-[*O,S*-chelating palladium(II)] complexes was carried out in two steps. Firstly, **HL1-3** were deprotonated using sodium acetate (NaOAc) in MeCN solution to generate the sodium salt. The latter was then treated with half equivalent of bis(benzonitrile)palladium(II) chloride and stirred overnight at room temperature. After workup through extraction with diethyl ether, the desired homoleptic complexes [Pd(L1)<sub>2</sub>] (**4**), [Pd(L2)<sub>2</sub>] (**5**), and [Pd(L3)<sub>2</sub>] (**6**) could be obtained as red-volatile crystalline solids in moderate yields as shown in Scheme 2 (path 2). The isolated complexes **4-6** were characterized by spectroscopic methods (<sup>1</sup>H NMR, <sup>13</sup>C{<sup>1</sup>H} NMR and IR), mass spectrometry, elemental analysis and X-ray crystallography for **6**. The <sup>1</sup>H NMR spectra of **4-6** complexes display the disappearance of the proton belonging to the hydroxyl group located at 15.10 ppm in the parent ligands **HL1-3**. The signal of the methine proton in these complexes was also detected at 6.71 ppm, which is shifted downfield relative to those of **HL1-3**. The <sup>13</sup>C{<sup>1</sup>H} NMR spectra of **4-6** display a signal at 184.6 ppm for the thiocarbonyl carbon atom and a signal at 174.9 ppm for the β-oxo carbon atom (average values given). These two signals (184.6 and 174.9 ppm) are shifted upfield, like those of **1-3** complexes. The signal of the carbon atom of the methine moiety was also detected at 111.8 ppm (average values given), which is shifted downfield relative to those of parent ligands **HL1-3**.

### ***Molecular structures***

Recrystallization from CH<sub>2</sub>Cl<sub>2</sub> and cyclohexane mixture (1:1) of complexes **2** and **6** at -20 °C provided suitable single crystals for X-ray diffraction studies. Figure 2 depicts the molecular structures of complexes **2** and **6** with ellipsoids drawn at the 50% probability level. It is evident from Figure 2 that the geometry around each metal center present the typical square-planar configuration of Pt/Pd(II) complexes. In the case of complex **2**, the central atom is Pt surrounded by one sulfur atom and one oxygen atom of the chelate ligand as well as one chloride atom in the *trans* position and one sulfur atom of the DMSO unit in *cis* position regarding the sulfur atom of the chelate ligand. On the other hand, the central atom in complex **6** is Pd, which surrounded by two *cis* sulfur atoms and two *cis* oxygen atoms of the bidentate *O,S*-ligands.



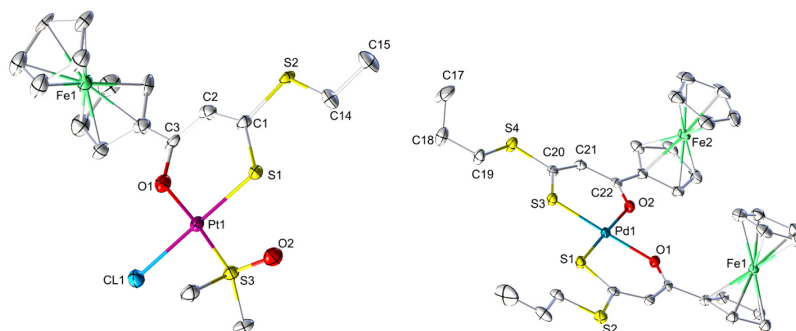


**Figure 2.** Molecular structures (50% probability) of complexes **2** (left) and **6** (right). Hydrogen atoms have been omitted for clarity.

The structure around the sulfur atom of the DMSO unit in **2**, can be best described as a distorted tetrahedral configuration due to the bending of the oxygen atom towards the methyl groups. Moreover, the S3–O2 bond length is reduced while it is extended for the S3–C bonds in comparison to that of free DMSO [46]. Bond lengths of the coordinated donor atoms around platinum increase in the order: Pt–O1 (2.018(10)) < Pt–S3 (2.191(3)) < Pt–S1 (2.258(3)) < Pt–Cl (2.353(4)). Additionally, the angle in the inner coordination sphere of complex **2** is unequal, in which it comes close to 90° for S3–Pt–Cl (90.56(13)°) and S1–Pt–S3 (88.62(13)°), is smaller for O1–Pt–Cl (85(3)°) and larger for O1–Pt–S1 (95.8(3)°). In the case of complex **6**, it comes higher than 90° for O1–Pd–S1 (96.22(5)°) and O2–Pd–S3 (95.97(5)°) whereas it is smaller than 90° for the angles O1–Pd–O2 (82.38(6)°) and S1–Pd–S3 (85.42(2)°). Coordination of all *O,S*-chelating ligands to the metal center in **2** and **6** results in elongation of the S1–C1 bond of complex **2** and S3–C20 bond of complex **6** as well as shortening of the C3–O1 bond in complex **2** and C22–O2 bond in complex **6**. This behavior is in agreement with the  $^{13}\text{C}\{^1\text{H}\}$  NMR data obtained for both complexes and consistent with those of *O,S*-chelating platinum(II) analogues [36–38]. The angles of the carbon framework are almost identical and hence confirm the delocalization of electrons in the six-membered chelating ring.

### ***Electrochemical studies***

In order to obtain more vision into the anodic electrochemistry of *O,S*-chelating complexes, cyclic voltammetry (CV) experiments were performed in 0.1 M CH<sub>2</sub>Cl<sub>2</sub>-[*n*-Bu<sub>4</sub>N][BF<sub>4</sub>] solutions. Representative CVs are given in Figure 3 for complexes **2** and **5** at a scan rate of 0.2 V/s since these complexes are only different in the alkyl substituent and hence give similar behavior.

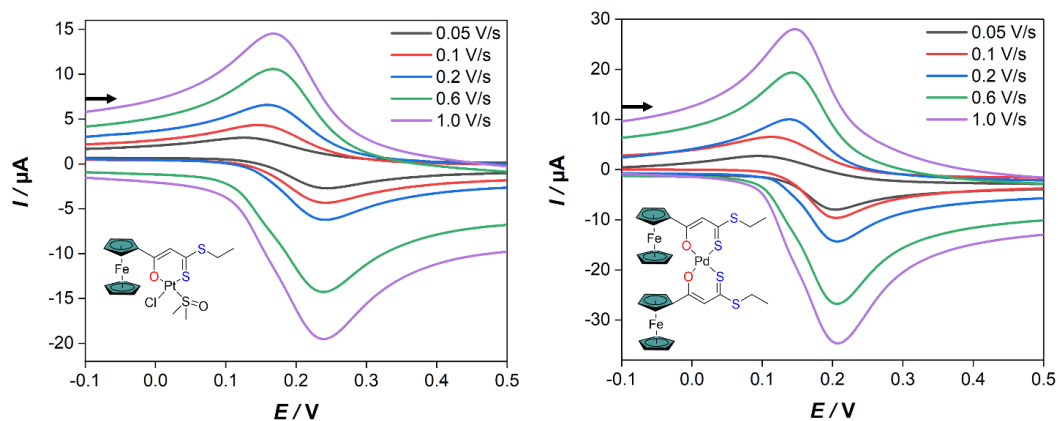


**Figure 3.** Cyclic voltammetry of 1.0 mM solutions of complexes **2** (left) and **5** (right) in  $\text{CH}_2\text{Cl}_2$ - $[n\text{-Bu}_4\text{N}][\text{BF}_4]$  (0.1 M) registered at a 0.2 V/s scan rate. The arrow indicates the scan direction. The potentials  $E$  are given in V and are referenced to the  $\text{Fc}^+/\text{Fc}$  couple.

On initiating the electrochemical scan in the anodic potential region between 0 and +1 V at a scan rate of 0.2 V/s, complexes **2** and **5** showed the appearance of a quasi-reversible oxidation peak at  $E_{1/2} = 0.20$  and 0.17 V, respectively as shown in Figure 3. These oxidation events could be assigned to the oxidation process of  $\text{Fe(II)} \rightarrow \text{Fe(III)}$  of the ferrocene moiety in accordance with the literature [29]. It is worth noting that even complex **5** containing two ferrocenyl moieties, its electrochemical behavior shows only one oxidation event ( $E_{1/2} = 0.17$  V) without splitting or even broadening of the wave. This suggests that simultaneous two-electron transfers at the same potential are occurred, and hence there is no significant electronic communication between the two ferrocenyl redox centers. This result is in accordance with the measurements carried out on similar reported analogous [29,47,48].

### **Biological activity**

Motivated by our results showing a high cytotoxic activity of  $\beta$ -hydroxy-dithiocinnamic acid derived palladium(II), platinum(II), ruthenium(II) and osmium(II) complexes [31-33, 38] we analyzed the ligands **HL1-3** and the complexes **1-6** for the anti-proliferative activity against the epithelial ovarian cancer cell lines A2780 and SKOV3 and their Cisplatin resistant subcultures (Tab. 1). Albeit the calculated  $\text{IC}_{50}$  values are more than one magnitude higher than  $\text{IC}_{50}$  values of Cisplatin or the aforementioned metal complexes the results enable insights into structure-activity-relationships. Several compounds show  $\text{IC}_{50}$  values outside the tested concentration range ( $> 100\mu\text{M}$ ), thus they should be evaluated as ineffective and calculated values are estimates only. However, the actual data confirm earlier

observations. Specifically,  $\beta$ -hydroxy-dithiocinnamic acid derived compounds are (i) not affected by the Cisplatin-resistance mechanisms and resistance factors (RF =  $IC_{50}$  resistant cells /  $IC_{50}$  sensitive cells) are smaller or equal than 1 and (ii) Pt(II)-compounds and free ligands with longer alkyl chains as substituent R show higher cytotoxic activity (Tab. 1) [31,38].

**Table 1.**  $IC_{50}$  values  $\pm$  SD of analyzed compounds [ $\mu$ M]

		A2780	A2780 Cis	RF A2780	Skov3	Skov3 Cis	RF Skov3	mean IC50
<b>Ligand</b>	<b>HL 1</b>	226.9 $\pm$ 81.2	780.1 $\pm$ 115.7	3.4	1831.2 $\pm$ 258.1	301.7 $\pm$ 65.5	0.2	785.0
	<b>HL 2</b>	183.5 $\pm$ 31.6	61.1 $\pm$ 14.6	0.3	289.4 $\pm$ 94.5	435.3 $\pm$ 105.1	1.5	242.3
	<b>HL 3</b>	124.1 $\pm$ 47.1	118.5 $\pm$ 39.2	1.0	195.2 $\pm$ 24.2	70.4 $\pm$ 16.2	0.4	127.0
		540.4 $\pm$ 100.5	118.1 $\pm$ 29.2	0.2	2509.7 $\pm$ 752.4	408.5 $\pm$ 103.2	0.2	894.2
<b>Pt complex</b>	<b>2</b>	37.8 $\pm$ 11.7	62.9 $\pm$ 21.4	1.7	149.0 $\pm$ 25.3	42.6 $\pm$ 19.2	0.3	73.1
	<b>3</b>	17.9 $\pm$ 4.8	58.6 $\pm$ 19.1	3.3	103.6 $\pm$ 31.6	46.8 $\pm$ 22.0	0.5	56.7
	<b>4</b>	970.5 $\pm$ 273.3	231.3 $\pm$ 35.9	0.2	1018.6 $\pm$ 328.9	424.0 $\pm$ 315.1	0.4	661.1
<b>Pd complex</b>	<b>5</b>	n.c.	n.c.		881.7 $\pm$ 215.6	1543.3 $\pm$ 485.1	0.5	677.5
	<b>6</b>	n.c.	n.c.		0	273.4 $\pm$ 76.1	0.2	908.4

(RF – resistance factor, n.c. – could not be calculated by regression analysis)

Regarding the new compounds we observed a higher activity of the Pt(II) compounds (**1-3**) in comparison to both the free ligands (**HL1-3**) and the Pd(II) complexes **4-6** (Tab. 1, Fig. 4). Altogether, this points to the specific contribution of the metal ion itself and to a reduced activity of the compounds with ferrocenyl-derivates of  $\beta$ -hydroxy-dithiocinnamic acid as ligands. Both Pt(II) and Pd(II) complexes with  $\beta$ -hydroxy-dithiocinnamic acid ligands exhibit a higher cytotoxic activity [31,38]. This may be caused by a different stability of the ferrocenyl-based compounds or steric effects inhibiting the binding to the target biomolecules (DNA, proteins).

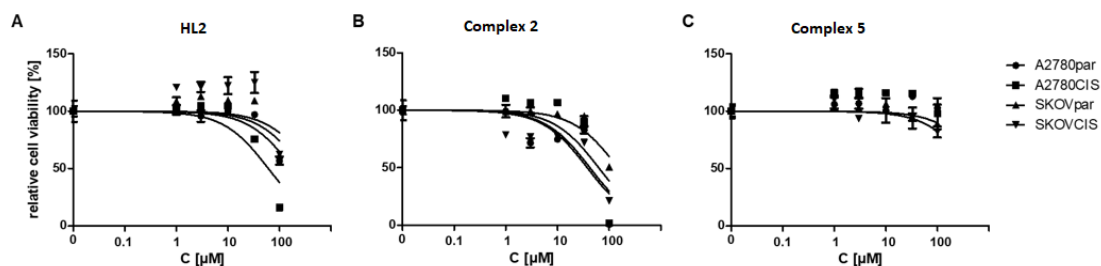


**Figure 4.** Exemplary dose-response curves for  $IC_{50}$  determination of the free ligand **HL2** (A), the Pt(II) complex **2** (B) and the Pd(II) complex **5** (C)

## Conclusion

This study elucidates the synthesis of  $\beta$ -hydroxy-dithioesters ferrocenyl derivatives **HL1-3** that used as proligands to react with the precursor complex *cis*-[PtCl<sub>2</sub>(DMSO)<sub>2</sub>] and bis(benzonitrile)palladium(II) chloride, respectively. The resulting heteroleptic platinum(II) and homoleptic palladium(II) complexes (**1-6**) bearing a conserved *O,S* binding moiety were fully characterized by use of <sup>1</sup>H, <sup>13</sup>C{<sup>1</sup>H}, and <sup>195</sup>Pt NMR as well as IR spectroscopy, mass spectrometry, elemental analysis, and X-ray crystallography for **2** and **6**. The influence of the ferrocene moiety on the redox behavior of complexes **2** and **5** (as representative example) was studied using cyclic voltammetry. As a result, both complexes display a quasi-reversible oxidation event at  $E_{1/2} = 0.20$  (for **2**) and 0.17 (for **5**) V. The cytotoxic activity of presented organo-metal complexes with  $\beta$ -hydroxy-dithioesters ferrocenyl derivatives as ligands is limited and reduced in comparison to the same compounds without the ferrocenyl substituent. However, structure-activity relationships are similar with an improved activity by longer alkyl rests.

## Experimental Section

### *Materials and Techniques*

All syntheses were carried out under an inert gas (nitrogen) atmosphere using the conventional Schlenk technique. The <sup>1</sup>H, <sup>13</sup>C{<sup>1</sup>H}, <sup>195</sup>Pt NMR spectra were recorded with a Bruker Avance 400 MHz spectrometer. Chemical shifts are given in parts per million with references to internal SiMe<sub>4</sub> (<sup>1</sup>H, <sup>13</sup>C{<sup>1</sup>H}). The IR spectra were recorded with a Bruker Equinox 55 spectrometer equipped with an ATR unit. Elemental analysis was performed with a Leco CHNS-932 apparatus. TLC was performed by using Merck TLC aluminum sheets (Silica gel 60 F254). Solvents from Fisher Scientific and other chemicals from Across and Aldrich were used without further purification. All solvents were dried and distilled prior to use according to standard methods. Compounds dimethyltrithiocarbonate (**A**), S,S-diethyltrithiocarbonate (**B**), S,S-dipropyltrithiocarbonate (**C**) and *cis*-[PtCl<sub>2</sub>(DMSO)<sub>2</sub>] were synthesized according to the literature procedure [40,43].

### *Structure Determinations*

The intensity data for the compounds were collected on a Nonius KappaCCD diffractometer using graphite-monochromated Mo-K $\alpha$  radiation. Data were corrected for Lorentz and polarization effects; absorption was taken into account on a semi-empirical basis using multiple-scans [49-51]. The structures were solved by direct methods (SHELXS) [52] and refined by full-matrix least squares techniques against Fo<sup>2</sup> SHELXL-2018) [53]. All hydrogen atoms were located by difference Fourier synthesis and refined isotropically. The crystal of **2** was a non-merohedral twin [54]. The twin law was 1.000 0.000 0.000) (-0.149 -1.000 0.000) -0.467 0.000 -1.000). The contribution of the main component was refined to 0.730(8). All non-hydrogen atoms were refined anisotropically [53]. MERCURY was used for structure representations [55].

### *Crystal Data for 2*

C<sub>17</sub>H<sub>21</sub>ClFeO<sub>2</sub>PtS<sub>3</sub>, Mr = 639.91 g mol<sup>-1</sup>, red-brown prism, size 0.082 x 0.044 x 0.042 mm<sup>3</sup>, triclinic, space group P  $\bar{1}$ , a = 7.1055(7), b = 11.8777(9), c = 12.8066(9) Å,  $\alpha$  = 112.261(5),  $\beta$  = 97.436(4),  $\gamma$  = 92.556(6)°, V = 986.69(14) Å<sup>3</sup>, T = -140 °C, Z = 2,  $\rho_{\text{calcd.}}$  = 2.154 g cm<sup>-3</sup>,  $\mu$  (Mo-K $\alpha$ ) = 82.78 cm<sup>-1</sup>, multi-scan, transmin: 0.5428, transmax: 0.7456, F(000) = 616, 4448 reflections in h(-9/9), k(-15/15), l(-16/16), measured in the range 2.906° ≤  $\Theta$  ≤ 27.482°, completeness  $\Theta_{\text{max}}$  = 98.5%, 4448 independent reflections, R<sub>int</sub> = 0.0495, 3943 reflections with F<sub>o</sub> > 4 $\sigma$ (F<sub>o</sub>), 230 parameters, 30 restraints, R<sub>1obs</sub> = 0.0728, wR<sub>2obs</sub> = 0.1964, R<sub>1all</sub> = 0.0829, wR<sub>2all</sub> = 0.2051, GOOF = 1.128, largest difference peak and hole: 6.203 / -5.815 e Å<sup>-3</sup>.

### *Crystal Data for 6*

C<sub>32</sub>H<sub>34</sub>Fe<sub>2</sub>O<sub>2</sub>PdS<sub>4</sub>, Mr = 796.93 g mol<sup>-1</sup>, red-brown prism, size 0.108 x 0.102 x 0.098 mm<sup>3</sup>, orthorhombic, space group P c c n, a = 17.9485(3), b = 27.1924(4), c = 12.7899(2) Å, V = 6242.27(17) Å<sup>3</sup>, T = -140 °C, Z = 8,  $\rho_{\text{calcd.}}$  = 1.696 g cm<sup>-3</sup>,  $\mu$  (Mo-K $\alpha$ ) = 17.84 cm<sup>-1</sup>, multi-scan, transmin: 0.6462, transmax: 0.7456, F(000) = 3232, 46577 reflections in h(-23/23), k(-35/35), l(-16/16), measured in the range 2.094° ≤  $\Theta$  ≤ 27.478°, completeness  $\Theta_{\text{max}}$  = 99.8%, 7151 independent reflections, R<sub>int</sub> = 0.0542, 6411 reflections with F<sub>o</sub> > 4 $\sigma$ (F<sub>o</sub>), 372 parameters, 0 restraints, R<sub>1obs</sub> =

0.0296,  $wR^2_{\text{obs}} = 0.0542$ ,  $R1_{\text{all}} = 0.0363$ ,  $wR^2_{\text{all}} = 0.0566$ , GOOF = 1.090, largest difference peak and hole: 0.522 / -0.655 e Å<sup>-3</sup>.

### ***Electrochemistry***

Corrections for the  $iR$  drop were performed for all experiments. Cyclic voltametric measurements were conducted in three-electrode technique [glassy carbon disk (diameter = 1.6 mm) as working electrode, Ag/Ag<sup>+</sup> in MeCN as reference electrode, Pt wire as counter electrode] using a Reference 600 Potentiostat (Gamry Instruments). All experiments were performed in CH<sub>2</sub>Cl<sub>2</sub> solutions (concentration of the complexes 1.0 mM) containing 0.1 M [*n*-Bu<sub>4</sub>N][BF<sub>4</sub>] at room temperature. The solutions were purged with N<sub>2</sub> and a stream of it was maintained over the solutions during the measurements. The vitreous carbon disk was polished on a felt tissue with alumina before each measurement. All potential values reported in this paper are referenced to the potential of the ferrocenium/ferrocene (Fc<sup>+</sup>/Fc) couple.

### ***IC<sub>50</sub> determination***

Cancer cell lines were cultured under standard conditions (5 % CO<sub>2</sub>, 37 °C, 90 % humidity) in RPMI medium supplemented with 10 % FCS, 100 U/ml penicillin and 100 µg/ml streptomycin (Life Technologies, Germany). The tested compounds were dissolved in DMSO. Determinations of IC<sub>50</sub> values were carried out using the CellTiter96 non-radioactive proliferation assay (MTT assay, Promega). After seeding 5000 cells per well in a 96 well plate cells were allowed to attach for 24 h and were incubated for 48 h with different concentrations of the substances ranging from 0 to 100 µM (0, 1, 3, 10, 33, 100 µM). Each measurement was done in triplicate and repeated 3-times. The proportion of live cells was quantified by the MTT assay and after background subtraction relative values compared to the mean of medium controls were calculated. Non-linear regression analyses applying the Hill-slope were run in GraphPad 5.0 software.

### ***General procedure for the synthesis of the free ligands HLI-3.***

Acetylferrocene (1.69 g, 7.4 mmol) in DMF (10 mL) was added slowly to a suspension of NaH (0.442 g, 18.4 mmol) in DMF:hexane mixture (10:1; 11 mL) in an ice bath under a N<sub>2</sub> atmosphere. The reaction mixture was stirred for 1 h then a

solution of S,S-dimethyltrithiocarbonate (1.02 g, 7.4 mmol) (for **HL1**), S,S-diethyltrithiocarbonate (1.23 g, 7.4 mmol) (for **HL2**) and S,S-dipropyltrithiocarbonate (1.44 g, 7.4 mmol) (for **HL3**) in 3 ml hexane was added slowly to the mixture, respectively. After that, the mixture was stirred overnight at room temperature. The reaction mixture was poured into saturated aqueous ammonium chloride solution (40 mL), and the product was extracted three times with 50 mL portions of dichloromethane, washed with brine solution and water, and dried over anhydrous Na<sub>2</sub>SO<sub>4</sub>. The products obtained was purified via silica gel chromatography using hexane:ethyl acetate (6:1) as the eluent to collect crystalline shiny violet solid.

*Methyl 3-hydroxy-3-ferroceneprop-2-enedithioate (HL1)*

violet solid; yield; 0.89 g (38%); mp 96 °C; R<sub>f</sub> = 0.8 (hexane/EtOAc, 6:1); <sup>1</sup>H NMR (400 MHz, CDCl<sub>3</sub>): δ = 15.08 (s, 1H, OH), 6.61 (s, 1 H), 4.82 (s, 2 H, Fc-H), 4.55 (s, 2 H, Fc-H), 4.22 (s, 5 H, Fc-H), 2.62 (s, 3 H). <sup>13</sup>C {<sup>1</sup>H} NMR (100 MHz, CDCl<sub>3</sub>): δ = 212.3, 176.4, 107.5, 72.4, 70.7, 68.3, 16.7. FTIR (KBr): 3090, 1603, 1485, 1256, 757 cm<sup>-1</sup>. Elemental analysis for FeC<sub>14</sub>H<sub>14</sub>S<sub>2</sub>O: C 52.83, H 4.43, S 20.15; found: C 52.52; H 4.60; S 20.28. DEI-MS: m/z = 318 [M]<sup>+</sup>

*Ethyl 3-hydroxy-3-ferroceneprop-2-enedithioate (HL2)*

violet solid; yield: 1.67 g (68%); m.p 74 °C; R<sub>f</sub> = 0.8 (hexane/EtOAc, 6:1). <sup>1</sup>H NMR (400 MHz, CDCl<sub>3</sub>): δ = 15.14 (s, 1H, OH), 6.56 (s, 1 H), 4.81 (s, 2 H, Fc-H), 4.54 (s, 2 H, Fc-H), 4.22 (s, 5 H, Fc-H), 3.25 (q, J = 7.52 Hz, 2 H), 1.38 (t, J = 7.48 Hz, 3H). <sup>13</sup>C {<sup>1</sup>H} NMR (100 MHz, CDCl<sub>3</sub>): δ = 211.5, 176.8, 107.5, 73.2, 70.7, 68.3, 27.7, 13.2. FTIR (solid): 3089, 1601, 1489, 1255, 755 cm<sup>-1</sup>. Elemental analysis for FeC<sub>15</sub>H<sub>16</sub>S<sub>2</sub>O: C, 54.22; H, 4.85; S, 19.30; found: C, 54.73; H, 4.94; S, 19.31. DEI-MS: m/z = 332 [M]<sup>+</sup>.

*Propyl 3-hydroxy-3-ferroceneprop-2-enedithioate (HL3)*

violet solid; yield: 1.85 g (72%); m.p 55 °C; R<sub>f</sub> = 0.8 (hexane/EtOAc, 6:1). <sup>1</sup>H NMR (400 MHz, CDCl<sub>3</sub>): δ = 15.11 (s, 1H, OH), 6.58 (s, 1 H), 4.81 (s, 2 H, Fc-H), 4.54 (s, 2 H, Fc-H), 4.22 (s, 5 H, Fc-H), 3.21 (t, J = 6.9 Hz, 2 H), 1.76 (m, 2 H), 1.06 (t, J = 7.0 Hz, 3H). <sup>13</sup>C {<sup>1</sup>H} NMR (100 MHz, CDCl<sub>3</sub>): δ = 211.8, 176.6, 107.6, 72.2, 70.5, 68.2, 35.2, 21.7, 13.8. FTIR (KBr): 3090, 1602, 1485, 1256, 750 cm<sup>-1</sup>. Elemental

analysis for  $\text{FeC}_{16}\text{H}_{18}\text{S}_2\text{O}$ : C, 55.49; H, 5.24; S, 18.59; found: C, 55.61; H, 5.34; S, 19.01. DEI-MS:  $m/z = 346$   $[\text{M}]^+$ .

### ***General procedure for the Synthesis of complexes 1-3***

Compounds **HL1-3** (1 equiv.) (180, 98.3 and 123 mg, respectively) in  $\text{CH}_2\text{Cl}_2$  (10 mL) was added slowly and separately to a stirred solution of *cis*- $[\text{PtCl}_2(\text{DMSO})_2]$ , (1 equiv.) (238, 125 and 150 mg, respectively) in  $\text{CH}_2\text{Cl}_2$  (10 mL). The resulting solution was stirred for 30 min. The yellow solution turned deep red, and the solvent was removed under reduced pressure. The residue was purified by short column chromatography using cyclohexane/ethyl acetate (5:1) as eluent. The complexes were collected from the second fraction and collected as a red solid.

#### ***[Pt(L1)(DMSO)Cl] (1)***

Red solid; yield: 241 mg (69%);  $R_f = 0.2$  (hexane/EtOAc, 5:1).  $^1\text{H}$  NMR (400 MHz,  $\text{CDCl}_3$ ):  $\delta = 6.68$  (s, 1 H), 4.88 (s, 2 H, Fc-H), 4.53 (s, 2 H, Fc-H), 4.20 (s, 5 H, Fc-H), 3.63 (s w/Pt satellites,  $^3J_{\text{Pt-H}} = 21.72$  Hz, 6H,  $\text{CH}_3$  (DMSO)) 2.63 (s, 3 H).  $^{13}\text{C}\{^1\text{H}\}$  NMR (100 MHz,  $\text{CDCl}_3$ ):  $\delta = 181.6$ , 173.5, 111.6, 72.6, 70.6, 69.7, 46.8 (s w/Pt satellites,  $^2J_{\text{Pt-C}} = 59.6$  Hz,  $\text{CH}_3$ (DMSO)), 17.3.  $^{195}\text{Pt}$  NMR (85.7 MHz,  $\text{CDCl}_3$ ) = -3123.5 ppm. FTIR (solid): 3091, 1600, 1484, 1252, 750  $\text{cm}^{-1}$ . Elemental analysis for  $\text{PtFeC}_{16}\text{H}_{19}\text{S}_3\text{O}_2\text{Cl}$ : C, 30.70; H, 3.06; S, 15.36. Found: C, 30.46; H, 3.26; S, 15.43. ESI-MS: (positive mode  $m/z$ ) = 644  $[\text{M}+\text{H}_2\text{O}+\text{H}]^+$ .

#### ***[Pt(L2)(DMSO)Cl] (2)***

Red solid; yield: 135.70 mg (72%);  $R_f = 0.2$  (hexane/EtOAc, 5:1).  $^1\text{H}$  NMR (400 MHz,  $\text{CDCl}_3$ ):  $\delta = 6.68$  (s, 1 H), 4.89 (s, 2 H, Fc-H), 4.54 (s, 2 H, Fc-H), 4.20 (s, 5 H, Fc-H), 3.63 (s w/Pt satellites,  $^3J_{\text{Pt-H}} = 22.12$  Hz, 6H,  $\text{CH}_3$  (DMSO)), 3.23 (q,  $J = 7.56$  Hz, 2 H), 1.43 (t,  $J = 7.40$  Hz, 3H).  $^{13}\text{C}\{^1\text{H}\}$  NMR (100 MHz,  $\text{CDCl}_3$ ):  $\delta = 181.8$ , 172.6, 111.8, 72.6, 70.6, 69.7, 46.8 (s w/Pt satellites,  $^2J_{\text{Pt-C}} = 57$  Hz,  $\text{CH}_3$ (DMSO)), 28.4, 13.4.  $^{195}\text{Pt}$  NMR (85.7 MHz,  $\text{CDCl}_3$ ) = -3124.2 ppm. FTIR (solid): 3090, 1601, 1486, 1254, 752  $\text{cm}^{-1}$ . Elemental analysis for  $\text{PtFeC}_{17}\text{H}_{21}\text{S}_3\text{O}_2\text{Cl}$ : C, 31.91; H, 3.31; S, 15.03. Found: C, 31.88; H, 3.24; S, 15.32. ESI-MS: (positive mode  $m/z$ ) = 658  $[\text{M}+\text{H}_2\text{O}+\text{H}]^+$ .



*[Pt(L3)(DMSO)Cl] (3)*

Red solid; yield: 165 mg (72%); R<sub>f</sub> = 0.2 (hexane/EtOAc, 5:1). <sup>1</sup>H NMR (400 MHz, CDCl<sub>3</sub>): δ = 6.69 (s, 1 H), 4.88 (s, 2 H, Fc-H), 4.53 (s, 2 H, Fc-H), 4.21 (s, 5 H, Fc-H), 3.63 (s w/Pt satellites, <sup>3</sup>J<sub>Pt-H</sub> = 22.24 Hz, 6H, CH<sub>3</sub> (DMSO)), 3.19 (t, J = 7.4 Hz, 2 H), 1.81 (m, 2 H), 1.08 (t, J = 7.32 Hz, 3H). <sup>13</sup>C{<sup>1</sup>H} NMR (100 MHz, CDCl<sub>3</sub>): δ = 181.7, 172.9, 111.9, 72.6, 70.6, 69.7, 46.8 (s w/Pt satellites, <sup>2</sup>J<sub>Pt-C</sub> = 58 Hz, CH<sub>3</sub>(DMSO)), 35.9, 21.8, 13.5. <sup>195</sup>Pt NMR (85.7 MHz, CDCl<sub>3</sub>) = -3121.4 ppm. FTIR (solid): 3091, 1600, 1488, 1254, 755 cm<sup>-1</sup>. Elemental analysis for PtFeC<sub>18</sub>H<sub>23</sub>S<sub>3</sub>O<sub>2</sub>Cl: C, 33.06; H, 3.54; S, 14.71. Found: C, 33.37; H, 3.73; S, 14.54. ESI-MS: (positive mode *m/z*) = 672 [M+H<sub>2</sub>O+H]<sup>+</sup>.

***General procedure for the Synthesis of complexes 4-6.***

Bis(benzonitrile)palladium(II) chloride (191 mg, 0.50 mmol) in acetonitrile solution was added dropwise to a stirred solution of the corresponding ligand **HL1-3** (1.0 mmol) (318, 332 and 346 mg, respectively) and sodium acetate trihydrate (136 mg, 1.0 mmol) in 15 mL acetonitrile. The reaction mixture was stirred overnight at room temperature. The red-volatile precipitated were filtered, followed by extraction with diethyl ether to afford the complexes **4-6** as red-volatile crystalline solid.

*[Pd(L1)<sub>2</sub>] (4)*

Red-volatile crystalline solids; yield: 186 mg (50%). <sup>1</sup>H NMR (400 MHz, CDCl<sub>3</sub>): δ = 6.71 (s, 2 H), 4.90 (t, J = 1.9 Hz, Fc-H, 4H), 4.55 (t, J = 1.9 Hz, Fc-H, 4H), 4.24 (s, 10 H, Fc-H), 2.65 (s, 6 H). <sup>13</sup>C{<sup>1</sup>H} NMR (100 MHz, CDCl<sub>3</sub>): δ = 184.5, 175.4, 111.5, 72.1, 70.4, 69.4, 17.3. FTIR (solid): 3091, 1600, 1484, 1252, 755 cm<sup>-1</sup>. Elemental analysis for PdFe<sub>2</sub>C<sub>28</sub>H<sub>26</sub>S<sub>4</sub>O<sub>2</sub>: C, 45.39; H, 3.54; S, 17.31. Found: C, 45.14; H, 3.50; S, 17.01. ESI-MS: (positive mode *m/z*) = 762.9 [M+Na]<sup>+</sup>.

*[Pd(L2)<sub>2</sub>] (5)*

Red-volatile crystalline solids; yield: 211.85 mg (55%). <sup>1</sup>H NMR (400 MHz, CDCl<sub>3</sub>): δ = 6.71 (s, 2 H), 4.89 (t, J = 1.9 Hz, Fc-H, 4H), 4.54 (t, J = 1.9 Hz, Fc-H, 4H), 4.24 (s, 10 H, Fc-H), 3.23 (q, J = 7.52 Hz, 4 H), 1.42 (t, J = 7.50 Hz, 6H). <sup>13</sup>C{<sup>1</sup>H} NMR (100 MHz, CDCl<sub>3</sub>): δ = 184.7, 174.5, 111.9, 72.1, 70.4, 69.4, 28.8, 13.9. FTIR (solid): 3087, 1600, 1484, 1252, 759 cm<sup>-1</sup>. Elemental analysis for PdFe<sub>2</sub>C<sub>28</sub>H<sub>26</sub>S<sub>4</sub>O<sub>2</sub>: C, 45.39; H, 3.54; S, 17.31. Found: C, 45.14; H, 3.50; S, 17.01. ESI-MS: (positive mode *m/z*) = 762.9 [M+Na]<sup>+</sup>.

PdFe<sub>2</sub>C<sub>30</sub>H<sub>30</sub>S<sub>4</sub>O<sub>2</sub>: C, 46.86; H, 3.93; S, 16.68. Found: C, 47.04; H, 3.92; S, 16.83. ESI-MS: (positive mode  $m/z$ ) = 790.9 [M+Na]<sup>+</sup>.

### *[Pd(L3)<sub>2</sub>] (6)*

Red-volatile crystalline solids; yield: 216.52 mg (54%). <sup>1</sup>H NMR (400 MHz, CDCl<sub>3</sub>): δ = 6.71 (s, 2 H), 4.89 (t, J = 1.9 Hz, Fc-H, 4H), 4.54 (t, J = 1.9 Hz, Fc-H, 4H), 4.23 (s, 10 H, Fc-H), 3.19 (t, J = 7.32 Hz, 4 H), 1.80 (m, 4 H), 1.08 (t, J = 7.36 Hz, 6H). <sup>13</sup>C {<sup>1</sup>H} NMR (100 MHz, CDCl<sub>3</sub>): δ = 184.7, 174.7, 111.9, 72.1, 70.4, 69.4, 36, 22.3, 13.6. FTIR (solid): 3091, 1600, 1484, 1252, 748 cm<sup>-1</sup>. Elemental analysis for PdFe<sub>2</sub>C<sub>32</sub>H<sub>34</sub>S<sub>4</sub>O<sub>2</sub>: C, 48.22; H, 4.29; S, 16.09. Found: C, 48.18; H, 4.23; S, 16.21. ESI-MS: (positive mode  $m/z$ ) = 818.80 [M+Na]<sup>+</sup>.

### **Acknowledgments**

M.K.F. is grateful to the Katholischer Akademischer Ausländer-Dienst (KAAD) for a Ph.D. scholarship. The authors would further like to thank Umicore AG & Co. KG Hanau-Wolfgang, Germany for the donation of K<sub>2</sub>PtCl<sub>4</sub>.

### **Supporting Information available**

Crystallographic data (excluding structure factors) has been deposited with the Cambridge Crystallographic Data Centre as supplementary publication CCDC-2169443 for **2**, and CCDC-2169444 for **6**. Copies of the data can be obtained free of charge on application to CCDC, 12 Union Road, Cambridge CB2 1EZ, UK [E- mail: [deposit@ccdc.cam.ac.uk](mailto:deposit@ccdc.cam.ac.uk)].

### **Disclosure statement**

No potential conflict of interest was reported by the author(s).

### **References**

- [1] Guo Z, Sadler PJ. Metals in Medicine. *Angew Chem Int Ed.* 1999;38(11):1512-1531.
- [2] Chen X, Wu Y, Dong H, et al. Platinum-Based Agents for Individualized Cancer Treatment. *Curr Mol Med.* 2013;13(10):1603-1612
- [3] Mavligit GM, Zukwiski AA, Ellis LM, et al. Gastrointestinal leiomyosarcoma metastatic to the liver. Durable tumor regression by hepatic

- chemoembolization infusion with cisplatin and vinblastine. *Cancer*. 1995;75(8):2083-2088.
- [4] Dasari S, Bernard Tchounwou P. Cisplatin in cancer therapy: Molecular mechanisms of action. *Eur J Pharmacol*. 2014;740:364-378.
- [5] Muggia FM, Bonetti A, Hoeschele JD, et al. Platinum Antitumor Complexes: 50 Years Since Barnett Rosenberg's Discovery. *J Clin Oncol*. 2015;33(35):4219-26.
- [6] Messori L, Merlino A. Cisplatin binding to proteins: A structural perspective. *Coord Chem Rev*. 2016;315:67-89.
- [7] Dilruba S, Kalayda GV. Platinum-based drugs: past, present and future. *Cancer Chemother Pharmacol*. 2016;77(6):1103-24.
- [8] Arany I, Safirstein RL. Cisplatin nephrotoxicity. *Semin Nephrol*. 2003;23(5):460-464.
- [9] Oun R, Moussa YE, Wheate NJ. The side effects of platinum-based chemotherapy drugs: a review for chemists. *Dalton trans*. 2018;47(19):6645-6653.
- [10] Reedijk J. Platinum Anticancer Coordination Compounds: Study of DNA Binding Inspires New Drug Design. *Eur J Inorg Chem*. 2009;2009(10):1303-1312.
- [11] Amable L. Cisplatin resistance and opportunities for precision medicine. *Pharmacol Res*. 2016;106:27-36.
- [12] El Arbi M, Pigeon P, Top S, et al. Evaluation of bactericidal and fungicidal activity of ferrocenyl or phenyl derivatives in the diphenyl butene series. *J Organomet Chem*. 2011;696(5):1038-1048.
- [13] Patra M, Gasser G, Metzler-Nolte N. Small organometallic compounds as antibacterial agents. *Dalton trans*. 2012;41(21):6350-6358.
- [14] Braga SS, Silva AMS. A New Age for Iron: Antitumoral Ferrocenes. *Organometallics*. 2013;32(20):5626-5639.
- [15] Osella D, Ferrali M, Zanello P, et al. On the mechanism of the antitumor activity of ferrocenium derivatives. *Inorganica Chim Acta*. 2000;306(1):42-48.
- [16] Top S, Tang J, Vessières A, et al. Ferrocenyl hydroxytamoxifen: a prototype for a new range of oestradiol receptor site-directed cytotoxics. *Chem Commun*. 1996(8):955-956.

- [17] Top S, Vessières A, Cabestaing C, et al. Studies on organometallic selective estrogen receptor modulators. (SERMs) Dual activity in the hydroxyferrocifen series. *J Organomet Chem.* 2001;637-639:500-506.
- [18] Top S, Vessières A, Leclercq G, et al. Synthesis, Biochemical Properties and Molecular Modelling Studies of Organometallic Specific Estrogen Receptor Modulators (SERMs), the Ferrocifens and Hydroxyferrocifens: Evidence for an Antiproliferative Effect of Hydroxyferrocifens on both Hormone-Dependent and Hormone-Independent Breast Cancer Cell Lines. *Chem - Eur J.* 2003;9(21):5223-5236.
- [19] Ferreira AP, da Silva JLF, Duarte MT, et al. Synthesis and Characterization of New Organometallic Benzo[b]thiophene Derivatives with Potential Antitumor Properties. *Organometallics.* 2009;28(18):5412-5423.
- [20] Plazuk D, Vessières A, Hillard EA, et al. A [3]Ferrocenophane Polyphenol Showing a Remarkable Antiproliferative Activity on Breast and Prostate Cancer Cell Lines. *J Med Chem.* 2009;52(15):4964-4967.
- [21] Pigeon P, Top S, Vessières A, et al. A new series of ferrocifen derivatives, bearing two aminoalkyl chains, with strong antiproliferative effects on breast cancer cells. *New J Chem.* 2011;35(10):2212-2218.
- [22] Młostoń G, Hamera-Fałdyga R, Celeda M, et al. Efficient synthesis of ferrocifens and other ferrocenyl-substituted ethylenes via a 'sulfur approach'. *Org Biomol Chem.* 2018;16(23):4350-6.
- [23] Rajput J, Moss JR, Hutton AT, et al. Synthesis, characterization and cytotoxicity of some palladium(II), platinum(II), rhodium(I) and iridium(I) complexes of ferrocenylpyridine and related ligands. Crystal and molecular structure of trans-dichlorobis(3-ferrocenylpyridine)palladium(II). *J Organomet Chem.* 2004;689(9):1553-1568.
- [24] Schulz J, Renfrew AK, Císařová I, et al. Synthesis and anticancer activity of chalcogenide derivatives and platinum(II) and palladium(II) complexes derived from a polar ferrocene phosphanyl-carboxamide. *Appl Organomet Chem.* 2010;24(5):392-397.
- [25] Gadre S, Manikandan M, Duari P, et al. A Rationally Designed Bimetallic Platinum (II)-Ferrocene Antitumor Agent Induces Non-Apoptotic Cell Death and Exerts in Vivo Efficacy. *Chem - Eur J.* 2022;28(46):e202201259.

- [26] Ma L, Li L, Zhu G. Platinum-containing heterometallic complexes in cancer therapy: advances and perspectives. *Inorg Chem Front.* 2022;9(11):2424-53.
- [27] Xu SD, Wu XH. Bimetallic DppfM(II) (M = Pt and Pd) dithiocarbamate complexes: Synthesis, characterization, and anticancer activity. *J Chem Res.* 2019;43(9-10):437-42.
- [28] Zhang Z, Du G, Gong G, et al. A novel ferrocene-palladium metal complex: synthesis, single crystal structure, in vitro cytotoxicity study and molecular docking. *J Mol Struct.* 2021;1232:130021.
- [29] Nieto D, González-Vadillo AM, Bruña S, et al. Heterometallic platinum(ii) compounds with  $\beta$ -aminoethylferrocenes: synthesis, electrochemical behaviour and anticancer activity. *Dalton trans.* 2012;41(2):432-441.
- [30] Farh MK, Gruschwitz FV, Ziegenbalg N, et al. Dual Function of  $\beta$ -Hydroxy Dithiocinnamic Esters: RAFT Agent and Ligand for Metal Complexation. *Macromol Rapid Commun.* 2022;(n/a):2200428.
- [31] Hildebrandt J, Häfner N, Görls H, et al. Novel Nickel(II), Palladium(II), and Platinum(II) Complexes with O,S Bidendate Cinnamic Acid Ester Derivatives: An In Vitro Cytotoxic Comparison to Ruthenium(II) and Osmium(II) Analogues. *Int J Mol Sci [Internet].* 2022; 23(12).
- [32] Hildebrandt J, Häfner N, Kritsch D, et al. Highly Cytotoxic Osmium(II) Compounds and Their Ruthenium(II) Analogues Targeting Ovarian Carcinoma Cell Lines and Evading Cisplatin Resistance Mechanisms. *Int J Mol Sci [Internet].* 2022; 23(9).
- [33] Hildebrandt J, Görls H, Häfner N, et al. Unusual mode of protein binding by a cytotoxic  $\pi$ -arene ruthenium(ii) piano-stool compound containing an O,S-chelating ligand. *Dalton trans.* 2016;45(31):12283-12287.
- [34] Schubert K, Alpermann T, Niksch T, et al. Synthese und Charakterisierung funktionalisierter  $\beta$ -Hydroxydithiozimsäuren und deren Ester. Komplexchemisches Verhalten gegenüber Nickel(II), Palladium(II) und Platin(II). *Z Anorg Allg Chem* 2006;632(6):1033-1042.
- [35] Schubert K, Saumweber R, Görls H, et al. Funktionalisierte  $\beta$ -Hydroxydithiozimsäurederivate als Liganden. Kristallstrukturanalyse von 4'-Hydroxy- $\beta$ -hydroxydithiozimsäuremethylester. *Z Anorg Allg Chem.* 2003;629(12-13):2091-2096.

- [36] Mügge C, Marzo T, Massai L, et al. Platinum(II) Complexes with O,S Bidentate Ligands: Biophysical Characterization, Antiproliferative Activity, and Crystallographic Evidence of Protein Binding. *Inorg Chem.* 2015;54(17):8560-8570.
- [37] Mügge C, Liu R, Görls H, et al. Novel platinum(ii) compounds with O,S bidentate ligands: synthesis, characterization, antiproliferative properties and biomolecular interactions. *Dalton trans.* 2014;43(8):3072-3086.
- [38] Hildebrandt J, Häfner N, Görls H, et al. Platinum(ii) O,S complexes as potential metallodrugs against Cisplatin resistance. *Dalton trans.* 2016;45(47):18876-18891.
- [39] van Staveren DR, Metzler-Nolte N. Bioorganometallic Chemistry of Ferrocene. *Chem Rev.* 2004;104(12):5931-5986.
- [40] Aoyagi N, Ochiai B, Mori H, et al. Mild and Efficient One-Step Synthesis of Trithiocarbonates Using Minimum Amount of CS<sub>2</sub>. *Synlett.* 2006;2006(04):0636-0638.
- [41] Singh PP, Yugandar S, Kumar SV, et al. Synthesis of Novel Five- and Six-Membered Ferrocene-Containing Heterocycles and Heteroaromatics via Cyclocondensation of 1-Ferrocenyl-3,3-bis(methylthio)prop-2-en-1-one with Various Bifunctional Nucleophiles. *Synthesis.* 2017;49(12):2700-2710.
- [42] Ahamed BN, Arunachalam M, Ghosh P. Thiomethoxychalcone-Functionalized Ferrocene Ligands as Selective Chemodosimeters for Mercury(II): Single-Crystal X-ray Structural Signature of the [Hg<sub>8</sub>(μ<sub>8</sub>-S)(SCH<sub>3</sub>)<sub>12</sub>]<sub>2+</sub> Cluster. *Inorg Chem.* 2010;49(10):4447-4457.
- [43] Price JH, Williamson AN, Schramm RF, et al. Palladium(II) and platinum(II) alkyl sulfoxide complexes. Examples of sulfur-bonded, mixed sulfur- and oxygen-bonded, and totally oxygen-bonded complexes. *Inorg Chem.* 1972;11(6):1280-1284.
- [44] Fulmer GR, Miller AJM, Sherden NH, et al. NMR Chemical Shifts of Trace Impurities: Common Laboratory Solvents, Organics, and Gases in Deuterated Solvents Relevant to the Organometallic Chemist. *Organometallics.* 2010;29(9):2176-2179.
- [45] Chauhan RS, Cordes DB, Slawin AMZ, et al. Reactivity of hemilabile pyridyl- and methyl-substituted pyrimidylselenolates with [MCl<sub>2</sub>(dppf)]

- (M = Pd, pt; dppf = bis(diphenylphosphino)ferrocene). *Inorganica Chim Acta*. 2018;478:125-129.
- [46] McLain SE, Soper AK, Luzar A. Orientational correlations in liquid acetone and dimethyl sulfoxide: A comparative study. *J Chem Phys*. 2006;124(7):074502.
- [47] Mahrholdt J, Noll J, Korb M, et al. Isocyano- and cyanoferrocenes in the synthesis of palladium, gold and zinc complexes. *Inorganica Chim Acta*. 2022;534:120829.
- [48] Flanagan JB, Margel S, Bard AJ, et al. Electron transfer to and from molecules containing multiple, noninteracting redox centers. Electrochemical oxidation of poly(vinylferrocene). *J Am Chem Soc*. 1978;100(13):4248-4253.
- [49] Nonius BV. COLLECT, Data Collection Software. Netherlands, 1998.
- [50] Otwinowski Z, Minor W. Processing of X-ray diffraction data collected in oscillation mode. *Methods Enzymol*. 1997;276:307-326.
- [51] Krause L, Herbst-Irmer R, Sheldrick GM, et al. Comparison of silver and molybdenum microfocus X-ray sources for single-crystal structure determination. *J Appl Cryst*. 2015;48(1):3-10.
- [52] Sheldrick GM. A short history of SHELX. *Acta Cryst A*. 2008;64(1):112-122.
- [53] Sheldrick GM. SHELXT - Integrated space-group and crystal-structure determination. *Acta Cryst A*. 2015;71(1):3-8.
- [54] Spek AL. PLATON SQUEEZE: a tool for the calculation of the disordered solvent contribution to the calculated structure factors. *Acta Cryst C*. 2015;71(1):9-18.
- [55] Macrae CF, Edgington PR, McCabe P, et al. Mercury: visualization and analysis of crystal structures. *J Appl Cryst*. 2006;39(3):453-457.

# **Platinum(II) and palladium(II) complexes mediated by $\beta$ -hydroxy-dithioesters ferrocenyl derivatives: synthesis, characterization and Antiproliferative Activity.**

Micheal K. Farh,<sup>a,b</sup> Ikrame Louzi,<sup>a</sup> Hassan Abul-Futouh,<sup>c\*</sup> Helmar Görls,<sup>a</sup> Norman Häfner,<sup>d</sup> Ingo B. Runnebaum,<sup>d\*</sup> Wolfgang Weigand<sup>a,e\*</sup>

<sup>a</sup> *Department of Inorganic and Analytical Chemistry (IAAC), Friedrich Schiller University Jena, Humboldtstraße 8, 07743 Jena, Germany. [wolfgang.weigand@uni-jena.de](mailto:wolfgang.weigand@uni-jena.de).*

<sup>b</sup> *Department of Chemistry, Faculty of Science, Assiut University, Assiut 71515, Egypt.*

<sup>c</sup> *Department of Chemistry, Faculty of Science, The Hashemite University, P.O. Box 330127, Zarqa 13133, Jordan. [h.abulfutouh@hu.edu.jo](mailto:h.abulfutouh@hu.edu.jo).*

<sup>d</sup> *Department of Gynecology, Jena University Hospital- Friedrich Schiller University Jena, Am Klinikum 1, 07747 Jena, Germany. [norman.haefner@med.uni-jena.de](mailto:norman.haefner@med.uni-jena.de).*

<sup>e</sup> *Jena Center for Soft Matter (JCSM), Friedrich Schiller University Jena, Philosophenweg 7, 07743 Jena, Germany*



### Synthesis of S,S-dialkyltrithiocarbonate A-C

A mixture of CS<sub>2</sub> (0.391 g, 0.31 mL, 5.0 mmol) and Cs<sub>2</sub>CO<sub>3</sub> (1.63g, 5.0 mmol) in DMF (5 mL) was stirred at room temperature for 15 min until the formation of red solution, then a solution of Iodomethane (0.71g, 0.311 mL, 5.0 mmol), Iodoethane (0.78g, 0.402 mL, 5.0 mmol) and Iodopropane (0.85g, 0.487 mL, 5.0 mmol) in DMF (1 mL) was added for S,S-dimethyltrithiocarbonate, S,S-diethyltrithiocarbonate and S,S-dipropyltrithiocarbonate respectively. Stirring of the reaction mixture was continued for 24h. The reaction was quenched by pouring into ice-water. The product was extracted with n-pentene, dried over anhydrous Na<sub>2</sub>SO<sub>4</sub>, filtered, and evaporated to give NMR pure product.

S,S-dimethyltrithiocarbonate (**A**), Light yellow oil; yield: 1.28 g (37%); <sup>1</sup>H NMR (400 MHz, CDCl<sub>3</sub>) δ = 2.77 (s, 3H, SCH<sub>3</sub>), <sup>13</sup>C{<sup>1</sup>H} NMR (CDCl<sub>3</sub>) δ = 225.59 (C=S), 20.09 (SCH<sub>3</sub>).

S,S-diethyltrithiocarbonate (**B**), Light yellow oil; yield: 1.40 g (34%); <sup>1</sup>H NMR (400 MHz, CDCl<sub>3</sub>) δ= 3.30 (q, J = 7.5 Hz, 4 H, SCH<sub>2</sub>), 1.28 (t, J = 7.5 Hz, 6 H, CH<sub>3</sub>), <sup>13</sup>C{<sup>1</sup>H} NMR (CDCl<sub>3</sub>) δ= 224.21 (C=S), 31.10 (SCH<sub>2</sub>), 13.14 (CH<sub>3</sub>).

S,S-dipropyltrithiocarbonate (**C**), Light yellow oil; yield: 3.25 g (67%); <sup>1</sup>H NMR (400 MHz, CDCl<sub>3</sub>) δ= 3.27 (t, J = 7.5 Hz, 4H, SCH<sub>2</sub>), 1.67 (sext, 4H, -CH<sub>2</sub>), 0.95 (t, J = 7.5 Hz, 6 H, CH<sub>3</sub>); <sup>13</sup>C{<sup>1</sup>H} NMR (CDCl<sub>3</sub>) δ= 224.75 (C=S), 38.69 (SCH<sub>2</sub>), 21.61 (CH<sub>2</sub>), 13.49 (CH<sub>3</sub>).

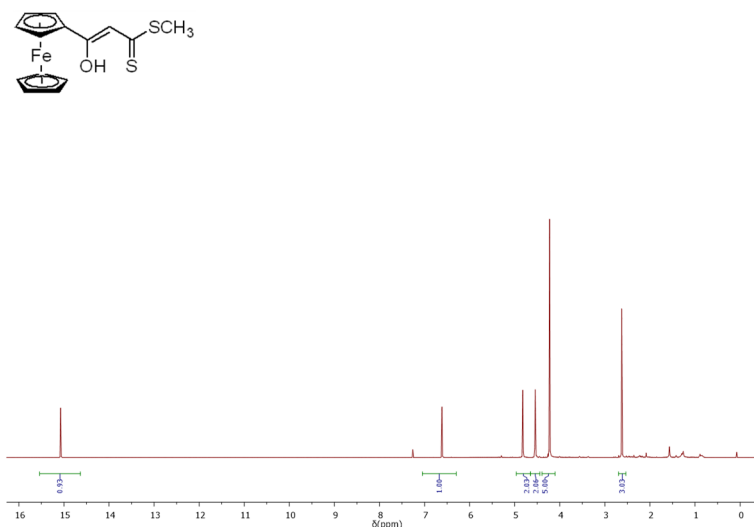


Figure S1. <sup>1</sup>H-NMR (400 MHz, CDCl<sub>3</sub>): (**HL1**)

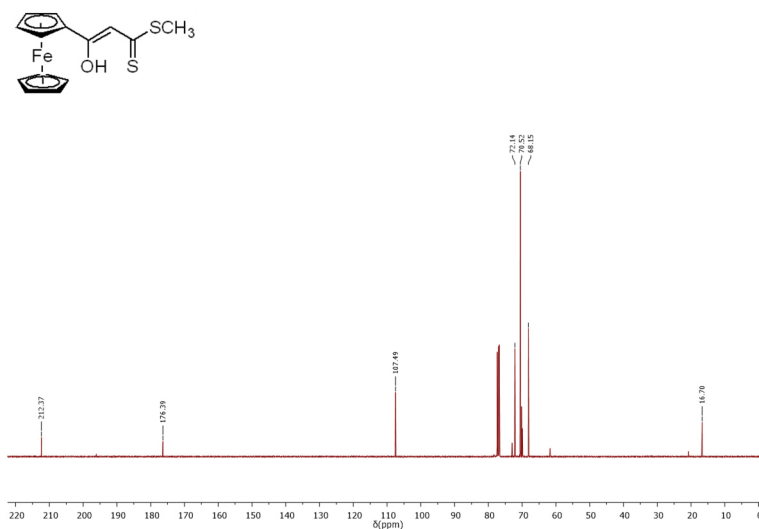


Figure S2.  $^{13}\text{C}\{^1\text{H}\}$  NMR (101 MHz,  $\text{CDCl}_3$ ): (HL1)

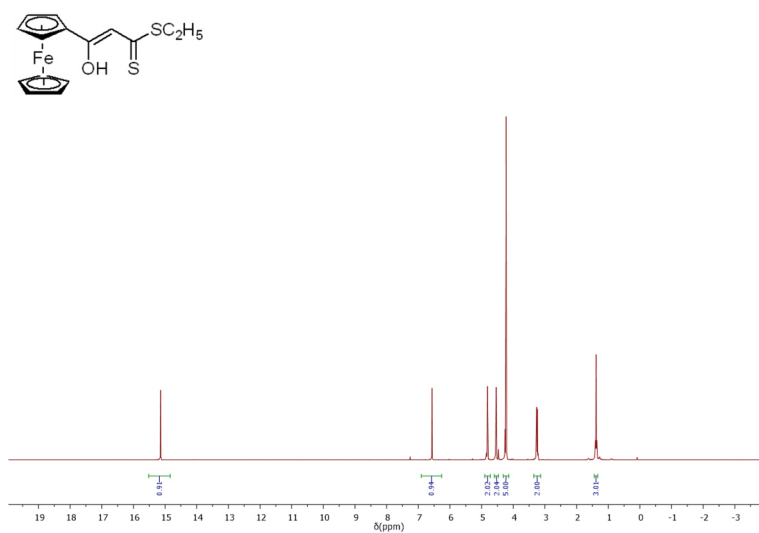


Figure S3.  $^1\text{H}$ -NMR (400 MHz,  $\text{CDCl}_3$ ): (HL2)

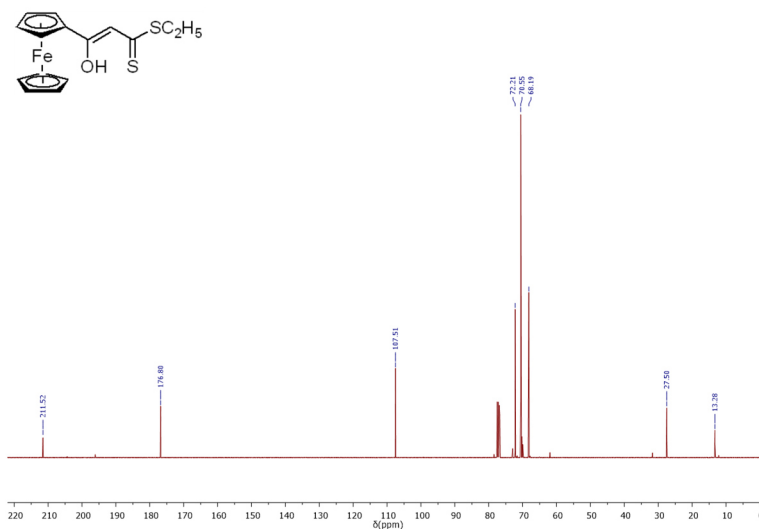


Figure S4.  $^{13}\text{C}\{^1\text{H}\}$  NMR (101 MHz,  $\text{CDCl}_3$ ): (HL2)

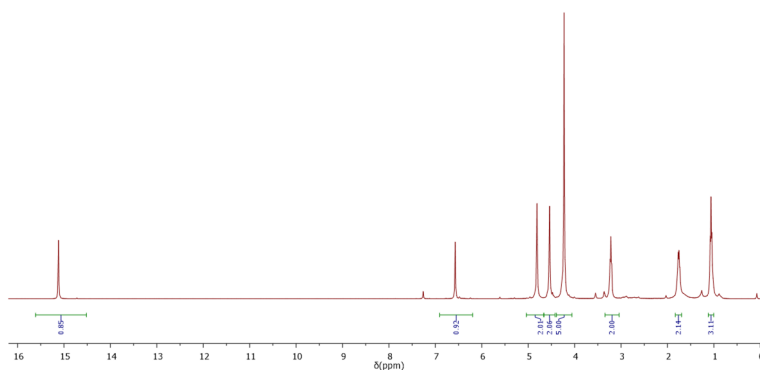
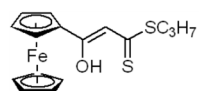


Figure S5.  $^1\text{H-NMR}$  (400 MHz,  $\text{CDCl}_3$ ): (**HL3**)

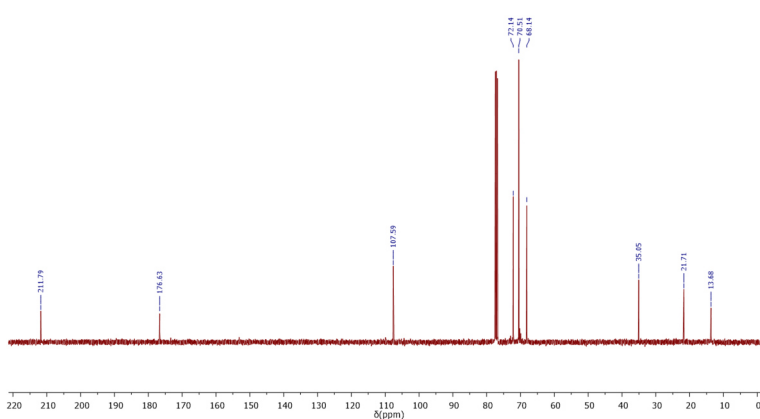
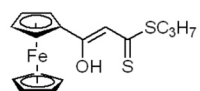


Figure S6.  $^{13}\text{C}\{^1\text{H}\}$  NMR (101 MHz,  $\text{CDCl}_3$ ): (**HL3**)

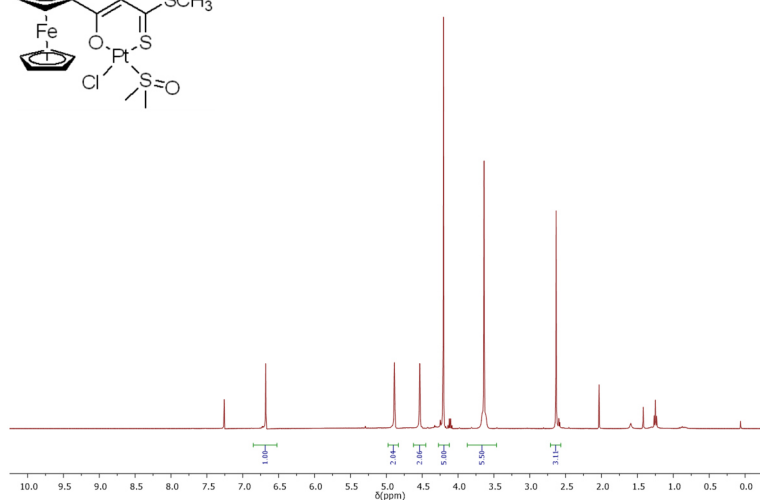
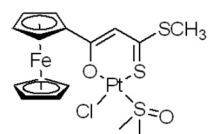


Figure S7.  $^1\text{H-NMR}$  (400 MHz,  $\text{CDCl}_3$ ):  $[\text{Pt}(\text{L1})(\text{DMSO})\text{Cl}]$  (**1**)

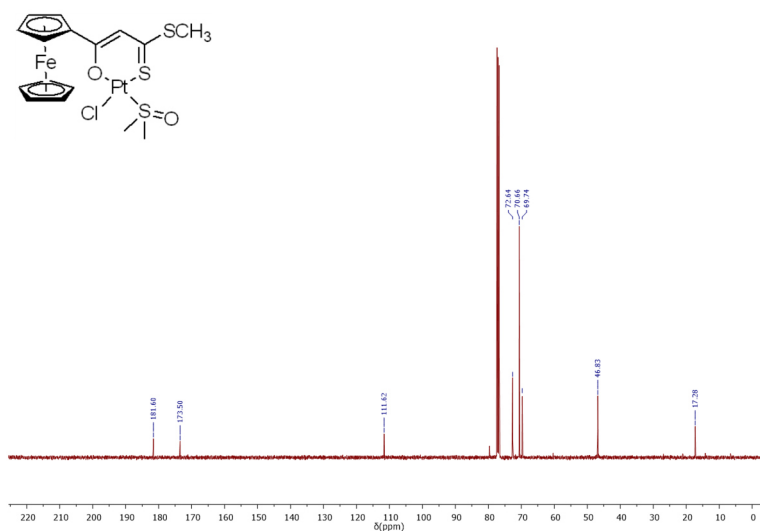


Figure S8.  $^{13}\text{C}\{^1\text{H}\}$  NMR (101 MHz,  $\text{CDCl}_3$ ): [Pt(L1)(DMSO)Cl] (**1**)

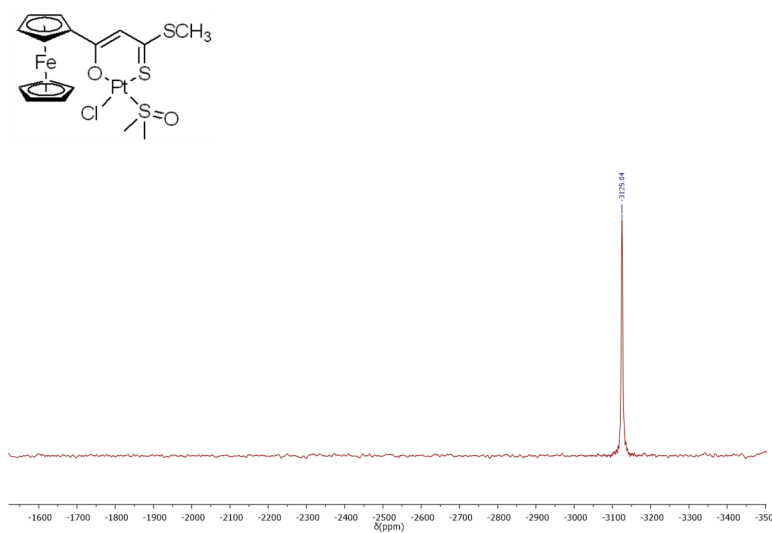


Figure S9.  $^{195}\text{Pt}$  NMR (85.7 MHz,  $\text{CDCl}_3$ ): [Pt(L1)(DMSO)Cl] (**1**)

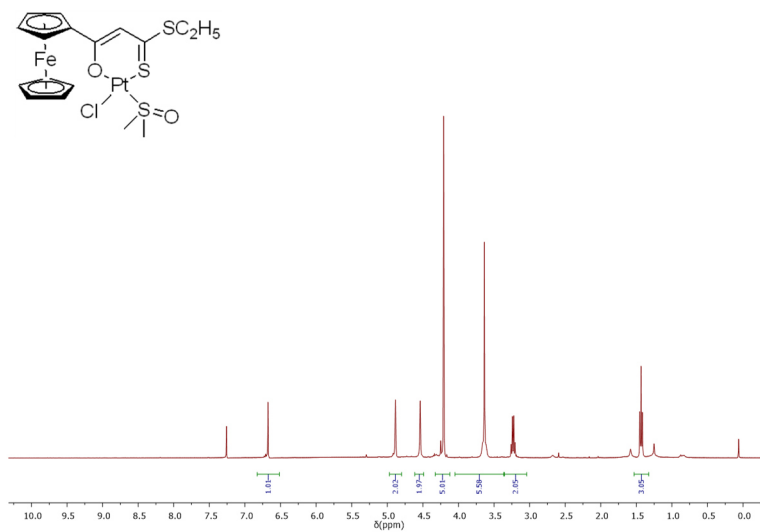


Figure S10.  $^1\text{H}$ -NMR (400 MHz,  $\text{CDCl}_3$ ): [Pt(L2)(DMSO)Cl] (**2**)

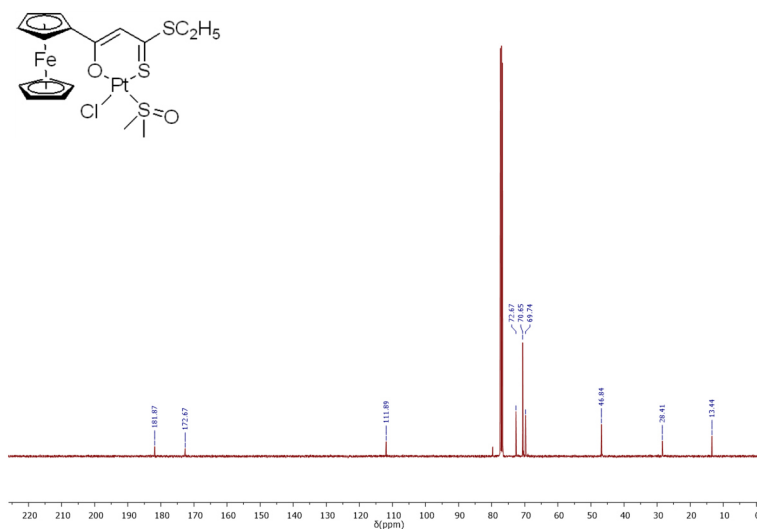


Figure S11.  $^{13}\text{C}\{^1\text{H}\}$  NMR (101 MHz,  $\text{CDCl}_3$ ): [Pt(L2)(DMSO)Cl] (2)

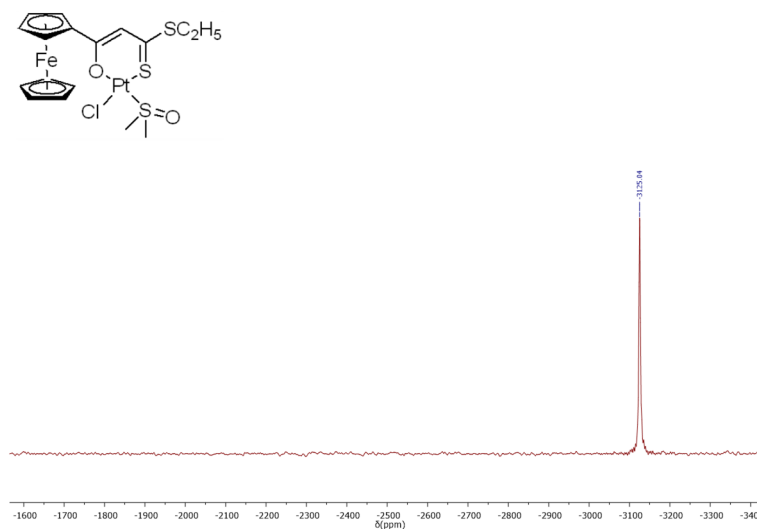


Figure S12.  $^{195}\text{Pt}$  NMR (85.7 MHz,  $\text{CDCl}_3$ ): [Pt(L2)(DMSO)Cl] (2)

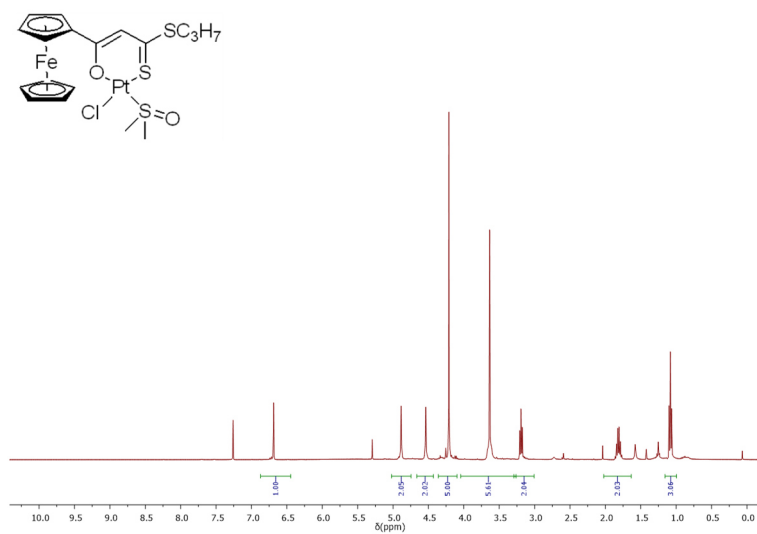


Figure S13.  $^1\text{H}$ -NMR (400 MHz,  $\text{CDCl}_3$ ): [Pt(L3)(DMSO)Cl] (3)

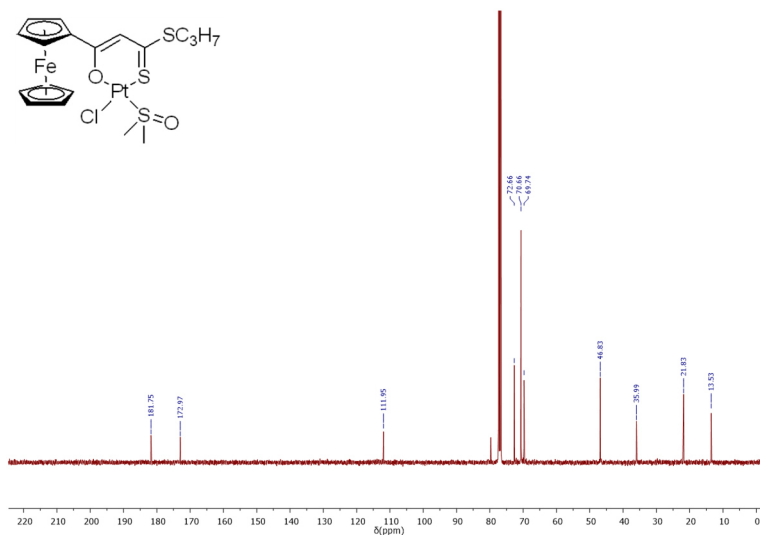


Figure S14.  $^{13}C\{^1H\}$  NMR (101 MHz,  $CDCl_3$ ):  $[Pt(L3)(DMSO)Cl]$  (3)

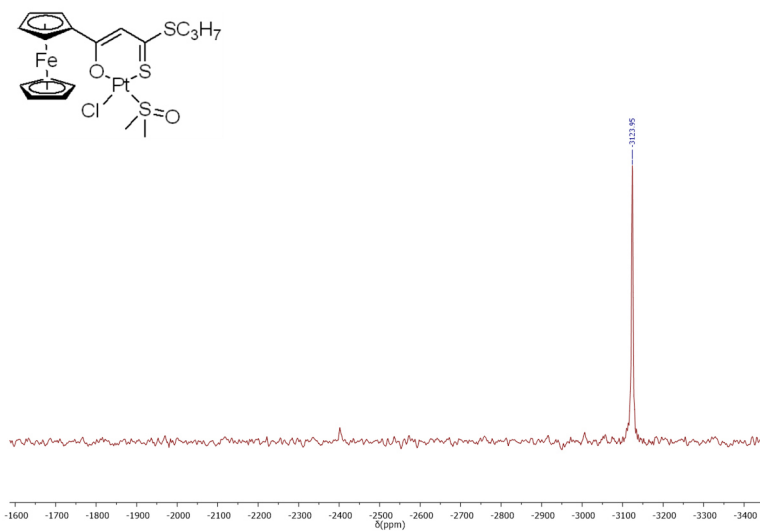


Figure S15.  $^{195}Pt$  NMR (85.7 MHz,  $CDCl_3$ ):  $[Pt(L3)(DMSO)Cl]$  (3)

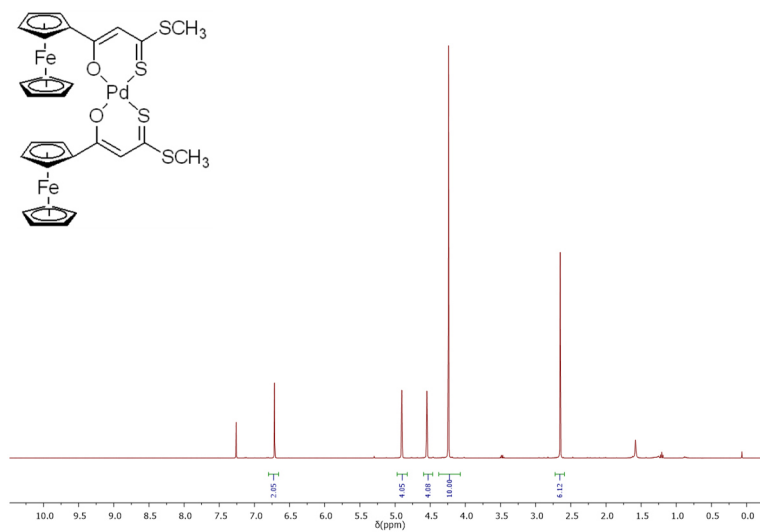


Figure S16.  $^1H$ -NMR (400 MHz,  $CDCl_3$ ):  $[Pd(L1)_2]$  (4)

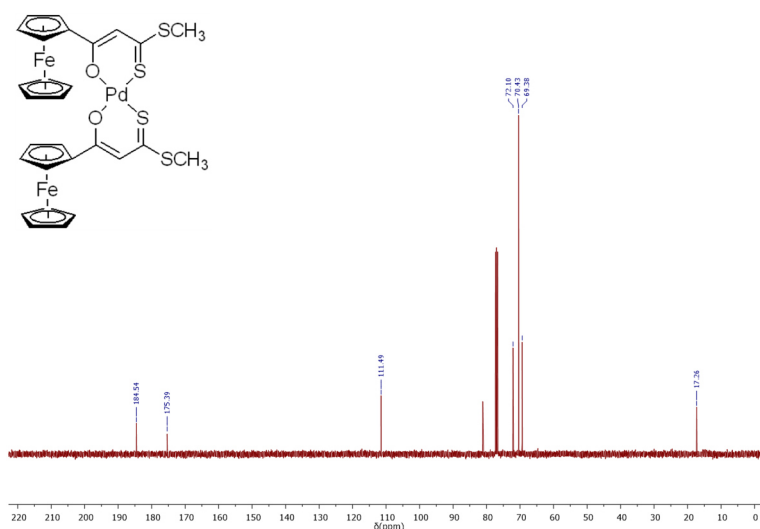


Figure S17. <sup>13</sup>C{<sup>1</sup>H} NMR (101 MHz, CDCl<sub>3</sub>): [Pd(L1)<sub>2</sub>] (4)

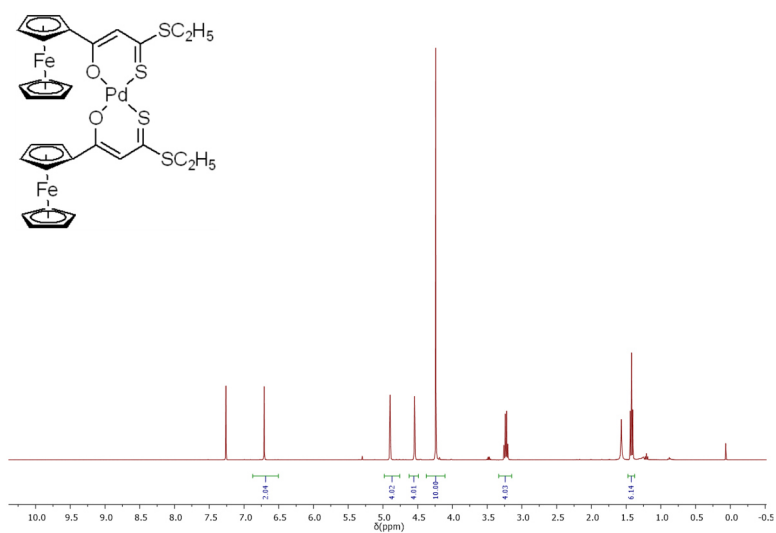


Figure S18. <sup>1</sup>H-NMR (400 MHz, CDCl<sub>3</sub>): [Pd(L2)<sub>2</sub>] (5)

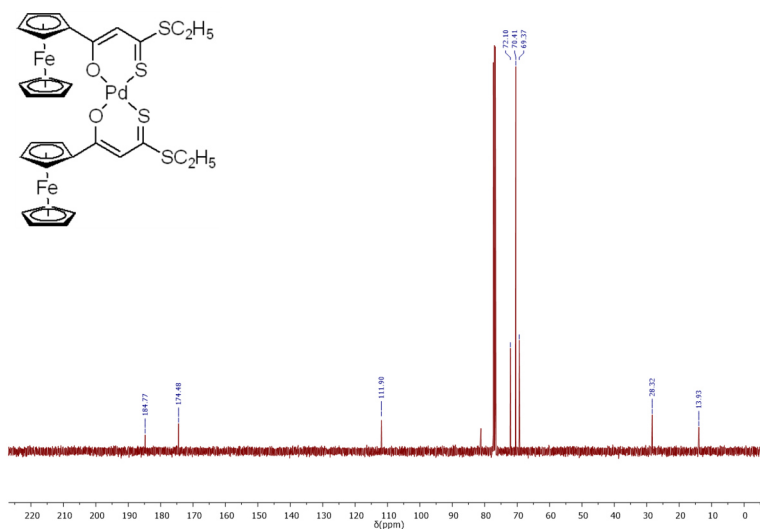


Figure S19. <sup>13</sup>C{<sup>1</sup>H} NMR (101 MHz, CDCl<sub>3</sub>): [Pd(L2)<sub>2</sub>] (5)

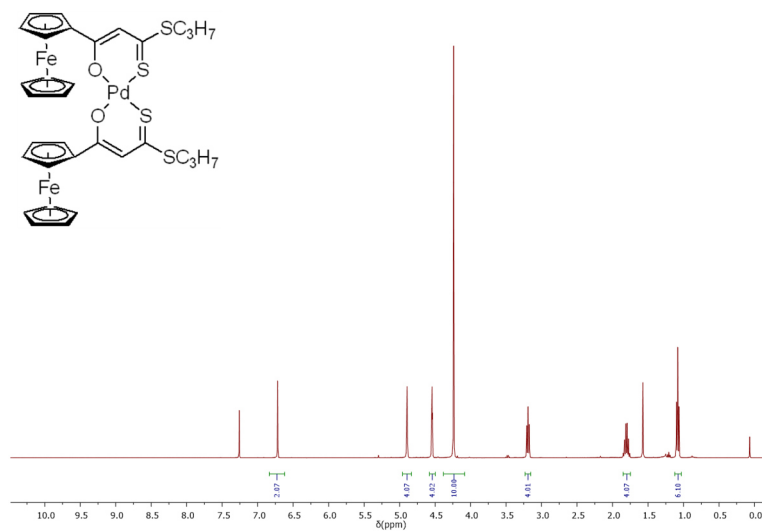


Figure S20.  $^1\text{H-NMR}$  (400 MHz,  $\text{CDCl}_3$ ):  $[\text{Pd}(\text{L}3)_2]$  (**6**)

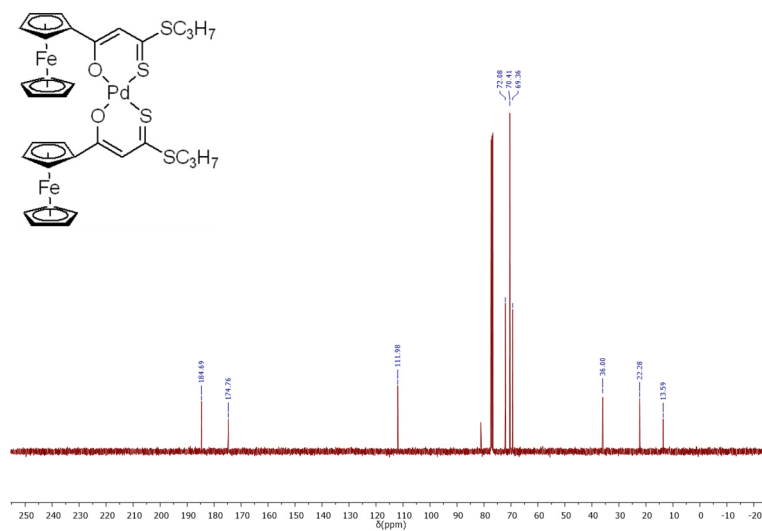


Figure S21.  $^{13}\text{C}\{^1\text{H}\}$  NMR (101 MHz,  $\text{CDCl}_3$ ):  $[\text{Pd}(\text{L}3)_2]$  (**6**)

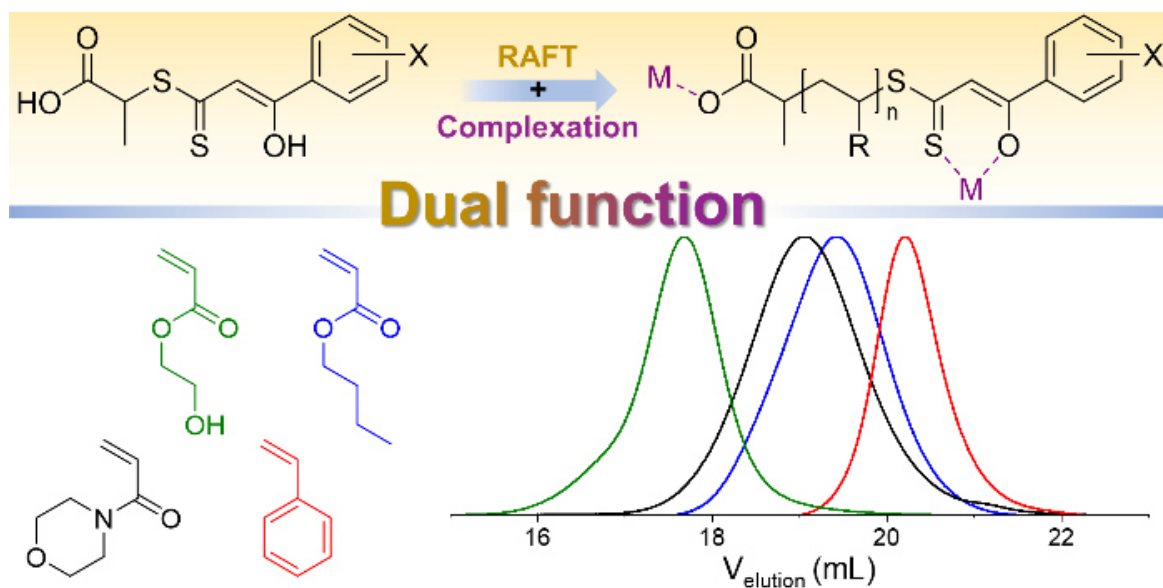


### 5.3 [ME-3]

#### Dual Function of $\beta$ -Hydroxy Dithiocinnamic Esters: RAFT Agent and Ligand for Metal Complexation

Micheal K. Farh, Franka V. Gruschwitz, Nicole Ziegenbalg, Hassan Abul-Futouh, Helmar Görls, Wolfgang Weigand, Johannes C. Brendel

Macromolecular Rapid Communications **2022**, 2200428.



This is an open-access article under the terms of the Creative Commons Attribution-NonCommercial License, which permits use, distribution, and reproduction in any medium, provided the original work is properly cited and is not used for commercial purposes. license link (<https://creativecommons.org/licenses/by-nc/4.0/>).

# Dual Function of $\beta$ -Hydroxy Dithiocinnamic Esters: RAFT Agent and Ligand for Metal Complexation

Micheal K. Farh, Franka V. Gruschwitz, Nicole Ziegenbalg, Hassan Abul-Futouh, Helmar Görls, Wolfgang Weigand,\* and Johannes C. Brendel\*

The reversible addition-fragmentation chain-transfer (RAFT) process has become a versatile tool for the preparation of defined polymers tolerating a large variety of functional groups. Several dithioesters, trithiocarbonates, xanthates, or dithiocarbamates have been developed as effective chain transfer agents (CTAs), but only a few examples have been reported, where the resulting end groups are directly considered for a secondary use besides controlling the polymerization. Herein, it is demonstrated that  $\beta$ -hydroxy dithiocinnamic esters represent a hitherto overlooked class of materials, which are originally designed for the complexation of transition metals but may as well act as reversible CTAs. Modified with a suitable leaving group (R-group), these vinyl conjugated dithioesters indeed provide reasonable control over the polymerization of acrylates, acrylamides, or styrene via the RAFT process. Kinetic studies reveal linear evolutions of molar mass with conversion, while different substituents on the aromatic unit has only a minor influence. Block extensions prove the livingness of the polymer chains, although extended polymerization times may lead to side reactions. The resulting dithiocinnamic ester end groups are still able to form complexes with platinum, which verifies that the structural integrity of the end group is maintained. These findings open a versatile new route to tailor-made polymer-bound metal complexes.

with defined length.<sup>[1–5]</sup> Among them, the reversible addition-fragmentation chain-transfer (RAFT) process enables a plethora of possibilities for polymeric architectures, meanwhile being suitable for a broad variety of monomers.<sup>[6–13]</sup> Generally, trithiocarbonates and aromatic dithioesters are used to polymerize more activated monomers, such as styrenes, (meth)acrylates or (meth)acrylamides, while less activated monomers such as vinyl esters or *N*-vinyl amides require xanthates or dithiocarbamates to maintain control.<sup>[14,15]</sup> This versatility makes the RAFT process highly attractive for the preparation of various functional polymers.<sup>[16,17]</sup> Furthermore, the process tolerates the incorporation of several reactive end groups as an attractive opportunity to create  $\alpha,\omega$ -heterotelechelic polymers for site-specific modifications or conjugations.<sup>[18–22]</sup> In fact, the literature is rich with numerous examples of chain transfer agents (CTA) that contain reactive moieties either attached to the functional leaving group R or the stabilizing unit Z.<sup>[23–36]</sup> Another alternative is the

cleavage of the dithioesters, xanthates, or trithiocarbonates to release the thiol end group, which however requires additional synthetic steps post polymerization.<sup>[37–41]</sup>

## 1. Introduction

Reversible deactivation radical polymerization methods are considered as a versatile tool to create narrowly distributed polymers


M. K. Farh, H. Görls, W. Weigand  
Department of Inorganic and Analytical Chemistry (IAAC)  
Friedrich Schiller University Jena  
Humboldtstraße 8, 07743 Jena, Germany  
E-mail: wolfgang.weigand@uni-jena.de

M. K. Farh  
Department of Chemistry  
Faculty of Science  
Assiut University  
Assiut 71515, Egypt

M. K. Farh, H. Abul-Futouh  
Department of Chemistry  
Faculty of Science  
The Hashemite University  
P.O. Box 330127, Zarqa 13133, Jordan

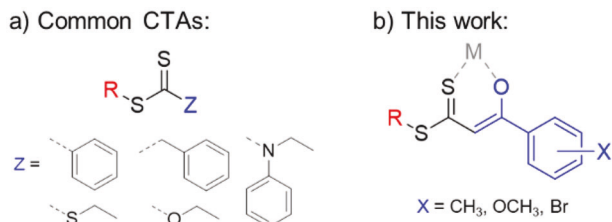
F. V. Gruschwitz, N. Ziegenbalg, J. C. Brendel  
Laboratory of Organic and Macromolecular Chemistry (IOMC)  
Friedrich Schiller University Jena  
Humboldtstraße 10, 07743 Jena, Germany  
E-mail: johannes.brendel@uni-jena.de

F. V. Gruschwitz, W. Weigand, J. C. Brendel  
Jena Center for Soft Matter (JCSM)  
Friedrich Schiller University Jena  
Philosophenweg 7, 07743 Jena, Germany

 The ORCID identification number(s) for the author(s) of this article can be found under <https://doi.org/10.1002/marc.202200428>

© 2022 The Authors. Macromolecular Rapid Communications published by Wiley-VCH GmbH. This is an open access article under the terms of the Creative Commons Attribution-NonCommercial License, which permits use, distribution and reproduction in any medium, provided the original work is properly cited and is not used for commercial purposes.

DOI: 10.1002/marc.202200428



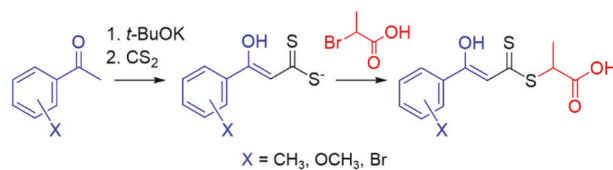
**Scheme 1.** a) Chemical structure of most common CTAs<sup>[11]</sup>; b) chemical structure of  $\beta$ -hydroxydithiocinnamic acid derivatives and their metal (M) coordinating site.

A far more elegant attempt relies on a direct utilization of the functional CTA end group as frequently reported for anchoring of trithiocarbonate or dithiobenzoates end groups onto gold surfaces or nanoparticles.<sup>[42–46]</sup> The group of Barner-Kowollik further successfully established efficient hetero-Diels–Alder reactions using either specifically designed CTAs or light-induced reactions on conventional dithioester benzoates.<sup>[47–53]</sup> Nevertheless, the bivalent uses of the inherent RAFT motif as a reactive moiety remain scarce in the literature, which is partly related to the limited option in the structural design of the CTA without sacrificing its ability to control the polymerization.<sup>[14,54]</sup> Interesting, but so far overlooked compounds are  $\beta$ -hydroxydithiocinnamic esters, which are well known for their ability to form complexes with a variety of metals including Pt, Pd, Ni, Cu, or Ru.<sup>[55–65]</sup> The structure differs from common CTAs based on trithiocarbonates or dithiobenzoates (**Scheme 1**), but the conjugation of the vinyl benzene moiety (Z-group) might still be sufficient to stabilize the intermediate radical in the RAFT process.

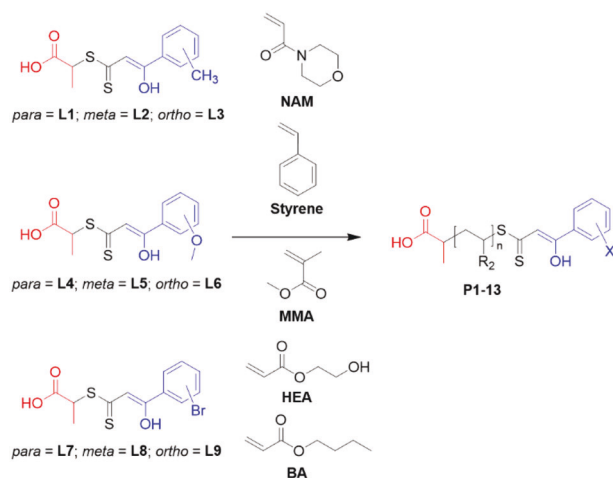
The group of Destarac and co-workers have previously examined dithiocinnamic acid derivatives as CTAs in RAFT, but the vinylogous character of their RAFT agents caused a severe retardation during polymerization.<sup>[66]</sup> The  $\beta$ -hydroxy modified ligands presented in this work might circumvent the observed degeneration by a Diels–Alder reaction, as the additional hydroxy group increases the steric hindrance and electron density at the vinyl group. The present work focuses on testing the suitability of these modified ligands (**Scheme 1**) as CTAs in the RAFT process. Moreover, we have investigated the reaction of the resulting polymers with Pt(II) metal, which were subsequently characterized by spectroscopic and elemental analysis techniques.

## 2. Results and Discussion

The described  $\beta$ -hydroxydithiocinnamic acid derivatives (**L1–L9**) can be prepared in one step from the corresponding acetophenone derivatives in accordance with previously reported routes (**Scheme 2**).<sup>[55,56]</sup> Interestingly, the free acid group simplifies the purification procedure and pure compounds are conveniently obtained after washing and recrystallization without the need for column chromatography. The specific experimental conditions as well as the synthetic pathways are described in the ESI, which further contains detailed characterization data including crystallographic data (molecular structure given in Figure S1, Supporting Information) and UV-vis spectra in solution (Figure S2, Supporting Information).



**Scheme 2.** General procedure for the synthesis of the  $\beta$ -hydroxydithiocinnamic acid derivatives.



**Scheme 3.** Chemical structures of the ligands, monomers, and the resulting polymers.

**Scheme 3** depicts an overview of the examined  $\beta$ -hydroxydithiocinnamic acid derivatives and the set of monomers tested during the RAFT polymerization. The polymerization procedure and the corresponding characterization by NMR and size exclusion chromatography (SEC) are described in the ESI. The tested monomers include the acrylates *n*-butyl acrylate (BA) and 2-hydroxyethyl acrylate (HEA), the acrylamide *N*-acryloyl morpholine (NAM), and styrene which are all known to be polymerizable with common trithiocarbonate and aromatic dithioester based RAFT-agents. Methyl methacrylate (MMA) was further included as a representative for methacrylates, but the *R*-group of our  $\beta$ -hydroxydithiocinnamic acid derivatives might not be suitable for efficient chain transfer. In all cases, azobisisobutyronitrile (AIBN) was used as the initiator (CTA/initiator ratio: 20/1). Given a temperature of 70 °C and a polymerization time of 24 h, around 95% of the initiator should be decomposed resulting in a theoretical livingness of all polymers of >95%, if an initiator efficiency of 0.5 is assumed.

**L1** was chosen to first evaluate the general potential of these compounds for controlling the polymerization of the different monomer types. The impact of different substituents on the benzene ring was investigated using the monomer *N*-acryloyl morpholine (NAM).

An overview of all combinations and the resulting polymers (after 24 h of polymerization) is given in **Table 1** (SEC traces for polymers **P1–P5** are given in the ESI, Figure S3, Supporting Information). Narrowly distributed polymers were obtained for the acrylates and styrene ( $\bar{D} < 1.2$ ), while the dispersity is slightly increased for NAM. MMA, however, could not be controlled by

**Table 1.** Summary of all prepared polymers.

Polymer	Monomer	CTA (X)	Conversion, <sup>a)</sup> 24 h [%]	$M_{n,theos}$ <sup>b)</sup> [kg mol <sup>-1</sup> ]	$M_{n,NMR}$ <sup>c)</sup> [kg mol <sup>-1</sup> ]	$M_{n,SEC}$ <sup>d)</sup> [kg mol <sup>-1</sup> ]	$\bar{D}$ <sup>d)</sup>
P1	NAM	L1 (Me)	79	5.9	7.8	7.1	1.24
P2	BA	L1 (Me)	92	6.2	8.2	8.4	1.18
P3	Styrene	L1 (Me)	18	1.2	2.4	2.9	1.11
P4	HEA	L1 (Me)	96	5.9	6.3	10.4	1.18
P5	MMA	L1 (Me)	60	–	–	213.0	1.88
P6	NAM	L2 (Me)	68	5.1	6.6	5.8	1.23
P7	NAM	L3 (Me)	67	5.0	5.6	5.3	1.23
P8	NAM	L6 (OMe)	83	6.2	8.3	6.4	1.29
P9	NAM	L5 (OMe)	78	5.8	6.4	5.5	1.31
P10	NAM	L4 (OMe)	82	6.1	6.8	5.8	1.31
P11	NAM	L9 (Br)	71	5.4	6.6	5.9	1.26
P12	NAM	L8 (Br)	40	3.2	4.0	2.6	1.40
P13	NAM	L7 (Br)	55	4.2	5.0	4.4	1.32

<sup>a)</sup> Determined from <sup>1</sup>H-NMR; <sup>b)</sup> Calculated from conversion and the targeted DP of 50; <sup>c)</sup> Precipitated polymers, determined from ratio of aromatic signals to signals of repeating units in <sup>1</sup>H NMR (precipitated polymers); <sup>d)</sup> Precipitated polymers, determined by SEC (Eluent: DMAc + 0.21 wt% LiCl, PMMA-calibration).

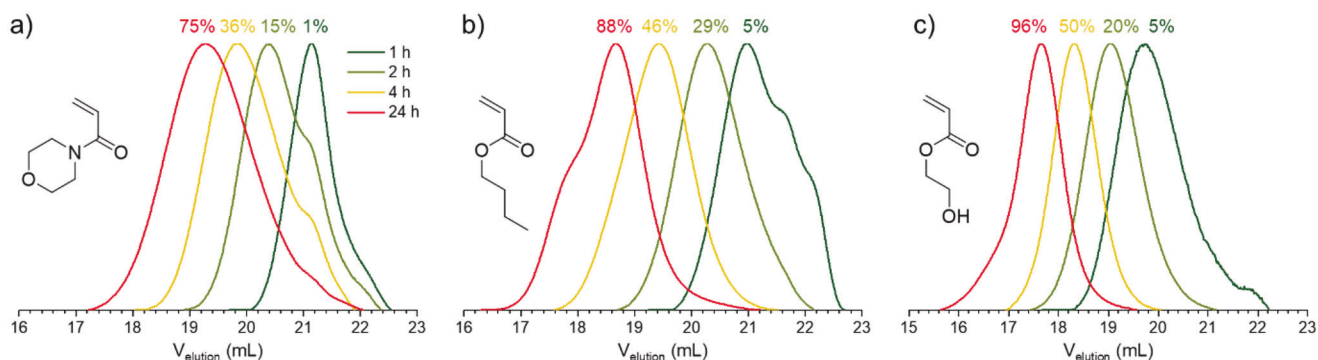


**Figure 1.** Normalized SEC traces of samples (1, 2, 4, and 24 h) taken during the polymerization of a) NAM (P1), b) BA (P2), and c) HEA (P4) (DMAc/LiCl, RI-detection).

these compounds, which corresponds to observations for established CTAs with similar poor leaving groups R.

Analyzing the progress of the reaction, SEC samples were taken at different time points of the polymerizations. Exemplarily chosen SEC traces for the polymerizations of NAM (P1), BA (P2), and HEA (P4) are depicted in Figure 1 (corresponding graphs normalized to conversion are given in Figure S4, Supporting Information, while an overview of all taken samples is given in Figure S6, Supporting Information).

A closer look at the corresponding conversions revealed pseudo-linear kinetics in the first hours after a short induction period for all polymerizations (Figure 2). The apparent reaction rates  $k_p^{app}$  are in the range of 0.17–0.23 for both acrylates, but one order of magnitude lower for styrene, which is expected due to the low propagation rate of the latter.

Interestingly and against our expectations, the polymerization rate for NAM is lower than for the acrylates, which coincides with the broader dispersity observed for the acrylamide. Nevertheless, a linear evolution of molar mass is observed for all polymers, but a closer look at the SEC traces of polymerizations of NAM (Figure 1 and Figure S6, Supporting Information) reveals a gradually

disappearing shoulder at high elution volume. As this signal is most prominent in the first samples, where the conversion was still close to zero, we initially assumed it corresponds to the CTA. However, the elution times did not match with the corresponding SEC measurements of the pure CTA (Figure S5a, Supporting Information). A closer look at the <sup>1</sup>H NMR spectra of the kinetic samples taken at the beginning of the polymerization (0 h) and after 1 h revealed that indeed the characteristic signal for tertiary CH group (on the R-group) next to the dithioester disappeared (Figure S5b, Supporting Information). Unfortunately, the signal of the newly formed CH group could not be identified, but we nevertheless consider that the species formed in the first hour of the polymerization corresponds to the single monomer insertion of NAM during the preequilibrium of the RAFT polymerization. This species is then continuously consumed during the main equilibrium. More detailed studies were, however, not considered. More interesting were the courses of the polymerization of the acrylates. In the case of BA, a shoulder at higher molar masses appears at late stages and high conversions (>80%) of the polymerization (Figure 1 and Figure S6, Supporting Information). Even in the case of HEA a similar trend becomes apparent



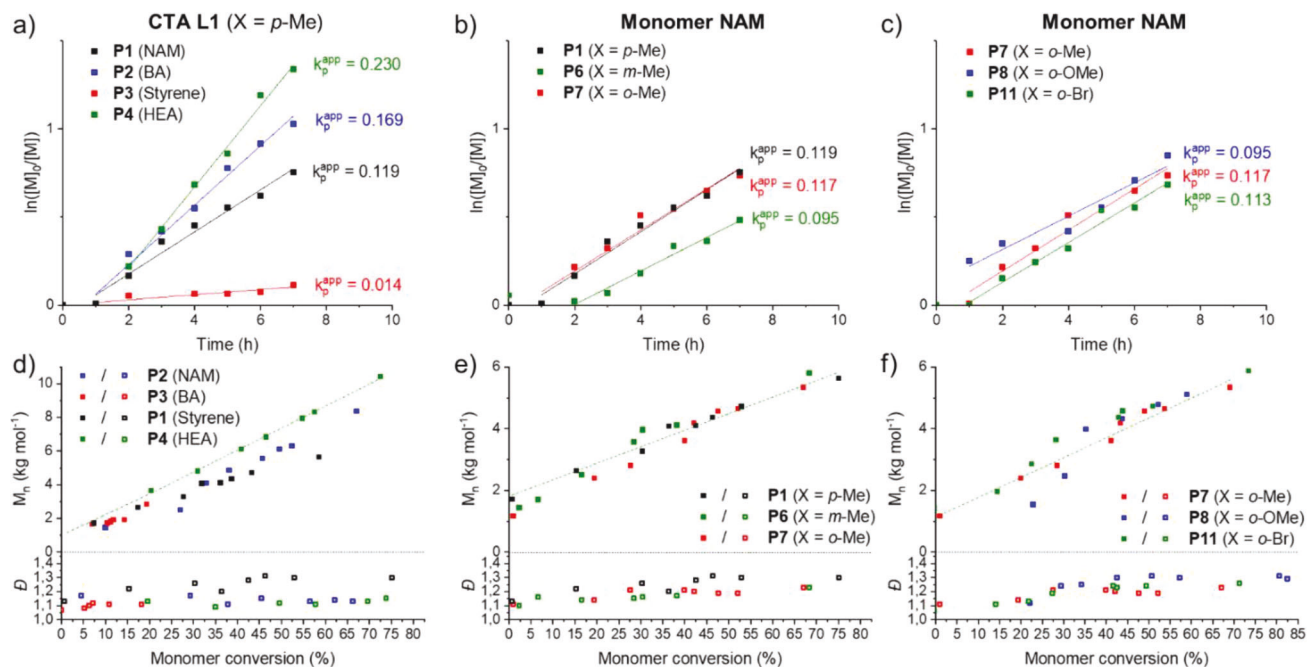


**Figure 2.** Polymerization kinetics (including apparent rate constants  $k_p^{app}$ ) in dependence of a) the type of monomer using L1 as CTA, b) the position of the methyl substitution at the aromatic ring (X), and c) the type of substituent on the aromatic ring (both b) and c) using NAM as monomer); d)-f) evolution of molar mass ( $M_n$ ) and dispersity  $\bar{D}$  with monomer conversion of the corresponding polymerizations shown above.

at very long polymerization times (24 h). Shoulders at higher molar masses have previously been reported for acrylates and particularly for BA as a result of a formation of a PBA macromonomer by backbiting  $\beta$ -scission.<sup>[67]</sup> In our case, however, the shoulder was quite prominent compared to the previous reports, which is why we consider that additional side reactions might contribute to this formation of a high molar mass shoulder. Common termination by combination seems not to play a major role, since the  $\beta$ -hydroxydithiocinnamic ester end group is still present as indicated by a similar intense UV-vis signal (detection at 350 nm) in the SEC trace (Figure S7, Supporting Information). However, a chain-chain coupling by radical reaction of a propagating chain end with the double bond of the cinnamic acid end group cannot be excluded as well, as if high conversions are reached even less reactive vinyl groups might react.<sup>[68]</sup>

Comparing the different substitution patterns on the benzene ring of the CTAs, no significant influence of the position of the methyl group on the reactivity becomes apparent as similar kinetics for all compounds are observed (Figure 2). Apart from varying the position, the substituent was exchanged for either a methoxy group (L4–L6) or the halogen bromine (L7–L9). While the first should induce a strong electron-donating effect on the aromatic system, the latter should cause the opposite. However, comparing the results of the polymerization of NAM, no significant differences in the reaction rate were found for L3, L6, and L9 (Figure 2C). Interestingly, changing the *ortho*-substitution (L9) of the bromo-ligands to a *meta* (L8) or *para* (L7) position, increases the dispersities of the polymers and reduces the reaction rate (Figure S8, Supporting Information). We assume that the more accessible *meta* and particular the *para* position of the bromine group might favor side reactions, or the latter positions induce an unfa-

vorable inductive effect. In the case of the methoxy substituent, only a slight decrease in the reaction rate for the *ortho* position is observed (Figure S8), which might be due to steric effects.

Intrigued by the surprisingly good control, we further examined whether the RAFT end group remains intact and is capable of reinitiating a chain extension.<sup>[69]</sup> Therefore, another batch of PBA (P14) was prepared from the CTA L1, but the polymerization was stopped after 4 h to minimize the previously mentioned side reaction. A monomodal distribution ( $\bar{D} = 1.10$ ) was obtained in this case and the polymer was purified by precipitation. Subsequently, this polymer was again dissolved in BA and a new initiator was added to initiate a potential chain extension of this macro-CTA. The comparison of the SEC traces (Figure 3) at each step reveals a clear and nearly complete shift of the signal for the macro-CTA (P14) after formation of the second block in the chain extension experiment. The newly formed polymer (P15) again features a monomodal distribution with narrow dispersity ( $\bar{D} = 1.11$ ) if the reaction time was kept at 4 h. The reactivity or livingness of the chains seems therefore be mostly preserved during the polymerization underlining the good control provided by this RAFT agent, if extended polymerization times are avoided.

Another key question is whether the  $\beta$ -hydroxydithiocinnamic ester end group is still capable of fulfilling its second function, the complexation of metals. Therefore, we have exemplarily chosen the water-soluble polymers P1 and P6–P11 and added  $K_2PtCl_4$  to form the corresponding complexes PtP1 and PtP6–11. NMR spectroscopy and inductively coupled plasma atomic emission spectroscopy (ICP-AES) revealed that all reactions yielded Pt(II) complexes. The <sup>1</sup>H NMR spectra of the resulting complexes PtP1 and PtP6–11 are very similar compared to the spectra of the

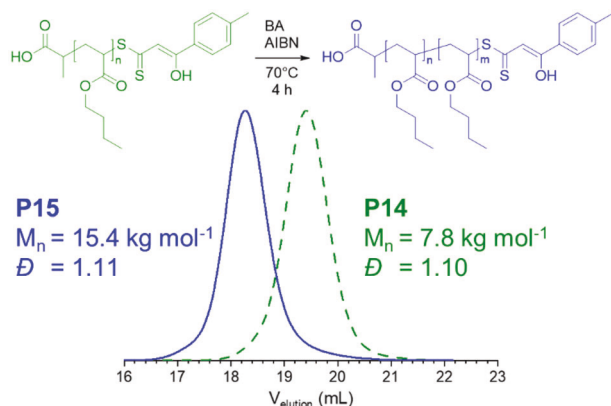


**Figure 3.** Scheme of the polymerization starting from the purified PBA (P14) using BA as monomer and the corresponding SEC traces of the macro-CTA P14 (dashed green line) and the resulting polymer P15 (solid blue line) after the chain extension (DMAc/LiCl, RI-detection, PMMA-calibration).

corresponding precursors polymer P1 and P6-11. However, the disappearance of the signal around 15 ppm indicates that the coordination occurred through the  $\beta$ -oxo-carbon atom. Furthermore, the  $^{13}\text{C}\{^1\text{H}\}$  NMR spectra of PtP1 and PtP6-11 display a downfield shift ( $\approx 3\text{--}7$  ppm) for the methine carbon atom and a high field shift ( $\approx 27\text{--}37$  ppm) for the quaternary thiocarbonyl carbon atom, which further corroborates that the coordination occurs through the  $\beta$ -hydroxydithiocinnamic ester moiety. We further used ICP-AES to quantify the amount of bound Pt in the polymers P1 and P6-11.<sup>[70–73]</sup> Interestingly, in most polymers a Pt content was found, which is considerably higher than expected for a complexation of one equivalent of Pt, despite excessive washing steps and thorough purification. These calculations were based on average molar masses or number of repeating units, respectively, estimated from the  $^1\text{H}$  NMR signals (aromatic protons vs protons of repeating units) of the precipitated polymers (Table 1). Although the  $M_n$  values might deviate from absolute molar masses (e.g., by the loss of the end group), this determination should still reflect the real content of active complexation sites in the sample independent of the molar masses. Therefore, these deviations cannot be related to false molar mass values. Instead, we assume that the additional binding of Pt is caused by the carboxylic acid groups present at the  $\alpha$  end of the polymer chains (Figure 4a), which were initially chosen to simplify the purification of the  $\beta$ -hydroxydithiocinnamic esters. The SEC analysis of the exemplarily chosen complex PtP6 further corroborated our assumption, as a bimodal distribution is observed (Figure 4b), which reflects the expected composition comprising a polymer distribution close to the initial polymer P6 and second distribution representing a coupled species at double molar mass.

Given the proposed two structures, we estimated that PtP6 must consist of 42% A and 58% B considering a measured Pt content of 47.16 mg(Pt)/g(sample) and an  $M_n$  (NMR) of 6.6 kg mol<sup>-1</sup> for the polymer P6. Independent of the discrepancies in the expected and observed Pt content, the high amount of Pt bound in the polymers can only be explained if the  $\beta$ -hydroxydithiocinnamic ester moiety is still able to bind the metal.

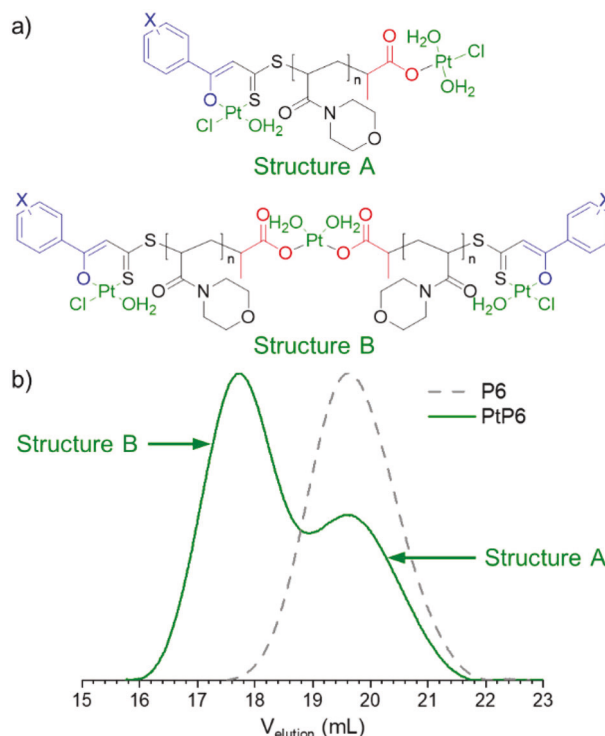


**Figure 4.** a) Scheme of the two potentially formed structures during the complexation of Pt by the RAFT-polymers based on NAM; b) corresponding SEC of the complex PtP1 (green solid line) in comparison with the initial polymer P1 (grey dashed line) (DMAc/LiCl, RI-detection, PMMA-calibration).

Therefore, this data confirms that the functionality of the end group is maintained during the polymerization and the desired Pt complexes can be formed. Considering the unexpected formation of the Pt-carboxylate complexes, we would like to emphasize that although these simple complexes appear quite robust, significantly higher binding constants can be expected for the Pt-complexes with  $\beta$ -hydroxydithiocinnamic esters considering the bidentate character of these O,S ligands.<sup>[74]</sup> The carboxylic acid moiety at the R-group further represents a versatile group for additional modifications of the polymers with regard to potential applications. Further studies in this direction are under consideration in our groups, which should further underline the importance of the dual use of the presented CTAs.

### 3. Conclusion

In summary, we could demonstrate that derivatives of  $\beta$ -hydroxydithiocinnamic esters are suitable chain transfer agents to control the polymerization of various acrylic or styrene-based monomers. Detailed kinetic studies revealed a linear evolution of molar masses with conversion. It has however to be considered that the increased reactivity of the vinyl moiety in the Z-group might still cause side reaction, if extended reaction times are applied. Nevertheless, the resulting polymer chains can successfully be chain extended, if shorter polymerization times are applied, verifying a high-end group fidelity and the living character of the polymerization. The substitution pattern

on the adjacent benzene has overall only a minor impact on the polymerization behavior. Only in the case of the rather reactive bromine substituents reduced conversions and a broadening of the molar mass distribution was observed, which became particularly prominent for the meta and para-substituted compounds. Most interestingly, the polymers appear to be still capable of binding Pt (II) and afford the corresponding platinum complexes. These types of dual-function compounds are attractive candidates to directly prepare functional polymers for application as catalysts in a variety of organic reactions,<sup>[62,64,65]</sup> anti-leishmanial agents,<sup>[58]</sup> potential anti-cancer agent,<sup>[56,57,59,60]</sup> inhibitors of amyloid aggregation,<sup>[63]</sup> or in wastewater treatment due to the ability to act as chelating ligands for noble metals.<sup>[75]</sup> Furthermore, such complexes might find use in bio-imaging by replacing the Pt element with Ti and Gd.<sup>[76]</sup>

## Supporting Information

Supporting Information is available from the Wiley Online Library or from the author.

## Acknowledgements

M.K.F. and F.V.G. contributed equally to this work. M.K.F. is grateful to the Katholischer Akademischer Ausländer-Dienst (KAAD) for a Ph.D. scholarship. J.C.B., F.V.G., and N.Z. further thank the German Science Foundation (DFG) for generous funding within the Emmy-Noether Programme (Project-ID: 358263073). Prof. U.S. Schubert is furthermore acknowledged for his continuous support and access to excellent research facilities. The authors would further like to thank Umicore AG & Co. KG Hanau-Wolfgang, Germany for donation of K<sub>2</sub>PtCl<sub>4</sub>.

Open access funding enabled and organized by Projekt DEAL.

## Conflict of Interest

The authors declare no conflict of interest.

## Data Availability Statement

The data that support the findings of this study are available from the corresponding author upon reasonable request.

## Keywords

controlled radical polymerization, ligands, platinum complexes, RAFT polymerization

Received: May 5, 2022

Revised: June 12, 2022

Published online:

- [1] W. A. Braunecker, K. Matyjaszewski, *Prog. Polym. Sci.* **2007**, *32*, 93.  
[2] P. B. Zetterlund, S. C. Thickett, S. Perrier, E. Bourgeat-Lami, M. Lansalot, *Chem. Rev.* **2015**, *115*, 9745.  
[3] P. Gurnani, S. Perrier, *Prog. Polym. Sci.* **102**, **2020**, 101209.

- [4] A. Anastasaki, V. Nikolaou, D. M. Haddleton, *Polym. Chem.* **2016**, *7*, 1002.  
[5] A. Anastasaki, V. Nikolaou, G. Nurumbetov, P. Wilson, K. Kempe, J. F. Quinn, T. P. Davis, M. R. Whittaker, D. M. Haddleton, *Chem. Rev.* **2016**, *116*, 835.  
[6] M. Semsarilar, V. Abetz, *Macromol. Chem. Phys.* **2021**, *222*, 2000311.  
[7] F. D'Agosto, J. Rieger, M. Lansalot, *Angew. Chem., Int. Ed.* **2019**, *59*, 8368.  
[8] S. Perrier, *Macromolecules* **2017**, *50*, 7433.  
[9] J. Rieger, *Macromol. Rapid Commun.* **2015**, *36*, 1458.  
[10] G. Moad, E. Rizzardo, S. H. Thang, *Aust. J. Chem.* **2005**, *58*, 379.  
[11] G. Moad, E. Rizzardo, S. H. Thang, *Aust. J. Chem.* **2012**, *65*, 985.  
[12] A. Gregory, M. H. Stenzel, *Prog. Polym. Sci.* **2012**, *37*, 38.  
[13] M. D. Nothling, Q. Fu, A. Reyhani, S. Allison-Logan, K. Jung, J. Zhu, M. Kamigaito, C. Boyer, G. G. Qiao, *Adv. Sci.* **2020**, *7*, 2001656.  
[14] D. J. Keddie, G. Moad, E. Rizzardo, S. H. Thang, *Macromolecules* **2012**, *45*, 5321.  
[15] M. Destarac, *Polym. Rev.* **2011**, *51*, 163.  
[16] M. R. Hill, R. N. Carmean, B. S. Sumerlin, *Macromolecules* **2015**, *48*, 5459.  
[17] B. D. Fairbanks, P. A. Gunatillake, L. Meagher, *Adv. Drug Delivery Rev.* **2015**, *91*, 141.  
[18] D. Quemener, T. P. Davis, C. Barner-Kowollik, M. H. Stenzel, *Chem. Commun.* **2006**, 5051.  
[19] G. Moad, E. Rizzardo, S. H. Thang, *Polym. Int.* **2011**, *60*, 9.  
[20] A. S. Goldmann, M. Glassner, A. J. Inglis, C. Barner-Kowollik, *Macromol. Rapid Commun.* **2013**, *34*, 810.  
[21] M. Kaupp, T. Tischer, A. F. Hirschbiel, A. P. Vogt, U. Geckle, V. Trouillet, T. Hofe, M. H. Stenzel, C. Barner-Kowollik, *Macromolecules* **2013**, *46*, 6858.  
[22] P. J. Roth, M. Haase, T. Basché, P. Theato, R. Zentel, *Macromolecules* **2010**, *43*, 895.  
[23] B. V. K. J. Schmidt, M. Hetzer, H. Ritter, C. Barner-Kowollik, *Macromolecules* **2011**, *44*, 7220.  
[24] I. Kulai, O. Brusylovets, Z. Voitenko, S. Harisson, S. Mazières, M. Destarac, *ACS Macro Lett.* **2015**, *4*, 809.  
[25] S. Pearson, C. St Thomas, R. Guerrero-Santos, F. D'Agosto, *Polym. Chem.* **2017**, *8*, 4916.  
[26] G. Gody, C. Rossner, J. Moraes, P. Vana, T. Maschmeyer, S. Perrier, *J. Am. Chem. Soc.* **2012**, *134*, 12596.  
[27] J. C. Brendel, L. Martin, J. Zhang, S. Perrier, *Polym. Chem.* **2017**, *8*, 7475.  
[28] G. Gody, D. A. Roberts, T. Maschmeyer, S. Perrier, *J. Am. Chem. Soc.* **2016**, *138*, 4061.  
[29] J. C. Brendel, G. Gody, S. Perrier, *Polym. Chem.* **2016**, *7*, 5536.  
[30] V. Ladmiraal, T. M. Legge, Y. Zhao, S. Perrier, *Macromolecules* **2008**, *41*, 6728.  
[31] S. Vandewalle, S. Billiet, F. Driessen, F. E. Du Prez, *ACS Macro Lett.* **2016**, *5*, 766.  
[32] Z. Zhang, N. Vanparijs, S. Vandewalle, F. E. Du Prez, L. Nuhn, B. G. De Geest, *Polym. Chem.* **2016**, *7*, 7242.  
[33] C. Boyer, M. H. Stenzel, T. P. Davis, *J. Polym. Sci., Part A: Polym. Chem.* **2011**, *49*, 551.  
[34] W. H. Binder, R. Sachsenhofer, *Macromol. Rapid Commun.* **2008**, *29*, 952.  
[35] T. A. Wright, M. S. Rahman, C. Bennett, M. R. Johnson, H. Fischesser, N. Ram, A. Tyler, R. C. Page, D. Konkolewicz, *Bioconjugate Chem.* **2021**, *32*, 2447.  
[36] G. Delaitre, N. K. Guimard, C. Barner-Kowollik, *Acc. Chem. Res.* **2015**, *48*, 1296.  
[37] J. Xu, L. Tao, C. Boyer, A. B. Lowe, T. P. Davis, *Macromolecules* **2010**, *43*, 20.  
[38] S. Chen, D. Ströhl, W. H. Binder, *ACS Macro Lett.* **2015**, *4*, 48.

- [39] M. Dietrich, M. Glassner, T. Gruending, C. Schmid, J. Falkenhagen, C. Barner-Kowollik, *Polym. Chem.* **2010**, *1*, 634.
- [40] M. Scherger, H. J. Räder, L. Nuhn, *Macromol. Rapid Commun.* **2021**, *42*, e2000752.
- [41] B. A. Abel, C. L. McCormick, *Macromolecules* **2016**, *49*, 6193.
- [42] M. Liang, I. C. Lin, M. R. Whittaker, R. F. Minchin, M. J. Monteiro, I. Toth, *ACS Nano* **2010**, *4*, 403.
- [43] C. Boyer, M. R. Whittaker, C. Nouvel, T. P. Davis, *Macromolecules* **2010**, *43*, 1792.
- [44] C. Boyer, M. R. Whittaker, M. Luzon, T. P. Davis, *Macromolecules* **2009**, *42*, 6917.
- [45] C.-A. Fustin, C. Colard, M. Filali, P. Guillet, A.-S. Duwez, M. A. R. Meier, U. S. Schubert, J.-F. Gohy, *Langmuir* **2006**, *22*, 6690.
- [46] A.-S. Duwez, P. Guillet, C. Colard, J.-F. Gohy, C.-A. Fustin, *Macromolecules* **2006**, *39*, 2729.
- [47] A. J. Inglis, S. Sinnwell, M. H. Stenzel, C. Barner-Kowollik, *Angew. Chem., Int. Ed.* **2009**, *48*, 2411.
- [48] S. Sinnwell, A. J. Inglis, T. P. Davis, M. H. Stenzel, C. Barner-Kowollik, *Chem. Commun.* **2008**, 2052.
- [49] M. Langer, J. O. Mueller, A. S. Goldmann, F. H. Schacher, C. Barner-Kowollik, *ACS Macro Lett.* **2016**, *5*, 597.
- [50] A. Belouqui, S. R. Mane, M. Langer, M. Glassner, D. M. Bauer, L. Fruk, C. Barner-Kowollik, G. Delaître, *Angew. Chem., Int. Ed.* **2020**, *59*, 19951.
- [51] M. Glassner, G. Delaître, M. Kaupp, J. P. Blinco, C. Barner-Kowollik, *J. Am. Chem. Soc.* **2012**, *134*, 7274.
- [52] N. Zydziak, C. M. Preuss, V. Winkler, M. Bruns, C. Hübner, C. Barner-Kowollik, *Macromol. Rapid Commun.* **2013**, *34*, 672.
- [53] K. K. Oehlenschlaeger, J. O. Mueller, N. B. Heine, M. Glassner, N. K. Guimard, G. Delaître, F. G. Schmidt, C. Barner-Kowollik, *Angew. Chem., Int. Ed.* **2013**, *52*, 762.
- [54] M. L. Coote, D. J. Henry, *Macromolecules* **2005**, *38*, 1415.
- [55] M. S. Singh, G. C. Nandi, T. Chanda, *RSC Adv.* **2013**, *3*, 14183.
- [56] C. Mügge, R. Liu, H. Görls, C. Gabbiani, E. Michelucci, N. Rüdiger, J. H. Clement, L. Messori, W. Weigand, *Dalton Trans.* **2014**, *43*, 3072.
- [57] C. Mügge, T. Marzo, L. Massai, J. Hildebrandt, G. Ferraro, P. Rivera-Fuentes, N. Metzler-Nolte, A. Merlino, L. Messori, W. Weigand, *Inorg. Chem.* **2015**, *54*, 8560.
- [58] M. K. Yadav, G. Rajput, K. Srivastava, R. K. Singh, R. Mishra, M. G. B. Drew, N. Singh, *New J. Chem.* **2015**, *39*, 6358.
- [59] J. Hildebrandt, N. Häfner, H. Görls, D. Kritsch, G. Ferraro, M. Dürst, I. B. Runnebaum, A. Merlino, W. Weigand, *Dalton Trans.* **2016**, *45*, 18876.
- [60] C. Mügge, D. Musumeci, E. Michelucci, F. Porru, T. Marzo, L. Massai, L. Messori, W. Weigand, D. Montesarchio, *J. Inorg. Biochem.* **2016**, *160*, 198.
- [61] M. K. Yadav, A. K. Maurya, G. Rajput, K. K. Manar, M. Vinayak, M. G. B. Drew, N. Singh, *J. Coord. Chem.* **2017**, *70*, 565.
- [62] C. L. Yadav, G. Rajput, K. K. Manar, K. Kumari, M. G. B. Drew, N. Singh, *Dalton Trans.* **2018**, *47*, 16264.
- [63] D. Florio, A. M. Malfitano, S. Di Somma, C. Mügge, W. Weigand, G. Ferraro, I. Iacobucci, M. Monti, G. Morelli, A. Merlino, D. Marasco, *Int. J. Mol. Sci.* **2019**, *20*, 829.
- [64] K. Kumari, S. Kumar, K. N. Singh, M. G. B. Drew, N. Singh, *New J. Chem.* **2020**, *44*, 12143.
- [65] C. L. Yadav, Anamika, G., Rajput, K. Kumar, M. G. B. Drew, N. Singh, *Inorg. Chem.* **2020**, *59*, 11417.
- [66] M. Destarac, I. Gauthier-Gillaizeau, C.-T. Vuong, S. Z. Zard, *Macromolecules* **2006**, *39*, 912.
- [67] A. Postma, T. P. Davis, G. Li, G. Moad, M. S. O'Shea, *Macromolecules* **2006**, *39*, 5307.
- [68] M. Naguib, K. L. Nixon, D. J. Keddie, *Polym. Chem.* **2022**, *13*, 1401.
- [69] M. H. Stenzel, C. Barner-Kowollik, *Mater. Horiz.* **2016**, *3*, 471.
- [70] A. Goncalves, J. R. Domínguez, J. Alvarado, *Talanta* **2008**, *75*, 523.
- [71] A. Calvo Fornieles, A. García de Torres, E. Vereda Alonso, J. M. Cano Pavón, *Microchem. J.* **2016**, *124*, 82.
- [72] M. M. L. Guerrero, E. V. Alonso, A. García de Torres, J. M. C. Pavón, *J. Anal. At. Spectrom.* **2017**, *32*, 2281.
- [73] F. C. Pinheiro, A. I. Barros, J. A. Nóbrega, *Microchem. J.* **2019**, *146*, 948.
- [74] S. E. Livingstone, *Coord. Chem. Rev.* **1971**, *7*, 59.
- [75] J.-J. Liñ, K.-Y. Yeh, C.-Y. Liu, *Fresenius' J. Anal. Chem.* **1990**, 336, 12.
- [76] M. d. C. Mancilla-González, V. Jancik, D. Martínez-Otero, M. Moya-Cabrera, I. García-Orozco, *J. Organomet. Chem.* **2014**, *770*, 35.



[M]acro-  
molecular  
Rapid Communications

Supporting Information

for *Macromol. Rapid Commun.*, DOI 10.1002/marc.202200428

Dual Function of  $\beta$ -Hydroxy Dithiocinnamic Esters: RAFT Agent and Ligand for Metal Complexation

*Micheal K. Farh, Franka V. Gruschwitz, Nicole Ziegenbalg, Hassan Abul-Futouh, Helmar Görls, Wolfgang Weigand\* and Johannes C. Brendel\**

## Supporting information

### Dual function of $\beta$ -Hydroxy dithiocinnamic esters: RAFT agent and ligand for metal complexation

Micheal K. Farh,<sup>a,b,†</sup> Franka V. Gruschwitz,<sup>c,d,†</sup> Nicole Ziegenbalg,<sup>c,d</sup> Hassan Abul-Futouh,<sup>c</sup>  
Helmar Görls,<sup>a</sup> Wolfgang Weigand,<sup>a,d,\*</sup> Johannes C. Brendel,<sup>c,d,\*</sup>

<sup>a</sup> *Department of Inorganic and Analytical Chemistry (IAAC), Friedrich Schiller University  
Jena, Humboldtstraße 8, 07743 Jena, Germany*

<sup>b</sup> *Department of Chemistry, Faculty of Science, Assiut University, Assiut 71515, Egypt.*

<sup>c</sup> *Laboratory of Organic and Macromolecular Chemistry (IOMC), Friedrich Schiller  
University Jena, Humboldtstraße 10, 07743 Jena, Germany*

<sup>d</sup> *Jena Center for Soft Matter (JCSM), Friedrich Schiller University Jena, Philosophenweg 7,  
07743 Jena, Germany*

<sup>e</sup> *Department of Chemistry, Faculty of Science, The Hashemite University, P.O. Box 330127,  
Zarqa 13133, Jordan.*

† These authors contribute equally.

\* Corresponding authors: [wolfgang.weigand@uni-jena.de](mailto:wolfgang.weigand@uni-jena.de); [johannes.brendel@uni-jena.de](mailto:johannes.brendel@uni-jena.de)

## Materials and Methods

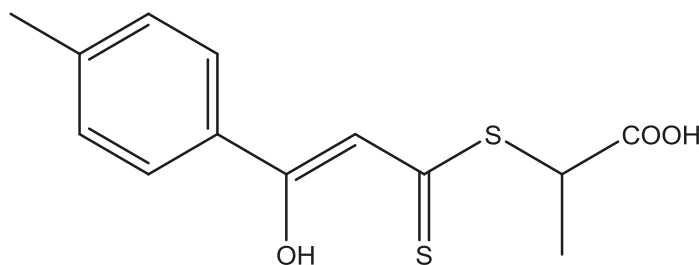
All reactions were performed using standard Schlenk and vacuum-line techniques under a nitrogen atmosphere. The NMR spectra were recorded with a Bruker Avance 300 MHz, 400 MHz or 500 MHz spectrometer. Chemical shifts are given in ppm with reference to SiMe<sub>4</sub>. Mass spectra were recorded with a Finnigan MAT SSQ 710 instrument. Elemental analysis was performed with a Leco CHNS-932 apparatus. TLC was performed using Merck TLC aluminum sheets (Silica gel 60 F254). Chemicals were purchased from Sigma-Aldrich, Merck, abcr or TCI and were used without further purification. All solvents were dried and distilled prior to use according to standard methods. Size-exclusion chromatography (SEC) of the polymers was performed on a Shimadzu system equipped with an SCL-10A system controller, an LC-10AD pump, a RID-10A refractive index detector and a PSS SDV column with N,N-dimethylacetamide (DMAc) + 0.21% LiCl. The column oven was set to 50 °C.

## Synthesis of the -β-hydroxydithiocinnamic acid derivatives

General procedure:

The desired acetophenone derivative (ca. 3-4 g, 1 eq.) is dissolved in dry diethyl ether (50 mL) and transferred into a precooled suspension of potassium- tert-butoxylate (t-BuOK, 2 eq.) in dry diethyl ether (40 mL) at -78 °C. Carbon disulfide (CS<sub>2</sub>, 1.4 eq.) is added dropwise to the solution under vigorous stirring, the mixture maintained at -78 °C for 3 hours and allowed to warm up to room temperature. 2-Bromopropionic acid (1 eq.) in dry diethyl ether (10 mL) is added dropwise with stirring to the formed dithiolate anion, the mixture is stirred protected from light at room temperature for a further 18 hours. For workup, the Solvent was removed, and dichloromethane (100 ml) was added to the yellow crude product. Sulfuric acid (aqueous solution, 2M, 100 ml) was added to the suspension and stirred for 30 minutes at room temperature. The two-phased system was separated, and the aqueous phase extracted with dichloromethane (3x35 ml). The combined organic phases were washed with water (3x20 ml), dried with sodium sulfate. After filtration, the solvent was removed, and the yellow crude product washed three times with n-pentane then recrystallized from (dichloromethane/acetone) affording the pure products 1–9 with yields ranging from 28% to 73%. All compounds were characterized by NMR spectroscopy, mass spectrometry and elemental analyses.

#### 4-Methyl- $\beta$ -hydroxydithiocinnamic acid $\beta'$ - propionic acid (L1)



Synthesis was performed according to general procedure 1. Using 4'-methylacetophenone (2.67 ml, 20 mmol), *t*-BuOK (4.48 g, 40 mmol), CS<sub>2</sub> (1.7 ml, 28 mmol) and 2-Bromopropionic acid (1.81 ml, 20 mmol). The compound was crystallized from dichloromethane/ acetone (1:1).

Yield: 2.73 g (48.47%) as yellow crystals.

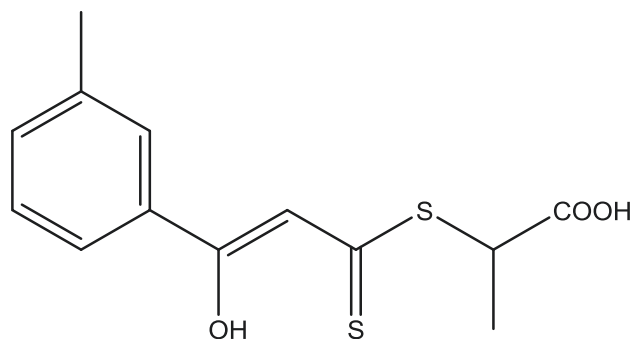
<sup>1</sup>H NMR (400 MHz, Acetone-d<sub>6</sub>):  $\delta$  = 1.66 (d, <sup>3</sup>*J*<sub>H-H</sub> = 7.3 Hz, 3H, CH-CH<sub>3</sub>); 2.46 (s, 3H, -CH<sub>3</sub>); 4.74 (q, <sup>3</sup>*J*<sub>H-H</sub> = 7.3 Hz, 1H, S-CH-); 7.21 (s, 1H, =CH-); 7.35 (d, <sup>3</sup>*J*<sub>H-H</sub> = 8.1 Hz, 2H, -Ar-*o*-H); 7.95 (d, <sup>3</sup>*J*<sub>H-H</sub> = 8.3 Hz, 2H, -Ar-*m*-H); 11.48 (s, 1H, -COOH); 15.16 (s, 1H, -C-OH).

<sup>13</sup>C {<sup>1</sup>H} NMR (101 MHz, Acetone-d<sub>6</sub>):  $\delta$  = 16.55 (CH<sub>3</sub>); 20.90 (-Ar-CH<sub>3</sub>); 44.80 (S-CH-); 107.10 (=CH-); 126.94 (2C, -Ar-*o*-C); 129.67 (2C, -Ar-*m*-C); 133.90 (-Ar-C1); 143.61 (-*p*-Ar-CH<sub>3</sub>); 171.11 (COOH); 171.67 (-C-OH); 214.10 (-C=S).

MS (ESI) *m/z* = 281.10 [M-H]<sup>-</sup>.

Elemental analysis: calculated for C<sub>13</sub>H<sub>14</sub>O<sub>3</sub>S<sub>2</sub> C: 55.30%; H: 5.00%; S: 22.71%, found: C: 55.72%; H: 5.03%; S: 22.58%.

### 3-Methyl- $\beta$ -hydroxydithiocinnamic acid $\beta'$ - propionic acid (L2)



Synthesis was performed according to general procedure 1. Using 3'-methylacetophenone (2.72 ml, 20 mmol), *t*-BuOK (4.48 g, 40 mmol), CS<sub>2</sub> (1.7 ml, 28 mmol) and 2-Bromopropionic acid (1.81 ml, 20 mmol). The compound was crystallized from dichloromethane/ acetone (1:1).

Yield: 1.58 g (27.88 %) as yellow crystals.

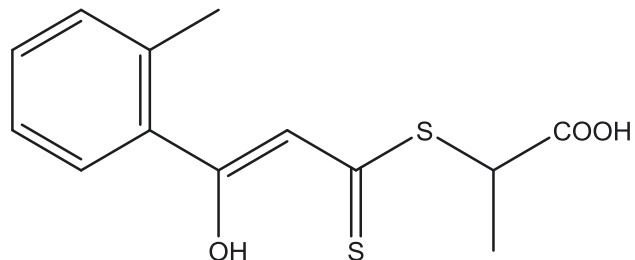
<sup>1</sup>H NMR (400 MHz, Acetone-d<sub>6</sub>):  $\delta$  = 1.66 (d, <sup>3</sup>*J*<sub>H-H</sub> = 7.3 Hz, 3H, CH-CH<sub>3</sub>); 2.45 (s, 3H, -CH<sub>3</sub>); 4.75 (q, <sup>3</sup>*J*<sub>H-H</sub> = 7.3 Hz, 1H, S-CH-); 7.22 (s, 1H, =CH-); 7.43 (m, 2H, -Ar-*m*-H, -Ar-*p*-H); 7.87 (m, 2H, -Ar-*o*-H); 11.44 (s, 1H, -COOH); 15.12 (s, 1H, -C-OH).

<sup>13</sup>C {<sup>1</sup>H} NMR (101 MHz, Acetone-d<sub>6</sub>):  $\delta$  = 17.50 (CH<sub>3</sub>); 21.50 (-Ar-CH<sub>3</sub>); 45.80 (S-CH-); 108.27 (=CH-); 124.95 (-Ar-*o*-C); 128.24 (-Ar-*o*-C); 129.78 (-Ar-*p*-C); 134.22 (-Ar-*m*-C); 134.55 (-Ar-C1); 139.70 (-*m*-Ar-CH<sub>3</sub>); 171.97 (COOH); 172.38 (-C-OH); 215.60 (-C=S).

MS (ESI) *m/z* = 281.10 [M-H]<sup>-</sup>.

Elemental analysis: calculated for C<sub>13</sub>H<sub>14</sub>O<sub>3</sub>S<sub>2</sub> C: 55.30%; H: 5.00%; S: 22.71%, found: C: 55.61%; H: 5.02%; S: 22.51%.

## 2-Methyl - $\beta$ -hydroxydithiocinnamic acid $\beta'$ - propionic acid (L3)



Synthesis was performed according to general procedure 1. Using 2'-methylacetophenone (2.62 ml, 20 mmol), *t*-BuOK (4.48 g, 40 mmol), CS<sub>2</sub> (1.7 ml, 28 mmol) and 2-Bromopropionic acid (1.81 ml, 20 mmol). The compound was crystallized from dichloromethane/acetone (1:1).

Yield: 2.64 g (46.74 %) as yellow crystals.

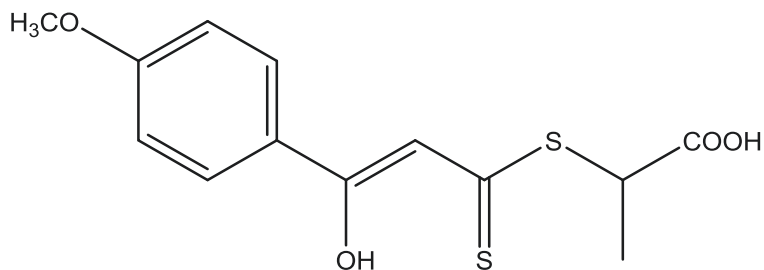
<sup>1</sup>H NMR (400 MHz, Acetone-d<sub>6</sub>):  $\delta$  = 1.66(d, <sup>3</sup>*J*<sub>H-H</sub> = 7.3 Hz, 3H, CH-CH<sub>3</sub>); 2.51 (s, 3H, -CH<sub>3</sub>); 4.75 (q, <sup>3</sup>*J*<sub>H-H</sub> = 7.3 Hz 1H, S-CH-); 6.71 (s, 1H, =CH-); 7.36 (m, 2H, -Ar-*m*-H, -Ar-*p*-H); 7.47 (m, 1H, -Ar-*m*-H); 7.56 (d, <sup>3</sup>*J*<sub>H-H</sub> = 7.8 Hz, -Ar- *o*-H); 11.49 (s, 1H, -COOH) ; 15.05 (s, 1H, -C-OH).

<sup>13</sup> C {<sup>1</sup>H} NMR (101 MHz, Acetone-d<sub>6</sub>):  $\delta$  = 16.40 (CH<sub>3</sub>); 20.40 (-Ar-CH<sub>3</sub>); 44.60 (S-CH-); 111.17 (=CH-); 126.22 (-Ar-*m*-C); 128.55 (-Ar-*o*-C); 131.05 (-Ar-*p*-C); 131.47 (-Ar-C1); 135.30 (-Ar-*m*-C); 136.10 (-*o*-Ar-CH<sub>3</sub>); 171.50 (COOH); 174.80 (-C-OH); 215.40 (-C=S).

MS (ESI) *m/z* = 281.10 [M-H].

Elemental analysis: calculated for C<sub>13</sub>H<sub>14</sub>O<sub>3</sub>S<sub>2</sub> C: 55.30%; H: 5.00%; S: 22.71%, found: C: 55.78%; H: 5.12%; S: 23.11%.

#### 4-Methoxy- $\beta$ -hydroxydithiocinnamic acid $\beta'$ - propionic acid (L4)



Synthesis was performed according to general procedure 1. Using 4'-methoxyacetophenone (3.00 g, 20 mmol), *t*-BuOK (4.48 g, 40 mmol), CS<sub>2</sub> (1.7 ml, 28 mmol) and 2-Bromopropionic acid (1.81 ml, 20 mmol). The compound was crystallized from dichloromethane/acetone (1:1).

Yield: 4.38 g (73.40%) as yellow crystals.

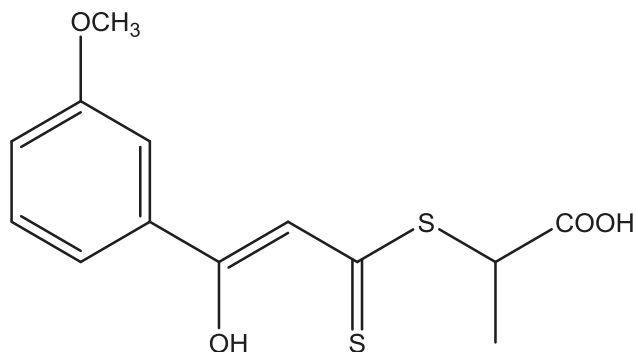
<sup>1</sup>H NMR (400 MHz, Acetone-d<sub>6</sub>):  $\delta$  = 1.65 (d, <sup>3</sup>*J*<sub>H-H</sub> = 7.3 Hz, 3H, CH-CH<sub>3</sub>); 3.93 (s, 3H, -CH<sub>3</sub>); 4.75 (q, <sup>3</sup>*J*<sub>H-H</sub> = 7.3 Hz, 1H, S-CH-); 7.20 (s, 1H, =CH-); 7.11 (m, 2H, -Ar-*o*-H); 8.06 (d, 2H, -Ar-*m*-H); 11.48 (s, 1H, -COOH); 15.19 (s, 1H, -C-OH).

<sup>13</sup>C {<sup>1</sup>H} NMR (101 MHz, Acetone-d<sub>6</sub>):  $\delta$  = 16.69 (CH<sub>3</sub>); 44.60 (-Ar-OCH<sub>3</sub>); 55.10 (S-CH-); 106.65 (=CH-); 114.60 (2C, -Ar-*o*-C); 126.00 (-Ar-C1); 129.20 (2C, -Ar-*m*-C); 163.68 (-*p*-Ar-OCH<sub>3</sub>); 171.13 (COOH); 171.98 (-C-OH); 212.70 (-C=S).

MS (ESI) *m/z* = 297.2 [M-H].

Elemental analysis: calculated for C<sub>13</sub>H<sub>14</sub>O<sub>4</sub>S<sub>2</sub> C: 52.32%; H: 4.73%; S: 21.49%, found: C: 52.60%; H: 4.59%; S: 21.23%.

### 3-Methoxy- $\beta$ -hydroxydithiocinnamic acid $\beta'$ - propionic acid (L5)



Synthesis was performed according to general procedure 1. Using 3'-methoxyacetophenone (2.75 ml, 20 mmol), *t*-BuOK (4.48 g, 40 mmol), CS<sub>2</sub> (1.7 ml, 28 mmol) and 2-Bromopropionic acid (1.81 ml, 20 mmol). The compound was crystallized from dichloromethane/acetone (1:1).

Yield: 2.66 g (44.50 %) as yellow crystals.

<sup>1</sup>H NMR (400 MHz, Acetone-d<sub>6</sub>):  $\delta$  = 1.67 (d, <sup>3</sup>*J*<sub>H-H</sub> = 7.3 Hz, 3H, CH-CH<sub>3</sub>); 3.91 (s, 3H, -CH<sub>3</sub>); 4.75 (q, <sup>3</sup>*J*<sub>H-H</sub> = 7.3 Hz, 1H, S-CH-); 7.21 (s, 1H, =CH-); 7.19 (dd, <sup>3</sup>*J*<sub>H-H</sub> = 8.4 Hz, <sup>4</sup>*J*<sub>H-H</sub> = 2.3 Hz, 1H, -Ar-*p*-H); 7.46 (t, <sup>3</sup>*J*<sub>H-H</sub> = 8.0 Hz, 1H, -Ar-*m*-H); 7.55 (s, 1H, -Ar-*o*-H); 7.62 (d, <sup>3</sup>*J*<sub>H-H</sub> = 7.9 Hz, 1H, -Ar-*o*-H); 11.44 (s, 1H, -COOH); 15.11 (s, 1H, -C-OH).

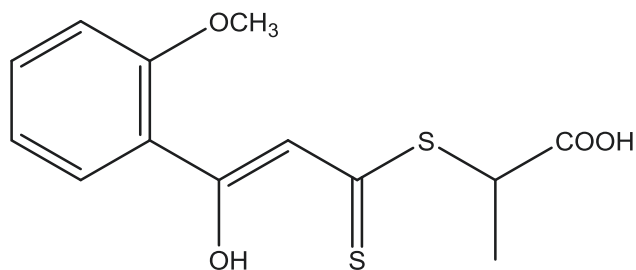
<sup>13</sup>C {<sup>1</sup>H} NMR (101 MHz, Acetone-d<sub>6</sub>):  $\delta$  = 16.68 (CH<sub>3</sub>); 44.70 (-Ar-CH<sub>3</sub>); 55.90 (S-CH-); 107.78 (=CH-); 111.87 (-Ar-*o*-C); 118.34 (-Ar-*p*-C); 119.208 (-Ar-*o*-C); 129.70 (-Ar-*m*-C); 135.40 (-Ar-C1); 160.00 (-*m*-Ar-OCH<sub>3</sub>); 171.10 (COOH); 177.10 (-C-OH); 213.10 (-C=S).

MS (ESI) *m/z* = 297.2 [M-H]<sup>-</sup>.

Elemental analysis: calculated for C<sub>13</sub>H<sub>14</sub>O<sub>4</sub>S<sub>2</sub> C: 52.32%; H: 4.73%; S: 21.49%, found: C: 52.49%; H: 4.71%; S: 21.24%.



## 2-Methoxy- $\beta$ -hydroxydithiocinnamic acid $\beta'$ - propionic acid (L6)



Synthesis was performed according to general procedure 1. Using 2'- methoxyacetophenone (2.75 ml, 20 mmol), *t*-BuOK (4.48 g, 40 mmol), CS<sub>2</sub> (1.7 ml, 28 mmol) and 2-Bromopropionic acid (1.81 ml, 20 mmol). The compound was crystallized from dichloromethane/acetone (1:1).

Yield: 3.05 g (51.03 %) as yellow crystals.

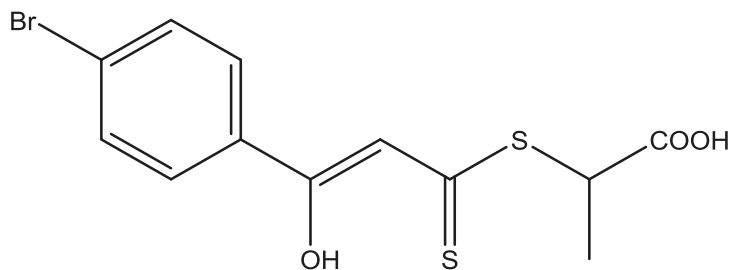
<sup>1</sup>H NMR (400 MHz, Acetone-d<sub>6</sub>):  $\delta$  = 1.66(d, <sup>3</sup>*J*<sub>H-H</sub> = 7.3 Hz, 3H, CH-CH<sub>3</sub>); 4.01 (s, 3H, -CH<sub>3</sub>); 4.72 (q, <sup>3</sup>*J*<sub>H-H</sub> = 7.3 Hz 1H, S-CH-); 7.11 (m, 1H, -Ar-*m*-H); 7.22 (d, <sup>3</sup>*J*<sub>H-H</sub> = 8.4 Hz, 1H, -Ar-*m*-H); 7.42 (s, 1H, =CH-); 7.58 (ddd, <sup>3</sup>*J*<sub>H-H</sub> = 8.8 Hz <sup>4</sup>*J*<sub>H-H</sub> = 1.8 Hz, 1H, -Ar- *p*-H); 7.91 (m, 1H, -Ar-*o*-H); 11.45 (s, 1H, -COOH) ; 15.14 (s, 1H, -C-OH).

<sup>13</sup> C {<sup>1</sup>H} NMR (101 MHz, Acetone-d<sub>6</sub>):  $\delta$  = 16.60 (CH<sub>3</sub>); 44.80 (-Ar-OCH<sub>3</sub>); 55.60 (S-CH-); 112.05 (=CH-); 112.34 (-Ar-C1); 120.74 (-Ar-*m*-C); 122.33 (-Ar-*m*-C); 129.90 (-Ar-*o*-C); 133.49 (-Ar-*p*-C); 158.46 (-*o*-Ar-OCH<sub>3</sub>); 169.16 (COOH); 171.45 (-C-OH); 213.90 (-C=S).

MS (DEI) *m/z* = 298.

Elemental analysis: calculated for C<sub>13</sub>H<sub>14</sub>O<sub>4</sub>S<sub>2</sub> C: 52.32%; H: 4.73%; S: 21.49%, found: C: 52.46%; H: 4.69%; S: 21.38%.

#### 4-Bromo- $\beta$ -hydroxydithiocinnamic acid $\beta'$ - propionic acid (L7)



Synthesis was performed according to general procedure 1. Using 4'-Bromoacetophenone (2.7 ml, 20 mmol), *t*-BuOK (4.48 g, 40 mmol), CS<sub>2</sub> (1.7 ml, 28 mmol) and 2-Bromopropionic acid (1.81 ml, 20 mmol). The compound was crystallized from dichloromethane/acetone (1:1).

Yield: 3.75 g (54%) as yellow crystals.

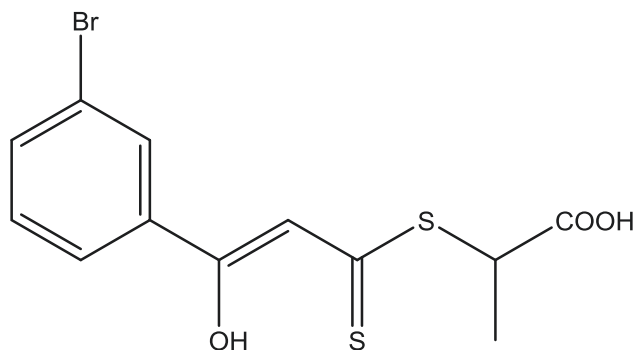
<sup>1</sup>H NMR (400 MHz, Acetone-d<sub>6</sub>):  $\delta$  = 1.67 (d, <sup>3</sup>*J*<sub>H-H</sub> = 7.3 Hz, 3H, CH-CH<sub>3</sub>); 4.76 (q, <sup>3</sup>*J*<sub>H-H</sub> = 7.3 Hz, 1H, S-CH-); 7.23 (s, 1H, =CH-); 7.77 (m, 2H, -Ar-*o*-H); 8.01 (m, 2H, -Ar-*m*-H); 11.02 (s, 1H, -COOH); 15.03 (s, 1H, -C-OH).

<sup>13</sup>C {<sup>1</sup>H} NMR (101 MHz, Acetone-d<sub>6</sub>):  $\delta$  = 16.40 (CH<sub>3</sub>); 45.10 (S-CH-); 107.50 (=CH-); 126.47 (-*p*-Ar-Br); 128.68 (-Ar-*o*-C); 132.24 (-Ar-*m*-C); 133.01 (-Ar-C1); 169.30 (COOH); 171.50 (-C-OH); 215.70 (-C=S).

MS (DEI) *m/z* = 346

Elemental analysis: calculated for C<sub>12</sub>H<sub>11</sub>O<sub>3</sub>S<sub>2</sub>Br C: 41.51%; H: 3.19%; S: 18.50%, Br: 23.01%, found: C: 41.82%; H: 3.17%; S: 18.62%; Br: 22.94%.

### 3-Bromo- $\beta$ -hydroxydithiocinnamic acid $\beta'$ - propionic acid (L8)



Synthesis was performed according to general procedure 1. Using 3'-Bromoacetophenone (2.7 ml, 20 mmol), *t*-BuOK (4.48 g, 40 mmol), CS<sub>2</sub> (1.7 ml, 28 mmol) and 2-Bromopropionic acid (1.81 ml, 20 mmol). The compound was crystallized from dichloromethane/acetone (1:1).

Yield: 1.95 g (28.10%) as yellow crystals.

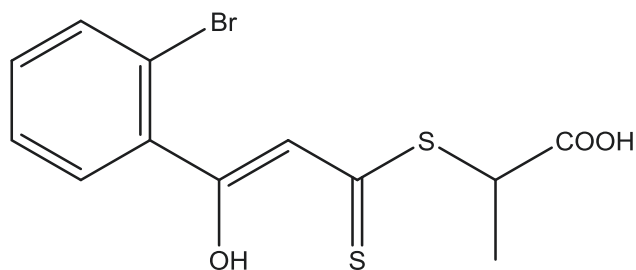
<sup>1</sup>H NMR (400 MHz, Acetone-d<sub>6</sub>):  $\delta$  = 1.68 (d, <sup>3</sup>*J*<sub>H-H</sub> = 7.3 Hz, 3H, CH-CH<sub>3</sub>); 4.75 (q, <sup>3</sup>*J*<sub>H-H</sub> = 7.3 Hz, 1H, S-CH-); 7.27 (s, 1H, =CH-); 7.52 (t, <sup>3</sup>*J*<sub>H-H</sub> = 8.0 Hz, 1H, -Ar-*m*-H); 7.80 (d, <sup>3</sup>*J*<sub>H-H</sub> = 8.0 Hz, 1H, -Ar-*p*-H); 8.05 (d, <sup>3</sup>*J*<sub>H-H</sub> = 7.9 Hz, 1H, -Ar-*o*-H); 8.20 (s, 1H, Ar-*o*-H); 11.47 (s, 1H, -COOH); 15.04 (s, 1H, -C-OH).

<sup>13</sup>C {<sup>1</sup>H} NMR (101 MHz, Acetone-d<sub>6</sub>):  $\delta$  = 17.60 (CH<sub>3</sub>); 46.20 (S-CH-); 108.70 (=CH-); 123.70 (-*m*-Ar-Br); 126.60 (-Ar-*o*-C); 130.30 (-Ar-*m*-C); 136.10 (-Ar-*p*-C); 132.00 (-Ar-*o*-C); 137.00 (-Ar-C1); 169.40 (COOH); 172.40 (-C-OH); 216.20 (-C=S).

MS (ESI) *m/z* = 345 [M-H]<sup>-</sup>.

Elemental analysis: calculated for C<sub>12</sub>H<sub>11</sub>O<sub>3</sub>S<sub>2</sub>Br C: 41.51%; H: 3.19%; S: 18.50%, Br: 23.01%, found: C: 41.50%; H: 3.06%; S: 18.72%; Br: 22.87%.

## 2-Bromo- $\beta$ -hydroxydithiocinnamic acid $\beta'$ - propionic acid (L9)



Synthesis was performed according to general procedure 1. Using 2'-Bromoacetophenone (2.7 ml, 20 mmol), *t*-BuOK (4.48 g, 40 mmol), CS<sub>2</sub> (1.7 ml, 28 mmol) and 2-Bromopropionic acid (1.81 ml, 20 mmol). The compound was crystallized from dichloromethane/acetone (1:1).

Yield: 2.10 g (30.24%) as yellow crystals.

<sup>1</sup>H NMR (400 MHz, Acetone-d<sub>6</sub>):  $\delta$  = 1.67 (d, <sup>3</sup>*J*<sub>H-H</sub> = 7.3 Hz, 3H, CH-CH<sub>3</sub>); 4.75 (q, <sup>3</sup>*J*<sub>H-H</sub> = 7.3 Hz, 1H, S-CH-); 6.72 (s, 1H, =CH-); 7.48 (td, <sup>3</sup>*J*<sub>H-H</sub> = 7.7 Hz, <sup>4</sup>*J*<sub>H-H</sub> = 1.6 Hz, 1H, -Ar-*m*-H); 7.55 (td, <sup>3</sup>*J*<sub>H-H</sub> = 7.5 Hz, <sup>4</sup>*J*<sub>H-H</sub> = 1.0 Hz, 1H, -Ar-*m*-H); 7.66 (dd, <sup>3</sup>*J*<sub>H-H</sub> = 7.6 Hz, <sup>4</sup>*J*<sub>H-H</sub> = 1.6 Hz, 1H, -Ar-*p*-H); 7.77 (dd, <sup>3</sup>*J*<sub>H-H</sub> = 7.9 Hz, <sup>4</sup>*J*<sub>H-H</sub> = 0.8 Hz, 1H, Ar-*o*-H); 11.52 (s, 1H, -COOH); 14.89 (s, 1H, -C-OH).

<sup>13</sup>C {<sup>1</sup>H} NMR (101 MHz, Acetone-d<sub>6</sub>):  $\delta$  = 16.70 (CH<sub>3</sub>); 45.30 (S-CH-); 109.58 (=CH-); 112.20 (-*o*-Ar-Br); 120.70 (-Ar-*p*-C); 127.90 (-Ar-*m*-C); 130.20 (-Ar-*o*-C); 132.30 (-Ar-*m*-C); 134.20 (-Ar-C1); 171.22v (COOH); 171.45 (-C-OH); 216.20 (-C=S).

MS (ESI) *m/z* = 345.2 [M-H].

Elemental analysis: calculated for C<sub>12</sub>H<sub>11</sub>O<sub>3</sub>S<sub>2</sub>Br C: 41.51%; H: 3.19%; S: 18.50%, Br: 23.01%, found: C: 41.69%; H: 3.06%; S: 18.80%; Br: 23.07%.

## Structure Determinations.

The intensity data for the compounds were collected on a Nonius KappaCCD diffractometer using graphite-monochromated Mo-K $\alpha$  radiation. Data were corrected for Lorentz and polarization effects; absorption was taken into account on a semi-empirical basis using multiple-scans<sup>[1-3]</sup>. The structures were solved by direct methods (SHELXS<sup>[4]</sup>) and refined by full-matrix least squares techniques against Fo<sup>2</sup> SHELXL-2018<sup>[5]</sup>. All hydrogen atoms (with exception of the methyl-group C12 of **L6**) were located by difference Fourier synthesis and refined isotropically. The hydrogen atoms bonded to C12 of **L6** were included at calculated positions with fixed thermal parameters. All non-hydrogen atoms were refined anisotropically<sup>[5]</sup>. MERCURY was used for structure representations<sup>[6]</sup>.

*Crystal Data for L6:* C<sub>13</sub>H<sub>14</sub>O<sub>4</sub>S<sub>2</sub>, Mr = 298.36 g mol<sup>-1</sup>, yellow prism, size 0.102 x 0.092 x 0.088 mm<sup>3</sup>, monoclinic, space group P 2<sub>1</sub>/c, a = 12.5849(3), b = 10.3771(2), c = 10.9319(2) Å,  $\beta$  = 104.836(1)°, V = 1380.05(5) Å<sup>3</sup>, T = -140 °C, Z = 4,  $\rho_{\text{calcd.}}$  = 1.436 g cm<sup>-3</sup>,  $\mu$  (Mo-K $\alpha$ ) = 3.92 cm<sup>-1</sup>, multi-scan, transmin: 0.7190, transmax: 0.7456, F(000) = 624, 10180 reflections in h(-16/16), k(-13/13), l(-14/14), measured in the range 1.674° ≤  $\Theta$  ≤ 27.445°, completeness  $\Theta_{\text{max}}$  = 99.3%, 3143 independent reflections, R<sub>int</sub> = 0.0213, 3033 reflections with F<sub>o</sub> > 4 $\sigma$ (F<sub>o</sub>), 217 parameters, 0 restraints, R<sub>1obs</sub> = 0.0670, wR<sub>2obs</sub><sup>2</sup> = 0.1631, R<sub>1all</sub> = 0.0686, wR<sub>2all</sub><sup>2</sup> = 0.1642, GOOF = 1.100, largest difference peak and hole: 1.476 / -0.948 e Å<sup>-3</sup>.

*Crystal Data for L5:* C<sub>13</sub>H<sub>14</sub>O<sub>4</sub>S<sub>2</sub>, Mr = 298.36 g mol<sup>-1</sup>, yellow prism, size 0.100 x 0.082 x 0.080 mm<sup>3</sup>, monoclinic, space group P 2<sub>1</sub>/c, a = 5.40870(10), b = 11.3630(2), c = 21.5531(4) Å,  $\beta$  = 92.936(1)°, V = 1322.89(4) Å<sup>3</sup>, T = -140 °C, Z = 4,  $\rho_{\text{calcd.}}$  = 1.498 g cm<sup>-3</sup>,  $\mu$  (Mo-K $\alpha$ ) = 4.09 cm<sup>-1</sup>, multi-scan, transmin: 0.7146, transmax: 0.7456, F(000) = 624, 8072 reflections in h(-6/7), k(-14/14), l(-21/27), measured in the range 2.027° ≤  $\Theta$  ≤ 27.484°, completeness  $\Theta_{\text{max}}$  = 99.7%, 3018 independent reflections, R<sub>int</sub> = 0.0147, 2848 reflections with F<sub>o</sub> > 4 $\sigma$ (F<sub>o</sub>), 228 parameters, 0 restraints, R<sub>1obs</sub> = 0.0256, wR<sub>2obs</sub><sup>2</sup> = 0.0652, R<sub>1all</sub> = 0.0273, wR<sub>2all</sub><sup>2</sup> = 0.0665, GOOF = 1.035, largest difference peak and hole: 0.369 / -0.208 e Å<sup>-3</sup>.

**Supporting Information available:** Crystallographic data (excluding structure factors) has been deposited with the Cambridge Crystallographic Data Centre as supplementary publication CCDC-2110906 for **L6**, and CCDC-2110907 for **L5**. Copies of the data can be obtained free of charge on application to CCDC, 12 Union Road, Cambridge CB2 1EZ, UK [E- mail: deposit@ccdc.cam.ac.uk].

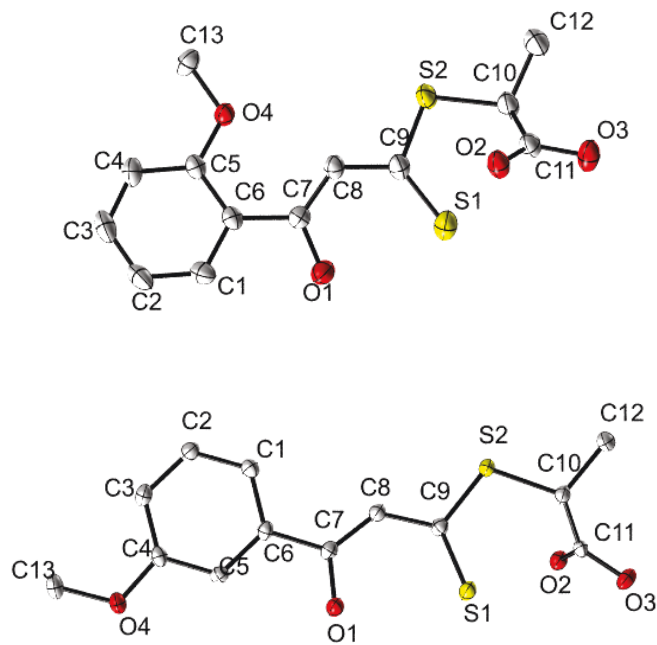


**Figure S1** Molecular structures of **L6** (up) and **L5** (down) (probability 50%). Hydrogen atoms are removed for clarity.

### UV-vis spectra.

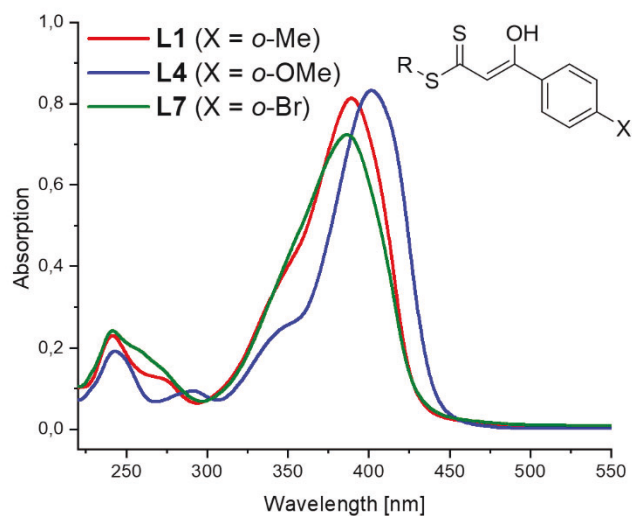


**Figure S2** UV-vis spectra of the compounds **L1**, **L4**, and **L7** dissolved in THF at a concentration of  $2.5 \times 10^{-5}$  mol/L.

## Polymerizations and kinetics

### poly(*N*-acryloylmorpholine), L1 (P1)

In a 20 mL microwave vial (Z)-2-((3-hydroxy-3-(*p*-tolyl)prop-2-enethiyl)thio)propanoic acid (L1) (40 mg, 0.142 mmol), *N*-acryloylmorpholine (1 g, 7.08 mmol), AIBN (58.15 mg of a 2 wt% solution in dioxane, 7.08  $\mu$ mol) and trioxane as an internal standard were added. The mixture was dissolved in dioxane (2.5 mL) and after degassing for 20 min with a stream of bubbled nitrogen in a sealed vial with a rubber septum, the reaction was started by inserting the vial in a preheated oil bath at 70 °C. After 24 h the reaction was cooled down and the polymer precipitated in diethyl ether. <sup>1</sup>H-NMR was performed after lyophilization.

<sup>1</sup>H-NMR (CD<sub>2</sub>Cl<sub>2</sub>, 400 MHz):  $\delta$  = 14.94 (s, 1H, -OH), 7.81-7.29 (m, 4H, -CH<sub>aromat</sub>), 6.97 (s, 1H, -CH-), 3.62-3.29 (m, morpholine), 2.64-2.41 (m, 42H, backbone), 1.68-1.26 (m, 108H, backbone), 1.15 (d, 3H, -CH<sub>3</sub>)

<sup>13</sup>C {<sup>1</sup>H} NMR (125.80 MHz, CD<sub>2</sub>Cl<sub>2</sub>):  $\delta$  = 18.51 (CH<sub>3</sub>); 21.59 (CH<sub>3</sub>-Ar); 35.56 (s, CH<sub>2</sub>-CH); 42.17, 45.97 (d, CH<sub>2</sub>-N); 45.30 (-CH-); 66.71 (s, CH<sub>2</sub>-O); 108.07 (=CH-); 126.89, 129.60, 129.70, 141.10 (CH of Ar); 171.88 (COOH); 173.14 (s, N-C=O); 177.89 (-C-OH); 204.39 (-C=S).

SEC (eluent: DMAc + 0.21% LiCl, PMMA-Standard):  $M_n$ : 7095 g mol<sup>-1</sup>,  $M_w$ : 8783 g mol<sup>-1</sup>, and  $D$  = 1.24.

### poly(butyl acrylate), L1 (P2)

In a 20 mL microwave vial (Z)-2-((3-hydroxy-3-(*p*-tolyl)prop-2-enethiyl)thio)propanoic acid (L1) (40 mg, 0.142 mmol), butyl acrylate (908 mg, 7.08 mmol), AIBN (58.15 mg of a 2 wt% solution in dioxane, 7.08  $\mu$ mol) and trioxane as an internal standard were added. The mixture was dissolved in dioxane (2.48 mL) and after degassing for 20 min with a stream of bubbled nitrogen in a sealed vial with a rubber septum, the reaction was started by inserting the vial in a preheated oil bath at 70 °C. After 24 h the reaction was cooled down and the polymer precipitated in mixture methanol:water (1:1).

<sup>1</sup>H-NMR (CDCl<sub>3</sub>, 300 MHz):  $\delta$  = 14.92 (s, 1H, -OH), 7.78 (d, 2H, -CH<sub>aromat</sub>), 7.27 (d, 2H, -CH<sub>aromat</sub>), 6.90 (s, 1H, -CH<sub>vinyl</sub>-), 4.03 (m, 123H, -O-CH<sub>2</sub>-), 2.41 (s, 3H, -CH<sub>3</sub>), 2.28-1.91 (m, 87H, backbone), 1.61-1.38 (m, 359H, backbone and -CH<sub>2</sub>-CH<sub>2</sub>- (butyl group)), 0.93 (t, 196H, -CH<sub>3</sub> (butyl group)).

SEC (eluent: DMAc + 0.21% LiCl, PMMA-Standard):  $M_n$ : 9817 g mol<sup>-1</sup>,  $M_w$ : 11790 g mol<sup>-1</sup>, and  $D$  = 1.18.

### **poly(styrene), L1 (P3)**

In a 20 mL microwave vial (Z)-2-((3-hydroxy-3-(p-tolyl)prop-2-enethioyl)thio)propanoic acid (L1) (40 mg, 0.142 mmol), styrene (738 mg, 7.08 mmol), AIBN (58.15 mg of a 2 wt% solution in dioxane, 7.08  $\mu$ mol) and trioxane as an internal standard were added. The mixture was dissolved in dioxane (2.48 mL) and after degassing for 20 min with a stream of bubbled nitrogen in a sealed vial with a rubber septum, the reaction was started by inserting the vial in a preheated oil bath at 70 °C. After 24 h the reaction was cooled down and the polymer precipitated in MeOH.

$^1\text{H-NMR}$  ( $\text{CDCl}_3$ , 300 MHz):  $\delta$  = 7.72 (s, 1H, -CH-), 7.13 (br, 4H,  $-\text{CH}_{\text{aromat(styrene)}}$ ), 6.62 (br,  $-\text{CH}_{\text{aromat(styrene)}}$ ), 2.37 (s, 3H,  $-\text{CH}_3$ ), 2.10-1.54 (m, br, backbone), 0.83 (br, 3H,  $-\text{CH}_3$ ).

SEC (eluent: DMAc + 0.21% LiCl, PS-Standard):  $M_n$ : 3261  $\text{g mol}^{-1}$ ,  $M_w$ : 3689  $\text{g mol}^{-1}$ , and  $D$  = 1.11.

### **poly(hydroxyl ethylacrylat), L1 (P4)**

In a 20 mL microwave vial (Z)-2-((3-hydroxy-3-(p-tolyl)prop-2-enethioyl)thio)propanoic acid (L1) (40 mg, 0.142 mmol), hydroxyl ethylacrylate (822 mg, 7.08 mmol), AIBN (58.15 mg of a 2 wt% solution in dioxane, 7.08  $\mu$ mol) and trioxane as an internal standard were added. The mixture was dissolved in dioxane (2.48 mL) and after degassing for 20 min with a stream of bubbled nitrogen in a sealed vial with a rubber septum, the reaction was started by inserting the vial in a preheated oil bath at 70 °C. After 24 h the reaction was cooled down and the polymer precipitated in diethyl ether.

$^1\text{H-NMR}$  ( $\text{D}_2\text{O}$ , 300 MHz):  $\delta$  = 7.84 (d, 2H,  $-\text{CH}_{\text{aromat}}$ ), 7.33 (d, 2H,  $-\text{CH}_{\text{aromat}}$ ), 4.12 (m, 110H,  $-\text{CH}_2(\text{HEA})^-$ ), 3.73 (m,  $-\text{CH}_2(\text{HEA})^-$ ), 2.38 - 1.58 (m br, 171H, backbone), 1.03 (d, 3H,  $-\text{CH}_3$ ).

SEC (eluent: DMAc + 0.21% LiCl, PEG-Standard):  $M_n$ : 10021  $\text{g mol}^{-1}$ ,  $M_w$ : 12203  $\text{g mol}^{-1}$ , and  $D$  = 1.18.

### **poly(methyl methacrylate), L1 (P5)**

In a 20 mL microwave vial (Z)-2-((3-hydroxy-3-(p-tolyl)prop-2-enethioyl)thio)propanoic acid (L1) (40 mg, 0.142 mmol), methyl methacrylate (709 mg, 7.08 mmol), AIBN (58.15 mg of a 2 wt% solution in dioxane, 7.08  $\mu$ mol) and trioxane as an internal standard were added. The mixture was dissolved in dioxane (2.48 mL) and after degassing for 20 min with a stream of bubbled nitrogen in a sealed vial with a rubber septum, the reaction was started by inserting the vial in a preheated oil bath at 70 °C. After 24 h the reaction was cooled down and the polymer precipitated in diethyl ether.



$^1\text{H-NMR}$  ( $\text{CDCl}_3$ , 300 MHz):  $\delta = 3.59$  (s, 3H,  $-\text{OCH}_3$ ), 1.80-0.84(m, 5H, backbone).

SEC (eluent: DMAc + 0.21% LiCl, PMMA-Standard):  $M_n$ : 215630  $\text{g mol}^{-1}$ ,  $M_w$ : 371900  $\text{g mol}^{-1}$ , and  $D = 1.70$ .

### **poly(N-acryloylmorpholine), L2 (P6)**

In a 20 mL microwave vial (Z)-2-(3-hydroxy-3-m-tolylprop-2-enethioylthio)propanoic acid (L2) (40 mg, 0.142 mmol), *N*-acryloylmorpholine (1 g, 7.08 mmol), AIBN (58.15 mg of a 2 wt% solution in dioxane, 6.70  $\mu\text{mol}$ ) and trioxane as an internal standard were added. The mixture was dissolved in dioxane (2.5 mL) and after degassing for 20 min with a stream of bubbled nitrogen in a sealed vial with a rubber septum, the reaction was started by inserting the vial in a preheated oil bath at 70 °C. After 24 h the reaction was cooled down and the polymer precipitated in diethyl ether.  $^1\text{H-NMR}$  was performed after lyophilization.

$^1\text{H-NMR}$  ( $\text{CD}_2\text{Cl}_2$ , 400 MHz):  $\delta = 14.92$  (s, 1H,  $-\text{OH}$ ), 7.73-7.00 (m, 5H,  $-\text{CH}_{\text{aromat}}$ ), 3.61-3.28 (m, morpholine), 2.64-2.54 (m, 45H, backbone), 1.78-1.25 (m, 90H, backbone), 1.15 (t, 3H,  $-\text{CH}_3$ )

$^{13}\text{C}\{^1\text{H}\}$  NMR (125.80 MHz,  $\text{CD}_2\text{Cl}_2$ ):  $\delta = 18.26$  ( $\text{CH}_3$ ); 21.13 ( $\text{CH}_3\text{-Ar}$ ); 35.51 (s,  $\text{CH}_2\text{-CH}$ ); 42.20, 45.94 (d,  $\text{CH}_2\text{-N}$ ); 45.21 ( $-\text{CH}-$ ); 66.77 (s,  $\text{CH}_2\text{-O}$ ); 107.80 ( $=\text{CH}-$ ); 124.10, 127.48, 128.79, 133.41, 133.57, 138.95 (CH of Ar); 171.68 (COOH); 172.94 (s,  $\text{N-C=O}$ ); 177.61 ( $-\text{C-OH}$ ); 204.60 ( $-\text{C=S}$ ).

SEC (eluent: DMAc + 0.21% LiCl, PMMA-Standard):  $M_n$ : 5939  $\text{g mol}^{-1}$ ,  $M_w$ : 7388  $\text{g mol}^{-1}$ , and  $D = 1.23$ .

### **poly(N-acryloylmorpholine), L3 (P7)**

The procedure was analogous to the above-mentioned synthesis.

$^1\text{H-NMR}$  ( $\text{CD}_2\text{Cl}_2$ , 400 MHz):  $\delta = 14.75$  (s, 1H,  $-\text{OH}$ ), 7.70-6.65 (m, 5H,  $-\text{CH}_{\text{aromat}}$ ), 3.65-3.31 (m, morpholine), 2.67-2.45 (m, 46H, backbone), 1.82-1.29 (m, 85H backbone), 1.18 (t, 3H,  $-\text{CH}_3$ )

$^{13}\text{C}\{^1\text{H}\}$  NMR (125.80 MHz,  $\text{CD}_2\text{Cl}_2$ ):  $\delta = 18.39$  ( $\text{CH}_3$ ); 20.60 ( $\text{CH}_3\text{-Ar}$ ); 35.64 (s,  $\text{CH}_2\text{-CH}$ ); 42.37, 46.08 (d,  $\text{CH}_2\text{-N}$ ); 43.70 ( $-\text{CH}-$ ); 66.97 (s,  $\text{CH}_2\text{-O}$ ); 111.79 ( $=\text{CH}-$ ); 126.24, 128.71, 131.14, 131.62, 134.90, 137.44 (CH of Ar); 172.69 (COOH); 173.07 (s,  $\text{N-C=O}$ ); 177.70 ( $-\text{C-OH}$ ); 204.60 ( $-\text{C=S}$ ).

SEC (eluent: DMAc + 0.21% LiCl, PMMA-Standard):  $M_n$ : 5095  $\text{g mol}^{-1}$ ,  $M_w$ : 6414  $\text{g mol}^{-1}$ , and  $D = 1.23$ .

### **poly(N-acryloylmorpholine), L6 (P8)**

In a 20 mL microwave vial (Z)-2-((3-hydroxy-3-(2-methoxyphenyl)prop-2-enethioyl)thio)propanoic acid (L6) (40 mg, 0.134 mmol), *N*-acryloylmorpholine (946 mg, 6.70 mmol), AIBN (55.05 mg of a 2 wt% solution in dioxane, 6.70  $\mu$ mol) and trioxane as an internal standard were added. The mixture was dissolved in dioxane (2.5 mL) and after degassing for 20 min with a stream of bubbled nitrogen in a sealed vial with a rubber septum, the reaction was started by inserting the vial in a preheated oil bath at 70 °C. After 24 h the reaction was cooled down and the polymer precipitated in diethyl ether. <sup>1</sup>H-NMR was performed after lyophilization.

<sup>1</sup>H-NMR (CD<sub>2</sub>Cl<sub>2</sub>, 400 MHz):  $\delta$  = 14.99 (s, 1H, -OH), 7.92-7.06 (m, 5H, -CH<sub>aromat</sub>), 3.66-3.32 (m, morpholine), 2.68-2.46 (m, 62H, backbone), 1.82-1.29 (m, 113H, backbone), 1.18 (t, 3H, -CH<sub>3</sub>)

<sup>13</sup>C{<sup>1</sup>H} NMR (125.80 MHz, CD<sub>2</sub>Cl<sub>2</sub>):  $\delta$  = 18.50 (CH<sub>3</sub>); 35.89 (s, CH<sub>2</sub>-CH); 42.40, 46.13 (d, CH<sub>2</sub>-N); 46.13 (-CH-); 55.96 (CH<sub>3</sub>O-Ar); 66.94 (s, CH<sub>2</sub>-O); 112.00 (=CH-); 112.90, 120.96, 130.34, 131.11, 133.70, 158.46 (CH of Ar); 169.83 (COOH); 173.15 (s, N-C=O); 177.87 (-C-OH); 204.60 (-C=S).

SEC (eluent: DMAc + 0.21% LiCl, PMMA-Standard):  $M_n$ : 6676 g mol<sup>-1</sup>,  $M_w$ : 8665 g mol<sup>-1</sup>, and  $D$  = 1.29.

### **poly(N-acryloylmorpholine), L5 (P9)**

The procedure was analogous to the above-mentioned synthesis.

<sup>1</sup>H-NMR (CD<sub>2</sub>Cl<sub>2</sub>, 400 MHz):  $\delta$  = 14.92 (s, 1H, -OH), 7.47-7.10 (m, 5H, -CH<sub>aromat</sub>), 3.66-3.30 (m, 344H, morpholine), 2.63-2.41 (m, 43H, backbone), 1.77-1.25 (m, 85H, backbone), 1.15 (s, 3H, -CH<sub>3</sub>)

<sup>13</sup>C{<sup>1</sup>H} NMR (125.80 MHz, CD<sub>2</sub>Cl<sub>2</sub>):  $\delta$  = 18.20 (CH<sub>3</sub>); 35.72 (s, CH<sub>2</sub>-CH); 42.23, 45.97 (d, CH<sub>2</sub>-N); 45.97 (-CH-); 55.48 (CH<sub>3</sub>O-Ar); 66.78 (s, CH<sub>2</sub>-O); 107.84 (=CH-); 112.05, 118.33, 119.17, 129.92, 135.10, 160.02 (CH of Ar); 171.12 (COOH); 172.97 (s, N-C=O); 177.64 (-C-OH); 204.10 (-C=S).

SEC (eluent: DMAc + 0.21% LiCl, PMMA-Standard):  $M_n$ : 5482 g mol<sup>-1</sup>,  $M_w$ : 7176 g mol<sup>-1</sup>, and  $D$  = 1.31.

### **poly(N-acryloylmorpholine)<sub>45</sub> L4 (P10)**

The procedure was analogous to the above-mentioned synthesis.

<sup>1</sup>H-NMR (CD<sub>2</sub>Cl<sub>2</sub>, 400 MHz): δ = 15.06 (s, 1H, -OH), 7.95 (s, 2H, -CH<sub>aromat</sub>), 7.35 (s, 1H, -CH-), 7.01 (d, 2H, -CH<sub>aromat</sub>), 3.65-3.32 (br, 372H, morpholine), 2.67-2.45 (m, 46H, backbone), 1.81-1.29 (m, backbone), 1.19 (s, 3H, -CH<sub>3</sub>)

<sup>13</sup>C {<sup>1</sup>H} NMR (125.80 MHz, CD<sub>2</sub>Cl<sub>2</sub>): δ = 18.37 (CH<sub>3</sub>); 35.90 (s, CH<sub>2</sub>-CH); 42.41, 46.13 (d, CH<sub>2</sub>-N); 46.13 (-CH-); 55.77 (CH<sub>3</sub>O-Ar); 66.91 (s, CH<sub>2</sub>-O); 107.11 (=CH-); 114.51, 129.22, 131.27, 163.70 (CH of Ar); 171.77 (COOH); 173.18 (s, N-C=O); 177.99 (-C-OH); 204.39 (-C=S).

SEC (eluent: DMAc + 0.21% LiCl, PMMA-Standard): M<sub>n</sub>: 5756 g mol<sup>-1</sup>, M<sub>w</sub>: 7639 g mol<sup>-1</sup>, and *D* = 1.31.

### **poly(N-acryloylmorpholine), L9 (P11)**

In a 20 mL microwave vial (Z)-2-(3-(2-bromophenyl)-3-hydroxyprop-2-enethioylthio)propanoic acid (L9) (40 mg, 0.115 mmol), N-acryloylmorpholine (813 mg, 5.76 mmol), AIBN (47.3 mg of a 2 wt% solution in dioxane, 5.76 μmol) and trioxane as an internal standard were added. The mixture was dissolved in dioxane (2.5 mL) and after degassing for 20 min with a stream of bubbled nitrogen in a sealed vial with a rubber septum, the reaction was started by inserting the vial in a preheated oil bath at 70 °C. After 24 h the reaction was cooled down and the polymer precipitated in diethyl ether. <sup>1</sup>H-NMR was performed after lyophilization.

<sup>1</sup>H-NMR (CD<sub>2</sub>Cl<sub>2</sub>, 400 MHz): δ = 14.75 (s, 1H, -OH), 7.70-7.39 (m, 4H, -CH<sub>aromat</sub>), 6.65 (s, 1H, -CH-), 3.57-3.34 (m, morpholine), 2.67-2.45 (m, 46H, backbone) 1.63-1.02 (m, 85H, backbone), 1.18 (t, 3H, -CH<sub>3</sub>)

<sup>13</sup>C {<sup>1</sup>H} NMR (125.80 MHz, CD<sub>2</sub>Cl<sub>2</sub>): δ = 18.50 (CH<sub>3</sub>); 35.67 (s, CH<sub>2</sub>-CH); 42.41, 46.14 (d, CH<sub>2</sub>-N); 46.14 (-CH-); 66.93 (s, CH<sub>2</sub>-O); 107.92 (=CH-); 123.09, 125.60, 130.06, 130.64, 131.85, 135.29 (CH of Ar); 169.40 (COOH); 173.19 (s, N-C=O); 177.95 (-C-OH); 214.40 (-C=S).

SEC (eluent: DMAc + 0.21% LiCl, PMMA-Standard): M<sub>n</sub>: 5831 g mol<sup>-1</sup>, M<sub>w</sub>: 7429 g mol<sup>-1</sup>, and *D* = 1.27.

### **poly(N-acryloylmorpholine), L8 (P12)**

The procedure was analogous to the above-mentioned synthesis.

$^1\text{H-NMR}$  ( $\text{CD}_2\text{Cl}_2$ , 400 MHz):  $\delta = 14.88$  (s, 1H, -OH), 8.10-7.41 (s, 4H,  $-\text{CH}_{\text{aromat}}$ ), 6.99 (s, 1H, -CH-), 3.68-3.33 (br, 209H, morpholine), 2.69-2.45 (m, 30H, backbone), 1.83-1.30 (m, 52H, backbone), 1.20 (s, 3H,  $-\text{CH}_3$ )

$^{13}\text{C}\{^1\text{H}\}$  NMR (125.80 MHz,  $\text{CD}_2\text{Cl}_2$ ):  $\delta = 18.39$  ( $\text{CH}_3$ ); 35.90 (s,  $\text{CH}_2\text{-CH}$ ); 42.40, 46.13 (d,  $\text{CH}_2\text{-N}$ ); 46.13 (-CH-); 66.94 (s,  $\text{CH}_2\text{-O}$ ); 112.41 ( $=\text{CH-}$ ); 120.89, 127.83, 130.48, 132.07, 134.13, 136.17 (CH of Ar); 171.68 (COOH); 173.15 (s,  $\text{N-C=O}$ ); 177.81 (-C-OH); 214.60 (-C=S).

SEC (eluent: DMAc + 0.21% LiCl, PMMA-Standard):  $M_n$ :  $3166 \text{ mol}^{-1}$ ,  $M_w$ :  $4554 \text{ g mol}^{-1}$ , and  $D = 1.44$ .

### **poly(N-acryloylmorpholine), L7 (P13)**

The procedure was analogous to the above-mentioned synthesis.

$^1\text{H-NMR}$  ( $\text{CD}_2\text{Cl}_2$ , 400 MHz):  $\delta = 14.88$  (s, 1H, -OH), 8.10-7.41 (s, 4H,  $-\text{CH}_{\text{aromat}}$ ), 6.99 (s, 1H, -CH-), 3.68-3.33 (br, 209H, morpholine), 2.69-2.45 (m, 30H, backbone), 1.83-1.30 (m, 52H, backbone), 1.20 (s, 3H,  $-\text{CH}_3$ )

$^{13}\text{C}\{^1\text{H}\}$  NMR (125.80 MHz,  $\text{CD}_2\text{Cl}_2$ ):  $\delta = 18.22$  ( $\text{CH}_3$ ); 35.75 (s,  $\text{CH}_2\text{-CH}$ ); 42.26, 45.97 (d,  $\text{CH}_2\text{-N}$ ); 45.97 (-CH-); 66.76 (s,  $\text{CH}_2\text{-O}$ ); 107.51 ( $=\text{CH-}$ ); 127.07, 128.37, 132.18, 132.70 (CH of Ar); 171.84 (COOH); 173.03 (s,  $\text{N-C=O}$ ); 177.80 (-C-OH); 213.21 (-C=S).

SEC (eluent: DMAc + 0.21% LiCl, PMMA-Standard):  $M_n$ :  $4857 \text{ mol}^{-1}$ ,  $M_w$ :  $6871 \text{ g mol}^{-1}$ , and  $D = 1.41$ .

### **poly(butyl acrylate) macro CTA, L1 (P14)**

In a 20 mL microwave vial (Z)-2-((3-hydroxy-3-(p-tolyl)prop-2-enethiioyl)thio)propanoic acid (L1) (81 mg, 0.287 mmol), butyl acrylate (3.64 g, 28.4 mmol), AIBN (121.7 mg of a 2 wt% solution in dioxane, 14.7  $\mu$ mol) and trioxane as an internal standard were added. The mixture was dissolved in dioxane (2.49 mL) and after degassing for 20 min with a stream of bubbled nitrogen in a sealed vial with a rubber septum, the reaction was started by inserting the vial in a preheated oil bath at 70 °C. After 4 h the reaction was cooled down and the polymer precipitated in mixture methanol:water (1:1).

$^1\text{H-NMR}$  ( $\text{CDCl}_3$ , 300 MHz):  $\delta$  = 14.92 (s, 1H, -OH), 7.78 (d, 2H,  $-\text{CH}_{\text{aromat}}$ ), 7.27 (d, 2H,  $-\text{CH}_{\text{aromat}}$ ), 6.90 (s, 1H,  $-\text{CH}_{\text{vinyl-}}$ ), 4.03 (m, 109H,  $-\text{O-CH}_2-$ ), 2.41-1.91 (m, 88H,  $-\text{CH}_3$ , backbone), 1.61-1.38 (m, 295H, backbone and  $-\text{CH}_2-\text{CH}_2-$  (butyl group)), 0.93 (t, 160H,  $-\text{CH}_3$  (butyl group)).

SEC (eluent: DMAc + 0.21% LiCl, PMMA-Standard):  $M_n$ : 7780  $\text{g mol}^{-1}$ ,  $M_w$ : 8590  $\text{g mol}^{-1}$ , and  $D = 1.10$ .

### **poly(butyl acrylate) chain extension (P15) from the macro-CTA P14**

In a 20 mL microwave vial poly(butyl acrylate) macro CTA (P14) (454 mg, 76  $\mu$ mol), butyl acrylate (983 mg, 7.67 mmol), AIBN (126.6 mg of a 2 wt% solution in dioxane, 15.3  $\mu$ mol) and trioxane as an internal standard were added. The mixture was degassed for 20 min with a stream of bubbled nitrogen in a sealed vial with a rubber septum, and the reaction was started by inserting the vial in a preheated oil bath at 70 °C. After 4 h the reaction was cooled down and the polymer precipitated in mixture methanol:water (1:1).

$^1\text{H-NMR}$  ( $\text{CDCl}_3$ , 300 MHz):  $\delta$  = 14.92 (s, 1H, -OH), 7.78 (d, 2H,  $-\text{CH}_{\text{aromat}}$ ), 7.27 (d, 2H,  $-\text{CH}_{\text{aromat}}$ ), 6.90 (s, 1H,  $-\text{CH}_{\text{vinyl-}}$ ), 4.03 (m, 275H,  $-\text{O-CH}_2-$ ), 2.41-1.91 (m, 220H,  $-\text{CH}_3$ , backbone), 1.61-1.38 (m, 747H, backbone and  $-\text{CH}_2-\text{CH}_2-$  (butyl group)), 0.93 (t, 407H,  $-\text{CH}_3$  (butyl group)).

SEC (eluent: DMAc + 0.21% LiCl, PMMA-Standard):  $M_n$ : 15420  $\text{g mol}^{-1}$ ,  $M_w$ : 17180  $\text{g mol}^{-1}$ , and  $D = 1.11$ .

## Evaluation of polymerization kinetics:

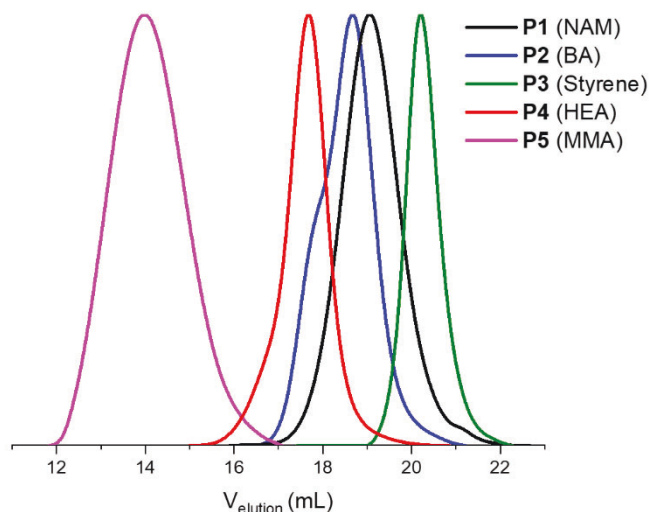


**Figure S3.** SEC traces for the polymers with L1 as CTA after precipitation (DMAc/LiCl, RI-detection).

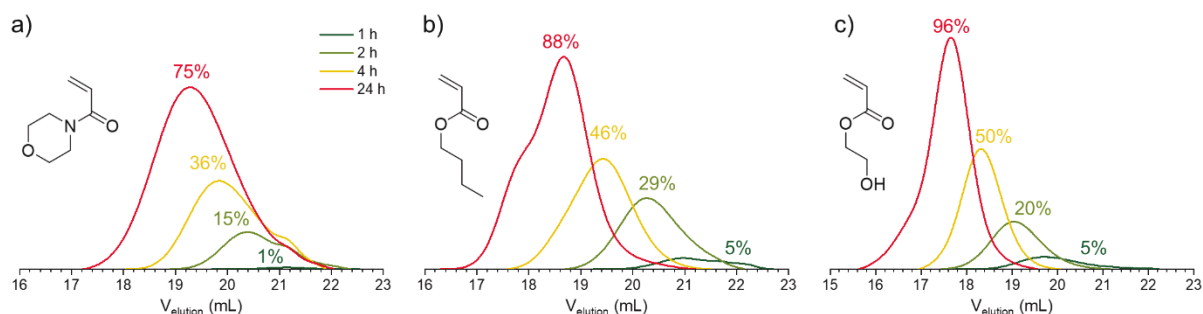


**Figure S4.** SEC traces normalized to conversions of samples (1h, 2h, 4h, and 24h) taken during the polymerization of a) NAM (P1), b) BA (P2), and c) HEA (P4) (DMAc/LiCl, RI-detection).

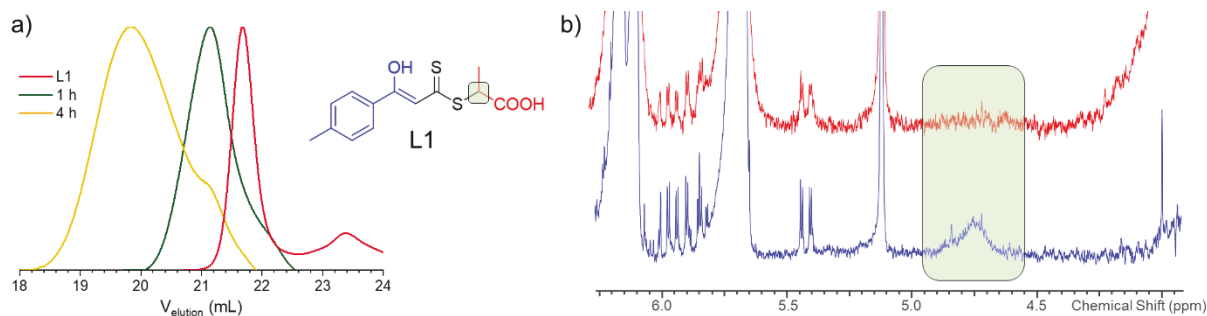


**Figure S5.** a) Normalized SEC trace of the CTA L1 in comparison to the 1h and 4h samples taken during the polymerization NAM (P1) (DMAc/LiCl, RI-detection); b)  $^1\text{H}$  NMR spectra of the kinetic samples taken at the beginning of the polymerization (blue) and after 1h (red), where the region for the signal of the CH group (marked in the structure) is highlighted.

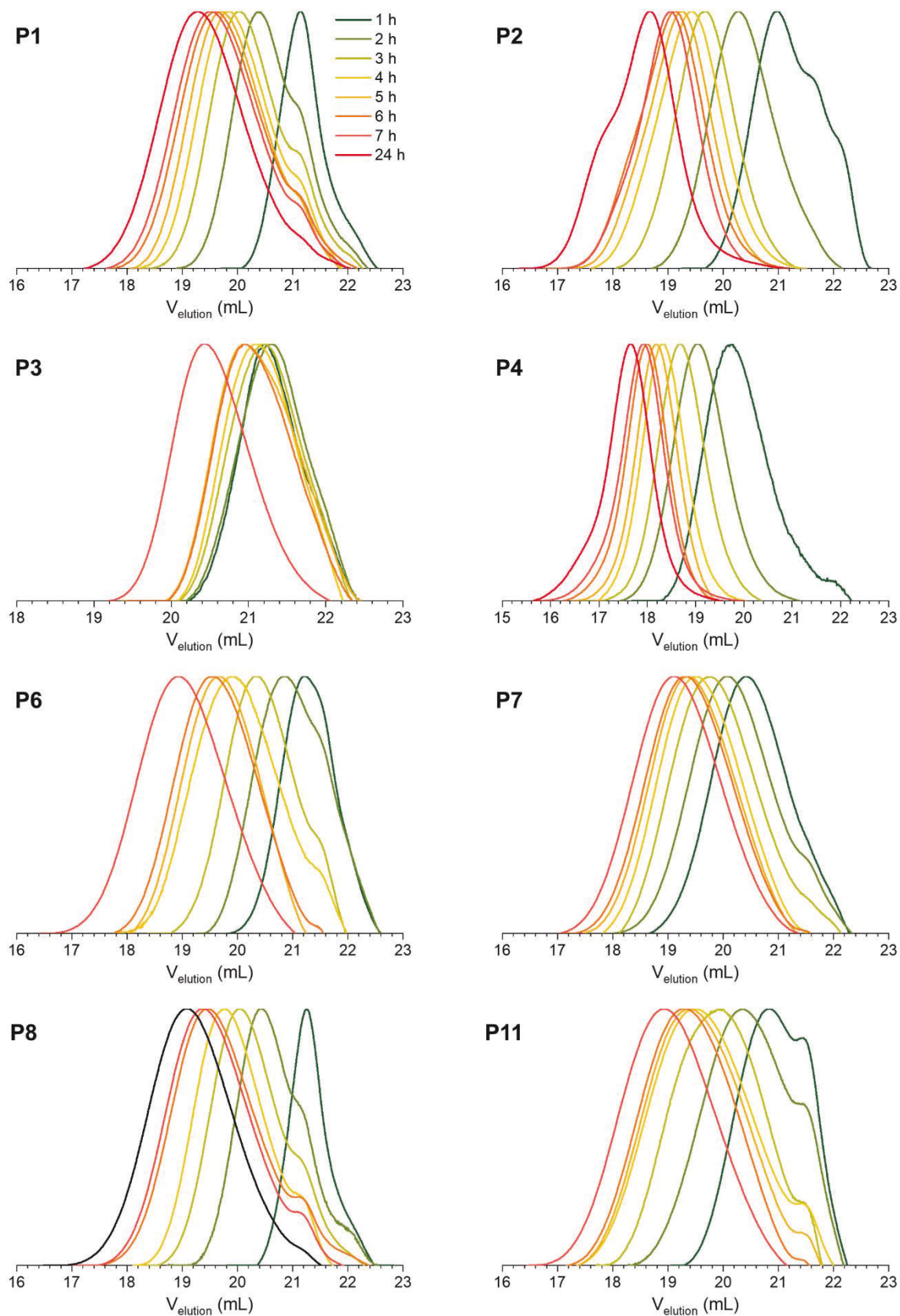


**Figure S6.** SEC traces of the kinetic samples (1h - 24h) taken during the polymerization of **P1-P4, P6-P8, and P11** (DMAc/LiCl, RI-detection).



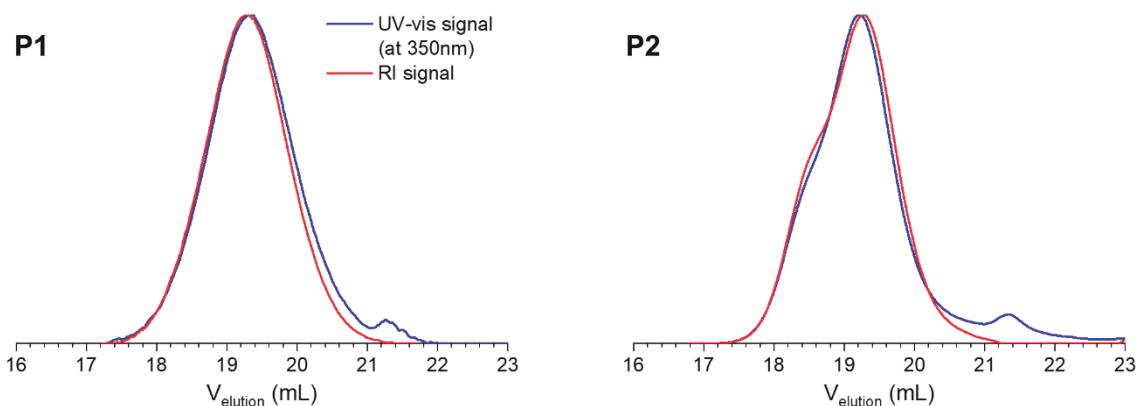


**Figure S7.** SEC traces (DMAc/LiCl, UV-Vis detection at 350 nm and RI detection) for the polymers P1 (a) and P2 (b) prepared with L1 as CTA after precipitation.

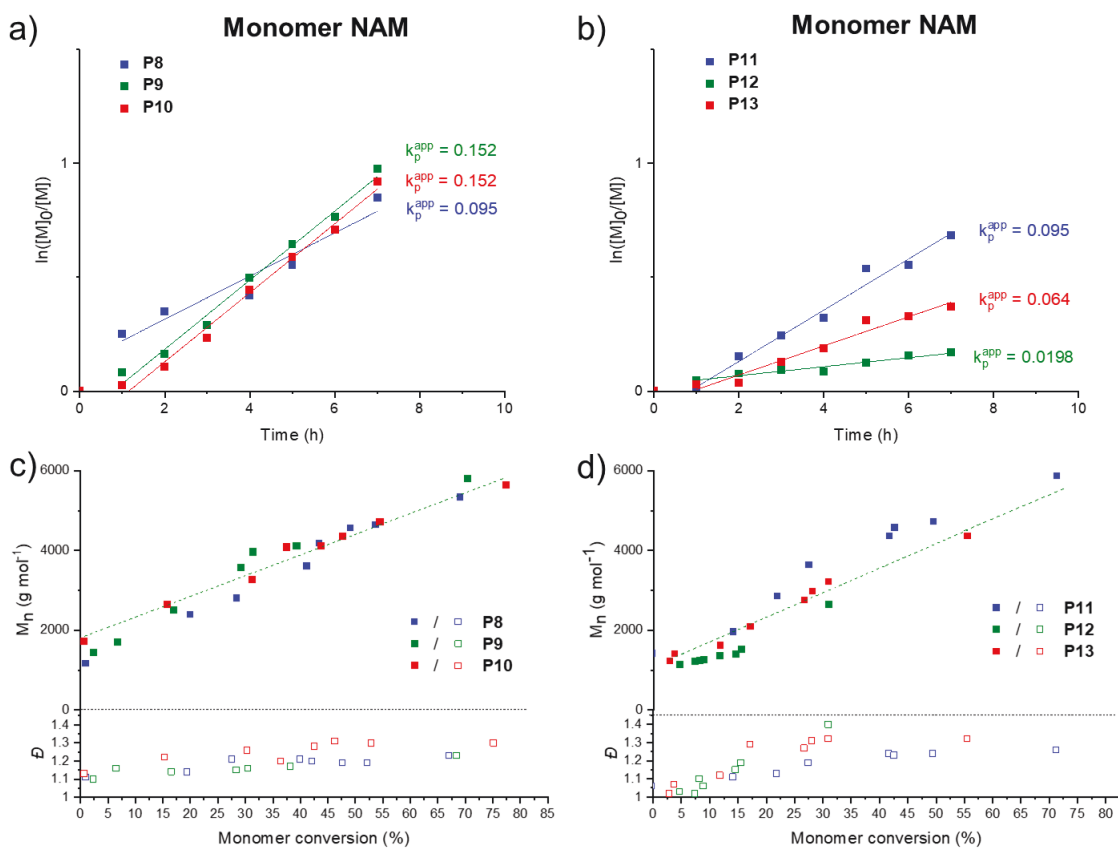


**Figure S8.** a)-b) Polymerization kinetics and c)-d) evolution of molar mass ( $M_n$ ) and dispersity  $D$  with conversion for L4-L6 (a) and c)) or L7-L9 (b) and d)).



## Preparation of the Pt(II) complexes

### General procedure 2

#### Pt(II) complexes of $\beta$ -hydroxydithiocinnamic acid modified polymers.

Potassium tetrachloro platinate ( $K_2PtCl_4$ ; 1.6-2 eq., 7-24 mg) is dissolved in 2 ml water. The  $\beta$ -hydroxydithiocinnamic acid modified polymers (1 eq., 71-200 mg) are dissolved in 5 ml water and added slowly to the metal solution in water path in 30 min. Then the mixture was stirred at room temperature overnight. The solvent was removed under reduced pressure to dryness resulting in yellow-orange powder. The product was extracted with DCM ( $3 \times 10$  ml). The combined organic phases are dried over sodium sulphate. After that, the solvent was removed. Finally, the Pt-functionalized polymers were dialyzed against water for 1 week.

#### Pt(II) Complex of P1 (PtP1)

Synthesis was performed according to general procedure 2. Using Potassium tetrachloro platinate ( $K_2PtCl_4$ ; 7.57 mg, 0.0182 mmol), **P1** (72 mg, 0.0093 mmol).

Isolated yield: 74 mg (97.61%)

$^1H$  NMR (400 MHz,  $CD_2Cl_2$ ):  $\delta$  = 1.18 (t, 3H,  $-CH_3$ ); 1.21-2.18 (m, 100H, backbone); 2.31-2.83 (m, 3H,  $-CH_3$ -Ar, 50H, backbone); 3.05-4.42 (m, 400H, morpholine); 4.94 (m, 1H,  $-CH-CH_3$ ); 7.00-9.15 (m, 1H,  $=CH-$ , 4H,  $-Ar-H$ ).

$^{13}C\{^1H\}$  NMR (125.80 MHz,  $CD_2Cl_2$ ):  $\delta$  = 18.39 ( $CH_3$ ); 21.62 ( $CH_3$ -Ar); 35.88 (s,  $CH_2-CH$ ); 42.39, 46.12 (d,  $CH_2-N$ ); 44.68 ( $-CH-$ ); 66.94 (s,  $CH_2-O$ ); 114.30 ( $=CH-$ ); 128.42, 129.88, 130.06, 140.13 ( $CH$  of Ar); 171.00 ( $COOH$ ); 173.12 (s,  $N-C=O$ ); 177.76 ( $-C-OH$ ); 177.82 ( $-C=S$ ).

### **Pt(II) Complex of P6 (PtP6)**

Synthesis was performed according to general procedure 2. Using Potassium tetrachloro platinate ( $K_2PtCl_4$ ; 24.53 mg, 0.059 mmol), **P6** (200 mg, 0.0301 mmol).

Isolated yield: 182.01 mg (85.51%)

$^1H$  NMR (400 MHz,  $CD_2Cl_2$ ):  $\delta$  = 1.19 (t, 3H,  $-CH_3$ ); 1.22-2.06 (m, 90H, backbone); 2.33-2.86 (m, 3H,  $-CH_3$ -Ar, 45H, backbone); 3.04-4.63 (m, 360H, morpholine); 4.96 (m, 1H,  $-CH-CH_3$ ); 6.82-9.42 (m, 1H,  $=CH-$ , 4H,  $-Ar-H$ ).

$^{13}C\{^1H\}$  NMR (125.80 MHz,  $CD_2Cl_2$ ):  $\delta$  = 18.35 ( $CH_3$ ); 21.28 ( $CH_3$ -Ar); 35.64 (s,  $CH_2-CH$ ); 42.40, 46.13 (d,  $CH_2-N$ ); 44.43 ( $-CH-$ ); 66.93 (s,  $CH_2-O$ ); 112.30 ( $=CH-$ ); 125.70, 127.70, 129.88, 130.07, 134.00, 138.80 (CH of Ar); 171.66 (COOH); 173.16 (s,  $N-C=O$ ); 176.94 ( $-C-OH$ ); 177.92 ( $-C=S$ ).

### **Pt(II) Complex of P7 (PtP7)**

Synthesis was performed according to general procedure 2. Using Potassium tetrachloro platinate ( $K_2PtCl_4$ ; 12.45 mg, 0.030 mmol), **P7** (100 mg, 0.0177 mmol).

Isolated yield: 107.08 mg (99.90%)

$^1H$  NMR (400 MHz,  $CD_2Cl_2$ ):  $\delta$  = 1.19 (t, 3H,  $-CH_3$ ); 1.21-2.18 (m, 76H, backbone); 2.30-2.86 (m, 3H,  $-CH_3$ -Ar, 38H, backbone); 2.95-4.60 (m, 304H morpholine); 4.91 (m, 1H,  $-CH-CH_3$ ); 6.95-9.40 (m, 1H,  $=CH-$ , 4H,  $-Ar-H$ ).

$^{13}C\{^1H\}$  NMR (125.80 MHz,  $CD_2Cl_2$ ):  $\delta$  = 18.34 ( $CH_3$ ); 20.26 ( $CH_3$ -Ar); 35.64 (s,  $CH_2-CH$ ); 42.40, 46.12 (d,  $CH_2-N$ ); 44.40 ( $-CH-$ ); 66.91 (s,  $CH_2-O$ ); 115.60 ( $=CH-$ ); 126.01, 127.73, 129.87, 130.06, 132.00, 134.10 (CH of Ar); 171.40 (COOH); 173.16 (s,  $N-C=O$ ); 176.88 ( $-C-OH$ ); 177.88 ( $-C=S$ ).

### **Pt(II) Complex of P8 (PtP8)**

Synthesis was performed according to general procedure 2. Using Potassium tetrachloro platinate ( $K_2PtCl_4$ ; 7.44 mg, 0.0179 mmol), **P8** (71 mg, 0.0085 mmol).

Isolated yield: 71.78 mg (96.22%)

$^1H$  NMR (400 MHz,  $CD_2Cl_2$ ):  $\delta$  = 1.18 (t, 3H,  $-CH_3$ ); 1.21-2.25 (m, 96H, backbone); 2.34-2.88 (m, 48H, backbone); 2.94-4.42 (m, 384H, morpholine); 4.00 (s, 3H,  $CH_3O-Ar$ ); 4.948 (m, 1H,  $-CH-CH_3$ ); 6.75-9.61 (m, 1H,  $=CH-$ , 4H,  $-Ar-H$ ).

$^{13}C\{^1H\}$  NMR (125.80 MHz,  $CD_2Cl_2$ ):  $\delta$  = 18.38 (CH<sub>3</sub>); 35.89 (s, CH<sub>2</sub>-CH); 42.40, 46.13 (d, CH<sub>2</sub>-N); 44.39 ( $-CH-$ ); 55.82 ( $CH_3O-Ar$ ); 66.94 (s, CH<sub>2</sub>-O); 117.20 ( $=CH-$ ); 118.60, 120.80, 128.88, 129.89, 130.07, 145.20 (CH of Ar); 168.00 (COOH); 173.14 (s, N-C=O); 176.81 ( $-C-OH$ ); 177.61 ( $-C=S$ ).

### **Pt(II) Complex of P9 (PtP9)**

Synthesis was performed according to general procedure 2. Using Potassium tetrachloro platinate ( $K_2PtCl_4$ ; 21.46 mg, 0.0517 mmol), **P9** (200 mg, 0.0314 mmol).

Isolated yield: 187.20 mg (87.74%)

$^1H$  NMR (400 MHz,  $CD_2Cl_2$ ):  $\delta$  = 1.18 (t, 3H,  $-CH_3$ ); 1.20-2.27 (m, 86H, backbone); 2.28-3.00 (m, 43H, backbone); 3.15-3.17 (m, 344H, morpholine); 4.03 (s, 3,  $CH_3O-Ar$ ); 4.96 (m, 1H,  $-CH-CH_3$ ); 6.51-9.461 (m, 1H,  $=CH-$ , 4H,  $-Ar-H$ ).

$^{13}C\{^1H\}$  NMR (125.80 MHz,  $CD_2Cl_2$ ):  $\delta$  = 18.39 (CH<sub>3</sub>); 35.89 (s, CH<sub>2</sub>-CH); 42.40, 46.13 (d, CH<sub>2</sub>-N); 44.37 ( $-CH-$ ); 55.74 ( $CH_3O-Ar$ ); 66.94 (s, CH<sub>2</sub>-O); 112.70 ( $=CH-$ ); 120.80, 122.60, 129.89, 130.07, 137.80, 160.02 (CH of Ar); 169.53 (COOH); 173.15 (s, N-C=O); 176.90 ( $-C-OH$ ); 177.89 ( $-C=S$ ).

### **Pt(II) Complex of P10 (PtP10)**

Synthesis was performed according to general procedure 2. Using Potassium tetrachloro platinate ( $K_2PtCl_4$ ; 20.48 mg, 0.0493 mmol), **P10** (200 mg, 0.0295 mmol).

Isolated yield: 176.26 mg (83.08%)

$^1H$  NMR (400 MHz,  $CD_2Cl_2$ ):  $\delta$  = 1.18 (t, 3H,  $-CH_3$ ); 1.20-2.27 (m, 90H, backbone); 2.29-2.87 (m, 45H, backbone); 2.95-4.67 (m, 360H, morpholine); 4.00 (s, 3H,  $CH_3O-Ar$ ); 4.95 (m, 1H,  $-CH-CH_3$ ); 6.74-9.12 (m, 1H,  $=CH-$ , 4H,  $-Ar-H$ ).

$^{13}C\{^1H\}$  NMR (125.80 MHz,  $CD_2Cl_2$ ):  $\delta$  = 18.28 ( $CH_3$ ); 35.88 (s,  $CH_2-CH$ ); 42.37, 46.09 (d,  $CH_2-N$ ); 44.40 ( $-CH-$ ); 55.77 ( $CH_3O-Ar$ ); 66.91 (s,  $CH_2-O$ ); 113.74 ( $=CH-$ ); 114.40, 130.04, 130.80, 163.90 ( $CH$  of  $Ar$ ); 168.30 ( $COOH$ ); 173.10 (s,  $N-C=O$ ); 177.57 ( $-C-OH$ ); 177.82 ( $-C=S$ ).

### **Pt(II) Complex of P11 (PtP11)**

Synthesis was performed according to general procedure 2. Using Potassium tetrachloro platinate ( $K_2PtCl_4$ ; 23.24 mg, 0.056 mmol), **P11** (200 mg, 0.0305 mmol).

Isolated yield: 186.43 mg (87.56%)

$^1H$  NMR (400 MHz,  $CD_2Cl_2$ ):  $\delta$  = 1.18 (t, 3H,  $-CH_3$ ); 1.2-2.26 (m, 88H, backbone); 2.29-2.85 (m, 44H, backbone); 2.88-4.73 (m, 352H, morpholine); 4.94 (m, 1H,  $-CH-CH_3$ ); 6.88-9.27 (m, 1H,  $=CH-$ , 4H,  $-Ar-H$ ).

$^{13}C\{^1H\}$  NMR (125.80 MHz,  $CD_2Cl_2$ ):  $\delta$  = 18.30 ( $CH_3$ ); 35.63 (s,  $CH_2-CH$ ); 42.39, 46.12 (d,  $CH_2-N$ ); 44.39 ( $-CH-$ ); 66.94 (s,  $CH_2-O$ ); 110.00 ( $=CH-$ ); 119.79, 125.54, 128.33, 129.88, 130.08, 134.30 ( $CH$  of  $Ar$ ); 168.20 ( $COOH$ ); 173.18 (s,  $N-C=O$ ); 176.84 ( $-C-OH$ ); 177.88 ( $-C=S$ ).

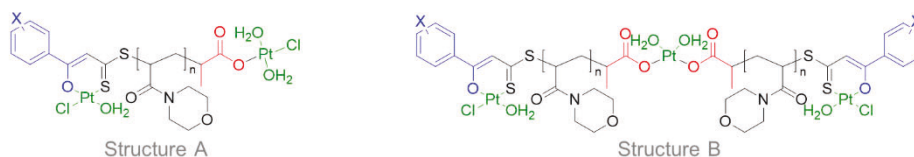
## Determination the concentration of Platinum in the prepared complexes using ICP-AES

### Microwave Digestion Method

The samples were digested in ETHOS ONE advanced microwave digestion system, equipped with easy prep plus extra high-pressure Teflon TFM vessels (The NOVA-8 rotor holds 8 TFM vessels with a volume of 75 ml, high pressures and temperatures up to 300°C) were used in the acid digestions of the samples. The microwave oven was operated in a temperature-controlled mode. Platinum samples of 5 -11 mg were weighed into the microwave digestion vessel, then 15 milliliters aqua regia was added to the digestion vessels. The vessels were closed, and the samples were digested in the microwave oven with a two-stage program. Stage (1) heating to 220 °C within 15 min, Stage (2) holding at 220 °C for 40 min. The solutions were allowed to cool to room temperature before opening the vessels. The solutions were transferred to 250 ml volumetric flasks and filled to the mark with 4% HCl (v/v) solution. The samples were further diluted with 4% HCl (v/v) before the ICP-AES determination.

### Calculations of compositions

More than one equivalent of Pt was found per chain in all samples, which is explained by the formation of the following to potential structures:



The experimentally determined mass of Pt for 1 g of sample is related to the ratio of the two proposed structures according to the equation

$$m(Pt) = \left[ x(A) \frac{2}{M(A)} + x(B) \frac{3}{M(B)} \right] A(Pt)$$

where  $x(A)$  and  $x(B)$  are the molar ratios of structures A and B in the sample,  $M(A)$  and  $M(B)$  are the average molar masses of the corresponding structures (average degrees of polymerization ( $n$ ) were estimated from the  $^1\text{H}$  NMR spectra of the precipitated polymers), and  $A(Pt)$  is the atomic weight of Pt. The numbers 2 and 3 in the numerators correspond to the number of Pt atoms in the corresponding structures A and B, respectively.

With  $x(B) = 1 - x(A)$  we can resolve the equation to estimate  $x(A)$  according to

$$x(A) = \left[ \frac{m(Pt)}{M(Pt)} - \frac{3}{M(B)} \right] / \left[ \frac{2}{M(A)} - \frac{3}{M(B)} \right]$$

**Table S 1. Concentrations on the Pt emission signal at 214.423 nm using ICP-AES.**

Pt(II) complexes	Pt content (theo.) [mg/g]	Pt content (experim.) [mg/g]	Calculated composition x(A) + x(B) (in %)
<b>PtP1 (structure A)</b> Pt <sub>2</sub> C <sub>384</sub> H <sub>601</sub> N <sub>53</sub> O <sub>112</sub> S <sub>2</sub> Cl <sub>2</sub> M.W.= 8277.48 g/mol	47.14		
<b>PtP1 (structure B)</b> Pt <sub>3</sub> C <sub>768</sub> H <sub>1198</sub> N <sub>106</sub> O <sub>222</sub> S <sub>4</sub> Cl <sub>2</sub> M.W.= 16252.94 g/mol	36.01	39.60	32% (A) + 68% (B)
<b>PtP6 (structure A)</b> Pt <sub>2</sub> C <sub>328</sub> H <sub>513</sub> N <sub>45</sub> O <sub>96</sub> S <sub>2</sub> Cl <sub>2</sub> M.W.= 7148.12 g/mol	54.58		
<b>PtP6 (structure B)</b> Pt <sub>3</sub> C <sub>656</sub> H <sub>1022</sub> N <sub>90</sub> O <sub>190</sub> S <sub>4</sub> Cl <sub>2</sub> M.W.= 13994.22 g/mol	41.82	47.16	42% (A) + 58% (B)
<b>PtP7 (structure A)</b> Pt <sub>2</sub> C <sub>279</sub> H <sub>436</sub> N <sub>38</sub> O <sub>82</sub> S <sub>2</sub> Cl <sub>2</sub> M.W.= 6159.93 g/mol	63.34		
<b>PtP7 (structure B)</b> Pt <sub>3</sub> C <sub>558</sub> H <sub>868</sub> N <sub>76</sub> O <sub>162</sub> S <sub>4</sub> Cl <sub>2</sub> M.W.= 12017.84 g/mol	48.70	52.80	28% (A) + 72% (B)
<b>PtP8 (structure A)</b> Pt <sub>2</sub> C <sub>412</sub> H <sub>645</sub> N <sub>57</sub> O <sub>121</sub> S <sub>2</sub> Cl <sub>2</sub> M.W.= 8858.16 g/mol	44.05		
<b>PtP8 (structure B)</b> Pt <sub>3</sub> C <sub>824</sub> H <sub>1286</sub> N <sub>114</sub> O <sub>240</sub> S <sub>4</sub> Cl <sub>2</sub> M.W.= 17414.30 g/mol	33.61	37.8	40% (A) + 60% (B)
<b>PtP9 (structure A)</b> Pt <sub>2</sub> C <sub>314</sub> H <sub>491</sub> N <sub>43</sub> O <sub>93</sub> S <sub>2</sub> Cl <sub>2</sub> M.W.= 6881.78 g/mol	56.70		
<b>PtP9 (structure B)</b> Pt <sub>3</sub> C <sub>628</sub> H <sub>978</sub> N <sub>86</sub> O <sub>184</sub> S <sub>4</sub> Cl <sub>2</sub> M.W.= 13461.54 g/mol	43.48	48.90	41% (A) + 59% (B)
<b>PtP10 (structure A)</b> Pt <sub>2</sub> C <sub>335</sub> H <sub>524</sub> N <sub>46</sub> O <sub>99</sub> S <sub>2</sub> Cl <sub>2</sub> M.W.= 7305.29 g/mol	53.41		
<b>PtP10 (structure B)</b> Pt <sub>3</sub> C <sub>670</sub> H <sub>1044</sub> N <sub>92</sub> O <sub>196</sub> S <sub>4</sub> Cl <sub>2</sub> M.W.= 14308.56 g/mol	40.90	45.00	33% (A) + 67% (B)
<b>PtP11 (structure A)</b> Pt <sub>2</sub> C <sub>320</sub> H <sub>499</sub> N <sub>44</sub> O <sub>94</sub> S <sub>2</sub> BrCl <sub>2</sub> M.W.= 7071.82 g/mol	55.17	47.50	40% (A) + 60% (B)

**PtP11 (structure B)**

Pt<sub>3</sub>C<sub>640</sub>H<sub>994</sub>N<sub>88</sub>O<sub>186</sub>S<sub>4</sub>Br<sub>2</sub>Cl<sub>2</sub> 42.28

M.W.= 13841.62 g/mol

**References**

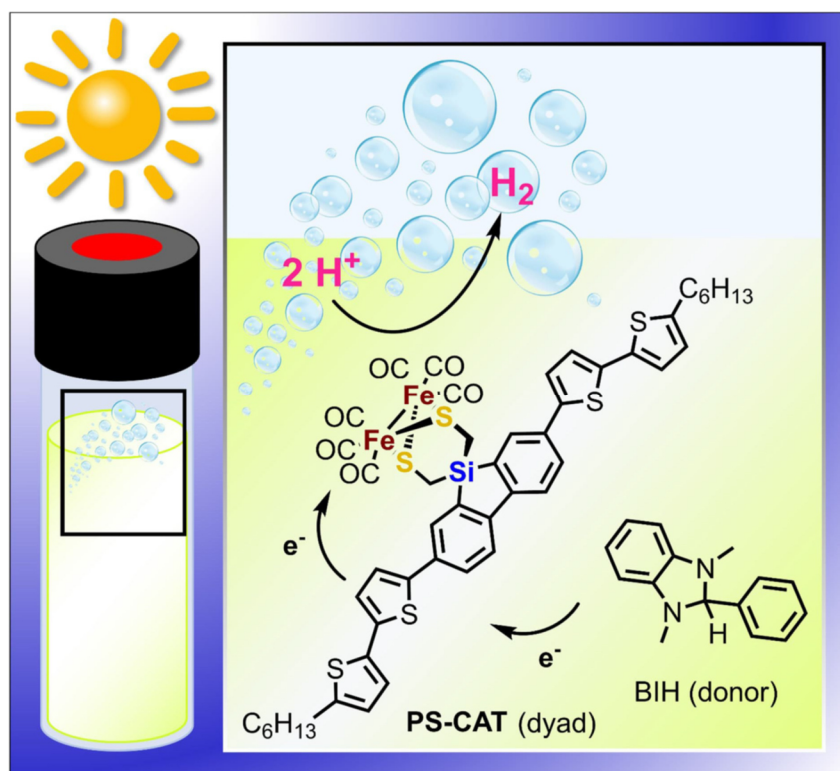
- [1] COLLECT, Data Collection Software; Nonius B.V., Netherlands, **1998**.
- [2] Z. Otwinowski, W. Minor, "Processing of X-ray diffraction data collected in oscillation mode", in *Methods Enzymol.*, Academic Press, 1997, p. 307.
- [3] L. Krause, R. Herbst-Irmer, G. M. Sheldrick, D. Stalke, *J. Appl. Crystallogr.* **2015**, *48*, 3.
- [4] G. Sheldrick, *Acta Crystallogr. Sect. A* **2008**, *64*, 112.
- [5] G. Sheldrick, *Acta Crystallogr. Sect. A* **2015**, *71*, 3.
- [6] C. F. Macrae, P. R. Edgington, P. McCabe, E. Pidcock, G. P. Shields, R. Taylor, M. Towler, J. van de Streek, *J. Appl. Crystallogr.* **2006**, *39*, 453.

## 5.4 [ME-4]

### Activating a [FeFe] Hydrogenase Mimic for Hydrogen Evolution under Visible Light

Philipp Buday, Chizuru Kasahara, Elisabeth Hofmeister, Daniel Kowalczyk, Micheal K. Farh, Saskia Riediger, Martin Schulz, Maria Wächtler, Shunsuke Furukawa, Masaichi Saito, Dirk Ziegenbalg, Stefanie Gräfe, Peter Bäuerle, Stephan Kupfer, Benjamin Dietzek-Ivanšić, Wolfgang Weigand

Angewandte Chemie International Edition **2022**, 61, e202202079.



This is an open-access article under the terms of the Creative Commons Attribution License, which permits use, distribution, and reproduction in any medium, provided the original work is properly cited. license link (<https://creativecommons.org/licenses/by/4.0/>).



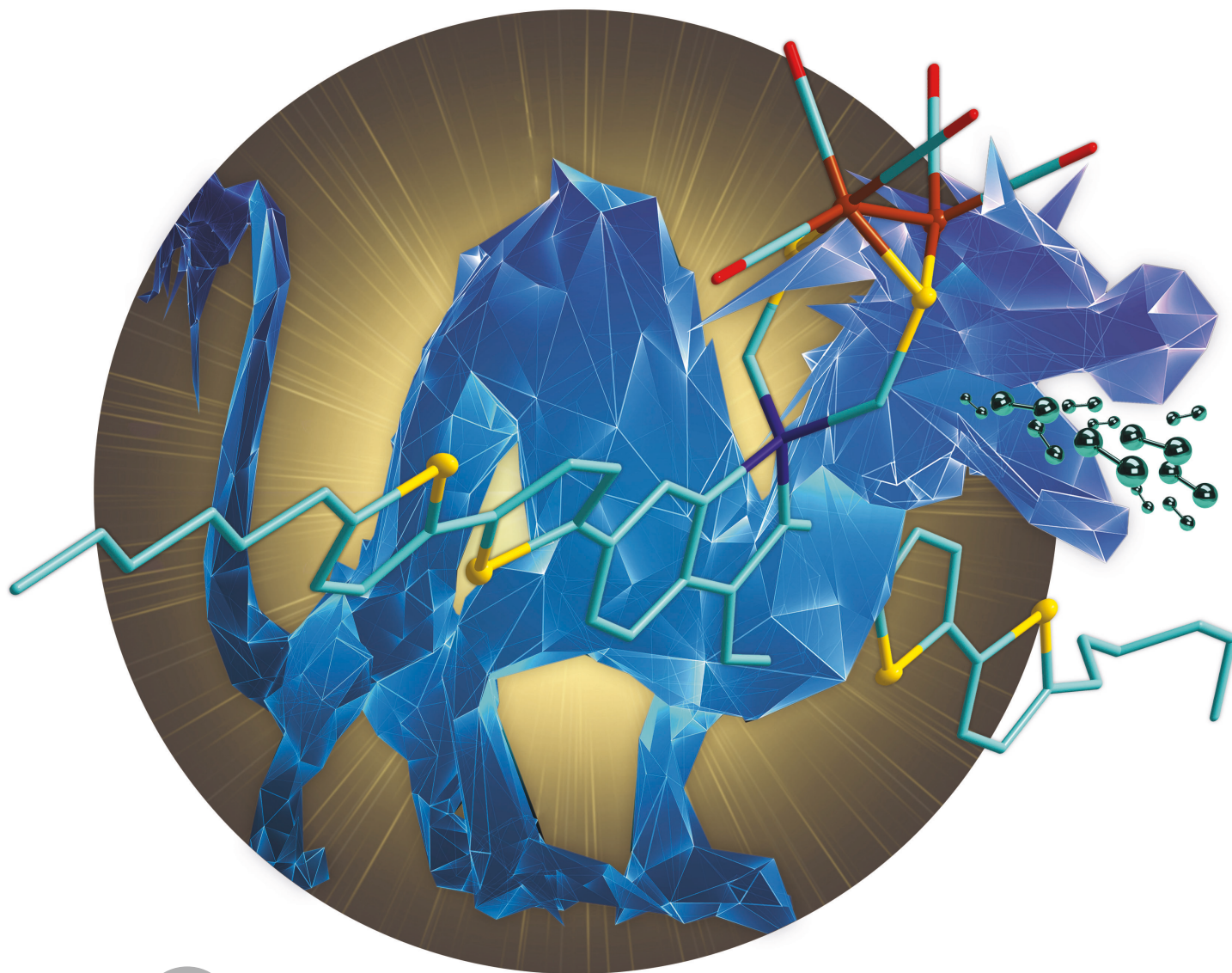
VIP Hydrogen Evolution Very Important Paper

How to cite: *Angew. Chem. Int. Ed.* **2022**, 61, e202202079  
International Edition: doi.org/10.1002/anie.202202079  
German Edition: doi.org/10.1002/ange.202202079

# Activating a [FeFe] Hydrogenase Mimic for Hydrogen Evolution under Visible Light\*\*

Philipp Buday<sup>+</sup>, Chizuru Kasahara<sup>+</sup>, Elisabeth Hofmeister, Daniel Kowalczyk, Micheal K. Farh, Saskia Riediger, Martin Schulz, Maria Wächtler, Shunsuke Furukawa, Masaichi Saito,\* Dirk Ziegenbalg, Stefanie Gräfe, Peter Bäuerle, Stephan Kupfer,\* Benjamin Dietzek-Ivanšić,\* and Wolfgang Weigand\*

Dedicated to Professor Wolfgang Beck on the occasion of his 90<sup>th</sup> birthday

Angewandte  
International Edition  
Chemie

**Abstract:** Inspired by the active center of the natural [FeFe] hydrogenases, we designed a compact and precious metal-free photosensitizer-catalyst dyad (**PS-CAT**) for photocatalytic hydrogen evolution under visible light irradiation. **PS-CAT** represents a prototype dyad comprising  $\pi$ -conjugated oligothiophenes as light absorbers. **PS-CAT** and its interaction with the sacrificial donor 1,3-dimethyl-2-phenylbenzimidazoline were studied by steady-state and time-resolved spectroscopy coupled with electrochemical techniques and visible light-driven photocatalytic investigations. *Operando* EPR spectroscopy revealed the formation of an active  $[\text{Fe}^{\text{I}}\text{Fe}^{\text{0}}]$  species—in accordance with theoretical calculations—presumably driving photocatalysis effectively (TON  $\approx$  210).

Nature provides paradigms for photocatalysis to generate solar fuels in a renewable and climate-neutral fashion. In this context, scientists have created various architectures to perform catalytic key processes, e.g. the hydrogen evolution reaction (HER), under light excitation. Commonly, 4d and 5d transition metals (e.g. Ru, Cd, Re, Ir, Pt) play a key role in molecular artificial HER photocatalysis—both as light-harvesters and catalysts—due to their favourable (photo)redox chemistry and stability.<sup>[1]</sup> However, rare abundance or undesired side effects (e.g. toxicity) hamper a larger scale application.

Nature uses earth-abundant, inexpensive reaction centers in the [FeFe] hydrogenase enzyme for HER.<sup>[2]</sup> Inspired by the natural paradigm, [FeFe] hydrogenase mimics have been reported.<sup>[3]</sup> Such catalysts, however, often rely on

photosensitizers based on precious metals. Few exceptions are given by e.g. xanthene dyes, (zinc) porphyrins<sup>[1a,4]</sup> or carbon dots<sup>[5]</sup> as light harvesters. Recently, we reported another fully precious metal-free example, a dibenzosilole photosensitizer directly attached to the catalyst, yield a TON of 539 for HER under UV light (254 nm).<sup>[6]</sup>  $\pi$ -Conjugated oligothiophenes present metal-free, readily accessible and strong light absorbers in the visible spectral region. The optical and redox properties of such dyes, which are used e.g. in organic<sup>[7]</sup> or dye-sensitized<sup>[8]</sup> solar cells, can be tuned easily. Recently, Hammarström and colleagues combined a  $\pi$ -conjugated oligothiophene photosensitizer and a [FeFe] hydrogenase mimic in a cosensitized NiO photocathode.<sup>[9]</sup>

We report a fully precious metal-free, visible-light absorbing, bioinspired and compact photocatalyst dyad **PS-CAT** as a prototype hybrid comprising  $\pi$ -conjugated oligothiophenes as photosensitizer for the light-driven HER. We present **PS-CAT**, its photocatalytic activity in the presence of the sacrificial donor 1,3-dimethyl-2-phenylbenzimidazoline (BIH) and a detailed mechanistic characterization. The oligothiophene sensitizer unit allows for a major improvement compared to the previously reported dibenzosilole light harvester, which is only active under UV irradiation.

**PS-CAT** combines the light-harvesting properties of  $\pi$ -conjugated oligothiophenes (PS) with a bioinspired [FeFe] hydrogenase mimic (CAT). It was synthesized according to Scheme 1 (also detailed in Scheme S1) from the bis-(thioacetate) **PS**. This pathway (iii–v) comprising a *N*-Methyl-2-pyrrolidone (NMP)-mediated<sup>[10]</sup> complexation reaction in step v) resulted in a better overall yield of **PS-CAT** (17%) compared to a direct conjunction (vi) with the  $[\text{2Fe}_2\text{S}]$  cluster (8%). Both, **PS** and **PS-CAT** were charac-

[\*] P. Buday,<sup>†</sup> C. Kasahara,<sup>†</sup> M. K. Farh, Prof. W. Weigand  
Institute of Inorganic and Analytical Chemistry  
Friedrich Schiller University Jena  
Humboldtstraße 8, 07743 Jena (Germany)  
E-mail: wolfgang.weigand@uni-jena.de

C. Kasahara,<sup>†</sup> Dr. S. Furukawa, Prof. M. Saito  
Department of Chemistry  
Graduate School of Science and Engineering,  
Saitama University  
Shimo-okubo, Sakura-ku, Saitama City, Saitama, 338-8570 (Japan)  
E-mail: masaichi@chem.saitama-u.ac.jp

E. Hofmeister, Dr. M. Schulz, Dr. M. Wächtler,  
Prof. B. Dietzek-Ivanšić  
Department Functional Interfaces  
Leibniz Institute of Photonic Technology Jena (Leibniz-IPHT)  
Albert-Einstein-Straße 9, 07745 Jena (Germany)

D. Kowalczyk, Prof. D. Ziegenbalg  
Institute of Chemical Engineering  
Ulm University  
Albert-Einstein-Allee 11, 89081 Ulm (Germany)

Dr. M. Schulz, Dr. M. Wächtler, Prof. S. Gräfe, Dr. S. Kupfer,  
Prof. B. Dietzek-Ivanšić  
Institute of Physical Chemistry  
Friedrich Schiller University Jena  
Helmholtzweg 4, 07743 Jena (Germany)  
E-mail: stephan.kupfer@uni-jena.de  
benjamin.dietzek@uni-jena.de

Dr. M. Wächtler, Prof. S. Gräfe, Prof. B. Dietzek-Ivanšić  
Abbe Center of Photonics (ACP)  
Friedrich Schiller University Jena  
Albert-Einstein-Straße 6, 07745 Jena (Germany)

S. Riediger, Prof. P. Bäuerle  
Institute of Organic Chemistry II and Advanced Materials  
Ulm University  
Albert-Einstein-Allee 11, 89081 Ulm (Germany)

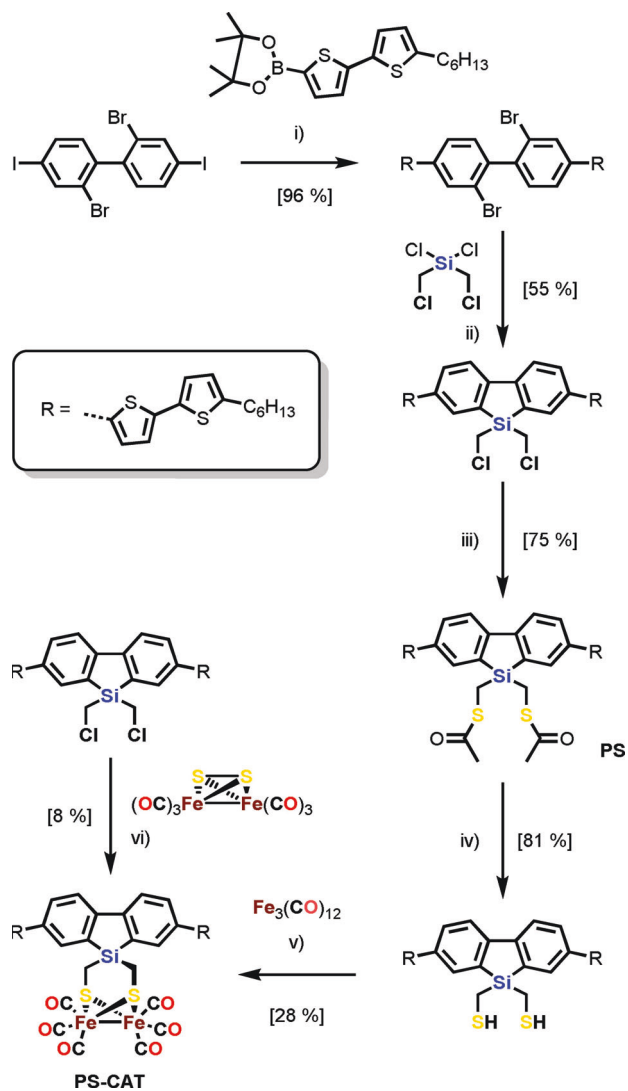
Prof. S. Gräfe, Prof. B. Dietzek-Ivanšić  
Center for Energy and Environmental Chemistry Jena (CEEC Jena)  
Friedrich Schiller University Jena  
Philosophenweg 8, 07743 Jena (Germany)

Prof. S. Gräfe  
Fraunhofer Institute for Applied Optics and Precision Engineering  
Albert-Einstein-Straße 7  
07745 Jena (Germany)

[†] These authors contributed equally to this work.

[\*\*] A previous version of this manuscript has been preprint deposited on a server (<https://doi.org/10.26434/chemrxiv-2021-1wh3l-v3>).

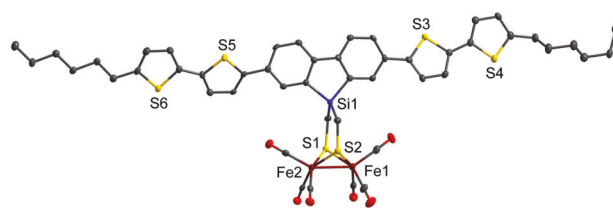
© 2022 The Authors. Angewandte Chemie International Edition published by Wiley-VCH GmbH. This is an open access article under the terms of the Creative Commons Attribution License, which permits use, distribution and reproduction in any medium, provided the original work is properly cited.



**Scheme 1.** Synthetic pathway to **PS-CAT** via **PS**. i)  $\text{BnNEt}_3\text{Cl}$ ,  $[\text{Pd}(\text{PPh}_3)_4]$ ,  $\text{K}_2\text{CO}_3$ , toluene;  $60^\circ\text{C}$ , 12 h; ii)  $n\text{-BuLi}$ , THF;  $-78^\circ\text{C}$  to r. t., 12 h; iii)  $\text{KSCoCH}_3$ , THF; r. t., 20 h; iv)  $\text{LiAlH}_4$ ,  $\text{Et}_2\text{O}$ ;  $0^\circ\text{C}$  to r. t., 12 h; v)  $\text{Fe}_3(\text{CO})_{12}$ , toluene/NMP (20:1); r. t., 12 h; vi)  $\text{LiBHET}_3$ , THF,  $-90^\circ\text{C}$  to r. t., 14 h.

terized by NMR, IR spectroscopy and mass spectrometry. The molecular structure of **PS-CAT** (Figure 1; Figure S2 and Table S1/S2; Supporting Information for crystallographic details) reveals a similar binding mode compared to that of a previous reported, structurally related complex.<sup>[6]</sup> A view on the ab plane shows stacking of planar **PS-CAT** molecules (Figure S2b). The cyclic voltammogram of **PS-CAT** in  $\text{CH}_2\text{Cl}_2$  at a scan rate of  $0.2 \text{ V s}^{-1}$  shows a quasi-reversible reduction event at  $E_{1/2}^{\text{Red1}} = -1.61 \text{ V}$  vs.  $\text{Fc}^+/\text{Fc}$  (Figure S9a).

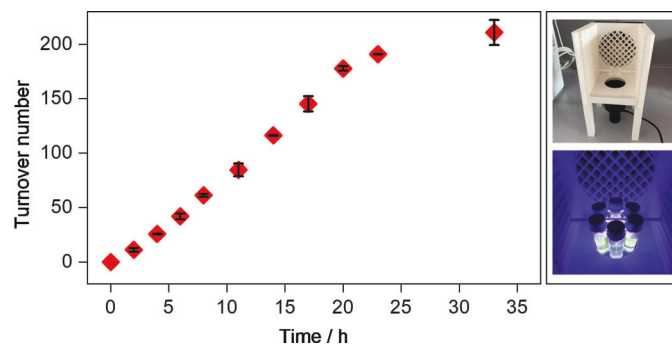
The photocatalytic proton reduction behaviour of **PS-CAT** was studied under irradiation with visible light in a 5:1 mixture of  $\text{CH}_3\text{CN}$  and NMP and with the two-electron, one-proton sacrificial donor  $\text{BIH}^{[12]}$  (1000 equivalents). The solvent mixture ensures solubility and a good catalytic performance due to an overall high dielectric constant.



**Figure 1.** Molecular structure and atom labeling scheme of **PS-CAT**.<sup>[11]</sup> The ellipsoids represent a probability of 50%. Hydrogen atoms are omitted for clarity. For selected bond lengths and angles see Table S2.

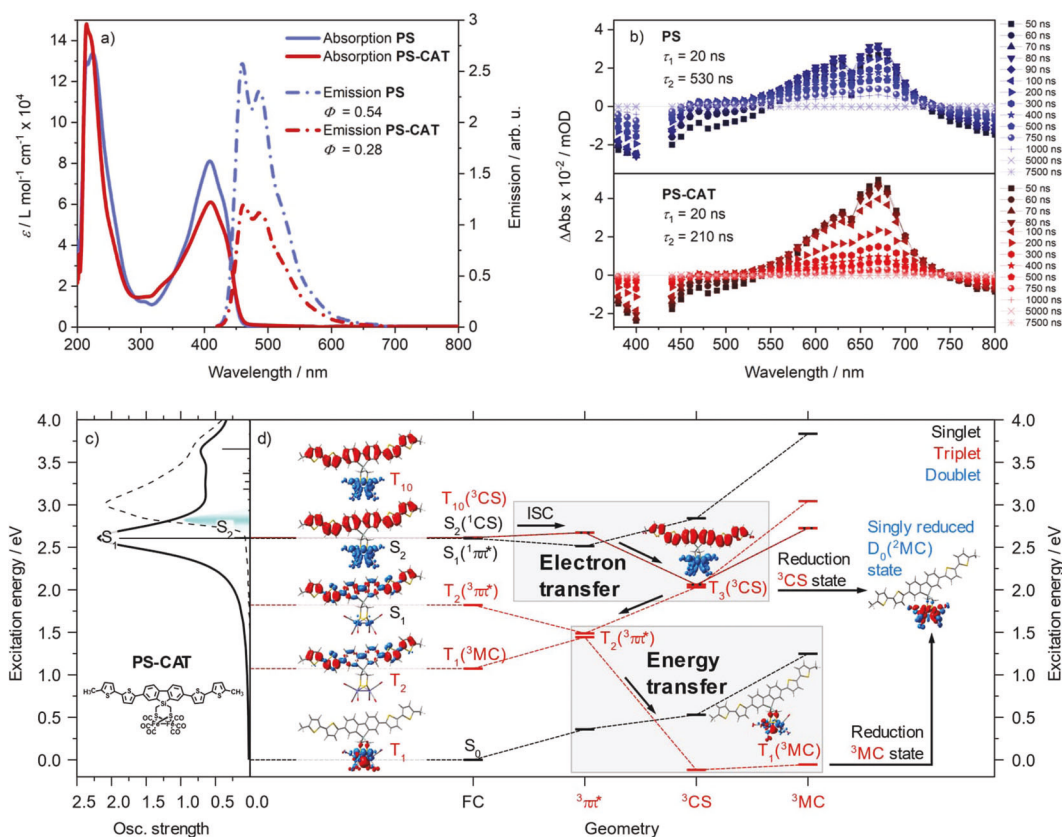
Moreover, the weak base NMP can potentially react with the oxidized donor ( $\text{BIH}^{*+}$ ) to capture the proton, thus inhibiting potential back electron transfer processes.<sup>[13]</sup> The photocatalytic reactions were performed in a custom-made, modular 3D printed photoreactor setup (Figure S1). Figure 2 shows the hydrogen evolution time profile. Within the initial 23 hours the catalytic turnover increases slightly sigmoidally, before the hydrogen evolution reaches a plateau at  $\text{TON} \approx 210$  ( $\text{TOF} \approx 6.4 \text{ h}^{-1}$ ). This visible light activity is the highest reported for molecular dyads employing  $[\text{FeFe}]$  hydrogenase mimics.<sup>[1a,4,14]</sup> No hydrogen was detected in corresponding experiments without **PS-CAT**, BIH or both or in the dark. Further photocatalytic results are given in Table S3. The major advance of **PS-CAT** over our previous reported photocatalyst dyad<sup>[6]</sup> is its pronounced catalytic performance under visible light irradiation (455 nm LED) even under comparatively low intensities of  $10 \text{ mW cm}^{-2}$ . Moreover, **PS-CAT** shows a significantly prolonged catalytic turnover up to 33 hours (7 hours in our earlier work<sup>[6]</sup>). This is likely a consequence of the lower energy light used here with respect to the previous study (UV light irradiation) and hence avoidance of side reactions. In the latter small amounts of hydrogen were detected in the absence of the dyad, which was not the case in this work.

Figure 3a depicts the UV/Vis spectra of **PS** and **PS-CAT**, which show a strong absorption in the visible spectral region ( $\lambda_{\text{max}} = 409 \text{ nm}$ ,  $\epsilon \approx 8.1 \cdot 10^4 \text{ L mol}^{-1} \text{ cm}^{-1}$  for **PS** and  $\lambda_{\text{max}} = 410 \text{ nm}$ ,  $\epsilon \approx 6.1 \cdot 10^4 \text{ L mol}^{-1} \text{ cm}^{-1}$  for **PS-CAT**) resulting



**Figure 2.** Photocatalytic hydrogen production by **PS-CAT** ( $10 \mu\text{M}$ ) in  $\text{CH}_3\text{CN}/\text{NMP}$  (5:1) with BIH (1000 equivalents) upon irradiation at 455 nm in a 3D printed photoreactor platform (see pictures on the right side). Hydrogen was quantified by GC-TCD with samples drawn from the head space. Each point was determined in duplicate and the error bars give the range of variation.





**Figure 3.** a) Steady-state UV/Vis absorption (solid lines) of **PS** (red) and **PS-CAT** (blue) and emission (dashed lines) in deaerated THF excited at 410 nm. b) Transient absorption spectra at indicated delay times of **PS** (top, blue) and **PS-CAT** (bottom, red) upon excitation at 420 nm in deaerated THF. c) Experimental (black, dashed) and simulated UV/Vis absorption spectrum of **PS-CAT** in THF; electronic transitions of interest are labelled. d) Potential excited state relaxation cascades associated to electron and energy transfer competing with radiative recombination; relative energies of involved singlet (black) and triplet states (red) are given within their respective equilibrium structures. Electron transfer and energy transfer pathways both leading to singly reduced **PS-CAT** ( $D_0$ ,  ${}^2\text{MC}$ , blue) upon BIH reduction are highlighted. Electronic characters are indicated by charge-density differences (CDDs, electronic transitions) and spin densities (open-shell ground state); charge transfer takes place from red to blue (Table S7).

from a  $\pi\pi^*$  transition localized within the oligothiophene moiety (see  $S_1$  in Figure 3d). For **PS-CAT** TDDFT reveals a dipole allowed charge-transfer transition in the visible region (see  $S_2$  in Figure 3d) shifting electron density from a photosensitizer-localized  $\pi$  orbital to the [FeFe] hydrogenase mimic unit, i.e. into the  $\sigma^*$  orbital of the Fe–Fe bond, contributing to the absorption in the visible range (Figure S13).

Emission spectra ( $\lambda_{\text{exc}} = 410$  nm) of both **PS** and **PS-CAT** display three nearly identical vibronic peaks at 455, 484 and 515 nm (shoulder) spaced by  $1250 \text{ cm}^{-1}$ , corresponding to a ground state vibrational mode coupled to the electronic transition (Table S6). The emission lifetimes were determined to 1 ns and the quantum yields are  $\Phi_{\text{F}} = 0.54$  in **PS** and  $\Phi_{\text{F}} = 0.28$  in **PS-CAT**. The reduced emission quantum yield in **PS-CAT** is associated with the population of a charge-separated state ( $S_2$ ) by quantum chemical simulations.  $S_2$ , which is not available in **PS**, is in close energetic proximity to the  $\pi\pi^*$   $S_1$  state.

Nanosecond-transient absorption spectroscopy was performed to detect the impact of the [FeFe] hydrogenase mimic on the relaxation of the triplet state populated via

intersystem crossing (ISC). The data (Figure 3b, Figure S7) for **PS** and **PS-CAT** exhibit similar spectral features. Both **PS** and **PS-CAT** show a negative signal between 350 and 550 nm, which arises from ground-state bleach and emission contributions between 460 and 550 nm.<sup>[15]</sup> Excited state absorption (ESA) is detected at wavelengths longer than 550 nm for both **PS** and **PS-CAT** which is characteristic for the  ${}^3\pi\pi^*$  state of the sensitizer unit.<sup>[16]</sup> TDDFT simulations on the dipole-allowed triplet-triplet excitations of **PS-CAT** within the equilibrium structure of the  ${}^3\pi\pi^*$  ground state, see  $T_2({}^3\pi\pi^*)$  in Figure 3d, associate these ESA features to  ${}^3\pi\pi^*$  transitions of the excited oligothiophene at 600 and 529 nm, respectively (see  $T_{11}$  and  $T_{16}$  in Figure S15), confirming this assignment.<sup>[17]</sup> At wavelengths above  $\approx 750$  nm there is a second negative signal which can be assigned to the triplet phosphorescence of the thiophenes.<sup>[17]</sup> Both transient signals of **PS** and **PS-CAT** decay biexponentially with lifetimes of  $\tau_1 = 20$  ns (reflecting the time-resolution of the experimental setup) and  $\tau_2 = 530$  ns for **PS** and  $\tau_1 = 20$  ns and  $\tau_2 = 210$  ns for **PS-CAT**. The fast component indicates the decay of the residual emission, the long-lived component is associated with the decay of the  ${}^3\pi\pi^*$  state of the sensitizer unit. The

shortening in  $\tau_2$  reflects changes in the  $^3\pi\pi^*$  state lifetime of the excited sensitizer in **PS-CAT** indicating the presence of additional relaxation channels occurring from the  $^3\pi\pi^*$  state with an estimated time constant of 348 ns. Nevertheless, besides the changes in lifetime of the triplet state we do not observe any absorption features at 400, 580 and 700 nm, which could be ascribed to the reduced [FeFe] moiety according to literature and UV/Vis SEC data (Figure S11/S12). Hence, no direct indication for a charge-separated state ( $^3\text{CS}$ , Figure 3d) is observed.<sup>[15a,18]</sup> The absence of these features indicates either that no charge transfer takes place to reduce the Fe–Fe unit or that the CS state is too short-lived, recombines quickly and escapes experimental detection in the absence of an electron donor.

Quantum chemical simulations indicate two relaxation pathways for **PS-CAT**: i) electron transfer causing charge separation which is accessible from the initially excited singlet states. ii) Energy transfer deactivating the  $^3\pi\pi^*$  state (Figure 3d). The electron transfer pathway leads from the initially excited  $^1\pi\pi^*$  state via ISC to the adjacent charge-separated  $T_{10/3}(\text{FC}/^3\text{CS equilibria})$  state (Figure 3d), resulting in a pronounced elongation of the Fe–Fe bond (Table S4) of the formally  $[\text{Fe}^1\text{Fe}^0]$  active site. Upon population of the  $^3\pi\pi^*$  state, either via  $^1\pi\pi^* \rightarrow ^3\pi\pi^*$  ISC or via relaxation from the  $^3\text{CS}$  state, an energy transfer pathway is available. In this case, hole transfer from the photooxidized photosensitizer to the photoreduced iron cluster yields an excited metal centered ( $^3\text{MC}$ ) state. During this process, the ESA decays as the initial configuration of the oligothiophene-based chromophore is reformed (Figure S15) in agreement with the experimental observations. In this  $^3\text{MC}$  state cleavage of the Fe–Fe bond (Table S4) occurs as both the  $\sigma_{\text{Fe-Fe}}$  and the  $\sigma_{\text{Fe-Fe}}^*$  orbitals are singly populated (bond order: 0). The population of the  $^3\text{MC}$  state can be an explanation for the missing signatures of a CS state in the transient absorption experiment. These findings indicate that the presence of sacrificial agent is crucial for the photoinduced reduction of the [FeFe] unit, a key step of the light-induced catalytic process. In this case, according to TDDFT simulations, both relaxation channels, i.e. electron transfer and energy transfer, yield the same singly reduced doublet species of  $[\text{Fe}^1\text{Fe}^0]$  character (see  $D_0$  spin density in Figure 3d, blue)—either upon reduction of the charge-separated species ( $^3\text{CS}$ ) or the  $^3\text{MC}$  state by BIH. Alternatively, the sacrificial agent could also interfere with the described relaxation processes already in an initial stage of the relaxation cascade reducing the sensitizer directly after excitation. The quenching behaviour of the fluorescence of **PS-CAT** by BIH gives the first indication for such a fast process (Figure S5).

The role of the sacrificial agent was elucidated by *operando* UV/Vis spectroscopy in the presence of sacrificial donor BIH (1000 equivalents) upon irradiation at 455 nm. After 30 minutes of irradiation, the absorption band of **PS-CAT** at 403 nm in  $\text{CH}_3\text{CN}/\text{NMP}$  (5:1) disappeared in favour of a characteristic band at 399 nm, which continues to build up within 17 hours (Figure S3a). Upon irradiation in the absence of the donor the absorption at 403 nm decays only slowly, indicating the light-mediated interaction of **PS-CAT** with BIH (Figure S3c). The newly formed species decom-

posed slowly in the dark and quite rapidly in the presence of oxygen (Figure S3b). It is tentatively attributed to a sensitive follow-up product of the catalytic species, not to the catalytic species itself.

*Operando* electron paramagnetic resonance (EPR) spectroscopy reveals the formation of a reduced  $[\text{FeFe}]$  moiety under photocatalytic conditions. The catalytic mixture (30  $\mu\text{M}$  **PS-CAT**, 1000 equivalents BIH) was illuminated in the resonator at 270 K and measured at 4 K. The data show the formation of a paramagnetic  $[\text{Fe}^1\text{Fe}^0]$  intermediate (Figure 4), which has been postulated as key species in the light-induced HER mechanism.<sup>[6c]</sup> No signal was detected in the dark or at room temperature (Figure S8a). The  $g$  values ( $g_1=2.003$ ,  $g_2=1.99557$ ,  $g_3=1.86197$ ) derived from the EPR data are similar to those reported on  $[\text{Fe}^1\text{Fe}^0]$  species with the third  $g$  tensor being shifted further low-field.<sup>[19]</sup> This shift could be due to a low concentration of the  $[\text{Fe}^1\text{Fe}^0]$  intermediate in photochemical reduction, consequently leading to a lower EPR spectral resolution compared to that resulting from (electro)chemical reduction processes.<sup>[19,20]</sup>

In summary, we synthesized a precious metal-free photocatalyst dyad **PS-CAT** for photocatalytic hydrogen generation under visible light. The dyad as prototype comprising  $\pi$ -conjugated oligothiophenes as light absorbers shows a remarkable, long-term photocatalytic activity, the best reported for comparable complexes in the visible spectral range. In accordance with theory, *operando* EPR spectroscopy using BIH as sacrificial donor reveals the generation of an active  $[\text{Fe}^1\text{Fe}^0]$  species, which presumably drives the light-induced hydrogen generation.

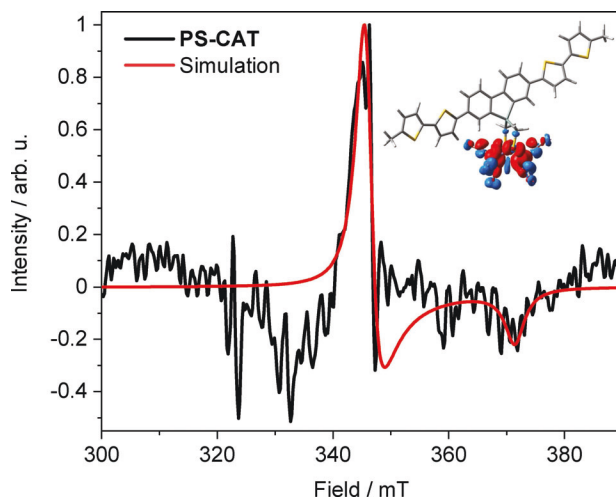


**Figure 4.** EPR spectrum of **PS-CAT** after four hours of illumination under catalytic conditions (30  $\mu\text{M}$  **PS-CAT**). Illumination was carried out in a MD5 resonator and the EPR measurement was done at 4 K. The negative signal at 330 mT stems from resonator background. Inset: Spin density localized at the  $[\text{FeFe}]$  moiety of the singly reduced **PS-CAT** (doublet).

## Acknowledgements

M. K. F. thanks the 'Katholischer Akademischer Ausländer-Dienst' (KAAD) for the scholarship. C. K. is grateful to the 'Deutscher Akademischer Austauschdienst' (DAAD) for an internship (ERASMUS+). The authors thank Professor C. Robl and H. Elbeheiry for helpful discussions, S. Benndorf for recording the IR SEC spectrum and Y. Carstensen for supervising the emission spectroscopy. Professor C. Kay is thanked for valuable discussion on the EPR measurements. Financial support by the German Research Foundation (DFG) via the TRR234 CataLight is gratefully acknowledged (project number 364549901, projects A2, C5 and Z2). All calculations were performed at the Universitätsrechenzentrum of the Friedrich Schiller University Jena. Open Access funding enabled and organized by Projekt DEAL.

## Conflict of Interest

The authors declare no conflict of interest.

## Data Availability Statement

The data that support the findings of this study are available from the corresponding author upon reasonable request.

**Keywords:** H<sub>2</sub> Production · Oligothiophene · *Operando* EPR Spectroscopy · Photocatalysis · [FeFe] Hydrogenase Mimics

- [1] a) W. T. Eckenhoff, *Coord. Chem. Rev.* **2018**, *373*, 295–316; b) W. T. Eckenhoff, R. Eisenberg, *Dalton Trans.* **2012**, *41*, 13004–13021; c) A. J. Esswein, D. G. Nocera, *Chem. Rev.* **2007**, *107*, 4022–4047; d) X.-B. Li, C.-H. Tung, L.-Z. Wu, *Nat. Rev. Chem.* **2018**, *2*, 160–173; e) S. Ott, M. Kritikos, B. Åkermark, L. Sun, *Angew. Chem. Int. Ed.* **2003**, *42*, 3285–3288; *Angew. Chem.* **2003**, *115*, 3407–3410; f) H. Ozawa, M.-a. Haga, K. Sakai, *J. Am. Chem. Soc.* **2006**, *128*, 4926–4927; g) H. Ozawa, K. Sakai, *Chem. Commun.* **2011**, *47*, 2227–2242; h) H.-L. Wu, X.-B. Li, C.-H. Tung, L.-Z. Wu, *Chem. Commun.* **2020**, *56*, 15496–15512; i) L.-Z. Wu, B. Chen, Z.-J. Li, C.-H. Tung, *Acc. Chem. Res.* **2014**, *47*, 2177–2185; j) Y.-J. Yuan, Z.-T. Yu, D.-Q. Chen, Z.-G. Zou, *Chem. Soc. Rev.* **2017**, *46*, 603–631.
- [2] W. Lubitz, H. Ogata, O. Rüdiger, E. Reijerse, *Chem. Rev.* **2014**, *114*, 4081–4148.
- [3] a) C. Tard, C. J. Pickett, *Chem. Rev.* **2009**, *109*, 2245–2274; b) T. R. Simmons, G. Berggren, M. Bacchi, M. Fontecave, V. Artero, *Coord. Chem. Rev.* **2014**, *270–271*, 127–150.
- [4] a) K. E. Dalle, J. Warnan, J. J. Leung, B. Reuillard, I. S. Karmel, E. Reisner, *Chem. Rev.* **2019**, *119*, 2752–2875; b) J. Amaro-Gahete, M. V. Pavliuk, H. Tian, D. Esquivel, F. J. Romero-Salguero, S. Ott, *Coord. Chem. Rev.* **2021**, *448*, 214172.
- [5] K. Holá, M. V. Pavliuk, B. Németh, P. Huang, L. Zdražil, H. Land, G. Berggren, H. Tian, *ACS Catal.* **2020**, *10*, 9943–9952.
- [6] a) R. Goy, U.-P. Apfel, C. Elleouet, D. Escudero, M. Elstner, H. Görls, J. Talarmin, P. Schollhammer, L. González, W. Weigand, *Eur. J. Inorg. Chem.* **2013**, 4466–4472; b) R. Goy, L. Bertini, H. Görls, L. De Gioia, J. Talarmin, G. Zampella, P. Schollhammer, W. Weigand, *Chem. Eur. J.* **2015**, *21*, 5061–5073; c) R. Goy, L. Bertini, T. Rudolph, S. Lin, M. Schulz, G. Zampella, B. Dietzek, F. H. Schacher, L. De Gioia, K. Sakai, W. Weigand, *Chem. Eur. J.* **2017**, *23*, 334–345.
- [7] A. Mishra, P. Bäuerle, *Angew. Chem. Int. Ed.* **2012**, *51*, 2020–2067; *Angew. Chem.* **2012**, *124*, 2060–2109.
- [8] A. Mishra, M. K. R. Fischer, P. Bäuerle, *Angew. Chem. Int. Ed.* **2009**, *48*, 2474–2499; *Angew. Chem.* **2009**, *121*, 2510–2536.
- [9] M. G. Gatty, S. Pullen, E. Sheibani, H. Tian, S. Ott, L. Hammarström, *Chem. Sci.* **2018**, *9*, 4983–4991.
- [10] S. Benndorf, E. Hofmeister, M. Wächter, H. Görls, P. Liebing, K. Peneva, S. Gräfe, S. Kupfer, B. Dietzek-Ivanšić, W. Weigand, *Eur. J. Inorg. Chem.* **2022**, e202100959.
- [11] Deposition Number 2106348 contains the supplementary crystallographic data for this paper. These data are provided free of charge by the joint Cambridge Crystallographic Data Centre and Fachinformationszentrum Karlsruhe Access Structures service.
- [12] X.-Q. Zhu, M.-T. Zhang, A. Yu, C.-H. Wang, J.-P. Cheng, *J. Am. Chem. Soc.* **2008**, *130*, 2501–2516.
- [13] Y. Tamaki, K. Koike, T. Morimoto, O. Ishitani, *J. Catal.* **2013**, *304*, 22–28.
- [14] a) H. Cui, M. Hu, H. Wen, G. Chai, C. Ma, H. Chen, C. Chen, *Dalton Trans.* **2012**, *41*, 13899–13907; b) A. Mazzeo, S. Santalla, C. Gaviglio, F. Doctorovich, J. Pellegrino, *Inorg. Chim. Acta* **2021**, *517*, 119950.
- [15] a) Y. Na, J. Pan, M. Wang, L. Sun, *Inorg. Chem.* **2007**, *46*, 3813–3815; b) Y. Na, M. Wang, J. Pan, P. Zhang, B. Åkermark, L. Sun, *Inorg. Chem.* **2008**, *47*, 2805–2810.
- [16] a) Z. Xu, T. Jin, Y. Huang, K. Mulla, F. A. Evangelista, E. Egap, T. Lian, *Chem. Sci.* **2019**, *10*, 6120–6124; b) S. Rentsch, J. P. Yang, W. Paa, E. Birkner, J. Schiedt, R. Weinkauff, *Phys. Chem. Chem. Phys.* **1999**, *1*, 1707–1714; c) J. P. Yang, W. Paa, S. Rentsch, *Synth. Met.* **1999**, *101*, 624–625.
- [17] D. Wasserberg, P. Marsal, S. C. J. Meskers, R. A. J. Janssen, D. Beljonne, *J. Phys. Chem. B* **2005**, *109*, 4410–4415.
- [18] S. J. Borg, T. Behrsing, S. P. Best, M. Razavet, X. Liu, C. J. Pickett, *J. Am. Chem. Soc.* **2004**, *126*, 16988–16999.
- [19] P. S. Singh, H. C. Rudbeck, P. Huang, S. Ezzaher, L. Eriksson, M. Stein, S. Ott, R. Lomoth, *Inorg. Chem.* **2009**, *48*, 10883–10885.
- [20] a) M. Razavet, S. J. Borg, S. J. George, S. P. Best, S. A. Fairhurst, C. J. Pickett, *Chem. Commun.* **2002**, 700–701; b) A. Silakov, J. L. Shaw, E. J. Reijerse, W. Lubitz, *J. Am. Chem. Soc.* **2010**, *132*, 17578–17587; c) D. Streich, M. Karnahl, Y. Astuti, C. W. Cady, L. Hammarström, R. Lomoth, S. Ott, *Eur. J. Inorg. Chem.* **2011**, 1106–1111.

Manuscript received: February 8, 2022

Accepted manuscript online: February 17, 2022

Version of record online: March 23, 2022

## Supporting Information

### **Activating a [FeFe] Hydrogenase Mimic for Hydrogen Evolution under Visible Light**

*P. Buday, C. Kasahara, E. Hofmeister, D. Kowalczyk, M. K. Farh, S. Riediger, M. Schulz, M. Wächter, S. Furukawa, M. Saito\*, D. Ziegenbalg, S. Gräfe, P. Bäuerle, S. Kupfer\*, B. Dietzek-Ivanšić\*, W. Weigand\**

**Table of Contents**

Materials and instrumentation .....	3
Synthesis and characterization .....	6
NMR spectra .....	11
Single crystal X-ray structure determination.....	16
Photocatalysis.....	19
UV-vis-monitored photocatalysis .....	21
Fluorescence quenching in presence of BIH.....	22
Time-resolved spectroscopy.....	25
EPR spectroscopy.....	27
Electrochemical characterization .....	28
Computational details.....	32
References .....	39
Author Contributions.....	40



## SUPPORTING INFORMATION

**Materials and instrumentation**

The following materials were synthesized according to the corresponding literature procedures: 2,2'-dibromo-[1,1'-biphenyl]-4,4'-diamine (1),<sup>[1]</sup> 2-(5'-Hexyl-2,2'-bithien-5-yl)-4,4,5,5-tetramethyl-1,3,2-dioxaborolan,<sup>[2]</sup>  $\text{SiCl}_2(\text{CH}_2\text{Cl})_2$ ,<sup>[3]</sup> 1,3-Dimethyl-2-phenylbenzimidazoline (BIH) from 2-phenyl-1H-benzo[d]imidazole.<sup>[4]</sup> All other chemicals and solvents were commercially available (Sigma-Aldrich, Acros, TCI, Alfa Aesar, abcr). Column chromatography was performed with Geduran Si 60 (0.063-0.200 mm), TLC monitoring on TLC Silica gel 60 F254.

**Melting points:** Melting points were determined with an APOTEC apparatus and are uncorrected.

**NMR:** NMR spectra were recorded with Bruker 600 MHz and 400 MHz spectrometers (Avance III).

**IR:** IR spectroscopy was performed with a Tensor 27 FT-IR spectrometer.

**MS:** High resolution mass spectrometry was carried out using a Thermo Scientific Q Exactive plus Orbitrap mass spectrometer coupled to an atmospheric pressure chemical ionization source (APCI). EI spectra were measured on a Finnigan MAT SSQ710 using the direct evaporation probe (DEP) technique and electron ionization (EI) at 70 eV.

**Elemental analysis:** For Elemental analysis an Euro Vector EA3000 element Analyser was utilized.

**X-ray:** The intensity data were collected on a Bruker Apex II diffractometer using graphite-monochromated Mo-K $\alpha$  radiation. Data were corrected for Lorentz and polarization effects; absorption was taken into account on a semi-empirical basis using multiple scans. Structure refinement made use of SHELXL.<sup>[5]</sup> Hydrogen atoms were included at calculated positions with isotropic displacement parameters.

**Photocatalysis / UV-vis:** Photocatalytic investigations with subsequent hydrogen quantification (7820A GC-TCD; Agilent Technologies) took place in a novel standard, 3D printed photoreactor utilizing a M455L3 Mounted LED from Thorlabs connected with a COP1-A Collimation Adapter (Thorlabs) (LED power:  $\approx 10 \text{ mW cm}^{-2}$ ). For monitoring photocatalysis by UV-vis spectroscopy, a V-780 Spectrophotometer (JASCO) was used to record the spectra between irradiation intervals with a M455L3 Mounted LED connected with a collimation lens (effective LED power:  $\approx 180 \text{ mW}$ ).

**Utilized Photoreactor:** Photocatalytic experiments were carried out in a custom made, modular 3D printed, photoreactor platform. The irradiation chamber of the reactor had the dimensions of 90x90x100 mm (Figure S1 (i)). The photoreactor was manufactured from polylactic acid using Fused Deposition Modeling. Due to its reflecting properties in the visible wavelength range, white filament was used. The irradiation chamber consisted of two walls with slots (Figure S1 (ii)), in which a sample holder can be installed. Circularly arranged vials can be irradiated from the bottom with an irradiation module at a defined (adjustable) distance from the light source. 8 4 mL GC-vials were placed in a circular holder with a diameter of 46 mm (measured from the center of two opposing vials). The holder was placed in the third slot (distance 30 mm) measured from the bottom of the irradiation module. At the bottom an adapter module for a Thorlabs collimator was installed together with a 455 nm LED (M455L3 Mounted LED from Thorlabs) (Figure S1 (iii)). The LED was operated at (100 %) of its maximum power. A third wall of the corpus was equipped with an opening. Here, a fan was installed to temper the inner of the irradiation chamber (Figure S1 (iv)). A fourth wall is used to close the reactor. It is equipped with an opening which works as exhaust for the ventilation air (Figure S1 (v)). The reaction chamber was ventilated using a fan ( $26.43 \text{ L s}^{-1}$ ) to avoid heat accumulation in the reaction chamber. The reactor was closed from above using a cover (Figure S1 (vi)). The complete modular reactor platform is depicted in Figure S1 (vii).

## SUPPORTING INFORMATION

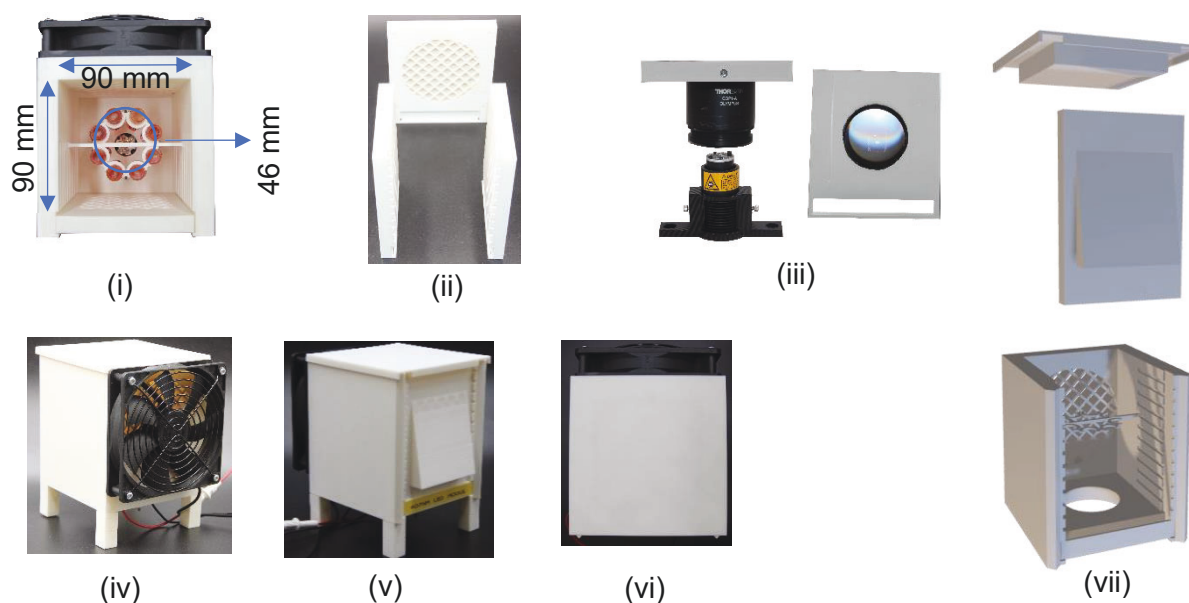


**Figure S1:** Modular photoreactor platform: irradiation chamber (i), side walls (ii), adapter module for Thorlabs collimator (iii), back wall with fan (iv), front wall with ventilation opening (v), reactor cover (vi) and model of whole reactor setup (vii).

**Steady-state spectroscopy:** UV-vis absorption spectroscopy was carried out with a V-780 Spectrophotometer (JASCO) and a SPECORD S600 (Analytik Jena). Emission spectroscopy and emission quenching experiments were performed with a FLS980 Spectrometer (Edinburgh Instruments), absolute fluorescence quantum yields were determined with an FLS980 Integrating Sphere (Edinburgh Instruments).

**Time-resolved spectroscopy:**

*Streak camera* – The two-dimensional (time and wavelength) emission decay profiles were measured using a Hamamatsu streak scope C4334 in photon counting mode using a time window of 500 ns. After excitation with the frequency-doubled output of a Ti-sapphire laser (Tsunami, Newport Spectra-Physics GmbH; pulse-to-pulse repetition rate 400 kHz after passing a pulse selector, model 3980, Newport Spectra-Physics GmbH) at  $\lambda_{\text{ex}} = 460$  nm, the luminescence of the sample was collected in a  $90^\circ$ -arrangement.

*Nanosecond transient absorption* – The excitation light source for measurements on the submicro-second time scale is based on a Nd:YAG laser (Continuum Surelite), yielding 5 ns pulses at 1064 nm with a repetition rate of 10 Hz. The fundamental pump pulses were frequency-tripled (yielding 355 nm), which was used as input for generating pump pulses centered at 420 nm using an optical parametric oscillator (Continuum Surelite). The kinetics were studied using a probe light provided by a 75 W xenon arc lamp, which was focused on the sample by a concave mirror. After passing through the sample, the probe pulses were spectrally dispersed (Acton Princeton Instrument 2300), detected on a photomultiplier (Hamamatsu R928), and processed (Pascher Instruments AB). TA kinetics were detected as a single-wavelength kinetic between 380 and 800 nm in steps of 10 nm. For all measurements, the power of the pump beam was kept at 0.35 mJ. A long pass filter (435 nm) to eliminate the pump scattering was used at wavelengths above 430 nm.

SUPPORTING INFORMATION

---

**EPR:** A X-Band ELEXSYS E500 spectrometer from Bruker with HE-flow cryostat equipped with a MD5 resonator at 5 K was used for EPR measurements. Illumination was carried out at room temperature at 420 nm. The samples were frozen under illumination. All experiments were carried out in an EPR tube for low temperature measurements (3 mm diameter). Simulation of experimental data was carried out with EasySpin in MatLab.<sup>[6]</sup>

**Electrochemistry:**

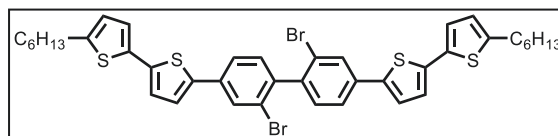
*Cyclic voltammetry (CV)* – Basic CV was accomplished with a three-electrode setup using a glassy carbon ( $d = 1.6$  mm) working electrode, a  $\text{Ag}^+/\text{Ag}$  (in acetonitrile) reference electrode and a Pt (wire) counter electrode, driven by a Reference 600 Potentiostat/Galvanostat/ZRA from Gamry Instruments.

*Spectroelectrochemistry (SEC)* – The measurements were executed with a BioLogic SP-50 Potentiostat. IR SEC was carried out in a Specac Omni-Cell with a Pt (mesh) working and counter electrode and an Ag (wire) reference electrode using a Tensor 27 FT-IR spectrometer. UV-vis SEC was done with a glassy carbon working electrode, a Pt (wire) counter electrode and an Ag (wire) reference electrode making use of a SPECORD S600 UV-vis spectrometer. The glassy carbon electrode has a hole cut in to ensure maximum concentration of the desired compound during measurements.



## SUPPORTING INFORMATION

**5',5''-(2,2'-dibromo-[1,1'-biphenyl]-4,4'-diyl)bis(5-hexyl-2,2'-bithiophene) (3)**. The reaction was performed under an argon atmosphere. In a three-necked flask 2,2'-dibromo-4,4'-diiodo-1,1'-biphenyl (**2**) (1.33 g, 2.37 mmol), 2-(5'-hexyl-[2,2'-bithiophen]-5-yl)-4,4,5,5-tetramethyl-1,3,2-dioxaborolane (2.12 g, 5.64 mmol, 2.38 eq), benzyltriethylammonium chloride (1.3 g, 5.7 mmol, 2.42 eq) and [Pd(PPh<sub>3</sub>)<sub>4</sub>] (816 mg, 0.71 mmol, 15 mol%) were dissolved in dry toluene (40 mL). After heating to 60 °C, K<sub>2</sub>CO<sub>3</sub> (23 mL of 2 M solution, 46 mmol) was added and the solution was refluxed for 12 hours. The heating bath was removed and the reaction mixture allowed to cool down to room temperature, followed by the addition of water (20 mL). Subsequently, dichloromethane (80 mL) was added and the organic layer was separated. The latter was washed with brine and water and then dried over Na<sub>2</sub>SO<sub>4</sub>. After removing the solvent under reduced pressure, the residue was purified by wet silica gel filtration using *n*-hexane for removing any impurities and then a mixture of *n*-hexane/dichloromethane = 3:1 to get **3** (1.84 g, 2.28 mmol, 96 %) as light yellow solid.



$R_f = 0.76$  (*n*-hexane/CH<sub>2</sub>Cl<sub>2</sub> = 2:1).

m. p.: 135-136 °C.

<sup>1</sup>H NMR (400 MHz, CD<sub>2</sub>Cl<sub>2</sub>):  $\delta = 0.91$  (t,  $J=7.02$  Hz, 6 H (overlap with *n*-hexane), hexyl), 1.29 – 1.46 (m, 12 H (overlap with *n*-hexane), hexyl), 1.70 (quin,  $J=7.45$  Hz, 4 H, hexyl), 2.82 (t,  $J=7.60$  Hz, 4 H, hexyl), 6.73 (d,  $J=3.80$  Hz, 2 H, het-Ar), 7.06 (d,  $J=3.51$  Hz, 2 H, het-Ar), 7.11 (d,  $J=3.80$  Hz, 2 H, het-Ar), 7.28 (d,  $J=7.89$  Hz, 2 H, Ar), 7.31 (d,  $J=3.80$  Hz, 2 H, het-Ar), 7.61 (dd,  $J=8.04, 1.90$  Hz, 2 H, Ar), 7.93 ppm (d,  $J=1.75$  Hz, 2 H).

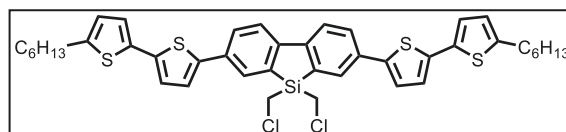
<sup>13</sup>C{<sup>1</sup>H} NMR (101 MHz, CD<sub>2</sub>Cl<sub>2</sub>):  $\delta = 14.4, 23.2, 29.3, 30.7, 32.2, 32.2, 124.3, 124.5, 124.6, 124.7, 125.5, 125.6, 129.6, 132.1, 134.8, 136.2, 139.0, 140.4, 140.8, 146.8$  ppm.

HRMS (APCI+):  $m/z$  calcd for C<sub>40</sub>H<sub>41</sub>Br<sub>2</sub>S<sub>4</sub><sup>+</sup> ([M+H]<sup>+</sup>): 807.0452; found: 807.0447.

Elemental analysis calcd (%) for C<sub>40</sub>H<sub>40</sub>Br<sub>2</sub>S<sub>4</sub>: C 59.40, H 4.99, S 15.86; found C 58.89, H 4.87, S 15.63.

IR:  $\tilde{\nu} = 3060$  (w), 2953 (w), 2922 (m), 2852 (m), 1594 (m), 1488 (m), 1444 (m), 1377 (m), 1199 (m), 1084 (m), 1040 (m), 997 (m), 970 (m), 864 (m), 779 (s), 746 (m), 667 (m) cm<sup>-1</sup>.

**5,5-bis(chloromethyl)-3,7-bis(5'-hexyl-[2,2'-bithiophen]-5-yl)-5H-dibenzo[*b,d*]silole (4)**. Referring to literature.<sup>[8]</sup> The reaction was performed under nitrogen gas. *n*-BuLi (2.1 mL, 2.5 M in hexane, 5.21 mmol, 2.03 eq) was added dropwise within 2



minutes to a stirred suspension of **3** (2.07 g, 2.57 mmol) in THF (30 mL) at -78 °C. After addition the suspension cleared up and then another suspension occurred. The temperature was held at -78 °C for 30 minutes and after that at room temperature for 10 minutes. The reaction mixture was cooled again to -78 °C and stirred for 30 minutes, followed by the addition of SiCl<sub>2</sub>(CH<sub>2</sub>Cl)<sub>2</sub> (0.5 mL, 3.73 mmol, 1.45 eq) in THF (5 mL) within 3 minutes. The suspension was allowed to slowly warm up to room temperature overnight resulting in a dark reddish-brown solution with some precipitate. Dry silica was added and the solvent was evaporated under reduced pressure. Wet silica column chromatography (different mixtures of CHCl<sub>3</sub>/*n*-hexane and toluene/*n*-hexane) did not afford pure, yellow **4** (about 1.10 g, 1.42 mmol, 55 %) since some side product could not be removed. In another unsuccessful trial an

## SUPPORTING INFORMATION

excess of *n*-BuLi (4 eq) and SiCl<sub>2</sub>(CH<sub>2</sub>Cl)<sub>2</sub> (12.14 eq) was used to avoid the formation of any side product, so **4** was used without further purification.

$R_f = 0.67$  (*n*-hexane/CHCl<sub>3</sub> = 2:1).

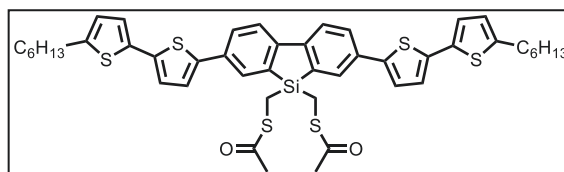
<sup>1</sup>H NMR (400 MHz, CDCl<sub>3</sub>):  $\delta = 0.91$  (t,  $J=6.87$  Hz, 6 H (overlap with *n*-hexane), hexyl), 1.29 – 1.47 (m, 12 H (overlap with *n*-hexane), hexyl), 1.70 (quin,  $J=7.45$  Hz, 4 H (overlap with *n*-hexane), hexyl), 2.81 (t,  $J=7.45$  Hz, 4 H (overlap with *n*-hexane), hexyl), 3.37 (s, 4 H, SiCH<sub>2</sub>), 6.71 (d,  $J=3.51$  Hz, 2 H, het-Ar), 7.04 (d,  $J=3.51$  Hz, 2 H, het-Ar), 7.09 (d,  $J=3.80$  Hz, 2 H, het-Ar), 7.25 – 7.29 (d (overlap with CDCl<sub>3</sub>),  $J=3.80$  Hz, 2 H, het-Ar), 7.71 (dd,  $J=8.18$ , 1.75 Hz, 2 H, het-Ar), 7.76 – 7.83 (m, 2 H, Ar), 8.00 ppm (d,  $J=1.75$  Hz, 2 H, Ar).

<sup>13</sup>C{<sup>1</sup>H} NMR (151 MHz, CDCl<sub>3</sub>):  $\delta = 14.1$ , 22.6, 25.2 (SiCH<sub>2</sub>), 28.8, 30.2, 31.6, 121.7, 123.4, 123.9, 124.0, 124.9, 129.0, 131.2, 132.7, 133.7, 134.7, 137.7, 141.7, 145.7, 147.1 ppm.

HRMS (APCI+):  $m/z$  calcd for C<sub>42</sub>H<sub>45</sub>Cl<sub>2</sub>S<sub>4</sub>Si<sup>+</sup> ([M+H]<sup>+</sup>): 775.1556; found: 775.1545.

IR:  $\tilde{\nu} = 3067$  (w), 2952 (w), 2922 (m), 2853 (m), 2360 (w), 1600 (w), 1486 (m), 1456 (m), 1379 (m), 1055 (m), 871 (m), 792 (s), 723 (s), 695 (m), 633 (m) cm<sup>-1</sup>.

**S,S'-((3,7-bis(5'-hexyl-[2,2'-bithiophen]-5-yl)-5H-dibenzo[b,d]silole-5,5-diyl)bis(methylene)) diethanethioate (5)**. Referring to literature.<sup>[9]</sup> **4** (693 mg, 0.90 mmol) was added as solid to a suspension of potassium thioacetate (340 mg, 2.98



mmol, 3.3 eq) in THF (40 mL) and the orange suspension was stirred at room temperature for 20 hours. The solvent was removed by a nitrogen flow and the residue dissolved in a mixture of *n*-hexane/toluene (4:1). Wet silica column chromatography (*n*-hexane/toluene = 4:1 to pure toluene) afforded **5** (570 mg, 0.67 mmol, 75 %) as yellow solid.

$R_f = 0.54$  (toluene).

m. p.: 96.5-97.5 °C.

<sup>1</sup>H NMR (400 MHz, CDCl<sub>3</sub>):  $\delta = 0.92$  (t,  $J=6.87$  Hz, 6 H, hexyl), 1.25 – 1.47 (m, 12 H (overlap with *n*-hexane), hexyl), 1.64 – 1.77 (m, 4 H, hexyl), 2.35 (s, 6 H, COCH<sub>3</sub>), 2.57 (s, 4 H, SiCH<sub>2</sub>), 2.82 (t,  $J=7.45$  Hz, 4 H, hexyl), 6.71 (d,  $J=3.51$  Hz, 2 H, het-Ar), 7.04 (d,  $J=3.51$  Hz, 2 H, het-Ar) 7.09 (d,  $J=3.80$  Hz, 2 H, het-Ar) 7.27 (d,  $J=3.51$  Hz, 2 H, het-Ar) 7.65 (dd,  $J=8.18$ , 1.75 Hz, 2 H, Ar) 7.70 - 7.78 (m, 2 H, Ar) 7.94 ppm (d,  $J=1.75$  Hz, 2 H, Ar).

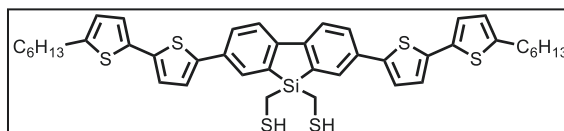
<sup>13</sup>C{<sup>1</sup>H} NMR (101 MHz, CDCl<sub>3</sub>):  $\delta = 10.2$  (SiCH<sub>2</sub>), 14.1, 22.6, 28.8, 30.1, 30.2, 31.6, 121.5, 123.4, 123.8, 123.9, 124.8, 128.4, 130.7, 133.4, 134.8, 135.1, 137.5, 142.1, 145.6, 147.0, 196.2 ppm (COCH<sub>3</sub>).

HRMS (APCI+):  $m/z$  calcd for C<sub>46</sub>H<sub>51</sub>O<sub>2</sub>S<sub>6</sub>Si<sup>+</sup> ([M+H]<sup>+</sup>): 855.1977; found: 855.1970.

Elemental analysis calcd (%) for C<sub>46</sub>H<sub>50</sub>O<sub>2</sub>S<sub>6</sub>Si: C 64.59, H 5.89, S 22.49; found C 64.41, H 5.85, S 22.55.

IR:  $\tilde{\nu} = 3066$  (w), 2922 (m), 2853 (m), 2361 (w), 2334 (w), 1694 (m), 1674 (m), 1456 (m), 1352 (m), 1138 (m), 1056 (m), 953 (m), 825 (m), 789 (vs), 617 (s) cm<sup>-1</sup>.

**(3,7-bis(5'-hexyl-[2,2'-bithiophen]-5-yl)-5H-dibenzo[b,d]silole-5,5-diyl)dimethanethiol (6)**. Referring to literature.<sup>[9]</sup> The reaction was carried out under an Ar





## SUPPORTING INFORMATION

atmosphere. **5** (275 mg, 0.32 mmol) was added as solid to a cooled suspension of lithium aluminium hydride (550 mg, 14.5 mmol, 45 eq) in diethyl ether (80 mL) at 0 °C. The cold bath was removed and the greenish yellow suspension was stirred at room temperature for 12 hours. After cooling to 0 °C, hydrochloric acid (2 M, 10 mL) was added carefully, followed by the addition of chloroform. The organic phase was separated and the aqueous phase extracted two times with chloroform. The combined organic solutions were dried over sodium sulfate and the solvent was removed under reduced pressure. Wet silica gel filtration (CHCl<sub>3</sub>) afforded **6** (200 mg, 0.26 mmol, 81 %) as yellow solid, which was used without further purification.

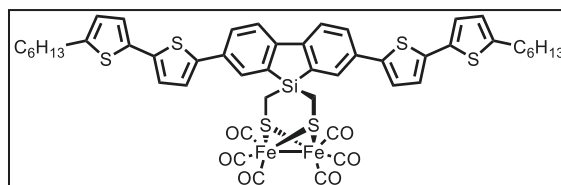
<sup>1</sup>H NMR (400 MHz, CDCl<sub>3</sub>): δ = 0.91 (t, *J*=6.58 Hz, 6 H (overlap with *n*-hexane), hexyl), 1.28 – 1.43 (m, 12 H (overlap with *n*-hexane), hexyl), 1.47 (t, *J*=7.75 Hz, 2 H, SH), 1.70 (quin, *J*=7.38 Hz, 4 H (overlap with *n*-hexane), hexyl), 2.23 (d, *J*=7.89 Hz, 4 H, SiCH<sub>2</sub>), 2.82 (t, *J*=7.60 Hz, 4 H (overlap with *n*-hexane), hexyl), 6.71 (d, *J*=3.51 Hz, 2 H, het-Ar), 7.04 (d, *J*=3.22 Hz, 2 H, het-Ar), 7.10 (d, *J*=3.51 Hz, 2 H, het-Ar), 7.28 (d (in overlap with CDCl<sub>3</sub>), 2 H, het-Ar), 7.71 (d, *J*=8.18 Hz, 2 H, Ar), 7.81 (d, *J*=8.18 Hz, 2 H, Ar), 7.99 ppm (s, 2 H, Ar).

<sup>13</sup>C{<sup>1</sup>H} NMR (101 MHz, CDCl<sub>3</sub>): δ = 3.0 (SiCH<sub>2</sub>) 14.1, 22.6, 28.8, 30.2, 31.6, 121.6, 123.4, 123.9, 124.9, 128.5, 130.7, 133.5, 134.6, 134.7, 137.6, 141.9, 145.7, 147.2 ppm.

HRMS (APCI+): *m/z* calcd for C<sub>42</sub>H<sub>47</sub>S<sub>6</sub>Si<sup>+</sup> ([M+H]<sup>+</sup>): 771.1766; found: 771.1758.

IR:  $\tilde{\nu}$  = 2921 (w), 2852 (w), 2361 (w), 2334 (w), 1456 (w), 1376 (w), 1261 (w), 1055 (w), 871 (w), 814 (w), 792 (m), 774 (m), 724 (m) cm<sup>-1</sup>.

[(C<sub>42</sub>H<sub>44</sub>S<sub>4</sub>SiS<sub>2</sub>)Fe<sub>2</sub>(CO)<sub>6</sub>] (**7**). Referring to literature.<sup>[8]</sup> **6** (58 mg, 81 μmol) was dissolved in a mixture of toluene and *N*-Methyl-2-pyrrolidone (NMP) (20:1, 21 mL). Fe<sub>3</sub>(CO)<sub>12</sub> (80 mg, 159 μmol, 2 eq) was added as solid and the resulting green solution was stirred at room temperature for 12 hours. The reddish solution was concentrated to a small volume with a nitrogen flow and the residue was purified by column chromatography (*n*-hexane/toluene = 1:1). **6** (23 mg, 28 %) was obtained as orange brown solid.



In another protocol, referring to literature,<sup>[10]</sup> LiBHET<sub>3</sub> (1 M in THF, 2.49 mmol, 2.5 eq) was added dropwise to a stirred solution of [(μ-S)<sub>2</sub>Fe<sub>2</sub>(CO)<sub>6</sub>] (428 mg, 1.24 mmol, 1 eq) in THF (50 mL) at -78 °C. The temperature was held at -90 °C for 2 hours and after that at room temperature for 5 minutes. The reaction mixture was cooled again to -90 °C, followed by the addition of **4** (955 mg, 1.23 mmol, 1 eq) in THF (32 mL) and subsequently was allowed to slowly warm up to room temperature overnight. After solvent removal under reduced pressure, the residue was dissolved in chloroform. The organic phase was washed with water, then dried over magnesium sulfate and removed in vacuo. The crude material was purified by flash wet silica column chromatography (*n*-hexane/CHCl<sub>3</sub> = 3:1 to 1:1) and further by gel permeation chromatography. The product was washed with *n*-hexane and obtained as orange powder (104 mg, 0.099 mmol, 8 %).

*R*<sub>f</sub> = 0.58 (*n*-hexane/toluene = 2:1).

<sup>1</sup>H NMR (400 MHz, CDCl<sub>3</sub>): δ = 0.87 – 0.96 (m, 6 H (overlap with *n*-hexane), hexyl), 1.22 – 1.47 (m, 12 H (overlap with *n*-hexane), hexyl), 1.66 – 1.78 (m, 4 H (overlap with *n*-hexane), hexyl), 2.00 (s, 4 H, SiCH<sub>2</sub>), 2.83 (t, *J*=7.60 Hz, 4 H, hexyl), 6.73 (d, *J*=3.51 Hz, 2 H, het-Ar), 7.05 (d, *J*=3.51 Hz, 2 H, het-Ar), 7.11 (d, *J*=3.80 Hz, 2 H, het-Ar), 7.25 (d, *J*=3.80 Hz, 2 H, het-Ar), 7.66 (dd, *J*=8.20, 1.80 Hz, 2 H, Ar), 7.72 (d, *J*=8.2 Hz, 2 H, Ar), 7.97 ppm (d, *J*=1.75 Hz, 2 H, Ar).

SUPPORTING INFORMATION

---

$^{13}\text{C}\{^1\text{H}\}$  NMR (101 MHz,  $\text{CDCl}_3$ ):  $\delta$  = 1.7 ( $\text{SiCH}_2$ ), 14.1, 22.6, 28.8, 30.2, 31.6, 121.5, 123.5, 123.9, 124.0, 124.9, 128.4, 129.8, 134.1, 134.7, 136.1, 137.8, 141.6, 145.8, 146.1, 207.3 ppm (CO).

MS: Applied mass spectrometric techniques (APCI, EI) gave no molecular ion or significant fragment peaks.

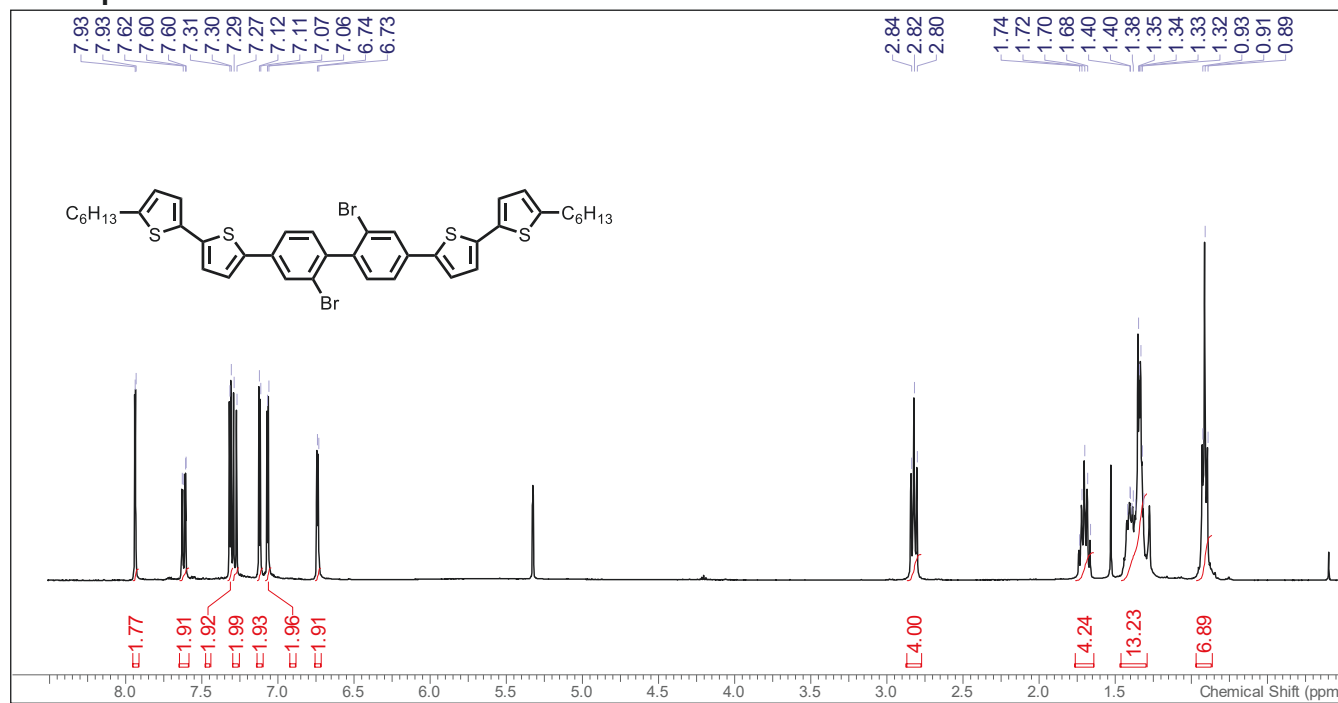
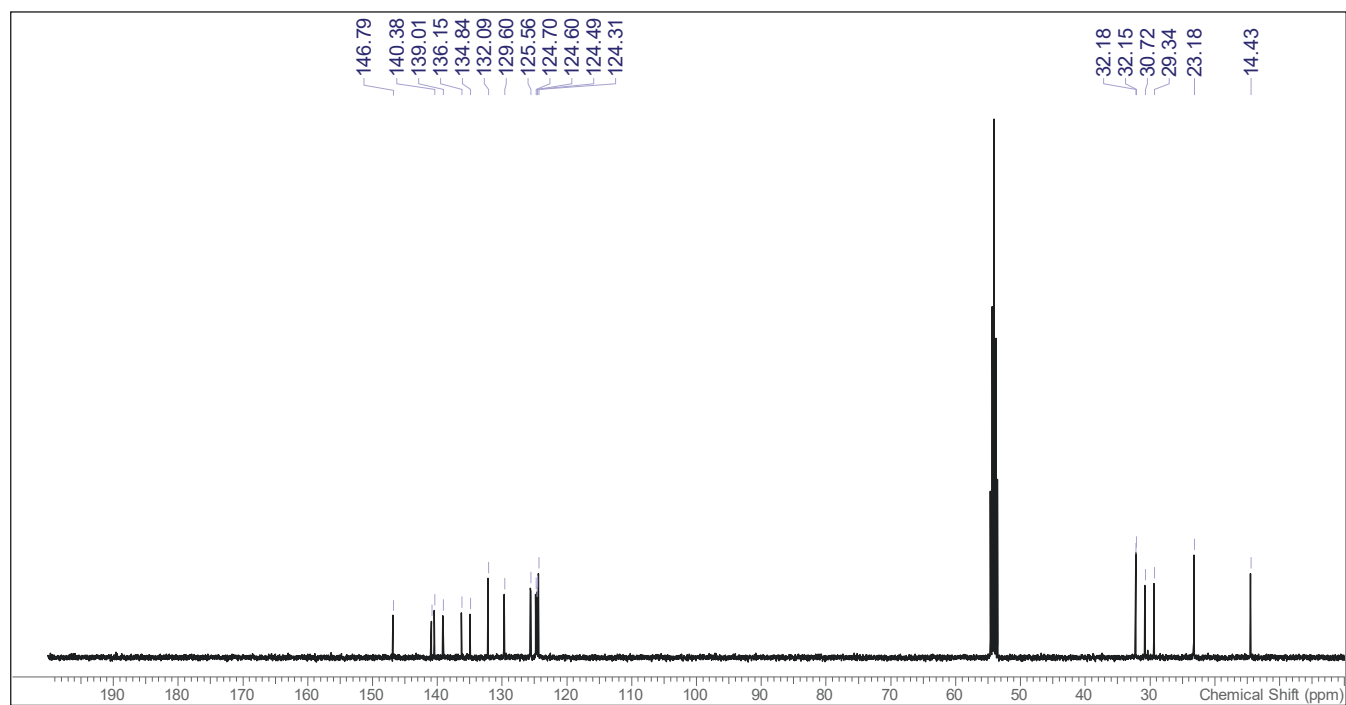
Elemental analysis calcd (%) for  $\text{C}_{48}\text{H}_{44}\text{Fe}_2\text{O}_6\text{S}_6\text{Si}$ : C 54.96, H 4.23, S 18.34; found C 55.51, H 4.28, S 18.14.

IR:  $\tilde{\nu}$  = 3065 (w), 2927 (m), 2854 (m), 2361 (w), 2070 (s), 2019 (s), 1982 (vs), 1961 (vs), 1484 (m), 1135 (m), 1057 (m), 872 (w), 789 (s), 720 (m), 620 (m), 606 (m)  $\text{cm}^{-1}$ .

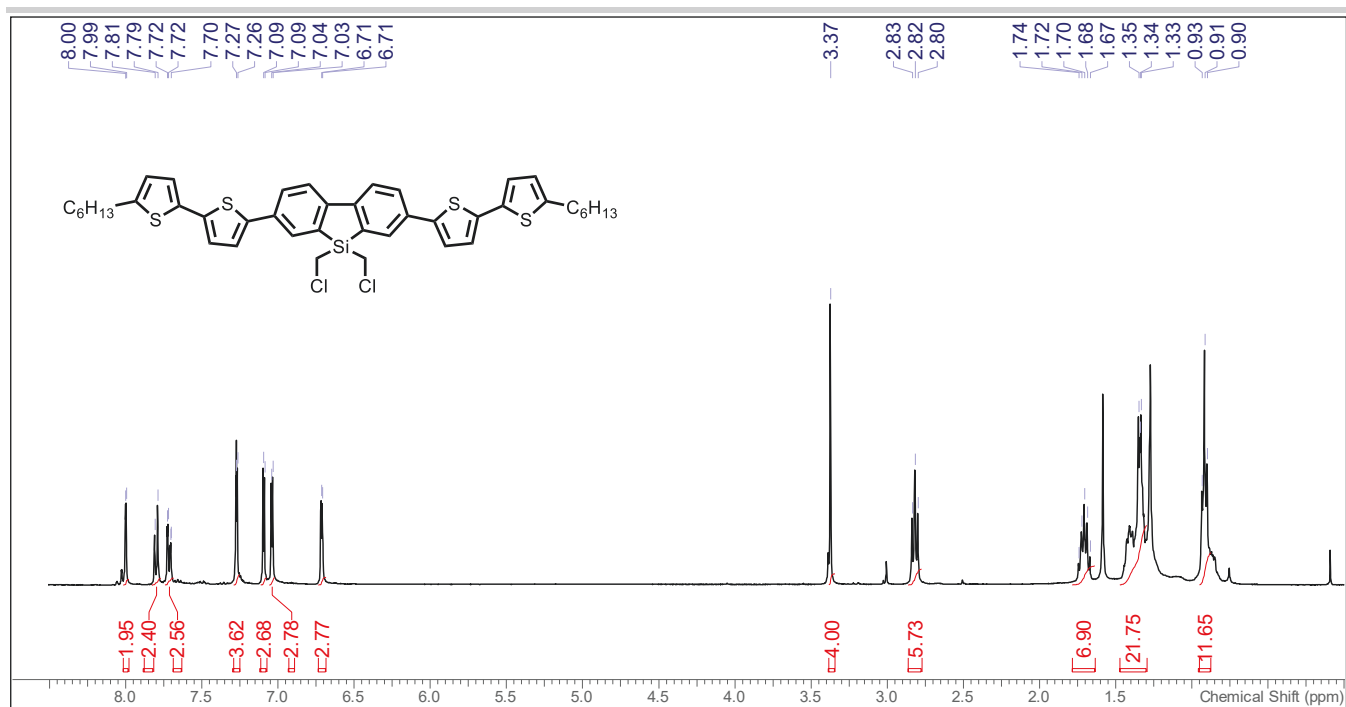


## SUPPORTING INFORMATION

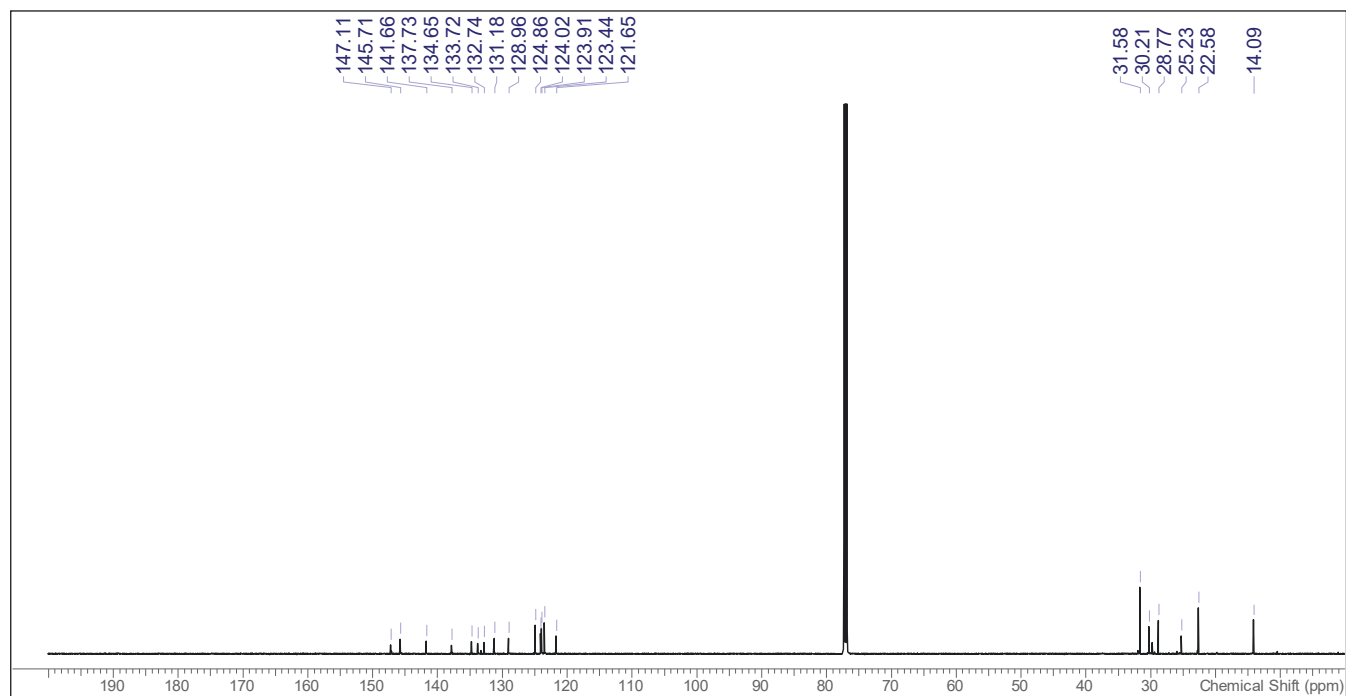
## NMR spectra

<sup>1</sup>H NMR spectrum (CD<sub>2</sub>Cl<sub>2</sub>, 400 MHz) of **3**.<sup>13</sup>C{<sup>1</sup>H} NMR spectrum (CD<sub>2</sub>Cl<sub>2</sub>, 101 MHz) of **3**.

## SUPPORTING INFORMATION

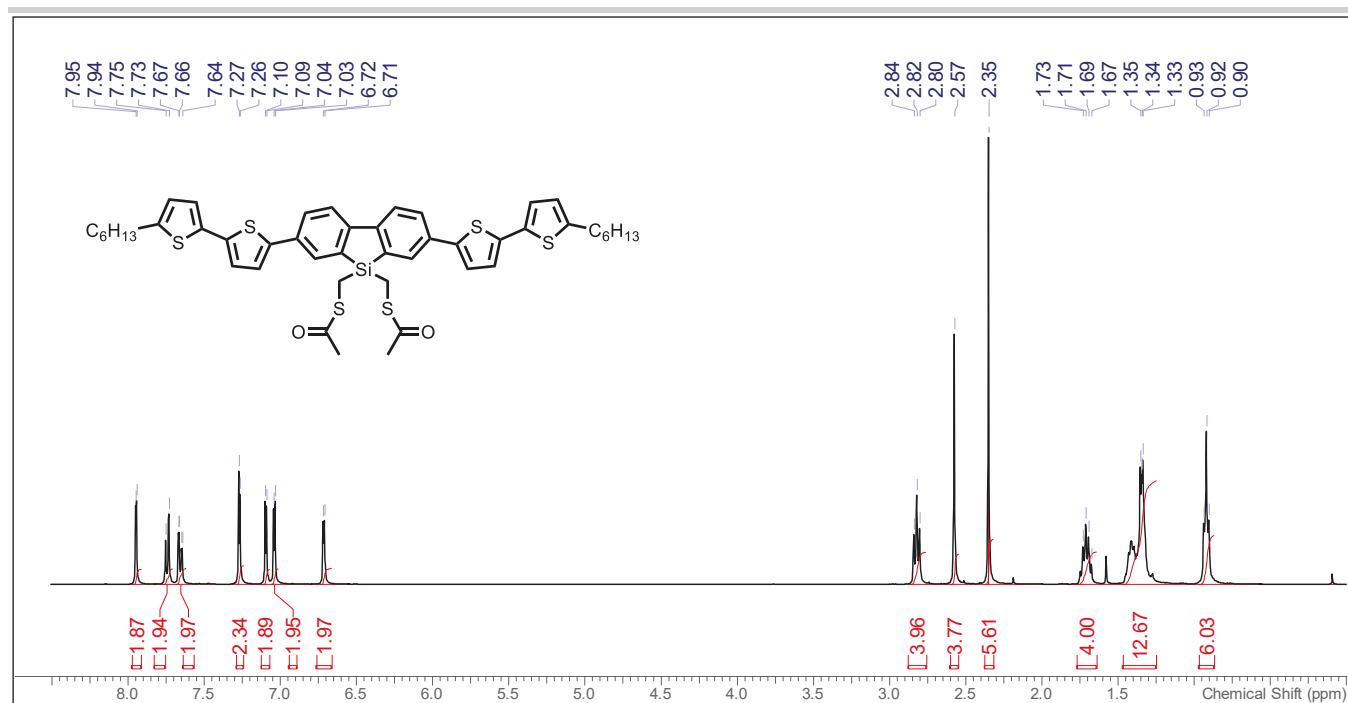


<sup>1</sup>H NMR spectrum (CDCl<sub>3</sub>, 400 MHz) of **4**.

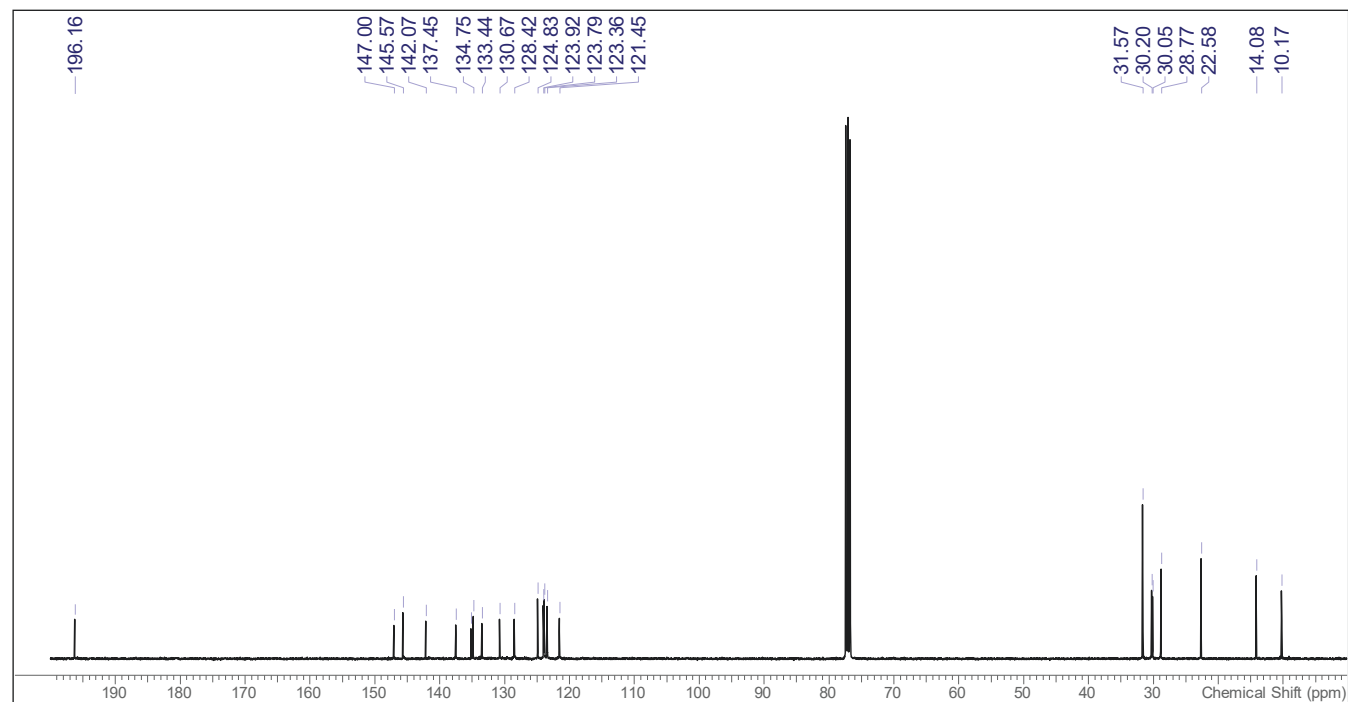


<sup>13</sup>C{<sup>1</sup>H} NMR spectrum (CDCl<sub>3</sub>, 151 MHz) of **4**.

## SUPPORTING INFORMATION

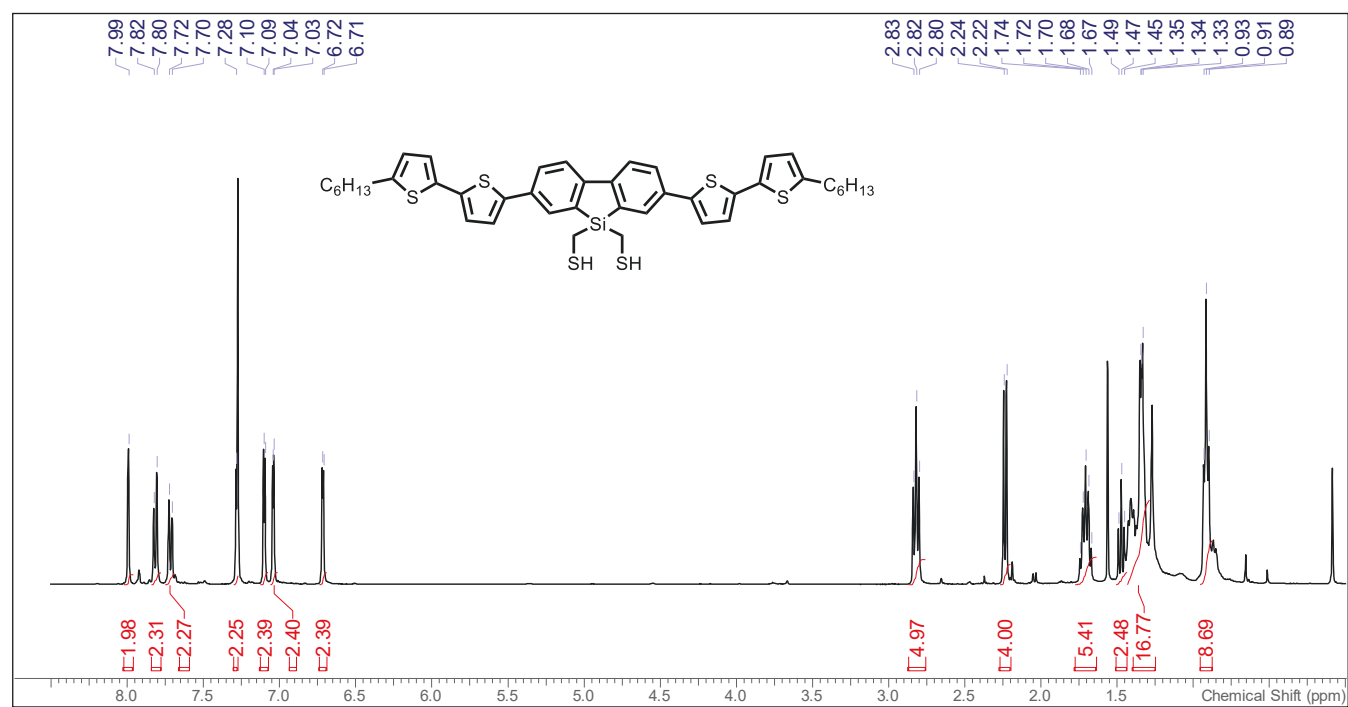


**<sup>1</sup>H NMR spectrum (CDCl<sub>3</sub>, 400 MHz) of **5 (PS)**.**

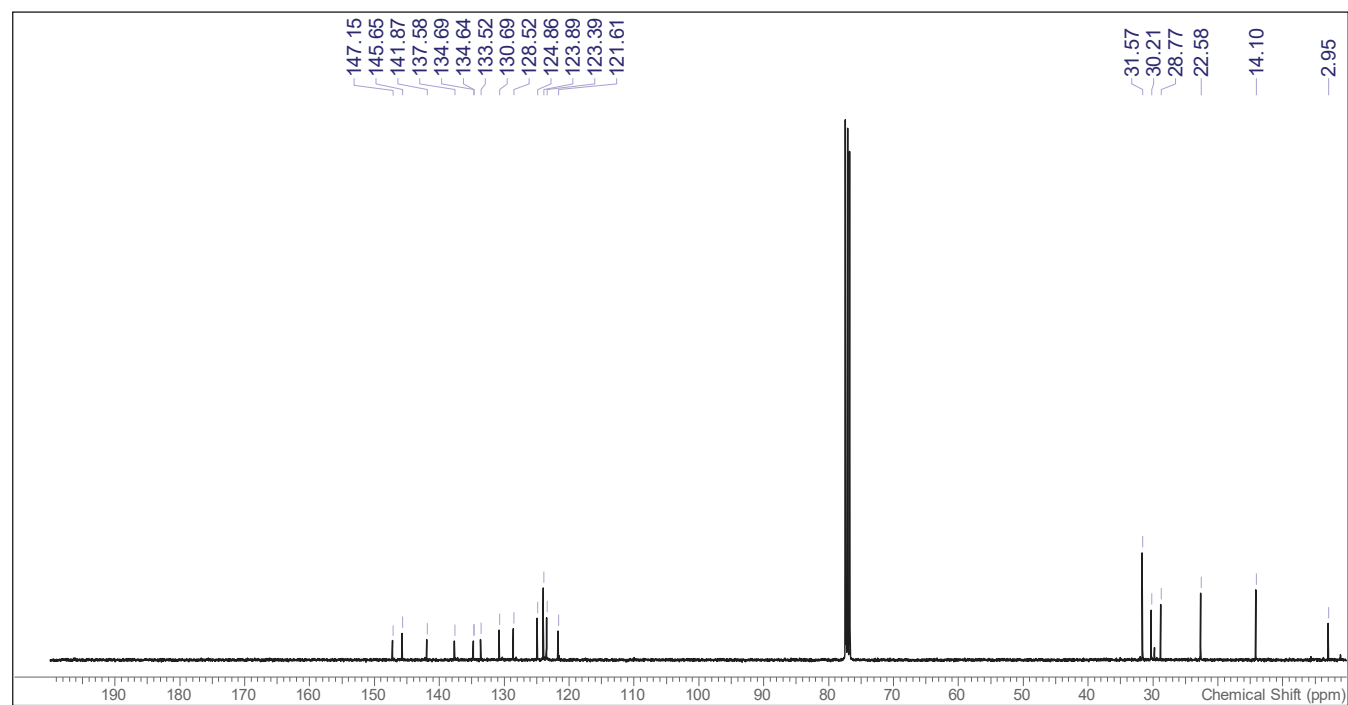


**<sup>13</sup>C{<sup>1</sup>H} NMR spectrum (CDCl<sub>3</sub>, 101 MHz) of **5 (PS)**.**

## SUPPORTING INFORMATION

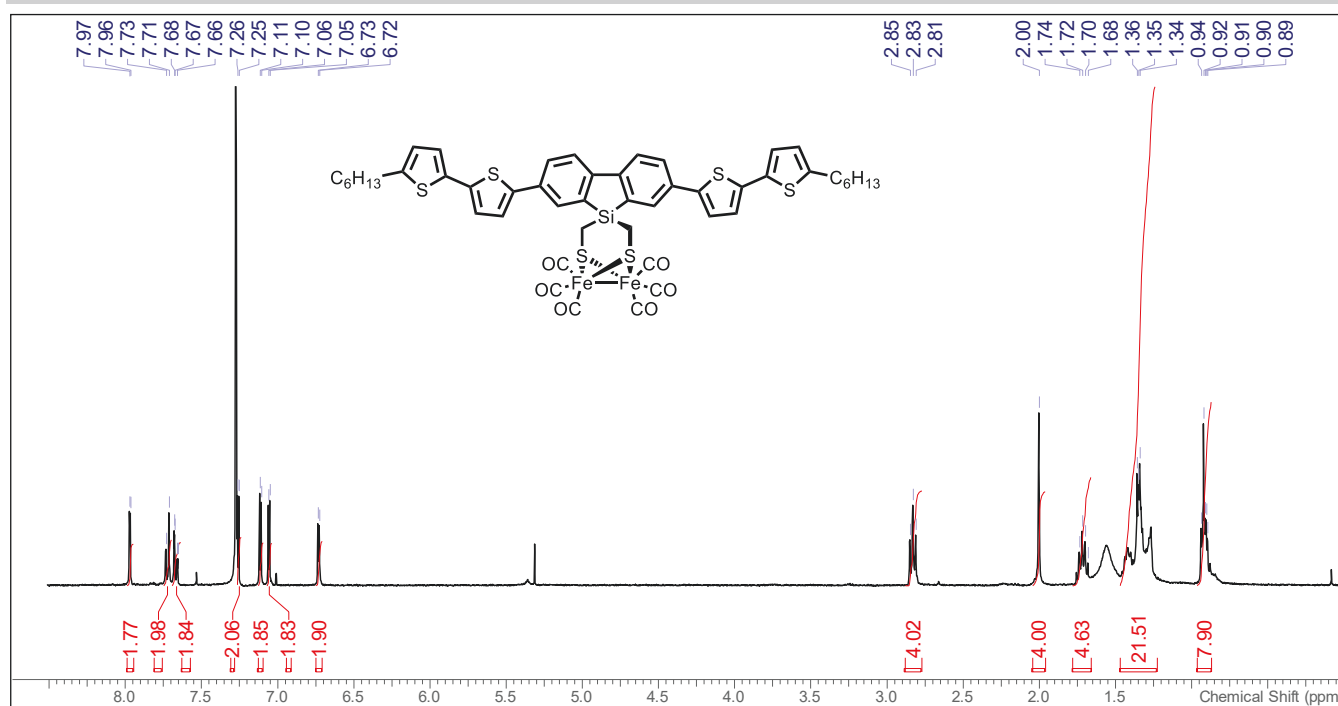
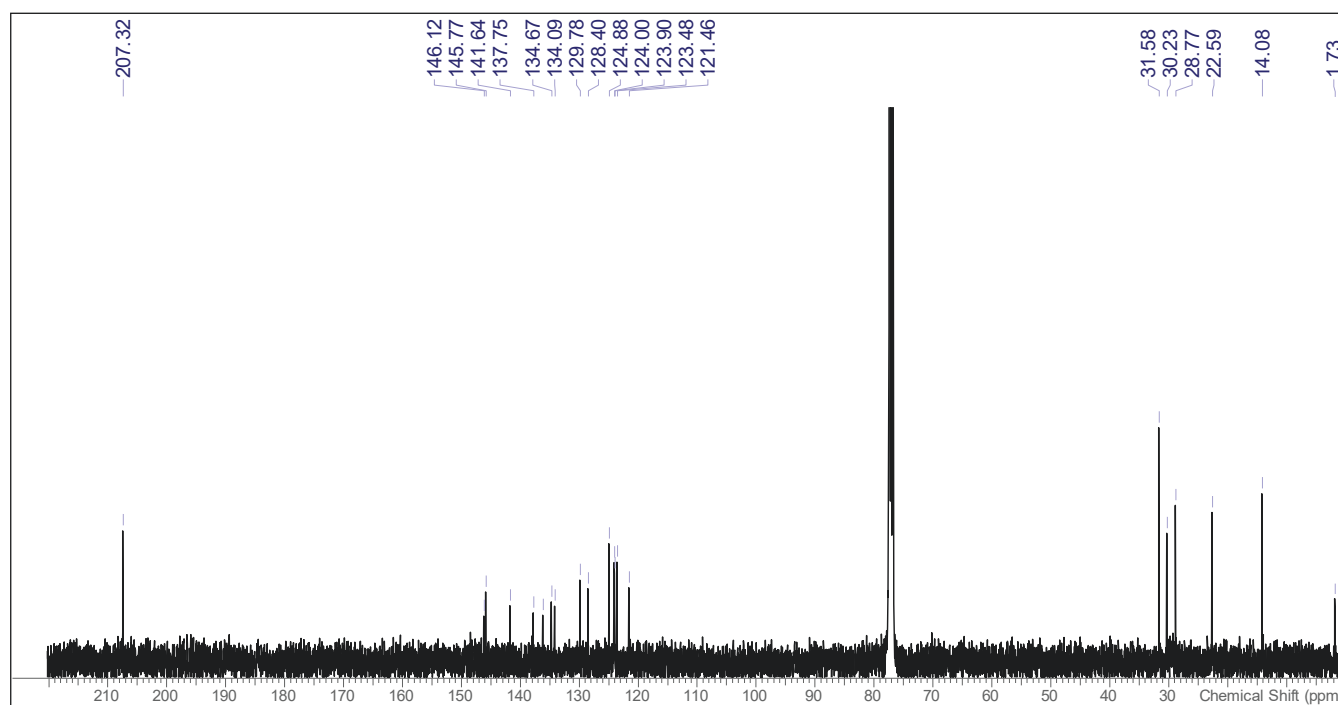


<sup>1</sup>H NMR spectrum (CDCl<sub>3</sub>, 400 MHz) of **6**.



<sup>13</sup>C{<sup>1</sup>H} NMR spectrum (CDCl<sub>3</sub>, 101 MHz) of **6**.

## SUPPORTING INFORMATION

<sup>1</sup>H NMR spectrum (CDCl<sub>3</sub>, 400 MHz) of **7** (PS-CAT).<sup>13</sup>C{<sup>1</sup>H} NMR spectrum (CDCl<sub>3</sub>, 101 MHz) of **7** (PS-CAT).

## SUPPORTING INFORMATION

## Single crystal X-ray structure determination

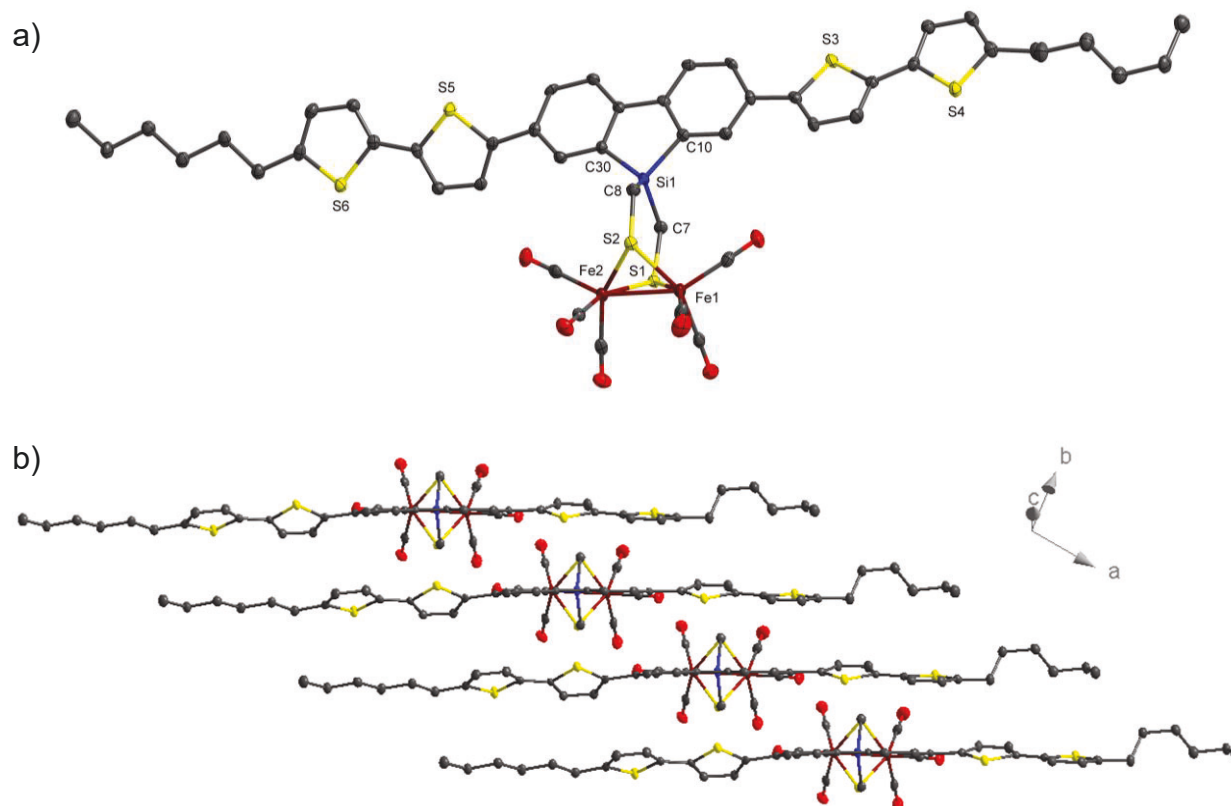


**Figure S2:** a) Molecular structure and atom labeling scheme of **PS-CAT**. b) View on the ab plane of stacked **PS-CAT** molecules. The stacking distance is 3.7672 Å. The ellipsoids represent a probability of 30 %, hydrogen atoms are omitted for clarity. Orange crystals suitable for X-ray structure determination were isolated from slow evaporation of a concentrated  $\text{CDCl}_3$  solution.

**Supporting Information available:** Crystallographic data have been deposited with the Cambridge Crystallographic Data Center as supplementary publication CCDC-2106348. Copies of the data can be obtained free of charge on application to CCDC, 12 Union Road, Cambridge CB2 1EZ, UK [E-mail: [deposit@ccdc.cam.ac.uk](mailto:deposit@ccdc.cam.ac.uk)].

**Table S1:** Crystallographic data of **PS-CAT**.

Formula	$\text{C}_{48}\text{H}_{44}\text{Fe}_2\text{O}_6\text{S}_6\text{Si}$
fw ( $\text{g}\cdot\text{mol}^{-1}$ )	1048.98
$T/\text{K}$	100
crystal system	Triclinic
space group	P-1 no. 2
$a/\text{Å}$	7.4430(12)
$b/\text{Å}$	16.584(3)
$c/\text{Å}$	19.525(3)
$\alpha/^\circ$	102.765(2)
$\beta/^\circ$	99.356(2)
$\gamma/^\circ$	95.671(2)

## SUPPORTING INFORMATION

$V/\text{\AA}^3$	2296.4(6)
$Z$	2
$\rho/\text{g}\cdot\text{cm}^{-3}$	1.517
$\mu/\text{cm}^{-1}$	9.8 (MoK $\alpha$ )
F(000)	1084
reflections collected	17149
$\Theta_{\text{max}}/^\circ$	23
unique reflections ( $R_{\text{int}}$ )	6208 (0.0360)
reflections with $ F  > 4\sigma_{ F }$	4907
$wR_2$ (all data, on $ F ^2$ ) <sup>a</sup>	0.0884
$R_1$ ( $ F  > 4\sigma_{ F }$ ) <sup>a</sup>	0.0321
parameters refined	570
$S^b$	1.036
max. features in final difference Fourier synthesis / $\text{e}\cdot\text{\AA}^{-3}$	0.426/-0.359
absorpt.corr. method	multi-scan
absorpt corr $T_{\text{min}}/\text{max}$	0.977/0.990
CCDC No.	2106348

<sup>a</sup>) Definition of the  $R$  indices:  $R_1 = (\sum || F_o | - F_c |) / \sum | F_o |$ ;

$wR_2 = \{\sum [w(F_o^2 - F_c^2)^2] / \sum [w(F_o^2)^2]\}^{1/2}$  with  $w^{-1} = \sigma^2(F_o^2) + (aP)^2 + bP$ ;  $P = [2F_c^2 + \text{Max}(F_o^2)]/3$ ;

<sup>b</sup>)  $S = \{\sum [w(F_o^2 - F_c^2)^2] / (N_o - N_p)\}^{1/2}$

**Table S2:** Selected bond lengths and angles of **PS-CAT**.

Formation	Bond length / $\text{\AA}$	Formation	Angle / $^\circ$
Fe(1)–Fe(2)	2.5084(8)	Fe(1)–Fe(2)–S(1)	55.79(3)
Fe(1)–S(1)	2.2378(11)	Fe(1)–Fe(2)–S(2)	56.33(3)
Fe(1)–S(2)	2.2540(11)	Fe(1)–S(1)–Fe(2)	67.97(3)
Fe(2)–S(1)	2.2494(10)	Fe(1)–S(2)–Fe(2)	67.84(3)
Fe(2)–S(2)	2.2412(10)	S(1)–C(7)–Si(1)	123.19(19)
S(1)–C(7)	1.812(3)	S(2)–C(8)–Si(1)	123.2(2)
S(2)–C(8)	1.815(3)	C(7)–Si(1)–C(8)	112.29(16)
C(7)–Si(1)	1.865(3)	C(10)–Si(1)–C(30)	91.47(15)
C(8)–Si(1)	1.873(4)	C(7)–Si(1)–C(10)	110.68(15)
Si(1)–C(10)	1.857(3)	C(8)–Si(1)–C(30)	115.38(16)

## SUPPORTING INFORMATION

---

Si(1)–C(30)	1.866(4)	C(10)–Si(1)–C(8)	111.70(15)
		C(30)–Si(1)–C(7)	113.59(16)



## SUPPORTING INFORMATION

## Photocatalysis

Irradiation experiments were executed in LABSOLUTE clear glass screw neck vials (ND13) and screw seals (ND13, butyl red / PTFE grey) (total volume 5 mL) filled with 10  $\mu\text{M}$  **PS-CAT** complex solutions with 1000 equivalents of BIH as sacrificial donor in  $\text{CH}_3\text{CN}/\text{NMP}$  (5:1). The samples were prepared under a nitrogen atmosphere to exclude any oxygen, solvents were deaerated thoroughly with an argon flow. Additionally, the vials were sealed with parafilm. Hydrogen quantification was carried out from each separate vials taking 200  $\mu\text{L}$  headspace volume.

*Detailed results*

Photocatalytic series were started with a M420LX Mounted LED from Thorlabs due to an appropriate overlapping between absorption (**PS-CAT**) and emission spectra (LED). However, a red-shifted M455L3 Mounted LED could even improve the photocatalytic performance (420 nm: TON = 72 after 16 h; 455 nm: TON = 145 after 17 h), although the spectral overlapping is less. The difference could also arise from a different LED power (420 nm:  $\approx 7$   $\text{mW cm}^{-2}$ , photon density  $\approx 2.5\text{E-}8$  mol photons  $\text{s}^{-1} \text{cm}^{-2}$ ; 455 nm:  $\approx 10$   $\text{mW cm}^{-2}$ , photon density  $\approx 3.8\text{E-}8$  mol photons  $\text{s}^{-1} \text{cm}^{-2}$ ; vial area: 1.23  $\text{cm}^2$ ), respectively.

Initially ( $\lambda_{\text{em,LED}} = 420$  nm), the experiments were carried out in a solvent mixture of  $\text{CH}_3\text{CN}/\text{THF}$  (5:1). Replacement of THF by NMP significantly increased the catalytic turnover, e.g., after 16 hours of irradiation: TON  $\approx 5$  from  $\text{CH}_3\text{CN}/\text{THF}$  (5:1) solution, TON = 72 from  $\text{CH}_3\text{CN}/\text{NMP}$  (5:1) solution. This can be explained by the basic properties of NMP, capturing the proton of the oxidized donor ( $\text{BIH}^{+\bullet}$ ) and thus inhibiting potential back electron transfer processes.<sup>[11]</sup>

According to their redox potential, even other electron donors should be suitable to drive HER under light, as (TD)DFT calculations revealed an energy gap between ( $\text{T}_3|\text{D}_0$ ) (**PS-CAT**) and ( $\text{D}_0|\text{S}_0$ ) ( $\text{Fc}^+/\text{Fc}$ ) of  $\Delta\Delta E = -0.45$  eV (Table S7), which in principle means, that sacrificial donors with a redox potential less positive than 0.45 V should be capable of reducing the system and to drive HER. However, as shown in Table S3, several experiments with potential donors, partly in combination with an additional proton source, yielded in very low catalytic rates after a moderate irradiation ( $\lambda_{\text{em,LED}} = 420$  nm) time. It should be noted that the given redox potentials are roughly recalculated against  $\text{Fc}^+/\text{Fc}$  from original data (for details see Table S3). What also contributes to the imprecision of the listed values, is the relation to an aqueous (ascorbic acid: HAsc, triethanolamine: TEOA) or pure  $\text{CH}_3\text{CN}$  solution (benzyl mercaptan: BnSH, 1,3-dimethyl-2-phenylbenzimidazoline: BIH, 1-Benzyl-1,4-dihydronicotinamide: BNAH).<sup>[12]</sup>

**Table S3:** Results of selected photocatalytic experiments of 10  $\mu\text{M}$  **PS-CAT** with common electron donors and  $\lambda_{\text{em,LED}} = 420$  nm. Redox potentials are roughly recalculated against  $\text{Fc}^+/\text{Fc}$  from original data by subtracting  $-0.63$  V<sup>a[13]</sup> (published vs. NHE) or  $-0.38$  V<sup>b[13]</sup> (published vs. SCE).<sup>[12]</sup>

Electron donor	Proton donor	$\approx E$ vs. $\text{Fc}^+/\text{Fc} < 0.45$ V	Solvent	Time	TON
HAsc 1000/10000 eq 5000 eq		0.08 V <sup>a</sup>	THF/ $\text{H}_2\text{O}$ (20:1) NMP	12 h 23 h	< 1 < 1
TEOA 10000 eq	TFA 5000 eq	0.19-0.44 V <sup>a</sup>	$\text{CH}_3\text{CN}/\text{THF}$ (3:1)	16 h	< 1
BnSH 1000/10000 eq		-0.48 V <sup>b</sup>	$\text{CH}_3\text{CN}/\text{THF}$ (3:1)	15.5 h	< 1

## SUPPORTING INFORMATION

BnSH 10000 eq	TFA 5000 eq	-0.48 V <sup>b</sup>	CH <sub>3</sub> CN/THF (3:1)	16 h	< 1
BIH 1000 eq 1000 eq 1000 eq		-0.05 V <sup>b</sup>	CH <sub>3</sub> CN/THF (3:1) CH <sub>3</sub> CN/THF (5:1) CH <sub>3</sub> CN/NMP (5:1)	16.5 h 16 h 16 h	≈ 2 ≈ 5 ≈ 72
BNAH 1000 eq		0.19 V <sup>b</sup>	CH <sub>3</sub> CN/NMP (5:1)	16 h	< 1

## SUPPORTING INFORMATION

## UV-vis-monitored photocatalysis

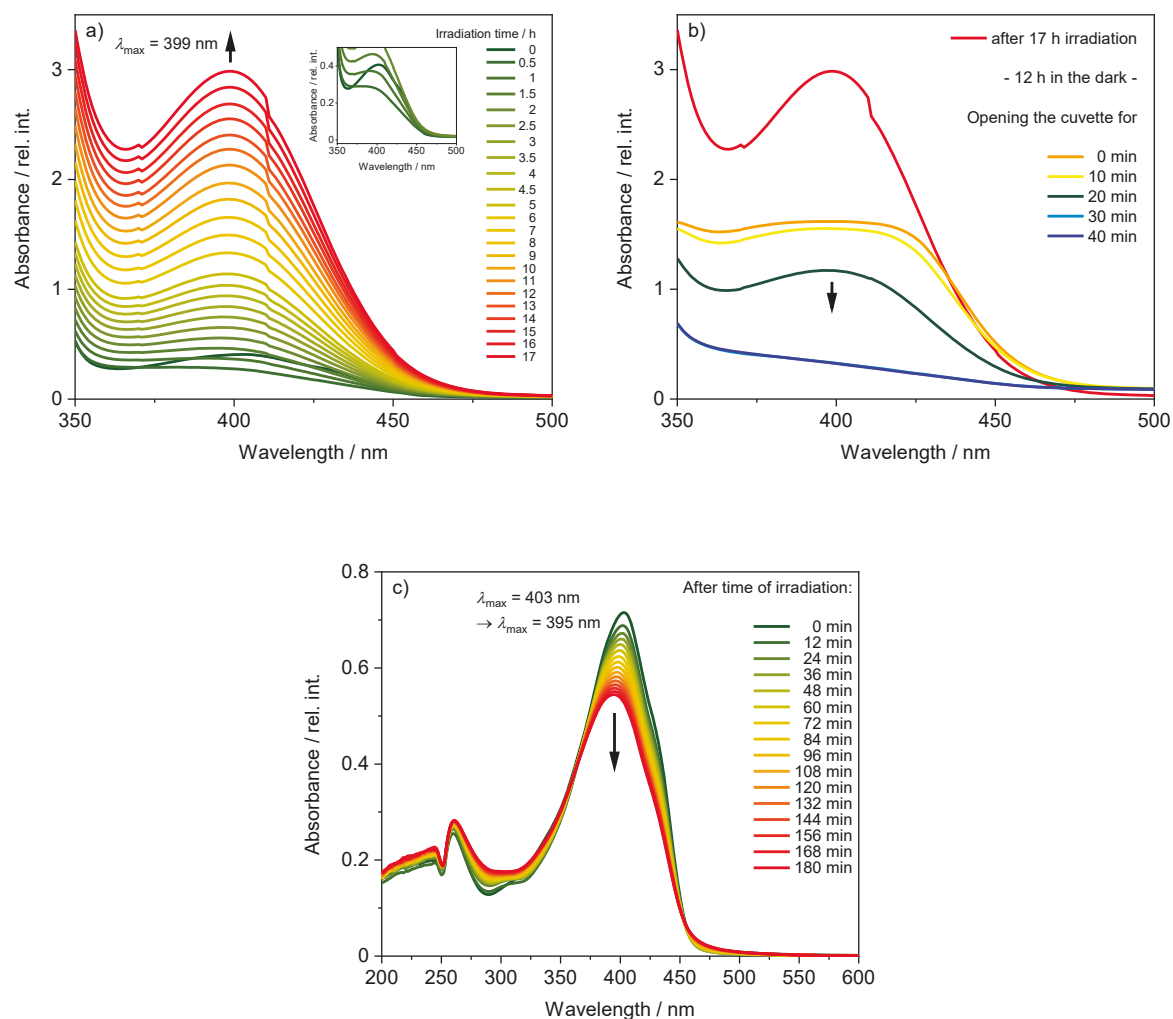


**Figure S3:** a) UV-vis spectroscopic monitoring of a photocatalytic experiment (10  $\mu\text{M}$  **PS-CAT** and 1000 eq BIH in  $\text{CH}_3\text{CN}/\text{NMP} = 5:1$ ,  $V = 1 \text{ mL}$ ) over a period of 17 h. During the UV-vis measurement the stirrer and the LED light (455 nm) were turned off. b) UV-vis spectroscopic monitoring of the dark and oxygen quenching process for the newly formed species. c) UV-vis spectroscopic monitoring of the photostability of **PS-CAT** in  $\text{CH}_3\text{CN}/\text{NMP} = 5:1$  upon irradiation (455 nm). All measurements were carried out in a 1 cm x 0.5 cm inert cuvette. After irradiation of the narrow cuvette side (LED power  $\approx 180 \text{ mW}$ ), the UV-vis measurement was executed throughout the wide cuvette side.

## SUPPORTING INFORMATION

## Fluorescence quenching in presence of BIH

Emission quenching experiments were performed to investigate potential interaction between **PS** and **PS-CAT** with the quencher BIH. The quenching experiments were performed by adding increasing equivalents of BIH to a solution of **PS** and **PS-CAT** in a titration experiment. Not only changes in emission intensity (and spectral shape of the emission spectra) have been followed, but also in parallel absorption spectra of the solutions with increasing BIH concentration were collected during this experiment.

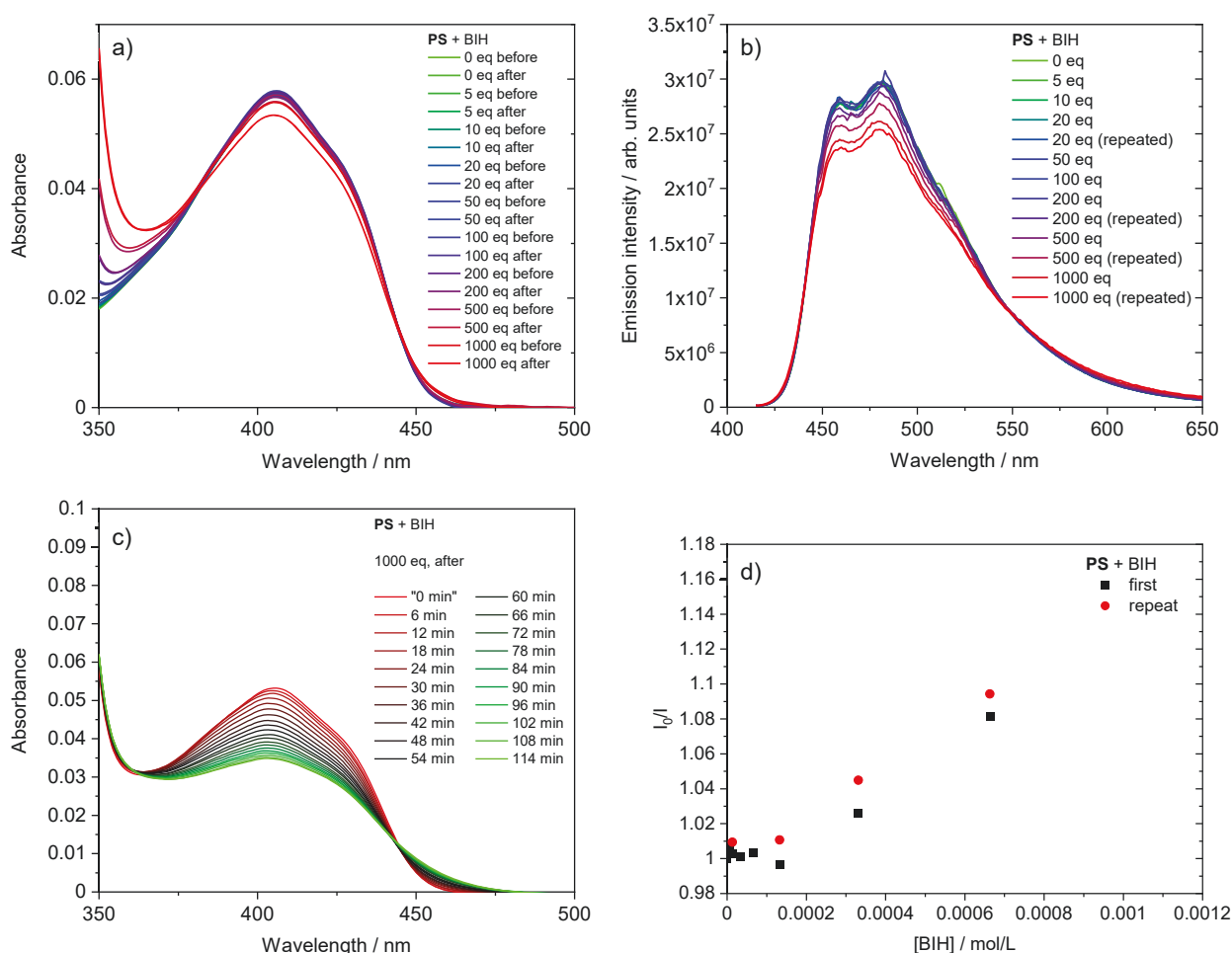


**Figure S4:** a) Absorption spectra of **PS** ( $c = 6.63 \cdot 10^{-7}$  mol/L) and b) emission spectra of **PS** upon addition of equivalents of BIH in dry and deaerated acetonitrile. All spectra are corrected for dilution effects occurring upon addition of increasing amounts of BIH. Absorption spectra were recorded for each concentration before and after the respective emission measurements to observe potential changes in the absorption spectrum during this time. For chosen concentrations several emission spectra were recorded sequentially to test for changes in emission intensity with time. c) Development of absorption spectra after addition of BIH. d) Respective plot of  $I_0/I$  vs. the concentration of BIH illustrating the changes in emission intensity in the presence of increasing amounts of BIH. For selected concentrations several sequential emission spectra were recorded. The repeated measurements after few minutes are represented by red circles.

For **PS** we noticed that in the solvent mixture ( $\text{CH}_3\text{CN}/\text{NMP} = 5:1$ ) applied in the catalytic experiment, **PS** apparently is lacking necessary stability, which shows in a decrease of absorbance and decreasing emission intensity with time, even without addition of BIH or additional irradiation. This behaviour is induced by the presence of NMP and the experiments for **PS** were performed in pure acetonitrile, where **PS** was stable. Upon addition of BIH, at low equivalents, we observe negligible quenching up to 200 equivalents. Only in the presence of 500 and 1000 equivalents the emission intensity of **PS** is significantly decreased, and the extent of quenching increases with time

## SUPPORTING INFORMATION

as shown by sequentially collected emission spectra at the same concentration. This correlates with slight changes in the absorption spectra which we recorded in parallel. A decrease of the absorption band with time after addition of BIH can be observed. In our series of experiments, we recorded absorption spectra before and after each emission measurement at a certain BIH concentration and we performed an additional experiment upon addition of 1000 equivalents following the development of a time range of longer than 100 minutes. After this time scale the absorption spectra is changed significantly, represented by a loss of absorbance of the visible absorption band. Whether this effect is caused by an aggregation effect or by a reaction between **PS** and BIH, which is changing the chromophore, is not clear at the current state of research. Under these conditions an evaluation of the quenching experiment following classical Stern-Volmer formalism is not possible.

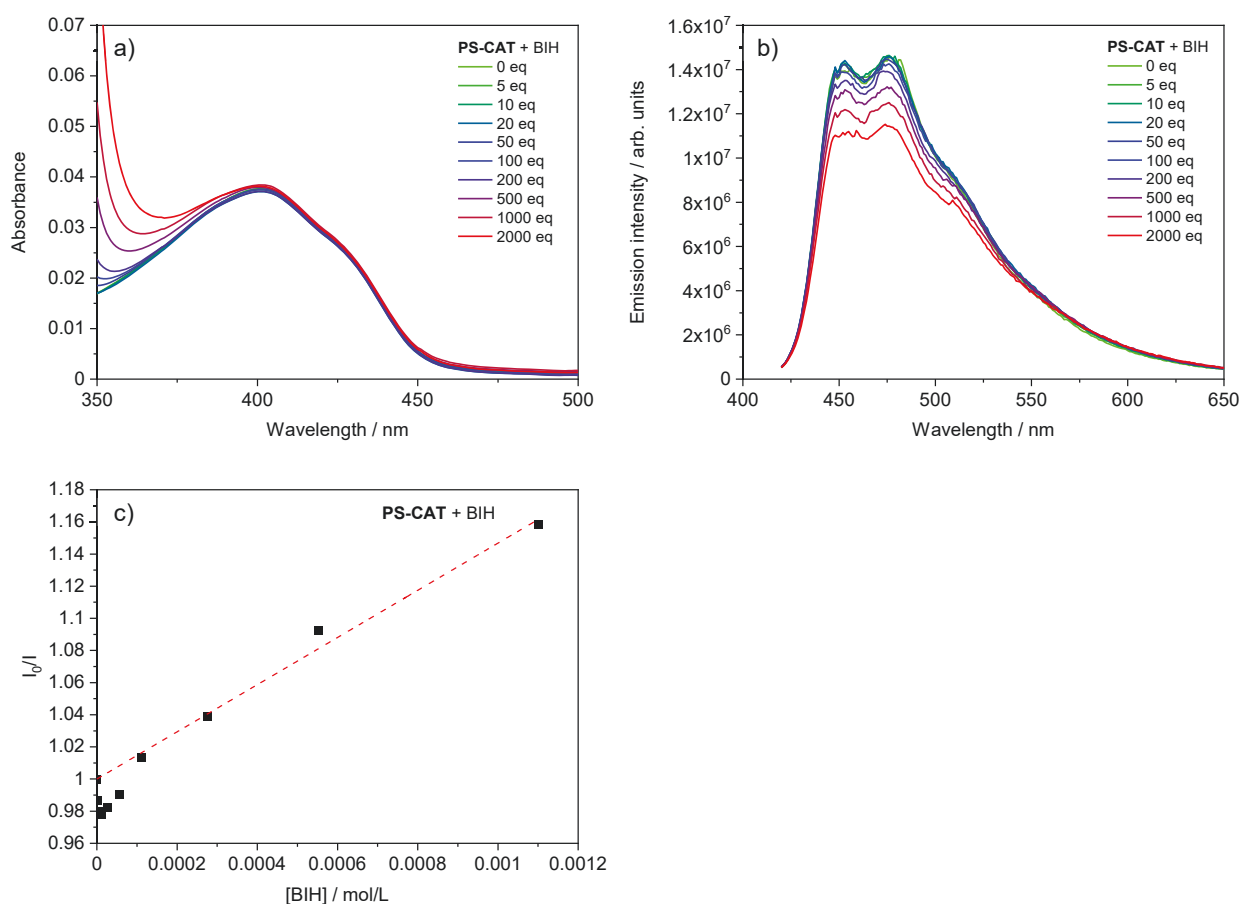


**Figure S5:** a) Absorption spectra of **PS-CAT** ( $c = 5.51 \cdot 10^{-7}$  mol/L) and b) emission spectra of **PS-CAT** upon addition of equivalents of BIH in a dry and deaerated mixture of  $\text{CH}_3\text{CN}/\text{NMP} = 5:1$ . All spectra are corrected for dilution effects occurring upon addition of increasing amounts of BIH. c) Respective plot of  $I_0/I$  vs. the concentration of BIH illustrating the changes in emission intensity in the presence of increasing amounts of BIH. The red dashed line is the respective Stern-Volmer fit.

In analogy to the investigations for **PS**, quenching experiments were also performed by adding BIH to a solution of **PS-CAT** with parallel monitoring of the absorption spectra of the solutions with increasing amount of BIH. These experiments were performed in a mixture of  $\text{CH}_3\text{CN}/\text{NMP} = 5:1$ . For **PS-CAT** the presence of NMP was essential to gain solubility and the complex is stable under these conditions. In contrast to **PS**, **PS-CAT** does not show any changes in the absorption spectra under these conditions during the quenching experiment, which means the processes leading to the changes in absorbance for **PS** in presence of BIH are not occurring for **PS-CAT**. The emission intensity decreases noticeably. A Stern-Volmer analysis was performed in this case. For collisional quenching the following relation applies:

SUPPORTING INFORMATION

---

$$\frac{I_0}{I} = 1 + K_D[Q] = 1 + k_q\tau[Q]$$

with  $I_0$  the integral intensity of the emission band in absence of quencher,  $I$  the integral intensity in presence of quencher,  $K_D$  the dynamic Stern-Volmer constant [L/mol],  $[Q]$  the quencher concentration [mol/L],  $k_q$  the bimolecular quenching rate constant [L/mol s],  $\tau$  lifetime of the fluorophore in absence of the quencher [s].

For static quenching with complex formation

$$\frac{I_0}{I} = 1 + K_S[Q]$$

with  $K_S$  the static Stern-Volmer constant [L/mol] or association constant applies.

For a system following the Stern-Volmer relation (independent of dynamic or static quenching) plotting  $I_0/I$  vs.  $[Q]$  results in a linear relation.

The fit reveals a Stern-Volmer constant of 146 L/mol, which results with a lifetime of the emission of 1 ns a bimolecular quenching constant of  $1.5 \cdot 10^{11}$  L/mol s. This is larger than the typical range for diffusion limited processes and can be an indication for a static quenching process playing a role, which in principle enables ultrafast quenching.

## SUPPORTING INFORMATION

## Time-resolved spectroscopy

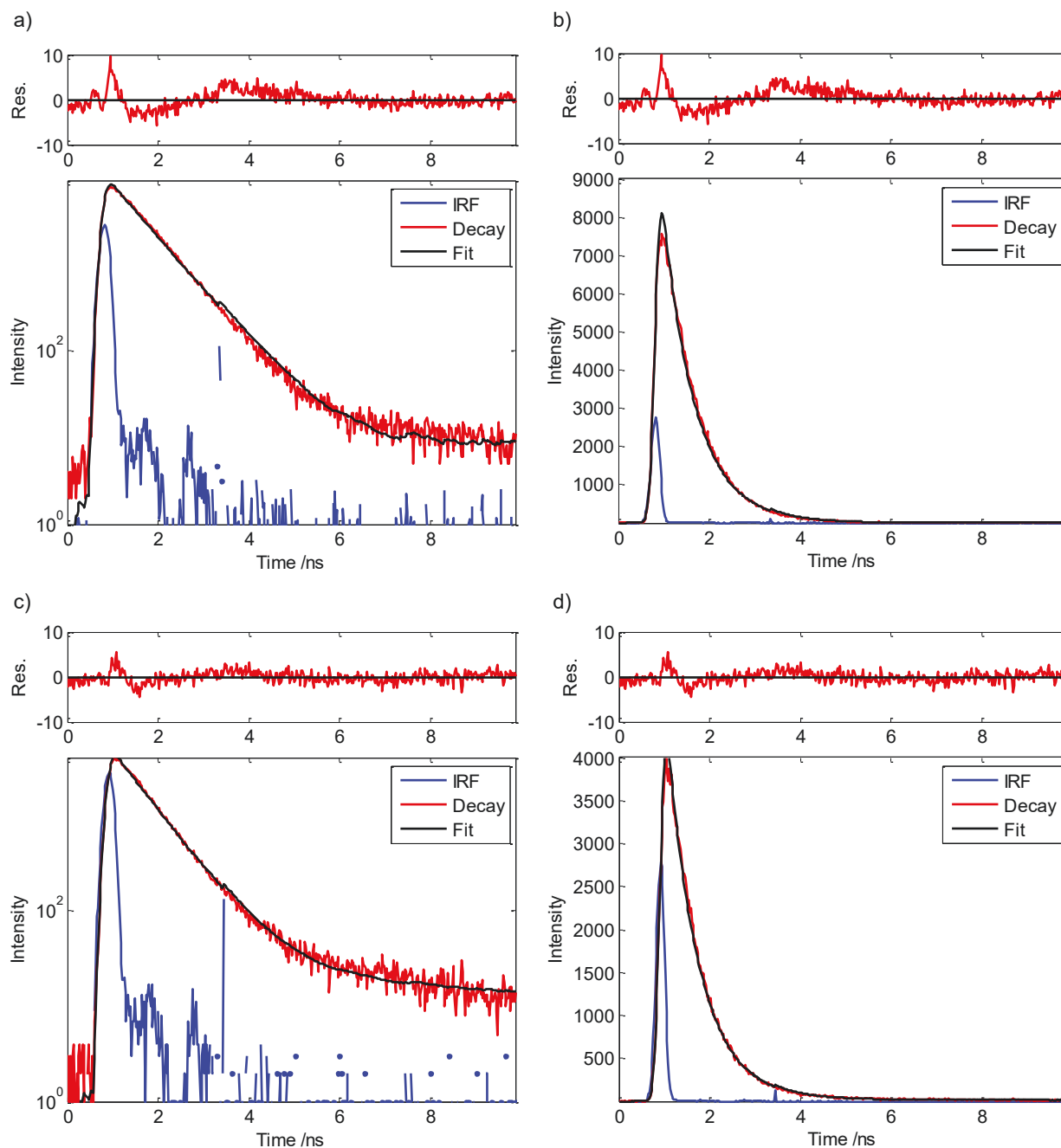


**Figure S6:** Streak camera measurements of **PS** (a, b) and **PS-CAT** (c, d). a, c) Trace on the regular scale. b, d) Trace on the logarithmic scale. The samples were prepared to yield an optical density of 0.1 at the excitation wavelength in a 1.0 cm inert quartz cuvette using deaerated, spectroscopic grade THF.

Emission lifetimes were determined for **PS** ( $\tau_1 = 1$  ns) and **PS-CAT** ( $\tau_1 = 1$  ns) in deaerated THF at an optical density of about 0.1. The absence of emission lifetime changes indicates that a potential quenching process leading to decreased emission quantum yields occurs on the ultrafast timescale or quasi instantaneously upon excitation, *e.g.* via partial population of the charge-separated singlet state ( $S_2$ ) predicted by TDDFT and cannot be resolved in the emission lifetime measurements due to limited temporal resolution.

## SUPPORTING INFORMATION

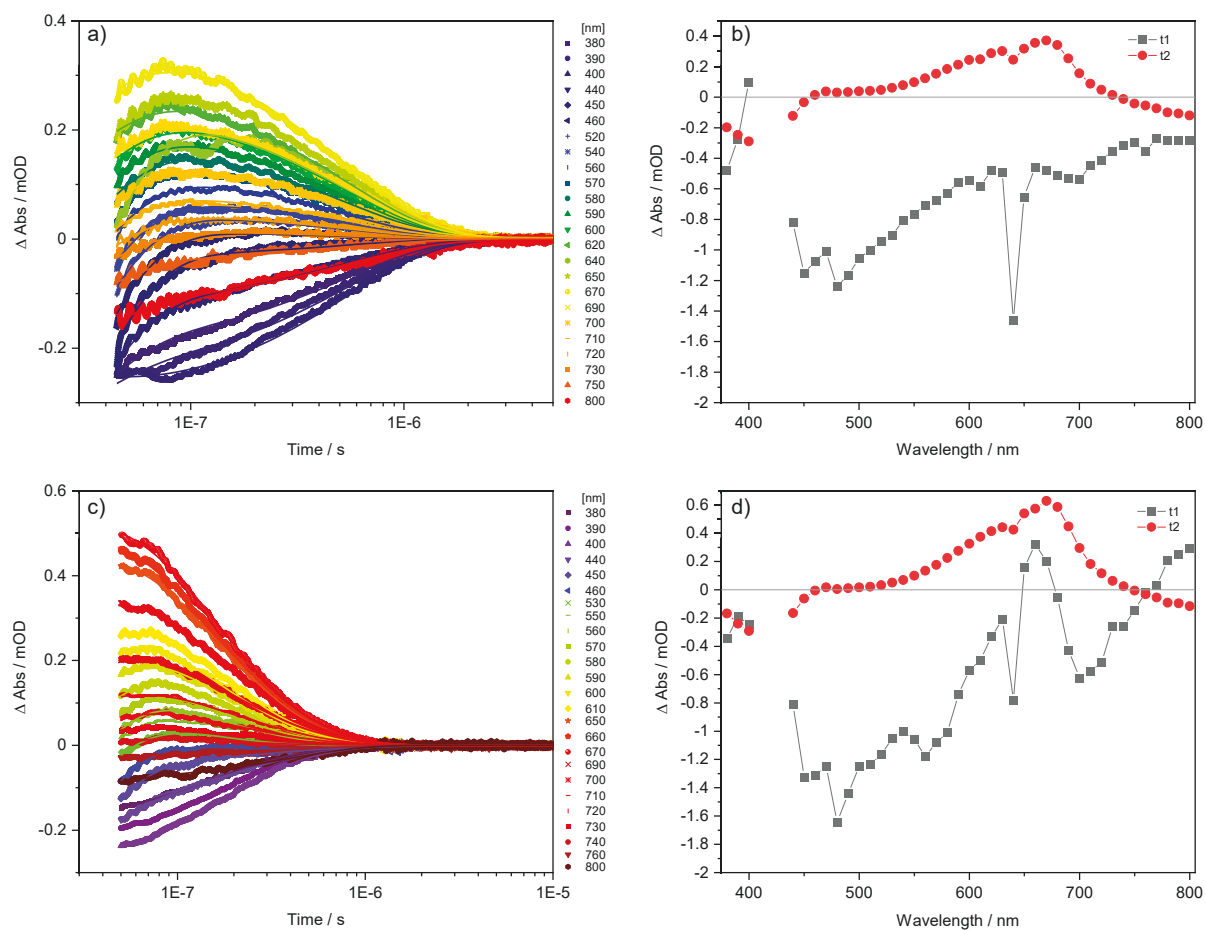


**Figure S7:** Pulsed ns-TA measurements of **PS** (a, b) and **PS-CAT** (c, d). a, c) Selected kinetic traces with corresponding biexponential fit. b, d) Decay associated spectra resulted from the global fit of the kinetic data. The samples were measured in 1 cm path length cuvettes at an optical density of around 0.25 at the excitation wavelength.



## SUPPORTING INFORMATION

## EPR spectroscopy

EPR spectroscopy was carried out under catalytic conditions with a **PS-CAT** concentration of 30  $\mu\text{M}$  to increase the concentration of the paramagnetic species. Samples were prepared under inert gas in the glovebox by solving **PS-CAT** in NMP and  $\text{CH}_3\text{CN}$  and adding 1000 equivalents of BIH. The solution was filled into an EPR tube with 3 mm diameter. Illumination was carried out at 270 K for 4 hours in the resonator, afterwards the system was cooled down to 4 K for the measurement. Measurement conditions – Microwave frequency: 9.387026 GHz, modulation amplitude: 0.2 mT, microwave power: 1.5 mW, 4 scans.

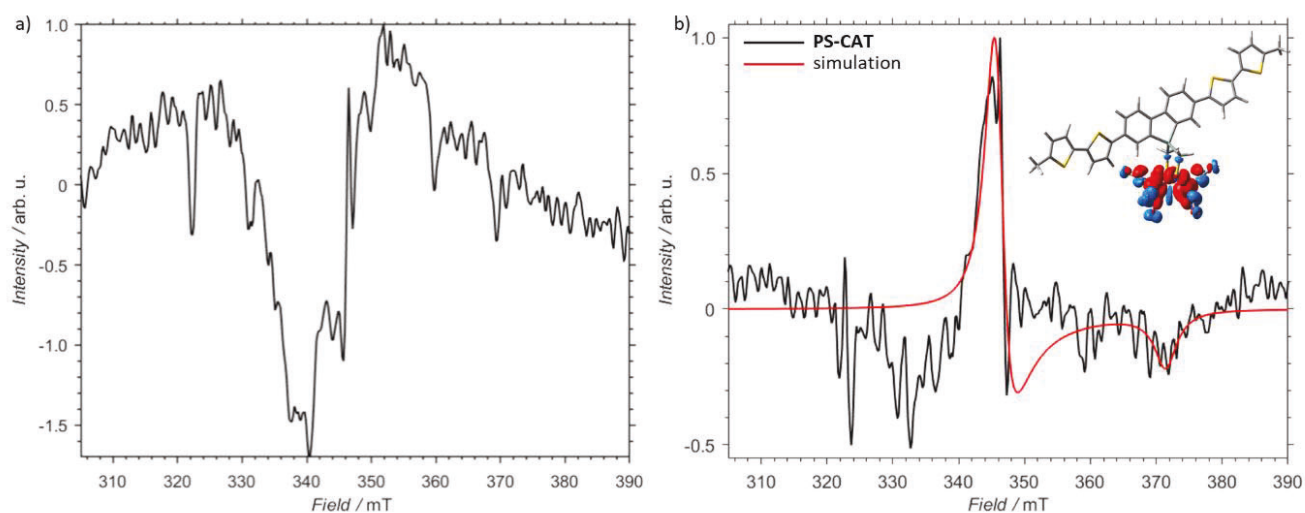


**Figure S8:** a) **PS-CAT** before illumination of the sample at 4 K. Dip at 340 mT stems from the resonator. b) **PS-CAT** after 4 hours illumination. Baseline is subtracted for better visibility of the peak; spin density localized at the [FeFe] moiety of the singly reduced **PS-CAT** (doublet).

## SUPPORTING INFORMATION

## Electrochemical characterization

CV was carried out in dry and deaerated 0.1 M  $\text{CH}_2\text{Cl}_2$ -[*n*-NBu<sub>4</sub>][BF<sub>4</sub>] solutions with a complex concentration of 1 mM. The working electrode was polished with alumina after each measurement. Oxygen-free environment in the measuring cell was realized by purging both headspace (permanently) and solution (during opening the cell) with a nitrogen flow. The ferrocenium/ferrocene (Fc<sup>+</sup>/Fc) couple served as reference.

**PS-CAT** shows a (quasi-)reversible reduction wave at  $E_{1/2}^{\text{Red1}} = -1.61$  V in  $\text{CH}_2\text{Cl}_2$  (Figure S9a), which is assigned to the reduction of [Fe<sup>I</sup>Fe<sup>I</sup>] to [Fe<sup>I</sup>Fe<sup>0</sup>] and similar to previous reported complexes in this solvent.<sup>[10, 14]</sup> The current function  $I_{\text{pc}} / (c\nu^{1/2})$  for different scan rates ( $0.2 \leq \nu \leq 20$  Vs<sup>-1</sup>) (Figure S9b)) reveals a one-electron transfer for this process, based on a comparison between a one- [(pdt)Fe<sub>2</sub>(CO)<sub>6</sub>]<sup>[15]</sup> (pdt = propane-1,3-dithiolate) and a two-electron [(bdt)Fe<sub>2</sub>(CO)<sub>6</sub>]<sup>[16]</sup> (bdt = benzo-1,3-dithiolate) transfer reference. This is underlined by the observed vibrational shift of the original  $\nu(\text{CO})$  (2072, 2033, 2000 and 1988 cm<sup>-1</sup>) upon electrochemical CAT reduction (Figure S10). Here, *i.e.*, the IR bands at 2072 and 2033 cm<sup>-1</sup> presumably are shifted to 2020 and 1970 cm<sup>-1</sup>, which is of a similar order of magnitude as for the one-electron reference [(pdt)Fe<sub>2</sub>(CO)<sub>6</sub>] (shift by ca. 70 cm<sup>-1</sup> upon electrochemical reduction).<sup>[15]</sup> As opposed to this, the two-electron reference [(bdt)Fe<sub>2</sub>(CO)<sub>6</sub>] shows shifts in the region of 110-140 cm<sup>-1</sup>, respectively.<sup>[16]</sup>

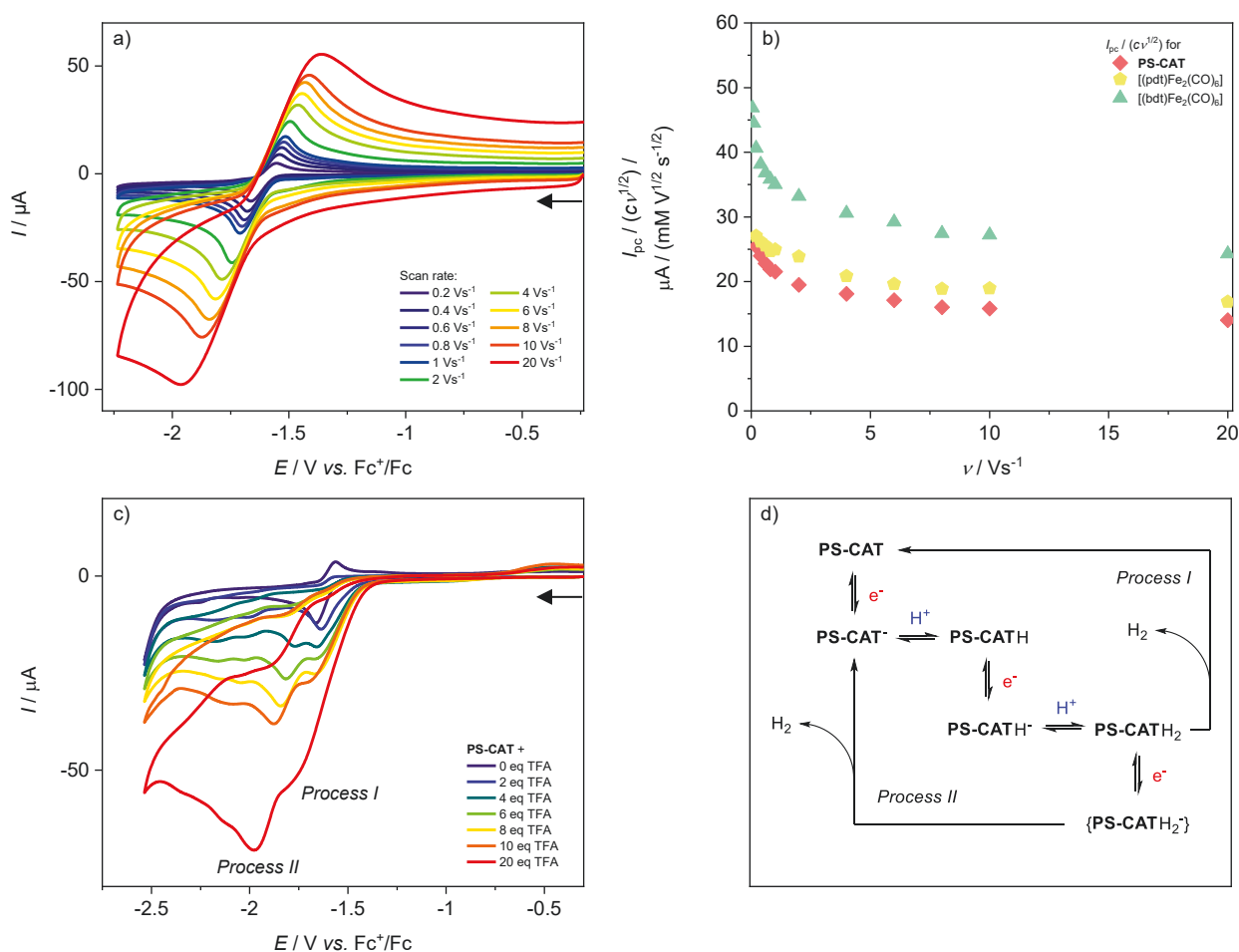


**Figure S9:** a) Cyclic voltammograms of 1 mM **PS-CAT** in 0.1 M  $\text{CH}_2\text{Cl}_2$ -[*n*-NBu<sub>4</sub>][BF<sub>4</sub>] at different scan rates. b) Corresponding current function of **PS-CAT**, compared with these for [(pdt)Fe<sub>2</sub>(CO)<sub>6</sub>] and [(bdt)Fe<sub>2</sub>(CO)<sub>6</sub>]. c) Cyclic voltammograms of 1 mM

## SUPPORTING INFORMATION

**PS-CAT** in 0.1 M  $\text{CH}_2\text{Cl}_2$ -[*n*-NBu<sub>4</sub>][BF<sub>4</sub>] at a scan rate of 0.2 Vs<sup>-1</sup> and different amounts of TFA. d) Proposed mechanism for the electrochemical proton reduction cycle of **PS-CAT** with TFA. Arrows indicate the scan direction.

The electrocatalytic property of **PS-CAT** was investigated by the addition of various amounts of trifluoroacetic acid (TFA) (Figure S9c), since only strong acids are capable of protonating a monoanionic species (one-electron transfer).<sup>[15]</sup> Upon addition of acid, the reduction potential of [Fe<sup>I</sup>Fe<sup>I</sup>] to [Fe<sup>I</sup>Fe<sup>0</sup>] is shifted from  $E_{\text{pc}} = -1.66$  V (without acid, formation of **PS-CAT**<sup>-</sup>) to -1.64 V (two equivalents of TFA) due to the follow-up protonation and generation of **PS-CATH**. For higher acid amounts (up to 20 equivalents of TFA) the current for this reduction is increasing, which exposes a first catalytic process (process I). Likewise, another catalytic reduction process (process II) emerges at four equivalents of TFA ( $E_{\text{pc}} = -1.77$  V, shifts to -1.98 V at 20 equivalents of TFA) and becomes more and more dominant up to 20 equivalents of TFA. Based on the behaviour of [(pdt)Fe<sub>2</sub>(CO)<sub>6</sub>] towards a strong acid (TfOH),<sup>[15]</sup> **PS-CAT** could follow a similar proton reduction cycle (Figure S9d).

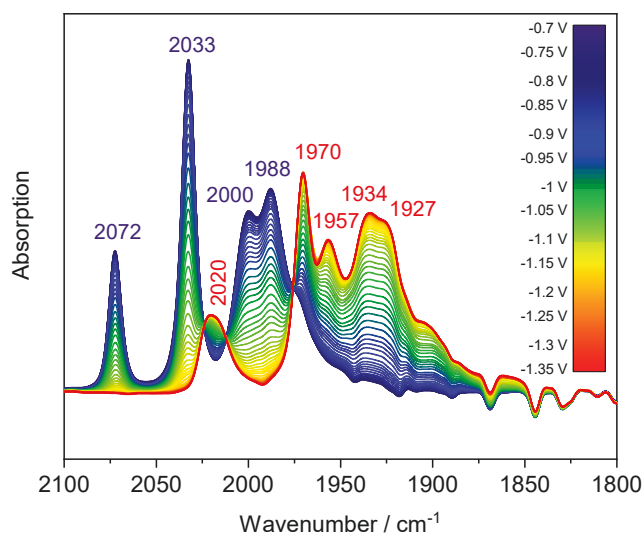


**Figure S10:** IR SEC of 2 mM **PS-CAT** (THF) during reduction.

## SUPPORTING INFORMATION

UV-vis SEC (Figure S11/S12) was achieved by using a UV-vis SEC cuvette with a 1 mm pathway equipped with a glassy carbon electrode as the working electrode, platinum wire as the counter electrode and silver wire as the reference electrode. The glassy carbon electrode has a hole in the center of the measurement window to ensure a high concentration of oxidized and reduced species is available for the measurement. The setup was degassed by a constant N<sub>2</sub> flow 15 min before solution was added and during the measurements. Both **PS** and **PS-CAT** were solved in THF at a concentration of  $2 \cdot 10^{-4}$  M with 0.1 M [*n*-NBu<sub>4</sub>][BF<sub>4</sub>] as the electrolyte. Oxidation and reduction were carried out with fresh solutions respectively.

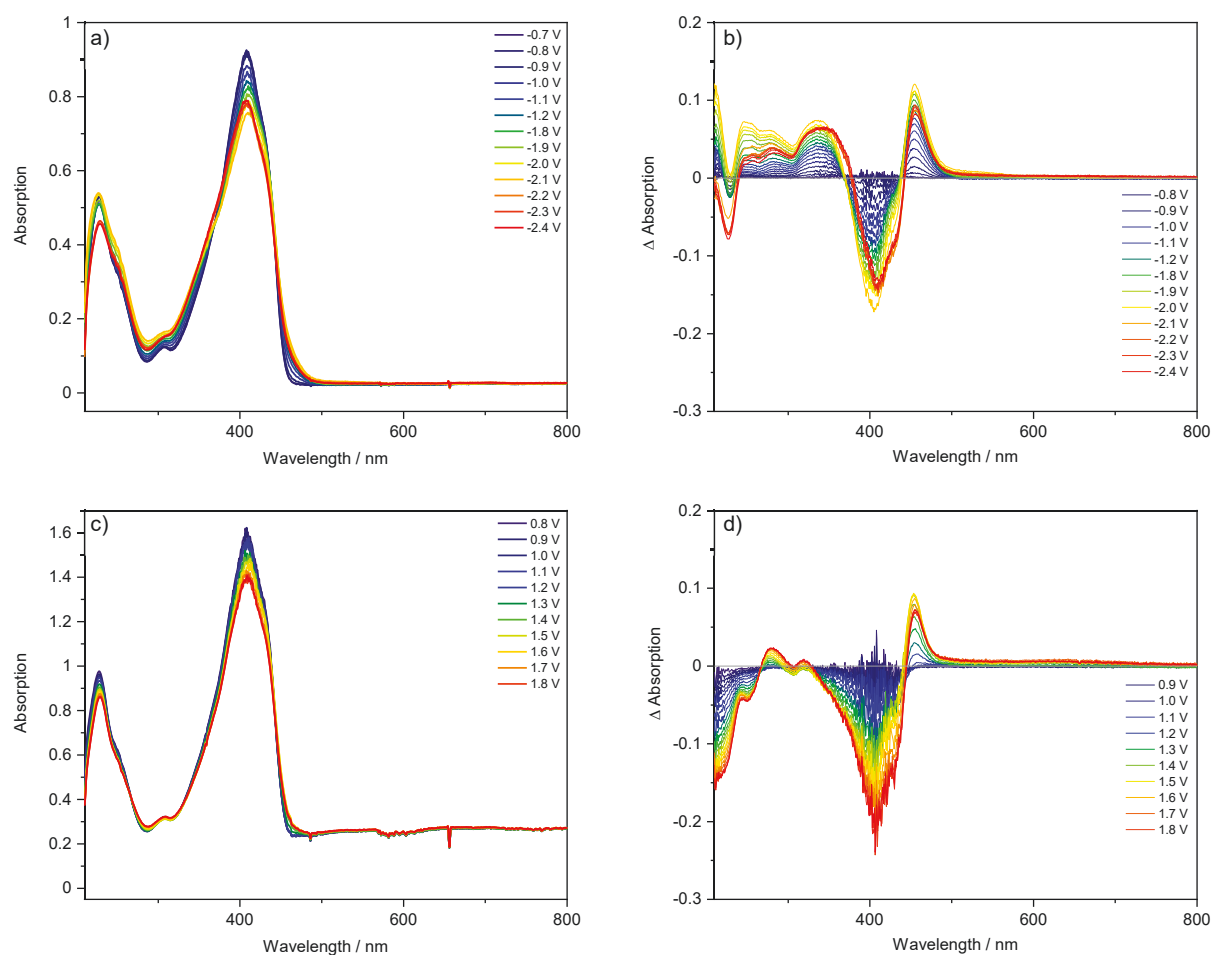


**Figure S11:** UV-vis SEC of **PS**. a) Reduction. b) differential spectrum of reduction. c) Oxidation. d) differential spectrum of oxidation.

## SUPPORTING INFORMATION

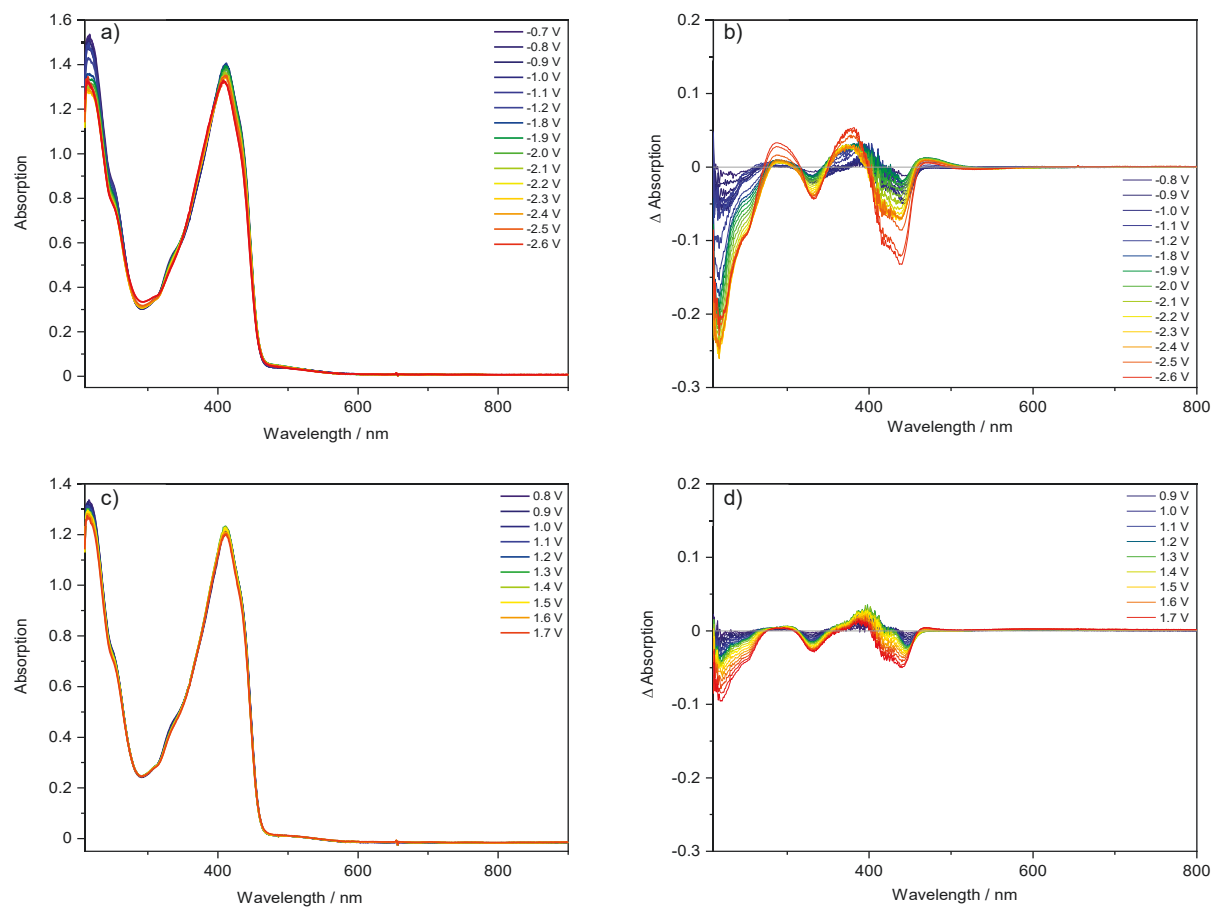


**Figure S12:** UV-vis SEC of PS-CAT. a) Reduction. b) differential spectrum of reduction. c) Oxidation. d) differential spectrum of oxidation.

## SUPPORTING INFORMATION

## Computational details

All quantum chemical calculations determining structural and electronic properties of **PS-CAT** were performed using the Gaussian 16 program.<sup>[17]</sup> To reduce the computational demand without affecting the photophysical properties of the present photocatalyst, the terminal alkyl groups of the thiophene-based chromophore were approximated by methyl groups. The fully relaxed equilibrium geometry of **PS-CAT** was obtained within the singlet ground state at the density functional level of theory (DFT) by means of the B3LYP<sup>[18]</sup> XC functional. The def2-SVP<sup>[18]</sup> basis set was applied for all atoms. A vibrational analysis was carried out to verify that a minimum on the potential energy (hyper)surface (PES) was obtained. To correct for the lack of anharmonicity and the approximate treatment of electron correlation, the harmonic frequencies were scaled by the factor 0.97.<sup>[19]</sup>

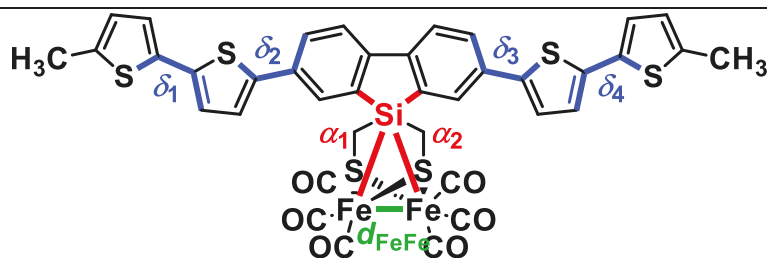
Subsequently, excited state properties such as excitation energies, oscillator strengths and electronic characters were calculated within the Franck-Condon (FC) structure at the time-dependent DFT (TDDFT) level of theory. Therefore, the 100 lowest singlet and the 100 lowest triplet excited states were calculated, while the same XC functional and basis set were applied as for the preceding ground state calculations. Several computational as well as joint spectroscopic-theoretical studies on structurally related [FeFe]-hydrogenase mimics showed that this computational protocol enables an accurate prediction of ground and excited states properties with respect to experimental data, e.g. structural and electrochemical properties as well as with respect to UV-vis absorption.<sup>[20]</sup> In particular, a reliable description of the singlet-triplet splitting is of uttermost importance to elucidate excited state relaxation processes for hydrogenase mimics. State-of-the-art *ab initio* simulations, e.g. via CASPT2, RASPT2 and CCSD(T), show that B3LYP is able to predict such singlet-triplet splitting with reasonable accuracy for structurally related hydrogenase mimics,<sup>[21]</sup> while protonation of the active site may hamper an accurate description at the B3LYP level of theory.<sup>[22]</sup> Such protonated species were not investigated in the present study. Several theoretical studies addressing the photophysics of the active site of such [FeFe]-hydrogenase models point to a dependency of the amount of exact exchange on the excited state properties of interest. However, in case of transition metal complexes, e.g. **PS-CAT**,<sup>[20a, 23]</sup> a balanced description – as provided by the present computational setup – is essential that allows to investigate the excited state properties of the photosensitizer, of the catalytic center as well as the intramolecular interactions among both moieties.<sup>[24]</sup> The extraordinary rich photophysics and photochemistry of such transition metal complexes originates from the manifold of excited states involved, i.e., metal-to-ligand charge transfer (MLCT), ligand-to-metal charge transfer (LMCT), ligand-to-ligand charge transfer (LLCT), intra-ligand charge transfer (ILCT), intra-ligand (IL) and metal-centered (MC) character. The present computational protocol, as provided by the present computational setup, is essential to assess the photophysics of transition metal complexes. Effects of interaction with a solvent (tetrahydrofuran, THF:  $\epsilon = 7.4257$ ,  $n = 1.407$ ) were taken into account on the ground and excited states properties by the solute electron density (SMD) variant of the integral equation formalism of the polarizable continuum model.<sup>[25]</sup> The non-equilibrium procedure of solvation was used for the calculation of the excitation energies within the Franck-Condon point, which is well adapted for processes where only the fast reorganization of the electronic distribution of the solvent is important. All calculations were performed including D3 dispersion correction with Becke-Johnson damping.<sup>[26]</sup>

Furthermore, excited state relaxation pathways associated to photo-induced electron transfer as well as energy transfer were studied. Therefore, fully relaxed equilibrium structures were obtained at the DFT and TDDFT for prominent triplet states, involved in the electron and energy transfer channels. Starting from the FC point, the triplet ground state ( $T_1$ ) of **PS-CAT** was optimized at the DFT level of theory. This metal-centered ( ${}^3MC$ ) state features one unpaired electron in the  $\sigma_{FeFe}$  orbital and one unpaired electron in the  $\sigma_{FeFe}^*$  orbital. Thus, the Fe-Fe bond order is decreased from one to zero upon population transfer from  $S_0$  to  $T_1$ . This decreased bond order is well reflected

## SUPPORTING INFORMATION

by the increased Fe-Fe distance from 2.503 (FC point) to 3.137 Å (<sup>3</sup>MC equilibrium structure). Furthermore, the locally excited <sup>3</sup>ππ\* state of the thiophene-based chromophore, T<sub>2</sub>, as well as the triplet charge-separated (<sup>3</sup>CS) were optimized at the TDDFT level of theory using pysisyphus<sup>[27]</sup> – our lately introduced external optimizer which is also aware of excited states. Structural relaxation within both states leads to a planarization of the in the FC point slightly twisted chromophore, see Table S4. As expected, the Fe-Fe bond is unaffected by the equilibration of the <sup>3</sup>ππ\* state ( $d_{\text{FeFe}} = 2.501$  Å), while the LMCT from the chromophore to the active site of the [Fe<sub>2</sub>S<sub>2</sub>]-cluster (<sup>3</sup>CS state) leads to an elongation of the Fe-Fe to  $d_{\text{FeFe}} = 2.753$  Å. This elongation is a result of the decreased bond order from one (S<sub>0</sub>) to 0.5 upon electron transfer into the  $\sigma_{\text{FeFe}}^*$  orbital. The equilibrium procedure of solvation was used for all ground and excited state optimizations. Finally, the redox potential of the <sup>3</sup>CS state (T<sub>2</sub>, see Table S7  $\Delta\Delta E = -0.45$  eV) was obtained based on its equilibrium energy and the ground state energy of the singly reduced **PS-CAT** (D<sub>0</sub>) with respect to the Fc<sup>+</sup>/Fc redox couple – obtained at the same level of theory.

**Table S4:** Selected structural properties such as bond lengths ( $d_{\text{FeFe}}$ ), bond angles ( $\alpha_i$ ) and dihedral angles ( $\delta_i$ ) of **PS-CAT** within its fully optimized equilibrium structures, *i.e.* at the Franck-Condon (FC) point, the locally excited intraligand triplet state (<sup>3</sup>ππ\*), the triplet charge-separated state (<sup>3</sup>CS) and the triplet metal-centered (<sup>3</sup>MC).



Geometry	$d_{\text{FeFe}} / \text{Å}$	$\alpha_1 / ^\circ$	$\alpha_2 / ^\circ$	$\delta_1 / ^\circ$	$\delta_2 / ^\circ$	$\delta_3 / ^\circ$	$\delta_4 / ^\circ$
FC	2.5030	110.7	123.0	11.5	-14.7	-18.0	9.0
<sup>3</sup> ππ*	2.5013	110.3	123.5	5.6	-7.9	-0.3	-0.1
<sup>3</sup> CS	2.7530	109.4	120.9	0.1	-2.8	0.3	0.7
<sup>3</sup> MC	3.1366	91.2	130.1	10.6	-6.4	-15.1	5.6

## SUPPORTING INFORMATION

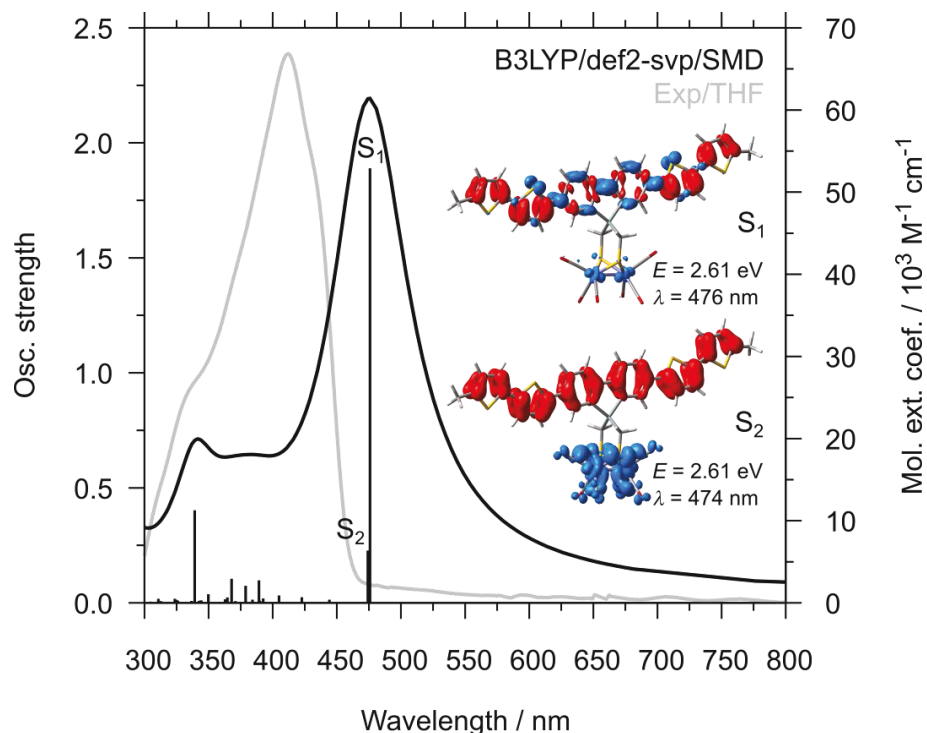


**Figure S13:** Experimental (grey) and simulated (black) UV-vis absorption spectrum of **PS-CAT** in THF. The nature of electronic transitions (into  $S_1$  and  $S_2$ ) is illustrated by charge density differences (CDDs); charge transfer takes place from red to blue.

**Table S5:** Excitation energies ( $\Delta E$ ), excitation wavelengths ( $\lambda$ ), oscillator strengths ( $f$ ) and electronic character of spin-allowed singlet-singlet and spin-forbidden singlet-triplet excitations within the equilibrium structure of the singlet ground state ( $S_0$ , Franck-Condon (FC) point) as well as spin-allowed doublet-doublet excitations within the equilibrium structure of the doublet ground state of the singly reduced species. Experimental excitation wavelengths ( $\lambda_{\text{exp}}$ ) are assigned.

Spin-allowed $S_0 \rightarrow S_i$ excitations (FC point)				
Excitation (Character)	$\Delta E / \text{eV}$	$\lambda / \text{nm}$	$f$	$\lambda_{\text{exp}} / \text{nm}$
$S_1$ (IL)	2.61	476	1.8895	412
$S_2$ (LMCT)	2.61	474	0.2273	412
Spin-forbidden $S_0 \rightarrow T_i$ excitations (FC point)				
Excitation (Character)	$\Delta E / \text{eV}$	$\lambda / \text{nm}$	$f$	$\lambda_{\text{exp}} / \text{nm}$
$T_1$ (MC)	1.07	1155	-	-
$T_2$ (IL)	1.82	681	-	-
$T_{10}$ (LMCT)	2.62	474	-	-
Spin-allowed $D_0 \rightarrow D_i$ excitations (singly reduced $D_0$ equilibrium structure)				
Excitation (Character)	$\Delta E / \text{eV}$	$\lambda / \text{nm}$	$f$	$\lambda_{\text{exp}} / \text{nm}$
$D_4$ (MC)	1.76	704	0.0721	580
$D_{25}$ (IL)	2.64	469	2.0524	399



## SUPPORTING INFORMATION

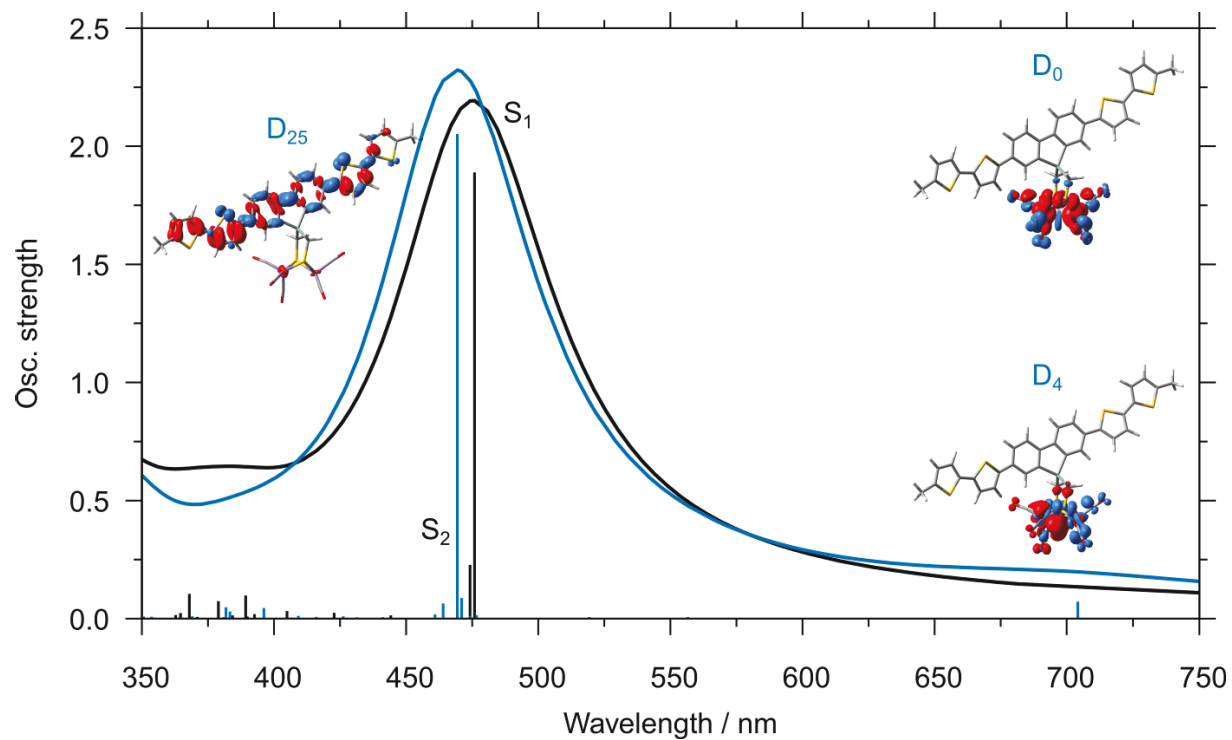


**Figure S14:** Simulated UV-vis absorption spectrum of the non-reduced singlet (black) and the singly reduced doublet (blue) species of **PS-CAT** in THF. The spin density of the doublet ground state ( $D_0$ ) show that single reduction occurs at the [FeFe]-center, *i.e.* population of the  $\sigma_{\text{FeFe}^*}$  molecular orbital. The nature of the  $D_0 \rightarrow D_{25}$  transitions is illustrated by a charge density difference (CDD); charge transfer takes place from red to blue.

## SUPPORTING INFORMATION

**Table S6:** Vibrational normal modes associated to the vibrational structure in the electronic absorption spectrum of **PS-CAT** in Figure 3a). All vibrational modes (modes 162 to 165) in vicinity of the measured vibrational feature ( $\sim 1250\text{ cm}^{-1}$ ) correspond to CC stretching and CH bending accounting for the altered electronic structure of the aromatic system upon  $\pi\pi^*$  excitation. All frequencies were scaled by a factor for 0.97.

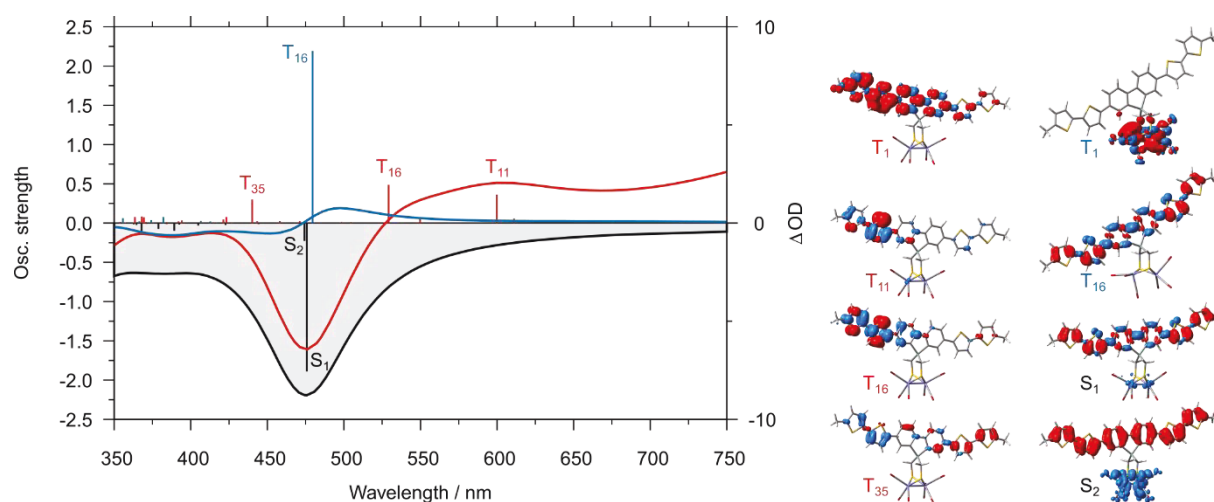
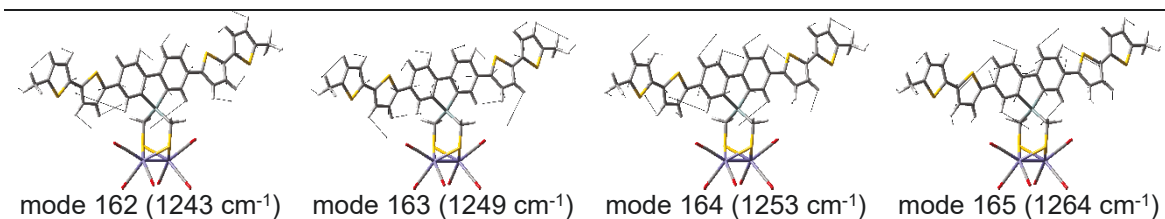
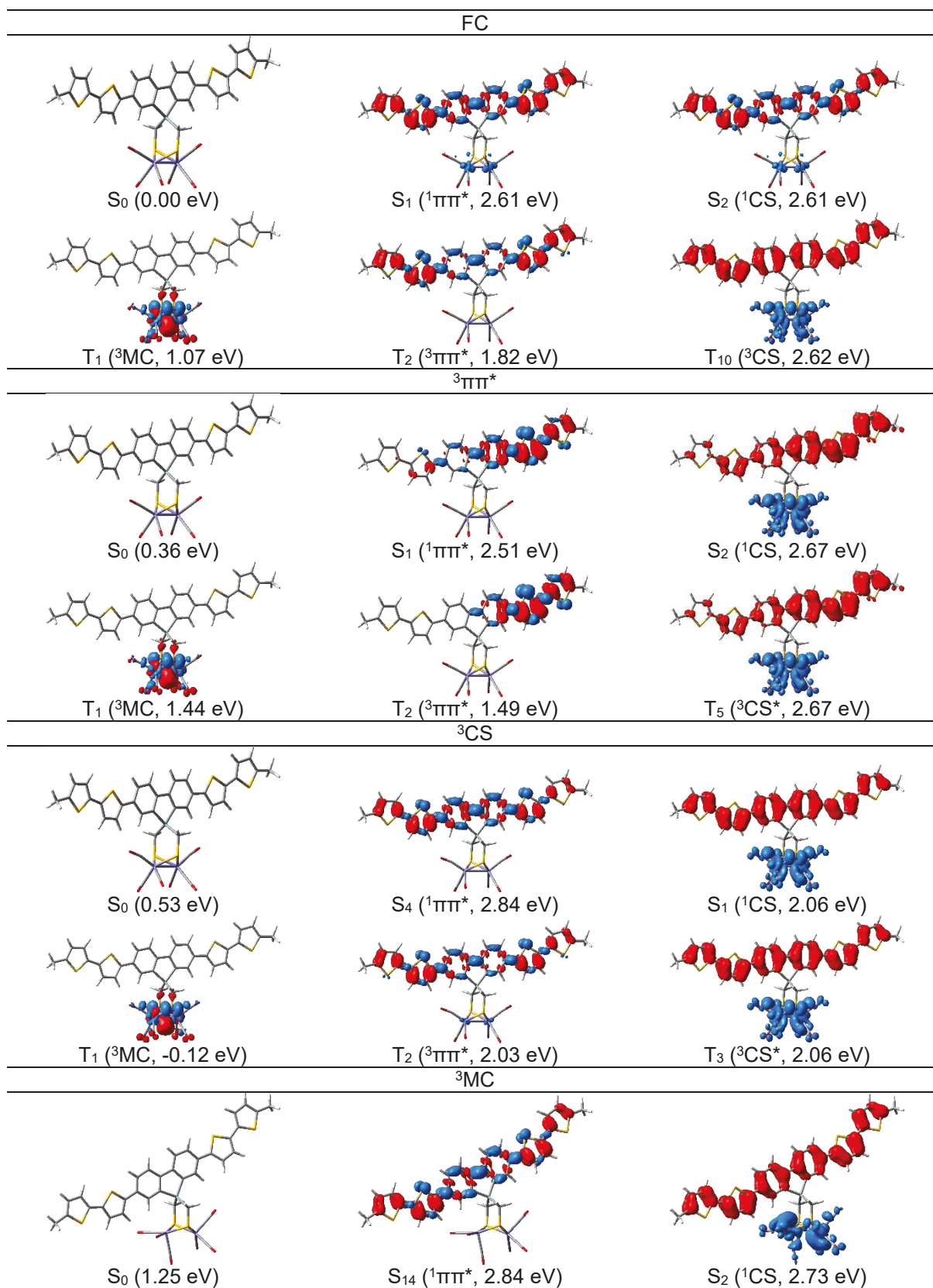


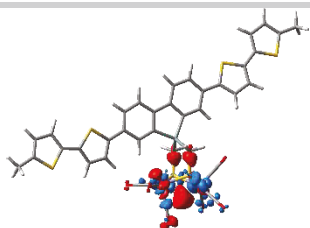
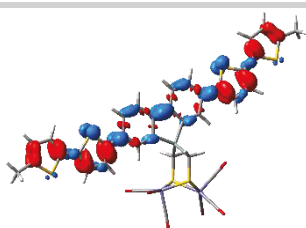
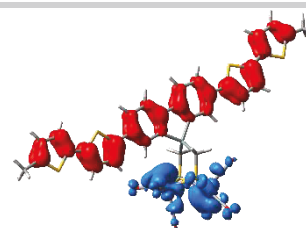
**Figure S15:** Simulated transient absorption spectra of **PS-CAT**. Positive signals (excited state absorption) originate from spin-allowed triplet-triplet excitations within the equilibrium structures of  ${}^3\pi\pi^*$  (red) and  ${}^3\text{MC}$  (blue), respectively. Negative signals (ground state bleach) stem from spin-allowed singlet-singlet excitations (black) within the equilibrium structure of the singlet ground state. Excitations of interest are labelled in red and blue accordingly. Spin densities of the triplet ground states ( $T_1$ ) obtained within  ${}^3\pi\pi^*$  (red) and  ${}^3\text{MC}$  (blue) and charge density differences (CDDs) illustrating the respective electronic transitions are shown; charge transfer takes place from red to blue.

## SUPPORTING INFORMATION

**Table S7:** Relative energies and charge density differences of all states involved in the proposed excited state relaxation scheme, see Figure 3. Energies are given with respect to the singlet ground state ( $S_0$ ) in the Franck-Condon point (FC,  $S_0$  equilibrium structure). Charge transfer takes place from red to blue.



## SUPPORTING INFORMATION

 $T_1$  ( ${}^3MC$ , -0.06 eV) $T_{10}$  ( ${}^3\Pi\Pi^*$ , 3.04 eV) $T_5$  ( ${}^3CS^*$ , 2.73 eV)

## SUPPORTING INFORMATION

## References

- [1] J.-C. Chen, Y.-C. Liu, J.-J. Ju, C.-J. Chiang, Y.-T. Chern, *Polymer* **2011**, *52*, 954-964.
- [2] a) S. D. Oosterhout, V. Savikhin, J. Zhang, Y. Zhang, M. A. Burgers, S. R. Marder, G. C. Bazan, M. F. Toney, *Chem. Mater.* **2017**, *29*, 3062-3069; b) S. A. Ponomarenko, E. A. Tatarinova, A. M. Muzafarov, S. Kirchmeyer, L. Brassat, A. Mourran, M. Moeller, S. Setayesh, D. de Leeuw, *Chem. Mater.* **2006**, *18*, 4101-4108.
- [3] a) V. I. Handmann, R. Bertermann, C. Burschka, R. Tacke, *J. Organomet. Chem.* **2000**, *613*, 19-25; b) J. O. Daiss, K. A. Barth, C. Burschka, P. Hey, R. Ilg, K. Klemm, I. Richter, S. A. Wagner, R. Tacke, *Organometallics* **2004**, *23*, 5193-5197.
- [4] D. Hong, Y. Tsukakoshi, H. Kotani, T. Ishizuka, T. Kojima, *J. Am. Chem. Soc.* **2017**, *139*, 6538-6541.
- [5] G. M. Sheldrick, *Acta Cryst. C* **2015**, *71*, 3-8.
- [6] S. Stoll, A. Schweiger, *J. Magn. Reson.* **2006**, *178*, 42-55.
- [7] C. Gu, D. Zhu, M. Qiu, L. Han, S. Wen, Y. Li, R. Yang, *New J. Chem.* **2016**, *40*, 7787-7794.
- [8] R. Goy, L. Bertini, T. Rudolph, S. Lin, M. Schulz, G. Zampella, B. Dietzek, F. H. Schacher, L. De Gioia, K. Sakai, W. Weigand, *Chem. - Eur. J.* **2017**, *23*, 334-345.
- [9] U.-P. Apfel, C. R. Kowol, E. Morera, H. Görls, G. Lucente, B. K. Keppler, W. Weigand, *Eur. J. Inorg. Chem.* **2010**, *2010*, 5079-5086.
- [10] R. Goy, U.-P. Apfel, C. Elleouet, D. Escudero, M. Elstner, H. Görls, J. Talarmin, P. Schollhammer, L. Gonzalez, W. Weigand, *Eur. J. Inorg. Chem.* **2013**, *2013*, 4466-4472.
- [11] Y. Tamaki, K. Koike, T. Morimoto, O. Ishitani, *J. Catal.* **2013**, *304*, 22-28.
- [12] Y. Pellegrin, F. Odobel, *C. R. Chim.* **2017**, *20*, 283-295.
- [13] V. V. Pavlishchuk, A. W. Addison, *Inorg. Chim. Acta* **2000**, *298*, 97-102.
- [14] a) R. Goy, L. Bertini, H. Görls, L. De Gioia, J. Talarmin, G. Zampella, P. Schollhammer, W. Weigand, *Chem. - Eur. J.* **2015**, *21*, 5061-5073; b) R. Goy, L. Bertini, T. Rudolph, S. Lin, M. Schulz, G. Zampella, B. Dietzek, F. H. Schacher, L. De Gioia, K. Sakai, W. Weigand, *Chem. - Eur. J.* **2017**, *23*, 334-345.
- [15] S. J. Borg, T. Behrsing, S. P. Best, M. Razavet, X. Liu, C. J. Pickett, *J. Am. Chem. Soc.* **2004**, *126*, 16988-16999.
- [16] M. Mirmohades, S. Pullen, M. Stein, S. Maji, S. Ott, L. Hammarström, R. Lomoth, *J. Am. Chem. Soc.* **2014**, *136*, 17366-17369.
- [17] M. J. Frisch, G. W. Trucks, H. B. Schlegel, G. E. Scuseria, M. A. Robb, J. R. Cheeseman, G. Scalmani, V. Barone, G. A. Petersson, H. Nakatsuji, et al., in *Gaussian 16 Rev. B.01*, Wallingford, CT, **2016**.
- [18] a) F. Weigend, R. Ahlrichs, *Phys. Chem. Chem. Phys.* **2005**, *7*, 3297-3305; b) F. Weigend, *Phys. Chem. Chem. Phys.* **2006**, *8*, 1057-1065.
- [19] J. P. Merrick, D. Moran, L. Radom, *J. Phys. Chem. A* **2007**, *111*, 11683-11700.
- [20] a) P. E. M. Siegbahn, R.-Z. Liao, *J. Phys. Chem. A* **2020**, *124*, 10540-10549; b) R. Goy, L. Bertini, C. Elleouet, H. Görls, G. Zampella, J. Talarmin, L. De Gioia, P. Schollhammer, U.-P. Apfel, W. Weigand, *Dalton Trans.* **2015**, *44*, 1690-1699; c) P. Buday, P. Seeber, C. Zens, H. Abul-Futouh, H. Görls, S. Graefe, P. Matczak, S. Kupfer, W. Weigand, G. Mloston, *Chem. - Eur. J.* **2020**, *26*, 11412-11416; d) L. Bertini, C. Greco, L. De Gioia, P. Fantucci, *J. Phys. Chem. A* **2009**, *113*, 5657-5670; e) H. Abul-Futouh, Y. Zagranyski, C. Müller, M. Schulz, S. Kupfer, H. Görls, M. El-khateeb, S. Gräfe, B. Dietzek, K. Peneva, W. Weigand, *Dalton Trans.* **2017**, *46*, 11180-11191.
- [21] a) M. G. Delcey, K. Pierloot, Q. M. Phung, S. Vancoillie, R. Lindh, U. Ryde, *Phys. Chem. Chem. Phys.* **2014**, *16*, 7927-7938; b) P. E. M. Siegbahn, R.-Z. Liao, *ACS Catal.* **2020**, *10*, 5603-5613.
- [22] a) G. Dong, U. Ryde, *J. Biol. Inorg. Chem.* **2016**, *21*, 383-394; b) G. Dong, Q. M. Phung, S. D. Hallaert, K. Pierloot, U. Ryde, *Phys. Chem. Chem. Phys.* **2017**, *19*, 10590-10601; c) S. Qiu, Q. Li, Y. Xu, S. Shen, C. Sun, *Wiley Interdiscip. Rev. Comput. Mol. Sci.* **2020**, *10*, e1422.
- [23] a) J. L. Bingaman, C. L. Kohnhorst, G. A. Van Meter, B. A. McElroy, E. A. Rakowski, B. W. Caplins, T. A. Gutowski, C. J. Stromberg, C. E. Webster, E. J. Heilweil, *J. Phys. Chem. A* **2012**, *116*, 7261-7271; b) M. Sensi, C. Baffert, L. Fradale, C. Gauquelin, P. Soucaille, I. Meynial-Salles, H. Bottin, L. de Gioia, M. Bruschi, V. Fourmond, C. Léger, L. Bertini, *ACS Catal.* **2017**, *7*, 7378-7387.
- [24] a) D. Escudero, in *Transition Metals in Coordination Environments: Computational Chemistry and Catalysis Viewpoints* (Eds.: E. Broclawik, T. Borowski, M. Radoń), Springer International Publishing, Cham, **2019**, pp. 259-287; b) L. González, D. Escudero, L. Serrano-Andrés, *ChemPhysChem* **2012**, *13*, 28-51; c) C. Latouche, D. Skouteris, F. Palazzetti, V. Barone, *J. Chem. Theory Comput.* **2015**, *11*, 3281-3289; d) G. E. Shillito, T. B. J. Hall, D. Preston, P. Traber, L. Wu, K. E. A. Reynolds, R. Horvath, X. Z. Sun, N. T. Lucas, J. D. Crowley, M. W. George, S. Kupfer, K. C. Gordon, *J. Am. Chem. Soc.* **2018**, *140*, 4534-4542; e) L. Zedler, A. K. Menzele, K. M. Ziem, Y. Zhang, M. Wächter, S. Gräfe, T. Pascher, S. Rau, S. Kupfer, B. Dietzek, *Angew. Chem. Int. Ed.* **2019**, *58*, 13140-13148.
- [25] a) A. V. Marenich, C. J. Cramer, D. G. Truhlar, *J. Chem. Phys. B* **2009**, *113*, 6378-6396; b) B. Mennucci, C. Cappelli, C. A. Guido, R. Cammi, J. Tomasi, *J. Phys. Chem. A* **2009**, *113*, 3009-3020.
- [26] S. Grimme, S. Ehrlich, L. Goerigk, *J. Comput. Chem.* **2011**, *32*, 1456-1465.
- [27] J. Steinmetzer, S. Kupfer, S. Gräfe, *Int. J. Quantum Chem.* **2021**, *121*, e26390.

SUPPORTING INFORMATION

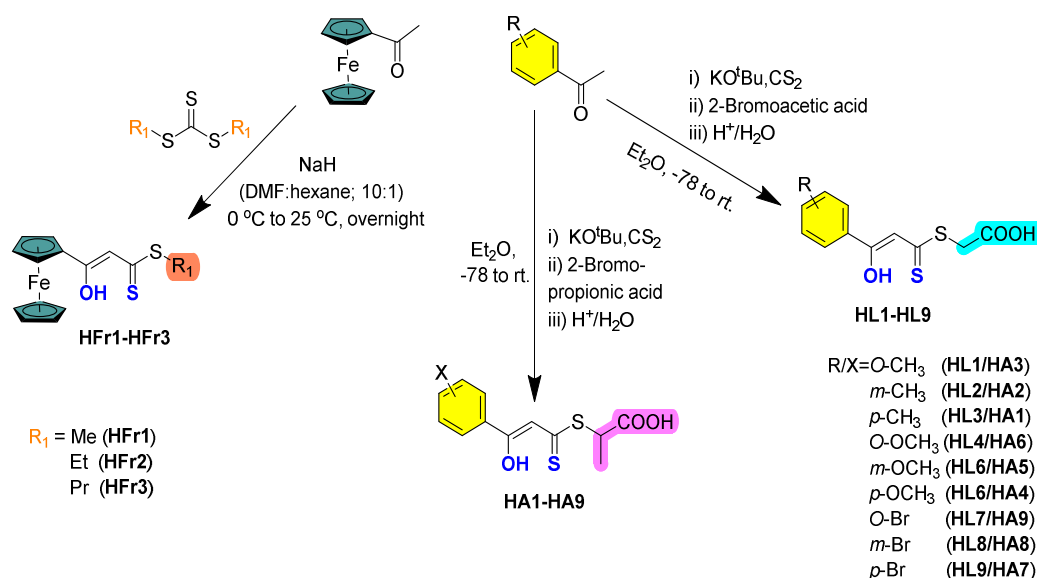
---

**Author Contributions**

Philipp Buday (synthesis, photocatalysis experiments, writing of original draft, equal contribution), Chizuru Kasahara (synthesis, equal contribution), Elisabeth Hofmeister (EPR and SEC experiments), Daniel Kowalczyk (development 3D photoreactor platform), Micheal K. Farh (synthesis, supporting), Saskia Riediger (synthesis, supporting), Martin Schulz (irradiation experiments, supporting), Maria Wächtler (photophysical experiments), Shunsuke Furukawa (co-supervision), Masaichi Saito (supervision), Dirk Ziegenbalg (development 3D photoreactor platform), Stefanie Gräfe (quantum chemical simulation), Peter Bäuerle (supervision, conceptualization), Stephan Kupfer (quantum chemical simulation, lead), Benjamin Dietzek-Ivanšić (supervision, photophysical experiments, lead), and Wolfgang Weigand (supervision, conceptualization, writing manuscript, lead)

## 6. Summary

Herein, the dissertation illustrates in detail the synthesis and characterization of three novel models based on the structural motif of the  $\beta$ -hydroxydithiocinnamic esters compounds as shown in Scheme I. Each model was designed for a separate project, which will be described later. The HL1-HL9 and HA1-HA9 ligands were synthesized according to the Thuillier method with some modification, affording finally the new class of  $\beta$ -hydroxydithiocinnamic ligands (HL1-HL9) and (HA1-HA9), that bearing *O*-/*m*-/*p*-(CH<sub>3</sub>, OCH<sub>3</sub>, or Br) as substituent R/X in the aromatic moiety as shown in Scheme I. While the  $\beta$ -hydroxy-dithioesters ferrocenyl Ligands (HFr1-HFr3) were prepared with different alkyl chain lengths (CH<sub>3</sub>-, C<sub>2</sub>H<sub>5</sub>-, or C<sub>3</sub>H<sub>7</sub>-) for HFr1, HFr2, and HFr3, respectively (Scheme I). All compounds were characterized by spectroscopic methods (<sup>1</sup>H NMR, <sup>13</sup>C{<sup>1</sup>H} NMR, and IR), mass spectrometry, and elemental analysis. Recrystallization of HL3, HA5, and HA6 produced suitable single crystals for X-ray diffraction studies.



Scheme I: Synthesis of the three model-systems  $\beta$ -hydroxydithiocinnamic ligands.

**[ME-1]. Novel Homoleptic and Heteroleptic Pt(II)  $\beta$ -oxodithiocinnamic ester Complexes: Synthesis, Characterization, Interactions with 9-methylguanine and Antiproliferative Activity.**

This article represents the first project and describes the synthesis of (HL1-HL9) ligands (Scheme I), as well as their homoleptic and heteroleptic Pt(II) complexes depicted in Figure I. Moreover, It also focuses on determining the molecular structures, studying the stability of some representative Pt(II) complexes, investigating how such Pt(II) complexes interact with 9-MeG as a DNA-model system, and finally, the anti-proliferative activity for the heteroleptic Pt(II) complexes was examined.

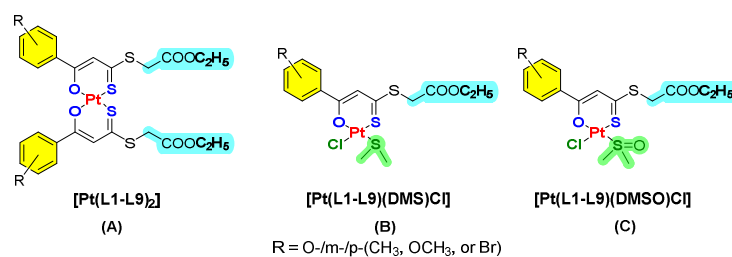


Fig. 1: Structures of A) Homoleptic Pt(II)-β-oxodithiocinnamic ester Complexes, B) and C) Heteroleptic Pt(II)-β-oxodithiocinnamic ester Complexes.

Where the free ligands (HL1–HL9) reacted with a precursor complex  $cis-[PtCl_2(DMS)(DMSO)]$  in ethanolic solution. After column chromatography, three different species of platinum(II) complexes obtained. Among them nine homoleptic complexes  $[Pt(L1-L9)_2]$ , where two β-hydroxydithiocinnamic ester ligands coordinated *cis* to each other, and 18 heteroleptic complexes  $[Pt(L1-L9)(DMS)Cl]$  and  $[Pt(L1-L9)(DMSO)Cl]$  with DMS or DMSO and chloride co-ligands. Structure determination was conceivable for the HL3 ligand as well as the Pt(II) complexes  $[Pt(L2)_2]$ ,  $[Pt(L2)(DMSO)Cl]$  and  $[Pt(L6)(DMS)Cl]$ . The solvolysis and the 9-MeG binding studies of three representative complexes  $[Pt(L6)_2]$ ,  $[Pt(L6)(DMS)Cl]$ , and  $[Pt(L6)(DMSO)Cl]$  in  $CH_3CN$ -PBS (pH 7.4; 1:1) at 37 °C for 72 hours was monitored by LC-ESI-MS spectroscopy (positive ion mode). In the solvolysis of the  $[Pt(L6)(DMSO)Cl]$  complex, both chloride and DMSO ligands were rapidly replaced by two  $CH_3CN$  molecules, affording only the bi-solvolysis species  $[(Pt(L6)(CH_3CN)_2)]^+$ . The interaction of the this complex with 9-MeG resulted in the formation of the bi-functional adduct  $[Pt(L6)(9-MeG)_2]^+$ , and the N7,O6-bidentate 9-MeG adduct  $[Pt(L6)(N7,O6-9-MeG)]^+$  could be also observed. Alternatively, the solvolysis of  $[Pt(L6)(DMS)Cl]$  complex gives both the mono-solvolysis  $[(Pt(L6)(DMS)(CH_3CN)]^+$  and the bi-solvolysis  $[(Pt(L6)(CH_3CN)_2]^+$  species, which also reflected on the interaction with the 9-MeG. Where the monofunctional adduct  $[Pt(L6)(DMS)(9-MeG)]^+$  as well as the bifunctional  $[Pt(L6)(9-MeG)_2]^+$  and the N7,O6-bidentate 9-MeG  $[Pt(L6)(N7,O6-9-MeG)]^+$  adducts were obtained. In contrast,  $[Pt(L6)_2]$  complex shows a peak corresponding to the non-solvolysed complex and a less abundant peak for the bi-solvolysis species  $[(Pt(L6)(CH_3CN)_2]^+$ . In agreement with its non-solvolysis behavior, this bis-chelate complex also exhibited the lowest 9-MeG binding. Based on these findings, the O,S-Pt(II) chelate units are almost stable under the study conditions, while the chloride, DMS, and DMSO ligands undergo solvolysis. Furthermore, such complexes, especially the heteroleptic mono-chelate complexes are capable of binding DNA-purine bases as well as forming stable mono- and bifunctional adducts. In addition, the biological activity of the heteroleptic complexes  $[Pt(L1-L9)(DMS)Cl]$ , and  $[Pt(L1, L2, L4, L5, \text{ and } L7-L9)(DMSO)Cl]$  was assayed against the epithelial ovarian cancer cell lines A2780 and Skov3 and their



cisplatin-resistant subcultures A2780cis and Skov3cis. Even though the compounds are less cytotoxic than cisplatin, they exhibit interesting activity patterns (Figure II). Most compounds affected both sensitive and cisplatin-resistant cells similarly or showed higher activity against resistant cells resulting in resistance factors ( $RF = IC_{50, resistant} / IC_{50, sensitive}$ )  $RF \leq 1$ . Moreover, for several compounds, the calculated  $IC_{50}$  values are outside the range of analyzed concentrations ( $>100 \mu M$ ). Therefore, these compounds should be evaluated as ineffective and not represented in the column graph (Figure II).

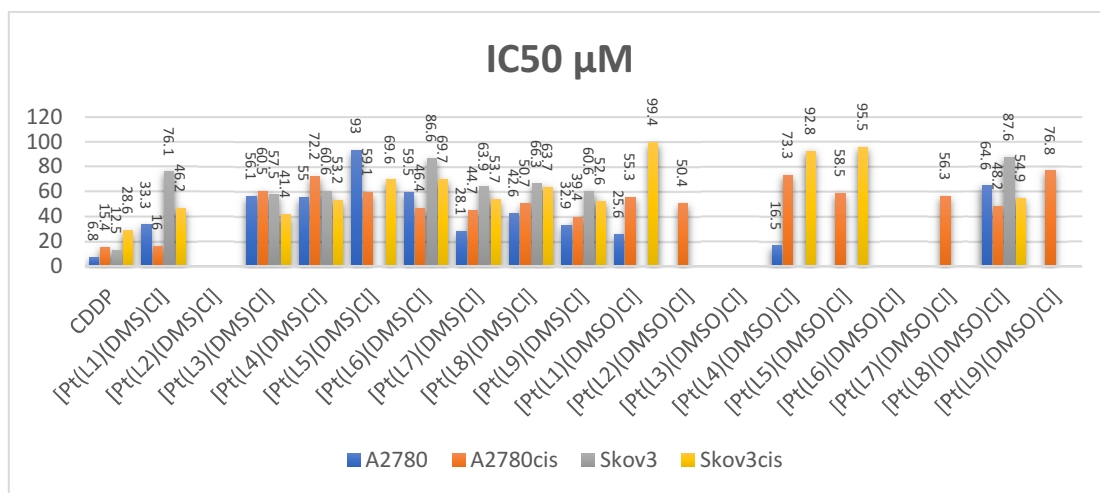


Fig. II:  $IC_{50}$  values of [Pt(L1-L9)(DMS)Cl], and [Pt(L1, L2, L4, L5, and L7-L9)(DMSO)Cl] complexes, compounds with ( $IC_{50} > 100 \mu M$ ) not shown in the column graph.

**[ME-2].** Platinum(II) and palladium(II) complexes mediated by  $\beta$ -hydroxy-dithioesters ferrocenyl derivatives: synthesis, characterization and antiproliferative activity.

This article represents the second project, which includes the synthesis of (HFr1-HFr3) ferrocenyl-containing ligands (Scheme I), as well as their heteroleptic Pt(II) and homoleptic Pd(II) complexes depicted in Figure III. In addition, this project elucidates the molecular structures of the Pt(II) and Pd(II) ferrocenyl-containing complexes, studying the action between a representative Pt(II) complex with 9-MeG, then the cytotoxic screening of the synthesized ligands and their Pt/Pd complexes.

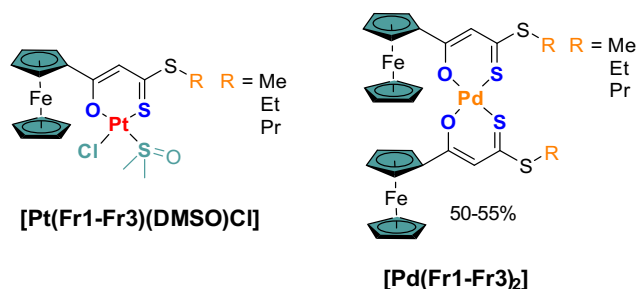


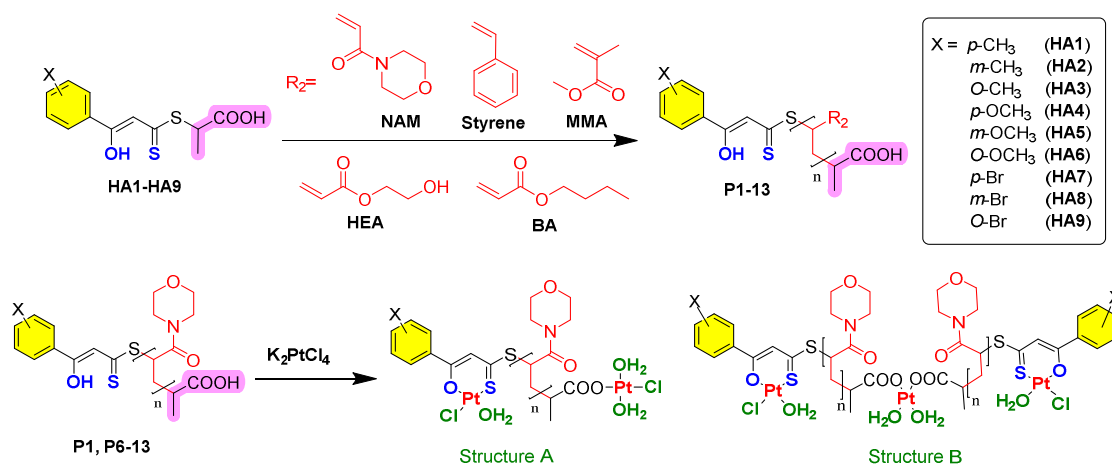
Fig. III: Structures of Pt(II)- and Pd(II)  $\beta$ -hydroxy-dithioesters ferrocenyl complexes.

The free ligands HFr1-HFr3 were reacted with *cis*-[PtCl<sub>2</sub>(DMSO)<sub>2</sub>], to obtain the heteroleptic complexes [Pt(Fr1-Fr3)(DMSO)Cl] in 69-72% yield. Whereas, they reacted with half equivalent of PdCl<sub>2</sub>(PhCN)<sub>2</sub>, and afforded the desired homoleptic complexes [Pd(Fr1-Fr3)<sub>2</sub>] in moderate yields (50-55%). Structure determination was conceivable for [Pt(Fr2)(DMSO)Cl], and [Pd(Fr3)<sub>2</sub>] complexes, and square-planar geometry was found. Moreover, the electrochemical properties of the obtained complexes were studied, where the influence of the ferrocene moiety on the redox behavior of complexes [Pt(Fr2)(DMSO)Cl] and [Pd(Fr2)<sub>2</sub>] as representative examples was investigated using cyclic voltammetry. As a result, both complexes display a quasi-reversible oxidation event at  $E_{1/2} = 0.20$  and  $0.17$  V, respectively. As a DNA model, 9-MeG was selected to react with [Pt(Fr1)(DMSO)Cl] complex in CH<sub>3</sub>CN-PBS (pH 7.4; 2:1) at 37 °C for 72 hours, and the reaction was analyzed by LC-ESI-MS to identify the formed Pt/9-MeG adducts. After 12 h, two major peaks were found, assignable to the monofunctional adducts [Pt(Fr1)(DMSO)(9-MeG)]<sup>+</sup>, and [Pt(Fr1)(CH<sub>3</sub>CN)(9-MeG)]<sup>+</sup>. The ESI spectra clearly show an additional peak assigned to [(Pt(Fr1)(CH<sub>3</sub>CN)<sub>2</sub>]<sup>+</sup>, which indicates the solvolysis of both co-ligands (Cl and DMSO), even though no bifunctional adduct was observed after 12 h. As the incubation time was extended to 24 h, the compounds decomposed into brown precipitates, and no adducts were detected, which might explain the lower cytotoxic activity of such ferrocenyl-based complexes. Anti-proliferative activity of the synthesized ligands and their Pt/Pd metal complexes against the epithelial ovarian cancer cell lines A2780 and Skov3 and their cisplatin resistant subcultures was analyzed. Overall, the Pt(II) complexes [Pt(Fr1-Fr3)(DMSO)Cl] showed higher activity than both free ligands (HFr1-HFr3) and the Pd(II) complexes [Pd(Fr1-Fr3)<sub>2</sub>]. The alkyl substituent strongly influenced the activity of these complexes and the free ligands, where the cytotoxic activity increases with the length of the alkyl chain. Both the Pt (II) and Pd(II) complexes with  $\beta$ -hydroxydithiocinnamic acid ligands that reported before in the Weigand group exhibited a higher cytotoxic activity than those ferrocenyl-based compounds. This may be caused by the lower stability of Pt/9-MeG adducts or steric effects inhibiting the binding to the target biomolecules.

### **[ME-3]. Dual Function of $\beta$ -hydroxydithiocinnamic esters: RAFT Agent and Ligand for Metal Complexation.**

Platinum drugs based on polymers and liposomes have the potential to enhance drug delivery and reduce apparent cytotoxicity. In this project, we represented a new design for  $\beta$ -hydroxydithiocinnamic ester ligands, which can be utilized as chain transfer agents (CTA-agents) for RAFT polymerization of acrylates, acrylamides, and styrene (Scheme II). Consequently, we could synthesized the Pt(II) complexes from the water-

soluble NAM- $\beta$ -hydroxydithiocinnamate- $\beta'$ -2- propionic acid polymers (Scheme II). And finally examining their cytotoxic activity.

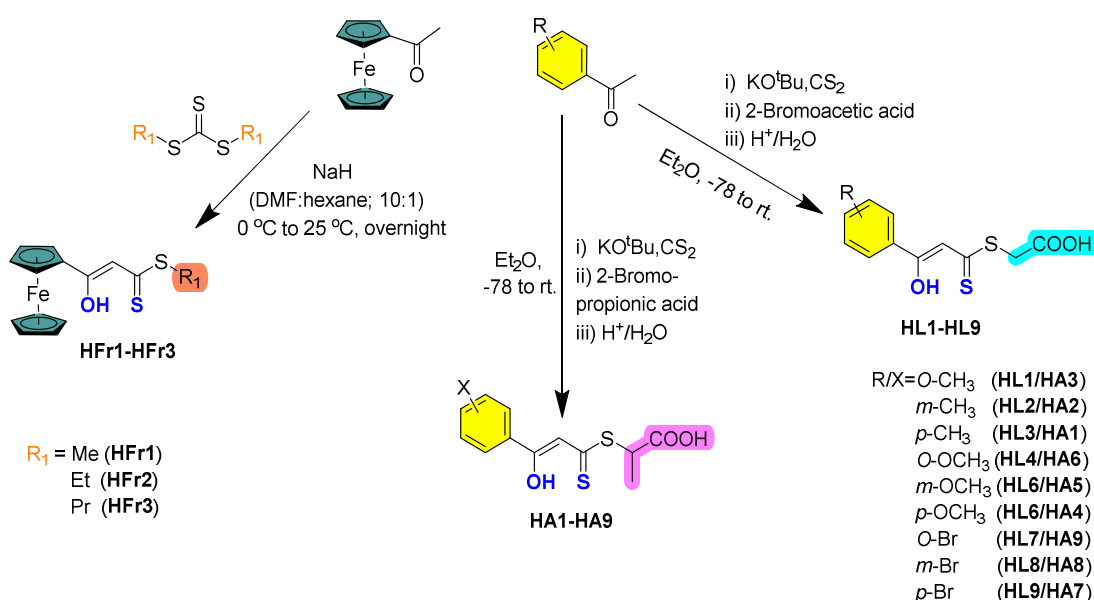


Scheme II: Structures of the ligands (HA1-HA9), monomers ( $R_2$ ), resulting polymers (P1-P13), and the Pt(II) complexes with the NAM- based polymers.

Succinctly, we could demonstrate that derivatives of  $\beta$ -hydroxydithiocinnamic esters are suitable chain transfer agents to control the polymerization of various acrylic or styrene-based monomers. Detailed kinetic studies revealed a linear evolution of molar masses with conversion. It has however to be considered that the increased reactivity of the vinyl moiety in the stabilizing group (Z-group) might still cause side reaction, if extended reaction times are applied. Nevertheless, the resulting polymer chains can successfully be chain extended, if shorter polymerization times are applied, verifying a high-end group fidelity and the living character of the polymerization. Intrinsically, the N-acryloylmorpholine-polymers appear to be still capable of binding Pt (II) and afford the two potentially platinum complexes as shown in Scheme II (structures A and B). The anti-proliferative activity of selected samples from NAM- $\beta$ -hydroxydithiocinnamic esters polymers (P6, P10, and P11) as well as their Pt complexes (PtP6, PtP10, and PtP11) against the epithelial ovarian cancer cell lines A2780 and Skov3 and their cisplatin-resistant subcultures was determined. They were evaluated as ineffective. Nevertheless, structure modifications, for instance, the polymerization of other monomers that can bind to a known anticancer drug might improve the cytotoxicity of such kind of promising compounds. Furthermore, these dual-function compounds are attractive candidates to directly prepare functional polymers for several applications, for instance, wastewater treatment since they could chelate many transition and heavy metals. Additionally, replacing the Pt element with Ti, Gd, or Lu might make them useful for bioimaging.

## 7. Zusammenfassung

In dieser Dissertation wird die Synthese und Charakterisierung von drei neuartigen Komplexen auf der Grundlage des in Schema I dargestellten Strukturmotivs der  $\beta$ -Hydroxydithiozimsäureester-Liganden im Detail beschrieben. Jeder Komplex wurde für ein separates Projekt entwickelt, welches später beschrieben wird. Die Liganden HL1-HL9 und HA1-HA9 wurden nach der Thuillier-Methode mit einigen Modifikationen synthetisiert, was schließlich die neue Klasse der  $\beta$ -Hydroxydithiozimsäure-Liganden (HL1-HL9) und (HA1-HA9) ergab, die *O*-/*m*-/*p*-(CH<sub>3</sub>, OCH<sub>3</sub> oder Br) als Substituenten R/X im aromatischen Teil tragen, wie in Schema I gezeigt. Die  $\beta$ -Hydroxydithioesterferrocenyl-Liganden (HFr1-HFr3) wurden mit unterschiedlichen Alkylkettenlängen (CH<sub>3</sub>-, C<sub>2</sub>H<sub>5</sub>- oder C<sub>3</sub>H<sub>7</sub>-) für HFr1, HFr2 bzw. HFr3 hergestellt (Schema I). Alle Verbindungen wurden Mittels spektroskopischer Methoden (<sup>1</sup>H NMR, <sup>13</sup>C{<sup>1</sup>H} NMR und IR), Massenspektrometrie und Elementaranalyse charakterisiert. Die Umkristallisation von HL3, HA5 und HA6 ergab geeignete Einkristalle für Röntgenbeugungsstudien.



Schema I: Synthese der drei Komplexentypen mit  $\beta$ -Hydroxydithiozimsäure-Liganden.

**[ME-1]. Neue homoleptische und heteroleptische Pt(II)  $\beta$ -Oxidithiozimsäureester-Komplexe: Synthese, Charakterisierung, Wechselwirkungen mit 9-Methylguanin und antiproliferative Aktivität.**

Dieser Artikel stellt das erste Projekt dar und beschreibt die Synthese von (HL1-HL9)-Liganden (Schema I) sowie deren homoleptische und heteroleptische Pt(II)-Komplexe, die in Abbildung I dargestellt sind. Darüber hinaus werden die Molekülstrukturen bestimmt, die Stabilität einiger repräsentativer Pt(II)-Komplexe sowie die Wechselwirkung dieser Pt(II)-Komplexe mit 9-MeG als DNA-Modellsystem untersucht und schließlich die antiproliferative Aktivität der heteroleptischen Pt(II)-Komplexe betrachtet.

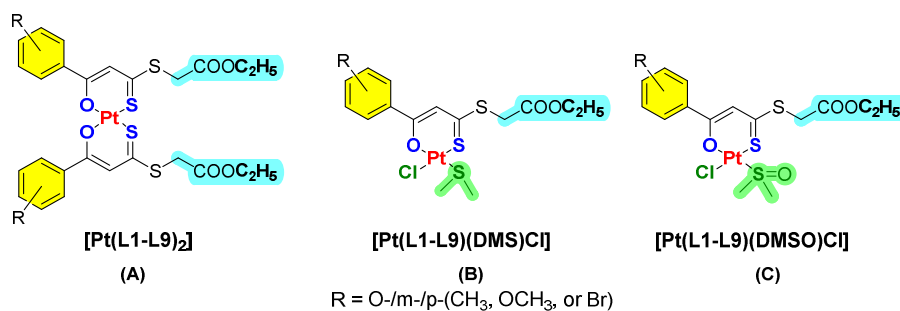


Abb. 1 Strukturen von A) homoleptischen Pt(II)- $\beta$ -Oxidithiocinnamidsäureester-Komplexen, B) und C) heteroleptischen Pt(II)- $\beta$ -Oxidithiocinnamidsäureester-Komplexen.

Dabei reagierten die freien Liganden (HL1-HL9) mit dem Vorläuferkomplex *cis*-[PtCl<sub>2</sub>(DMS)(DMSO)] in ethanolischer Lösung. Nach der Säulenchromatographie wurden drei verschiedene Arten von Platin(II)-Komplexen erhalten. Darunter neun homoleptische Komplexe [Pt(L1-L9)<sub>2</sub>], bei denen zwei  $\beta$ -Hydroxydithiozimtsäureester-Liganden in *cis*-Position miteinander koordinieren und 18 heteroleptische Komplexe [Pt(L1-L9)(DMS)Cl] und [Pt(L1-L9)(DMSO)Cl] mit DMS oder DMSO und Chlorido-Coliganden. Ein Strukturvorschlag wurde sowohl für den HL3-Liganden als auch für die Pt(II)-Komplexe [Pt(L2)<sub>2</sub>], [Pt(L2)(DMSO)Cl] und [Pt(L6)(DMS)Cl] erstellt. Die Solvolyse und die 9-MeG-Bindungsstudien von drei repräsentativen Komplexen [Pt(L6)<sub>2</sub>], [Pt(L6)(DMS)Cl] und [Pt(L6)(DMSO)Cl] in CH<sub>3</sub>CN-PBS (pH 7,4; 1:1) bei 37 °C für 72 Stunden wurden mit LC-ESI-MS-Spektroskopie (Positiv-Ionen-Modus) verfolgt. Bei der Solvolyse des [Pt(L6)(DMSO)Cl]-Komplexes wurden sowohl die Chlorido- als auch die DMSO-Liganden rasch durch zwei CH<sub>3</sub>CN-Moleküle ersetzt, so dass nur die Bi-Solvolysespezies [(Pt(L6)(CH<sub>3</sub>CN)<sub>2</sub>]<sup>+</sup> entstand. Die Wechselwirkung dieses Komplexes mit 9-MeG führte zur Bildung des bifunktionellen Addukts [Pt(L6)(9-MeG)<sub>2</sub>]<sup>+</sup> und das N7,O6-bidentate 9-MeG-Addukt [Pt(L6)(N7,O6-9-MeG)]<sup>+</sup> konnte ebenfalls beobachtet werden. Alternativ ergibt die Solvolyse des [Pt(L6)(DMS)Cl]-Komplexes sowohl die mono-solvolysierte [(Pt(L6)(DMS)(CH<sub>3</sub>CN)]<sup>+</sup> als auch die bi-solvolysierte [(Pt(L6)(CH<sub>3</sub>CN)<sub>2</sub>]<sup>+</sup> Spezies, die ebenfalls die Wechselwirkung mit dem 9-MeG widerspiegelt. Dabei wurden sowohl das monofunktionelle Addukt [Pt(L6)(DMS)(9-MeG)]<sup>+</sup> als auch das bifunktionelle [Pt(L6)(9-MeG)<sub>2</sub>]<sup>+</sup> und das N7,O6-zweiseitige 9-MeG [Pt(L6)(N7,O6-9-MeG)]<sup>+</sup>-Addukt erhalten. Im Gegensatz dazu zeigt der [Pt(L6)<sub>2</sub>]-Komplex einen Peak, der dem nichtsolvolysierten Komplex entspricht sowie einen weniger intensiven Peak für die Bi-Solvolysespezies [(Pt(L6)(CH<sub>3</sub>CN)<sub>2</sub>]<sup>+</sup>. In Übereinstimmung mit seinem Nicht-Solvolysverhalten wies dieser Bischelat-Komplex auch die geringste 9-MeG-Bindung auf. Diese Ergebnisse zeigen, dass die O,S-Pt(II)-Chelateinheiten unter den Untersuchungsbedingungen nahezu stabil sind, während die Chlorido-, DMS- und DMSO-Liganden der Solvolyse unterliegen. Darüber hinaus sind diese Komplexe, insbesondere die heteroleptischen Monochelat-Komplexe, in der Lage, DNA-Purinbasen zu binden und stabile mono- und bifunktionelle Addukte zu bilden. Des Weiteren wurde die biologische Aktivität der heteroleptischen Komplexe [Pt(L1-L9)(DMS)Cl] und [Pt(L1, L2, L4, L5 und L7-L9)(DMSO)Cl] gegenüber epithelialen Ovarialkarzinom-Zelllinien A2780 und Skov3 sowie deren Cisplatin-resistente Subkulturen A2780cis und Skov3cis untersucht. Obwohl die Verbindungen weniger

zytotoxisch sind als Cisplatin, weisen sie interessante Aktivitätsmuster auf (Abbildung II). Die meisten Verbindungen wirkten auf empfindliche und cisplatinresistente Zellen in ähnlicher Weise oder zeigten eine höhere Aktivität gegen resistente Zellen, was zu Resistenzfaktoren ( $R_F = IC_{50, \text{resistent}} / IC_{50, \text{empfindlich}}$ )  $R_F \leq 1$  führte. Außerdem liegen die berechneten  $IC_{50}$ -Werte für mehrere Verbindungen außerhalb des Bereichs der analysierten Konzentrationen ( $>100 \mu\text{M}$ ). Daher sollten diese Verbindungen als unwirksam eingestuft und nicht im Säulendiagramm (Abbildung II) dargestellt werden.

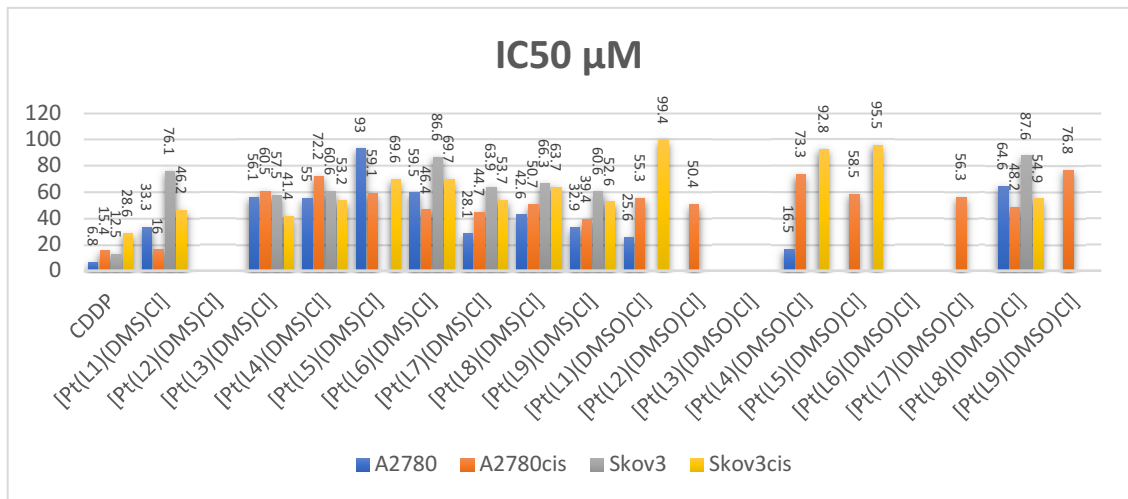


Abb. II:  $IC_{50}$ -Werte der  $[Pt(L1-L9)(DMS)Cl]$ - und  $[Pt(L1, L2, L4, L5 \text{ und } L7-L9)(DMSO)Cl]$ -Komplexe, Verbindungen mit ( $IC_{50} > 100 \mu\text{M}$ ) nicht im Säulendiagramm dargestellt.

**[ME-2]. Platin(II)- und Palladium(II)-Komplexe, vermittelt durch  $\beta$ -Hydroxydithioesterferrocenylderivate: Synthese, Charakterisierung und antiproliferative Aktivität.**

Dieser Artikel stellt das zweite Projekt dar, das die Synthese von (HFr1-HFr3) ferrocenylhaltigen Liganden (Schema I) sowie deren heteroleptische Pt(II)- und homoleptische Pd(II)-Komplexe umfasst, die in Abbildung III dargestellt sind. Darüber hinaus werden in diesem Projekt die Molekülstrukturen der Pt(II)- und Pd(II)-Ferrocenylhaltigen Komplexe aufgeklärt, die Wirkung eines repräsentativen Pt(II)-Komplexes mit 9-MeG untersucht und anschließend die zytotoxischen Eigenschaften der synthetisierten Liganden und ihrer Pt/Pd-Komplexe überprüft.

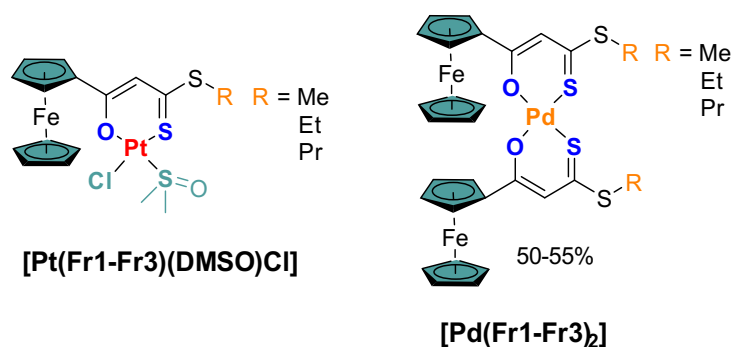


Abb. III: Strukturen von Pt(II)- und Pd(II)- $\beta$ -Hydroxydithioester-Ferrocenyl-Komplexen.

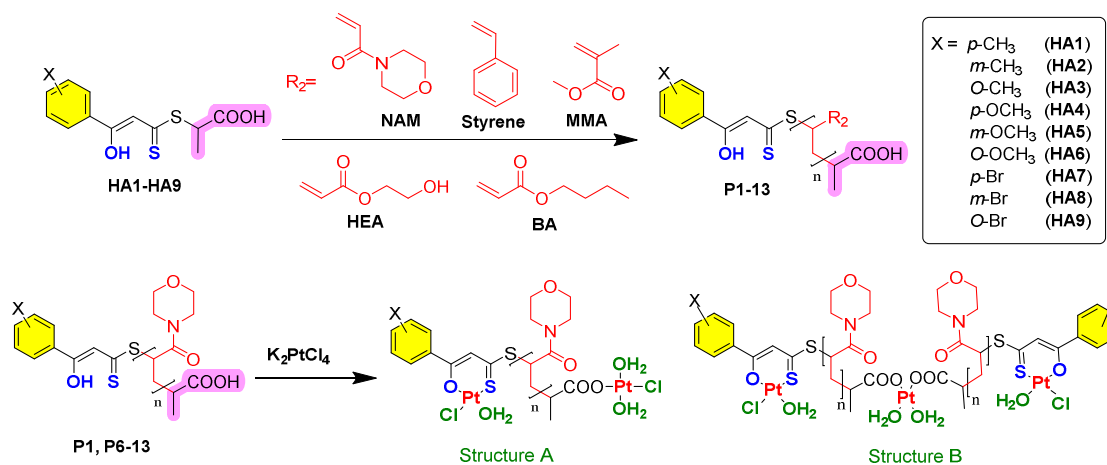


Die freien Liganden HFr1-HFr3 wurden mit *cis*-[PtCl<sub>2</sub>(DMSO)<sub>2</sub>] umgesetzt, um die heteroleptischen Komplexe [Pt(Fr1-Fr3)(DMSO)Cl] in 69-72 % Ausbeute zu erhalten. Sie reagierten dagegen mit einem halben Äquivalent PdCl<sub>2</sub>(PhCN)<sub>2</sub> und lieferten die gewünschten homoleptischen Komplexe [Pd(Fr1-Fr3)<sub>2</sub>] in mäßiger Ausbeute (50-55 %). Für die Komplexe [Pt(Fr2)(DMSO)Cl] und [Pd(Fr3)<sub>2</sub>] war eine Strukturbestimmung denkbar. Dabei wurde eine quadratisch-planare Anordnung der Liganden gefunden. Darüber hinaus wurden die elektrochemischen Eigenschaften der erhaltenen Komplexe untersucht, wobei der Einfluss des Ferrocenanteils auf das Redoxverhalten der Komplexe [Pt(Fr2)(DMSO)Cl] und [Pd(Fr2)<sub>2</sub>] als repräsentative Beispiele mittels zyklischer Voltammetrie (CV) untersucht wurde. Das Ergebnis: Beide Komplexe zeigen ein quasi-reversibles Oxidationsereignis bei E<sub>1/2</sub> = 0,20 bzw. 0,17 V. Als DNA-Modell wurde 9-MeG ausgewählt, um mit dem [Pt(Fr1)(DMSO)Cl]-Komplex in CH<sub>3</sub>CN-PBS (pH 7,4; 2:1) bei 37 °C 72 Stunden lang zu reagieren. Die Reaktion wurde mittels LC-ESI-MS analysiert, um die gebildeten Pt/9-MeG-Addukte zu identifizieren. Nach 12 Stunden wurden zwei Hauptpeaks gefunden, die den monofunktionellen Addukten [Pt(Fr1)(DMSO)(9-MeG)]<sup>+</sup> und [Pt(Fr1)(CH<sub>3</sub>CN)(9-MeG)]<sup>+</sup> zugeordnet werden konnten. Die ESI-Spektren zeigen deutlich einen zusätzlichen Peak, der [(Pt(Fr1)(CH<sub>3</sub>CN)<sub>2</sub>]<sup>+</sup> zugeordnet ist, was auf die Solvolyse beider Co-Liganden (Cl und DMSO) hinweist, obwohl nach 12 Stunden kein bifunktionelles Addukt beobachtet wurde. Als die Inkubationszeit auf 24 Stunden verlängert wurde, zersetzten sich die Verbindungen in braune Präzipitate. Es wurden keine Addukte nachgewiesen, was die geringere zytotoxische Aktivität solcher Komplexe auf Ferrocenylbasis erklären könnte. Die antiproliferative Aktivität der synthetisierten Liganden und ihrer Pt/Pd-Metallkomplexe gegen die epithelialen Ovarialkarzinom-Zelllinien A2780 und Skov3 sowie deren cisplatinresistente Subkulturen wurde analysiert. Insgesamt zeigten die Pt(II)-Komplexe [Pt(Fr1-Fr3)(DMSO)Cl] eine höhere Aktivität als sowohl die freien Liganden (HFr1-HFr3) als auch die Pd(II)-Komplexe [Pd(Fr1-Fr3)<sub>2</sub>]. Der Alkylsubstituent beeinflusste die Aktivität dieser Komplexe und der freien Liganden stark, wobei die zytotoxische Aktivität mit der Länge der Alkylkette zunahm. Sowohl die Pt(II)- als auch die Pd(II)-Komplexe mit β-Hydroxydithiozimtsäure-Liganden, über die zuvor in der Weigand-Gruppe berichtet wurde, wiesen eine höhere zytotoxische Aktivität auf als die auf Ferrocenyl-basierenden Verbindungen. Dies könnte auf die geringere Stabilität der Pt/9-MeG-Addukte oder auf sterische Effekte zurückzuführen sein, die die Bindung an die Ziel-Biomoleküle verhindern.

### [ME-3]. Doppelfunktion von β-Hydroxydithiozimtsäureestern: RAFT-Mittel und Ligand für die Metallkomplexierung.

Platinmedikamente auf der Basis von Polymeren und Liposomen haben das Potenzial, die Medikamentenabgabe zu verbessern und die scheinbare Zytotoxizität zu verringern. In diesem Projekt haben wir ein neues Design für β-Hydroxydithiozimtsäureester-Liganden vorgestellt, die als CTA (Kettenübertragungsmittel)-Agenten für die RAFT-Polymerisation von Acrylaten, Acrylamiden und Styrol verwendet werden können (Schema II). Folglich konnten wir die Pt(II)-Komplexe aus den wasserlöslichen NAM-β-Hydroxydithiocinnamate-β'-2-

Propionsäure-Polymeren synthetisieren (Schema II). Und schließlich untersuchten wir ihre zytotoxische Aktivität.



Schema II: Strukturen der Liganden (HA1-HA9), der Monomere (R<sub>2</sub>), der resultierenden Polymere (P1-P13) und der Pt(II)-Komplexe mit den NAM-basierten Polymeren.

Zusammenfassend konnten wir zeigen, dass Derivate von  $\beta$ -Hydroxydithiozimatesteren als Kettenüberträger geeignet sind, um die Polymerisation von verschiedenen Monomeren auf Acryl- oder Styrolbasis zu steuern. Detaillierte kinetische Studien zeigten eine lineare Entwicklung der Molmassen mit dem Umsatz. Es ist jedoch zu bedenken, dass die erhöhte Reaktivität der Vinyleneinheit in der Stabilisierungsgruppe (Z-Gruppe) bei längeren Reaktionszeiten immer noch zu Nebenreaktionen führen kann. Dennoch können die resultierenden Polymerketten erfolgreich verlängert werden, wenn kürzere Polymerisationszeiten angewendet werden, was eine hohe Gruppentreue und den lebendigen Charakter der Polymerisation bestätigt. Im Inneren scheinen die N-Acryloylmorpholin-Polymere immer noch in der Lage zu sein, Pt(II) zu binden und die beiden potenziellen Platinkomplexe zu bilden, wie in Schema II (Strukturen A und B) gezeigt. Die antiproliferative Aktivität ausgewählter Proben von NAM- $\beta$ -Hydroxydithiozimatester-Polymeren (P6, P10 und P11) sowie ihrer Pt-Komplexe (PtP6, PtP10 und PtP11) wurde gegen die epithelialen Ovarialkarzinom-Zelllinien A2780 und Skov3 sowie deren Cisplatin-resistente Subkulturen bestimmt. Sie wurden als unwirksam eingestuft. Durch Strukturveränderungen, z. B. durch die Polymerisation anderer Monomere, die an ein bekanntes Krebsmedikament binden können, ließe sich die Zytotoxizität dieser vielversprechenden Verbindungen jedoch möglicherweise verbessern. Darüber hinaus sind diese Verbindungen mit Doppelfunktion attraktive Kandidaten für die direkte Herstellung funktioneller Polymere für verschiedene Anwendungen, z. B. für die Abwasserbehandlung, da sie viele Übergangs- und Schwermetalle chelatisieren können. Durch den Ersatz von Platin durch Gd oder Lu könnten sie außerdem für bildgebende Methoden nützlich sein.



## 8. References

- [1] <https://www.cancer.gov/about-cancer/understanding/what-is-cancer>
- [2] <https://ncbi.nlm.nih.gov/books/NBK279410/>
- [3] <https://www.gesundheitsinformation.de/wie-krebszellen-wachsen-und-sich-ausbreiten.html>
- [4] A. Patel, JAMA Oncol. 2020, 6, 1488-1488.
- [5] J. Fares, M. Y. Fares, H. H. Khachfe, H. A. Salhab, Y. Fares, Signal Transduct. Target. Ther. 2020, 5, 28.
- [6] i. Db, J. mol. biomark. diagn. 2017, 8, 1-8.
- [7] K. L. Eales, K. E. R. Hollinshead, D. A. Tennant, Oncogenesis 2016, 5, e190-e190.
- [8] A. E. El-Kenawi, A. B. El-Remessy, Br. J. Pharmacol. 2013, 170, 712-729.
- [9] P. K. Vogt, West J Med 1993, 158, 273-278.
- [10] M. Papetti, I. M. Herman, Am. J. Physiol. Cell Physiol. 2002, 282, C947-C970.
- [11] G. A. Kwong, S. Ghosh, L. Gamboa, C. Patriotis, S. Srivastava, S. N. Bhatia, Nat. Rev. Cancer 2021, 21, 655-668.
- [12] Y. Zheng, H. Vioix, F. X. Liu, B. Singh, S. Sharma, D. Sharda, Future Oncol. 2021, 18, 505-518.
- [13] H. J. Burstein, J. J. Griggs, Surg. Oncol. Clin. N. Am. 2010, 19, 639-647.
- [14] H. I. Scher, K. Fizazi, F. Saad, M.-E. Taplin, C. N. Sternberg, K. Miller, R. de Wit, P. Mulders, K. N. Chi, N. D. Shore, A. J. Armstrong, T. W. Flaig, A. Fléchon, P. Mainwaring, M. Fleming, J. D. Hainsworth, M. Hirmand, B. Selby, L. Seely, J. S. de Bono, N. Engl. J. Med. 2012, 367, 1187-1197.
- [15] T. M. Beer, A. J. Armstrong, D. E. Rathkopf, Y. Loriot, C. N. Sternberg, C. S. Higano, P. Iversen, S. Bhattacharya, J. Carles, S. Chowdhury, I. D. Davis, J. S. de Bono, C. P. Evans, K. Fizazi, A. M. Joshua, C.-S. Kim, G. Kimura, P. Mainwaring, H. Mansbach, K. Miller, S. B. Noonberg, F. Perabo, D. Phung, F. Saad, H. I. Scher, M.-E. Taplin, P. M. Venner, B. Tombal, N. Engl. J. Med. 2014, 371, 424-433.
- [16] C. E. Kyriakopoulos, Y. H. Chen, M. A. Carducci, G. Liu, D. F. Jarrard, N. M. Hahn, D. H. Shevrin, R. Dreicer, M. Hussain, M. Eisenberger, M. Kohli, E. R. Plimack, N. J. Vogelzang, J. Picus, M. M. Cooney, J. A. Garcia, R. S. DiPaola, C. J. Sweeney, J. Clin. Oncol. 2018, 36, 1080-1087.
- [17] S. Kumar, M. Shelley, C. Harrison, B. Coles, T. J. Wilt, M. D. Mason, Cochrane Database Syst. Rev. 2006, 2006, Cd006019.
- [18] S. Jha, P. K. Sharma, R. Malviya, Achiev. Life Sci. 2016, 10, 161-167.
- [19] S. Y. Lee, G. Fiorentini, A. M. Szasz, G. Szigeti, A. Szasz, C. A. Minnaar, Front. Oncol. 2020, 10, 1690.
- [20] J. H. Correia, J. A. Rodrigues, S. Pimenta, T. Dong, Z. Yang, Pharmaceutics 2021, 13, 1332.
- [21] J. F. Algorri, M. Ochoa, P. Roldán-Varona, L. Rodríguez-Cobo, J. M. López-Higuera, Cancers (Basel) 2021, 13, 4447.

- [22] D. A. Palma, W. F. A. R. Verbakel, K. Otto, S. Senan, *Cancer Treat. Rev.* 2010, 36, 393-399.
- [23] M. Baumann, M. Krause, J. Overgaard, J. Debus, S. M. Bentzen, J. Daartz, C. Richter, D. Zips, T. Bortfeld, *Nat. Rev. Cancer* 2016, 16, 234-249.
- [24] R. Baskar, K. A. Lee, R. Yeo, K. W. Yeoh, *Int. J. Med. Sci.* 2012, 9, 193-199.
- [25] I. Abraha, C. Aristei, I. Palumbo, M. Lupattelli, S. Trastulli, R. Ciocchi, R. De Florio, V. Valentini, *Cochrane Database Syst. Rev.* 2018, 10, Cd002102.
- [26] A. D. Waldman, J. M. Fritz, M. J. Lenardo, *Nat. Rev. Immunol.* 2020, 20, 651-668.
- [27] K. Esfahani, L. Roudaia, N. Buhlaiga, S. V. Del Rincon, N. Papneja, W. H. Miller, Jr., *Curr. Oncol.* 2020, 27, S87-S97.
- [28] S. Akkin, G. Varan, E. Bilensoy, *Molecules* 2021, 26, 3382.
- [29] L. Zhong, Y. Li, L. Xiong, W. Wang, M. Wu, T. Yuan, W. Yang, C. Tian, Z. Miao, T. Wang, S. Yang, *Signal Transduct. Target. Ther.* 2021, 6, 201.
- [30] T. A. Baudino, *Curr. Drug. Discov. Technol.* 2015, 12, 3-20.
- [31] V. V. Padma, *Biomedicine (Taipei)* 2015, 5, 19.
- [32] X. Bai, *Cells* 2020, 9, 2193.
- [33] D.-T. Chu, T. T. Nguyen, N. L. B. Tien, D.-K. Tran, J.-H. Jeong, P. G. Anh, V. V. Thanh, D. T. Truong, T. C. Dinh, *Cells* 2020, 9, 563.
- [34] D. J. Benjamin, *Med. Hypotheses* 2014, 82, 412-420.
- [35] L. Wyld, R. A. Audisio, G. J. Poston, *Nat. Rev. Clin. Oncol.* 2015, 12, 115-124.
- [36] B. A. Chabner, T. G. Roberts, *Nat. Rev. Cancer* 2005, 5, 65-72.
- [37] B. L. Hoffman, J. O. Schorge, L. M. Halvorson, C. A. Hamid, M. M. Corton, J. I. Schaffer, in *Williams Gynecology, 4e*, McGraw-Hill Education, New York, NY, 2020.
- [38] D. J. Kerr, D. G. Haller, C. J. H. van de Velde, M. Baumann, *Oxford Textbook of Oncology*, Oxford University Press, 2016.
- [39] E. Å. Lundqvist, K. Fujiwara, M. Seoud, *Int. J. Gynaecol. Obstet.* 2015, 131, S146-S149.
- [40] M. M. Skubisz, S. Tong, *ISRN Obstet. Gynecol.* 2012, 2012, 637094.
- [41] S. S. Abolmaali, A. M. Tamaddon, R. Dinarvand, *Cancer Chemother. Pharmacol.* 2013, 71, 1115-1130.
- [42] P. Koźmiński, P. K. Halik, R. Chesori, E. Gniazdowska, *Int. J. Mol. Sci.* 2020, 21, 3483.
- [43] A. Paci, G. Veal, C. Bardin, D. Levêque, N. Widmer, J. Beijnen, A. Astier, E. Chatelut, *Eur. J. Cancer.* 2014, 50, 2010-2019.
- [44] L. de Sousa Cavalcante, G. Monteiro, *Eur. J. Pharmacol.* 2014, 741, 8-16.
- [45] H. Umezawa, K. Maeda, T. Takeuchi, Y. Okami, *J. Antibiot. (Tokyo)* 1966, 19, 200-209.
- [46] L. Du, C. Sánchez, M. Chen, D. J. Edwards, B. Shen, *Chem. Biol.* 2000, 7, 623-642.
- [47] L. H. Einhorn, *Proc. Natl. Acad. Sci. U.S.A.* 2002, 99, 4592-4595.

- [48] R. W. Carlson, B. I. Sikic, M. M. Turbow, S. C. Ballon, *J. Clin. Oncol.* 1983, 1, 645-651.
- [49] J. Chen, J. Stubbe, *Nat. Rev. Cancer* 2005, 5, 102-112.
- [50] V. Murray, J. K. Chen, L. H. Chung, *Int. J. Mol. Sci.* 2018, 19.
- [51] V. Murray, J. K. Chen, L. H. Chung, *Int. J. Mol. Sci.* 2018, 19.
- [52] A. J. Trevor, B. G. Katzung, M. Kruidering-Hall, in *Katzung & Trevor's Pharmacology: Examination & Board Review*, 11e, McGraw-Hill Education, New York, NY, 2015.
- [53] A. Fujiwara, T. Hoshino, J. W. Westley, *Crit. Rev. Biotechnol.* 1985, 3, 133-157.
- [54] R. B. Weiss, *Semin. Oncol.* 1992, 19, 670-686.
- [55] G. Minotti, P. Menna, E. Salvatorelli, G. Cairo, L. Gianni, *Pharmacol. Rev.* 2004, 56, 185.
- [56] M. Binaschi, M. Bigioni, A. Cipollone, C. Rossi, C. Goso, A. C. Maggi, G. Capranico, F. Animati, *Curr. Med. Chem. Anticancer Agents* 2001, 1, 113-130.
- [57] R. Bharadwaj, H. Yu, *Oncogene* 2004, 23, 2016-2027.
- [58] D. A. Brito, Z. Yang, C. L. Rieder, *J. Cell Biol.* 2008, 182, 623-629.
- [59] Y. Pommier, E. Leo, H. Zhang, C. Marchand, *Chem. Biol.* 2010, 17, 421-433.
- [60] C. Canel, R. M. Moraes, F. E. Dayan, D. Ferreira, *Phytochemistry* 2000, 54, 115-120.
- [61] R. K. Singh, S. Kumar, D. N. Prasad, T. R. Bhardwaj, *Eur. J. Med. Chem* 2018, 151, 401-433.
- [62] S. M. Rink, M. S. Solomon, M. J. Taylor, S. B. Rajur, L. W. McLaughlin, P. B. Hopkins, *J. Am. Chem. Soc.* 1993, 115, 2551-2557.
- [63] M. P. Frenay, D. Fontaine, F. Vandebos, C. Lebrun, *Eur. J. Neurol.* 2005, 12, 685-690.
- [64] S. Guohui, Z. Lijiao, Z. Rugang, *Anticancer Agents Med. Chem.* 2015, 16, 221-246.
- [65] W. J. Bodell, *J. Neuro-Oncol.* 2008, 91, 257.
- [66] O. M. Colvin, in *Encyclopedia of Cancer (Second Edition)* (Ed.: J. R. Bertino), Academic Press, New York, 2002, pp. 35-42.
- [67] M. J. v. Maanen, C. J. M. Smeets, J. H. Beijnen, *Cancer Treat. Rev.* 2000, 26, 257-268.
- [68] R. Bizanek, B. F. McGuinness, K. Nakanishi, M. Tomasz, *Biochemistry* 1992, 31, 3084-3091.
- [69] B. Lippert, *Cisplatin: chemistry and biochemistry of a leading anticancer drug*, Verlag Helvetica Chimica Acta, Zürich, 1999.
- [70] B. Rosenberg, L. Van Camp, T. Krigas, *Nature* 1965, 205, 698-699.
- [71] N. J. Wheate, S. Walker, G. E. Craig, R. Oun, *Dalton Trans.* 2010, 39, 8113-8127.
- [72] M. Watson, A. Barrett, R. Spence, C. Twelves, *Oncology*, Oxford University Press, Oxford, 2nd edn, 2006.

- [73] Martindale: The complete drug reference, ed. S. C. Sweetman, Pharmaceutical Press, London, 35th edn, 2007.
- [74] U. Frey, J. D. Ranford, P. J. Sadler, *Inorg. Chem.* 1993, 32, 1333-1340.
- [75] G. Chu, R. Mantin, Y.-M. Shen, G. Baskett, H. Sussman, *Cancer* 1993, 72, 3707-3714.
- [76] O. Rixe, W. Ortuzar, M. Alvarez, R. Parker, E. Reed, K. Paull, T. Fojo, *Biochem. Pharmacol.* 1996, 52, 1855-1865.
- [77] A. Kuwahara, M. Yamamori, K. Nishiguchi, T. Okuno, N. Chayahara, I. Miki, T. Tamura, T. Inokuma, Y. Takemoto, T. Nakamura, K. Kataoka, T. Sakaeda, *Int. J. Med. Sci.* 2009, 6, 305-311.
- [78] S. Zhang, K. S. Lovejoy, J. E. Shima, L. L. Lagpacan, Y. Shu, A. Lapuk, Y. Chen, T. Komori, J. W. Gray, X. Chen, S. J. Lippard, K. M. Giacomini, *Cancer Res.* 2006, 66, 8847-8857.
- [79] A. K. Holzer, G. H. Manorek, S. B. Howell, *Mol. Pharmacol.* 2006, 70, 1390-1394.
- [80] *Drugs in R & D* 2003, 4, 369-372.
- [81] D.-K. Kim, G. Kim, J. Gam, Y.-B. Cho, H.-T. Kim, J.-H. Tai, K. H. Kim, W.-S. Hong, J.-G. Park, *J. Med. Chem.* 1994, 37, 1471-1485.
- [82] K. Tanaka, T. Kunimatsu, J. Shimakura, M. Hanada, *Sumitomo Kagaku* 2011, 1-12.
- [83] Y. Chen, Z. Guo, S. Parsons, P. J. Sadler, *Chem. - Eur. J.* 1998, 4, 672-676.
- [84] J. Holford, S. Y. Sharp, B. A. Murrer, M. Abrams, L. R. Kelland, *Br. J. Cancer* 1998, 77, 366-373.
- [85] S. Y. Sharp, C. F. O'Neill, P. Rogers, F. E. Boxall, L. R. Kelland, *Eur. J. Cancer.* 2002, 38, 2309-2315.
- [86] P. Sood, K. B. Thurmond, J. E. Jacob, L. K. Waller, G. O. Silva, D. R. Stewart, D. P. Nowotnik, *Bioconjug. Chem* 2006, 17, 1270-1279.
- [87] D. P. Nowotnik, E. Cvitkovic, *Adv. Drug Deliv. Rev.* 2009, 61, 1214-1219.
- [88] T. Boulikas, *Expert Opin. Investig. Drugs* 2009, 18, 1197-1218.
- [89] G. P. Stathopoulos, T. Boulikas, *J. Drug Deliv.* 2012, 2012, 581363.
- [90] A. Bhargava, U. N. Vaishampayan, *Expert Opin. Investig. Drugs* 2009, 18, 1787-1797.
- [91] H. Choy, C. Park, M. Yao, *Clin. Cancer Res.* 2008, 14, 1633-1638.
- [92] T. C. Johnstone, K. Suntharalingam, S. J. Lippard, *Chem. Rev.* 2016, 116, 3436-3486.
- [93] T. C. Johnstone, J. J. Wilson, S. J. Lippard, *Inorg. Chem.* 2013, 52, 12234-12249.
- [94] S. Dilruba, G. V. Kalayda, *Cancer Chemother. Pharmacol.* 2016, 77, 1103-1124.
- [95] D. P. Gately, S. B. Howell, *Br. J. Cancer* 1993, 67, 1171-1176.
- [96] R. Safaei, *Cancer Lett.* 2006, 234, 34-39.
- [97] V. Brabec, O. Hrabina, J. Kasparkova, *Coord. Chem. Rev.* 2017, 351, 2-31.
- [98] A. M. J. Fichtinger-Schepman, J. L. Van der Veer, J. H. J. Den Hartog, P. H. M. Lohman, J. Reedijk, *Biochemistry* 1985, 24, 707-713.

- [99] R. C. Todd, S. J. Lippard, *Metallomics* 2009, 1, 280-291.
- [100] M. Selvakumaran, D. A. Pisarcik, R. Bao, A. T. Yeung, T. C. Hamilton, *Cancer Res.* 2003, 63, 1311-1316.
- [101] M. Duan, J. Ulibarri, K. J. Liu, P. Mao, *Int. J. Mol. Sci.* 2020, 21.
- [102] T. Furuta, T. Ueda, G. Aune, A. Sarasin, K. H. Kraemer, Y. Pommier, *Cancer Res.* 2002, 62, 4899-4902.
- [103] J. Zlatanova, J. Yaneva, S. H. Leuba, *FASEB J.* 1998, 12, 791-799.
- [104] S. U. Dunham, S. J. Lippard, *Biochemistry* 1997, 36, 11428-11436.
- [105] C. S. Chow, C. M. Barnes, S. J. Lippard, *Biochemistry* 1995, 34, 2956-2964.
- [106] S. J. Brown, P. J. Kellett, S. J. Lippard, *Science* 1993, 261, 603-605.
- [107] D. B. Zamble, D. Mu, J. T. Reardon, A. Sancar, S. J. Lippard, *Biochemistry* 1996, 35, 10004-10013.
- [108] J. C. Huang, D. B. Zamble, J. T. Reardon, S. J. Lippard, A. Sancar, *Proc. Natl. Acad. Sci. U.S.A.* 1994, 91, 10394-10398.
- [109] Q. He, C. H. Liang, S. J. Lippard, *Proc. Natl. Acad. Sci. U.S.A.* 2000, 97, 5768-5772.
- [110] L. Kelland, *Nat. Rev. Cancer* 2007, 7, 573-584.
- [111] A. K. Holzer, G. H. Manorek, S. B. Howell, *Mol. Pharmacol.* 2006, 70, 1390-1394.
- [112] J. Zisowsky, S. Koegel, S. Leyers, K. Devarakonda, M. U. Kassack, M. Osmak, U. Jaehde, *Biochem. Pharmacol.* 2007, 73, 298-307.
- [113] R. Safaei, A. K. Holzer, K. Katano, G. Samimi, S. B. Howell, *J. Inorg. Biochem.* 2004, 98, 1607-1613.
- [114] R. Safaei, *Cancer Lett.* 2006, 234, 34-39.
- [115] K. Nakayama, A. Kanzaki, K. Terada, M. Mutoh, K. Ogawa, T. Sugiyama, S. Takenoshita, K. Itoh, N. Yaegashi, K. Miyazaki, N. Neamati, Y. Takebayashi, *Clin. Cancer Res.* 2004, 10, 2804-2811.
- [116] T. Yang, M. Chen, T. Chen, A. Thakur, *Oncol. Lett.* 2015, 10, 2584-2590.
- [117] P. Borst, R. Evers, M. Kool, J. Wijnholds, *J. Natl. Cancer Inst.* 2000, 92, 1295-1302.
- [118] T. Ishikawa, *Trends Biochem. Sci.* 1992, 17, 463-468.
- [119] L. Galluzzi, L. Senovilla, I. Vitale, J. Michels, I. Martins, O. Kepp, M. Castedo, G. Kroemer, *Oncogene* 2012, 31, 1869-1883.
- [120] A. D. Lewis, J. D. Hayes, C. R. Wolf, *Carcinogenesis* 1988, 9, 1283-1287.
- [121] K. V. Ferry, T. C. Hamilton, S. W. Johnson, *Biochem. Pharmacol.* 2000, 60, 1305-1313.
- [122] A. Vaisman, M. Varchenko, A. Umar, T. A. Kunkel, J. I. Risinger, J. C. Barrett, T. C. Hamilton, S. G. Chaney, *Cancer Res.* 1998, 58, 3579-3585.
- [123] G. Gifford, J. Paul, P. A. Vasey, S. B. Kaye, R. Brown, o. b. o. t. S. G. C. T. Group, *Clin. Cancer Res.* 2004, 10, 4420-4426.

- [124] E. Bassett, A. Vaisman, K. A. Tropea, C. M. McCall, C. Masutani, F. Hanaoka, S. G. Chaney, *DNA Repair* 2002, 1, 1003-1016.
- [125] A. K. Srivastava, C. Han, R. Zhao, T. Cui, Y. Dai, C. Mao, W. Zhao, X. Zhang, J. Yu, Q.-E. Wang, *Proc. Natl. Acad. Sci. U.S.A.* 2015, 112, 4411-4416.
- [126] M. R. Albertella, C. M. Green, A. R. Lehmann, M. J. O'Connor, *Cancer Res.* 2005, 65, 9799-9806.
- [127] A. Gadducci, S. Cosio, S. Muraca, A. R. Genazzani, *Eur. J. Gynaecol. Oncol.* 2002, 23, 390-396.
- [128] Z. Yuan, K. Cao, C. Lin, L. Li, H. Y. Liu, X. Y. Zhao, L. Liu, H. X. Deng, J. Li, C. L. Nie, Y. Q. Wei, *Mol. Med.* 2011, 17, 1262-1274.
- [129] P. Saha, C. Descôteaux, K. Brasseur, S. Fortin, V. Leblanc, S. Parent, É. Asselin, G. Bérubé, *Eur. J. Med. Chem.* 2012, 48, 385-390.
- [130] C. Van Themsche, S. Parent, V. Leblanc, C. Descôteaux, A.-M. Simard, G. Bérubé, E. Asselin, *Endocr.-Relat. Cancer* 2009, 16, 1185-1195.
- [131] H. Li, X. Gao, R. Liu, Y. Wang, M. Zhang, Z. Fu, Y. Mi, Y. Wang, Z. Yao, Q. Gao, *Eur. J. Med. Chem.* 2015, 101, 400-408.
- [132] R. J. Shaw, *Curr. Opin. Cell Biol.* 2006, 18, 598-608.
- [133] B. E. Bowler, S. J. Lippard, *Biochemistry* 1986, 25, 3031-3038.
- [134] S. Jin, Y. Guo, Z. Guo, X. Wang, *Pharmaceuticals* 2021, 14.
- [135] J. P. Macquet, J. L. Butour, *J. Natl. Cancer Inst.* 1983, 70, 899-905.
- [136] M. J. Cleare, J. D. Hoeschele, *Bioinorg. Chem.* 1973, 2, 187-210.
- [137] S. Jin, Y. Guo, Z. Guo, X. Wang, *Pharmaceuticals* 2021, 14.
- [138] M. J. Cleare, J. D. Hoeschele, *Bioinorg. Chem.* 1973, 2, 187-210.
- [139] G. Y. Park, J. J. Wilson, Y. Song, S. J. Lippard, *Proc. Natl. Acad. Sci. U.S.A.* 2012, 109, 11987-11992.
- [140] T. C. Johnstone, K. Suntharalingam, S. J. Lippard, *Philos. Trans. Royal Soc.* 2015, 373, 20140185.
- [141] K. S. Lovejoy, R. C. Todd, S. Zhang, M. S. McCormick, J. A. D'Aquino, J. T. Reardon, A. Sancar, K. M. Giacomini, S. J. Lippard, *Proc. Natl. Acad. Sci. U.S.A.* 2008, 105, 8902-8907.
- [142] T. C. Johnstone, G. Y. Park, S. J. Lippard, *Anticancer Res.* 2014, 34, 471.
- [143] D. Wang, G. Zhu, X. Huang, S. J. Lippard, *Proc. Natl. Acad. Sci. U.S.A.* 2010, 107, 9584-9589.
- [144] G. Zhu, M. Myint, W. H. Ang, L. Song, S. J. Lippard, *Cancer Res.* 2012, 72, 790-800.
- [145] K. S. Lovejoy, M. Serova, I. Bieche, S. Emami, M. D'Incalci, M. Broggin, E. Erba, C. Gespach, E. Cvitkovic, S. Faivre, E. Raymond, S. J. Lippard, *Mol. Cancer Ther.* 2011, 10, 1709-1719.
- [146] Y. Zhao, C. Biertümpfel, M. T. Gregory, Y.-J. Hua, F. Hanaoka, W. Yang, *Proc. Natl. Acad. Sci. U.S.A.* 2012, 109, 7269-7274.
- [147] Z. H. Siddik, *Oncogene* 2003, 22, 7265-7279.

- [148] M. Galanski, A. M. Jakupec, K. B. Keppler, *Curr. Med. Chem.* 2005, 12, 2075-2094.
- [149] V. Cepeda, M. A. Fuertes, J. Castilla, C. Alonso, C. Quevedo, J. M. Perez, *Anti-Cancer Agents Med. Chem.* 2007, 7, 3-18.
- [150] D. Gibson, *Dalton Trans.* 2016, 45, 12983-12991.
- [151] J. J. Wilson, S. J. Lippard, *Chem. Rev.* 2014, 114, 4470-4495.
- [152] D. Gibson, *Journal of Inorganic Biochemistry* 2021, 217, 111353.
- [153] X. Li, Y. Liu, H. Tian, *Bioinorg. Chem. Appl.* 2018, 2018, 8276139.
- [154] R. G. Kenny, S. W. Chuah, A. Crawford, C. J. Marmion, *Eur. J. Inorg. Chem.* 2017, 2017, 1596-1612.
- [155] E. Wexselblatt, D. Gibson, *J. Inorg. Biochem.* 2012, 117, 220-229.
- [156] J. Z. Zhang, E. Wexselblatt, T. W. Hambley, D. Gibson, *Chem. Commun.* 2012, 48, 847-849.
- [157] Z. Xu, Z. Wang, Z. Deng, G. Zhu, *Coord. Chem. Rev.* 2021, 442, 213991.
- [158] G. R. Gibbons, S. Wyrick, S. G. Chaney, *Cancer Res.* 1989, 49, 1402-1407.
- [159] T. J. O'Rourke, G. R. Weiss, P. New, H. A. Burris, 3rd, G. Rodriguez, J. Eckhardt, J. Hardy, J. G. Kuhn, S. Fields, G. M. Clark, et al., *Anti-Cancer Drugs* 1994, 5, 520-526.
- [160] P. Bouchal, J. Jarkovsky, K. Hrazdilova, M. Dvorakova, I. Struharova, L. Hernychova, J. Damborsky, P. Sova, B. Vojtesek, *Proteome Sci.* 2011, 9, 68.
- [161] A. Kozubík, V. Horváth, L. Švihálková-Šindlerová, K. Souček, J. Hofmanová, P. Sova, A. Kroutil, F. Žák, A. Mistr, J. Turánek, *Biochem. Pharmacol.* 2005, 69, 373-383.
- [162] G. Milazzo, D. Mercatelli, G. Di Muzio, L. Triboli, P. De Rosa, G. Perini, F. M. Giorgi, *Genes* 2020, 11.
- [163] A. C. Chueh, J. W. T. Tse, L. Tögel, J. M. Mariadason, *Antioxid. Redox Signal.* 2014, 23, 66-84.
- [164] P. W. Atadja, in *Epigenetics and Disease: Pharmaceutical Opportunities* (Eds.: S. M. Gasser, E. Li), Springer Basel, Basel, 2011, pp. 175-195.
- [165] J. Yang, X. Sun, W. Mao, M. Sui, J. Tang, Y. Shen, *Mol. Pharm.* 2012, 9, 2793-2800.
- [166] M. Alessio, I. Zanellato, I. Bonarrigo, E. Gabano, M. Ravera, D. Osella, *J. Inorg. Biochem.* 2013, 129, 52-57.
- [167] R. Raveendran, J. P. Braude, E. Wexselblatt, V. Novohradsky, O. Stuchlikova, V. Brabec, V. Gandin, D. Gibson, *Chem. Sci.* 2016, 7, 2381-2391.
- [168] A. R. Z. Almotairy, V. Gandin, L. Morrison, C. Marzano, D. Montagner, A. Erxleben, *J. Inorg. Biochem.* 2017, 177, 1-7.
- [169] W. H. Ang, I. Khalaila, C. S. Allardyce, L. Juillerat-Jeanneret, P. J. Dyson, *J. Am. Chem. Soc.* 2005, 127, 1382-1383.
- [170] K. G. Z. Lee, M. V. Babak, A. Weiss, P. J. Dyson, P. Nowak-Sliwinska, D. Montagner, W. H. Ang, *ChemMedChem* 2018, 13, 1210-1217.
- [171] T. Soussi, *Ann. N. Y. Acad. Sci.* 2000, 910, 121-139.

- [172] S. Shangary, S. Wang, *Annu. Rev. Pharmacol. Toxicol.* 2009, 49, 223-241.
- [173] S. K. Kumar, E. Hager, C. Pettit, H. Gurulingappa, N. E. Davidson, S. R. Khan, J. *Med. Chem.* 2003, 46, 2813-2815.
- [174] L. Ma, R. Ma, Y. Wang, X. Zhu, J. Zhang, H. C. Chan, X. Chen, W. Zhang, S.-K. Chiu, G. Zhu, *Chem. Commun.* 2015, 51, 6301-6304.
- [175] T. Hussain, S. Gupta, H. Mukhtar, *Cancer Lett.* 2003, 191, 125-135.
- [176] A. M. De Marzo, E. A. Platz, S. Sutcliffe, J. Xu, H. Grönberg, C. G. Drake, Y. Nakai, W. B. Isaacs, W. G. Nelson, *Nat. Rev. Cancer* 2007, 7, 256-269.
- [177] S. Bacchi, P. Palumbo, A. Sponta, M. F. Coppolino, *Anti-Inflamm. Anti-Allergy Agents Med. Chem.* 2012, 11, 52-64.
- [178] D. Spector, O. Krasnovskaya, K. Pavlov, A. Erofeev, P. Gorelkin, E. Beloglazkina, A. Majouga, *Int. J. Mol. Sci.* 2021, 22.
- [179] R. K. Pathak, S. Marrache, J. H. Choi, T. B. Berding, S. Dhar, *Angew. Chem. Int. Ed.* 2014, 53, 1963-1967.
- [180] Q. Cheng, H. Shi, H. Wang, Y. Min, J. Wang, Y. Liu, *Chem. Commun.* 2014, 50, 7427-7430.
- [181] W. Neumann, B. C. Crews, L. J. Marnett, E. Hey-Hawkins, *ChemMedChem.* 2014, 9, 1150-1153.
- [182] W. Neumann, B. C. Crews, M. B. Sárosi, C. M. Daniel, K. Ghebreselasie, M. S. Scholz, L. J. Marnett, E. Hey-Hawkins, *ChemMedChem.* 2015, 10, 183-192.
- [183] D. A. Tolan, Y. K. Abdel-Monem, M. A. El-Nagar, *Appl. Organomet. Chem.* 2019, 33, e4763.
- [184] Y. Chen, Q. Wang, Z. Li, Z. Liu, Y. Zhao, J. Zhang, M. Liu, Z. Wang, D. Li, J. Han, *Dalton Trans.* 2020, 49, 5192-5204.
- [185] S. Jin, N. Muhammad, Y. Sun, Y. Tan, H. Yuan, D. Song, Z. Guo, X. Wang, *Angew. Chem. Int. Ed.* 2020, 59, 23313-23321.
- [186] D. V. Spector, K. G. Pavlov, R. A. Akasov, A. N. Vaneev, A. S. Erofeev, P. V. Gorelkin, V. N. Nikitina, E. V. Lopatukhina, A. S. Semkina, K. Y. Vlasova, D. A. Skvortsov, V. A. Roznyatovsky, N. V. Ul'yanovskiy, I. I. Pikovskoi, S. A. Sypalov, A. S. Garanina, S. S. Vodopyanov, M. A. Abakumov, Y. L. Volodina, A. A. Markova, A. S. Petrova, D. M. Mazur, D. A. Sakharov, N. V. Zyk, E. K. Beloglazkina, A. G. Majouga, O. O. Krasnovskaya, *J. Med. Chem.* 2022, 65, 8227-8244.
- [187] A. Houry, J. A. Sakoff, J. Gilbert, K. F. Scott, S. Karan, C. P. Gordon, J. R. Aldrich-Wright, *Pharmaceutics* 2022, 14, 787.
- [188] A. Janssen, T. J. Maier, S. Schiffmann, O. Coste, M. Seegel, G. Geisslinger, S. Grösch, *Eur. J. Pharmacol.* 2006, 540, 24-33.
- [189] M. G. Vander Heiden, L. C. Cantley, C. B. Thompson, *Science* 2009, 324, 1029-1033.
- [190] G. B. Stefano, R. M. Kream, *Med. Sci. Monit.* 2015, 21, 3736-3739.
- [191] S. Dhar, S. J. Lippard, *Proc. Natl. Acad. Sci. U.S.A.* 2009, 106, 22199-22204.
- [192] X. Xue, S. You, Q. Zhang, Y. Wu, G.-z. Zou, P. C. Wang, Y.-I. Zhao, Y. Xu, L. Jia, X. Zhang, X.-J. Liang, *Mol. Pharm.* 2012, 9, 634-644.



- [193] J. Ma, H. Liu, Z. Xi, J. Hou, Y. Li, J. Niu, T. Liu, S. Bi, X. Wang, C. Wang, J. Wang, S. Xie, P. G. Wang, *Front. Chem.* 2018, 6, 386.
- [194] Q. Wang, Z. Huang, J. Ma, X. Lu, L. Zhang, X. Wang, P. George Wang, *Dalton Trans.* 2016, 45, 10366-10374.
- [195] J. Ma, X. Yang, W. Hao, Z. Huang, X. Wang, P. G. Wang, *Eur. J. Med. Chem.* 2017, 128, 45-55.
- [196] J. Ma, Q. Wang, Z. Huang, X. Yang, Q. Nie, W. Hao, P. G. Wang, X. Wang, *J. Med. Chem.* 2017, 60, 5736-5748.
- [197] W. X. Ren, J. Han, S. Uhm, Y. J. Jang, C. Kang, J.-H. Kim, J. S. Kim, *Chem. Commun.* 2015, 51, 10403-10418.
- [198] J. Zhao, W. Hua, G. Xu, S. Gou, *J. Inorg. Biochem.* 2017, 176, 175-180.
- [199] N. Muhammad, N. Sadia, C. Zhu, C. Luo, Z. Guo, X. Wang, *Chem. Commun.* 2017, 53, 9971-9974.
- [200] W. Hu, L. Fang, W. Hua, S. Gou, *J. Inorg. Biochem.* 2017, 175, 47-57.
- [201] K. R. Barnes, A. Kutikov, S. J. Lippard, *Chem. Biol.* 2004, 11, 557-564.
- [202] W. Hu, J. Zhao, W. Hua, S. Gou, *Metallomics* 2018, 10, 346-359.
- [203] X. Qin, L. Fang, J. Zhao, S. Gou, *Inorg. Chem.* 2018, 57, 5019-5029.
- [204] Z.-Y. Ma, D.-B. Wang, X.-Q. Song, Y.-G. Wu, Q. Chen, C.-L. Zhao, J.-Y. Li, S.-H. Cheng, J.-Y. Xu, *Eur. J. Med. Chem.* 2018, 157, 1292-1299.
- [205] X. Qin, L. Fang, F. Chen, S. Gou, *Eur. J. Med. Chem.* 2017, 137, 167-175.
- [206] F. Chen, G. Xu, X. Qin, X. Jin, S. Gou, *J. Pharmacol. Exp. Ther.* 2017, 363, 221-239.
- [207] T. Yempala, T. Babu, S. Karmakar, A. Nemirovski, M. Ishan, V. Gandin, D. Gibson, *Angew. Chem. Int. Ed.* 2019, 58, 18218-18223.
- [208] E. Petruzzella, R. Sirota, I. Solazzo, V. Gandin, D. Gibson, *Chem. Sci.* 2018, 9, 4299-4307.
- [209] E. Petruzzella, J. P. Braude, J. R. Aldrich-Wright, V. Gandin, D. Gibson, *Angew. Chem. Int. Ed.* 2017, 56, 11539-11544.
- [210] Z. Dai, Z. Wang, *Molecules* 2020, 25.
- [211] H. Shi, C. Imberti, P. J. Sadler, *Inorg. Chem. Front.* 2019, 6, 1623-1638.
- [212] J. Gurruchaga-Pereda, Á. Martínez, A. Terenzi, L. Salassa, *Inorg. Chim. Acta.* 2019, 495, 118981.
- [213] N. A. Kratochwil, M. Zabel, K.-J. Range, P. J. Bednarski, *J. Med. Chem.* 1996, 39, 2499-2507.
- [214] A. Vogler, A. Kern, J. Hüttermann, *Angew. Chem. Int. Ed.* 1978, 17, 524-525.
- [215] A. F. Westendorf, A. Bodtke, P. J. Bednarski, *Dalton Trans.* 2011, 40, 5342-5351.
- [216] F. S. Mackay, J. A. Woods, H. Moseley, J. Ferguson, A. Dawson, S. Parsons, P. J. Sadler, *Chem. Eur. J.* 2006, 12, 3155-3161.

- [217] A. F. Westendorf, J. A. Woods, K. Korpis, N. J. Farrer, L. Salassa, K. Robinson, V. Appleyard, K. Murray, R. Grünert, A. M. Thompson, P. J. Sadler, P. J. Bednarski, *Mol. Cancer Ther.* 2012, 11, 1894-1904.
- [218] N. J. Farrer, J. A. Woods, L. Salassa, Y. Zhao, K. S. Robinson, G. Clarkson, F. S. Mackay, P. J. Sadler, *Angew. Chem. Int. Ed.* 2010, 49, 8905-8908.
- [219] H. Shi, C. Imberti, H. Huang, I. Hands-Portman, P. J. Sadler, *Chem. Commun.* 2020, 56, 2320-2323.
- [220] Z. Wang, N. Wang, S.-C. Cheng, K. Xu, Z. Deng, S. Chen, Z. Xu, K. Xie, M.-K. Tse, P. Shi, H. Hirao, C.-C. Ko, G. Zhu, *Chem* 2019, 5, 3151-3165.
- [221] H. Yao, S. Chen, Z. Deng, M.-K. Tse, Y. Matsuda, G. Zhu, *Inorg. Chem.* 2020, 59, 11823-11833.
- [222] J. Karges, T. Yempala, M. Tharaud, D. Gibson, G. Gasser, *Angew. Chem. Int. Ed.* 2020, 59, 7069-7075.
- [223] M. Ethirajan, Y. Chen, P. Joshi, R. K. Pandey, *Chem. Soc. Rev.* 2011, 40, 340-362.
- [224] J. Karges, F. Heinemann, M. Jakubaszek, F. Maschietto, C. Subecz, M. Dotou, R. Vinck, O. Blacque, M. Tharaud, B. Goud, E. Viñuelas Zahínos, B. Spingler, I. Ciofini, G. Gasser, *J. Am. Chem. Soc.* 2020, 142, 6578-6587.
- [225] S. B. França, P. R. d. S. Correia, I. B. D. d. Castro, E. F. d. Silva Júnior, M. E. d. S. B. Barros, D. J. d. P. Lima, *Res., Soc. Dev.* 2021, 10, e28010111691.
- [226] N. Ruwizhi, B. A. Aderibigbe, *Int. J. Mol. Sci.* 2020, 21.
- [227] P. De, M. Baltas, F. Bedos-Belval, *Curr. Med. Chem.* 2011, 18, 1672-1703.
- [228] F. F. Gan, K. K. Kaminska, H. Yang, C. Y. Liew, P. C. Leow, C. L. So, L. N. Tu, A. Roy, C. W. Yap, T. S. Kang, W. K. Chui, E. H. Chew, *Antioxid. Redox Signal.* 2013, 19, 1149-1165.
- [229] R. Wang, W. Yang, Y. Fan, W. Dehaen, Y. Li, H. Li, W. Wang, Q. Zheng, Q. Huai, *Bioorg. Chem.* 2019, 88, 102951.
- [230] Y.-X. Ge, Y.-H. Wang, J. Zhang, Z.-P. Yu, X. Mu, J.-L. Song, Y.-Y. Wang, F. Yang, N. Meng, C.-S. Jiang, H. Zhang, *Steroids* 2019, 152, 108499.
- [231] S. Sadeghi, A. Davoodvandi, M. H. Pourhanifeh, N. Sharifi, R. ArefNezhad, R. Sahebnaasagh, S. A. Moghadam, A. Sahebkar, H. Mirzaei, *Eur. J. Med. Chem.* 2019, 178, 131-140.
- [232] M. Imai, H. Yokoe, M. Tsubuki, N. Takahashi, *Biol. Pharm. Bull.* 2019, 42, 1134-1139.
- [233] Y. Luo, Y. Zhou, Y. Song, G. Chen, Y.-X. Wang, Y. Tian, W.-W. Fan, Y.-S. Yang, T. Cheng, H.-L. Zhu, *Bioorg. Med. Chem. Lett.* 2018, 28, 3634-3638.
- [234] D. Rathee, V. Lather, A. S. Grewal, H. Dureja, *Chem. Cent. J.* 2018, 12, 41.
- [235] P. Mabeta, K. Pavić, B. Zorc, *Acta Pharm.* 2018, 68, 337-348.
- [236] I. Perković, S. Raić-Malić, D. Fontinha, M. Prudêncio, L. Pessanha de Carvalho, J. Held, T. Tandarić, R. Vianello, B. Zorc, Z. Rajić, *Eur. J. Med. Chem.* 2020, 187, 111927.
- [237] Y. Ling, W.-J. Gao, C. Ling, J. Liu, C. Meng, J. Qian, S. Liu, H. Gan, H. Wu, J. Tao, H. Dai, Y. Zhang, *Eur. J. Med. Chem.* 2019, 168, 515-526.

- [238] E. Pontiki, D. Hadjipavlou-Litina, K. Litinas, G. Geromichalos, *Molecules* 2014, 19, 9655-9674.
- [239] A. Meeprom, C. B. Chan, W. Sompong, S. Adisakwattana, *Biomed. Pharmacother.* 2018, 101, 777-785.
- [240] N. Muhammad, M. Saeed, A. Adhikari, K. M. Khan, H. Khan, *J. Enzyme Inhib. Med. Chem.* 2013, 28, 997-1001.
- [241] V. D. Kortenska, M. P. Velikova, N. V. Yanishlieva, I. R. Totzeva, V. S. Bankova, M. C. Marcucci, *Eur. J. Lipid Sci. Technol.* 2002, 104, 19-28.
- [242] A. Garcia-Jimenez, F. García-Molina, J. A. Teruel-Puche, A. Saura-Sanmartin, P. A. Garcia-Ruiz, A. Ortiz-Lopez, J. N. Rodríguez-López, F. Garcia-Canovas, J. Munoz-Munoz, *Int. J. Biol. Macromol.* 2018, 119, 548-554.
- [243] Y. Nazir, A. Saeed, M. Rafiq, S. Afzal, A. Ali, M. Latif, J. Zuegg, W. M. Hussein, C. Fercher, R. T. Barnard, M. A. Cooper, M. A. T. Blaskovich, Z. Ashraf, Z. M. Ziora, *Bioorg. Med. Chem. Lett.* 2020, 30, 126722.
- [244] D. Ribeiro, C. Proença, C. Varela, J. Janela, E. J. Tavares da Silva, E. Fernandes, F. M. F. Roleira, *Bioorg. Chem.* 2019, 91, 103179.
- [245] B. Korošec, M. Sova, S. Turk, N. Kraševc, M. Novak, L. Lah, J. Stojan, B. Podobnik, S. Berne, N. Zupanec, M. Bunc, S. Gobec, R. Komel, *J. Appl. Microbiol.* 2014, 116, 955-966.
- [246] J. F. Malheiro, J. Y. Maillard, F. Borges, M. Simões, *Int. Biodeterior. Biodegrad.* 2019, 141, 71-78.
- [247] O. Forero-Doria, R. Araya-Maturana, A. Barrientos-Retamal, L. Morales-Quintana, L. Guzmán, *Molecules* 2019, 24, 3484.
- [248] A. Atmaram Upare, P. K. Gadekar, H. Sivaramakrishnan, N. Naik, V. M. Khedkar, D. Sarkar, A. Choudhari, S. Mohana Roopan, *Bioorg. Chem.* 2019, 86, 507-512.
- [249] C. Teixeira, C. Ventura, J. R. B. Gomes, P. Gomes, F. Martins, *Molecules* 2020, 25, 456.
- [250] Y. Wang, F. He, S. Wu, Y. Luo, R. Wu, D. Hu, B. Song, *Pestic. Biochem. Physiol.* 2020, 164, 115-121.
- [251] M. V. Kozlov, K. A. Konduktorov, A. Z. Malikova, K. A. Kamarova, A. S. Shcherbakova, P. N. Solyev, S. N. Kochetkov, *Eur. J. Med. Chem.* 2019, 183, 111723.
- [252] M. P. Rodrigues, D. C. Tomaz, L. Ângelo de Souza, T. S. Onofre, W. Aquiles de Menezes, J. Almeida-Silva, A. M. Suarez-Fontes, M. Rogéria de Almeida, A. Manoel da Silva, G. C. Bressan, M. A. Vannier-Santos, J. L. Rangel Fietto, R. R. Teixeira, *Eur. J. Med. Chem.* 2019, 183, 111688.
- [253] J.-S. Lan, R.-F. Zeng, X.-Y. Jiang, J.-w. Hou, Y. Liu, Z.-H. Hu, H.-X. Li, Y. Li, S.-S. Xie, Y. Ding, T. Zhang, *Bioorg. Chem.* 2020, 94, 103413.
- [254] S. Ghafary, R. Ghobadian, M. Mahdavi, H. Nadri, A. Moradi, T. Akbarzadeh, Z. Najafi, M. Sharifzadeh, N. Edraki, F. H. Moghadam, M. Amini, *DARU J. Pharm. Sci.* 2020, 28, 463-477.
- [255] Y. Bai, X. He, Y. Bai, Y. Sun, Z. Zhao, X. Chen, B. Li, J. Xie, Y. Li, P. Jia, X. Meng, Y. Zhao, Y. Ding, C. Xiao, S. Wang, J. Yu, S. Liao, Y. Zhang, Z. Zhu, Q. Zhang, Y. Zhao, F. Qin, Y. Zhang, X. Wei, M. Zeng, J. Liang, Y. Cuan, G. Shan, T.-P. Fan, B. Wu, X. Zheng, *Eur. J. Med. Chem.* 2019, 183, 111650.

- [256] X.-T. Xu, X.-Y. Deng, J. Chen, Q.-M. Liang, K. Zhang, D.-L. Li, P.-P. Wu, X. Zheng, R.-P. Zhou, Z.-Y. Jiang, A.-J. Ma, W.-H. Chen, S.-H. Wang, *Eur. J. Med. Chem.* 2020, 189, 112013.
- [257] R. Saumweber, C. Robl, W. Weigand, *Inorganica Chim. Acta* 1998, 269, 83-90.
- [258] K. Schubert, R. Saumweber, H. Görls, W. Weigand, *Z. Anorg. Allg. Chem.* 2003, 629, 2091-2096.
- [259] K. Schubert, T. Alpermann, T. Niksch, H. Görls, W. Weigand, *Z. Anorg. Allg. Chem.* 2006, 632, 1033-1042.
- [260] K. Schubert, H. Görls, W. Weigand, *Z. Naturforsch. B* 2007, 62, 475-482.
- [261] C. Mügge, R. Liu, H. Görls, C. Gabbiani, E. Michelucci, N. Rüdiger, J. H. Clement, L. Messori, W. Weigand, *Dalton Trans.* 2014, 43, 3072-3086.
- [262] C. Mügge, T. Marzo, L. Massai, J. Hildebrandt, G. Ferraro, P. Rivera-Fuentes, N. Metzler-Nolte, A. Merlino, L. Messori, W. Weigand, *Inorg. Chem.* 2015, 54, 8560-8570.
- [263] J. Hildebrandt, N. Häfner, H. Görls, D. Kritsch, G. Ferraro, M. Dürst, I. B. Runnebaum, A. Merlino, W. Weigand, *Dalton Trans.* 2016, 45, 18876-18891.
- [264] J. Hildebrandt, H. Görls, N. Häfner, G. Ferraro, M. Dürst, I. B. Runnebaum, W. Weigand, A. Merlino, *Dalton Trans.* 2016, 45, 12283-12287.
- [265] J. Hildebrandt, N. Häfner, D. Kritsch, H. Görls, M. Dürst, I. B. Runnebaum, W. Weigand, *Int. J. Mol. Sci.* 2022, 23, 4976.
- [266] J. Hildebrandt, N. Häfner, H. Görls, M.-C. Barth, M. Dürst, I. B. Runnebaum, W. Weigand, *Int. J. Mol. Sci.* 2022, 23, 6669.
- [267] M. K. Yadav, G. Rajput, K. Srivastava, R. K. Singh, R. Mishra, M. G. B. Drew, N. Singh, *New J. Chem.* 2015, 39, 6358-6366.
- [268] K. Kumari, A. S. Singh, K. K. Manar, C. L. Yadav, V. K. Tiwari, M. G. B. Drew, N. Singh, *New J. Chem.* 2019, 43, 1166-1176.
- [269] K. Kumari, S. Kumar, K. N. Singh, M. G. B. Drew, N. Singh, *New J. Chem.* 2020, 44, 12143-12153.
- [270] C. L. Yadav, Anamika, G. Rajput, K. Kumar, M. G. B. Drew, N. Singh, *Inorg. Chem.* 2020, 59, 11417-11431.
- [271] M. S. Singh, G. C. Nandi, T. Chanda, *RSC Adv.* 2013, 3, 14183-14198.
- [272] S. T. Bhaskaran, P. Mathew, *J. Mol. Struct.* 2022, 1251, 132071.
- [273] I. H. Chanu, L. M. Devi, T. P. Singh, S. J. Singh, R. R. Singh, O. Mukherjee Singh, *ChemistrySelect* 2020, 5, 7447-745.
- [274] R. K. Chellu, S. Kurva, A. K. Soda, S. K. Chilaka, J. B. Nanubolu, S. Madabhushi, *Asian J. Org. Chem.* 2021, 10, 1432-1435.
- [275] S. Soni, S. Koley, M. S. Singh, *Tetrahedron Lett.* 2017, 58, 2512-2516.
- [276] A. Thuillier, J. Vialle, *Bull. Soc. Chim. Fr.* 1962, 2182-2186.
- [277] G. Singh, S. S. Bhattacharjee, H. Ila, H. Junjappa, *Synthesis* 1982, 1982, 693-694.
- [278] H. Junjappa and H. Ila, *PCT Int. Appl.* 2004, 2004101530
- [279] P. Beslin, M. C. Houtteville, *Bull. Soc. Chim. Fr.*, 1989, 413-418.

- [280] S. K. Nair, R. Samuel, C. V. Asokan, *Synthesis*, 2001, 573–576.
- [281] S. K. Nair, C. V. Asokan, *Synth. Commun.*, 1999, 29, 791–798.
- [282] P. Kapoor, K. Löqvist, Å. Oskarsson, *J. Mol. Struct.* 1998, 470, 39-47.
- [283] G. R. Fulmer, A. J. M. Miller, N. H. Sherden, H. E. Gottlieb, A. Nudelman, B. M. Stoltz, J. E. Bercaw, K. I. Goldberg, *Organometallics* 2010, 29, 2176-2179.
- [284] M. Kazemnejadi, A. Shakeri, M. Nikookar, R. Shademani, M. Mohammadi, *R. Soc. Open Sci.* 2018, 5, 171541.
- [285] M. El Arbi, P. Pigeon, S. Top, A. Rhouma, S. Aifa, A. Rebai, A. Vessières, M.-A. Plamont, G. Jaouen, *J. Organomet. Chem.* 2011, 696, 1038-1048.
- [286] M. Patra, G. Gasser, N. Metzler-Nolte, *Dalton Trans.* 2012, 41, 6350-6358.
- [287] S. Top, J. Tang, A. Vessières, D. Carrez, C. Provot, G. Jaouen, *Chem. Commun.* 1996, 955-956.
- [288] S. Top, A. Vessières, C. Cabestaing, I. Laios, G. Leclercq, C. Provot, G. Jaouen, *J. Organomet. Chem.* 2001, 637-639, 500-506.
- [289] S. Top, A. Vessières, G. Leclercq, J. Quivy, J. Tang, J. Vaissermann, M. Huché, G. Jaouen, *Chem. Eur. J.* 2003, 9, 5223-5236.
- [290] J. Rajput, J. R. Moss, A. T. Hutton, D. T. Hendricks, C. E. Arendse, C. Imrie, *J. Organomet. Chem.* 2004, 689, 1553-1568.
- [291] J. Schulz, A. K. Renfrew, I. Císařová, P. J. Dyson, P. Štěpnička, *Appl. Organomet. Chem.* 2010, 24, 392-397.
- [292] D. Nieto, A. M. González-Vadillo, S. Bruña, C. J. Pastor, C. Ríos-Luci, L. G. León, J. M. Padrón, C. Navarro-Ranninger, I. Cuadrado, *Dalton trans.* 2012, 41, 432-441.
- [293] N. Aoyagi, B. Ochiai, H. Mori, T. Endo, *Synlett* 2006, 2006, 0636-0638.
- [294] R. S. Chauhan, D. B. Cordes, A. M. Z. Slawin, S. Yadav, C. Dash, *Inorganica Chim. Acta* 2018, 478, 125-129.
- [295] K. Ramesh, A. K. Mishra, J. K. Kim, Y. T. Jeong, Y.-S. Gal, K. T. Lim, in *Materials*, Vol. 13, 2020.
- [296] K. Ramesh, D. S. B. Anugrah, K. T. Lim, *React. Funct. Polym.* 2018, 131, 12-21.
- [297] A. J. van der Vlies, J. Xu, M. Ghasemi, C. Bator, A. Bell, B. Rosoff-Verbit, B. Liu, E. D. Gomez, U. Hasegawa, *Biomacromolecules* 2022, 23, 77-88.
- [298] M. Semsarilar, V. Abetz, *Macromol. Chem. Phys.* 2021, 222, 2000311.
- [299] F. D'Agosto, J. Rieger, M. Lansalot, *Angew. Chem. Int. Ed.* 2020, 59, 8368-8392.
- [300] S. Perrier, *Macromolecules* 2017, 50, 7433-7447.
- [301] J. Rieger, *Macromol. Rapid Commun.* 2015, 36, 1458-1471.
- [302] G. Moad, E. Rizzardo, S. H. Thang, *Aust. J. Chem.* 2005, 58, 379-410.
- [303] G. Moad, E. Rizzardo, S. H. Thang, *Aust. J. Chem.* 2012, 65, 985-1076.
- [304] A. Gregory, M. H. Stenzel, *Prog. Polym. Sci.* 2012, 37, 38-105.
- [305] M. D. Nothling, Q. Fu, A. Reyhani, S. Allison-Logan, K. Jung, J. Zhu, M. Kamigaito, C. Boyer, G. G. Qiao, *Adv. Sci.* 2020, 7, 2001656.

- [306] D. J. Keddie, G. Moad, E. Rizzardo, S. H. Thang, *Macromolecules* 2012, 45, 5321-5342.
- [307] M. Destarac, *Polym. Rev.* 2011, 51, 163-187.
- [308] B. V. K. J. Schmidt, M. Hetzer, H. Ritter, C. Barner-Kowollik, *Macromolecules* 2011, 44, 7220-7232.
- [309] I. Kulai, O. Brusylovets, Z. Voitenko, S. Harrisson, S. Mazières, M. Destarac, *ACS Macro Lett.* 2015, 4, 809-813.
- [310] S. Pearson, C. St Thomas, R. Guerrero-Santos, F. D'Agosto, *Polym. Chem.* 2017, 8, 4916-4946.
- [311] G. Gody, C. Rossner, J. Moraes, P. Vana, T. Maschmeyer, S. Perrier, *J. Am. Chem. Soc.* 2012, 134, 12596-12603.
- [312] J. C. Brendel, L. Martin, J. Zhang, S. Perrier, *Polym. Chem.* 2017, 8, 7475-7485.
- [313] G. Gody, D. A. Roberts, T. Maschmeyer, S. Perrier, *J. Am. Chem. Soc.* 2016, 138, 4061-4068.
- [314] J. C. Brendel, G. Gody, S. Perrier, *Polym. Chem.* 2016, 7, 5536-5543.
- [315] V. Ladmiral, T. M. Legge, Y. Zhao, S. Perrier, *Macromolecules* 2008, 41, 6728-6732.
- [316] S. Vandewalle, S. Billiet, F. Driessen, F. E. Du Prez, *ACS Macro Lett.* 2016, 5, 766-771.
- [317] Z. Zhang, N. Vanparijs, S. Vandewalle, F. E. Du Prez, L. Nuhn, B. G. De Geest, *Polym. Chem.* 2016, 7, 7242-7248.
- [318] C. Boyer, M. H. Stenzel, T. P. Davis, *J. Polym. Sci., Part A: Polym. Chem.* 2011, 49, 551-595.
- [319] W. H. Binder, R. Sachsenhofer, *Macromol. Rapid Commun.* 2008, 29, 952-981.
- [320] T. A. Wright, M. S. Rahman, C. Bennett, M. R. Johnson, H. Fischesser, N. Ram, A. Tyler, R. C. Page, D. Konkolewicz, *Bioconjugate Chem.* 2021, 32, 2447-2456.
- [321] G. Delaittre, N. K. Guimard, C. Barner-Kowollik, *Acc. Chem. Res.* 2015, 48, 1296-1307.
- [322] M. L. Coote, D. J. Henry, *Macromolecules* 2005, 38, 1415-1433.
- [323] M. Destarac, I. Gauthier-Gillaizeau, C.-T. Vuong, S. Z. Zard, *Macromolecules* 2006, 39, 912-914.
- [324] A. Goncalves, J. R. Domínguez, J. Alvarado, *Talanta* 2008, 75, 523-527.
- [325] A. Calvo Fornieles, A. García de Torres, E. Vereda Alonso, J. M. Cano Pavón, *Microchem. J.* 2016, 124, 82-89.
- [326] M. M. L. Guerrero, E. V. Alonso, A. García de Torres, J. M. C. Pavón, *J. Anal. At. Spectrom.* 2017, 32, 2281-2291.
- [327] F. C. Pinheiro, A. I. Barros, J. A. Nóbrega, *Microchem. J.* 2019, 146, 948-956.

## **9. Acknowledgements**

My research has been significantly influenced by many people who have helped in some way or another. Here, it is only appropriate that I acknowledge them and thank them for their support. My gratitude goes out to my supervisor, prof. Dr. Wolfgang Weigand, for his fruitful and kind guidance and for his encouragement and confidence in me, which have helped me become a more confident researcher. As far as research strategies are concerned, he always allowed me to follow my research and supported me in my endeavor.

In addition, I would like to thank Dr. Helmar Görls for the X-ray structure determination of my compounds, as well as everyone at the IAAC institute who measured NMR, Ms spectra and performed elemental analysis.

Moreover, I would like to express my gratitude to Dr. Johannes Brendel, Dr. Hassan Abul-Futouh, Dr. Franka Gruschwitz, Nicole Ziegenbalg, Philipp Buday, Chizuru Kasahara, and Ibrahim Basma for their productive collaborations.

I would also like to acknowledge Dr. Norman Häfner for the biological experiments he did, that complemented my work in a meaningful way. Likewise, I would like to thank prof. Dr. Matthias Dürst and prof. Dr. Ingo Runnebaum.

Many thanks to all my friends and colleagues, Hani Elbeheiry, Walid Al-Jammal, Mohamed Zayed, Abdulaziz Diab, Xiao Liu, Stefan Benndorf, Dr. Fadi Younis, Dr. Marius Alexander Wünsche, and Dr. Samuel Lawrence, who helped me with my research, German, and day-to-day life in Jena over the years.

I would like to thank the Journal of Sulfur Chemistry for permitting including the second article in my thesis.

Finance is of course essential for any Ph.D. student. I am grateful for the Katholischer Akademischer Ausländer-Dienst (KAAD), which granted me the Ph.D. scholarship, that is greatly appreciated.

Over the past years, my family has been an unwavering pillar of support. It is my pleasure to thank my family for their support in my life, especially my wife Nermeen Nageeb, a great mother, who took care of our children in Egypt while I was doing my Ph.D. in Germany. I greatly appreciate the kindness of my wife Nermeen Nageeb, my lovely daughter Miley Eshak, and my sweet son Asser Eshak, whom I missed terribly during my Ph.D.

## 10. Curriculum Vitae

### Micheal Eshak

Ph.D. Student at Institute of Inorganic  
and Analytical Chemistry,  
Friedrich-Schiller-Universität Jena



#### 1. Address

**Current Address:**

Institute of Inorganic and Analytical Chemistry, Humboldtstraße 8, 07743 Jena, Germany

**Permanent Address:**

Department of Chemistry, Faculty of Science, Assiut University, Assiut 71515, Egypt

Tel: +201227742042

Fax: +49 3641 9-48102

E-mail: [micheal\\_kamal\\_farh@science.au.edu.eg](mailto:micheal_kamal_farh@science.au.edu.eg)  
[micheal.eshak@uni-jena.de](mailto:micheal.eshak@uni-jena.de)

#### 2. Personal Background

**Date of Birth:** 8 June 1988

**Nationality:** Egyptian

**Place of Birth:** Assiut, Egypt

**Marital Status:** Married, 2 kids

#### 3. Objective

Efficient contribution in Medicinal Chemistry & Material Science.

#### 4. Educational Background

03/2011 – 11/2015	<b>Master's degree in</b> Inorganic Chemistry from Chemistry Department, Assiut University, Egypt. <b>Title of the thesis:</b> Transition Metal Complexes of N(4)-Substituted Thiosemicarbazones Derived From Pyridine-2-Carbaldehyde.
03/2010 – 03/2011	<b>Preparatory Year (Diploma) in</b> Inorganic Chemistry from Chemistry Department, Assiut University, Egypt with General grade (very good and the degree of honor, 82.86%).
09/2005 – 06/2009	<b>Bachelor of Science</b> in Chemistry from Chemistry Department, Assiut University, Egypt with General grade (very good and the degree of honor, 83.28%).
09/2002 – 06/2005	<b>High School</b> Science Division, Naser Secondary School, Assiut, Egypt with record of 91.5 %.



## 5. Courses Studied (selected)

Master (2010 – 2011)	1. Advanced Stereochemistry
	2. Advanced Inorganic Synthetic Chemistry
	3. Advanced Analytical Chemistry
	4. Advanced Electrochemical Chemistry
	5. Advanced Inorganic Chemistry
	6. Advanced IT course
	7. Advanced English course
Bachelor (2006 – 2009)	1. Inorganic Chemistry
	2. Molecular Spectroscopy
	3. Molecular Symmetry and Group Theory
	4. Stereochemistry
	5. Biochemistry
	6. Photochemistry
	7. Statistical Thermodynamics
	8. Thermodynamics
	9. Quantum Chemistry
	10. Organic Chemistry
	11. Analytical Chemistry
	12. Quantum Physics
	13. Physics of Vibrations and Waves
	14. Calculus (Differential and Integral)
	15. Differential equations
	16. Algebra and Linear Algebra
	17. Geometry
	18. Statistics
	19. Programming languages (FORTRAN and Basic)
	20. Crystallography

## 6. Employment Record and Research Experience

03/2010 – 11/2015	Demonstrator of Inorganic & Analytical Chemistry, Faculty of science, Assiut University.
12/2015 – 01/2018	Assistant Lecturer of Inorganic & Analytical Chemistry, Faculty of science, Assiut University.
07/2018 – until now	Ph.D. Student at IAAC, Friedrich-Schiller-Universität Jena

## 7. Technical Experience

UV-Vis spectroscopy	NMR	X-Ray
FT- IR spectroscopy	Mass spectrometry	HPLC-UV
Fluorescence spectroscopy	Elemental analyzer	Magnetic susceptibility
Molar conductometer	DTG 60-H thermal analyzer	Autoclaving
Reactions under inert conditions		

## 8. Teaching Experience

Course	Date	Target Ss	Place
Qualitative Analysis (Identification of simple inorganic salts).	03/2010 -01/2018	Science and Education Faculties Students (Students of 1 <sup>st</sup> year)	Assiut University
Volumetric Analysis.	03/2010 -01/2018	Science Faculty Students (Students of 1st and 2 <sup>nd</sup> year)	Assiut University
Gravimetric Analysis.	03/2010 -01/2018	Science Faculty Students (Students of 3rd year)	Assiut University
Practical Physical Chemistry.	03/2010 -01/2018	Science Faculty Students (Students of 3rd year)	Assiut University
Inorganic Synthesis	03/2010 -01/2018	Science Faculty Students (Students of 3rd year)	Assiut University
Instrumental Analysis.	03/2010 -01/2018	Science Faculty Students (Students of 4th year)	Assiut University

## 9. Training Courses

1. **SSDP** Student Skills Development Program by RTC (Recruitment & Training committee), Assiut University, Egypt (2009).
2. Pharmaceutical clinical Practice (clinical Pharmacology), Cairo University, Egypt (2008).
3. Summer internship Program In operations area, Raw mills & Kilns department, and Quality Assurance department, Assiut CEMEX Cement Company, Egypt (2007)
4. Training in Oil Refraining Labs, Assiut Oil Refining Company, Egypt (2007)

## 10. Conferences

1. S. A. El-Gyar, S. A. Ibrahim, M. A. El-Gahami, D. M. Fouad, **M. K. Farh**, Structural and Spectral studies of Novel Mn(II) Complexes of Substituted Thiosemicarbazone Derived from Pyridine-2-Carbaldehyde, The 5<sup>th</sup> International Conference for Young Researchers, Assiut University, Egypt, April (2016).
2. S. A. El-Gyar, S. A. Ibrahim, M. A. El-Gahami, D. M. Fouad, **M. K. Farh**, Synthesis and Characterization of Novel Ni(II) and Cu(II) Complexes of Substituted Thiosemicarbazone Derived from Pyridine-2-Carbaldehyde, The 4<sup>th</sup> International Conference for Young Researchers, Assiut University, Egypt, April (2014).

## 11. Publications

1. A. B. M. Ibrahima, **M. K. Farh**, S. A. El-Gyara, M.A. EL-Gahamia, D. M. Fouad, F. o Silva, I. C. Santos, A. Paulo, Synthesis, structural studies and antimicrobial activities of manganese, nickel and copper complexes of two new tridentate 2-formylpyridine thiosemicarbazone ligands, *Inorg. Chem. Commun.*, **2018**, 96, 194–201.
2. A. B. M. Ibrahima, **M. K. Farh**, P. Mayer, Copper complexes of new thiosemicarbazone ligands: Synthesis, structural studies and antimicrobial activity, *Inorg. Chem. Commun.*, **2018**, 94, 127–132.

- A. B. M. Ibrahima, **M. K. Farh**, J. R Plaisier, E. M. Shalaby, Synthesis, structural and antimicrobial studies of binary and ternary complexes of a new tridentate thiosemicarbazone, *FutureMed. Chem.*, **2018**, 10(21), 2507–2519.
- A. B. M. Ibrahima, **M. K. Farh**, P. Mayer, Synthesis, structural studies, and antimicrobial evaluation of nickel (II) complexes of NNS tridentate thiosemicarbazone based ligands, *Appl. Organometal. Chem.*, **2019**, 33, e4883.
- A. B. M. Ibrahima, **M. K. Farh**, I. C. Santos, A. Paulo, Nickel Complexes Bearing SNN and SS Donor Atom Ligands: Synthesis, Structural Characterization and Biological activity, *Appl. Organometal. Chem.*, **2019**, 33, e5088.
- P. Buday, C. Kasahara, E. Hofmeister, D. Kowalczyk, **M. K. Farh**, S. Riediger, M. Schulz, M. Wächtler, S. Furukawa, M. Saito, D. Ziegenbalg, S. Gräfe, P. Bäuerle, S. Kupfer, B. Dietzek-Ivanšić, W. Weigand, Activating a [FeFe] Hydrogenase Mimic for Hydrogen Evolution under Visible Light, *Angew. Chem. Int. Ed.* 2022, 61, e202202079; *Angew. Chem.* **2022**, 134, e202202079.
- M. K. Farh**, F. V. Gruschwitz, N. Ziegenbalg, H. Abul-Futouh, H. Görls, W. Weigand, J. C. Brendel, Dual Function of  $\beta$ -Hydroxy Dithiocinnamic Esters: RAFT Agent and Ligand for Metal Complexation, *Macromol. Rapid Commun.*, **2022**, n/a, 2200428.
- M. K. Farh**, I. Louzi, H. Abul-Futouh, H. Görls, N. Häfner, I. B. Runnebaum, W. Weigand, Platinum(II) and palladium(II) complexes mediated by  $\beta$ -hydroxy-dithioesters ferrocenyl derivatives: synthesis, characterization and Antiproliferative Activity, *J. Sulphur Chem.*, **2022**, DOI: 10.1080/17415993.2022.2152285.

## 12. Language Proficiency

**English:** Very Good

**German:** Elementary

**Arabic:** Native language

## 13. Personal Skills

Excellent communication Skills, Self-Confidence, Able to work under pressure, Self-motivated, Creative, Hard worker, Well-organized, Quick learner and Enjoy challenges.

## 14. Hobbies

Traveling, Football and Handball

## 15. References

- Prof. Dr. **Wolfgang Weigand** Professor of Inorganic and Analytical Chemistry, Institute of inorganic und analytical chemistry, Humboldtstraße 8, 07743 Jena, Germany, **E-mail:** [wolfgang.weigand@uni-jena.de](mailto:wolfgang.weigand@uni-jena.de)
- Prof. Dr. **Said Ahmed Ibrahim** Professor of Inorganic Chemistry, Department of Chemistry, Faculty of Science, Assiut University, Assiut 71516, Egypt, **E-mail:** [saidib@aun.edu.eg](mailto:saidib@aun.edu.eg)

.....  
Micheal Eshak

## **11. Declaration of Authorship**

I declare that this thesis and the work presented herewith are my own and have been generated by me as the result of my own original research.

## **12. Selbstständigkeitserklärung**

Ich erkläre, dass ich die vorliegende Arbeit selbstständig und unter Verwendung der angegebenen Hilfsmittel, persönlichen Mitteilungen und Quellen angefertigt habe.

Jena,

---

Micheal Eshak